e-ISSN : 2320-0847
p-ISSN : 2320-0936

American Journal of Engineering Research (AJER)

Volume 2 Issue 10 – October 2013

www.ajer.org ajer.research@gmail.com

Editorial Board

American Journal of Engineering Research (AJER)

Volume-2 Issue-10

American Journal of Engineering Research (AJER)
e-ISSN : 2320-0847 p-ISSN : 2320-0936
Volume-02, Issue-10, pp-01-10
www.ajer.org

Research Paper Open Access

Polyethylene Terephthalate (Pete) And High Density Polyethylene (Hdpe) Mixture To Fuel Production

Moinuddin Sarker[1], Mohammad Mamunor Rashid[2]
[1,2] Natural State Research, Inc., Department of Research and Development, 37 Brown House Road (2nd Floor), Stamford, CT-06902, USA

Abstract: - High density polyethylene (HDPE) and polyethylene terephthalate (PETE) mixture to fuel production process was performed with Ferric Oxide (Fe_2O_3) and activated carbon. HDPE waste plastic was use 75 gm, PETE was use 25 gm, activated carbon was use 5 gm as a 5% and Ferric Oxide was use 2 gm as a 1%. PETE and HDPE waste plastics mixture to fuel production process temperature was use 420 ºC and reactor was use Pyrex glass reactor. Total waste plastics sample was 100 gm and 100 gm of waste plastic mixture to fuel was collected 50.1 gm. PETE and HDPE waste plastic mixture to fuel density is 0.76 gm/ml. Liquid fuel was analysis by FT-IR, GC/MS and DSC for fuel functional group, compounds structure and enthalpy value determination. Product fuel is ignited and fuel can use an internal combustion engine.

Keywords: - *HDPE, PETE, fuel, thermal, catalyst, hydrocarbon, waste plastics, FT-IR*

I. INTRODUCTION

In modern life, the application of polymers is common. This kind of material is present in packaging, the electrical industry, in toys, etc. High-density polyethylene (HDPE), low-density polyethylene (LDPE), polypropylene (PP), polyvinyl chloride (PVC), polystyrene (PS), and polyethylene terephtalate (PET) are the most extensively used plastics. The polyethylene plastics (HDPE and LDPE) are the major components of the total plastic content of municipal solid waste. [1-4] Volume of plastics currently represent 24% of the MSW, due to their low density. Moreover, medical red-bag (infectious) waste contains a much higher fraction of plastics, as high as 40 wt %. The current methods for dealing with the environmental problems resulting from this solid waste include source reduction, reuse, recycling, landfill, and waste-to-energy conversion. Most solid wastes are disposed through landfilling. However, with the lack of landfill space and with current challenges both in implementing the recycling of plastics and in finding markets for the recyclables, combustion of these materials in waste-to-energy (WTE) plants offers an alternative of technological and economic interest. Combustion of waste plastics provides a number of advantages, such as destruction of hazardous contaminants, reduction of mass and volume (by more than 90%), and energy recovery, as well as rendering the waste unrecognizable from its original form (which is often a requirement for medical waste). [5]

Recycling of plastics has a positive environmental impact; in most cases it is not yet economically attractive. So far, industry has focused efforts in plastics recycling on the recovery and reuse of polymers by mechanical processing. However, mechanical technologies require relatively clean feedstocks that are expensive to collect and separate. For this reason, commercial recycling has not had a significant impact with the collection rate of less than 5% of total annual resin sales.[6] Producing hydrogen from waste plastics could complement conventional recycling techniques because it could use more complex materials that are not handled by existing processes, e.g. mixed plastics, polyester-cotton blends, rigid polyurethane foams. The challenge is to efficiently convert these polymers to hydrogen at a cost similar to that for the existing natural-gas-based technologies. Plastics have a high calorific value (i.e., polyethylene 43 MJ/ kg, polypropylene 44 MJ/kg, polyvinyl chloride 20 MJ/kg), and their combustion can be an alternative to removing them. [7]This alternative must, however, be subjected to severe environmental controls in order to fulfill the legal restrictions concerning the emission of solid particles and gaseous effluents.[7,8,9] Landfills have also been used for plastic disposal, but these can pose a danger through the environment product degradation and the subsequent pollutant generation.[8,9] A promising alternative for the reprocessing of waste plastics is feedstock recycling, which

involves the conversion of plastics residue into raw chemicals, monomers for plastics or hydrocarbon feedstocks. In this way, thermal degradation has been used to convert different polyolefins into hydrocarbon mixtures. [10-12]

The thermal decomposition of polyolefins at temperatures of 400 °C or higher produce a mixture of hydrocarbons that is formed by a gas fraction (C_1-C_4), a liquid fraction (C_5-C_{18}), and a solid residue (C_{19}-C_{70}). For each number of C atoms, three main components are produced: the corresponding n-paraffin, α-olefin, and α, ω-diene. The relative proportion of these products is dependent on the thermal degradation operating conditions, which are determined mainly by the temperature.[13] The thermal degradation of polyolefins involves complex reactions through a radical mechanism, and their extension is very dependent on temperature, pressure, reactor geometry, and heat- and mass-transfer rates, as well as mixing intensity. Polymerssand particularly polyolefins shave high viscosity, which hinders mass- and heat-transfer phenomena.[14,15] The terminal double bond of α-olefins presents a high reactivity, in regard to a wide variety of chemicals, and, therefore, they are used to produce any derivative requiring an even-numbered, straight carbon chain. In this sense, α-olefins are utilized as intermediates in the manufacture of many commercial products, including plastics (e.g., HDPE and LDPE), synthetic lubricants (e.g., poly-α-olefins, polyol esters), surfactants (e.g., α-olefin sulfonates, alkyl benzene sulfonates, alkyl dimethyl amines), additives (e.g., alkenyl succinic anhydrides, and polyvinylchloride lubricants and stabilizers) and specialty chemicals (e.g., epoxides, halogenated α-olefins).[16]

II. MATERIALS

PETE waste was collected water bottle and HDPE was collected milk container for experimental purpose. Both waste plastics cut into small pieces and places into glass reactor chamber including activated carbon and Ferric Oxide. Activated carbon and Ferric Oxide (Fe_2O_3) was collected from VWR. Com Company. Ferric Oxide (Fe_2O_3) was powder type and activated carbon was pellet type.

III. PROCESS DESCRIPTION

PETE and HDPE mixture to fuel production process was performed under the laboratory fume hood and production process was batch process. Total sample was use for experiment 100 gm of waste plastics mixture. PETE was 25 gm and HDPE was 75 gm, ferric oxide was 2 gm and activated carbon was 5 gm. 25 gm of PETE and 75 gm of HDPE waste plastic to fuel production was determine from less percentage of PETE and high percentage of HDPE waste plastics mixture. Catalyst was use for reaction acceleration and helping to breakdown polymer bond by using thermal degradation process. For experimental temperature was use starting 180 ºC to up to 420 ºC and temperature was increase slowly. Experimental setup purpose was use boiling flask for raw sample melting and fuel collection, heat mental with temperature controller, condensation unit, clamp, grease, foil paper for cover up the heat loss. Small pieces waste plastics placed into boiling flask inside with Ferric Oxide and activated carbon. Then boiling flask was placed into heating chamber for waste plastic melting. Then condensation unit was setup with sample provided boiling neck and fuel collection boiling flask neck with thermal protect grease. Because during production period gas loss prevention. This experiment main goal was PETE and HDPE waste plastics to fuel production recover measurement. PETE waste plastic has carbon chain with hydrogen combination and PETE waste plastic has carbon, hydrogen, benzene with oxygen combination and PETE waste plastic oxygen percentage more than 30%. Both plastic was heated up at 180 ºC to up to 420 ºC. Experimental process was monitor closely inside laboratory fume hood because during fuel production period was notice that boiling flask inside gas was generated huge amount. Sometimes temperature profile was increase and sometimes temperature profile was decreased for quality fuel product. Production process flow chart is showing in figure 1. Production process flow chart is showing waste plastic and Ferric Oxide was placed into reactor chamber then condensation unit, and alkali solution was use for light gas cleaning NaOH, $NaHCO_3$ and water. Light gas was produce during fuel production period and gas was captured into Teflon bag by using small pump. Residue was collected after fuel production finished when is reactor was cool down. In mass balance calculation production result showed liquid fuel was 50.1 gm, light gas was produced 16.5 gm and residue and solid pest was 24.4 gm + 9 gm. During production period PETE waste plastic was unable to fuel conversion into fuel because PETE waste plastic has Oxygen content more than 30% which was not convertible. It's was coming as solid pest wise and it collected from condensation and weight was 9 gm. The PETE waste plastic to fuel production period its try to block the condensation unit and it coming out with liquid fuel which is shown in figure 2 and figure 3 and total experiment run time was 4 hour 35 minute. From liquid fuel to wax part was removing after filtering process and solid wax part keep into separate container. This type of solid wax portion was coming from PETE waste plastic because PETE has high percentage of Oxygen. Light gas analysis is under investigation. Liquid and light gas percentage was 66.6%, residue was 9% and solid pest was 24.4% which was not convertible see figure 2. Some portion of sediment part was come out with liquid fuel

and shown into figure 3. Fuel sediment was separated by filtering system. Fuel color is light yellow and fuel is ignite.

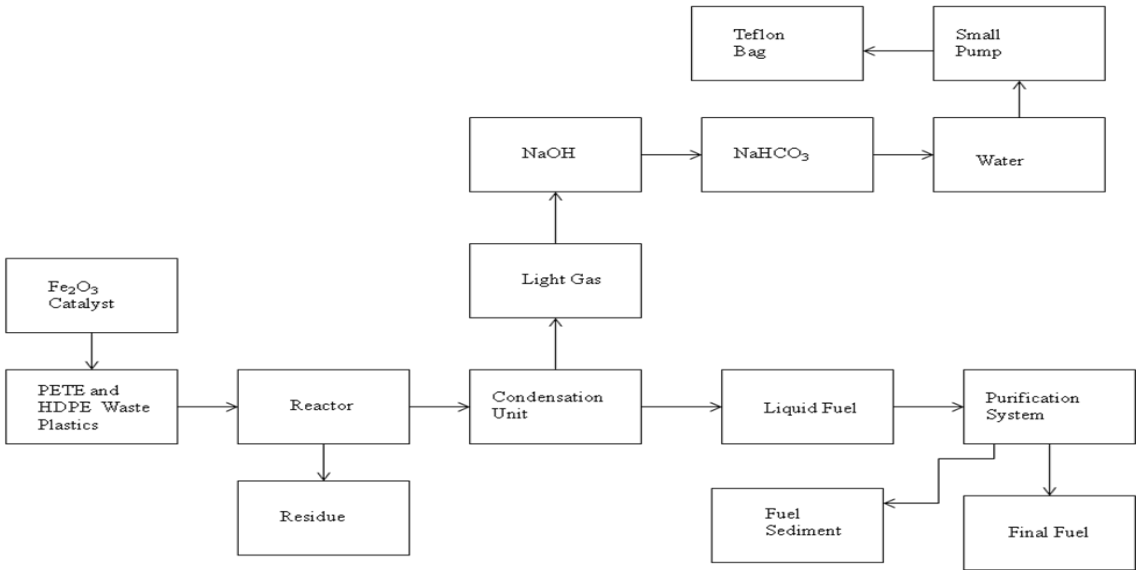

Figure 1: HDPE and PETE mixture to fuel production

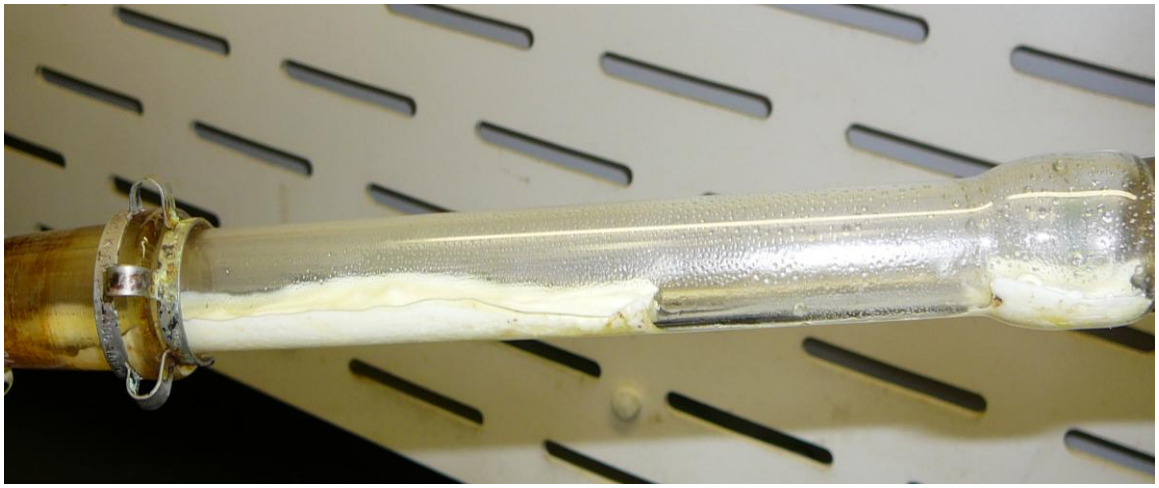

Figure 2: Wax type materials in the condensation pipe inside during PETE and HDPE waste plastic mixture to fuel production period.

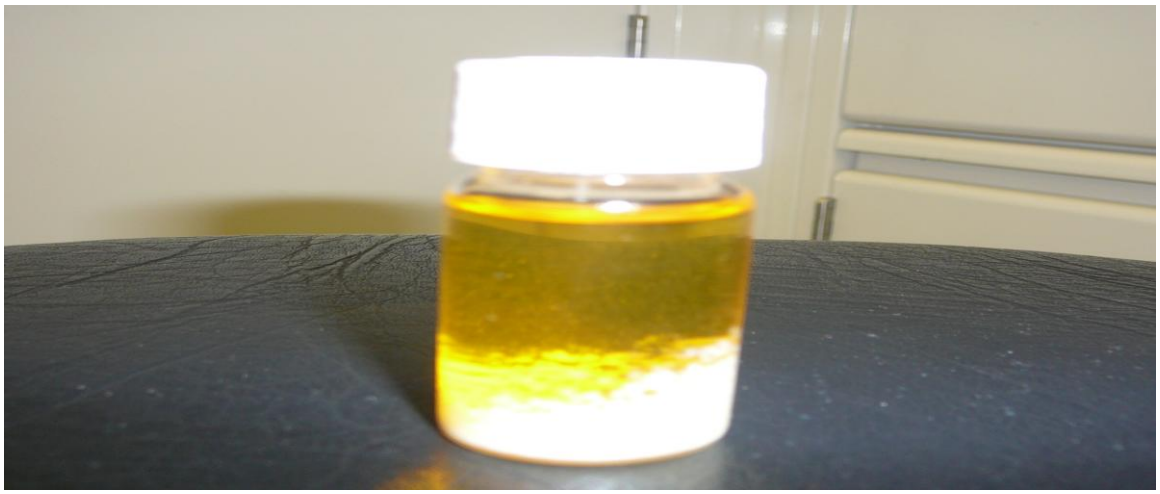

Figure 3: PETE and HDPE waste plastics mixture to fuel with wax

IV. RESULT AND DISCUSSION

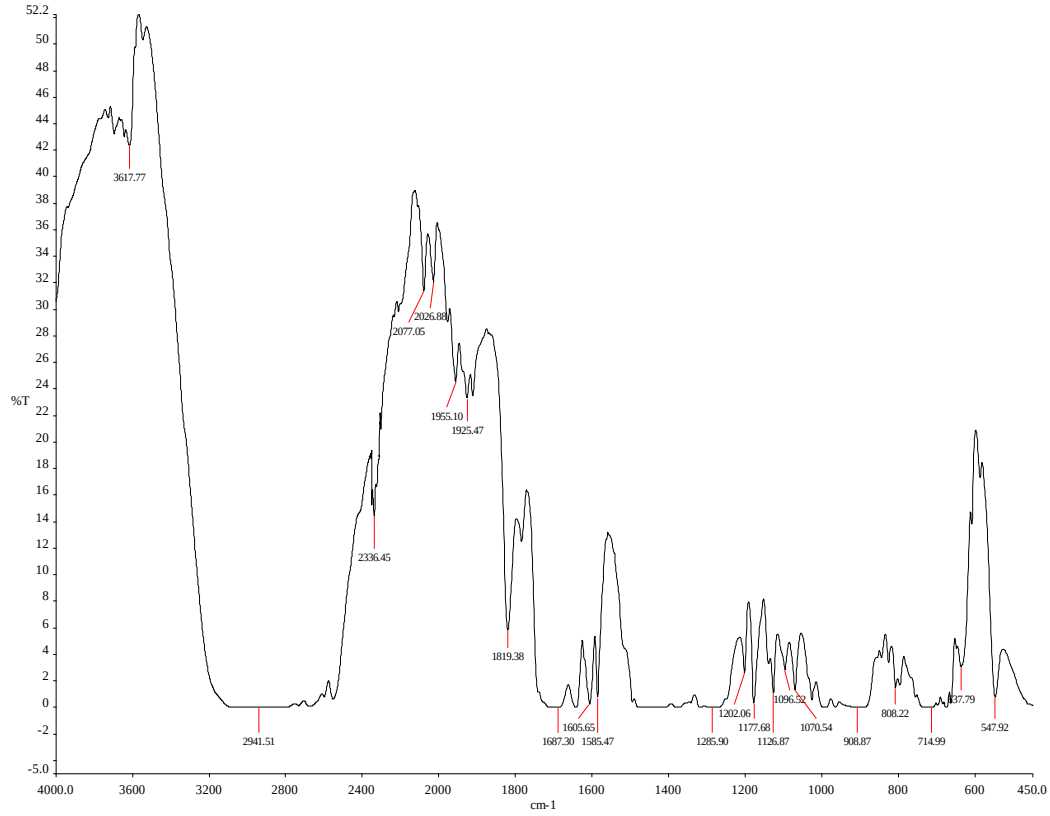

Figure 4: FT-IR spectrum of PETE and HDPE mixture to fuel

Table 1: FT-IR spectrum functional group list of PETE and HDPE mixture to fuel

Number of Wave	Wave Number	Compound/Functional Group
1	3617.77	Free OH
2	2941.51	C-CH_3
3	2336.45	
4	2077.05	C-C= -C-C= -CH
5	2026.88	
6	1955.10	
7	1925.47	
8	1819.38	Non-Conjugated
9	1687.30	Non-Conjugated
10	1605.65	Non-Conjugated
11	1585.47	Conjugated
12	1285.90	
13	1202.06	
14	1177.68	~Formates
15	1126.87	
16	1096.52	
17	1070.54	
18	908.87	-CH=CH_2-
19	808.22	
20	714.99	-CH=CH-(cis)
21	637.79	-CH=CH-(cis)
22	547.92	

FTIR analysis of 25% PETE and 75% HDPE with 5% Activated Carbon and 2% Fe_2O_3 to fuel (figure 4 and table 1) according to their wave number and spectrum band following types of functional groups are appeared in the analysis. In the spectrum field we noticed that higher wave number are emerged in the initial phase and middle index of the spectrum in higher wave number small and bulky both functional groups are available and

in low wave number double bond and single bond functional groups are available such as methane group,trans and alkene group etc. Hereafter wave number 3617.77 cm^{-1} functional group is Free OH, wave number 2941.51 cm^{-1}, functional group is C-CH_3, wave number 2077.05 cm^{-1}, functional group is C-C= -C-C= -CH, wave number 2186.56 cm^{-1} functional group is C-C=-C-C=-CH, wave number 1819.38 cm^{-1} , 1687.30 cm^{-1} and 1605.65 cm^{-1} functional group is Non-Conjugated, wave number 1585.47cm^{-1}, functional group is Conjugated , wave number 1177.68cm^{-1} functional group is ~Formates, wave number 908.87 cm^{-1} functional group is -CH=CH_2-, and ultimately wave number 714.99 cm^{-1} and 637.79 cm^{-1} functional group is -CH=CH-(cis) as well. Energy values are calculated, using formula is E=hυ, Where h=Planks Constant, h =$6.626x10^{-34}$ J, υ=Frequency in Hertz (sec^{-1}), Where υ=c/λ, c=Speed of light, where, c=299,792,458 m/s, W=1/λ, where λ is wave length and W is wave number in cm^{-1}. Therefore the equation E=hυ, can substitute by the following equation, E=hcW. According to their wave number several energy values are calculated such as for wave number 3671.77 (cm^{-1}) calculated energy, E=$7.18x10^{-20}$ J, wave number 2941.51 (cm^{-1}) calculated energy, E=$5.84x10^{-20}$ J, wave number 2077.05 (cm^{-1}), calculated energy, E=$4.12x10^{-20}$ J, wave number 1819.38 (cm^{-1}), calculated energy, E=$3.61x10^{-20}$ J, wave number 1585.47 (cm^{-1}), calculated energy, E=$3.14x10^{-20}$ J, wave number 908.87 (cm^{-1}), calculated energy, E=$1.80x10^{-20}$ J and ultimately wave number 714.99 (cm^{-1}), calculated energy, E=$1.42x10^{-20}$ J respectively .

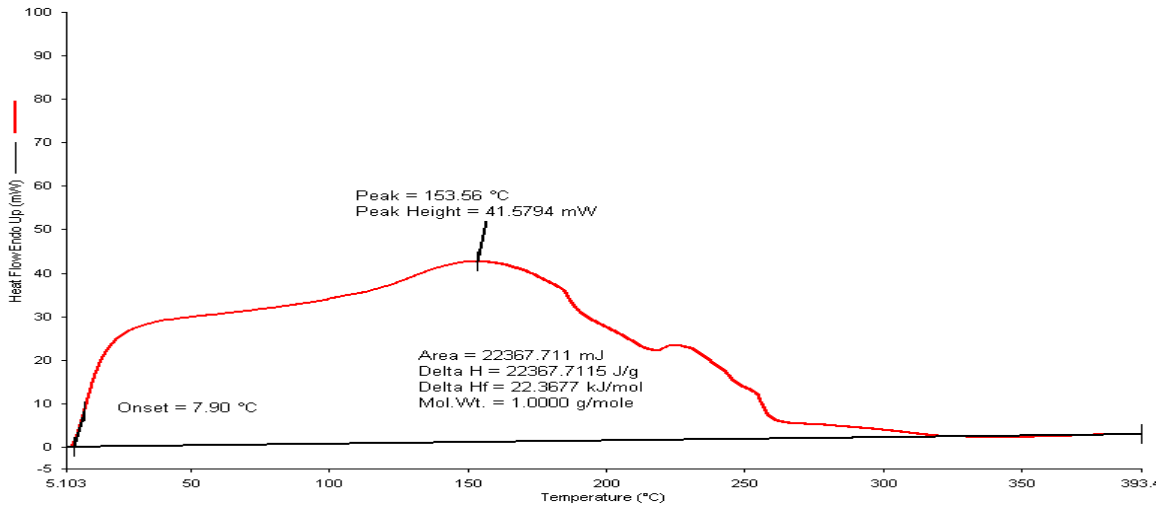

Figure 5: DSC graph of PETE and HDPE waste plastics mixture to fuel

PETE and HDPE waste plastics mixture to fuel product was analysis (Figure 5) by DSC for fuel enthalpy value. DSC run temperature was 5 ºC to 400 ºC and temperature ramping rate was 10 ºC. DSC carrier gas was use Nitrogen and pan was use aluminum. DSC fuel graph showed onset temperature is 7.90 ºC, Peak is 153.56 ºC and peak height is 41.5794 mW. Graph area is 22367.711 mJ, delta H value or enthalpy value is 22367.7115 J/g and a delta Hf value is 22.3677 kJ/mol.

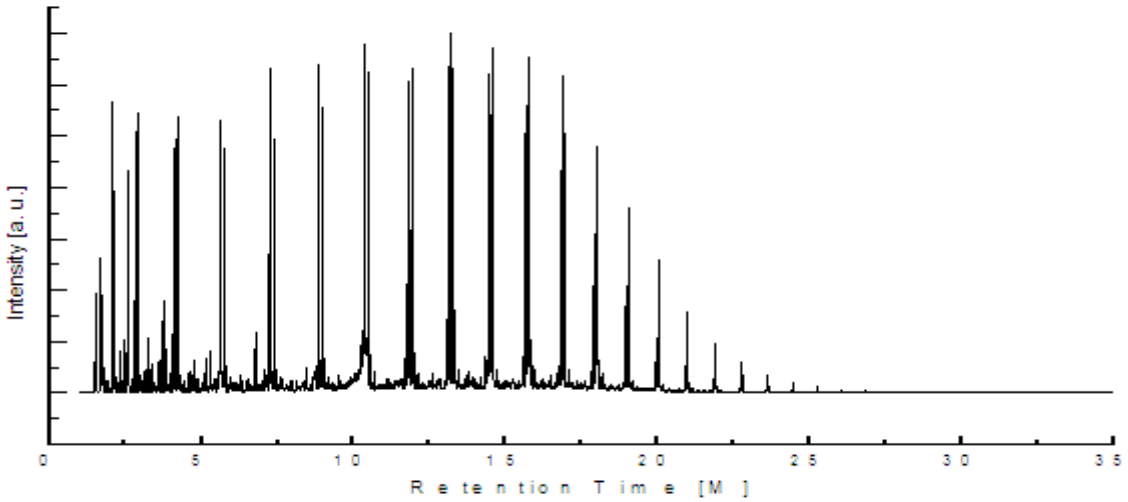

Figure 6: GC/MS Chromatogram of PETE and HDPE waste plastics mixture to fuel

Table 2: GC/MS Chromatogram compounds list of PETE and HDPE waste plastics mixture to fuel

Peak Number	Retention Time (M.)	Trace Mass (m/z)	Compound Name	Compound Formula	Molecular weight	Probability Percentage	NIST Library Number
1	1.48	41	Propane	C_3H_8	44	58.1	18863
2	1.54	41	Butane, 1-isocyano-	C_5H_9N	83	28.1	39412
3	1.69	42	Cyclopropane, ethyl-	C_5H_{10}	70	21.9	19072
4	1.71	43	Pentane	C_5H_{12}	72	83.4	114462
5	1.79	67	1,3-Pentadiene	C_5H_8	68	25.7	291890
6	1.95	42	Butane, 2,3-dimethyl-	C_6H_{14}	86	13.8	291518
7	2.08	56	Cyclopropane, 1-ethyl-2-methyl-, cis-	C_6H_{12}	84	20.9	113658
8	2.12	57	Hexane	C_6H_{14}	86	85.5	61280
9	2.16	55	3-Hexene, (Z)-	C_6H_{12}	84	22.9	114381
10	2.22	67	Cyclobutene, 3,3-dimethyl-	C_6H_{10}	82	7.91	62288
11	2.33	56	Cyclopentane, methyl-	C_6H_{12}	84	63.5	114428
12	2.41	79	1,3-Cyclopentadiene, 5-methyl-	C_6H_8	80	16.1	419
13	2.50	67	Cyclopentene, 1-methyl-	C_6H_{10}	82	13.8	107747
14	2.59	78	Benzene	C_6H_6	78	68.5	291514
15	2.76	67	Cyclohexene	C_6H_{10}	82	16.9	114431
16	2.85	56	1-Heptene	C_7H_{14}	98	36.4	107734
17	2.94	43	Heptane	C_7H_{16}	100	75.9	61276
18	3.02	41	2-Heptene	C_7H_{14}	98	28.0	113119
19	3.10	81	Cyclopropane, trimethylmethylene-	C_7H_{12}	96	9.97	63085
20	3.18	81	Cyclopentane, 1-methyl-2-methylene-	C_7H_{12}	96	12.4	62523
21	3.25	83	Cyclohexane, methyl-	C_7H_{14}	98	62.0	118503
22	3.36	69	Cyclopentane, ethyl-	C_7H_{14}	98	74.2	231044
23	3.47	81	Norbornane	C_7H_{12}	96	9.92	114371
24	3.57	81	Cyclobutane, (1-methylethylidene)-	C_7H_{12}	96	18.9	150272
25	3.62	67	1-Ethylcyclopentene	C_7H_{12}	96	42.5	114407
26	3.76	91	Toluene	C_7H_8	92	42.5	291301
27	3.82	81	Cyclohexene, 1-methyl-	C_7H_{12}	96	19.2	139432
28	3.96	79	3-Oxabicyclo[4.3.0]non-8-en-2-one, cis-	$C_8H_{10}O_2$	138	15.0	153194
29	4.09	55	1-Octene	C_8H_{16}	112	19.5	227923
30	4.13	55	Cyclopentane, 1-ethyl-2-methyl-	C_8H_{16}	112	17.7	150594
31	4.23	43	Octane	C_8H_{18}	114	42.3	229407
32	4.30	55	2-Octene, (Z)-	C_8H_{16}	112	24.2	113889
33	4.34	95	Bicyclo[3.1.0]hexan	C_8H_{14}	110	11.7	142175

			e, 1,5-dimethyl-				
34	4.62	67	1-Methyl-2-methylenecyclohexane	C_8H_{14}	110	32.2	113437
35	4.72	41	Cyclopentane, propyl-	C_8H_{16}	112	13.6	142655
36	4.77	83	Cyclohexane, ethyl-	C_8H_{16}	112	65.0	113476
37	4.82	43	2,4-Dimethyl-1-heptene	C_9H_{18}	126	60.1	113516
38	5.15	91	Ethylbenzene	C_8H_{10}	106	62.6	114918
39	5.29	81	Cyclohexane, ethylidene-	C_8H_{14}	110	10.7	118885
40	5.43	55	Cyclohexane, cyclopropyl-	C_9H_{16}	124	21.6	26670
10	5.47	41	1,8-Nonadiene	C_9H_{16}	124	27.3	227629
42	5.63	56	1-Nonene	C_9H_{18}	126	19.5	107756
43	5.77	43	Nonane	C_9H_{20}	128	34.9	228006
44	5.85	55	cis-2-Nonene	C_9H_{18}	126	15.2	113508
45	5.97	55	trans--4-Nonene	C_9H_{18}	126	12.9	113512
46	6.06	41	2,4-Undecadien-1-ol	$C_{11}H_{20}O$	168	10.4	136410
47	6.30	55	Cyclohexane, propyl-	C_9H_{18}	126	30.4	249350
48	6.53	67	Cyclopentene, 1-butyl-	C_9H_{16}	124	32.4	113491
49	6.79	77	Benzaldehyde	C_7H_6O	106	75.1	291541
50	7.10	55	1,9-Decadiene	$C_{10}H_{18}$	138	13.7	155383
51	7.26	41	1-Decene	$C_{10}H_{20}$	140	18.3	107686
52	7.31	55	Cyclopentanol, 1-(1-methylene-2-propenyl)-	$C_9H_{14}O$	138	14.0	152742
53	7.40	43	Decanes	$C_{10}H_{22}$	142	37.4	114147
54	7.46	55	cis-3-Decene	$C_{10}H_{20}$	140	14.0	113558
55	7.60	41	9-Oxabicyclo[6.1.0]nonane, 1-methyl-, cis-	$C_9H_{16}O$	140	10.3	46594
56	7.67	55	Cyclopentane, 1-methyl-3-(2-methylpropyl)-	$C_{10}H_{20}$	140	11.0	63333
57	8.46	105	Acetophenone	C_8H_8O	120	13.2	34989
58	8.70	41	1,10-Undecadiene	$C_{11}H_{20}$	152	11.0	113574
59	8.85	55	1-Undecene	$C_{11}H_{22}$	154	7.08	5022
60	8.91	41	Pentafluoropropionic acid, 10-undecenyl ester	$C_{14}H_{21}F_5O_2$	316	5.12	280071
61	8.99	57	Undecane	$C_{11}H_{24}$	156	39.3	114185
62	9.04	55	3-Undecene, (Z)-	$C_{11}H_{22}$	154	13.9	142598
63	9.53	105	Benzoyl bromide	C_7H_5BrO	184	6.12	226735
64	10.23	105	Cyclohexanamine, N-(benzoyloxy)-	$C_{13}H_{17}NO_2$	219	23.6	185471
65	10.38	55	1-Dodecene	$C_{12}H_{24}$	168	7.03	107688
66	10.50	57	Dodecane	$C_{12}H_{26}$	170	31.8	291499
67	10.55	55	3-Dodecene, (E)-	$C_{12}H_{24}$	168	11.2	113960

68	10.68	41	6-Dodecene, (Z)-	$C_{12}H_{24}$	168	11.9	142611
69	11.68	55	1,12-Tridecadiene	$C_{13}H_{24}$	180	14.3	7380
70	11.81	55	1-Tridecene	$C_{13}H_{26}$	182	14.9	107768
71	11.84	41	Z-10-Pentadecen-1-ol	$C_{15}H_{30}O$	226	6.23	245485
72	11.93	57	Tridecane	$C_{13}H_{28}$	184	51.0	114282
73	11.97	55	2-Tridecene, (Z)-	$C_{13}H_{26}$	182	9.81	142613
74	12.11	55	5-Tridecene, (E)-	$C_{13}H_{26}$	182	7.90	142619
75	13.05	55	E-10-Pentadecenol	$C_{15}H_{30}O$	226	5.13	245484
76	13.11	154	Biphenyl	$C_{12}H_{10}$	154	74.5	114218
77	13.17	55	1-Hexadecene	$C_{16}H_{32}$	224	6.44	118882
78	13.29	57	Tetradecane	$C_{14}H_{30}$	198	38.5	113925
79	13.32	55	3-Tetradecene, (E)-	$C_{14}H_{28}$	196	9.80	139981
80	14.46	55	1-Pentadecene	$C_{15}H_{30}$	210	8.21	69726
81	14.56	57	Pentadecane	$C_{15}H_{32}$	212	40.1	107761
82	14.59	55	Dichloroacetic acid, 3-pentadecyl ester	$C_{17}H_{32}Cl_2O_2$	338	3.63	280648
83	14.72	55	E-2-Hexadecacen-1-ol	$C_{16}H_{32}O$	240	12.8	131101
84	15.67	55	1-Hexadecene	$C_{16}H_{32}$	224	10.8	118882s
85	15.77	57	Hexadecane	$C_{16}H_{34}$	226	39.5	114191
86	15.80	55	1-Hexadecene	$C_{16}H_{32}$	224	6.50	118882
87	15.93	55	Cyclopentane, undecyl-	$C_{16}H_{32}$	224	4.54	10583
88	16.73	55	E-2-Octadecadecen-1-ol	$C_{18}H_{36}O$	268	14.0	131102
89	16.82	55	E-14-Hexadecenal	$C_{16}H_{30}O$	238	9.46	130980
90	16.91	57	Heptadecane	$C_{17}H_{36}$	240	36.1	107308
91	16.94	55	8-Heptadecene	$C_{17}H_{34}$	238	11.3	113620
92	17.91	55	E-15-Heptadecenal	$C_{17}H_{32}O$	252	19.6	130979
93	18.00	57	Octadecane	$C_{18}H_{38}$	254	29.9	57273
94	18.03	55	E-7-Octadecene	$C_{18}H_{36}$	252	8.53	130920
95	18.96	55	1-Nonadecene	$C_{19}H_{38}$	266	11.4	113626
96	19.04	57	Nonadecane	$C_{19}H_{40}$	268	15.1	114098
97	19.20	55	9-Nonadecene	$C_{19}H_{38}$	266	15.7	113627
98	19.95	55	1-Nonadecene	$C_{19}H_{38}$	266	7.73	113626
99	20.02	57	Eicosane	$C_{20}H_{42}$	282	33.2	290513
100	20.19	55	1-Eicosanol	$C_{20}H_{42}O$	298	7.62	113075
101	20.91	43	1-Docosene	$C_{22}H_{44}$	308	9.91	113878
102	20.97	57	Heneicosane	$C_{21}H_{44}$	296	30.0	107569
103	21.88	57	Heneicosane	$C_{21}H_{44}$	296	15.8	107569
104	22.06	55	10-Heneicosene (c,t)	$C_{21}H_{42}$	294	10.0	113073
105	22.72	43	1-Docosene	$C_{22}H_{44}$	308	15.0	113878
106	22.76	57	Heneicosane	$C_{21}H_{44}$	296	12.6	107569
107	23.62	57	Heneicosane	$C_{21}H_{44}$	296	12.6	107569
108	24.44	57	Heneicosane	$C_{21}H_{44}$	296	7.93	107569
109	25.25	57	Nonadecane	$C_{19}H_{40}$	268	8.83	114098

110	26.03	57	Eicosane	$C_{20}H_{42}$	282	7.88	149863
111	26.81	43	Heptacosane	$C_{27}H_{56}$	380	7.25	150574

PETE and HDPE waste plastic to fuel production process was thermal with Ferric Oxide catalyst to accelerated the reaction. Product fuel percentage was 66.6% and rest of percentage was residue and white color solid pest. Because PETE waste plastic has Oxygen content and it was not convertible. Product fuel was analysis by GC/MS (Figure 6) and chromatogram was analysis by using NIST library wise. In GC/MS analysis indicate that product fuel has hydrocarbon compounds including oxygen content, alcoholic group, aromatic group, nitrogen content and halogenated compounds. Analysis was perform base on retention time (m) and traces mass (m/z). During GC/MS analysis period fuel compounds, molecular weight, trace mass, probability percentage and NIST library number was determine showed into table 2. Initial compounds was detected from GC/MS chromatogram Propane (C_3H_8) (t=1.48, m/z=41) molecular weight 44 and probability percentage is 58.1%, and largest carbon number compounds is Heptacosane ($C_{27}H_{56}$) (t=26.81, m/z= 43) molecular weight is 380 and probability percentage is 7.25%. Aromatics group compounds is appeared into GC/MS analysis Toluene (C_7H_8) (t=3.36, m/z=91) molecular weight is 92 and probability percentage is 42.5%, Ethylbenzene (C_8H_{10}) (T=5.15, m/z=91) molecular weight is 106 and probability percentage is 62.6% and so on. Alcoholic compounds was detected 2,4-Undecadien-1-ol ($C_{11}H_{20}O$) (t=6.06, m/z=41) compound molecular weight is 168 and probability percentage is 10.4%, 1-(1-methylene-2-propenyl)-Cyclopentanol ($C_9H_{14}O$) (t=7.31, m/z=55) molecular weight is 138 and probability percentage is 14.0% and so on. Oxygen compounds appeared into GC/MS analysis and showed Benzaldehyde (C_7H_6O) (t=6.79, m/z=77) molecular weight is 106 and probability percentage is 75.1% E-14-Hexadecenal ($C_{16}H_{30}O$) (t=16.82, m/z=55) molecular weight is 238 and probability percentage is 9.46%. Nitrogen and halogen group compounds was appeared form GC/MS analysis such as 1-isocyano-Butane (C_5H_9N) (t=1.54, m/z=41) molecular weight is 83 and probability percentage is 28.1%, Dichloroacetic acid, 3-pentadecyl ester ($C_{17}H_{32}Cl_2O_2$) (t=14.59, m/z=55) molecular weight is 338 and probability percentage is 3.63%. Product fuel has short chain hydrocarbon C_3H_8 to long chain hydrocarbon $C_{27}H_{56}$ for that reason fuel can use as a diesel or heating fuel.

V. CONCLUSION

PETE and HDPE waste plastic to fuel production process was successfully with Fe_2O_3 and activated carbon. Laboratory scale batch process was under laboratory fume hood at temperature 420 ºC. Product fuel density is 0.76 g/ml and conversion rate was liquid and light gas 66.6 % and rest of percentage was wax and solid black residue. Fuel was analysis by FTIR to identify functional group inside fuel and found that C-CH_3, C-C= -C-C= -CH, -CH=CH_2-, -CH=CH-(cis), Non-Conjugated and Conjugated. Product fuel has enthalpy value. GC/MS analysis result indicates that fuel has hydrocarbon chain C_3 to C_{27}, aromatic group, alcoholic group, oxygen content, nitrogen content and halogen content. PETE and HDPE waste plastics mixture to fuel production period produce fuel and wax mixture can separated by using filtering system. Solid waxy portion can separate by micron filter process. Then fuel can use as a clean fuel in to internal combustion engine. Residue and catalyst recovery is under investigation. By using this technology PETE and HDPE to fuel recovery process can work easy ways at temperature 420 ºC. Although PETE has high percentage of Oxygen content (33.3%) and rest of percentage can convert as liquid fuel. The technology can solve the PETE and HDPE waste plastics dumping and landfill problem as well as environmental problem.

VI. ACKNOWLEDGEMENT

The authors acknowledge the support of Dr. Karin Kaufman, the founder and sole owner of Natural State Research, Inc. The author also acknowledges the valuable contributions NSR laboratory team members during the preparation of this manuscript.

REFERENCES

[1] Mastral, J. F.; Esperanza, E.; Garcia, P.; Juste, M. Pyrolysis of HDPE in a fluidised bed reactor. Influence of the temperature and residence time. J. Anal. Appl Pyrolysis 2002, 63, 1.
[2] Williams, P. T.; Williams, E. A. Fluidised bed pyrolysis of low density PE to produce petrochemical feedstock. J. Anal. Appl. Pyrolysis 1999, 51, 107.
[3] Kaminsky, W.; Schmidt, H.; Simon, C. M. Recycling of mixed plastics by pyrolysis in a fluidised bed. Macromol. Symp. 2000, 152, 191.
[4] Onu, P.; Vasile, C.; Ciocilteu, S.; Iojoiu, E.; Darie, H. Thermal and catalytic decomposition of PE and PP. J. Anal. Appl. Pyrolysis 1999, 49,145.

[5] Seeker, R. Combustion By-Product Formation: An Overview. In Proceedings of the Twenty-Third Symposium (International) on Combustion; The Combustion Institute: Pittsburgh, PA, 1990; pp 867-885.
[6] Stefan Czernik and Richard J. French, Production of Hydrogen from Plastics by Pyrolysis and Catalytic Steam Reform, Energy & Fuels 2006, 20, 754-758
[7] Arandes, J. M.; Abajo, I.; Lopez-Valerio, D.; Fernandez, I.; Azkoiti, M. J.; Olazar, M.; Bilbao, J. Transformation of several plastic wastes into fuels by catalytic cracking. Ind. Eng. Chem. Res. 1997, 36, 4523.
[8] Aguado, J.; Serrano, D. P.; Escola, J. M.; Garagorri, E.; Fernandez, J. A. Catalytic conversion of polyolefins into fuels over zeolite beta. Polym. Degrad. Stab. 2000, 69, 11.
[9] San You, Y.; Kim, J-H.; Seo, G. Liquid-phase catalytic degradation of polyethylene wax over MFI zeolites with different particle size. Polym. Degrad. Stab. 2000, 70, 365.
[10] Ranzi, E.; Dente, M.; Faravelli, T.; Bozzano, G.; Fabini, S.; Nava, R.; Cozzani, V.; Tognotti, L. Kinetic modeling of polyethylene and polypropylene thermal degradation. J. Anal. Appl. Pyrolysis 1997, 40-41, 305.
[11] Westerhout, R. W. J.; Waanders, J.; Kuipers, J. A. M.; van Swaaij, W. P. M. Recycling of polyethene and polypropene in a novel bench-scale rotating cone reactor by high-temperature pyrolysis. Ind. Eng. Chem. Res. 1998, 37, 2293.
[12] Bockhorn, H.; Hornung, A.; Hornung, U.; Schawaller, D. Kinetic study on the thermal degradation of polypropylene and polyethylene. J.Anal. Appl. Pyrolysis 1999, 48, 93.
[13] J. Aguado, D. P. Serrano, G. Vicente, and N. Sanchez, Enhanced Production of α-Olefins by Thermal Degradation of High-Density Polyethylene (HDPE) in Decalin Solvent: Effect of the Reaction Time and Temperature, Ind. Eng. Chem. Res. 2007, 46, 3497-3504
[14] Sato, S.; Murakata, T.; Baba, S.; Saito, Y.; Watanabe, S. Solvent effect on thermal degradation of polystyrene. J. Appl. Polym. Sci. 1990, 40, 2065.
[15] Karaduman, A.; Sü imsüek, E. H.; Cü icüek, B.; Bilgesu, A. Y. Thermal degradation of polystyrene wastes in various solvents. J. Anal. Appl. Pyrolysis 2002, 62, 273.
[16] J. Aguado, D. P. Serrano, G. Vicente, and N. Sanchez, Enhanced Production of α-Olefins by Thermal Degradation of High-Density Polyethylene (HDPE) in Decalin Solvent: Effect of the Reaction Time and Temperature, Ind. Eng. Chem. Res. 2007, 46, 3497-3504

American Journal of Engineering Research (AJER)
e-ISSN : 2320-0847 p-ISSN : 2320-0936
Volume-02, Issue-10, pp-11-21
www.ajer.org

Research Paper Open Access

Lightning Protection of Floating Roof Tanks

Adekitan, Aderibigbe Israel,
B.Sc., MNSE
Electrical and Electronic Engineering, University of Ibadan, Nigeria

Abstract: - Prior to export, processed crude oil is stored in Floating Roof Tanks (FRT) to further allow any trapped gas within the crude oil to escape, as this stabilises the crude oil. In the oil and gas industry, FRT's are vital in the processing of crude oil to the acceptable export specification.
In the tropics and other lightning prone regions, lightning induced floating roof tank fire constitutes a major threat to crude oil production. Among others, a single lightning incident could result in the loss of life, product and production time, avoidable incident review time, damaged equipment, wasted repair cost, bad publicity and loss of income.
This paper therefore, is aimed at providing an effective solution to the menace of lightning induced tank fire by focussing on the starting process of the lightning induced fire and proposing alternative concepts for breaking the fire triangle before fire ensues.

Keywords: *- crude oil, fire, floating roof tank, lightning protection, sparks*

I. INTRODUCTION

Lightning is more prevalent in the tropics than elsewhere in the world [10] and it is a natural phenomenon with an associated potential hazard. Lightning is a scientific phenomenon and contrary to common opinion lightning can be studied scientifically and using its empirical properties its occurrence can be predicted, detected and its impact mitigated.

Preventing static electricity and lightning related hazards such as step / touch voltage, lightning fire, equipment damage etc. is achieved by installing an effective Lightning Protection System (LPS) on the structure of concern. The effectiveness of such a Lightning Protection System is dependent on the nature and the thoroughness of the design of the grounding and bonding system implemented on and around the structure and how well it is maintained after installation.

In providing an effective solution to lightning issues several studies have been carried out and different approaches adopted overtime. Some of these approaches have been criticized and said to be based on junk science [4, 6, 7, 9]. There is therefore a need for a detailed analysis and definition of what qualifies as an effective lightning protection system especially as regards oil and gas facilities, which are particularly prone to lightning induced fire incidents because of the flammable nature of oil and gas products.

Unavoidably, analysis here focuses on accepted principles and guidelines as proposed by competent authorities on lightning protection.

II. INTERACTION OF LIGHTNING WITH A FLOATING ROOF TANK

"Tank fire statistics shows that 35% of all floating roof tank fires are caused by lightning related issues. It is presently estimated that 95% of rim seal fires are as a result of lightning strikes and 0.16% of all tanks with rim seals will experience a ream seal fire in any year [3]"

If 95% of all rim seal fires are as a result of lightning, then this raises the question "what is peculiar about the rim-seal region of a FRT that makes it susceptible to lightning?" By design to ensure ease of movement of the floating roof within the tank shell, there exist a gap between the tank shell and the edge of the floating roof. This eliminates friction, guarantees ease of movement but creates issues in the following areas when lightning strikes.

Sparking

When lightning strikes the floating roof the lightning current will flow over the roof towards the edge of the roof, and at the edge there exist a discontinuity because of the tank shell-roof gap this prevents the current from flowing through the tank shell to the ground. Lightning induced electrostatic field at ground level is in the order of 5KV/m and because of this high electric field a potential difference will exist between the roof and the tank shell.

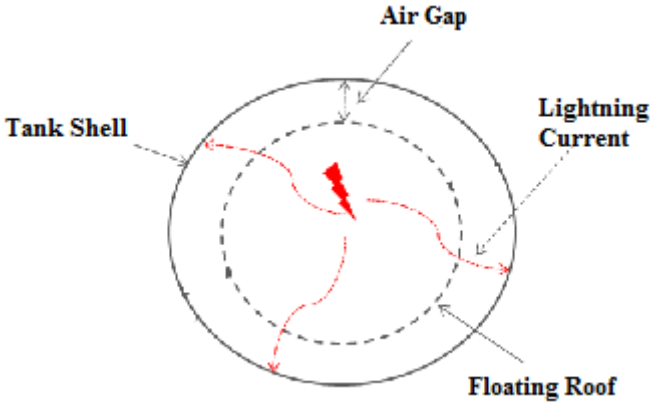

Figure 1: Tank shell-roof air gap

Because of the content of a floating roof tank which is crude oil, the tank contains flammable vapour, also oxygen is readily available in the environment and at a potential of about 3KV/mm the flammable air vapour (acting as a di-electric) within the gap will break down and conduct electricity in the form of a spark (arc). This completes the fire triangle resulting in a lightning induced floating roof tank fire.
According to API [1] there are two types of spark; thermal and voltage sparks.

Roof Surface Charging

Prior to an eventual lightning strike electric charges will accumulate in the sky, e.g. for a negative cloud to ground lightning, by induction positive charge will be induced on the surface of the shell and the roof of the tank. This will ultimately create a difference in potential between the roof and the shell which can result in transient currents.

Heating due to lightning strike

The flow of high energy lightning current can cause erosion and melting of thin metal sheets and this can generate incendiary particles even around the shell-roof gap. However tanks with a thickness greater than 5mm cannot be melted by lightning. The continuing current with over 200C of charges will only met a little over 1mm. Usually FRT tank shells are thicker than 5mm.

2.1 ROOF - SHELL CONNECTION

The discussion above shows that the gap between the roof and the tank shell is a major cause of lightning voltage spark. In order to mitigate this, standards on lightning protection recommends that a form of short circuit (direct connection) should be established between the roof and the shell so as to provide a flow path for the lightning current from the roof to the tank shell rather than through the air gap so as to drastically reduce the electric field build up within the air gap, and this takes the following forms:

2.1.1 Connection via the roof steers

The stairs that connects the tank shell to the top of the roof, for providing access to the roof so that technicians can service the instrumentation systems installed on the tank roof is metallic. Hence this can serve as a flow path for lightning current but this has a limitation in the sense that the stair is not solidly connected to the roof.

Figure 2: FRT Roof Access Ladder

The contact between the roof and the stairs is via movable rollers on rails that does not guarantee a good electrical connection and also there is a tendency for spark generation between the roller and the roof if gaps exist. Also because of the content of the tank that is crude oil, the roof is sometimes coated with oil and this further reduces the electrical conductivity between the roof and the roller. Hence this cannot be depended on for a good roof to shell connection.

2.1.2 Connection via bypass cable

It is also a common practise to connect the roof to the shell with a long length of cable at different points along the circumference at a maximum separation distance of 30m. The bypass conductor is installed to conduct the intermediate and the continuing current component of the lightning current. FRT are usually large in diameter e.g. for a tank with a diameter of 60m and 50m in height the cable must be long enough to connect the shell to the roof even when the tank is empty and the roof is at the bottom of the tank. For such a tank, if the cable is connected to the centre of the roof the cable length must be at least 58.3 m and definitely it will be longer as the cable cannot be taut.

When lightning impulse current with a frequency varying from hundreds of kilohertz to tens of megahertz flows through such a cable the resistance of the cable is no longer significant, what matters is the impedance which is highly determined by the frequency dependent inductance ($2\pi FL$). If the impedance becomes so high to the extent that a very high voltage develops across the cable as several kilo amperes flows through it, a flash over can occur. Flash over is when lightening current jumps through air to a nearby conducting medium or object when the voltage build up across its initial path is so high as to cause a dielectric breakdown of the insulating surrounding air.

Another issue with the use of cables is due to the rate of change of the lightning current (di/dt) as high as 200KA/μs. With a high inductance a very high voltage can easily be induced in nearby conductors or in the cable by faradays law of electromagnetic induction even when the current is not flowing directly through the cable. Hence the use of connecting cable is also not an optimal option.

2.1.3 Use of shunts

Towards resolving the roof-shell connection issue National Fire Protection Agency in their standard NFPA 780 and also according to API 545-A [1] which recommended that a thin sheet of metal called a shunt should be used to connect the roof to the shell at a separation distance of 3m round the circumference of the tank for conducting the component A and B of the lightning current. The shunt is sometimes used together with the bypass conductor. The shunt shall be made of austenitic stainless steel with a minimum of $20mm^2$ in cross sectional area and a minimum width of 51mm or could be of any other material with an equal current rating and corrosion resistant rating.

The installed shunt, by design is held in contact with the tank shell by tension with a spring like effect such that as the roof moves up and down the shunt moves with it and maintains contact with the shell.

Unfortunately the shunt also does not provide a perfect solution, the contact between the shunt and the shell is not a solid contact and as such there is a tendency for arcing. Also the conductivity of the shunt-shell interface is affected by the internal paint on the shell surface, the level of rusting and also by the insulating coating deposited by the heavy component of crude oil on the tank surface. API research shows that irrespective of the location of the shunt, always there is a spark generation at the shell shunt interface when lightning current flows, the only difference is that the magnitude of the spark is reduced compared to that without the shunt. Because the contact between the shell and shunt is dependent on the springy tension, on several tanks shunts can

be seen completely separated from the tank shell due to the lost tension thereby creating the spark gap it was installed to eliminate.

Figure 3: Shunt Not Making Contact with the Tank
Copyright: Lightning Eliminators and Consultants, Inc. 2012

Since there will always be sparking at the shunt-shell interface API recommended that the shunts should be installed submerged below the crude oil at a minimum depth of 0.3m in a region where flammable vapour does not exist such that even when sparks are generated the fire triangle will not be completed. Presently the submersible type of shunt is not available because the feasibility and effectiveness of such a design is not generally agreed on. This therefore challenges the effectiveness of shunts for current conduction.

2.1.4 Retractable Grounding Array (RGA)

Figure 4: Retractable Grounding Assembly Copyright: Lightning Eliminators and Consultants, Inc. 2012

Recent design came up with a device called a Retractable Grounding Array (RGA) which is basically a self-retracting conductor. The RGA retracts and extends based on the roof level thereby maintaining the shortest electrical connection possible and by so prevents the issue associated with the use of long cables. It is made of multiple weaved strands of low resistance tinned copper wire and is typically installed on the tank shell and connected to the edge of the roof.

RGA should be more effective due to the shortest electrical connection it provides, although more expensive compared to ordinary cables but RGA alone is not considered a complete lightning protection against direct strike.

III. LIGHTNING PROTECTION SYSTEM CONCEPT SELECTION

The approach to solving the lightning induced fire issue is centred on eliminating voltage differential and majorly breaking the fire triangle and this would take two forms.

a. Eliminating the chances of spark generation at the shunt-shell interface by ensuring that the lightning stroke does not terminate on the roof but on a preferred conductive part
b. Ensuring the absence of flammable fuel-air vapour in the shunt region by eliminating oxygen or limiting the volume of hydrocarbon fumes

This paper focuses on the first, and this would be achieved by implementing a conventional LPS on the FRT in a way that the lightning current would be almost if not completely routed from the tank's shell-shunt interface.

Concept 1: Air terminal installation on the tank rim

Description

Research findings clearly show that the shape and dimension of an air terminal determines its performance. In line with this, since the tank shell itself is not an air terminal though effectively conductive its ability to emit upward streamers and thereby attract the lightning to itself rather than to the roof could be impaired by its shape and properties, hence this option.

Based on oil and gas industry practices around the world and as proposed by the OISD [5].

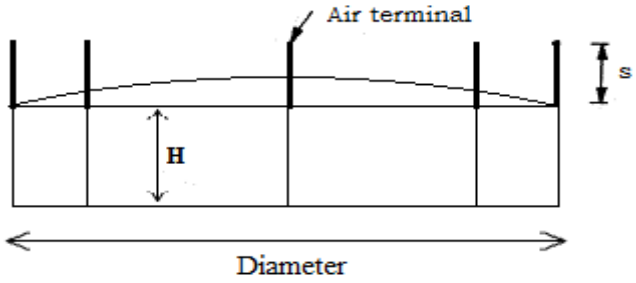

Figure 5: Air terminal rods on a FRT

1. Install blunt tip Franklin rods (preferably dia-19 mm) at every 20 m spacing around the tank rim [BS-6651 [2]]
2. The down conductor in this case shall be the tank shell [Since the tank shell thickness ≥ 4.8mm [NFPA [8]]]

The major limitation of this approach is that with a 5 m high air terminal only a maximum of 16.58 m distance on the roof from the edge of the shell is protected.

The key advantage is that this concept prevents direct strike to the shunt region, and if the stroke terminates somewhere around the centre, the lightning stroke current will be divided among the different shunts thereby reducing the magnitude of current through individual shunt. The protected zone can be improved by increasing the height of the air terminal, although a 5m high air terminal seems excessively long already.

With this concept a direct strike to the tank shell will still result in transients current flowing from the shell across the shunts to the roof, through other shunts, then over the shell again.

Concept 2: Use of suspended horizontal air terminal attached to the tank rim

Description

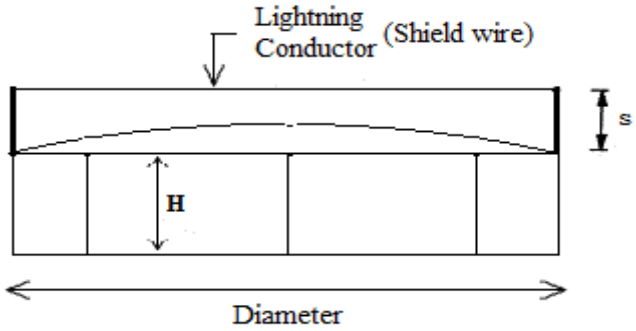

Figure 6: Shield wire attached to the tank shell

The focus of this option is to eliminate the weakness of concept 1 in terms of the limit of the protection radius of the air terminals. It utilizes an array of horizontal air terminals supported by steel rods welded to the tank rim to ensure a full protection zone cover of the tank roof.

The main flaw of this approach is that even without a lightning bypass to the roof, the flow of current through the support steel pole to the tank shell will still result in the flow of a portion of the current via the shunts to the roof, then through other shunts back to the shell and then down to the ground.

Concept 3: Use of suspended horizontal air terminal using support poles
Description

The protection is achieved using multiple suspended air terminations (overhead shield wires) at an adequate height above the area to be protected as recommended by BS 6651 [2] and NFPA 780 (#7.3.3) for explosive materials.

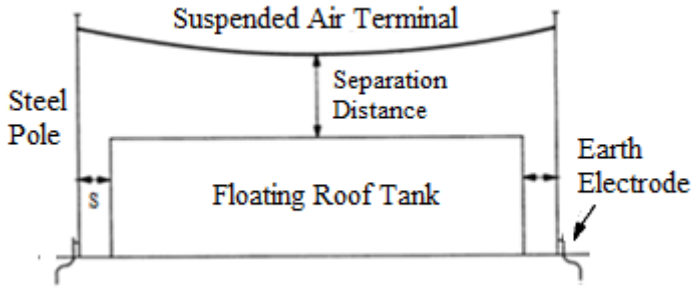

Figure 7: Pole supported shield wire

"Since lightning currents are difficult to prevent except by roofing over the tank with metal or having a mesh type catenary system over the entire tank, which is not very practicable". API 545-A [1] also recognizes the benefits of a conducting mesh over the tank

The setup is made up of low resistance, separately grounded steel poles used as support for low resistance catenary ground wire. The minimum separation distance between an overhead ground (horizontal shield) wire or a lightning mast and the structure being protected must be greater than or equal to the side flash distance (s) or the bonding distance, so as to prevent side flashes.
The main advantage of this option is that it completely keeps the lightning current from the tank provided there is no eventual bypass.

3.1 CRITERIA DEFINTION

The best option among the three concepts will be selected based on the following criterion.

Table 1: Project Selection Criteria Paired Comparison

	B	C	D	E	F	G	Criteria	Score	Weight	Ranking
A	B2	C3	D3	E2	A1F1	G2	A: Material Requirement	1	2%	6
B		B2	D2	B2	B2	B1G1	B: Constructability	9	20%	3
C			D2	C2	C2	G2	C: Extent of roof protection	7	15%	4
D				D3	D3	D1G1	D: Tendency of spark generation	14	30%	1
E					E2	G2	E: Ease of maintenance	4	9%	5
F						G2	F: Design flexibility	1	2%	6
							G: Tank isolation from lightning	10	22%	2
								46		

Preference Scoring

1 = About the Same
2 = Preferred
3 = Strongly Preferred

Material Requirement: This translates to the installation cost
Constructability: The ease / feasibility of the design installation in terms of material availability, space limitation, structural arrangement and the effect on production.
Extent of roof protection: The proportion of the FRT roof that is within the protection zone of the LPS.
Tendency of spark generation: The magnitude of lightning current that is likely to flow through the shell-shunt interface.

Ease of maintenance: Ease of access for maintenance activities, in terms of location / height challenges and impact on production activities.
Design flexibility: Design limitation on arrangement / physical setup as a measure of LPS interference with other equipment / tank component.
Tank isolation from lightning: The probability of a direct strike to the tank as a result of LPS lightning bypass / limitation of the zone of protection.

Table 2: Application of the weight of the criteria to each concept

	A: Material requirement	B:Constructa-bility	C: Extent of roof protection	D: Tendency of spark generation	E: Ease of maintenance	F: Design flexibility	G: Isolation from lightning	Concept Score	Concept Ranking
Design Concept	0.0217	0.1956	0.1521	0.3043	0.0869	0.0217	0.0217		
Air terminal installation on the tank rim	**7**	**4**	**6**	**6**	**7**	**6**	**4**	4.50	**3**
Use of suspended horizontal air terminal attached to the tank rim	**9**	**8**	**9**	**7**	**6**	**6**	**5**	6.02	**2**
Use of suspended horizontal air terminal using support poles	**6**	**8**	**9**	**9**	**5**	**6**	**9**	6.57	**1**

In line with preventing tank fire, concept 3 which utilizes horizontal air termination with support poles which has the highest concept score after comparison as shown in Table 1and Table 2 is the recommended concept. The main reasons are that this concept has the best protection zone and the least tendency of spark generation

3.2 Application of the rolling sphere to a floating roof tank protected using concept 3

Using the rolling sphere approach to air terminal design mathematical analysis were carried out to determine the relationship between the striking distance, the attractive radius and the penetration depth between two adjacent lightning shield wires. Using developed mathematical relationships and the recommendations of competent authorities on lightning protection, an application was developed which simplifies the intricacies of designing a LPS for a FRT using the recommended concept.

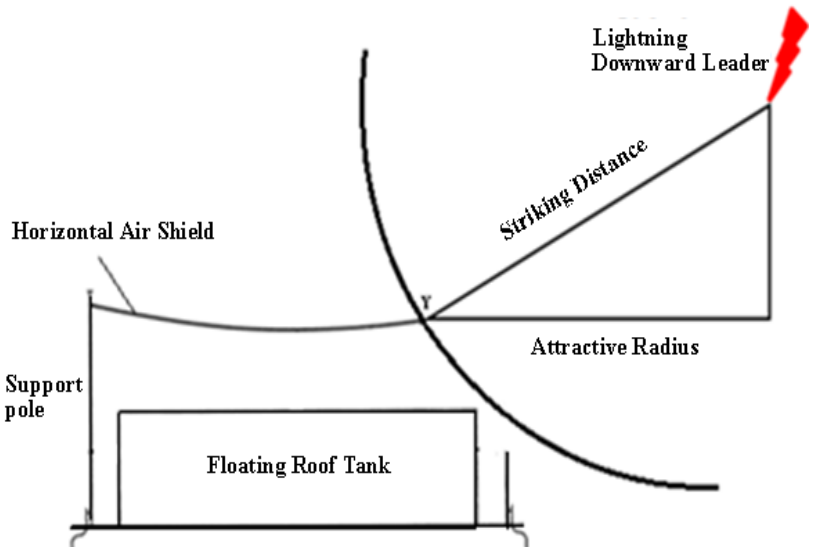

Figure 8: Striking distance to a point Y on the air terminal

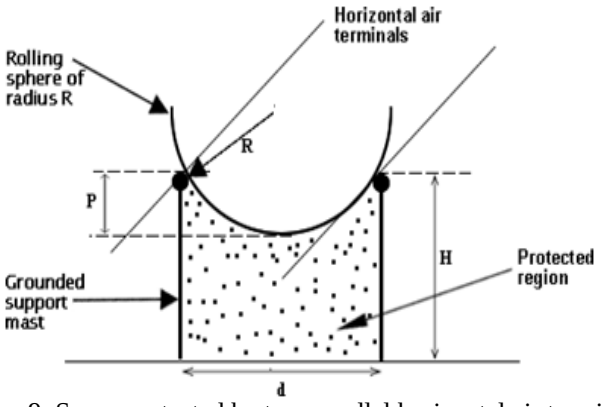

Figure 9: Space protected by two parallel horizontal air terminals

IV. THE APPLICATION

Based on the analysis and models developed around the selected concept a software application was developed which automates the LPS design.

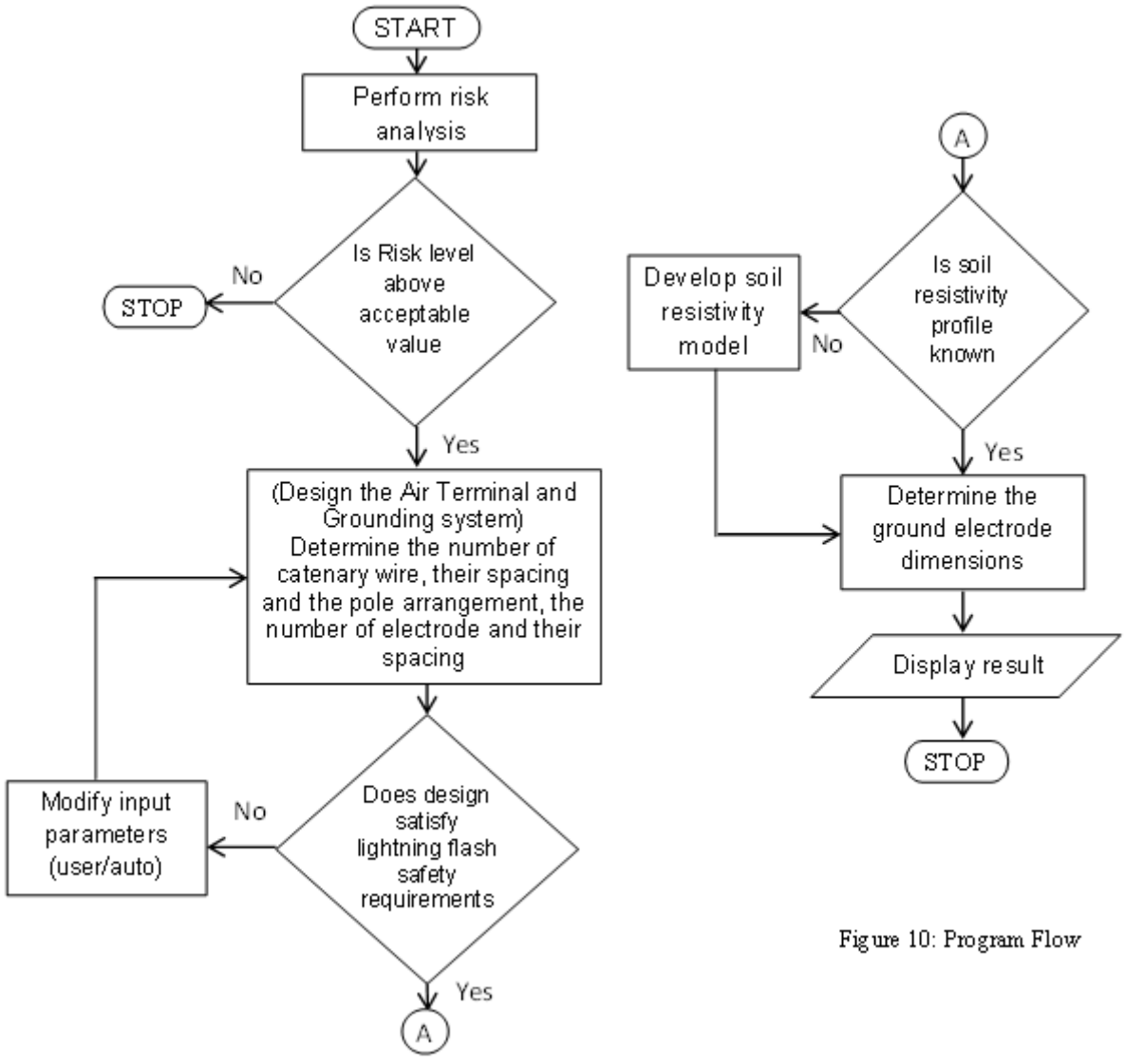

Figure 10: Program Flow

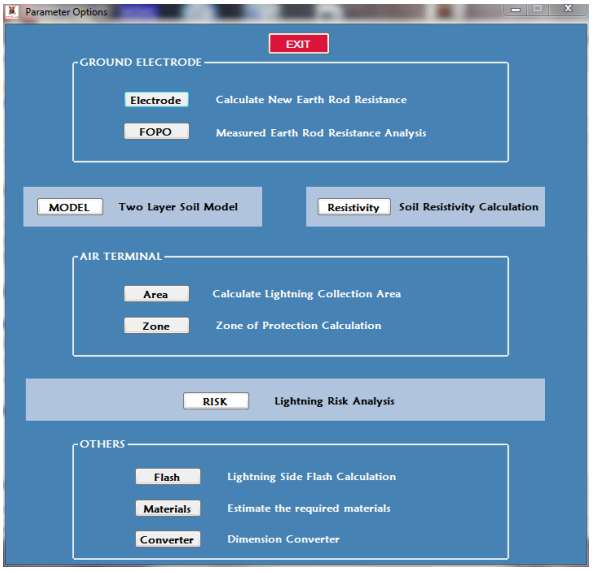

Figure 11: Parameter selection form

4.1 Setting up the Lightning Protection System

Setting up the LPS requires making technical decisions to determine the number of parallel lightning shield wires required, their spacing, the minimum height of the wire above the tank to prevent side flash and so on. The design process can be carried out in stages, with analysis done separately for the grounding system, the down conductor and the air terminal, doing this will require the user to make some enlightened decisions. This could be a little cumbersome for someone with a basic understanding of lightning protection and its requirements. To address this, a platform was created which only requires the dimension of the tank and the desired protection level, and the application will automatically compute the installation requirement in terms of spacing and air terminal height.

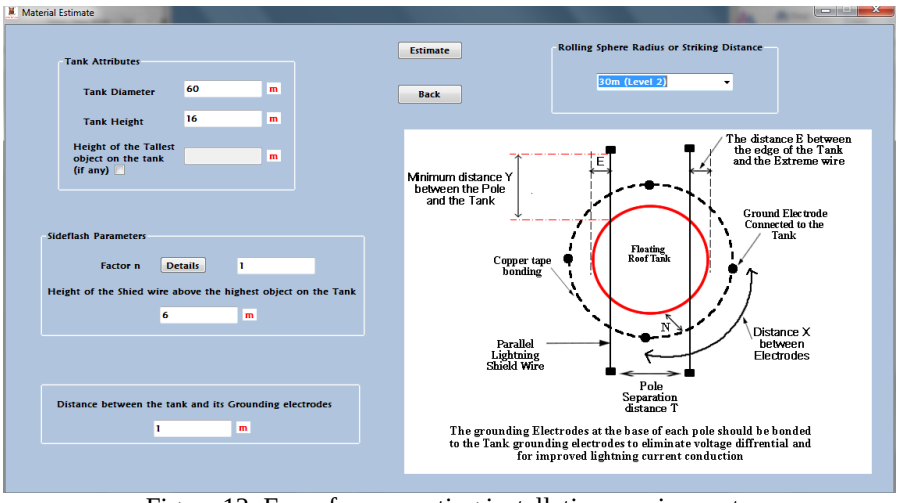

Figure 12: Form for computing installation requirements

Although the automatic computation considers necessary factors such as the tendency of a lightning flash and is thus accurate and sufficient for protection but it may not be the optimum design in terms of material usage where manually the application user can make decisions based on the physical structure and arrangement of equipment around and above the tank

The application generates an estimate of the materials (number of electrodes, length of copper tapes) needed. The position of the distance as given in the report can be determined by comparing it with reference diagram (tank plan) in the application form.

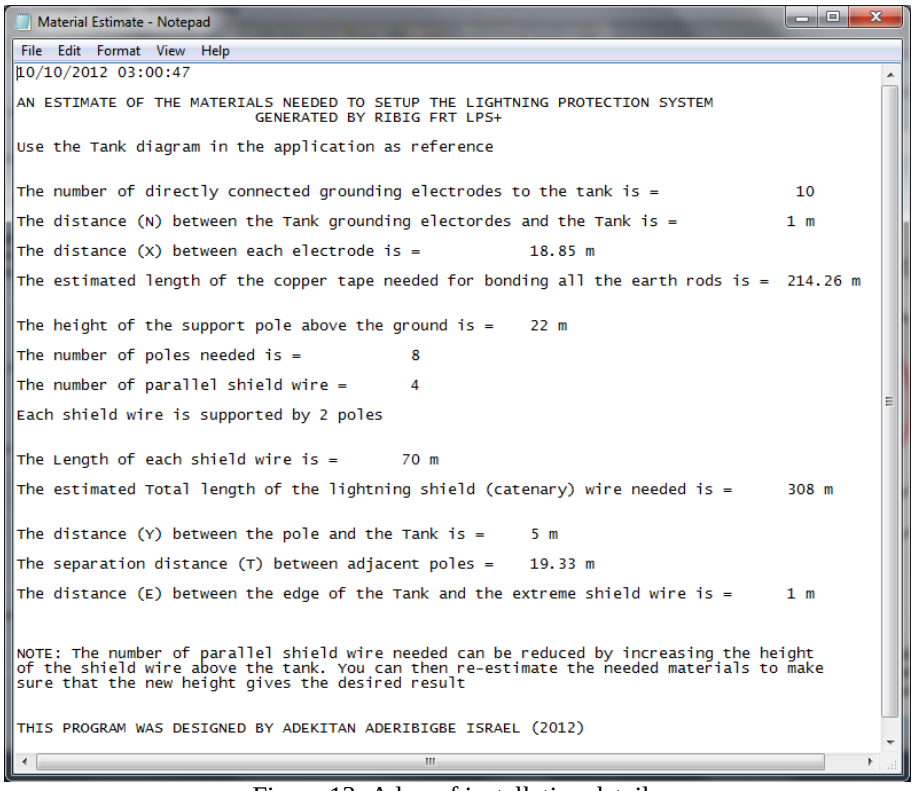

Figure 13: A log of installation details

The guidelines and data provided by the application, if duly adhered to will help in setting up an effective lightning protection system for floating roof tanks.

V. RISK MATRICES

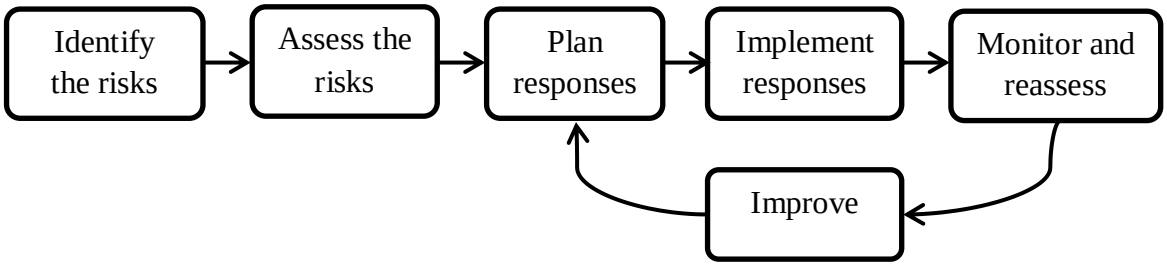

Figure 14: Risk analysis and management process

Risk based analysis using *EASY RISK* MANAGER shows that the associated risk with lightning induced floating roof tank fire can be effectively reduced from high-high to low-low in terms of the consequence and the probability of occurrence, by deploying an effective LPS as presented by this paper.

VI. CONCLUSION

This paper has presented the process of how lightning interacts with floating roof tanks. LPS models were proposed and the very best after a thorough comparison was selected. Using the selected concept this project mathematically analysed the lightning strike process to a tank and in the course of this formulas and algorithms were developed, also other relevant formulas were compiled from competent authorities on lightning protection.

Ultimately, a lightning protection system design software called RIBIG FRT LPS+ was developed which serves as a platform for fast and accurate design of LPS for floating roof tanks.

VII. ACKNOWLEGMENTS

Engr. Muyiwa Falade – Electrical Team Lead Shell Petroleum Development Company of Nigeria (SPDC)
Engr. Chidumga Okoye – Senior Electrical Engineer SPDC.

Mr Kalu Justice – Supervisor Electrical Team, Bonny oil and Gas Terminal, SPDC
Dr O. A. Fakolujo – Electrical and Electronic Engineering Department, Univeristy of Ibadan, Nigeria.

REFERENCES

[1] API, RR 545-A. (2009), Verification of lightning protection requirements for above ground hydrocarbon storage tanks. American Petroleum Institute.
[2] BS-6651 (1999), Code of practice for protection of structures against lightning. BSI Standards Publication, pg.41.
[3] Changa, James I.; Linb, Cheng-Chung (2005). A study of storage tank accidents. Department of safety, Health and Environmental Engineering, National Kaohsiung First University of Science and Technology, Kaohsiung, Taiwan, ROC.
[4] Committee on Atmospheric and Space Electricity of the American (2001). Scientific basis for Traditional Lightning Protection Systems.
EN 62305, B.S. (2006), Protection against lightning.
[5] GDN-180, OISD (1999), LIGHTNING PROTECTION. Oil Industry Safety Directorate, New Delhi, India
[6] Group, Federal Interagency Lightning Protection User (2001), The Basis of Conventional Lightning Protection Technology, A review of the scientific development of conventional lightning protection technologies and standards.
[7] Hartono, Z. A. & Robiah, I. (2006), Review of Studies of ESE & CTS in Malaysia. In 17th International Symposium EMC. Zurich, 2006.
[8] NFPA-780 (2004), Standard for the Installation of Lightning Protection Systems. National Fire Protection Association.
[9] Rison, William (2002) There Is No Magic To Lightning Protection:Charge Transfer Systems Do Not Prevent Lightning Strikes. New mexico: New Mexico Institute of Mining and Technology.
[10] Wikipedia (2011), Lightning. [Online] Available at: http://en.wikipedia.org/wiki/Lightning [Accessed 20 April 2012].

American Journal of Engineering Research (AJER)
e-ISSN : 2320-0847 p-ISSN : 2320-0936
Volume-02, Issue-10, pp-22-47
www.ajer.org

Research Paper Open Access

Performance of C.I Engine by Using Biodiesel-Mahua Oil.

sudheer nandi
Andhra Pradesh,INDIA-517502

Abstract: - India is looking at renewable alternative fuel sources to reduce its dependence on foreign imports of oils. As India imports 70% of the oil, the country has been hit hard by increasing cost and uncertainty. Recently the biomass resources are being used as alternative fuels and effective use of those fuels is gaining prominence as a substitute way to solve the problem of global warming and the energy crisis. Among all the alternative fuels existing mahua oil is also one. In this work, conventional laboratory equipment has been used for the transesterification of mahua oil. Various properties of esterified mahua oil have been tested for comparison with diesel fuel; further the investigations are carried out on a laboratory based diesel engine to study its performance.

An attempt has been made in the present work to find out the suitability of transesterified mahua oil as a fuel in C.I. engine. Experimental work was carried out on 7B.H.P single cylinder four stroke and vertical, water cooled Kirloskar diesel engine at rated speed of 1500rpm different blends of transesterified mahua oil with diesel were tested at 200bar injection pressure.

From the performance characteristics of transesterified mahua oil diesel blends the efficiencies obtained were found to be better with 75% transesterified mahua oil. The thermal efficiencies of transesterified mahua oil are higher at 25% diesel blends. The cost of transesterified mahua oil is low compared to the cost of diesel. Hence mahua oil blended with diesel is more economical and this can provide an immediate, though partial solution to the growing diesel scarcity in developing countries like ours.

i. INTRODUCTION

When Rudolf diesel first enunciated the concept of diesel engine, about a century back, the experimental evaluation was demonstrated on peanut oil indicating that the vegetable oils will be the prospective future fuels in diesel engines. In the context of fast depletion of fossil fuels and ever increasing diesel vehicle population, use of renewable fuels like vegetable oils has become more pertinent.

The various biomass based resources, which cab be used as an extender, or a complete substitute of diesel fuel may have very significant role in the development of agriculture, industrial and transport sectors in the energy crisis situation. The role of diesel fuel in these sectors cannot be denied because of its ever-increasing use. In fact agricultural and industrial sectors are almost diesel dependent.

Need for shifting towards alternative fuels

Probably in this century, it is believed that crude oil and petroleum products will become very scarce and costly to find and produce. Although fuel economy of engines is greatly improved, increase in the number of automobiles alone dictates that there will be a great demand for fuel in the near future. Alternative fuel technology, availability, and use must and will become more common in the coming decades.

Another reason motivating the development of alternative fuels for the IC-engine is concerned over the emission problems of gasoline engines. Combined with other air polluting systems, the large number of automobiles is a major contributor to the air quality problem of the world. A third reason for alternative fuel development is the fact that a large percentage of crude oil must be imported from other countries which control the larger oil fields.

Energy consumption as a measure of prosperity

Energy is an important input in all sectors of any countries economy. The standard of living of a given country can be directly related to the per capita energy consumption.

Energy crisis is due to the two reasons:
1. The population of the world has increased rapidly.
2. The standard of living of human beings has increased.

Supply and demand of energy

The energy plays an important role in everyday life. Growth of an economy is largely dependent on adequate supply of energy. Energy available in its original form in nature such as crude oil, natural gas, coal, solar heat, etc. is called primary energy sources. Many of these sources are not directly usable and can be used only after processing of or conversion. Crude oil is refined in a petroleum refinery and resulting petroleum products include petrol are termed as **secondary energy sources.**

Present demand and supply

World energy future in present trend countries, the world in the next 50 years will be more crowded than that of today. The world population may reach 10 billions. The conventional sources of energy are depleting and may be exhausted by the end of the century or at the beginning of the next century.
The various alternative fuel options researched for diesel are mainly bio-gas, producer gas, methanol, ethanol, and vegetable oils. Out of all these vegetable oils offer an advantage because of its comparable fuel properties with diesel. The various edible vegetable oils like sunflower, soyabean, peanut, cotton seed etc. have been tested successfully in diesel engine. Research in this direction with edible oils yielded encouraging results. But as India still imports huge quantity of edible oils, therefore, the use of non-edible oils of minor oilseeds like mahua (madhuca indica) oil has been tested as a diesel fuel extender.

The advantages of vegetable oils as diesel fuel are:
- Liquid nature-portability
- Ready availability
- Renewability
- High Cetane number
- Lower sulfur content
- Lower aromatic content
- Biodegradability

The disadvantages of vegetable oils as diesel fuel are:
- Higher viscosity
- Lower volatility
- The reactivity of unsaturated hydrocarbon chains

II. IMPORTANCE OF BIO-DIESEL

What is Bio-diesel?

Bio-diesel is a renewable fuel, biodegradable and non-toxic. It is an ester based oxygenated fuel made form any vegetable oil (edible or non-edible) or animal fat. Bio-diesel is produced by a simple chemical reaction between vegetable oil and alcohol in the presence of an acid or base as catalyst. It contains around 10% built-in oxygen by weight and has no sulphur and has excellent lubricity properties. Built-in-oxygen makes it more efficient fuel than petro-diesel hence its cetane number is higher than that of petro-diesel. It can be blended with petro-diesel in any proportion.

Bio-diesel is the name of the clean burning alternative fuel, produced from domestic, renewable resources. Bio-diesel contains no petroleum, but it can be blended at any level with petroleum diesel to create a bio-diesel blend. It can be used in compression-ignition (diesel) engines with little or no modifications. Bio-diesel is simple to use, biodegradable, nontoxic, and essentially free of sulphur and aromatics. It is defined as mono-alkyl esters of long chain fatty acids derived from vegetable oils or animal fats which confirm to ASTM D6751 specifications for use in diesel engines. Bio-diesel refers to the pure fuel before blending with diesel fuel.

Statistical report:

The National Bio-diesel Board (NBA) in the US reported that an estimated 5 million gallons of Bio-diesel were sold in 1999, followed by 2 million gallons in 2000, 5 millions gallons in 2001, 15 million gallons in 2002 and an estimated 25 million gallons in 2003 respectively. It is estimated that during 2004-2005, an estimated 35 million gallons of bio-diesel is made in the US and it is likely to reach 70 million gallons in the US in 2006. Bio-diesel operates in conventional engines. Just like petroleum diesel, bio-diesel operates in compression-ignition engines. Essentially no engine modifications are required, and bio-diesel maintains the payload capacity and range of diesel.

Pure bio-diesel is not compatible with natural rubber, sometimes found in pre 1994 vehicles. Because it is a solvent. It can degrade natural rubber hoses and gaskets. This is not a problem with B20 blends (20 percent biodiesel/80 percent diesel) and below. Bio-diesel does not require special storage. In fact, in its pure form or in blends, Bio-diesel can be stored wherever petroleum diesel is stored, except in concrete-lined tanks. It is handled like diesel and uses the same infrastructure for transport, storage and use. At higher blend levels, bio-diesel may deteriorate natural rubber or polyurethane foam materials. Bio-diesel exhaust is less offensive. The use of bio-diesel and bio-diesel blends results in a noticeable, less offensive change in exhaust odour, which can be a real benefit in confined spaces. In fact, equipment operators have compared it to the smell of French fries. Users also report having no eye irritation. Since bio-diesel is oxygenated, diesel engines have more complete combustion with bio-diesel than with petroleum. Bio-diesel is safer to use than petroleum diesel. The flash point (the point at which fuel ignites) for bio-diesel in its pure form is a minimum of 260 degrees versus about 125 degrees Fahrenheit for regular No.2 diesel. This makes bio-diesel one of the safest fuels to use, handle and store. Bio-diesel reduces emissions significantly.

Bio-diesel is the first alternative fuel to have fully completed the health effects testing requirements of the US Clear Air Act. The use of bio-diesel in a conventional diesel engine results substantial reduction of unburnt hydrocarbons, carbon monoxide, and particulate matter. Emissions of nitrogen oxides are either slightly reduced or slightly increased depending on the duty cycle and testing methods. The use of bio-diesel decreases the solid carbon fraction of particulate matter (since the oxygen in bio-diesel enables more complete combustion to CO_2), eliminates the sulfate fraction (as there is no sulfur in the fuel), while the soluble, or hydrocarbon, fraction stays the same or is increased. Bio-diesel works well with new technologies such as catalysts, particulate traps, and exhaust gas recirculation. So bio-diesel reduces carbon dioxide by 78 percent on a life cycle basis. No engine modifications are required up to 20 percent blend.

Bio-diesel is made from Rapeseed (UK), Soybean (USA, Brazil), Sunflower (Italy and Southern France), Oil palm (Malaysia), Linseed, Olive (Spain), Cotton seed (Greece) and tree borne, non-edible oilseeds like Mahua,Jatropha (Ratanjot) and Pongamia (Karanja) in India. Bio-diesel is produced from more than 20 countries in the world. Like USA, Australia, France, Italy, Hungary, Germany and Czechoslovakia. No tax is being levied on the production of bio-diesel by Germany and Italy. More than 100 bio-diesel plants were established in the world. Bio-diesel could be made from crude/natural vegetable oils, crude/refined fats, high acidity oil/fats, recovered fried oils, animal fats and waste oils.

Bio – Diesel Scenario in the World:

Bio-fuel used for school buses in the US

Pollution from school diesel buses has health implications to children. The use of Bio diesel can reduce such health risks. In view of this, several thousand school buses in the US are using blends of bio-diesel. In 1997, Medford, New Jersey school district used bio-diesel buses for transport of children to school. In August 2002, Olympia, Illinois school district used bio-diesel for 33 schools buses and travels around 4000 miles per day with 6 lakhs miles per annum. Clark country, Nevada school district used bio-diesel buses in May 2003 for 1200 schools. Similarly, Arlington County, Cirginia school district used bio-diesel buses for 200 schools, and in July 2004, Arkansas school district used bio-diesel buses for 149 schools respectively.

Bio-diesel passenger Cars & trucks in the US

America's big 3 Auto makers – general Motors, Ford and Daimler Chrysler each introduced new generation of vehicles with diesel electric hybrids. Diesel engines are about 30 percent more efficient than gasoline engines. This means that the diesel engine of the same displacement will produce about 30 percent more horse power or give 30 percent better fuel economy for 30 percent less carbon dioxide emissions. Today's diesel engines are quieter, cleaner burning and more responsive than earlier diesels. In Europe, where the cost of owning and operative of a passenger vehicle is significantly higher than in the US, stringent laws adopted by California and four north West States have slowed the introduction of diesel vehicles to the market. However, increasing fuel prices, the introduction of ultra low sulphur diesel, and new emissions, technology are making passenger diesel vehicles more attractive to customers leading to diesel option offerings by auto manufacturers.

Bio-diesel further enhances the advantages of diesel by reducing vehicle emissions. B20 reduces emissions of 12 percent. It reduces sulphur on average by 20 percent. Hundreds of US flights, representing over 25,000 vehicles for commercial, government, utility and transit use, currently run on bio-diesel blends nationwide. Bio-diesel blends are also used increasingly in the farming, mining and marine industries, as well as for heating oil and electrical generation applications. Most auto manufacturers approve Upto the use of B 55% percent bio-diesel for the diesel engines.

Bio-diesel in Indonesia from Castor Oil

Indonesia's scientists claimed to have developed bio-diesel from castor oil plant at Bogor Institute of Agriculture (IPB) and at the Ban dung Institute of Technology. They are currently developing bio-diesel oil from the castor oil plant in 400 ha of land in Bireun, Aceh. Each 400 ha of Castor oil plants can produce 4000 liters of bio-diesel.

Bio-diesel from Oliplam in Malaysia

Palm oil prices have been showing wide variation over the last 4 years despite rising production of the oil with in Malaysia, Palm oil (30 million tones) accounts for about 35 percent of global vegetable oil production (110mt) and close to 60 percent of world trade of (40 mt in vegetable oils. The industry estimates that up to five lakhs tones of crude palm oil will be used up annually for bio-fuel purposes, a development that would act as a stabilizing factor for the palm oil market; any quantity in excess of one million tones in stocks will be diverted for bio-diesel.

Energy Scenario in India

India's incremental energy demand for the next decade is projected to be among the highest in the world. With increasing growth rate of GDP, total primary commercial energy consumption has increased from 350 million metric tones of oil equivalent (MMToE) during 2003-04 to 380 MMToE at present.
Consumption of petroleum has increased form 3.5 million metric tones (MMT) in 1950-51 to 17.9 MMT in 1970 and 843 MMT in 1997-98 and to more than 120 MMT at present. It is estimated that the demand for petroleum is 234 MMT in 2019-20. Domestic production of oil in 2004-05 is 33 MMT. Diesel consumption in 2004-05 for import of petroleum products and it is estimated to cost approximately Rs. 1, 75, 000 .00 crores in 2005 respectively.

There is increase in the growth rate of expenditure on import of petroleum to the tine of 46 percent from 2004-05 and 2005-06. More than 70 percent of India's total petroleum consumption is imported from international market, which itself has become more volatile than ever. International crude prices are soaring to new highs. Petroleum is predominately (46 percent) consumed in transport sector. The fuel-mix in transport sector shows that about 80 percent consumption in this sector is a High Speed Diesel (HSD). The projected demand for HSD in the country by 2005-07 is 52 MMT and on present indications, by 2011-12, it could increase to 67 MMT. Petroleum resources are finite and therefore search for alternative fuels is continuing all over the world. Bio-diesel is a renewable fuel and it can be made from any edible, non-edible vegetable oil including waste oil development of Bio-diesel as an alternative and renewable source of energy for transport sector has become important in the national effort towards self-reliance, an important component of the strategy for energy security.

Bio-diesel Society of India (BDSI) formed

Keeping in view of the depleting oil reserves, increasing crude prices and rising global temperature, a group of like minded entrepreneurs, scientists, bureaucrats and social workers have formed a society to promote the use of bio-diesel. The objective of the society is to promote the consumption of bio-diesel. Due to availability of high yielding varieties, this may also results in reduction in import of petroleum products.

III. ALTERNATIVE FUELS

The selection of alternative fuels for IC-engines include the following factors

- Should be available in plenty and derived continuously from renewable sources.
- They should have high specific energy content.
- Should permit easy transportation and storage.
- Should cause less environmental pollution.
- Should be safe in handling.

The various alternative fuels for compression ignition engines are as follows.

ALCOHOLS:

Alcohol is an important renewable energy sources that can substitute petroleum products to certain extent. The two alcohols that are of main interest are

ETHANOL:

Ethanol is a convenient liquid fuel and can act as a substitute for petrol and diesel. Usually 95% (hydrous) ethanol can be directly used in modified engines. 100% (anhydrous) ethanol can be mixed with dry petrol to produce gasohol comprising 10% anhydrous ethanol with 90% petrol. The excellent combustion properties of ethanol enable an engine to produce up to 20% more power. Mass, density and calorific value of ethanol are less than that of petrol but on account of its improved combustion properties of ethanol fuel

consumption from for ethanol, gasohol or petrol is more or less than the same. Ethanol as petrol additive raises the octane rating of the mixture, as anhydrous ethanol is an octane fuel. Distinctive advantage of ethanol is that it can be produced by renewable sources unlike nonrenewable fossil fuels.

METHANOL:

Methanol like ethanol possesses octane enhancing capability when blended with unleaded petrol. Methanol has high toxicity, which makes it a less desirable fuel than ethanol. Methanol, in blends with petrol, up to a 10% can be used in existing S.I.engines without any modification. In view of its particular solubility, characteristics, methanol can not be blended with diesel for use in C.I engines. Methanol has a value of 15.5*10^6 to 17.7*10^6 joules per liter, which about half the heat value of petrol and 75% of ethanol. Apart from having higher flame speed, methanol possesses superior anti knocking properties that enable us to achieve a higher output. The concentration of carbon monoxide, unburnt hydrocarbons and oxides of nitrogen in the engine exhaust is less with methanol and methanol-petrol blends as compared to that of petrol. It is to be noted that methanol burns cleaner than petrol.

Table 1: important properties of methanol and ethanol

S.no	Property	Methanol	Ethanol
1	Chemical formula	CH_3OH	C_2H_5OH
2	Composition by weight %		
	Carbon	37.5	52
	Hydrogen	12.5	13
	Oxygen	50	35
3	Specific gravity at 15.5^{o}c	0.796	0.794
4	Boiling point	65	78
5	Lower calorific value (K cal/Kg)	4700	6400
6	Self ignition temperature (^{o}C)	478	420
7	Octane numbers		
	(a) research	114	111
	(b) motor	94	94
8	Cetane number	03	08

BIO-MASS:

Biomass is produced in nature through photo synthesis achieved by solar energy conversion. Bio-mass can be obtained from different sources comprising

1. Organic wastes that accumulate at specific locations such as municipal solid wastes (MSW), timber wastes and sewage sludge.
2. Bio-mass in non traditional form (converted in to liquid fuels).
3. Fermenting the biomass aerobically to obtain a gaseous fuel called biogas.

Bio-mass is a renewable energy so long as it is grown at a rate at least equal to the rate of its consumption.

BIO-GAS:

Bio-gas can be produced by fermenting organic materials in the absence of air or oxygen with the help of bacteria (micro organisms) to break down the materials into intermediates like alcohols and fatty acids and finally to methane, carbon dioxide and water. This process is called anaerobic fermentation. The appropriate fermentation. The appropriate composition of biogas produced is as follows: methane 50-60%, CO2 30-40%, hydrogen 5-10%, nitrogen 4-6%, oxygen 1-2% and hydrogen sulfide in traces. Methane and hydrogen when burnt with oxygen give energy in the form of heat.

1. $CH_4 + 2O_2 \rightarrow 2H_2O + CO_2 + 978.6$ KJ
2. $2H_2 + O_2 \rightarrow 2H_2O + 572.6448$ KJ

The CO2 in bio-mass does not contribute to the heat energy; indeed it is unfavorable to any burning process. The amount of heat energy generated is 36476.804 KJ/m^3 for methane and 11712.428 KJ/m^3 for hydrogen. It is impracticable to store large volumes of biogas at low pressure. It is therefore more economically used as it is produced, for example, to meet space and water heating or cooking needs in forms.

NATURAL GAS:

Natural gas is generally associated with petroleum and coal deposits. It consists of mainly methane with small percentages of ethane, propane, butane and CO2 and nitrogen. Natural gas is nearly odorless and colorless. The usual range of consumption is 68% to 96% of methane and 3% to 30% of ethane in natural gas. The range of calorific value of the natural gas is 37674-46046 KG/m^3. Gaseous fuel has number of advantages

over solid or liquid fuels as they burn without any smoke and ash. The control of gases relatively easy and main disadvantage is its storage.

HYDROGEN:

Hydrogen can play an important role as an alternative to conventional fuels provided, its technical problems of production, storage and transportation can be resolved satisfactorily and cost could be brought to the acceptable limits. One of the most attractive features of hydrogen as an energy carrier is that it can be produced from water, which is abundantly available in nature. Hydrogen has the highest energy content per unit if mass than any chemical fuel and can be substituted for hydrocarbons in a broad range of applications, often with increased combustion efficiency. Its burning process is non- polluting and it can be used in fuel cells to produce both electricity and useful heat.

METHANE:

Methane is clear gas with high calorific value. It can be used on site, and into the gas mines. Natural gas is 955-methane or converted into methanol by treatment with a catalyst at high temperature and pressure. It can also be compressed and used in limited range vehicles like tractors and forklift trucks. However, to store or transport the energy equivalent of a single gallon of petrol as compressed requires a large tank. At 115bar pressure the tank dimensions would need to be 0.45m in diameter and 1.45m in height.

LIQUIFIED PETROLEUM GAS:

During the refining of petroleum, large quantities of butane are liberated from the top of the column and from the other refining processes. These gases can be compressed and liquefied at atmospheric temperature. Butane and propane are also present in natural gas and can be separated and removed. Thus large volumes of the gas can be stored under pressure in steel cylinders. It is an ideal fuel for domestic and mobile use. LPG contains some fraction of methane and unsaturated hydro carbons in addition to butane and propane.

VEGETABLE OILS:

Vegetable oils can be classified as edible and non-edible oils. In India the consumption of edible oils is more than the production. Hence, we can depend on non-edible oils for use in CI engines. Edible oils such as sunflower, coconut, rice bran etc. can be used. Non-edible oils such as mahua, karanji, rapeseed, cottonseed etc. can be substituted in CI engines.

PROPERTIES OF VEGETABLE OILS:

If fuel shall be used in the existing engines, some required properties of the fuel such as kinematic-viscosity, the self ignition response, the net heating value, the grass heating value and density must be considered.

VISCOSITY:

The direction injection in open combustion chamber trough nozzle and pattern of fuel spray decides the case of combustion and thermal efficiency of the engine. Viscosity plays a vital role in the combustion. Low viscosity can lead to excessive internal pumping leakage where as high viscosity can increase system pressure to unacceptable levels and will effect injection during spray atomization. This effect is critical particularly at low speed or light load condition as pure vegetable oils have high viscosity. The derivatives of vegetable oils are called monsters and have low kinematics viscosity than that of oils. The monoesters are able to give stable solutions in wide range of proportions with diesel fuel, vegetable oils and with alcohol too. They can be solubilizers and can also make it possible to influence the viscosity of blended oils.

SELF-IGNITION RESPONSE:

It is expressed by the cetane number and for a good diesel fuel the value has to be not lower than 45. The cetane number of vegetable oils is less than the diesel. The cetane number of monoesters, on an average, is above that of vegetable oils. For example neem and karanji oils with diesel blends of 10% level have cetane number about 40-45 and at 20% level have cetane number about 35-40.

THE ENERGY CONTENT or HEATING VALUE:

The specific heating values of the different vegetable oils are nearly the same.

They range from 30.5-40.5MJ/Kg and for fuels it are approximately 42.4MJ/Kg. if calorific or heating value of vegetable oils is more, it helps to reduce the quantity handled and to maximize equipment operating range. It is always desirable for vegetable fuels to have heating value nearer to diesel oil.

DENSITY:
Density of the vegetable oils is 0.91-0.94gm/cc at 15^{o}C. In comparison to the density of diesel fuel (0.81-0.86gm/cc)the density of vegetable oils 10% higher, and for ester about 5% higher. For example mahua oil-0.92, neem oil-0.921 & karanji oil-0.95 while the density of ethyl and methyl ester of rape oil is 0.87 and 0.88gm/cc respectively.

POUR POINT, CLOUD POINT AND FLASH POINT:
First two properties are important for cold weather operation. For satisfactory working, the values of both are well below freezing point of oil used. Flash point is important from safety point of view. The temperature should be practically as high as possible. Typical values of vegetable fuels range between 50 & 110 c addition of vegetable oil with diesel to form a blend should not decrease the flash point temperature.

SEPERATION OF VEGETABLE OIL FUELS:
Solution to the viscosity problem has approached in at least four ways:

1. by dilution
2. by preparation of methyl esters transesterification
3. by micro emulsification
4. by Pyrolosis(or)thermal cracking

(a)DILUTION:
Dilution or blending of vegetable oil with neat diesel fuel, to improve fuel property of vegetable oil, is one of the well known methods. Dilution of sunflower oil with diesel fuel (1.3v/v) provides a fuel with a viscosity of 4.88 at 40 c, which is higher than the specified ASTM value of 4.0 at 40c. The viscosity is moderately less than that of neat sunflower oil. However Ziejewsks concluded that the blend could not be recommended for long term use in the direction diesel, engine because of closing of injector nozzle.

(b) METHYL ESTER TRANS ESTERFICATION:
The second method for reducing the viscosity is the conversion of the triglyceride oil to simple esters, which reduces the molecular weight of the original oil to 1/3 of its former value and so reduces the viscosity. Transesterification is a chemical reaction that aims at substituting the glycerol of the glycosides with their molecules of mono alcohols such as methanol and ethanol there by obtaining three molecules of methyl ester of the vegetable oil. A mixture of anhydrous alcohol and reagent (NaOH) in proper proportions is combined with moisture free vegetable oil. The materials are maintained at 65 to 75 c and allowed to settle by gravity for 24 hours.

Alkali catalyzed transesterification is known to proceed much fatter than acid catalyzed transesterification. Fatty acid methyl esters are considered as a possible substitute for a conventional automotive diesel engine.

Vegetable oil + alcohol ----------> glycerin + esters

(c)MICRO EMULSIFICATION:
Another method of reducing vegetable oil viscosity has been discovered through the formation micro emulsion with short chain as methanol (or) ethanol. A micro emulsion is defined as colloidal equilibrium dispersion of optically isotopic fluid micro
structures, with dimension generally in 1 to 150 square meter range, formed spontaneously from two normally immiscible liquids and one or more amhophilous.
The preliminary engine tests gave the following results for micro emulsions.

1. Lower exhaust temperature, and reduced emissions. Lower carbon monoxide/nitrogen oxide emissions than that is observed for diesel fuel.
2. Heat release4 patters indicated that the micro emulsion fuels burned faster than diesel fuel and had higher levels of pre mixed burning and lower levels of diffusion flame burning.

(d) PYROLYSIS OR THERMAL CRACKING:
Thermal and catalytic decomposition of vegetable oils to produce substitutes for diesel fuel has been studied by a number of researchers using a variety of methods. The method involves cleavage of chemical bonds to yield smaller molecules. Essentially two different methods of processing vegetable oils to obtain fuel have been used.

1. Passing of the oil over a heated catalyst in a tube.
2. Distillation of the oil while in the presence of metallic salts.,

PROPERTIES OF VEGETABLE OIL ESTER:

The physical characteristics of vegetable oil esters are close to those of diesel oil. A very positive gain by this process is the cetane number of esters. The fact that the cetane number of esters is in the range of 50 and above indicates their superiority in this respect. Viscosity is considerably reduced and is brought down to the level of what is usual for diesel oil. They heating value is slightly lower than that of the parent oil. The cloud point, though considerably reduced, is still high enough to cause flow problem in certain climates. The carbon residue of the esters is also low. There is only a marginal improvement in the volatility as a result of esterification. However this is not sufficient to eliminate starting problems in cold conditions. They mix easily with diesel oil. The characteristics being so close to those of the diesel oil that the esters become strong candidates to replace the diesel oil when need arises.

Table 2: vegetable oil properties

Oil	Flash point (^{o}c)	Density gm/cc	Kinematic Viscosity At 37.8^o c Sq.mm/sec	Cetane number	Cloud point (^{o}c)	Lower heating Value MJ/liter
Diesel oil	46	0.832	1.62	45.0	-17.8	35.3
Peanut oil	235	0.921	41.2	41.5	+3	34.1
Methyl ester peanut oil	176	0.883	4.9	54.0	+5	33.6
Soya bean oil	219	0.923	36.8	38.5	-4	34.0
Babassu oil	150	0.946	30.3	38.0	+20	33.4
Methyl babassu oil	127	0.879	3.6	63.0	+4	31.8
Palm oil	267	0.918	39.6	42.0	+31	35.0
Methyl ester of palm oil	164	0.880	5.7	62.0	+13	33.3
Sunflower oil	232	0.924	37.1	35.5	-5	34.0
Methyl ester of sunflower oil	183	0.880	4.6	49.0	+1	33.5

VEGETABLE OIL FUEL PERFORMANCE:

The vegetable oil based fuels are renewable biomass derived fuels. Further these fuels can be readily mixed with standard diesel and can be used in blends at any proportion. As far as the impact engine is concerned, there has been no evidence of material compatibility, problems using vegetable oil fuel when it is used in the proportion of 20 to 30% blend with diesel. A test in this regard was carried out by national Soya diesel.

According to NSDB(Development board USA) reports 100%esters of Soya bean oil indicated immersion incompatibility with certain rubbers and plastics, but not with metals. As far is durability is concerned most studies have shown no appreciable difference between vegetable oil based diesel and petrol. Vegetable oils based fuel can be substituted for diesel fuel with essential no engine modifications particularly at lower blending levels. Further, vegetable oil based fuel has a flash point of 64 c. vegetable oil fuel also has the advantage of not producing explosive fuel air mixtures.

PROBLEMS ASSOCIATING WITH VEGETABLE OIL FUEL:

1. Viscosity of vegetable oils is much higher than that of diesel. It can cause problems in fuel handling, pumping, atomization and fuel injection, incomplete combustion, poor cold startup, deposit formation and ring sticking.
2. Slower burning rate: vegetable oil gives rise to exhaust smoke, fuel impingements of oil on cylinder walls and lubricant oil contamination.
3. *VOLATALITY* of vegetable oils is very less which preclude their use in spark ignition engine.
4. *FLOW PROPERTIES* of the vegetable oils are poor which limit their utilization during cold weather in moderate temperature climates.

MODIFICATIONS:

The problems associated with viscosity can be reduced by heating the oil before entering into the engine.

1. Further the fuel injection problem can be increasing the injection pressure.
2. The problems associated with late/slow burning can be avoided by advancing fuel injection and preheating the fuel.
3. All the above problems can be eliminated up to certain extent by blending vegetable oils with diesel.
4. Low problems can be eliminated by winterization (popular technique for reducing high melting point by freezing them over a prescribed time period and drawing the liquid portion off separately)

POLLUTION ASPECT OF VEGETABLE OILS:

Vegetable oils have high carbon residue. Vegetable oil based fuel contribute less green house gases to the atmosphere and its use results in reduced air pollution to local levels. The parameters, which improve with vegetable oil based fuel, include smoke, polyrometric hydrocarbon, unburned hydrocarbon, sulphurdioxide, and acetaldehyde. One more important thing is that vegetable oil based fuels are biodegradable and non toxic. If spilled, it is at least 90% biodegradable with in three weeks. Therefore, its spill and leaks in mines and other sensitive areas will have less impact on disturbed aquifers. These characteristics make it a valuable fuel particularly in environmentally sensitive areas. Vegetable oil has good ignition qualities than lighter alcohols for diesel engines, since their cetane number is above 30.

ECONOMICAL ASPECT OF VEGETABLE OIL FUELS:

Vegetable oil based fuel is currently more expensive than petrol & diesel. But by increasing the production and by providing subsidies, the prices can be lowered down. Further, by using glycerin as bi-product, the prices can be brought down. While considering about cost factor, we have to think about petroleum sources. They will become scarce with in next 25-30 years, and by that time we must have some alternative sources to run out millions of vehicles with out disturbance. The alternative fuels available are LPG, alcohol, and vegetable oils etc., further these LPG sources are also limited. They may serve 30-40 years. So, next choice is to go for vegetable oils. These vegetable oil based fuels are promising once. Their use doesn't requiring major engine, vehicle or infrastructure modification in existing facilities. Because, these vegetable oils are renewable, the promising feature of vegetable oil based fuel cannot be over looked.

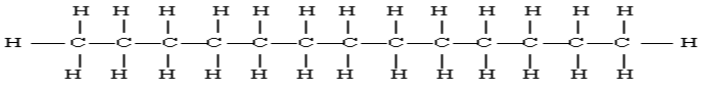

DIESEL FUEL STRUCTURE

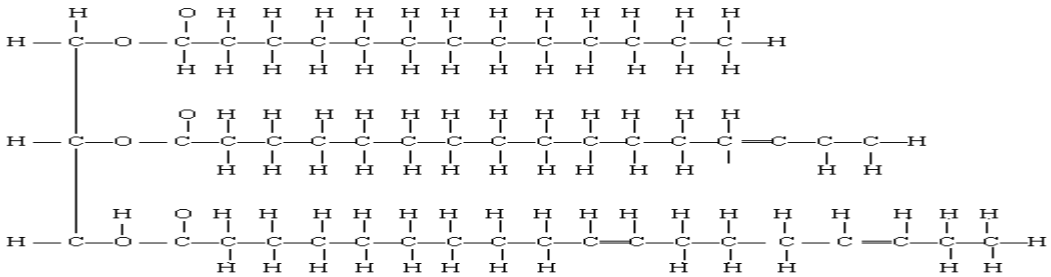

VEGETABLE OIL FUEL STRUCTURE

IV. MAHUA OIL – LITERARY SURVEY

Introduction:

Two species of the genus madhuca indica and madhuca longifolia are found in India. Mahua is known as *Illupai maram* in Tamil and *Hippi* in Kannada, which can be successfully grown in the wastelands and dry lands. The seeds of the tree, popularly known as `Indian butter tree. The specific gravity of mahua oil was 9.11% higher than that of diesel. The kinematic viscosity of mahua oil was 15.23times more than that of diesel at temperature of 40c. The kinematic viscosity of mahua oil reduced considerably with increase in temperature to 80c and by increasing the proportion of diesel in fuel blends.

Mahua oil tree plantations and seeds shown at the top right corner

Leaves and flowers of mahua oil tree

Edible oil:

The seeds contain 30-40 per cent fatty oil called mahua oil, which is edible and is also used in the manufacture of various products such as soap and glycerin. The oil cake is used as bio fertilizer, organic manure and as feed for fish and cattle. The leaves are used as fodder and as green manure. The flowers are used for extracting ethanol, which is used in making country liquor.

Potential income:

The tree is found in abundance in Thanjavur, Tiruchi and Perambalur regions of Tamil- Nadu and along the Cauvery River basin. About 30-40 percent of the tribal economy in north India such as in Bihar, Madhya Pradesh and Orissa is dependent on the mahua seeds and flowers. The tree has a potential of enhancing rural income. Being an evergreen variety, it reaches a height of 45-60 feet, and is well adapted to varied weather conditions. With its wide spreading branches and circular crown the trees present a visually appealing structure. Though the tree starts bearing seeds from the seventh year of planting, commercial harvesting of seeds can be done only from the tenth year. Seed yield ranges from 20-200 kg per tree every year, depending on its growth and development. Being hardy and pest resistant, the tree requires little attention once it has taken root.

Propagation technique:

Elaborating on the technique for propagating the trees, he said the variety can be propagated through seeds and transplanted seedlings. Seeds are sown at a depth of 1.5-2.5 cm on raised beds. The seeds germinate in about ten days. One-month-old seedlings are transplanted in plastic containers of 15 x 25 cm. Six to twelve-month old-seedlings are used for planting in the main field.

Comparison of mahua oil with diesel oil:

(a) **Calorific Value and Carbon Residue:** The calorific value of mahua oil was observed as 88.26% of diesel on weight basis and 96.30% on volume basis. The calorific value of mahua oil was found nearer to diesel fuel in comparison with other liquid fuel options like ethanol and methanol. The carbon residue of mahua oil was found higher than that of the limit specified for gradeA diesel and this may increase the chances of carbon deposition in the combustion chamber. The higher carbon residue may be due to the difference in chemical composition and molecular structure of mahua oil.

(b) **Flash point:** the flash point of mahua oil was very high as compared to diesel thus indicating its low volatile nature. The results of increase in concentration of mahua oil in diesel revealed that the power output decreases at all compression ratios.

(c) Brake thermal efficiency and a/f ratio: Brake thermal efficiency decreased with the increase of mahua oil in diesel at all three compression ratio in comparison with pure diesel. Exhaust gas temperature increased with the increase in concentration of mahua oil in diesel. The air-fuel ratio and volumetric efficiency decreased with increase in concentration of mahua oil in diesel.

Table 3: characteristics of mahua oil

Properties	Value
Refractive index	1.452-1.462
saponification value	187-197
Iodine value	55-70
Unsaponifiable matter, %	1-3
Palmitic acid, %	24.5
Stearic acid, %	22.7
Oleic acid, %	37.0
Linoleic acid,%	14.3

Table 4: Comparison of properties of different fuels

Properties	Diesel	Jatropha oil	Karanji oil	Rapeseed oil	Cotton seed oil	Rubber seed oil	Mahua oil	Transesterified mahua oil
Density gm/cc	0.840	0.918	0.927	0.918	0.874	0.920	0.918	0.844
Calorific value MJ/KWhr	42.93	39.774	35.8	36.89	39.648	38.957	38.863	36.914
Cetane number	45.55	45	40	39	45	40	34	65
Viscosity at 44 ° c	4.59	49.9	56	55	50	55.6	68.51	16.34
Flash point ° c	75	240	250	275	210	242	238	160
Carbon residueg	0.1	0.44	0.66	0.31	0.55	0.46	0.4215	0.38
Fire point ° c	78	244	255	279	215	246	244	165

V. TRANSESTERIFICATION

Introduction:

Transesterification is the process of using an alcohol (methanol, ethanol, proponol, or butanol) in the presence of catalyst to chemically break the molecule of the raw renewable oil into methyl or ethyl esters of the renewable oils with glycerol as by-product.

Transesterification of vegetable oils and fats:

The transesterification reaction proceeds with catalyst or without catalyst by using primary or secondary monohydric aliphatic alcohols having 1-8 carbon atoms as follows:

Triglycerides + monohydric alcohol ↔ glycerin + mono-alkyl esters

Transesterification means taking a triglyceride molecule or a complex fatty acid, neutralizing the free fatty acids, removing the glycerin, and creating an alcohol ester. Theoretically, transesterification reaction is an equilibrium reaction. In this reaction, however more amount of methanol was used to shift the reaction equilibrium to the right side and produce more methyl esters as the proposed product. A catalyst is usually used to improve the reaction rate and yield.

Alcohols are primary or secondary monohydric aliphatic alcohols having 1-8 carbon atoms. Among the alcohols that can be used in the transesterification reactions are Methanol, ethanol, proponol, or butanol or amyl alcohol. Methanol and ethanol are most frequently used. Ethanol is a preferred alcohol compared to methanol because it is derived from agricultural products and is biologically less objectionable in the environment. However methanol is preferable because if it's low cost and its physical and chemical advantages (polar and shortest chain alcohol). The transesterification can also be catalyzed by alkalis, acid or enzymes.

In the conventional transesterification of animal fats and vegetable oils for biodiesel production, free fatty acids and water always produce negative effects, since the presence of free fatty acids and water causes soap formation, consumes catalyst and reduces catalyst effectiveness, all of which resulting in a low conversion.

The transesterification reaction based on the catalyst usage is divided into two types namely

1. catalytic transesterification method
2. non- catalytic transesterification method

Reaction mechanism of transesterification:

Tranesterification consists of a number of consecutive, reversible reactions. Triglyceride is converted stepwise to diglyceride, monoglyceride and finally glycerol. The formation of alkyl esters form monoglycerides is believed as a step which determines the reaction rate, since monoglycerides are the most stable intermediate compound.

$$\textit{Triglyceride} + ROH \leftrightarrow \textit{diglyceride} + RCOOR_1$$
$$\textit{Diglyceride} + ROH \leftrightarrow \textit{glycerol} + RCOOR_2$$
$$\textit{Monoglyceride} + ROH \leftrightarrow \textit{glycerol} + RCOOR_3$$

Several aspects, including the type of catalyst (alkaline, acid or enzyme), alcohol/vegetable oil molar ratio, temperature, water content and free fatty acid content have an influence on the course of the tranesterification. In the tranesterification of vegetable oils and fats for bio-diesel production, free fatty acids and water always produce negative effects, since the presence of fatty acids and water causes soap formation, consumes catalyst and reduces catalyst effectiveness, all of which result in a low conversion. When the original ester is reacted with an alcohol, the transesterification process is called alcoholysis. The transesterification is an equilibrium reaction and the transformation occurs essentially by mixing the reactants. In the transesterification of vegetable oils, a triglyceride reacts with an alcohol in the presence of a strong acid or a base, producing a mixture of fatty acids alkyl esters and glycerol. The stoichiometric reaction requires 1mol of a triglyceride and

3mol of the alcohol. However an excess alcohol is used to increase the yield of the alkyl esters and to allow its phase separation from the glycerol formed.

In the below graph various reaction times are plotted against various percentage yields of methyl esters at two different temperatures.

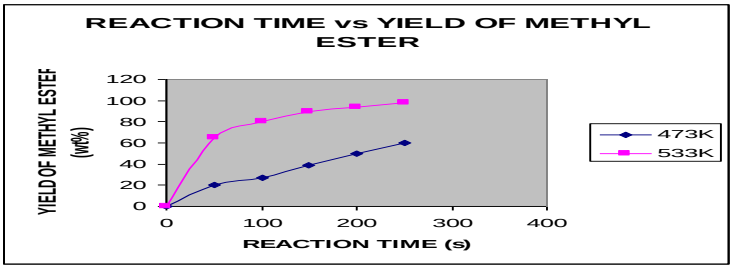

Based on the type of catalyst used the transesterification process is classified as follows:

1. Acid-catalyzed process
2. Alkali- catalyzed process
3. Enzyme- catalyzed process

Acid-catalyzed process:

The transesterification process is catalyzed by acids, preferably by sulphonic and sulphuric acids. These catalysts give very high yields in alkyl esters, but the reactions are slow**.** The alcohol/vegetable oil molar ratio is one of the main factors that influence the transesterification. An excess of alcohol favors the formation of products. On the other hand, an excessive amount of alcohol makes the recovery of glycerol difficult, so that the ideal alcohol/oil ratio has to be established empirically considering each individual process.

Alkali-catalyzed process:

The reaction mechanism for alkali-catalyzed transesterification was formulated in a simple manner. This reaction proceeds faster than that of the former one. The reaction mechanism will be explained in the later part.

Enzyme-catalyzed process:

This process is not yet commercially developed and also the reaction yields as well as the reaction times are still unfavorable compared to the base-catalyzed systems.

Transesterification procedure:

Table 5:

Sl.no	Chemical	Proportions
1	Mahua oil	500ml
2	Catalyst- NAOH	5.2gram
3	Methanol	225ml
4	Acetic acid + water	150ml + 850ml

- The catalyst is dissolved into methanol by vigorous stirring in a flask.
- The oil is transferred into a round bottomed flask and is heated in a water bath at 70c in water the prepared catalyst and alcohol mixture is added at first by constant stirring.
- The final mixture is stirred vigorously for 2hours at 340K in ambient pressure.
- A successful transesterification produces two liquid phases: ester and crude glycerol. Crude glycerol being heavier liquid is collected at the bottom of the flask after several hours of settling.
- Phase separation can be observed within 10min and can be completed within 2hours of settling in the separating funnel. Complete settling can take as long as 20hours.
- Before collecting the oil in the separating funnel it is mixed with acetic acid and water for distillation and easy phase separation.
- The separating funnel should be shaken well for two to three times while the mixture is allowed for phase separation.
- Finally, after 20hours, complete settling of oil and glycerol will take place.

VI. TRANSESTERIFICATION PROCESS

step1: weighing NaOH

step2: mixing methanol and NaOH

step3: heating sodium methoxide with 100ml mahua oil

step4: heated mahua oil in water bath and colour change appeared

step5: preparing dilute acetic acid solution (approx 130ml)

step6: mixing and shaking heated mahuaoil with acetic acid in a separating funnel

step7: finally obtained layers of biodiesel and glycerol after settling

step8: testing glycerol with acidified potassium permanganate solution

Precautions:

- The vegetable oil should have an acid value less than one and all materials should be substantially anhydrous. If acid value is more than one, more NaOH is injected to neutralize the free fatty acids.
- Water can cause soap formation and frothing. The resulting soaps can induce an increase in viscosity, formation of gels and foams, and made the separation of glycerol difficult.
- The stochiometric ratio for transesterification reaction requires 3mol of alcohol and 1mol of triglyceride to yield 3mol of fatty acid ester and 1mol of glycerol.
- Higher molar ratios result in greater ester production in a shorter time.
- Stirring plays a vital role in transesterification process. Constant stirring should be done for yielding of oil else it will be solidified.

Test for glycerol:

- The glycerol is tested for whether it is unsaturated or saturated fatty acid. For that it is taken in a flask.
- Then acidified potassium permanganate solution is added to that glycerol drop wise and observed carefully
- In this experiment it is observed that the acidified potassium permanganate solution decolorized the glycerol taken in the glass flask indication that it is unsaturated fatty acid.

FLOW CHART:

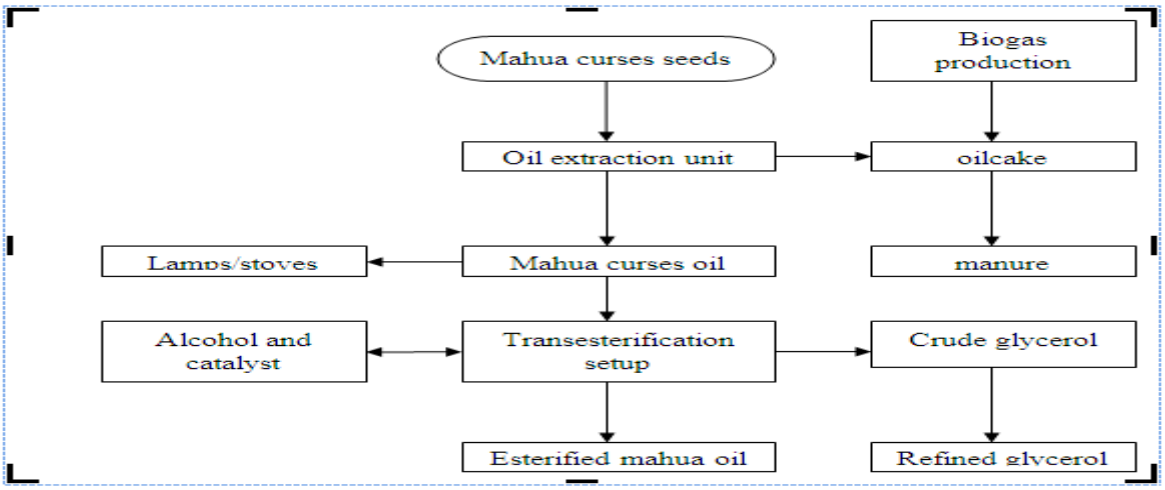

fig: flow chart for preparation of esterified mahua oil

VII. ACID AND HYDROCARBONS TEST

TEST WITH NaHCO3:

The esterified mahua oil is partially soluble in NaHCO3 and regeneration with dil.Hcl to this the oil contains "acidic groups".

TEST WITH NITRATION:

The esterified mahua oil and Nitration mixture (1:1 ratio of sulphuric acid and nitric acid) is collected in ice for about 15min and then heated in water bath for 20min and then poured into crushed ice then yellow precipitate is formed due to this the oil contains "hydrocarbons".

TEST WITH dil.Hcl:

The oil is insoluble in dil.Hcl due to this property the oil does not contain "basic groups".

VIII. DISTILLATION

What is distillation?

The process in which a liquid (or) vapour mixture of two (or) more substances is separated into its component factions of desired purity by the application and removal of heat. Distillation is the most common separation technique.

Introduction

Distillation Experiment

One of the major tasks of the synthetic organic chemist is the purification of starting materials and the isolation and purification of products. It is of particular importance to free a compound of impurities when its structure is to be established or its physical properties are to be precisely determined.

Distillation is a very old technique which is frequently used to purify compounds and to determine their boiling points. The boiling point is a useful molecular constant for the characterization and identification of pure compounds. Furthermore, the boiling point range is usually a good indicator of the purity of a liquid.

In this experiment you will perform several distillations. You will compare distillations of a mixture of methanol and water using the glassware set-up for a simple distillation and one for fractional distillation. You will also measure the boiling point-range for an unknown compound and use this information as an aid in its identification

Set Up

Distillation Experiment

The distillation flask, fractionation column and distillation head make up the part of the apparatus where the liquid components are volatilized and separated. (This unit should be constructed high enough on a ring stand to permit raising and lowering of the heating unit and assembled using the clamped flask as the foundation for the apparatus.) The rest of the apparatus serves to condense the hot vapor back to a liquid as it flows out the side-arm of the distillation head into the water-cooled condenser. (Caution: water should always flow from bottom to top of the condenser) Liquid flows down the condenser and through the adapter into a collection vessel. A thermometer is attached to the top of the distillation head by an adapter in order to determine the temperature of the vapor being collected. The animation shows the step-by-step assembly of a fractional distillation set-up.

A simple distillation apparatus is less efficient than a fractional distillation apparatus, but is used to purify materials containing only small amounts of impurities with much higher or lower boiling points.

IX. DISTILLATION PROCESS

Experiment

Distillation Experiment

The distillation flask is charged with the mixture of liquids and a couple of boiling chips. (Caution: never heat a liquid without boiling chips and always add new chips to a cooled solution before reheating.) After reattaching the flask, the liquid is heated to its boiling point to cause distillation. As the liquid travels up the fractionating column, there is constant contact of the vapor and condensed liquid flowing back down the column setting up equilibration all along the column. This results in the equivalent of a number of simple distillations, depending on the particular column being used. As the liquid is removed, the sample is depleted of the lower boiling component which is highly enriched at the top of the column until most of it is gone. An intermediate fraction consisting of the two components is usually collected until all of the lower boiling component is removed, at which point the pure higher boiling component is distilled. The progress of the distillation is followed by measuring the temperature of the vapor at the top of the column. In a reasonably efficient distillation, a fraction of each of the pure components will be obtained which boil over a small temperature range near the boiling points of the components with an intermediate fraction, whose boiling range is broad and between those of the pure components.

X. GLYCEROL REPRESENTATIONS:

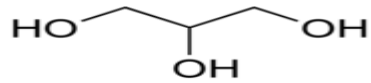

chemical structure of glycerol

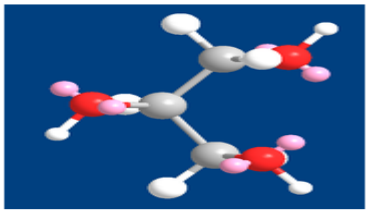

glycerol 3D model

GLYCEROL:

Glycerol, also well known as **glycerin** and **glycerine**, and less commonly as **propane-1,2,3-triol**, **1,2,3-propanetriol**, **1,2,3-trihydroxypropane**, **glyceritol**, and **glycyl alcohol** is a colorless, odorless, hygroscopic, and sweet-tasting viscous liquid. Glycerol is a sugar alcohol and has three hydrophilic alcoholic hydroxyl groups (OH^-) that are responsible for its solubility in water. Glycerol has a wide range of applications. Glycerol has a prochiral spatial arrangement of atoms.

Glycerol – uses and applications:

Glycerol literally has thousands of uses. However, those uses are in constant flux as new technologies are adapted. Here is an overview of the most common uses.

Foods and Beverages

Glycerol is used to moisten, sweeten and preserve foods and drinks.

Examples:

- Soft drinks
- Candies
- Cakes
- Casings for meats, cheese and dry pet foods

As an intermediate, glycerol also is used in margarine, salad dressings, frozen desserts and food coatings.

Drugs

Glycerol is one of the most widely used ingredients in drugs and pharmaceuticals, Uses include:

- Capsules
- Ear infection remedies
- Anesthetics
- Cough remedies
- Gargles
- As a vehicle for antibiotics and antiseptics

Cosmetics and Toiletries

Because glycerol is nontoxic, non-irritating and odorless, it is used as a moisturizing agent and emollient (softening agent) for cosmetics and toiletries, including:

- Toothpaste
- Skin creams and lotions
- Pre-shaving lotions
- Deodorants
- Make up
- Lipstick

Tobacco

Glycerol keeps tobacco moist and soft to prevent breaking and crumbling during processing; it also adds flavor to chewing and pipe tobaccos. Glycerol also is used to manufacture cigarette filter tips.

Paper and Printing

Glycerol is used to soften and reduce shrinkage during paper manufacturing.

Related uses:

- Grease-proof paper
- Food wrappers
- To manufacture printing ink

Textiles

Glycerol is used to size and soften yarn and fabric and to lubricate many kinds of fibers in spinning, knitting and weaving operations.

Other common uses:

- As a lubricant for food processing machinery
- To manufacture resin coatings
- To add flexibility to rubber and plastic
- As a building block in manufacturing flexible foams
- To manufacture dynamite
- To create a component used in radios and neon lights

XI. EXPERIMENTAL SETUP AND PROCEDURE

The schematic diagram of the experimental setup to test the performance of the engine with esterified mahua oil is shown in figure. The engine is rigidly fixed to engine bed by bolts and nuts. A surge tank is fixed to the stand and air enters into the surge tank through air filter and passes through an orifice plate. The difference in water column in two legs of U-tube manometer gives the pressure drop across orifice plate. This pressure drop is used to calculate the mass flow rate of air.

The dynamometer used here is brake dynamometer. It has a brake drum connected to the crankshaft. A belt runs over the brake drum one end connected to the spring balance and another end to the load carrying plate. The reading of the spring balance is taken as the net load on the engine.

EXPERIMENTS:

For better homogenization of the blends, they were prepared by mixing the required proportions in the fuel tank. The compressed air at 2-3 atmospheres from a compressor was bubbled through the mahua oil blend. This ensures a thorough mixing and homogenization of the blend. The blended fuel was then injected into the combustion chamber with the standard fuel injection system of the engine. The injection timing was optimized for the fuel at the rated load and this injection timing is maintained constant through the test.

The experimental setup consists of

1. Setup for investigation of the performance characteristics of C.I.engine using diesel and mahua oil blends.
2. Setup for the investigation of fuel properties.
3. Setup for the transesterification of mahua oil.
4. Setup for changing the pressure of the injector of the engine.

Kirloskar Single Cylinder 4-Stroke Diesel Engine

Experimental Setup For Investigation Of Performance Characteristics:

The experimental setup consists of single cylinder, 4-stroke, and water cooled KIRLOSKAR diesel engine. It is provided with accessories for the measurement of the load, fuel consumption, exhaust gas temperature, volume of air inducted. The experimental setup is shown in the figure.

Specification Of The Engine:

Name of the engine	: KIRLOSKAR
General details	: 4-stroke C.I, vertical, water cool
Number of cylinders	: 1
Bore	: 80mm
Stroke	: 110mm
Rated power	: 5bhp at 1500rpm
Brake drum diameter	: 310mm
Belt thickness	: 6mm

Arrangement For Measuring Load:

A rope runs over the brake drum one end connected to the spring balance and another end to the load carrying plate. The reading of the spring balance is taken as the net load on the engine. In the operation of the rope brake drum dynamometer, the engine is made to run at constant speed. The frictional torque due to the rope must be equal to the torque transmitted by the engine.

Apparatus For Measurement Of Fuel Consumption:

The fuel tank is attached with a graduated burette. The valve at the bottom of the tank is closed when fuel consumption rate is to be measured so that fuel is consumed only from the burette. The time taken for "X" amount of fuel consumption is recorded to measure the fuel consumption rate.

Experimental Set Up For The Investigation Of Fuel Properties:

For determination of properties of esterified mahua oil and diesel blends, the experimental setup consists of

(a) Apparatus to determine emission gases
(b) Apparatus to determine viscosity
(c) Apparatus to determine density
(d) Determination of aniline point and cetane number

Description Of Apparatus For Measuring Emission Gases:

(a) DC-5 GAS ANALYZER:

DC- 5 gas analyzer measures five emission gases, including hydrocarbons (HC), Carbon Monoxide (CO), Carbon Dioxide (Co2), Oxygen (O2) and oxides of Nitrogen (NOX).

It will also provide a read-out for an optional Tachometer that handles up to 30,000 r.p.m.

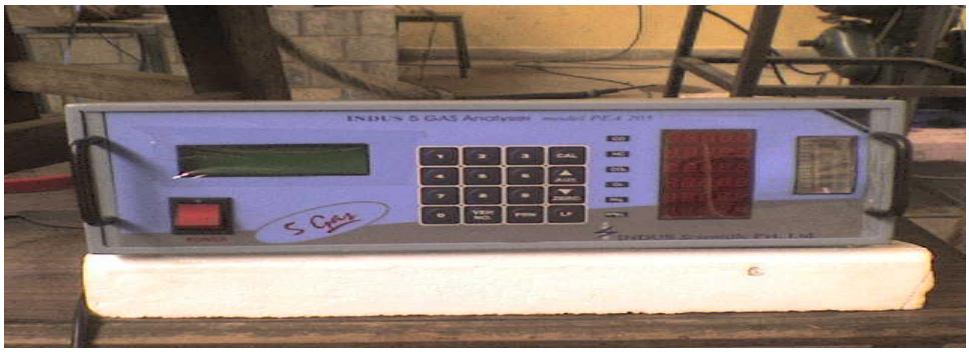

DC-5 GAS ANALYZER

(b)SMOKEMETER:

Many stationary sources discharge visible emissions into the atmosphere; these emissions are usually in the shape of plume. This smoke meter involves to determination of plume opacity.

SMOKE METER

Description Of Apparatus For Measuring Viscosity:

The viscosity of the vegetable oil blends is determined by using redwood viscometer. The description of apparatus is given below. The redwood viscometer consists of a copper cup, which is used to fill the liquid whose viscosity, is to be determined. The cylinder cup is surrounded by a water jacket. To maintain a uniform temperature throughout the volume of a stirrer is provided. A ball valve is provided to control the flow of liquid through the small hole located at the bottom of copper cup. A collecting flask and stopwatch are required to collect 50cc of oil and to determine the corresponding time.

Apparatus To Determine Density:

For measuring the density of fuel blends, the apparatus consists of gravity bottle is determined accurately with the help of physical balance and weight. A 50cc of trans esterified mahua oil is taken in the bottle and its weight is determined. From the readings obtained, the density of esterified mahua oil is determined

Apparatus For Determing Aniline Point And Cetane Number:

To determine the aniline point of fuel blends the apparatus consists of a water container in which a test tube with the aniline mixture placed. The setup is heated using the Bunsen burner and the heat is distributed to the stem by using a stirrer. Thermometer is placed in the mixture to, read the aniline mixture.

Experimental Technique:

The important fuel properties of esterified mahua oil where determined according to standard procedure. The kirloskar 5bhp, single cylinder, 4stroke, water cooled engine having a bore(80mm) and stroke (10mm) was used for this stud as shown in the figure 7.1.the experiments were conducted at constant speed of 1500rpm as applicable for stationary engine. The engine was coupled with a belt brake dynamometer. The standard instrumentation was used to measure the fuel consumption, exhaust temperature, coolant temperature(fig 1)for the stabilization of measuring parameters at each load setting and at the start of each test, time period of 10 min and 30min were allowed. Three blends of esterified mahua oil with diesel and pure oil were tested in the engine. The fuel blends were prepared in the proportion of 80% and 60% volume be volume

with diesel, respectively. Pure esterified mahua oil (100%) is also used as another blend to run the engine. The base line test was conducted with diesel only. In the process of testing with esterified mahua oil – diesel fuel blends, no change was made in the engine. The engine was directly started on the fuel blends with out a change over from diesel fuel. The engine performance was compared on the basis of parameter, i.e. power output, specific fuel consumption, brake thermal efficiency, and exhaust gas temperature, air/fuel ratio and volumetric efficiency.

The values of power output, specific fuel consumption (SFC) and brake thermal efficiency was calculated using the standard formula and compared with that of diesel.

Experimental Procedure:

The experimental procedure consists of

1. Tests for determination of fuel properties
2. Tests for finding out the performance characteristics

Test To Determine The Properties Of Blends:

A Procedure To Determine The Viscosity:

The apparatus is cleaned thoroughly. The ball valve is placed in position thus closing the orifice. The sample is poured into the cup up to gauge point. The standard 50 ml flask is kept under the orifice of the cup. The sample is heated to the required temperature, which is noted from the thermometer immersed in the oil. After heating to the desired temperature the ball valve is lifted off. The oil drains in to the flask placed beneath. The time taken to collect the oil up to the mark is measured using stop watch.

The kinematic viscosity of the sample is determined using the formula.

Kinematic viscosity = A*t – B/t in centistokes.

Density (Dt) = Dr-0.000675(T-Tr) in gm/cc.

Where t = Redwood seconds to collect the 50 ml sample.

A and B are constants given below

A = 0.26 and B = 171.5.

PROCEDURE TO CALCULATE CETANE NUMBER:

The aniline point is the lowest temperature at which equal parts of volume of freely distilled aniline and test sample are completely miscible in each other.

It is determined by mixing in jacketed test tube to clear solution and recording the temperature at which turbidity appears as mixture cools.

$$\text{Cetane number} = -\frac{\text{Aniline temperature in } {}^{o}C}{1.95} - 31.5$$

for pure esterified mahua oil, diesel blends that are mixable with aniline at room temperature, the mid boiling point is determined. From mid boiling point, the cetane number is determined.

The aniline point indicates the possible deterioration of rubber sealing, pacing, etc, in contact with the oil. The aniline point, the lower the percentage of aromatic hydrocarbons and higher the content of paraffin lower the aromatic content.

Procedure To Measure Density:

The gravity bottle is thoroughly cleaned and dried. The bottle is placed in the left pan of the balance and mass of bottle is determined b placing weights from the weight box in the right pan so the weights of the masses in the pans are balanced. The bottle is filled with the sample up to the mark, it is again placed on the pan and its mass is also determined. The volume of the sample in the bottle is 'X 'cc

Density of the sample = (b – a)/ X g/cc

Where

b = mass of fuel + bottle in g.

a = mass of bottle in g.

XII. PROCEDURE TO CHANGE INJECTOR PRESSURE:

Higher fuel-injection pressure increases the degree of atomization. The fineness of atomization reduces the ignition delay, due to higher surface volume ratio. Smaller droplet size will have low depth of penetration due to less momentum of the droplet and less velocity relative to air from where it has to find oxygen after vaporization. Because of this air utilization factor will be reduced due to fuel spray path being shorter. Also with smaller droplets, the aggregate area of inflammation will increase after ignition, resulting in higher pressure rise during the second stage of combustion. Thus, lower injection pressure, giving larger droplet size may give lower pressure rise during the second stage of combustion and probably smoother running.

Generally mean droplet size decreases with increase in the injection pressure. Also the rate of injection increases with the increase in injection pressure and there by the load on the injector push rod and cam increases which may affect the durability of the engine.

Injector to be pressure changed should be placed in the pressure changing setup. The lever is pulled down such that the nozzle sprays the fuel and the pressure reading is shown in the indicator in bar. Pressure can be changed by removing the head nut of the nozzle and by adjusting the screw, by operating the lever the pressure can be changed. The pressures we have used for injector is 200bar. The following steps show the procedure of pressure changing of the injector.


Step: 1


Step: 2


Step: 3


Step: 4


Step: 5


Step: 6

Experimental Procedure For The Determination Of Performance Characteristics

The procedure comprises of determining Brake Horse power, Brake Thermal efficiency, specific energy consumption, and Exhaust gas temperature. Before the actual tests are carried out the engine is checked for lubrication and fuel supply. Rotating the flywheel manually and operation the decompression lever start the engine. If the engine starting is difficult for blends, the engine is run on diesel initially. The nozzle injection pressure is set at 200 kg/cm2.

Determination of Brake Power

The equivalent load 'W' is recorded from the calibrated circular scale incorporated in the dynamometer setup.

$$B.P = W*N/1500 \quad KW$$

Where,

N is speed of engine in rpm,

W is load applied in kg

Determination Of Brake Thermal Efficiency

$$\text{Brake thermal efficiency} = (B.P * 3600)/ (F.C.H * C.V)$$

Where,

C.V = calorific value of the blend in kJ/kg

F.C.H = fuel consumption in kg/hr

Determation Of Specific Fuel Consumption

.

$$S.F.C = F.C.H / B.P \text{ kg / KW-hr}$$

Procedure To Obtain Exhaust Gas Temperature

The Exhaust gas temperature is measured using a Dail thermometer. The indicator on a graduated Dail directly reads the temperature in ^{o}C

Table: 6 Engine performance with 100 % diesel at an injection pressure of 200bar

Gas Analyser Readings					Smokometer Readings	
Co (%)	HC(ppm)	Nox(ppm)	Co2 (%)	O2 (%)	Opacity(N)	K
0.049	15	74	2.03	18.12	1.1	0.03
0.040	18	351	3.98	15.26	1.5	0.03
0.036	22	615	5.34	13.4	1.4	0.035
0.039	19	840	6.53	11.6	4.1	0.09
0.033	12	831	6.58	11.57	8	0.21
0.033	8	865	7	10.9	13.5	0.35
0.086	29	829	6.61	11.38	16.5	0.35

S.No	Load (Kg)	Speed (rpm)	Fuel Consumption (mf),Kg/hr		Exhaust Gas Temp.(°C)	B.P (kw)	F.C (kg/hr)	F.P (kw)	I.P (kw)	S.F.C (kg/kw-hr)	B.T.E (%)	I.T.E (%)	M.E (%)
			X(cc)	T(Sec)									
1	0	1500	30	187	105	0	0.49	5.2	5.2	∞	0	87.9	0
2	1	1490	30	141	140	0.99	0.66	5.2	6.19	0.66	12.58	78.6	15.99
3	2	1480	30	110	175	1.97	0.84	5.2	7.17	0.43	19.67	71.6	27.47
4	3	1460	30	97	205	2.92	0.96	5.2	8.12	0.33	25.51	70.1	35.96
5	4	1452	50	145	225	3.87	1.06	5.2	9.07	0.27	30.62	70	42.67
6	5	1440	50	129	240	4.8	1.2	5.2	10	0.25	33.54	69.8	48
7	6	1416	50	113	265	5.66	1.37	5.2	10.86	0.24	34.64	66.47	52.12

Table: 7 Engine performance with 25% esterified oil and 75% diesel at an injection pressure of 200bar

S.No	Load (Kg)	Speed (rpm)	Fuel Consumption (mf),Kg/hr		Exhaust Gas Temp.(°C)	B.P (kw)	F.C (kg/hr)	F.P (kw)	I.P (kw)	S.F.C (kg/kw-hr)	B.T.E (%)	I.T.E (%)	M.E (%)
			X(cc)	T(Sec)									
1	0	1500	30	176	110	0	0.54	4.5	4.5	∞	0	73.17	0
2	1	1493	30	141	130	0.99	0.67	4.5	5.49	0.68	12.97	71.94	18.03
3	2	1486	30	114	155	1.98	0.82	4.5	6.48	0.41	21.20	69.39	30.55
4	3	1474	30	99	175	2.94	0.95	4.5	7.45	0.31	27.26	68.86	39.59
5	4	1464	50	140	195	3.9	1.12	4.5	8.4	0.29	30.57	65.85	46.43
6	5	1451	50	123	215	4.84	1.27	4.5	9.34	0.26	33.46	64.57	51.82
7	6	1427	50	107	255	5.71	1.46	4.5	10.21	0.25	34.34	61.40	55.92

Gas Analyser Readings					Smokometer Readings	
Co (%)	HC(ppm)	Nox(ppm)	Co2 (%)	O2 (%)	Opacity(N)	K
0.048	10	169	3.12	16.46	0.4	0.01
0.045	13	307	3.72	15.37	0.7	0.01
0.039	17	616	5.20	13.63	1.6	0.02
0.037	19	710	5.68	12.96	3.4	0.05
0.035	13	897	6.49	11.78	6.8	0.17
0.041	13	951	8.16	10.5	10.5	0.25
0.069	33	1492	9.83	7.05	19.5	0.48

Table: 8 Engine performance with 50% esterified oil and 50% diesel at an injection pressure of 200bar

S.No	Load (Kg)	Speed (rpm)	Fuel Consumption (mf),Kg/hr		Exhaust Gas Temp.(°C)	B.P (kw)	F.C (kg/hr)	F.P (kw)	I.P (kw)	S.F.C (kg/kw-hr)	B.T.E (%)	I.T.E (%)	M.E (%)
			X(cc)	T(Sec)									
1	0	1500	30	191	90	0	0.5	4.1	4.1	∞	0	73.98	0
2	1	1496	30	141	140	0.99	0.67	4.1	5.09	0.68	13.33	68.54	19.45
3	2	1488	30	112	165	1.98	0.85	4.1	6.08	0.43	21.02	64.54	32.56
4	3	1478	30	94	185	2.96	1.01	4.1	7.06	0.34	26.44	63.07	41.92
5	4	1464	50	139	205	3.91	1.15	4.1	8.01	0.29	30.67	62.84	48.81
6	5	1451	50	120	230	4.84	1.32	4.1	8.94	0.28	33.08	61.11	54.14
7	6	1434	50	102	265	5.74	1.55	4.1	9.84	0.27	33.41	57.28	58.33

Gas Analyser Readings					Smokometer Readings	
Co (%)	HC(ppm)	Nox(ppm)	Co2 (%)	O2 (%)	Opacity(N)	K
0.043	10	97	2.61	17.28	0.8	0.02
0.038	11	344	4.17	15.11	1.2	0.03
0.037	12	518	4.9	14.01	1.4	0.03
0.033	13	778	5.91	12.67	2.5	0.05
0.031	15	1002	6.85	11.37	3.3	0.10
0.028	15	1142	8.09	9.56	9.6	0.25
0.061	23	1323	9.22	7.24	23.5	0.72

Table: 9 Engine performance with 75% esterified oil and 25% diesel at an injection pressure of 200bar

S.No	Load (Kg)	Speed (rpm)	Fuel Consumption (mf),Kg/hr		Exhaust Gas Temp.(°C)	B.P (kw)	F.C (kg/hr)	F.P (kw)	I.P (kw)	S.F.C (kg/kw-hr)	B.T.E (%)	I.T.E (%)	M.E (%)
			X(cc)	T(Sec)									
1	0	1500	30	210	85	0	0.46	3.2	3.2	∞	0	65.9	0
2	1	1499	30	151	120	.99	0.64	3.2	4.2	0.64	14.83	62.17	23.81
3	2	1494	30	121	155	1.99	0.8	3.2	5.19	0.4	23.57	61.46	38.34
4	3	1474	30	104	180	2.95	0.93	3.2	6.15	0.32	30.06	62.84	47.97
5	4	1466	50	141	200	3.91	1.15	3.2	7.11	0.29	32.21	58.57	54.99
6	5	1452	50	121	225	4.84	1.34	3.2	8.04	0.28	34.22	56.84	60.19
7	6	1434	50	102	250	5.74	1.59	3.2	8.94	0.27	34.30	53.27	64.21

Gas Analyser Readings					Smokometer Readings	
Co (%)	HC(ppm)	Nox(ppm)	Co2 (%)	O2 (%)	Opacity(N)	K
0.041	8	90	2.26	17.75	0.4	0.01
0.040	9	270	3.73	16.14	1.1	0.03
0.038	11	520	4.84	14.38	1.3	0.04
0.031	11	819	6.04	12.42	2.3	0.07
0.028	10	983	6.86	11.47	3.1	0.09
0.02	8	1036	7.86	10.61	8.9	0.23
0.058	19	1332	9.39	8.15	16.1	0.38

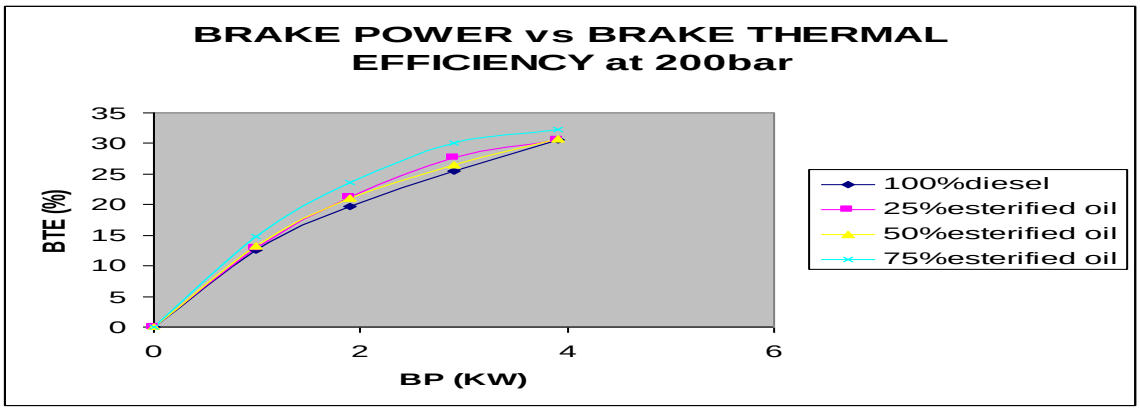
BRAKE POWER vs BRAKE THERMAL EFFICIENCY at 200bar
BTE (%)
35
30
25
20
15
10
5
0
0
2
4
6
BP (KW)
100%diesel
25%esterified oil
50%esterified oil
75%esterified oil

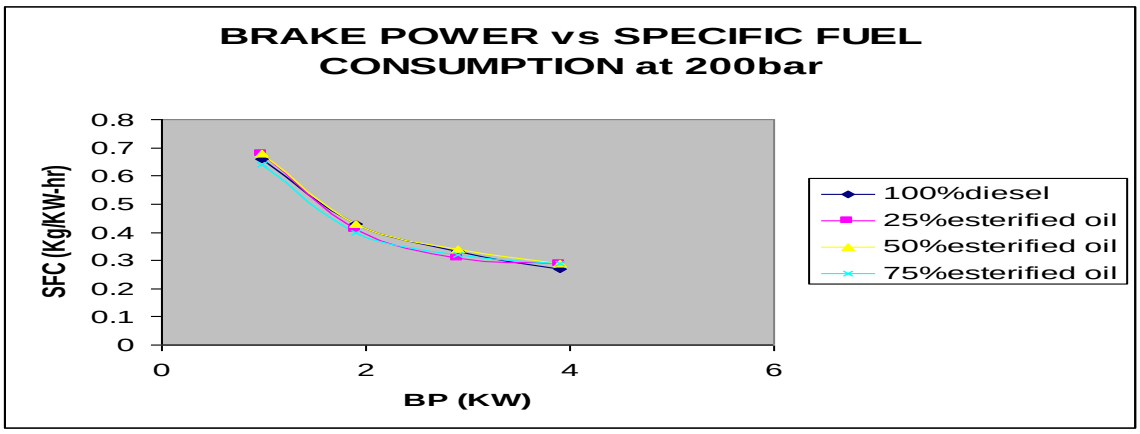
BRAKE POWER vs SPECIFIC FUEL CONSUMPTION at 200bar
SFC (Kg/KW-hr)
0.8
0.7
0.6
0.5
0.4
0.3
0.2
0.1
0
0
2
4
6
BP (KW)
100%diesel
25%esterified oil
50%esterified oil
75%esterified oil

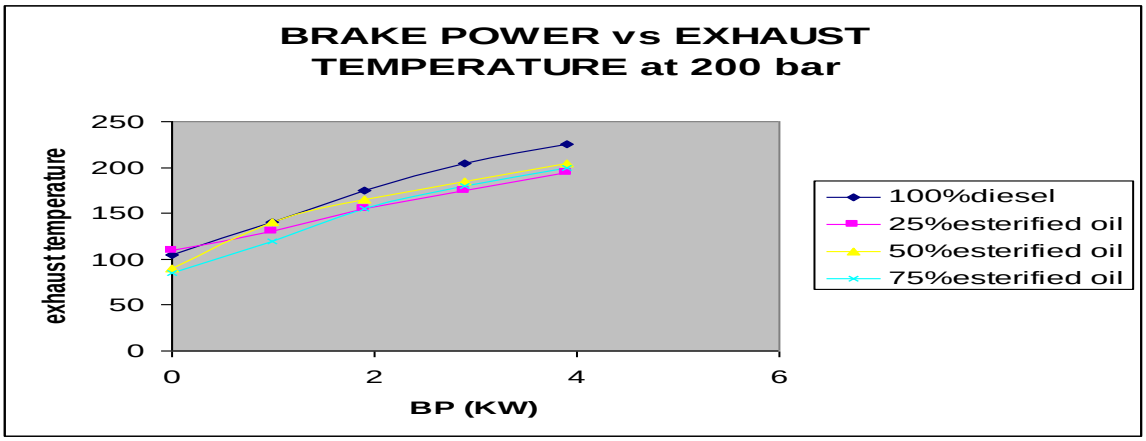
BRAKE POWER vs EXHAUST TEMPERATURE at 200 bar
exhaust temperature
250
200
150
100
50
0
0
2
4
6
BP (KW)
100%diesel
25%esterified oil
50%esterified oil
75%esterified oil

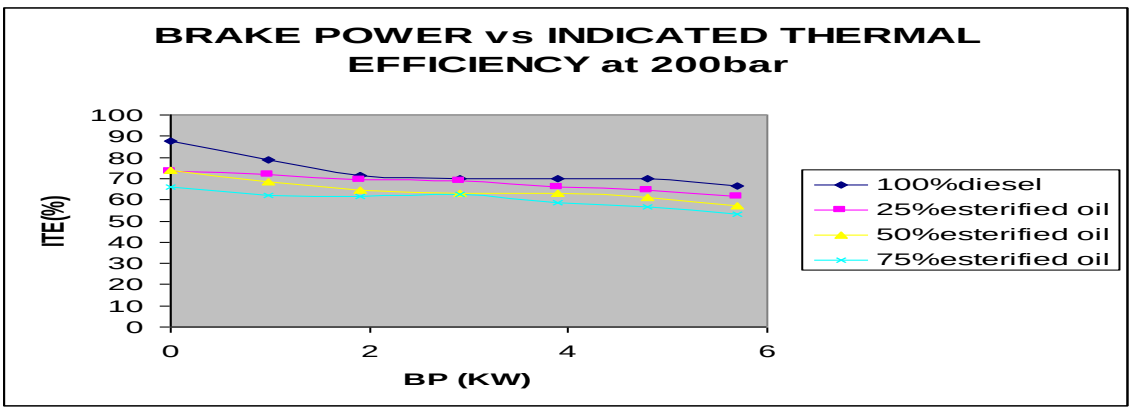
BRAKE POWER vs INDICATED THERMAL EFFICIENCY at 200bar
ITE(%)
100
90
80
70
60
50
40
30
20
10
0
0
2
4
6
BP (KW)
100%diesel
25%esterified oil
50%esterified oil
75%esterified oil

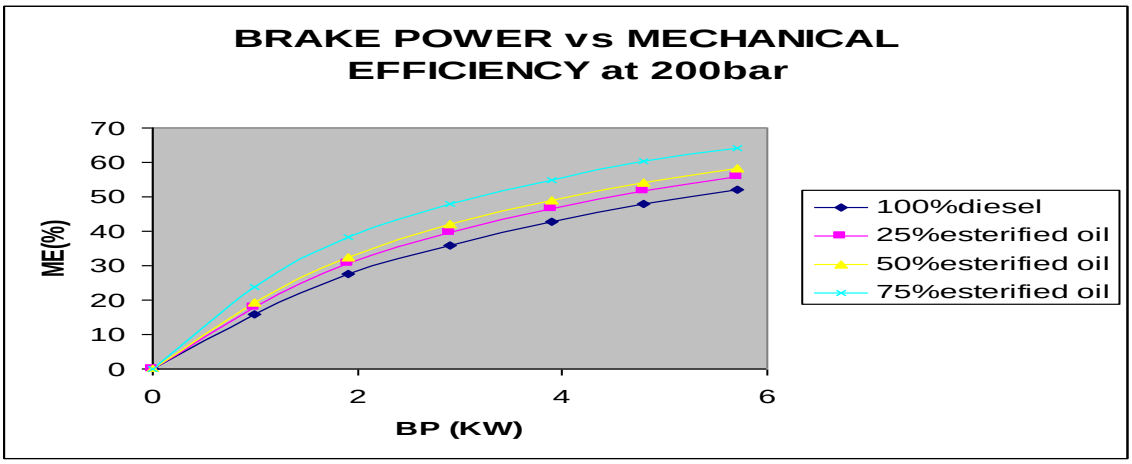
BRAKE POWER vs MECHANICAL EFFICIENCY at 200bar
ME(%)
70
60
50
40
30
20
10
0
0
2
4
6
BP (KW)
100%diesel
25%esterified oil
50%esterified oil
75%esterified oil

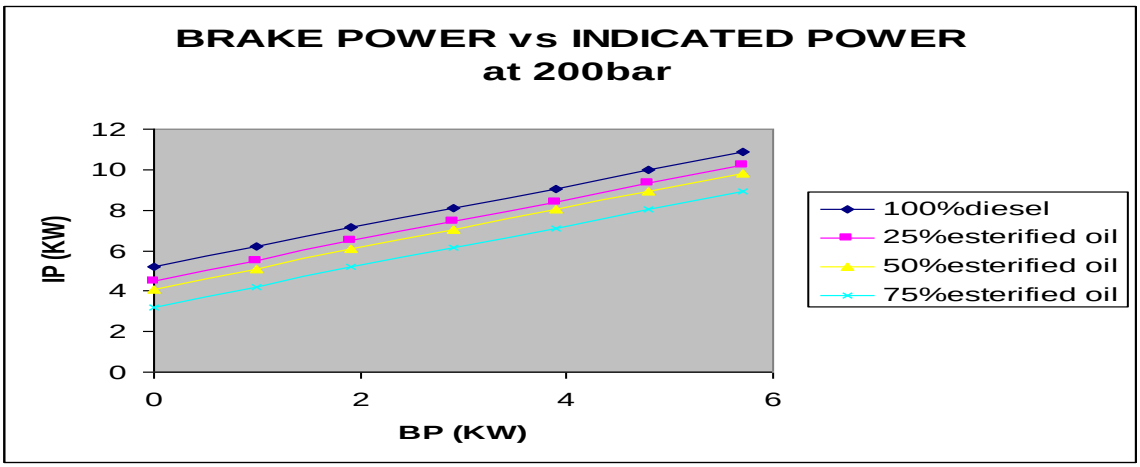
BRAKE POWER vs INDICATED POWER at 200bar
IP (KW)
12
10
8
6
4
2
0
0
2
4
6
BP (KW)
100%diesel
25%esterified oil
50%esterified oil
75%esterified oil

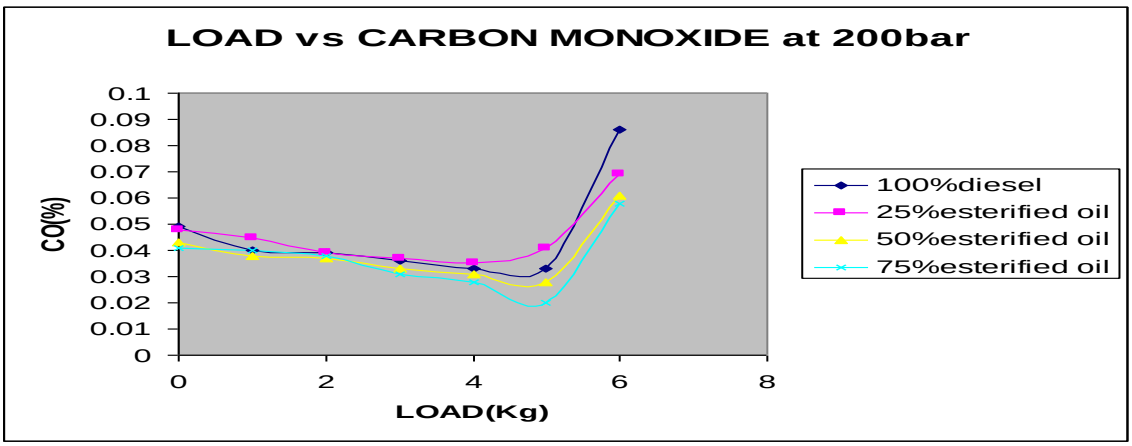
LOAD vs CARBON MONOXIDE at 200bar
CO(%)
0.1
0.09
0.08
0.07
0.06
0.05
0.04
0.03
0.02
0.01
0
0
2
4
6
8
LOAD(Kg)
100%diesel
25%esterified oil
50%esterified oil
75%esterified oil

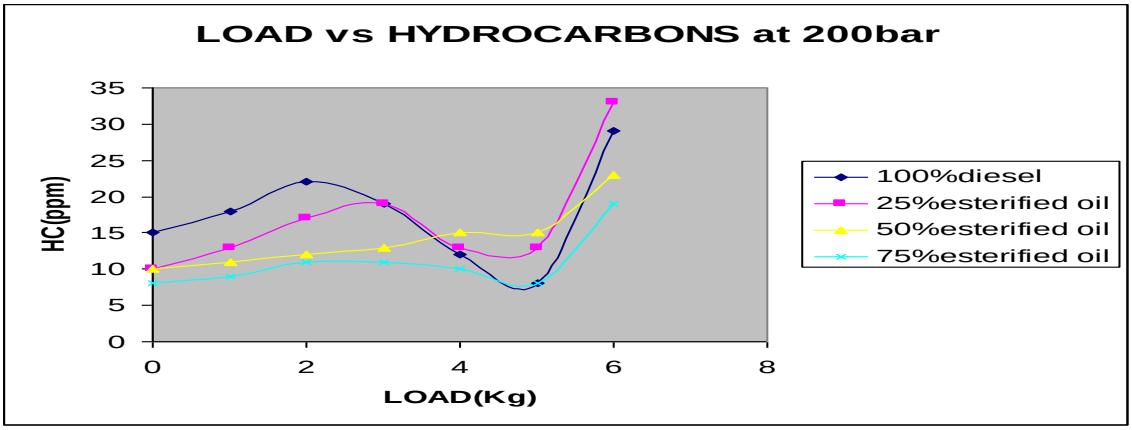
LOAD vs HYDROCARBONS at 200bar
HC(ppm)
35
30
25
20
15
10
5
0
0
2
4
6
8
LOAD(Kg)
100%diesel
25%esterified oil
50%esterified oil
75%esterified oil

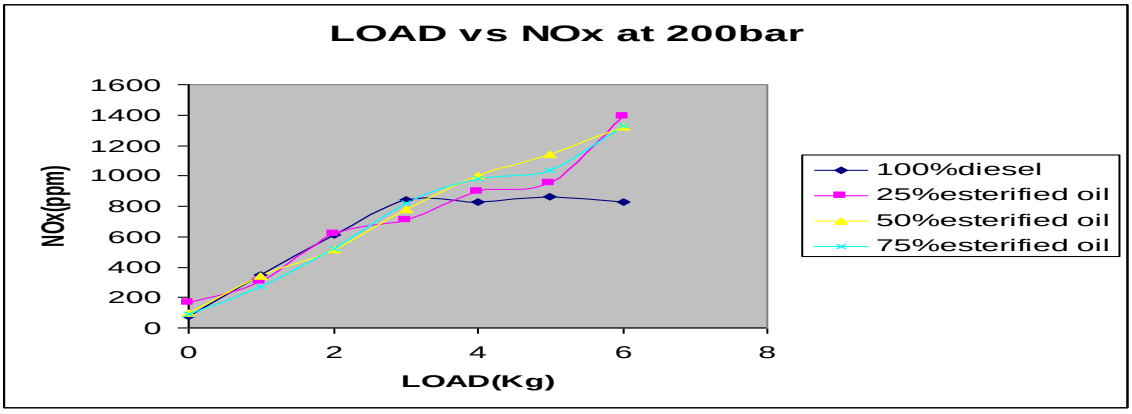
LOAD vs NOx at 200bar
NOx(ppm)
1600
1400
1200
1000
800
600
400
200
0
0
2
4
6
8
LOAD(Kg)
100%diesel
25%esterified oil
50%esterified oil
75%esterified oil

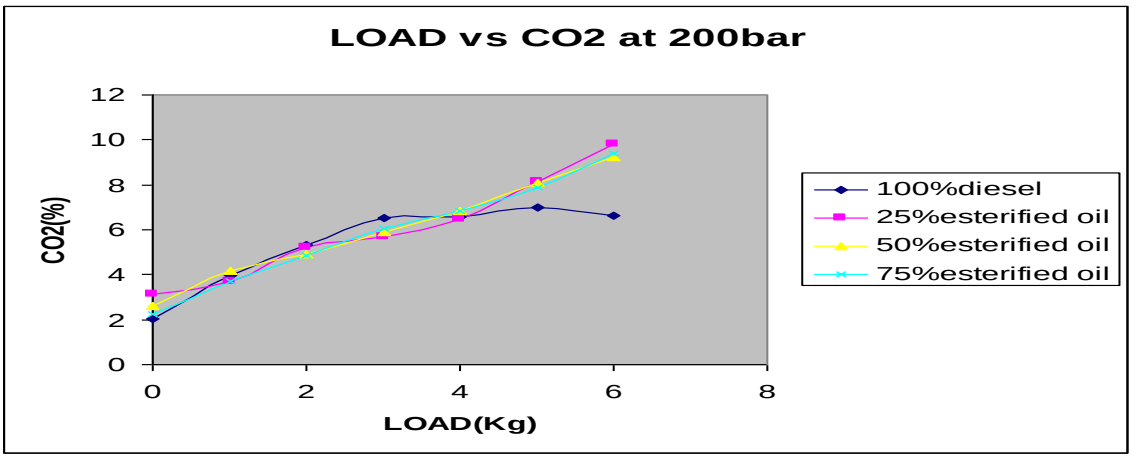
LOAD vs CO2 at 200bar
CO2(%)
12
10
8
6
4
2
0
0
2
4
6
8
LOAD(Kg)
100%diesel
25%esterified oil
50%esterified oil
75%esterified oil

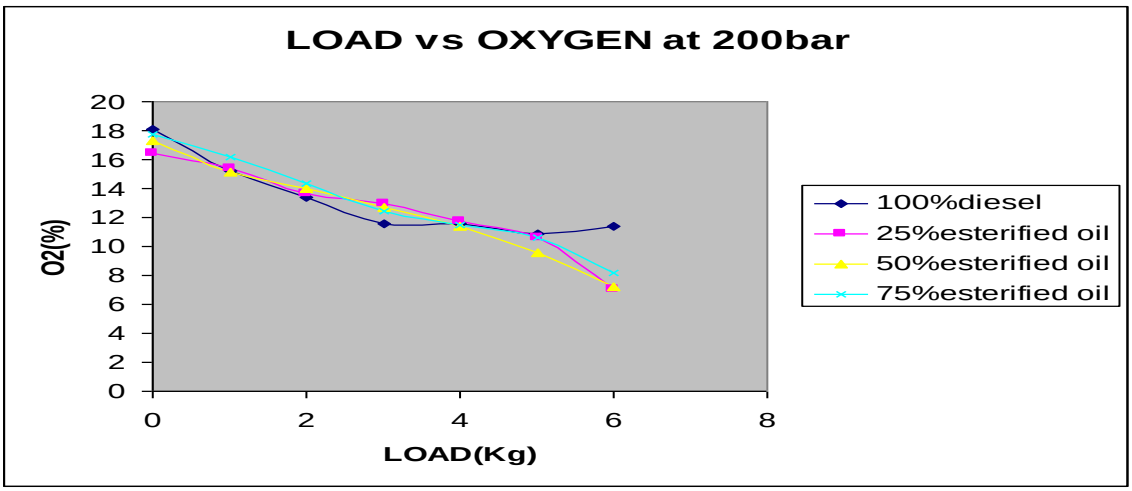
LOAD vs OXYGEN at 200bar
O2(%)
20
18
16
14
12
10
8
6
4
2
0
0
2
4
6
8
LOAD(Kg)
100%diesel
25%esterified oil
50%esterified oil
75%esterified oil

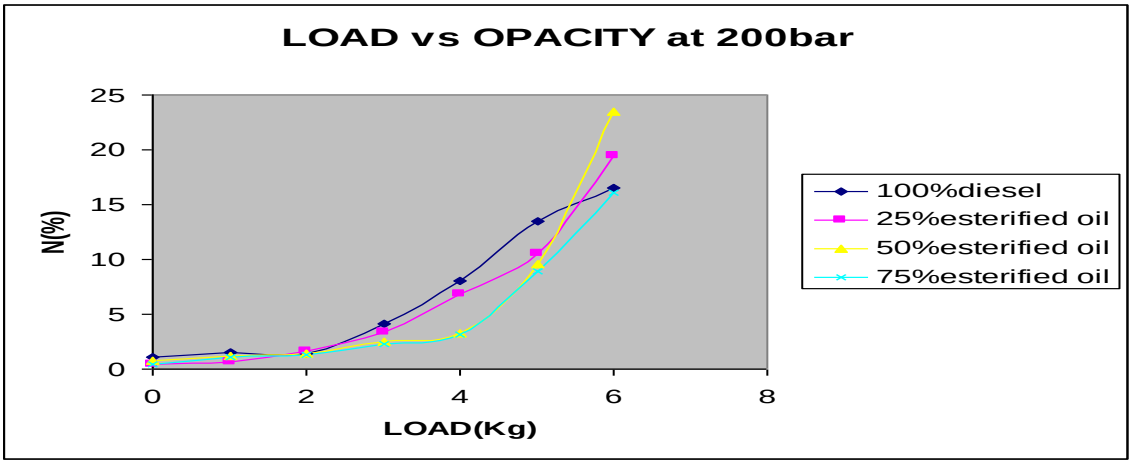

XIII. CONCLUSIONS

- 800-850ml of esterified mahua oil is extracted from 1000ml of mahua oil during esterification.
- Percentage increase in esterified mahua oil increases the viscosity of diesel.
- Increase in percentage of mahua oil increases the cetane number of the blend.
- Smooth running of engine is observed with esterified mahua oil compared with that of diesel.
- Slight increase in brake thermal efficiency and decrease in specific fuel consumption is observed in the case of esterified mahua oil (all blends especially 75% mahua oil) compared to that of diesel.
- Particulate matter is some what less in the case of esterified mahua oil than that of diesel which is observed by keeping a tissue paper at the outlet of the exhaust pipe.
- Among the injection pressures tested 200bar is the optimum pressure for esterified mahua oil.
- Observing the particulate matter esterified mahua oil is an eco-friendly fuel.

SCOPE FOR FUTURE WORK:

- Attempts are to be made to extract more pure esterified oil during esterification.
- Attempts are to be made to extract pure bio diesel of esterified mahua oil by using distillation process.
- Increase in production of mahua oil reduces the cost of fuel.

BIBLIOGRAPHY

[1] **IC ENGINES** by V.Ganesan
[2] **IC ENGINES** by Domukundwar
[3] **Mahua oil** (Madhuaca Indica seed oil) **methyl ester as biodiesel preparation** by Sukumar Puhan, N.Vedaraman, G.Sankarnarayanan and K.Jayachandran
[4] **Biodiesel production from vegetable oils via catalytic and non catalytic supercritical methanol transesterfifcation methods** by Ayhan Demirbas
[5] **www.elsevier.com**

American Journal of Engineering Research (AJER)
e-ISSN : 2320-0847 p-ISSN : 2320-0936
Volume-02, Issue-10, pp-48-51
www.ajer.org

Research Paper Open Access

Emotional and Spiritual Intelligence as Predictors of Eco Friendly Behavior of Undergraduate

Dr. Indira Sharma,
Associate Professor, Faculty of Education, DEI Deemed University, Dayalbagh, Agra.

Abstract: - The increase interference of human beings with Environmental processes has created environmental crisis. To check and make aware to this problem and to develop environmentally responsible behavior, environmental education is made compulsory subject. The present scenario is quite unsatisfactory as environment is deteriorating further. An effort is made to know the role of emotional and spiritual intelligence on eco-friendly behavior of undergraduate student. The co relational research design was used to conduct study. Random sampling technique was used to select 300 student of 1st year of graduation from 3 degree college of Agra city, 150 male and 150 female. The result indicated that educational and spiritual intelligence are powerful predictor of eco-friendly behavior of undergraduates and both variables accounted for 55% variance in their eco-friendly behavior.

I. INTRODUCTION

Nature is so fascinating and embodies the spirit of its creator. The nature has very intelligently evolved the human species on earth to provide protection to the entire spectrum of the existing natural resources. The great protector of the earth has today became potential predator of the entire natural environment and a prime decimator of the wild life resources. Rapid industrialization, voracious appetite, men's greed and unlimited exploitation has left us with polluted rivers, contaminated soil, depleted forest and wild life and exhausted natural resources.

One fact we must bear in mind is that the survival of man depend upon how judiciously has he manage the earth and maintains the quality of overall environment. In 1972, the leader of the international community met at Stockholm and expressed grave concern over the readily deteriorating environment. A number of well international declarations were made. Various institutions both at the national and international levels were set up. Since Stockholm to Copenhagen number of conference, summit & meets have been held all over the world and millions of dollars spent. From 1975 every nation is imparting environmental education and in India from academic session 2004-05 it has been made a compulsory subject at each level of education.

From the above facts, pertinent and fundamental question arise, why in spite of such efforts Stockholm (1972) to world summit of Copenhagen (2009), the world environment has deteriorated further and ecological imbalance intensified. This may be because thinking and actions of contemporary societies are being shaped by mechanical view of nature and thus little realization and sensitization that life and nature are inseparable parts of a cosmic web. So the need of today is to channelize the thought system of individuals, making him sensitive toward the nature and transforming their behavior consumerism to environment friendly. Some degree of emotional self awareness and empathy is an important foundation for successfully start our spiritual growth. Emotional intelligence makes us sensitive towards a thing or human being and to deal with own emotions and others effectively and appropriately. While spiritual intelligence leads to that state of mind in which we think the "Welfare of all". Thus an effort is made to know whether these two intelligence have any role in making our behavior eco-friendly.

II. OBJECTIVES

1. To study emotional intelligence of undergraduate students.
2. To study spiritual intelligence of undergraduate students.
3. To study eco friendly behavior of undergraduate students.
4. To ascertains the Zero order relationship between criterion and dependent variable.

5. To study the relative contributory role of criterion variable in determining the eco friendly behavior.

Hypothesis

1. There is no significant difference between the emotional intelligence of male & female undergraduate students.
2. Male and female undergraduate student do not differ in their spiritual intelligence.
3. No significant difference exists among eco friendly behavior of male and female undergraduate students.
4. No significant relationship exists among criterion and predictive variable.
5. Criterion variables do not play any role in determining the eco friendly behavior of students.

Variable

Independent variable – emotional & spiritual intelligence
Dependent variable – Eco friendly behavior

Method

The study involves correlation method.

Sample

Study is conducted on 300 students of undergraduates (Studying in 1st year of graduation) of both the sex (150 male and 150 female) from 3 colleges of Agra city affiliated with B.R. Ambedkar university by random sampling method.

Tools – The following tools are used for the collection of data.

1. Mangal emotional intelligence inventory by Mangal & Mangal.
2. Spiritual intelligence scale – self constructed.
3. Environmental friendly behavior measure – self constructed.

Statistical Techniques –

To analyses the data according to objective of study. Mean, S.D. C.R., product moment correlation and regression analyses are used.

Result & discussions – Objective I - Study of Emotional intelligence of undergraduates

Table 1 Statistical Preview of emotional intelligence scores of undergraduates

Sex / Statistics	Male	Female	Total
Mean	58.17	59.82	58.99
S.D.	38.57	38.72	38.62
C.R.	1.369		

The mean value (58.99) for total group indicates that undergraduate students have average level of emotional intelligence showing less ability of youth to cope with their emotions. The male and female undergraduates do not differ in their emotional intelligence as confirmed by statistically insignificant value of C.R. even at .05 level thus Null hypotheses is accepted.

Objective II - Study of spiritual intelligence of undergraduate students

Table – 2 Mean, S.D., C.R. of spiritual intelligence score of undergraduates

Sex / Statistics	Male N(150)	Female N (150)	Total N- 300
Mean	116.75	120.42	118.58
S.D.	24.12	26.74	25.06
C.R.	.917		

The perusal of above table reveals that undergraduate students have average level of spiritual intelligence as shown by mean (118.58), to some extent satisfactory as today's materialistic world our youth still have spiritual nature. Great variation is observed in spiritual intelligence score as shown by high value of standard deviation. The Male and female students do not differ in their spiritual intelligence inferred by value of C.R. 917 which is not significant even at .05 levels of confidence, thus for this objective also Null hypothesis is

accepted. This is quite surprising that boys also have faith in some supreme power and neglecting the common concept that females are more spiritualities than males.

Objective III - Study of eco friendly behavior of undergraduates

Table – 3 Statistical preview of eco friendly behavior score of undergraduates

Statistics / Sex	Mean	S.D.	C.R
Male	54.17	36.41	.466
Female	56.98	37.19	
Total group	55.57	36.12	

The perusal of mean values shown in table indicates that undergraduate students do not have favorable behavior towards environment as the obtained mean score of eco friendly is quite lower in comparison to the maximum scores of eco friendly behavior scale i.e. 120. This picture is quite unsatisfactory and compelled us to find the answer, why in spite of imparting compulsory environmental education in school and colleges, we are fail to develop eco friendly behavior among our students. The same results were found by study conducted by Japan science and technology agency in university of Tokyo on topic 'change, in environmental consciousness and behavior led by information concluded that environmental consciousness has been increasing in Japan, where as environmental friendly behavior has not. This may be the reason that our environmental education is imparting environmental awareness and knowledge among students but not channelizing our behavior toward beneficiary to environment.

The value of C.R. (.466) which is lower than the calculated table value even at .05 level of significance is revealing the fact that male and female undergraduate students do not differ in their eco friendly behavior and thus null hypothesis framed for this objective is accepted.

Objective IV- Zero order Correlation among predictive & criterion variable

Table – 4 Showing inter correlation among variable

Variable	(coefficient of correlation (r)		
	X1	X2	X3
X1 (eco friendly behavior)	-	.55	.68
X2 Emotional intelligence	.55	-	.41
X3 Spiritual intelligence	.68	.41	-

The values of coefficient of correlation shown in table between eco friendly behavior (X1) and scores of emotional intelligence (X2) and spiritual intelligence (X3) are .55 and .68 respectively which are positive and significant, thus indicating the high and positive relationship between criterion and predictive variable.

Objective V - Relative Contributory Role Of Predictive Variable On Criterion Variable

To determine the relative contributory role of each predictive variable in determination of eco friendly behavior of undergraduate students, multiple regression analysis is carried out. With the help of Zero order correlation matrix, value of Beta coefficient (B) regression coefficients (b), coefficient of multiple correlation (R), coefficient of multiple determination are computed.

Table – 5 Showing multiple correlation, Regression coefficient & common variable

Variable	r	R	R2	B	BXr	(b)
Emotional intelligence & Eco friendly behavior (X2)	.55		.5314	.372	.2156	.366
Spiritual Intelligence and eco friendly behavior (X3)	.68	.729	Variance 53.14%	.465	.3162	.670
Regression equation – X1 = .366 X2+ .670 X3 + K						

The values of positive regression weights shown in table confirming the effect of both predictive variables on eco friendly behavior of undergraduates. The value of R2 .5314 is the indicative of the fact that 53.14% variance in eco friendly behavior of undergraduates could be accounted by the cognitive predictive variables i.e. emotional and spiritual intelligence. The separate variance of emotional intelligence and spiritual intelligence for eco friendly behavior is 21.56% and 31.62% respectively and thus indicating, spiritual intelligence as more powerful predictor for development of eco friendly behavior that emotional intelligence.

III. CONCLUSION

On the basis of above analysis and discussion it can be inferred that Emotional and spiritual intelligence are powerful predicator of eco friendly behavior and accounted for 53.14% variance in eco friendly behavior of students, if we want to save our planet earth than we have to reconstruct our present environmental education curriculum and some activities should be added to utilize and enhance both the intelligence. Human beings are rational creatures who have an innate need to rationalize all their actions and thoughts. Spirituality provides the rationale and make them sensitive towards other beings and nature, make able to realize that man is not the owner but the steward or trustee of God's creation, and thus by the use of both intelligence we can develop sensitiveness towards nature and morality can be sprouted in student and by that we can save our planet earth.

REFERENCES

[1] 2008, Adegems, D.B. (2008), Emotional intelligence, religiosity & self efficacy as predictors of psychological well being among secondary school adolescent in Ogbomosho, Nigeria Ibadan.
[2] 2009,Bara Stewart, Factors influencing environmental attitude and behavior, U.K. Environment and behavior, vol. 39 No. 4, Pg, 435- 473
[3] 2006, Gihar sandya, sakina. M.G. level of awareness of environmental pollution among rural and urban women and its educational implications ,Experiment in education, Chennai, No. 4 page 25 –27
[4] 2008, Kalantari K, Femi A, Mohammad H.M. Investigating factors affecting environmental behavior of urban residents, American journal of environmental science.
[5] 2007, Padiyals and Godiyas S. environmental awareness among university students a case study of undergraduate student of Uttarakhand. Experiment in education, Chennai, vol. 35 No. 4, page 5-11
[6] 2008,Singh tirath, Arjindev and kaur B, Development of spiritual intelligence scale, psycho lingua research journal of cognitive information and communication process, vol. 38, No. 2
[7] http.//en.wikipedia.org/wiki/spiritual

American Journal of Engineering Research (AJER)
e-ISSN : 2320-0847 p-ISSN : 2320-0936
Volume-02, Issue-10, pp-52-62
www.ajer.org

Research Paper Open Access

Medical image processing using a service oriented Architecture and Distributed Environment

Himadri Nath Moulick[1], Moumita Ghosh[2]
[1]*CSE, Aryabhatta Institute of Engg & Management, Durgapur, PIN-713148, India*
[2]*CSE,University Institute Of Technology,(The University Of Burdwan) Pin -712104,India*

Abstract: **-** The aim of this paper is to present a services based architecture for medical image processing in assisted diagnosis. Service oriented architecture (SOA) improves the reusability and maintainability of distributed systems. In service oriented architectures, the most important element is the service, a resource provided to remote clients via a service contract. We propose a generic model for a service, based on a loosely coupled, message-based communication model. Our service model takes into account the possibility to integrate legacy applications. Specialized image processing services can be dynamically discovered and integrated into client applications or other services. Complex systems can be created with the help of some SOA concepts like Enterprise Service Bus (ESB). DIPE is a distributed environment that provides image processing services over integrated teleradiology services networks. DIPE integrates existing and new image processing software and employs sophisticated execution scheduling mechanisms for the efficient management of computational resources within a distributed environment. It can also be extended to provide various added-value services, such as management and retrieval of image processing software modules, as well as advanced charging procedures based on quality of service. DIPE can be viewed as the natural evolution of the legacy field of medical image processing towards a service over the emergent health care telematics networks.

Keywords: **-** *service oriented architecture, image processing, web service.*

I. INTRODUCTION

In service oriented systems, operational entities are distributed across the network in order to improve availability, performance and scalability. These entities are called *services.* The service provides access to its functionality. The whole system is viewed as a set of interactions among these services. SOA promotes the reuse of services. The system evolves through the addition of new services. SOA is not tied to a specific technology. It can be implemented using a large variety of technologies, programming languages and communication protocols. Interactions between services and clients in SOA are based on a very dynamic model [1]. A service can be discovered at runtime, can be replaced if has become unavailable or can be used to create a new service (and a new functionality). With these characteristics, SOA offers a powerful support for adaptability. The adaptability can take many forms, depending on the terminal capabilities, the network connection, etc. Microsoft has proposed a SOA based platform for healthcare [2]. Healthcare is an extremely fluid industry. Each change requires an adaptation of systems. Point-topoint integration becomes costly and complex to maintain for healthcare providers and consumers. The benefit of SOA to the healthcare industry is that it enables systems to communicate using a common framework, integration of new elements becomes less complex and the system can be adapted more rapidly. In recent years, advances in information technology and telecommunications have acted as catalysts for significant developments in the sector of health care. These technological advances have had a particularly strong impact in the field of medical imaging, where film radiographic techniques are gradually being replaced by digital imaging techniques, and this has provided an impetus to the development of integrated hospital information systems and integrated teleradiology services networks which support the digital transmission, storage, retrieval, analysis, and interpretation of distributed multimedia patient records [1]. One of the many added-value services that can be provided over an integrated teleradiology services network is access to high-performance computing facilities in order to execute computationally intensive image analysis and visualisation tasks [2]. In general, currently available products in the field of image processing (IP) meet only

specific needs of different end user groups. They either aim to provide a comprehensive pool of ready to use software within a user-friendly and application specific interface for those users that use IP software, or aim for the specialised IP researcher and developer, offering programmer‟ s libraries and visual language tools. However, we currently lack the common framework that will integrate all prior efforts and developments in the field and at the same time provide added-value features that support and in essence realise what we call a „service‟ . In the case of image processing, these features include: computational resource management and intelligent execution scheduling; intelligent and customisable mechanisms for the description, management, and retrieval of image processing software modules; mechanisms for the "plug-and-play" integration of already existing heterogeneous software modules; easy access and user transparency in terms of software, hardware, and network technologies; sophisticated charging mechanisms based on quality of service; and, methods for the integration with other services available within an integrated health telematics network. In this paper we present the architecture of DIPE, a novel distributed environment for image processing services. DIPE is based on a distributed, autonomous, co-operating agent architecture [3]. It is designed so that it is modular, scaleable and extensible, and it can be readily implemented on different hardware and software platforms, and over heterogeneous networks. DIPE consists of a functional core which supports the persistent distributed execution of IP algorithms, and can be extended to support other added-value services such as macros, resource management, algorithm retrieval, charging, etc. Here we describe the functional core of the system and discuss the mechanisms and notions employed to allow integration of third party IP algorithms and the development of new IP software. Finally, we describe the functional extensions of the core that support macro execution and resource management. DIPE has been developed to support distributed medical imaging processing, an added-value teleradiology service within the integrated regional health telematics network, currently under development by the Institute of Computer Science (ICS), Foundation for Research and Technology - Hellas (FORTH), on the island of Crete [4].

II. SOA BACKGROUND

The term Service Oriented Architecture, SOA for short, contains some important notions. We have the following definitions for these notions [3]: An **Architecture** is a formal description of a system, defining its purpose, functions, externally visible properties, and interfaces. It also includes the description of the system's internal components and their relationships, along with the principles governing its design, operation, and evolution. A **service** is a software component that can be accessed via a network to provide functionality to a service requester.The term **service-oriented architecture** refers to a style of building reliable distributed systems that deliver functionality as services, with the additional emphasis on loose coupling between interacting services.

1.Service

The **service** is the core element in SOA. A **service** is defined as "a mechanism to enable access to one or more capabilities, where the access is provided using a prescribed interface and is exercised consistent with constraints and policies as specified by the service description" [4]. A service can have the following characteristics: A service provides a contract defined by one or more interfaces (just like a software component). This allows the change of the service implementation without reconstructing the client as long as the contract is not changed. Implementation details (programming languages, operating systems, etc) of the service are not the concern of the service requestor. A service can be used as stand-alone piece of functionality or it may be integrated in a higher-level service (composition). This promotes reusability. Legacy applications can be transformed in services by using some wrapper techniques. Services communicate with their clients by exchanging messages. Typically, the request/ response message pattern is used. From the client point of view, a synchronous or asynchronous communication mechanism can be implemented. In SOA model is not fixed a specific communication protocol. Many protocols can be used: HTTP, RMI, DCOM, CORBA, etc. Services can participate in a workflow (the term is *service choreography* in SOA terminology). A workflow is "the movement of information and/or tasks through a work process" [5] and it's based on a workflow engine. Services need to be discovered at design time and run time by clients. This mechanism is provided by a service directory (service registry). A service provider can publish (register) his service. Services communicate with other services and clients using standard, dependency-reducing, decoupled message-based methods such as XML document exchanges. This characteristic is called **loose coupling** This term implies that the interacting software components minimize their knowledge of each other: more information is achieved at the time is needed. For instance, after discovering a service, a client can retrieve its capabilities, its policies, its location, etc. The characteristics of **loose coupling** are [6] Flexibility: A service can be located on any server and relocated as necessary (with the condition to update its registry information) and clients will be able to find it. Scalability: Services can be added and removed depending on the needs. Replaceability: With the condition that the original interfaces are preserved, a new implementation of a service can be introduced, and outdated

implementations can be retired, without affecting the service clients. Fault tolerance: If a server, a software component, or a network segment fails, or the service becomes unavailable for any other reason, clients can query the registry for alternate services that offer the required functionality, and continue to work in the same way.

2. SOA Interaction cycle

In figure 1 is depicted the basic case of using a service with three components: a service provider, a service requester and a service directory (service registry). Some simple, bi-directional interactions (synchronous request/response pattern) are represented as an *interaction cycle* [7]. A real-world implementation can be more complex. A SOA architecture has three important elements:

2.1 Service directory

It acts as an intermediary between providers and requesters. Usually, services are grouped by categories.

2.2 Service provider

The Service Provider defines a service description and publishes it to the service directory.

2.3 Service requester

The service requester can use the search capabilities offered by the service directory to find service descriptions and their respective providers.

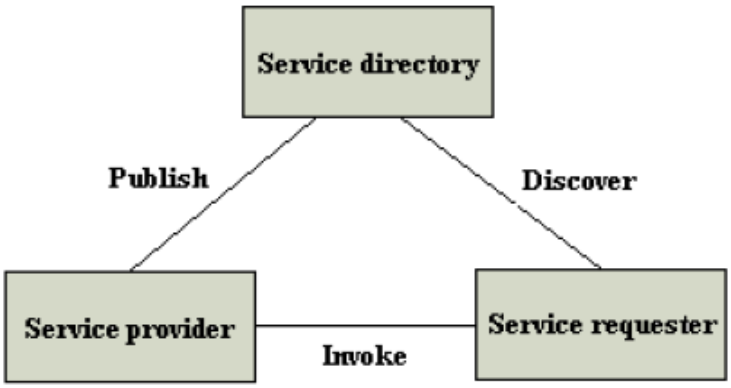

Fig 1. SOA interaction cycle

The service provider has to publish the service description in order to allow the requester to find it. Where it is published depends on the architecture. In the discovery the service requester retrieves a service description directly or queries the service registry for the type of service required. In this step the service requester invokes or initiates an interaction with the service at runtime using the binding details in the service description to locate, contact and invoke the service.

3. Enterprise Service Bus

The Enterprise Service Bus (ESB) is sometimes described as a *distributed infrastructure* [8] and it's a logical architectural component that provides an integration infrastructure consistent with the principles of SOA. Two different issues are being addressed: the *centralization of control*, and the *distribution of infrastructure* [9]. ESB and centralize control of configuration, such as the routing of service interactions, the naming of services, and so forth. ESB might deploy in a simple centralized infrastructure, or in a more sophisticated, distributed manner. ESB does not implement a service-oriented architecture (SOA) but provides the features with which one may be implemented. ESB is not mandatory in SOA but is usually used in large (enterprise) systems with many services. The ESB might be implemented as a distributed, heterogeneous infrastructure. Minimum ESB capabilities considered in IMB view [8, 9]:

3.1 Communications

Routing and addressing capabilities providing location transparency, administrations capabilities to control service addressing and at least one form of messaging (request/response, publish/subscribe, etc), support for at least one communication protocol (preferable a widely available protocols such HTTP).

3.2 Integration

Support for multiple means of integration to service providers, such as Java 2 Connectors, Web services, asynchronous messaging, adaptors, and so forth.

3.3 Service interactions
An open and implementation independent service messaging that should isolate application code from the specifics of routing services and transport protocols, and allow service implementations to be substituted.

III. MODEL FOR SOA-BASED IMAGE PROCESSING SYSTEMS

In this section we propose a model for implementing SOA-based system oriented to medical image processing. The model is generic enough to be used in other areas. The model contains a programming model, a service model and a messaging model.

1. Programming Model

The programming model, depicted in figure 2, is composed by four layers: the service layer, the component layer, the object layer and the technology layer.

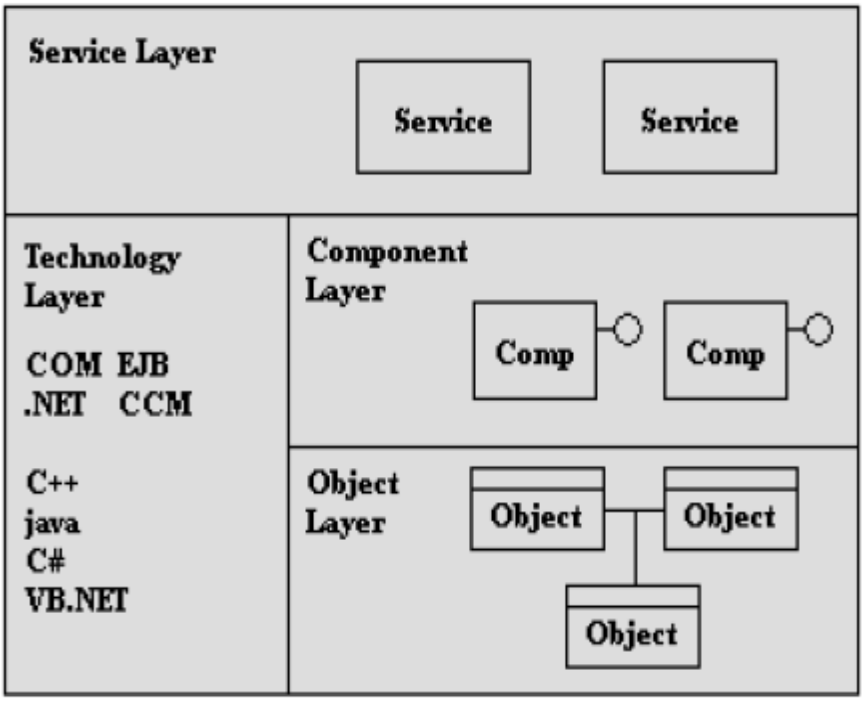

Fig 2. Programming model

Typically, a service is created using one or more components and a component is created using one or more objects. The service layer contains business services. A service is created with the help of the component oriented programming (COP). The component layer relies on software component technologies like: COM (component object model), EJB (Enterprise Java Beans), CCM (CORBA Component Model), OSGi (Open Services Gateway Initiative) or .NET Component Model. The software components can be of two types: functional components (business components) and non-functional components (like data access components, communication components or any other components). A component is implemented using object oriented techniques (the object layer). This layer is based on object oriented technologies (programming languages) like: C++, java, C#. Our model addresses the problem of integrating legacy applications (existent applications that are not servicebased). In order to integrate these applications, a wrapper pattern (adapter pattern) can be used. The wrapper can be applied in every layer. For instance, if the legacy application is object oriented but is not based on components, the wrapper should be applied in the component layer. If the legacy application is implemented in C, the wrapper should be applied in the object layer. This respect the proposed model: functionality is encapsulated in components, and components are created using objects.

2. Service Model

The service model is depicted in figure 3. It's composed from 3 layers: the interface layer, the business layer and the resource layer.

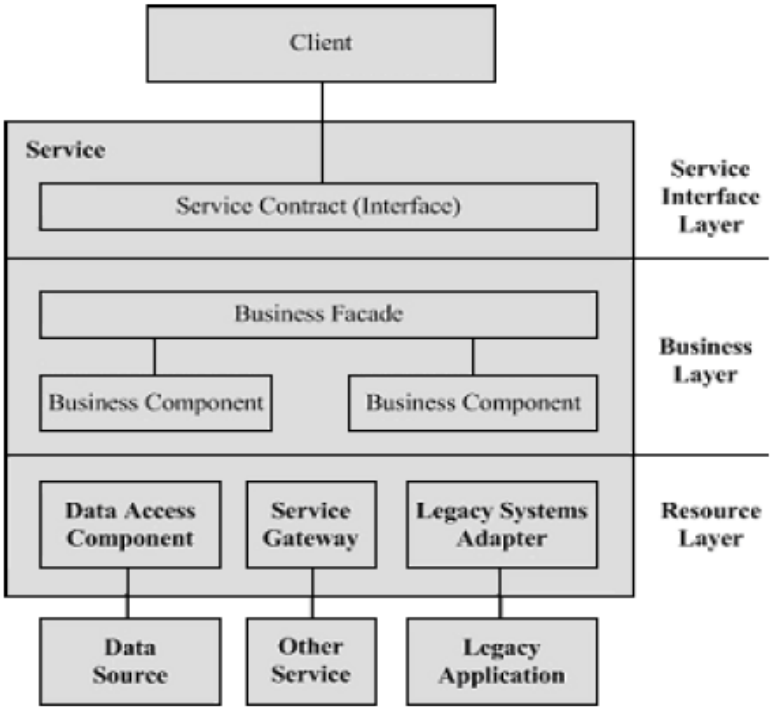

Fig 3. Service model

The Service Interface Layer contains the service contract (service interface) and it's detailed in the next section. The Business Layer contains a business façade and business components (sometimes called functional components). A business component performs (implements) operations described in the service contract. The business façade (façade pattern) is optional and it may be used in a complex architecture, with many business components. The resource layer contains different components (nonfunctional components) with the roll of interacting with external resources. In the figure are represented three of the most common types of resource access: a data access component for accessing database systems, a service gateway for accessing other services (in SOA a service can be a consumer for another service) and a wrapper (adapter) component for accessing legacy systems. The resource layer is not mandatory if the service does not use external resources. Accessing a legacy application was treated in section 3.1 from a programming point of view. The service model is extensible, new facilities like security, transactions or QoS capabilities can be introduced.

3. Messaging Model

Usually, a service communicates with its clients by sending and receiving well-defined messages. A proposed messaging model is presented in figure 4. A service interface is similar with an interface in object oriented programming. The service interface has the role to describe the service operations and the types of messages needed by those operations.

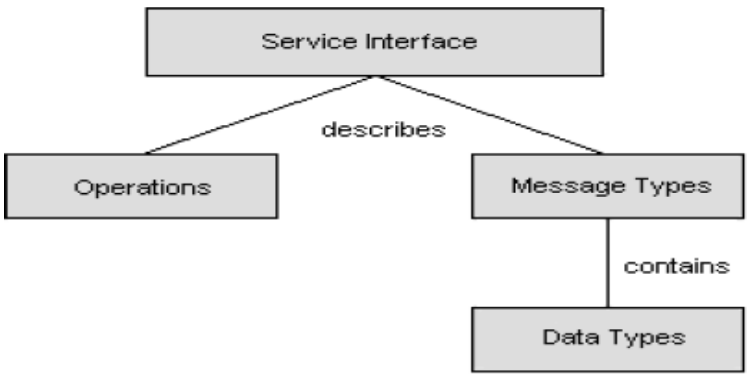

Fig 4. Messaging model

A message type contains one or many data types that can be translated in build-in or custom data types from a programming language. In many cases, marshalling techniques may be used to provide compatibility between server data types and client data types. Typically, this is the case when the client and the server are implemented using different technologies. For instance, an image processing service interface can describe a user defined data type (a class in object oriented programming) containing the image name, the image type, the image data (as a specific format), etc. If the service is implemented as a web service, the data types are encapsulated (serialized) in XML documents and send over network using SOAP. Messaging exchange patterns (MEP) can be used for accessing a service. The most common access pattern used is the request/response (also known as request/reply) pattern. In this case, the service consumer sends a request to the service and receives a response. This access pattern is used in the web services applications. The client can use a synchronous or asynchronous communication mechanism. The asynchronous mechanism is preferred when communication costs are high or the network is unpredictable. Another pattern that can be used is publish/subscribe. This pattern is based on the message queue paradigm. For instance, an image capture service allows to other services or clients to subscribe to it. When a new image is captured all subscribers receives the new image. The publish/subscribe pattern is typically used with an asynchronous communication mechanism.

IV. ARCHITECTURE AND IMPLEMENTATION

The core of the system consists of several communicating components: user applications, execution agents, pools of IP algorithms, and management agents. [20] The management agent is the central element. Its main purpose is to realise the network of individual modules (applications and execution agents) and initialise the communication among them. However, the main body of messages is communicated directly among the individual modules. The local cluster can be further expanded through a network of management agents, within the same or even different organisations. Thus, the management agent ensures the scaleability of the environment, a basic requirement of an integrated teleradiology services network [21]. Additionally, the management agent authenticates users and provides unique image ids by using standard digital signature technology.

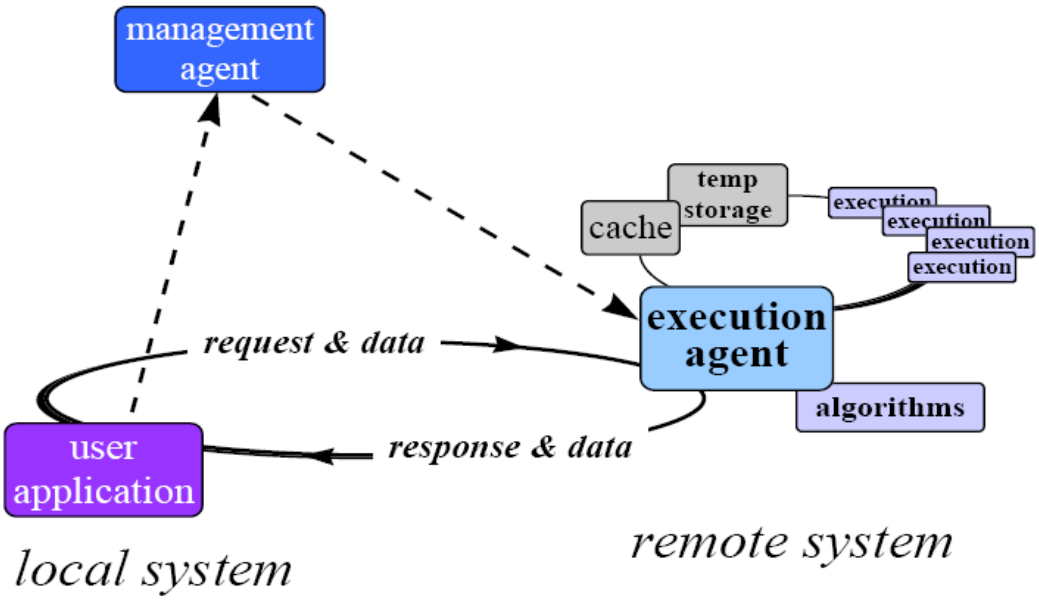

Fig 5 . Communication within a DIPE cluster

The execution agent is responsible for the execution of a specific algorithm. It receives requests for execution through the management agent and creates a communication link with the requesting application in order to receive further information and input data required for the execution (Figure 5). After this point, this agent can proceed autonomously to the execution of the algorithm. It stores input data into a local cache area and executes the requested algorithm. Output generated through the execution of the algorithm is sent back to the agent. The execution agent is responsible to forward this output to the requesting application. In case there is a network failure or the requesting application is not running any longer, the agent keeps the results of the execution in temporary storage for delivery upon request. This ensures persistent algorithm execution and enhances the robustness of the system. The user application is the front end of the system and consists primarily

of a customisable graphical user interface. A virtual temporary storage management module ensures that the application can handle synchronously a considerable number of large data sets. An important feature of the user application is that it incorporates certain image processing algorithms that require real-time response, and thus it is not sensible to redirect their execution to an agent or over the network. These include routines necessary for image visualisation (e.g., zoom, focus, resize, contrast adjustment, etc.), as well as certain algorithms for local, real-time image processing. Finally, the graphical user interface provides toolkits that support the various functionalities of the environment (algorithm insertion, monitoring of the system‟ s status, resource management, macro composition and execution, etc.). A typical screen of the application is shown in Figure 6 . The basic requirement that DIPE is readily implemented on various operating systems and over heterogeneous networks poses certain implementation constraints. Thus, inter-process communication is based on the TCP/IP network protocol, while operating system transparency is ensured by using ACE, an object-oriented network programming toolkit for developing communication software [5]. DIPE is now implemented on UNIX and Windows NT/95 workstations.

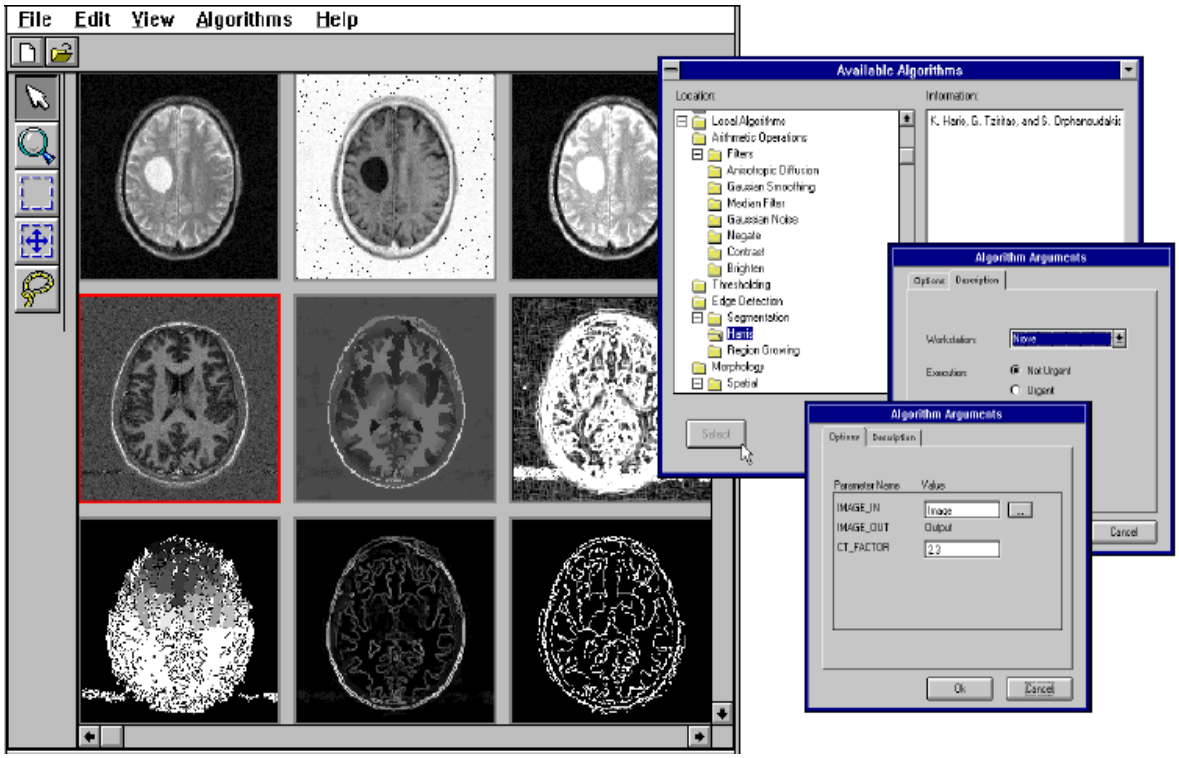

Fig 6. A typical screen of DIPE

1. The Algorithm Repository

The functional core of DIPE is the set of available image processing algorithms, private or public, local or network wide. An important feature of DIPE is that it allows easy integration of third party algorithms, i.e. software modules where only an executable is available and the only information known is the command line syntax, as well as the input and output data formats. The integration is achieved through the algorithm wrapper, a single generic process. The wrapper converts input data from the application format to the format that a specific IP algorithm requires, executes the algorithm and finally converts the output data of the algorithm to the format of the user application. While the algorithm is being executed, the wrapper is responsible to handle requests from the user application. Such requests include the termination or pause of the execution, or the resumption of a previously paused execution. Additionally, DIPE provides a library of ready-to-use routines for the development of new IP algorithms, which consists of basic routines related to the starting and ending phases of the algorithm, as well as of routines that support a more sophisticated mode of user-algorithm communication during execution. In routine medical image processing, a common situation involves processing images using the same set of algorithms often with a standard set of parameter values. DIPE provides the mechanisms to simplify the complicated process of executing individual algorithms sequentially, by grouping them together and thus creating a macro-algorithm (macro). In general, the DIPE macro is a set of individual algorithms that may be performed independently on the same or different data sets, or may be performed sequentially. There is no constraint on the complexity of algorithm combinations and the inter-relationships of their input and output

data. The execution of a macro is the responsibility of a special macro agent. The macro agent acts as a mediator for macro executions. It consists of three main functional parts: the interface with the application, the interface with the rest of the system (management and execution agents), and the module which is responsible for the management of the macro execution. The macro agent models macros as a directed acyclic graph, thus enabling macro decomposition and individual scheduling of its components.

2. Resource Management

Quality of service in DIPE is guaranteed by a sophisticated resource management and execution scheduling mechanism. The scheduling of a requested algorithm execution to the most appropriate processing element (PE) is a distributed decision making process based on the market metaphor, and is realised through the co-operation of the execution agents [16, 19]. Upon request for an algorithm execution, the management agent initialises an „auction" . The request is forwarded to the appropriate „bidders" , that is those execution agents that are able to perform the request. Each execution agent evaluates the request by taking into consideration the load of the local PE, the possible existence of the required input data in its local cache vs. the cost for transferring the data through the network, and the execution characteristics of the particular algorithm. Then, each execution agent makes a bid to the management agent by returning the estimated „cost" of the execution. The management agent evaluates all the bids it receives and assigns the execution to a particular execution agent. It is important to note that the execution characteristics of each algorithm are drawn from its execution profile, which includes information on size of input/output data, PE memory needed at runtime (relative to input data) and time needed for execution (normalised to input data and PE). A good approximation about the memory requirements and the execution time of an algorithm is derived from a statistical analysis based on previous execution profiles of the algorithm.

V. EXPERIMENTAL RESULTS

In this section we present two service implementation using web services standard and OSGi (Open services Gateway Initiative). OSGi [13] is a java-based service platform that implements a dynamic component model (from our point of view, OSGi is a component model).

1. Web service example

The first example is a service implementation according to our model. The service receives an image and returns a grayscale copy of that image. The service interface is named *GrayscaleFilter* (figure 7) and has a single operation, *transformImage*(). The business layer (functional layer) contains 2 components: *GrayscaleComponent* implementing the filter and *BitmapUtilsComponent* used to convert an image to byte array and vice versa. Non-functional aspects of the service like handling incoming connections are treated by the web service used to run our service. Also, on the client side, some tools (like Visual Studio .NET) greatly simplify the work with web services by generating the necessary code to access the service.

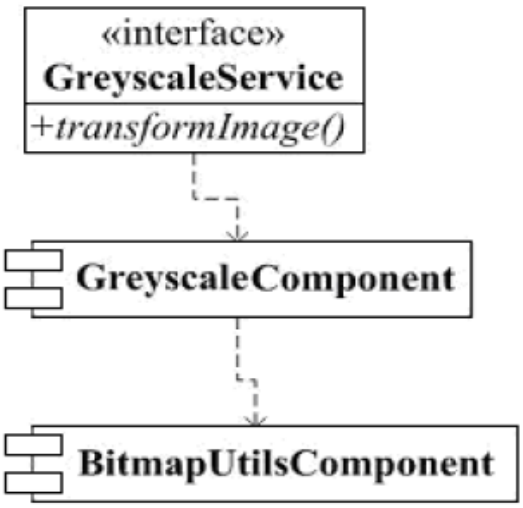

Fig 7. Web service component diagram

The class diagram is represented in figure 8. Every component is implemented by a single class.

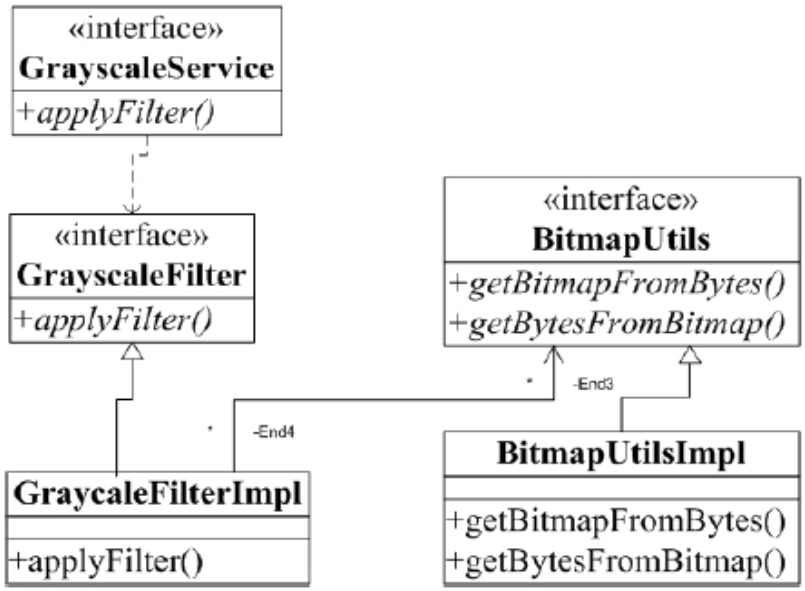

Fig 8. Web service class diagram

Note that in this simple example the business façade from our service model is not used and the resource layer is missing since no external resources are needed.

2. OSGi service example

In order to show that SOA is not based only on web services, the second example is an implementation of an image processing service using OSGi. We are using the *Knopflerfish* framework [14] as support for developing our service. In OSGi a deployment unit is called *bundle*. The framework manages the bundle lifecycle. A bundle functionality is contained typically in a jar file (java archive file). After the bundle is created it needs to be registered in the framework and other bundle can use the published service. Our OSGi service is more complex than the web service because it needs communication facilities (offered by a communication component) because OSGi does not specify a communication protocol like a web service. The component diagram for our service is depicted in figure 9

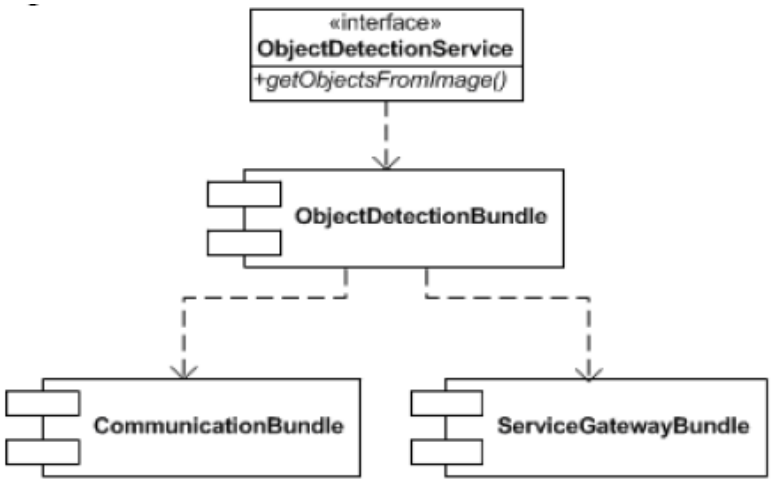

Fig 9.OSGi service component diagram

The service interface is called *ObjectDetectionService* and exposes a single operation, *getObjectsFromImage*. The input parameters (an image) and the return values (a collection of image objects) are not represented on this diagram. The *ObjectDetectionBundle* represent the functional part of the service (business layer). This component uses a communication component and a gateway component. In figure 11 is depicted the class diagram for the communication bundle.

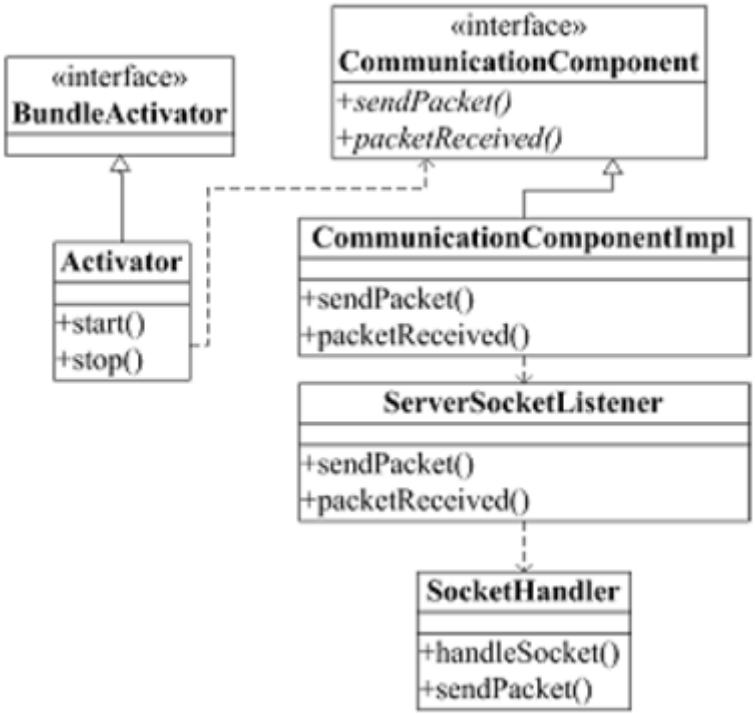

Fig 10. Communication component, class diagram

The component interface is called *CommunicationComponent* and provides two operations, one for sending a packet and the second for receiving a packet. A packet is a unit of information exchanged by the service. In our case the packet contains the image as a byte array. The Activator class implements *BundleActivator* interface and is necessary in order to allow the *Knopflerfish* framework to manage the bundle (start and stop the bundle). To be used, a bundle must be started. The bundle interface has an implementation provided by CommunicationComponentImpl. The communication is based on standard sockets (with the help of ServerSocketListener and SocketHandler). For this service, the resource layer contains a component (*ServiceGatewayBundle*) for accessing other services. The object detection algorithm implemented needs to use a grayscale image in order to provide good results. This component contains the logic to access our grayscale web service presented in section previous.

VI. CONCLUSIONS

In this paper, we have proposed a model for implementing SOA-based image processing systems. The model contains a programming model, a service model and a messaging model. We have focused on the concept of service. The service is represented as a layered architecture with a service interface layer, a business layer and an optional resource layer. The service interface layer contains the service contract (service interface). The business layer contains the service functionality, contained in business components. The resource layer contains non-functional components, used to access external resources like database systems, other services or legacy applications. Service Oriented Systems are very flexible. A service can be discovered at runtime, can be replaced if is unavailable or can be incorporated in a new service (a powerful support for adaptability). Our future goals are to create a SOA based platform for adaptation with applicability in medical domains. This platform may be based on ESB in order to provide full SOA facilities. DIPE has been designed and developed to offer image processing services over integrated health care services networks, and to act as an integration platform for diverse image processing software. It exhibits a modular, extensible and scaleable architecture that ensures system robustness and execution persistence. A sophisticated resource management and execution scheduling mechanism allows the medical expert to take full advantage of geographically distributed computational resources. Future research will address the development of intelligent and customisable mechanisms for the description, management, and retrieval of image processing software modules, as well as charging mechanisms based on quality of service. DIPE is currently being extended through its functional integration with other medical information systems that have been developed in our laboratory. Important examples include CoMed [17], a desktop conferencing application which allows interactive real-time co-operation among several medical experts, as well as TelePACS [16], an information system for medical image

management and communication. DIPE is one of the diverse telematics applications incorporated in the regional health telematics network, which is currently being developed by ICS-FORTH on the island of Crete.

REFERENCES

[1] Michael Herrmann, Muhammad Ahtisham Aslam, Oliver Dalferth, Applying Semantics (WSDL, WSDL-S, OWL) in Service Oriented Architectures (SOA), Universität Leipzig, Germany, Technical report, 2005.

[2] Microsoft Healthcare [online], http://www.microsoft.com/ industry/healthcare, (Jun, 2007).

[3] J. Treadwell, Open Grid Services Architecture Glossary of Terms, Hewlett-Packard, January 25, 2005.

[4] Organization for the Advancement of Structured Information Standards (OASIS), "Service Oriented Architecture (SOA) Reference Model," Public Review Draft 1.0, February 10, 2006.

[5] Workflow definition [online], http://en.wikipedia.org/wiki/ Workflow (June 2007).

[6] Latha Srinivasan and Jem Treadwell, An Overview of Service-oriented Architecture, Web Services and Grid Computing, , HP Software Global Business Unit, November 3, 2005.

[7] Armin Haller, Juan Miguel Gomez, Christoph Bussler, Exposing Semantic Web Service Principles in SOA to Solve EAI Scenarios, May, 2005.

[8] Rick Robinson, Understand Enterprise Service Bus scenarios and solutions in service-oriented architecture, IBM, Jun 15, 2004.

[9] Patterns: Implementing an SOA Using an Enterprise Service Bus (IBM Redbooks), IBM.Com/Redbooks, 2004.

[10] WS Specifications [online], http://www.w3schools.com/ webservices/default.asp, (Jun, 2007).

[11] Jeffrey Hasan, Expert Service-Oriented Architecture in C#: Using the Web Services Enhancements 2.0, Apress, 2004.

[12] SOAP Specifications [online], http://www.w3schools.com/ soap, (Jun, 2007).

[13] OSGi Service Platform, The Open Service Gateway Initiative, IOS Press, 2003.

[14] OSGi Tutorial A Step by Step Introduction to OSGi Programming Based on the Open Source Knopflerfish OSGi Framework , Sven Haiges, http://www.knopflerfish.org /tutorials, October 2004.

[15] S.C. Oprhanoudakis, E. Kaldoudi, and M. Tsiknakis, "Technological Advances in Teleradiology", Eur. J. Radiology, vol. 22, 205-217, 1996.

[16] S.C. Orphanoudakis, "Supercomputing in Medical Imaging" IEEE Eng Med Biol, vol. 7, 16-20, 1988.

[17] P. Maes, "Modelling Adaptive Autonomous Agents", Artificial Life Journal, ed. C. Langton, vol. 1, nos. 1&2, MIT Press, 1994.

[18] S.C. Orphanoudakis, M. Tsiknakis, C. Chronaki, S. Kostomanolakis, M. Zikos, and Y. Tsamardinos, "Development of an Integrated Image Management and Communication System on Crete". In: Lemke HU, Inamura K, Jaffe CC, Vanier MW, eds. Proc. of CAR" 95, Berlin, p. 481-487, 1995.

[19] D.C. Schmidt, "The ADAPTIVE Communication Environment: An Object-Oriented Network Programming Toolkit for Developing Communication Software", 12th Sun User Group Conference, San Francisco, California, June 14-17, 1993.

[20] D.F. Ferguson, Y. Yemini, C. Nikolaou, "Microeconomic Algorithms for Load Balancing in Distributed Computer Systems.", . In Proceedings of International Conference on Distributed Systems (ICDCS 88). San Jose, California: IEEE Press, 1988.

[21] M. Zikos, C. Stephanidis, and S.C. Orphanoudakis, "CoMed: Cooperation in Medicine", Proceedings of EuroPACS" 96, pp. 88-92, Heraklion, Greece, October 3-5, 1996.

American Journal of Engineering Research (AJER)
e-ISSN : 2320-0847 p-ISSN : 2320-0936
Volume-02, Issue-10, pp-63-73
www.ajer.org

Research Paper Open Access

An Efficient Spam Filtering Techniques for Email Account

S. Roy, A. Patra, S.Sau, K.Mandal, S. Kunar
[1,2,3]*Computer Science & Technology&*[4]*Mechanical Engineering, NITTTR, Kolkata, India*
[5]*Production Engineering, Jadavpur University, Kolkata, India*

Abstract: - *Unsolicited emails, known as spam, are one of the fast growing and costly problems associated with the Internet today. Electronic mail is used daily by millions of people to communicate around the globe and is a mission-critical application for many businesses. Over the last decade, unsolicited bulk email has become a major problem for email users. An overwhelming amount of spam is flowing into user's mailboxes daily. Not only is spam frustrating for most email users, it strains the IT infrastructure of organizations and costs businesses billions of dollars in lost productivity. The necessity of effective spam filters increases. In this paper, we presented an efficient spam filter techniques to spam email based on Naive Bayes Classifier. Bayesian filtering works by evaluating the probability of different words appearing in legitimate and spam mails and then classifying them based on those probabilities.*

Keywords: - *Spam, Filters, Bayesian, Content based spam filter and Email*

I. INTRODUCTION

The Internet is gradually becoming an integral part of everyday life. Internet usage is expected to continue growing and e-mail has become a powerful tool intended for idea and information exchange, as well as for users' commercial and social lives. Along with the growth of the Internet and e-mail, there has been a dramatic growth in spam in recent years. The majority of spam solutions deal with the flood of spam. However, it is amazing that despite the increasing development of anti-spam services and technologies, the number of spam messages continues to increase rapidly. The increasing volume of spam has become a serious threat not only to the Internet, but also to society. For the business and educational environment, spam has become a security issue. Spam has gone from just being annoying to being expensive and risky. The enigma is that spam is difficult to define. What is spam to one person is not necessarily spam to another. Fortunately or unfortunately, spam is here to stay and destinedto increase its impact around the world. It has become an issue that can no longer be ignored; an issue that needs to be addressed in a multi-layered approach: at the source, on the network, and with the end-user [1].

In this digital age, which is the era of electronics & computers, one of the efficient & power mode of communication is the email. Undesired, unsolicited email is a nuisance for its recipients; however, it also often presents a security threat. For ex., it may contain a link to a phony website intending to capture the user's login credentials (identity theft, phishing), or a link to a website that installs malicious software (malware) on the user's computer. Installed malware can be used to capture user information, send spam, host malware, host phish, or conduct denial of service attacks as part of a "bot" net. While prevention of spam transmission would be ideal, detection allows users & email providers to address the problem today [2].

Spam filtering has become a very important issue in the last few years as unsolicited bulk e-mail imposes large problems in terms of both the amount of time spent on and the resources needed to automatically filter those messages. Email communication has come up as the most effective and popular way of communication today. People are sending and receiving many messages per day, communicating with partners and friends, exchanging files and information. E-mail data's are now becoming the dominant form of inter and intra-organizational written communication for many companies and government departments. Emails are the essential part of life now just likes mobile phones & i-pods [3].

Emails can be of spam type or non-spam type. Spam mail is also called as junk mail or unwanted mail whereas non-spam mails are genuine in nature and meant for a specific person and purpose. Information

retrieval offers the tools and algorithms to handle text documents in their data vector form. The Statistics of spam are increasing in number. At the end of 2002, as much as 40 % of all email traffic consisted of spam. In 2003, the percentage was estimated to be about 50 % of all emails. In 2006, BBC news reported 96 % of all emails to be spam.

Spam can be defined as unsolicited (unwanted, junk) email for a recipient or any email that the user do not wanted to have in his inbox. It is also defined as "Internet Spam is one or more unsolicited messages, sent or posted as a part of larger collection of messages, all having substantially identical content." There are severe problems from the spam mails, viz., wastage of network resources (bandwidth), wastage of time, damage to the PC's & laptops due to viruses & the ethical issues such as the spam emails advertising pornographic sites which are harmful to the young generations[4].

Email is the most widely used medium for communication worldwide because it's Cheap, Reliable, Fast and easily accessible. Email is also prone to spam emails because of its wide usage, cheapness & with a single click you can communicate with anyone anywhere around the globe. It hardly cost spammers to send out 1 million emails than to send 10 emails. Hence, Email Spam is one of the major problems of the today's internet, bringing financial damage to companies and annoying individual users.

- **Rule based**

Handmade rules for detection of spam made by experts (needs domain experts & constant updating of rules).

- **Customer Revolt**

Forcing companies not to publicize personal email ids given to them (hard to implement).

- **Domain filters**

Allowing mails from specific domains only (hard job of keeping track of domains that are valid for a user).

- **Blacklisting**

Blacklist filters use databases of known abusers, and also filter unknown addresses (constant updating of the data bases would be required).

- **White list Filters**

Mailer programs learn all contacts of a user and let mail from those contacts through directly (every one should first be needed to communicate his email-id to the user and only then he can send email).

- **Hiding address**

Hiding ones original address from the spammers by allowing all emails to be received at temporary email-id which is then forwarded to the original email if found valid by the user (hard job of maintaining couple of email-ids).

- **Checks on number of recipients by the email agent programs.**
- **Government actions**

Laws implemented by government against spammers (hard to implement laws).

- **Automated recognition of Spam**

Uses machine learning algorithms by first learning from the past data available (seems to be the best at current). Here, follows a brief overview of e-mail spam filtering. Among the approaches developed to stop spam, filtering is an important and popular one. It can be defined as automatic classification of messages into spam and legitimate mail. It is possible to apply the spam filtering algorithms on different phases of email transmission at routers, at destination mail server or in the destination mailbox[5]. Filtering on the destination port solves the problems caused by spam only partially, i.e., prevents end users from wasting their time on junk messages, but it does not prevent resources misuse, because all the messages are delivered nevertheless. In general, a spam filter is an application which implements a function:

f(m, L) = { cspam, if the decision is "spam" cleg, otherwise }

Where 'm' is a message or Email to be classified, L is a vector of parameters, and cspam and cleg are labels assigned to the messages. Most of the spam filters are based on a machine learning classification techniques. In a learning-based technique the vector of parameters L is the result of training the classifier on a pre collected dataset:

L = R(M),

M = {(m1, y1),…… (mn, yn)}, yi∈ { cspam, cleg}

Where m1, m2…mn are previously collected messages, y1, y2…yn are the corresponding labels, and R is the training function. In order to classify new message, a spam filter can analyze them either separately (by just checking the presence of certain words) or in groups (consider the arrival of dozen of messages with same content in five minutes than arrival of one message with the same content). In addition, learning-based filter analyzes a collection of labeled training data (pre-collected messages with reliable judgment).

This paper explores statistical learning algorithms such as Bayesian techniques for classifying spam. This spam probability and non spam probability for every word occurred in incoming message by using training sets of

words. Every word contains two frequencies one is spam frequency and other is non-spam frequency. Using this frequency calculate spam and non-spam probability [6]. If spam probability greater than non-spam probability then incoming message is considered as spam email message. After that all words have been updated in trainings set. All time training sets will be updated.

II. GENERAL CHARACTERISTICS OF SPAM

Spam is not only offensive and annoying; it causes loss of productivity, decreases bandwidth and costs companies a lot of money. Therefore, every smart company that uses email must take measures in order to block spam from entering their email systems. Although it might not be possible to block out all spam, just blocking a large proportion of it will greatly reduce its harmful effects. In order to effectively filter out spam and junk mail, the proposed system is able to distinguish spam from legitimate messages and to do this it needs to identify typical spam characteristics & practices. Once these practices are known, suitable measures can be put into place to block these messages. Of course, spammers are continually improving their spam tactics, so it is important to keep up to date on new spam practices from time to time to ensure spam is still being blocked effectively.

Spam characteristics appear in two parts of a message; email headers and message content:

2.1 Email Header

Email headers show the route an email has taken in order to arrive at its destination. They also contain other information about the email, such as the sender and recipient, the message ID, date and time of transmission, subject and several other email characteristics. Most spammers try to hide their identity by forging email headers or by relaying mail to hide the real source of the message. Since they need to send mails to a large number of recipients, spammers use certain methods for mass mailing that can be classified as pure spam practices and can therefore be identified in the email headers. Although newsletters and legitimate mailings are also sent to a large number of recipients, these will generally not display the same characteristics since the message source does not need to be concealed.

Typical email header characteristics in spam messages:

Recipient's email address is not in the To: or Cc: fields
Empty To: field
To: field contains invalid email address
Missing To: field
From:
Missing From: field
Missing or malformed Message ID
More than 10 recipients in To: and/or Cc: fields
X-mailer field contains name of popular spam ware
Bcc: header exists
X-Distribution = bulk
X-UIDL header exists
Code and space sequence exists
Illegal HTML exists

Table 1. Statistics of spam based on spam characteristics

Spam Characteristics	% of Searched mails
Recipient address not in To: or Cc: field	64%
To: field missing	34%
To: field contains invalid email address	20%
No message ID	20%
Suspect message ID	20%
Cc: filed contains more than 15 recipients	17%
From: is same as the To: field	6%
Cc: field contains more between 5-15 recipients	3%
To: field contains more between 5-15 recipients	2%
Cc: field contains more than 5-15 recipients	1%
Bcc: field exists	0%
To: field is empty	0%
From: is blank or missing	0%

2.2 Message contents

Apart from headers, spammers tend to use certain language in their emails that companies can use to distinguish spam messages from others. Typical words are free, limited offer, click here, act now, risk free, lose weight, and earn money, get rich, and (over) use of exclamation marks and capitals in the text. Spam canbe blocked by checking for words in the email body and subject, but it is important that you filter words accurately since otherwise you might be blocking legitimate mails as well.

III. DEVELOPMENT OF THE PROPOSED SYSTEM

3.1 Overview of Design Methodology

The proposed system using naive bayes classifier to classify an email is spam or not. Proposed system should be good rate for false positive and false negative. While false positive means a good email can be identified as spam email. False negative means a spam emails identified by a good email.

3.1.1 Bayes Theorem

The probability of an event may depend on the occurrence or non-occurrence of another event. This dependency is written in terms of **conditional probability**:

P(A|B) = P(A∩B) / P(B)

P(B|A) = P(A∩B) / P(A)

P(A∩B) =P(B|A) P(A) = P(A|B) P(B)

An event A is INDEPENDENT from event B if the conditional probability is the same as the **marginal probability**.

P(B|A) = P(B)

P(A|B) = P(A)

From the formulas the Bayes Theorem States the Prior probability: Unconditional probabilities of our hypothesis before we get any data or any NEW evidence. Simply speaking, it is the state of our knowledge before the data is observed. Also stated is the posterior probability: A conditional probability about our hypothesis (our state of knowledge) after we revised based on the new data.

Likelihood is the conditional probability based on our observation data given that our hypothesis holds.

P(A|B) = P(B|A) P(A)/ P(B)

P(B|A) = P(B|A) P(B)/ P(A)

Where P (A|B) is the posterior probability, P(B|A) is the likelihood and P(A) prior probability.

Thomas Bayes (c. 1702 – 17 April 1761) was a British mathematician and Presbyterian minister, known for having formulated a specific case of the theorem that bears his name: Bayes' theorem, which was published posthumously.

The following are the mathematical formalisms, and the example on a spam filter, but keep in mind the basic idea.

The Bayesian classifier uses the Bayes theorem, which says:

P(cj | d) = P(d |cj) P(cj) / P(d)

Considering each attribute and class label as a random variable and given a record with attributes (A1,A2,…, An), the goal is to predict class C. Specifically, we want to find the value of C that maximizes P(C| A1,A2,…An).

The approach taken is to compute the posterior probability P(C| A1,A2,…An) for all values of C using the Bayes theorem.

P(C | A1 A2 ...An) = P(A1 A2 ....An | C) P(C) / P(A1 A2 ....An)

So you choose the value of C that maximizes P(C| A1,A2,…An). This is equivalent to choosing the value of C that maximizes P(A1,A2,…An | C) P(C).

3.2 Evaluation Process

Naïve Bayesian prediction requires each conditional probability be non zero. Otherwise, the predicted probability will be zero.

$$P(X \mid C_i) = \prod_{k=1}^{n} P(x_k \mid C_i)$$

In order to overcome this, we use probability estimation from one of the following:

$$\text{Original}: P(A_i \mid C) = \frac{N_{ic}}{N_c}$$

$$\text{Laplace}: P(A_i \mid C) = \frac{N_{ic} + 1}{N_c + c}$$

$$\text{m - estimate}: P(A_i \mid C) = \frac{N_{ic} + mp}{N_c + m}$$

c: number of classes
p: prior probability
m: parameter

In order to classify and predict a spam email from a non spam one, the following techniques and assumptions are used:

1. Sorting according to language (spam or non spam), then words, and then count.
2. If a word does not exist, consider to approximate P(word|class) using Laplacian.
3. A learning dataset for analysis.
4. The Learning Datasetcontains each word that content filtering uses to determine if a message is spam. Beside each word, there are two numbers. The first number is the number of times that the word has occurred in non-spam e-mail messages. The second number is the number of times that the word has occurred in spam e-mail messages.

Table 2.Example of learning dataset containing words

Word	Occurred in Non Spam	Occurred in Spam
Specializing	391	4022
Graciously	2095	380
Bringing	2772	11854
Mbps	425	823
Tantra	96	52

3.3 Algorithm of the Proposed System

Input: keyword list, stop word list, ignore list, email message

Step1:- Let m be an email message. Take two variables Nonspam percent and Spam percent initialized to 1. Convert all words to lower case.

Step2:- Find out all special character from m and remove all special character from m.

Step 3:- For each word w_i in m
If w_i found in stopword list
Then w is removed from m.
End If.
End For.

Step 4:-For each word w_j in m
If w_j found in learning keyword dataset
Take spam value and calculate the probability using spam value divided by total spam value and multiply this probability with Spam percent
Else Take spam value as 1(using Laplace) and calculate the Probability using 1 divided by total spam value and Multiply this probability with Spam percent. And add to keyword dataset.
End For.

Step 4:-For each word w_k in m
If w_k found in learning keyword dataset
Take non spam value and calculate the probability using non spam value divided by total non spam value and multiply this probability with NonSpam percent
Else take non spam value as 1(using Laplace) and calculate the Probability using 1 divided by total non spam value and Multiply this probability with NonSpam percent. And add to keyword dataset.
End For.

Step 5:- Find out spam and non spam probability from learning dataset and multiply spam probability with Spam percent to get all word spampercent and similarly multiply non spam probability with non spam percent to get all word non spam percent

Step 6:- If Spam percent >Nonspam percent
Then m will be identified as Spam Email.

Else m will be legitimate Email.

3.4 Explanation of Algorithm

Input of the above algorithm is ignoring list, stop word list, and keyword list. Ignore list contains set of special character like (~,!,@,#,$,%,^,&,*,<,>,.,? etc)

First to remove from email content this ignores character. Then remove stop word from email content. Stop word list like (am, is, are etc). Rest of the word contains in email is termed as keyword. To maintain a huge learning data set using this keyword. Learning datasets contain lots of word. And each word has two properties. One spam count and another is non spam count [7]. Where spam count is no of spam email contains this word. Non spam count is the no of non spam email that contains this word.

First find out probability of mail type from the training dataset. Probability of spam email will be

P (SpamMailType) = (Total spam count from learning set/ Total count)

Similarly probability for non spam email will be

P (NonSpamMailType) = (Total spam count from learning set/ Total count)

Then take two variable example spampercent and nonspampercent and initialized to 1. Then look for percent of word in non spam. Similarly look for percent of word in spam. Final probability by multiplying each word to the total probability. Compare spampercent with nonspampercent. If spam percent greater than nonspampercent, then email is considered as spam email.

IV. IMPLEMENTATION

To implement a system, there are some software and hardware required. Some softwares as well as hardwaresare used to implement the above proposed system.

Hardware Used: 1. Windows 7

Software Used: 1.Visual studio 2010
2. Sql Server 2008
3. IIS 7.0

Some of this system snapshot is given below.

Login page of this email system

Fig 4.1 Login page

After login successful page

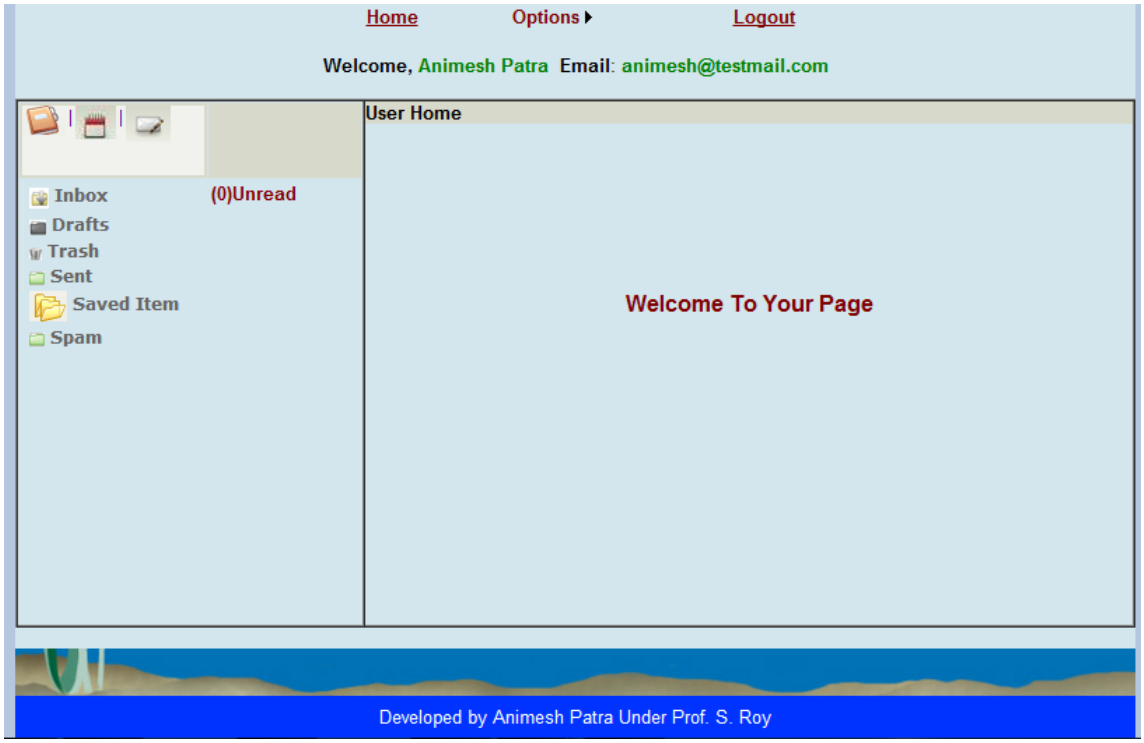

Fig 4.2. Home page

Compose mail

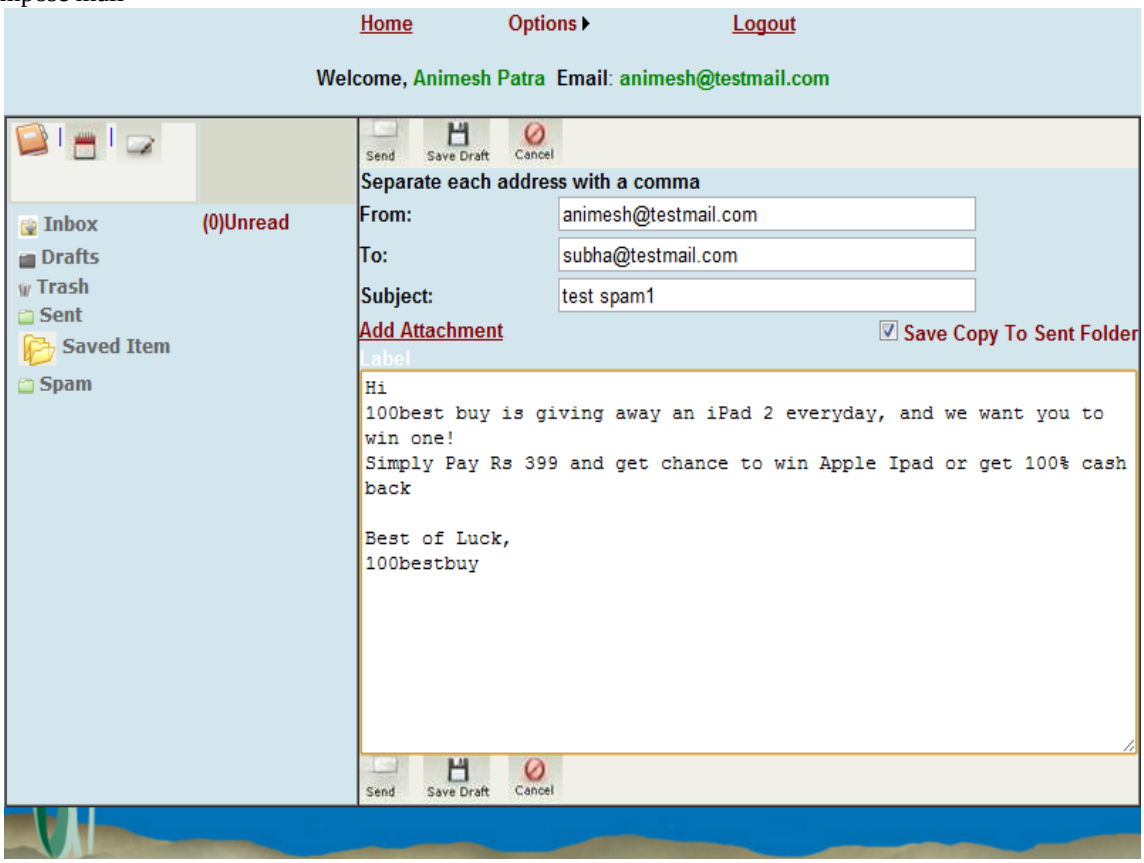

Fig 4.3 Compose mail page

After sending mail

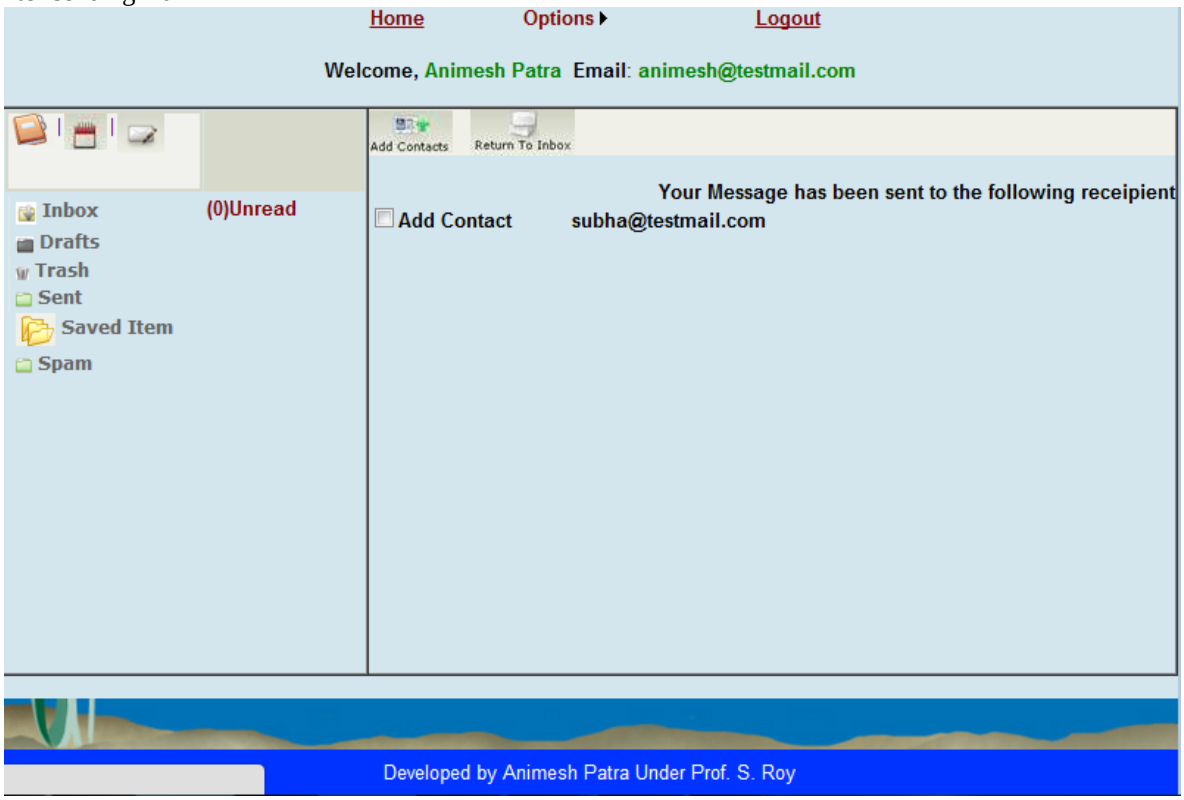

Fig.4.4 After email sending Page

After login successful page

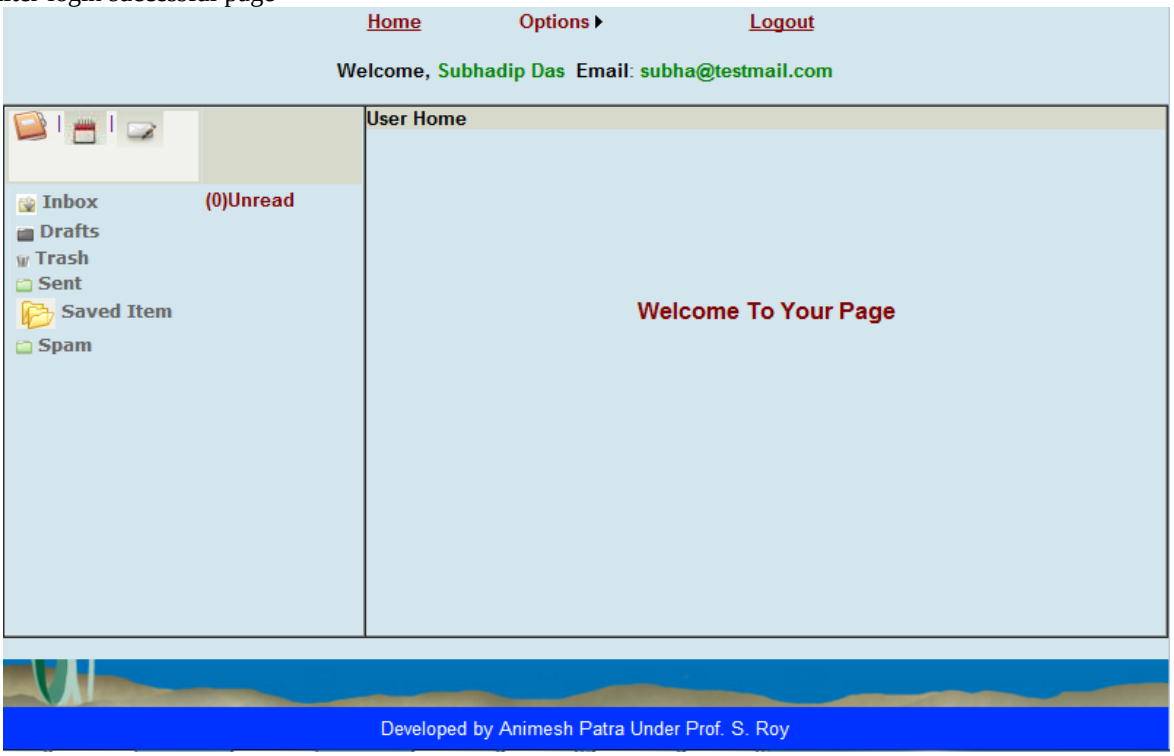

Fig. 4.5 After login to another account page

See spam folder contain the incoming email

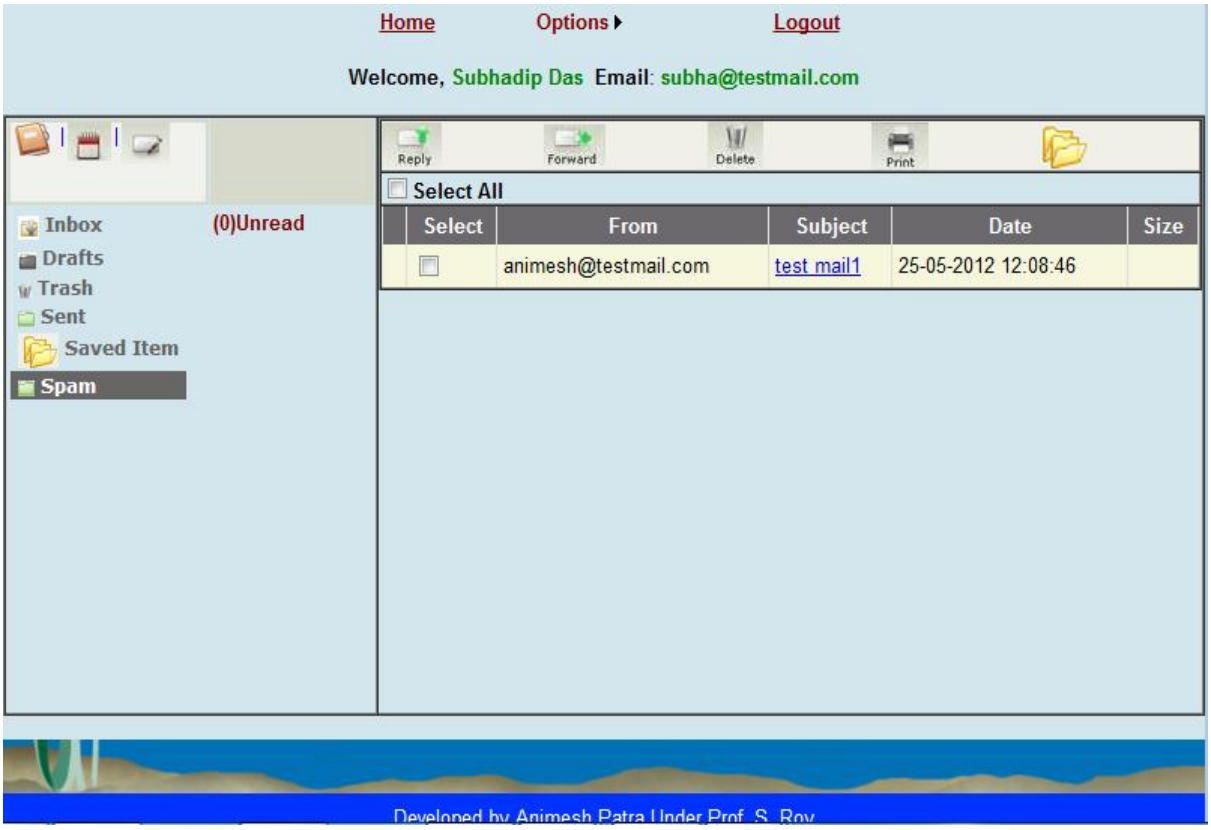

Fig. 4.6 Spam folder page

Login to another account

Fig.4.5 Another login page

Spam email content

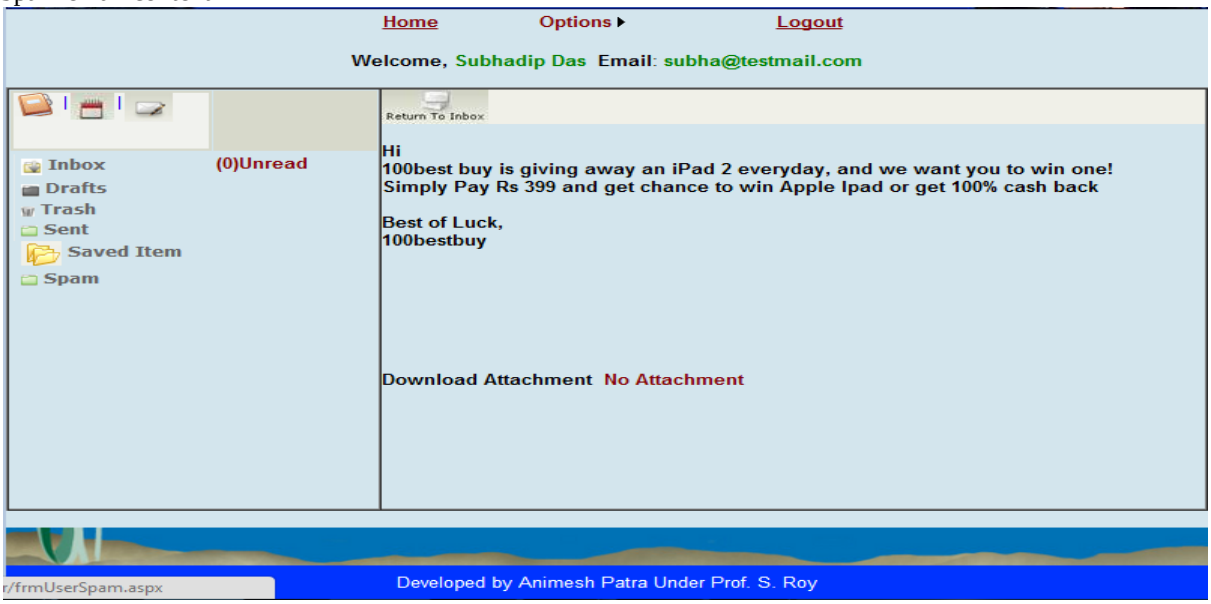

Fig. 4.7 Content of Spam Mail.

V. EXPERIMENTAL RESULT AND ANALYSIS

Estimating classifier accuracy is important in that it allows one to evaluate how accurately a given classifier will label the test data. It can be calculated using the formula discussed below. A classifier is trained to classify e-mails as non-spam and spam mails. An accuracy of 85 % may make the classifier accurate, but what if only 10-15 % of the training samples are actually "spam"? Clearly an accuracy of 85 % may not be acceptable-the classifier could be correctly labeling only the "non-spam" samples. Instead, we would like to be able to access how well the classifier can recognize "spam" samples (referred to as positive samples) how well it can recognize "non-spam" samples (referred to as negative samples)[8].The sensitivity (recall) and specificity measures can be used, respectively for this purpose.

The use precision to access the percentage of samples labeled as "spam" that actually are "spam" samples. The evaluation measures which are used in approach for testing process in our research work could be defined as follows:

True Positive (TP): This states the no. of spam documents correctly classified as spam

True Negative (TN): This states the number of non-spam documents correctly classified as non spam.

False Positive (FP): This states the number spam documents classified as non spam.

False Negative (FN): This states the number of non-spam document classified as spam.

Table.3: Measurement, Formula, and Meaning of TP, TN, FP and FN

Measurement	Formula	Meaning
Precision	TP / (TP + FP)	The percentage of positive predictions that is correct.
Recall / Sensitivity	TP / (TP + FN)	The percentage of positive labeled instances that ispredicted as positive.
Specificity	TN / (TN + FP)	The percentage of negative labeled instances that is predicted as negative.
Accuracy	(TP + TN) / (TP + TN + FP + FN)	The percentage of predictions that is correct.

500 spam document and 100 non spam document are tested. From the experimental result, out of 500 spam to identify 468 as a spam and from 100 non spam document to identify 86 documents as nonspam.

True Positive (TP) = 477

True Negative (TN) = 88
False Positive (FP) = 23
False Negative (FN) = 12
Precision = TP / (TP + FP) = 0.95
Recall / Sensitivity = TP / (TP + FN) = 0.97
Specificity = TN / (TN + FP) = 0.79
Accuracy = ((TP + TN) / (TP + TN + FN + FP))*100 = 94.16%

VI. CONCLUSION

In this Dissertation, the email client system that has capability to send email and receive email and project mainly concerned about an efficient email spam filtering techniques for an email account. For this system, we collected statistical data by which we create a training set. This dataset is updated time by time. The filtering techniques based on Naive bayes Theorem, which is a good one machine learning algorithm. The projectis concentrated only on text word not any other content. But the system is very much effective to identify spam from email for text based.

REFERENCES

[1] A. Androutsopoulos, J. Koutsias, K.V. Cbandrinos and C.D. Spyropoulos. An experimental comparison of naive Bayesian and keyword-based anti-spam filtering with personal e-mail messages. *In Proceedings of the 23rd ACM International Conference on Research and Developments in Information Retrieval*, Athens, Greece, 2000, 160–167.

[2] B.Klimt and Y.Yang. The Enron corpus: A new data set for e-mail classification research. *In Proceedings of the European Conference on Machine Learning*, 2004, 217–226.

[3] A. McCallum and K. Nigam. A comparison of event models for naive Bayes text classification. *In Proceedings of the AAAI Workshop on learning for text categorization*, 1998, 41–48.

[4] F.Sebastiani. Machine learning in automated text categorization. *ACM Computing Surveys*, 34(1):1–47, 2002.

[5] M. Sahami, S. Dumais, D. Heckerman and E. Horvitz. A Bayesian approach to filtering junk e-mail. *AAAI Technical Report WS-98-05*, Madison, Wisconsin, 1998.

[6] L. Zhang, J. Zhu and T. Yao. An evaluation of statistical spam filtering techniques. *ACM Transactions on Asian Language Information Processing*, 3(4):243–269, 2004.

[7] J. Golbeck and J. Hendler. Reputation network analysis for email filtering. *In Proceedings of the First Conference on Email and Anti-spam*,2004.

[8] T.M. Mitchell, *Machine Learning*, McGraw-Hill, New York, 1997.

American Journal of Engineering Research (AJER)
e-ISSN : 2320-0847 p-ISSN : 2320-0936
Volume-02, Issue-10, pp-74-76
www.ajer.org

Research Paper Open Access

Fuzzy gc-super Irresolute Mappings

M. K. Mishra, Manisha Shukla
Professor, EGS PEC Nagapattinam
And Asst.Prof. AGCW Karaikal

Abstract: - In this paper we study the concept of fuzzy gc-super irresolute mappings and introduced some of their basic properties in fuzzy topology.

Keywords: *- fuzzy super closure ,fuzzy super interior, fuzzy super closed set, fuzzy super open set ,fuzzy super continuity ,fuzzy g -super closed sets and fuzzy g –super open sets, fuzzy g -super continuous mappings.*

I. INTRODUCTION

After the introduction of fuzzy sets by Zadeh [15] in 1965 and fuzzy topology by chang [4] in 1967. Several researches were conducted on the generalizations of the notions of fuzzy sets and fuzzy topology. The concept of fuzzy sets was introduced by Atanassov [1] as a generalization of fuzzy sets . In the last 20 years various concepts of fuzzy mathematics have been extended for fuzzy sets. In 1997 Coker [5] introduced the concept of fuzzy topological spaces. Recently many fuzzy topological concepts such as fuzzy compactness [8], fuzzy connectedness [14], fuzzy multi functions [9] fuzzy g -super closed set [11] and fuzzy g -super continuity [12] have been generalized for fuzzy topological spaces. Topological space. In the present paper we introduce and study the concept of fuzzy gc-super irresolute mappings in fuzzy topological space.

II. PRELIMINARIES

Definition 2.1[8,9,12]**:** A fuzzy set A of a fuzzy topological space $(X,\Im)$ is called a

(a) fuzzy generalized super closed (fuzzy g -super closed) if $cl(A) \leq O$ Whenever $A \leq O$ and O is fuzzy super open.

(b) Fuzzy generalized super open if its complement is fuzzy generalized super closed.

Remark 2.1 [8,9,12]**:** Every fuzzy super closed set is fuzzy g -super closed set but its converse may not be true.

Definition 2.2[9]: Let $(X,\Im)$ and (Y,Φ) be two fuzzy topological spaces and let $f: X \to Y$ be a function. Then

(a) f is said to be fuzzy super continuous if the pre image of each fuzzy open set in Y is an fuzzy super open set in X.[8]

(b) f is said to be fuzzy g -super continuous if the inverse image of every fuzzy super closed set of Y is fuzzy g -super closed set in X.[13]

Definition 2.3[8,9,13]: An fuzzy topological space X is called fuzzy g -super connected if there is no proper fuzzy set of X which is both fuzzy g -super open and fuzzy g -super closed.

Definition 2.4[8,9,13]: An fuzzy set B of a fuzzy topological space $(X,\Im)$ is said to be fuzzy GO- super compact relative to X, if for every collection $\{A_i: i \in \wedge\}$ of fuzzy g –super open sets of X such that $B \leq \cup\{A_i: i \in \wedge\}$. There exists a finite subset $\wedge_0$ of $\wedge$ such that $B \leq \cup\{A_i: i \in \wedge_0\}$.

Definition 2.5[8,9,13] : A crisp subset Y of an fuzzy topological space $(X,\Im)$ is said to be fuzzy GO- super compact if Y is fuzzy GO- super compact as a fuzzy subspace of X.

Definition 2.6.[8,9,13]: Let (X, $\Im$) be an fuzzy topological space. The generalized closure of a fuzzy set A of X denoted by gcl(A) is the intersection of all fuzzy g -super closed sets of X which contains A.

III. FUZZY GC-SUPER IRRESOLUTE MAPPINGS

Definition 3.1: A mapping f from an fuzzy topological space (X,$\Im$) to another fuzzy topological space (Y,σ) is said to be fuzzy gc-super irresolute if the inverse image of every fuzzy g -super closed set of Y is fuzzy g -super closed in X.

Theorem 3.1: A mapping f : (X,$\Im$)$\rightarrow$(Y,σ) is fuzzy gc-super irresolute if and only if the inverse image of every fuzzy g –super open set in Y is fuzzy g -super open in X.

Proof: It is obvious because $f^{-1}(U^c) = (f^{-1}(U))^c$, for every fuzzy set U of Y.

Remark 3.1: Since every fuzzy closed set is fuzzy g -super closed it is clear that every fuzzy gc-super irresolute mapping is fuzzy g -super continuous but the converse may not be true.

Remark 3.2: Example (3.1) and example (3.2) asserts that the concepts of fuzzy gc-super irresolute and fuzzy super continuous mappings are independent.

Theorem 3.2: If a mapping f : (X,$\Im$)$\rightarrow$(Y,σ) is fuzzy gc-super irresolute then

(a) $f(gcl(A)) \leq gcl(f(A)$

(b) $gcl(f^{-1}(B)) \leq f^{-1}(gcl(B))$.

Proof: Obvious.

Theorem 3.3: Let f: (X,$\Im$)$\rightarrow$(Y,σ) is bijective fuzzy super open and fuzzy g -super continuous then f is fuzzy gc- super irresolute.

Proof: Let A be a fuzzy g -super closed set in Y and let $f^{-1}(A) \leq G$ where G is fuzzy open set in X. Then $A \leq f(G)$. Since f(G) is fuzzy super open and A is fuzzy g -super closed in Y, $cl(A) \leq f(G)$ and $f^{-1}(cl(A)) \leq G$. Since f is fuzzy g -super continuous and cl(A) is fuzzy super closed in Y, $cl(f^{-1}(cl(A))) \leq G$. And so $cl(f^{-1}(A)) \leq G$. Therefore $f^{-1}(A)$ is fuzzy g -super closed in X. Hence f is fuzzy gc- super irresolute.

Theorem 3.4: Let f : (X,$\Im$)$\rightarrow$(Y,σ) and g: (Y,σ)$\rightarrow$(Z,η) be two fuzzy gc-super irresolute mappings, then gof : (X,$\Im$)$\rightarrow$(Z, η) is fuzzy gc- super irresolute.

Proof : Obvious.

Theorem 3.5: Let f : (X,$\Im$) $\rightarrow$ (Y,σ) is fuzzy gc-super irresolute and g: (Y,σ)$\rightarrow$(Z,η) is fuzzy g -super continuous then the gof : (X,$\Im$)$\rightarrow$(Z, η) is fuzzy g -super continuous.

Proof: Obvious.

Theorem 3.6: Let f : (X,$\Im$)$\rightarrow$(Y,σ) is fuzzy gc-super irresolute mappings, then gof : (X,$\Im$)$\rightarrow$(Z, η) is fuzzy gc-super irresolute and if B is fuzzy GO- super compact relative to X, then the image f(B) is fuzzy GO- super compact relative to Y.

Proof : Let {Ai: i$\in\wedge$}be any collection of fuzzy g–super open set of Y such that $f(B) \leq \cup\{Ai: i\in\wedge\}$. Then $B \leq \cup\{f^{-1}(Ai): i\in\wedge\}$. By using the assumption, there exists a finite subset $\wedge_0$ of $\wedge$ such that $B \leq \cup\{f^{-1}(Ai): i\in\wedge_0\}$. Therefore, $f(B) \leq \{Ai: i\in\wedge_0\}$. Which shows that f(B) is fuzzy GO- super compact relative to Y.

Corollary 3. 1: A fuzzy gc-super irresolute image of a fuzzy GO- super compact space is fuzzy GO- super compact.

Theorem 3.8: Let (XxY, $\Im x\sigma$) be the fuzzy product space of non-empty fuzzy topological spaces (X,$\Im$) and (Y,σ). Then the projection mapping p: XxY$\rightarrow$X is fuzzy gc- super irresolute.

Proof: Let F be any fuzzy g -super closed set of X. Then $fx_1(= p^{-1}(F))$ is fuzzy g -super closed and hence p is fuzzy gc- super irresolute.

Theorem 3.9: If the product space (XxY, $\Im x\sigma$) of two non empty fuzzy topological spaces (X,$\Im$) and (Y,σ) is fuzzy GO-super compact, then each factor space is fuzzy GO- super compact.

Proof: Obvious.

Theorem: 3.10: Let f : (X,$\Im$)$\rightarrow$(Y,σ) is an fuzzy gc-super irresolute surjection and (X,$\Im$) is fuzzy GO- super connected, then (Y,σ) is fuzzy GO- super connected.

Proof: Suppose Y is not fuzzy GO- super connected then there exists a proper fuzzy set G of Y which is both fuzzy g -super open and Fuzzy g -super closed, therefore $f^{-1}(G)$ is a proper fuzzy set of X, which is both fuzzy g -super open and fuzzy g -super closed, because f is fuzzy g -super continuous surjection. Therefore X is not fuzzy GO- super connected, which is a contradiction. Hence Y is fuzzy GO- super connected.

Theorem 3.11: If the product space (XxY ,$\Im x\sigma$) of two non-empty fuzzy topological spaces (X,$\Im$) and (Y,σ) is fuzzy GO- super connected, then each factor fuzzy space is fuzzy GO- super connected.

Proof: Obvious.

REFERENCES

[1] K. Atanassova, Fuzzy Sets, In VII ITKR's Session, (V.Sgurev,Ed.) Sofia, Bulgaria, (1983)
[2] K. Atanassov and S. Stoeva., Fuzzy Sets, In Polish Symposium on Interval and Fuzzy Mathematics , Poznan, (1983), 23-26
[3] K. Atnassov, Fuzzy Sets. Fuzzy Sets and Systems, 20(1986), 87-96.
[4] C.L. Chang, Fuzzy Topological Spaces, J.Math.Anal.Appl. 24(1968) 182-190.
[5] D. Coker, An Introduction to Fuzzy Topological Spaces, Fuzzy Sets and Systems .88(1997), 81-89.
[6] D.Coker and A. Es. Hyder., On Fuzzy Compactness in Fuzzy Topological Spaces, The Journal of Fuzzy Mathematics, 3-4(1995),899-909.
[7] H. Gurcay, D. Coker and Es., A.Haydar, On Fuzzy Continuity in Fuzzy Topological Spaces. The Journal of Fuzzy Mathematics Vol.5, no.2, 1997, 365-378.
[8] Mishra M.K. ,et all on " Fuzzy super closed set" International Journal International Journal of Mathematics and applied Statistics.
[9] Mishra M.K. ,et all on " Fuzzy super continuity" International Review in Fuzzy Mathematics ISSN : 0973-4392July –December2012.
[10] Mishra M.K., Shukla M. "Fuzzy Regular Generalized Super Closed Set" Accepted for publication in International Journal of Scientfic and Research Publication ISSN2250-3153. July December 2012.
[11] N. Levine., Generalized Closed Sets In Topology, Rend. Cerc. Mat. Palermo.19(2), 1970, 571-599.
[12] O. Ozbakir and D. Coker., Fuzzy Multifunctions in Fuzzy Topological Spaces Notes on IFS 5(1999) No. 3.
[13] S.S. Thakur and Malviya R., Generalized Closed Sets In Fuzzy Topology, Math. Notae 38(1995), 137-140.
[14] N.Turnali and D. Coker, Fuzzy Connectedness in Fuzzy Topological Spaces. Fuzzy Sets And Systems 116(2000) (3), 369-375.
[15] L.A.Zadeh, Fuzzy Sets, Information and Control, 18(1965), 338-353.

American Journal of Engineering Research (AJER)
e-ISSN : 2320-0847 p-ISSN : 2320-0936
Volume-02, Issue-10, pp-77-85
www.ajer.org

Research Paper Open Access

Experimental Analysis of Particle Size Distribution using Electromagnetic Sieve

Ujam, A.J., and Enebe, K. O
a. Department of Mechanical and production Engineering Enugu State University of Science and Technology, Enugu, Nigeria
b. Scientific Equipment Development Institute, Enugu, Enugu State, Nigeria.

Abstract: - This work is aimed at grading the particle sizes of powders and granular distribution of particle sizes of a local agricultural product, **GARRI.** To be able to do this, an electromagnetic sieving machine which transforms electromagnetic energy to mechanical energy was designed and constructed. The Choice of **Electromagnetic Sieving Machine** was to increase the amplitude of oscillation and thereby reducing the time of sieving. With the aid of the machine, sieving was carried out three times at different voltage settings. The tests conducted show that with increase in voltage, the amplitude of oscillation also increased, thereby reducing the sieving time. Optimal output (from 1kg of Garri) was obtained in 120 seconds at a voltage setting of 255 volts which generated 5mm amplitude. The different particle sizes were evaluated by the use of an electronic microscope. The efficiency of the machine was evaluated to be 98%.

Key words: *- Particle size, Vibration, Sieve, Energy, magnetic flux*

I. INTRODUCTION

The **particle-size distribution (PSD)** of a powder, or granular material, or particles dispersed in fluid, is a list of values or a mathematical function that defines the relative amount, typically by mass, of particles present according to size.**[1]** PSD is also known as **grain size distribution**.**[2]**
The PSD of a material can be important in understanding its physical and chemical properties. It affects the strength and load-bearing properties of rocks and soils. It affects the reactivity of solids participating in chemical reactions, and needs to be tightly controlled in many industrial products such as the manufacture of printer toner and cosmetics.

The way PSD is usually defined is by the method by which it is determined. The most easily understood method of determination is **sieve analysis,** where powder is separated on sieves of different sizes. Thus, the PSD is defined in terms of discrete size ranges: e.g. "% of sample between 45 μm and 53 μm", when sieves of these sizes are used. The PSD is usually determined over a list of size ranges that covers nearly all the sizes present in the sample. Some methods of determination allow much narrower size ranges to be defined than can be obtained by use of sieves, and are applicable to particle sizes outside the range available in sieves. However, the idea of the notional "sieve", that "retains" particles above a certain size, and "passes" particles below that size, is universally used in presenting PSD data of all kinds.

One of the most important types of analytical work associated with producing resources and wares with desired properties, is particle size, shape, and distribution analysis. **[3]**
Sieving, microscopy, computerized image analysis, laser diffraction, sedimentation, and centrifugation, are some of the particle size analysis methods by which a samples particle characterization may be established.
The method one employs, has to do with the nature of the sample, ie...liquid or solid, the size range of the particles to be analyzed, the relevance of the results to the finished product properties, and cost. For some applications, like certain pharmaceuticals, particle shape characteristics may also have a bearing on the outcome of the finished good.
The use of sieves with different sized mesh is one of the oldest, most reliable, and most commonly used methods for providing an analysis of particle size distribution.

Although sieve shakers have limitations based on the assumption that all particles are spherical, they work well for a wide variety of applications, and because it is relatively inexpensive, is generally the first method employed by companies when a particle size distribution analysis program is initiated**. [3]**

A sieve analysis consists of using a single or set of screens (typically woven wire mesh), decreasing in opening size, to separate or classify a sample. Several mechanisms are used to disperse the sample and transport it through the screens (i.e. vibration, air entrainment or flowing liquid). While considered relatively low resolution, sieving's practical application lends itself well to quality control specifications. ASTM E-11 establishes acceptance criteria for the woven wire mesh opening tolerances of standard sieve sizes. For optimal quality control, PTL verifies its in-house sieves with an external vendor for compliance with the ASTM E-11. **[4]**

While sieving may appear rudimentary compared to more modern instrumental particle characterization techniques, it still requires several important considerations to obtain the best repeatable and precise results. Several factors must be considered when developing a robust sieving method or performing a routine quality analysis. Sample size, sieving duration, controlled agitation parameters and end point determination are all critical method variables which need to be addressed.

The vibrating sieve shaker applies the principle of electromagnetic induction. When the particles are characterized, the products are useful as a raw material or consumption purposes. Many dependent variables are considered in this work and the effectiveness of each of them contributes to the overall efficiency. Such dependent variables are the amplitude of vibration, voltage variation which is a function of magnetic flux density, the mass of product collected and the resident time for the sieving. The effectiveness of the designed sieve will help in particle separation in local industries, especially cassava (garri) processing industries.

The test sieve shakers electromagnetic design offers many equipment – feature benefit compared with manual motor driven units. The electromagnetic shaker combines sharp, vertical motion with rotary motion at 3,600 vibrations per minutes for optimum performance. This high speed straight to line vibratory actions minimizes particle detention, provide faster particle separation with improved accuracy and assure uniform particle size distribution. Electromagnetic drives also assure outstanding durability with virtually no maintenance or part replacement. There are no motor for overheat or burn out, no belt, gears, pulley or other moving components to wear and lubrication is not required. Operation is simple. The operator places the nested sieve on the top sieve and pushes the handle down to lock the sieve in position. The unit preset timer is actuated to test the material sample. The time control devices guarantees uniformly – timed sample analysis. A rheostat control can be set to a fixed voltage value to assure a consistence analysis of the design and operation noise level conform with standard. Test sieve shakers are compact, light weight. Each sieve shakers hold about six - eight – inch diameter standard screen full height testing sieves and a bottom pan, or twelve half height sieves and bottom pan Units operates at 230 volts, 50Hz single phase ac.

1.2 Mathematical models

Probability distributions

- The **log-normal distribution** is often used to approximate the particle size distribution of aerosols, aquatic particles and pulverized material.
- The **Weibull distribution** or Rosin Rammler distribution is a useful distribution for representing particle size distributions generated by grinding, milling and crushing operations.
- The **log-hyperbolic distribution** was proposed by Bagnold and Barndorff-Nielsen**[5]** to model the particle-size distribution of naturally occurring sediments. This model suffers from having non-unique solutions for a range of probability coefficients.
- The **skew log-Laplace model** was proposed by Fieller, Gilbertson and Olbricht **[6]** as a simpler alternative to the log-hyperbolic distribution.

Rosin-Rammler distribution

The Weibull distribution, now named for Waloddi Weibull was first identified by Fréchet (1927) and first applied by Rosin & Rammler (1933) to describe particle size distributions. It is still widely used in mineral processing to describe particle size distributions in comminution processes.

$$f(x; P_{80}, m) = \begin{cases} 1 - e^{ln(0.2)\left(\frac{x}{P_{80}}\right)^m} & x \geq 0, \\ 0 & x < 0, \end{cases}$$

where

x: Particle size

P_{80}: 80th percentile of the particle size distribution

m: Parameter describing the spread of the distribution
The inverse distribution is given by:

$$f(F; P_{80}, m) = \begin{cases} P_{80} \sqrt[m]{\frac{ln(1-F)}{ln(0.2)}} & F > 0, \\ 0 & F \leq 0, \end{cases}$$

where
F: Mass fraction

Parameter estimation

The parameters of the Rosin-Rammler distribution can be determined by refactoring the distribution function to the form**[7]**

$$\ln\left(-\ln\left(1-F\right)\right) = m\ln(x) + \ln\left(\frac{-\ln(0.2)}{(P_{80})^m}\right)$$

Hence the slope of the line in a plot of
$\ln\left(-\ln\left(1-F\right)\right)$ versus $\ln(x)$
yields the parameter m and P_{80} is determined by substitution into

$$P_{80} = \left(\frac{-\ln(0.2)}{e^{intercept}}\right)^{\frac{1}{m}}$$

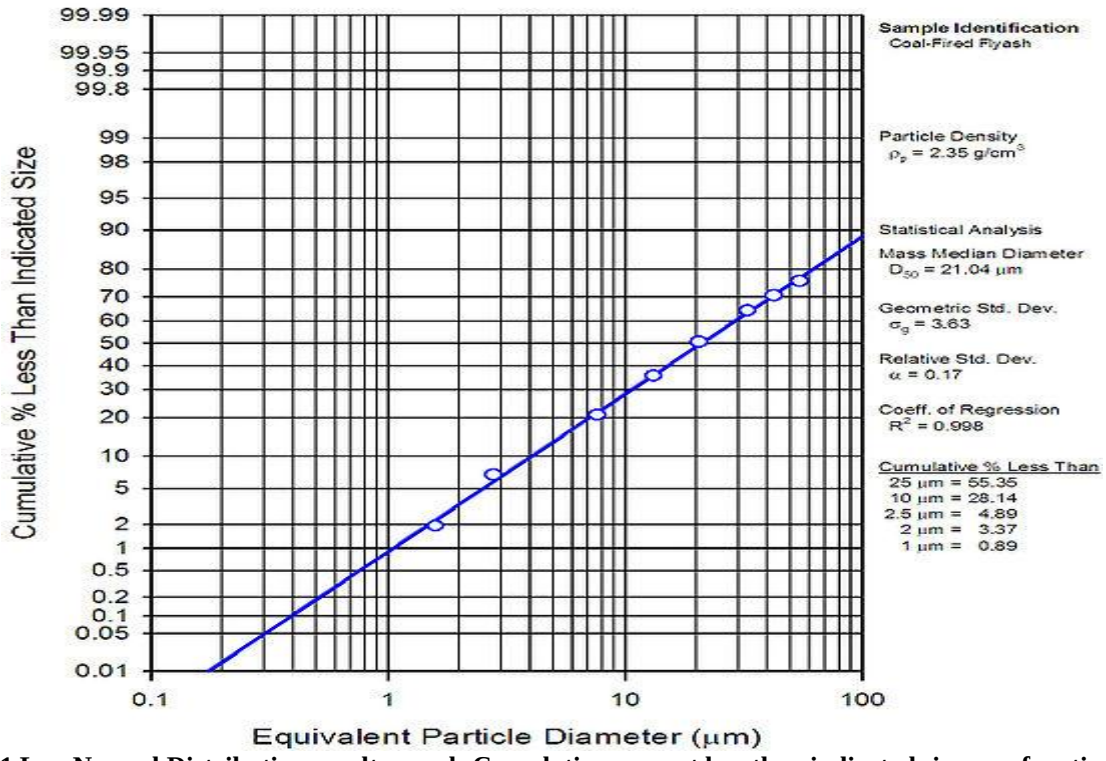

Fig.1 Log-Normal Distribution results graph-Cumulative percent less than indicated size as a function of particle size. [8]

II. MATERIALS AND METHODS

2.1 Sample Collection:

Cassava tubers are harvested wet, pealed and ground in the grinding machine. It is partially dried using the screw jack. The product "garri" is then fried in the frying pan and ready for consumption. But sometimes, it becomes difficult for consumption or other useful purposes due to sizes of the grain. The designed sieves however, solved a problem of difficulty posed by large sizes of the particles. The grading process using the electromagnetic sieve provides better particle sizes of the product that are exportable to other countries of the world.

2.2 – Equipment/Material used for Experiment

1. One Kilogram (1000g) of fried "garri" sample
2. A stop watch
3. A locally fabricated electromagnetic sieving machine.
4. Sieves
5. Voltage regulator (digital meter)
6. Springs

2.3: Experimental Procedures

1 kg (1000g) sample of "garri" was weighed using the weighing balance. The designed electromagnetic sieve was connected to the electric mains and voltage was adjusted with the regulator to read 235 volts. The sieve agitated as the voltage is varied and a stop watch is set to measure the time for a complete sieving. Different aggregate of "garri" particle sizes were collected on each sieve and weighed. The procedure was repeated with the voltage varied at 245, 255 and 265 volts. The corresponding time (seconds) for each experiment was noted. The particles sizes were also recorded and evaluated using the electronic microscope.

III. RESULTS

The result shows that the designed sieve is capable of grading the product "garri" at different aggregates. The mass of "garri" on each sieve was noted at different voltage variation in a particular time intervals. The results are tabulated below.

Table 1 Voltage Varied at 235 Volts: Time for sieving – 230 seconds

Mesh Nos	Weight of Mesh (Kg)	Weight of Mesh + Weight of Garri(Kg)	Weight of Garri(Kg)-Product	Particle Size (µ)
1	0.380	0.440	0.120	>18µm
2	0.480	0.770	0.290	18µm
3	0.480	0.720	0.240	24µm
4	0.680	1.020	0.340	30µm

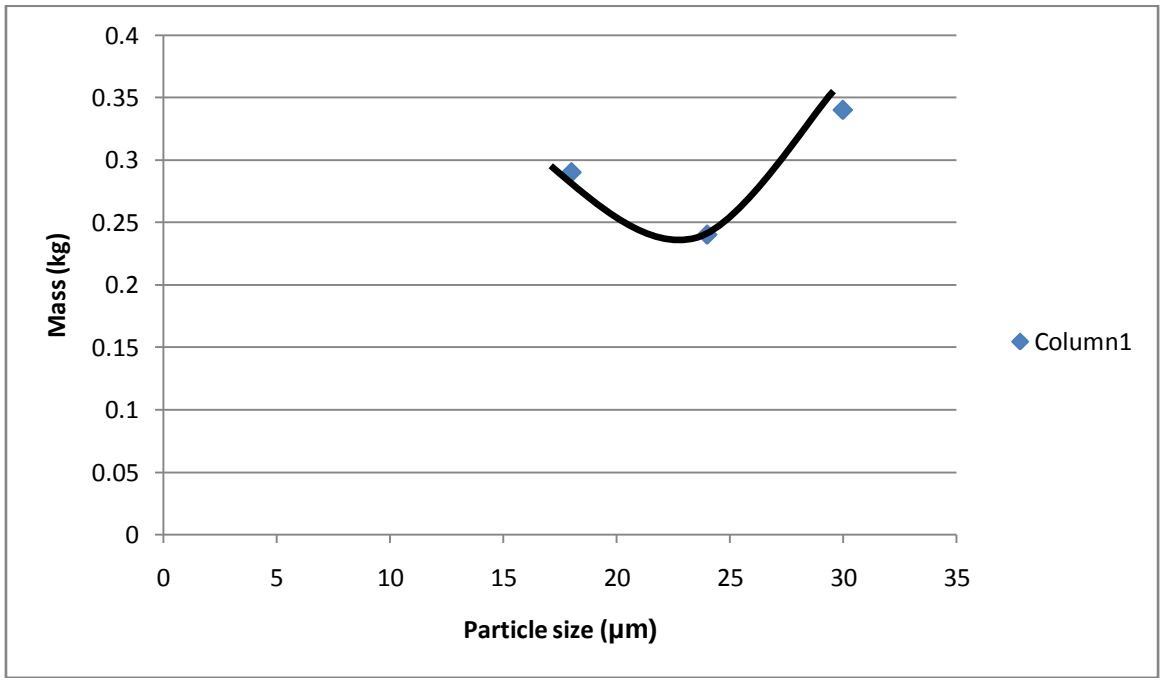

Fig 2: Graph of mass Vs Particle size for 235volts

.Table 2 Voltage varied at 245Volts. Time of sieving – 180seconds

Mesh Nos	Weight of Mesh (Kg)	Weight of Mesh + Weight of Garri(Kg)	Weight of Garri(Kg)- Product Y	Particle Size (µ)
1	0.380	0.420	0.040	>18µm
2	0.480	0.780	0.300	18µm
3	0.480	0.640	0.260	24µm
4	0.680	1.060	0.380	30µm

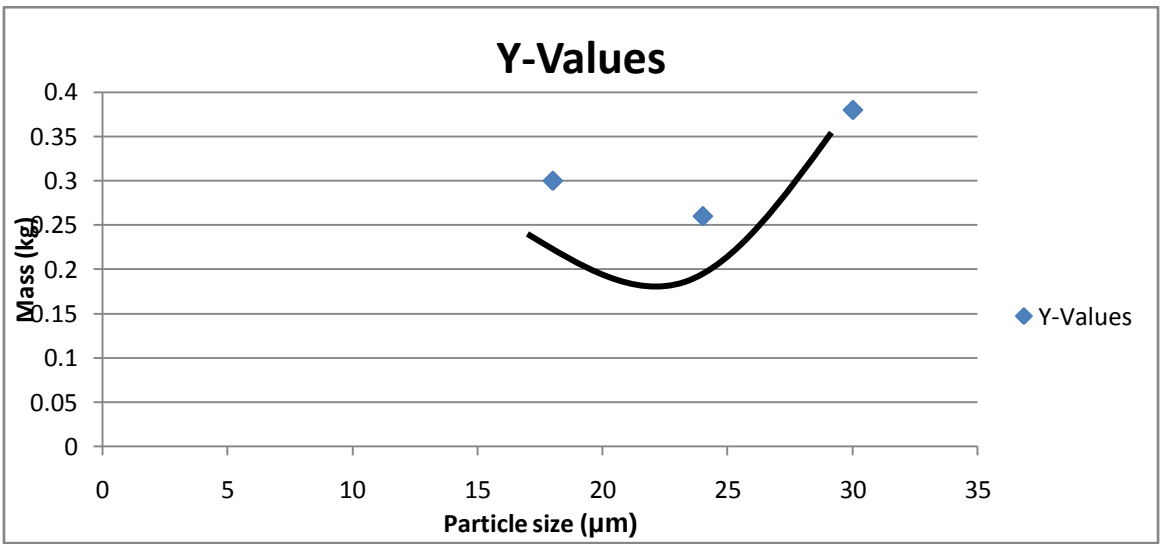

Fig 3: Graph of mass Vs Particle size for 245 volts

Table 3.Voltage varied at 255Volts. Time of sieving – 120 seconds

Mesh Nos	Weight of Mesh (Kg)	Weight of Mesh + Weight of Garri(Kg)	Weight of Garri(Kg)- Product Y	Particle Size (µ)
1	0.380	0.390	0.010	>18µm
2	0.480	0.780	0.300	18µm
3	0.480	0.760	0.280	24µm
4	0.680	1.080	0.400	30µm

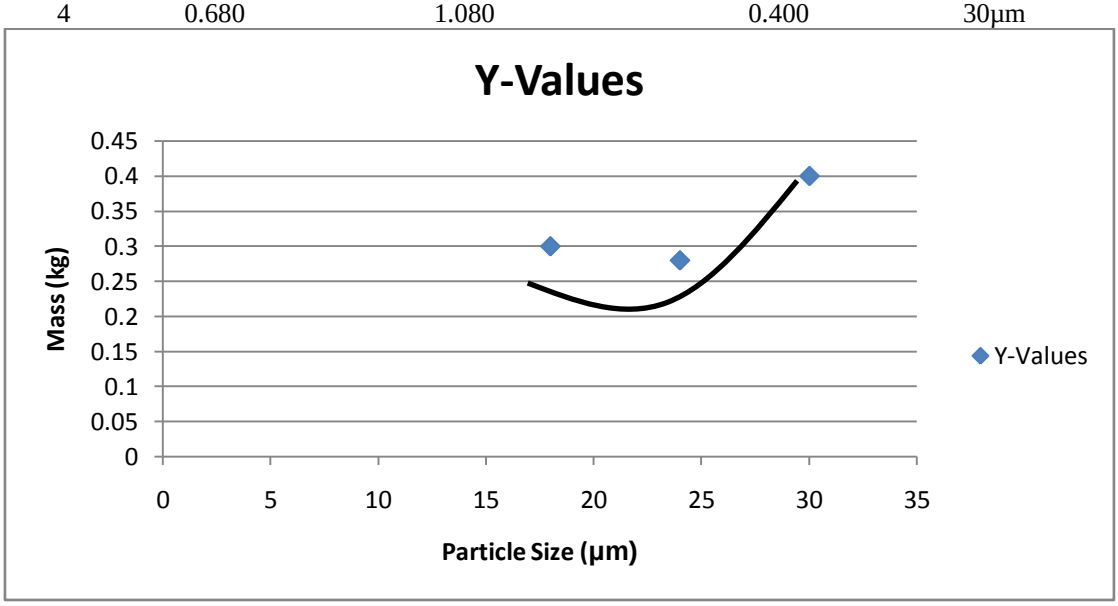

Fig 4 Graph of mass Vs Particle size for 255 volts

Table 4: Variation of voltage with time.

Voltage (Volts)	Time (Seconds)
235	230
245	180
255	120
265	90

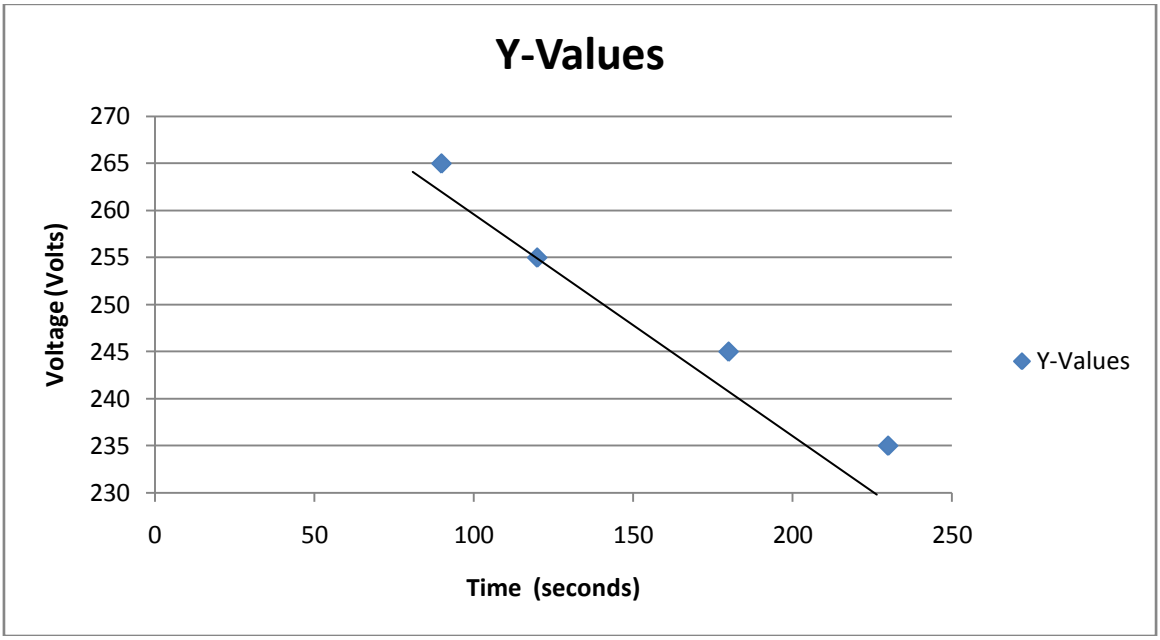

Fig 5: Graph of Voltage Vs time.

Table 5 Variation of average mass collected with time

Voltage (Volts)	Average mass(Kg)	Time (Seconds)
235	0.290	230
245	0.313	180
255	0.326	120

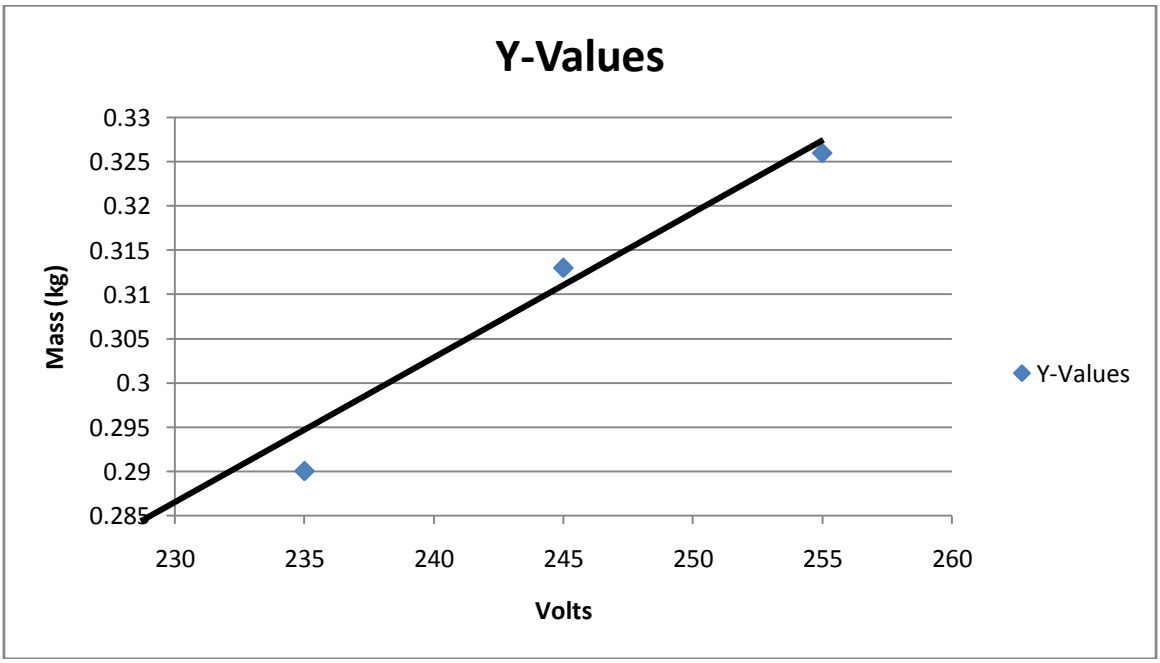

Fig 6 Graph of average mass Vs voltage

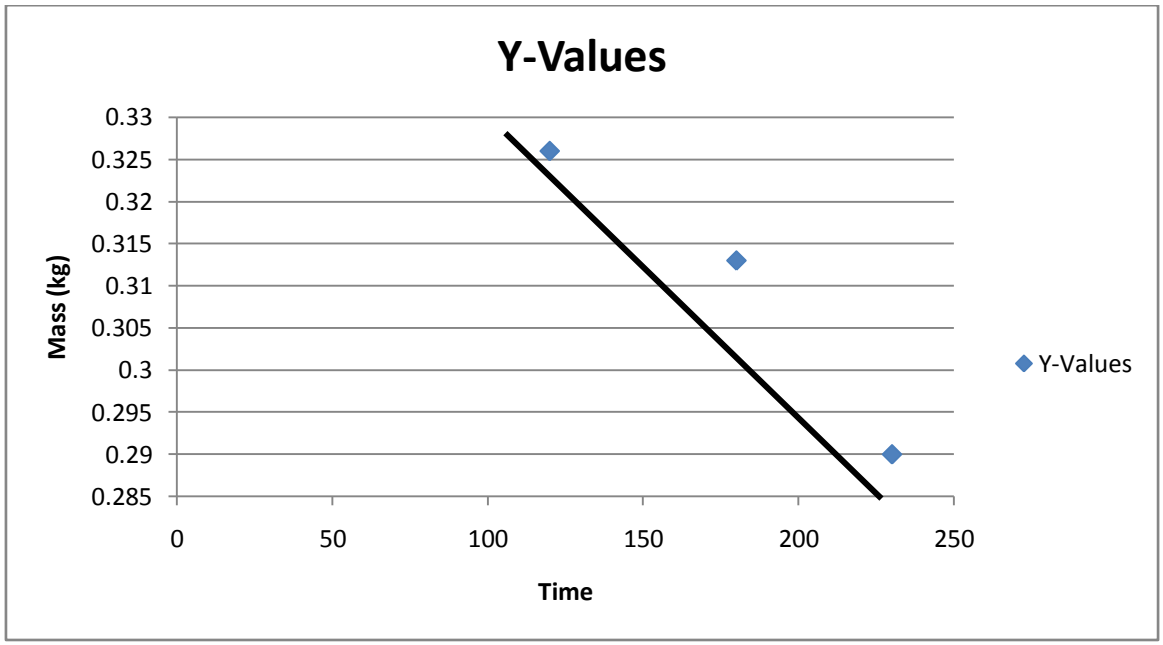

Fig 7: Graph of average mass Vs time at 255 volts.

IV. DISCUSSIONS

The designed electromagnetic sieve was operated with a combined action of electricity and magnetism. The shaking principle was also achieved with the help of spring (amplitude) displacement due to the increased magnetic flux existing between the air gap.

Fig. 2 indicates that there is an increase in mass collected at the sieves as the particle size decreases except in the second set of sieve when the voltage was varied at 235Volts. The decrease in mass at the second sieve can be attributed to the uneven distribution of the agitation.

Fig.3 indicates that there is an increase in mass collected at the sieves as the particle size decreases except in the second set of sieve as the voltage was varied at 245Volts. The decrease in mass at the second sieve may also be attributed to poor agitation at the middle sieve. There was also an increase in mass collected at the bottom due to the direct flux.

Fig.4 indicates that there is an increase in mass collected at the sieves as the particle size decreases except in the second set of sieve as usual. Here the voltage is varied at 255Volts and highest separation was achieved. This is known as the peak voltage. The decrease in mass at the second sieve may also be attributed to poor agitation.

Fig.5 indicates that as the voltage increases, the time of sieving decreases proportionally. This is as a result of increase in amplitude.

Fig.6 shows that mass collected from the sieves increases as the voltage increases.

The result shows that the designed sieve is capable of grading the product "garri" into different aggregates. The mass of "garri" on each sieve is noted at different voltage variation in a particular time intervals. It was observed that with increase in voltage sieving time was reduced.

V. CONCLUSION

Many natural and manufactured materials occur in a diverse form, which means that they consist of differently shaped and sized particles. The particle size distribution is responsible for important physical and chemical properties such as: Mechanical bulk behavior, Surface reaction, Taste, Miscibility, Filtration properties, Conductivity.

If the particle distribution changes during the manufacturing process then the quality of the finished product will also change. Only a continuous monitoring of the particle size distribution can guarantee a constant product quality.

The designed "Throw action" type utilizes the electromagnetic induction at varied voltages. The vertical oscillation is used to determine the amplitude of the vibration and hence maximum sample collected per sieve. The sieve is capable of handling up to one kilogramme (1000g) of garri sample at a batch. The three grades of particle sizes collected (30µm, 24µm and 18µm) are exportable to other countries of the world if labeled accordingly.

The result show that increased voltage gives a maximum collection of finest particle at a smallest resident time. The amplitude of the vibration and mass of the sieved samples, also increases as the voltage increases. But as the voltage increase arbitrarily, the mass of the finest particle decreases because the electromagnetic energy are not all converted to electromechanical energy. Therefore, several losses are encountered. The particle sizes collected at the different sieves was evaluated using an electronic microscope.

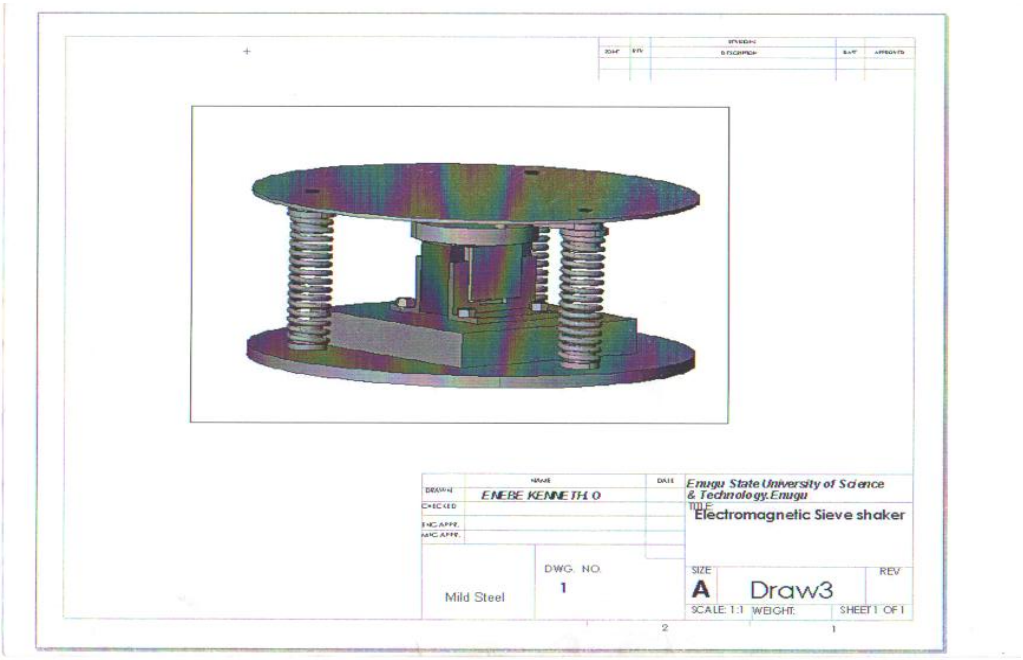

Fig. 8 Constructed electromagnetic sieve shaker

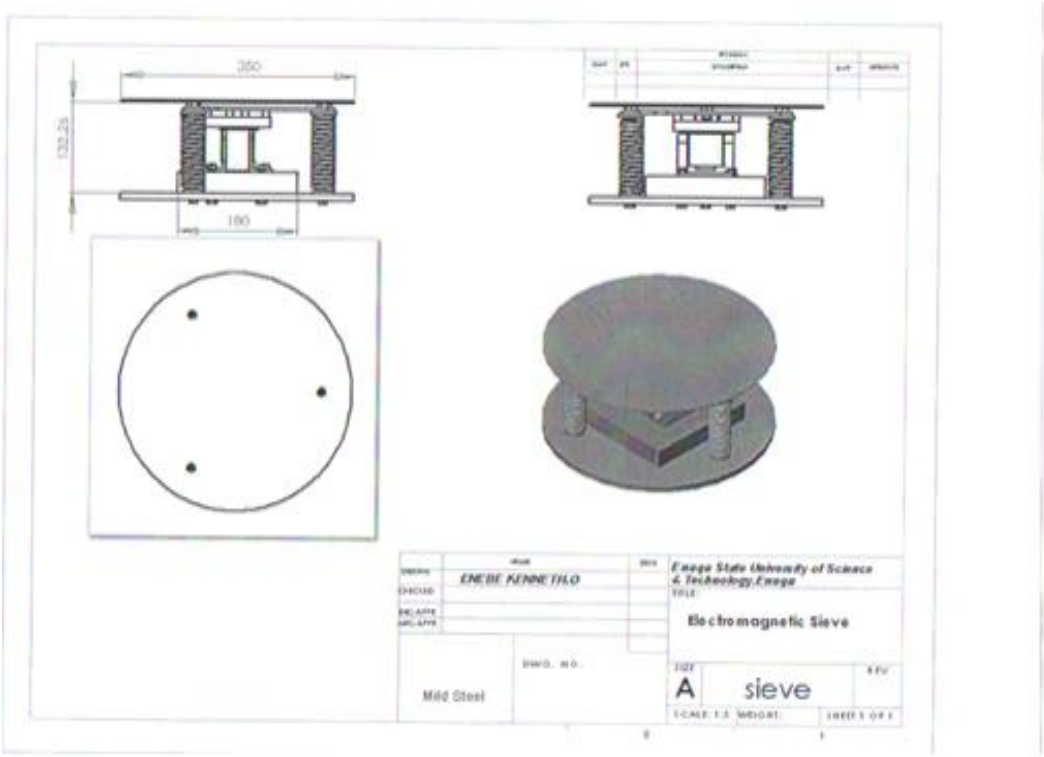

Fig.9 Views of the electromagnetic sieve shaker

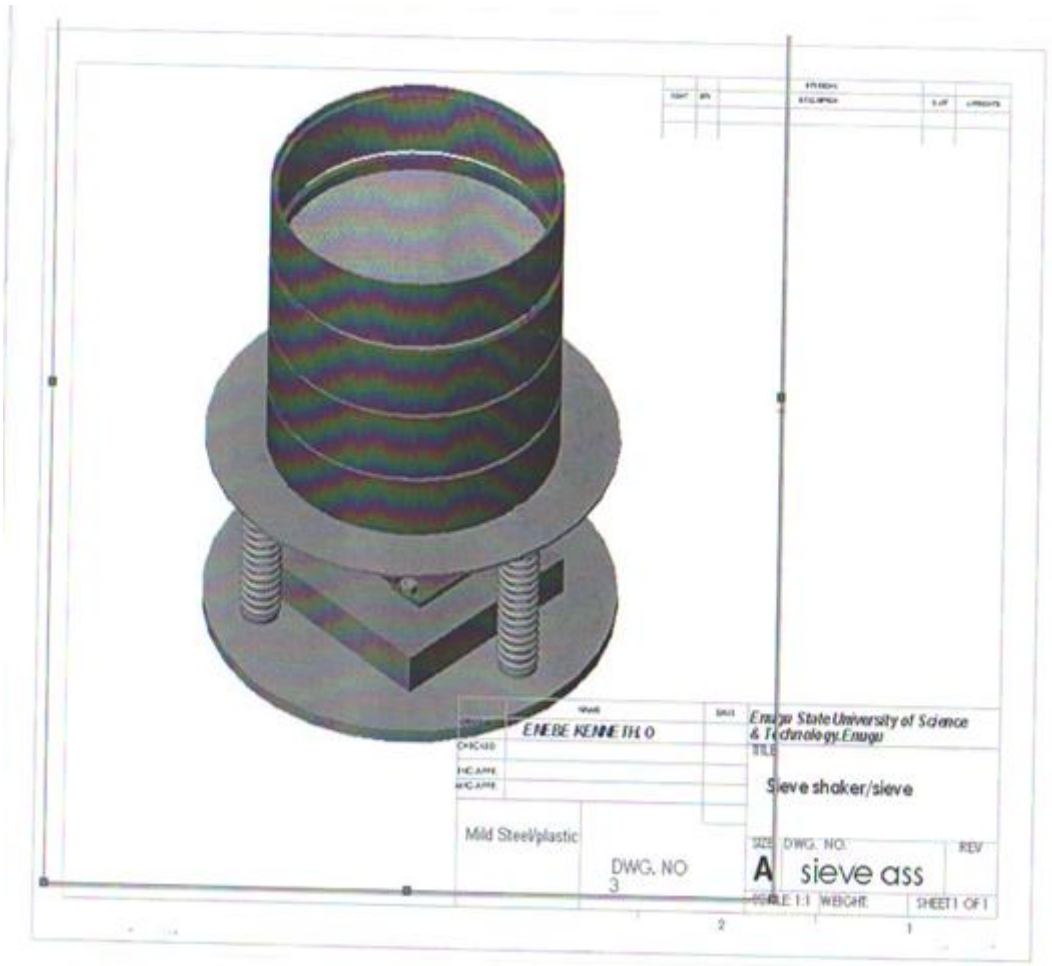

Fig.10. Assembled Sieve and Shaker

REFERENCES

[1] Jillavenkatesa, A; Dakpunas, S. J and Lin-Sien Lum (2001), **"Particle Size Characterization"**, NIST Special Publication, 960-1.

[2] Sivakugan, N. (2000), **"Soil Classification"**, James Cook University Geoengineering Lecture Handout www.coffeelabequipment.com (2013), **"Particle Size Analysis"**

[3] www.advantechmfg.com (1995), **"Principles and Procedures-manual with tables 2",**

[4] ASTM E11-04

[5] Bagnold, R. A and Barndoff-Nelson, O. (1980) **"The Pattern of natural distribution**", Sedimentology 27 (2); 199:207

[6] Fieller, N. R; Gilbertson, D. D and Olbricht, W. (1984), **"A new method of environmental analysis of particle size distribution data from shoreline sediments"**, Nature 311 (5987): 648-651.

[7] Wills, B. A and Napier-Munn. (2006), **"Mineral Processing Technology: an introduction to the practical aspects of ore treatment and mineral recovery"**, Elsevier, Great Britain, 7th Ed.

[8] www.wikipedia.org/wiki/user:Rhoades500. (2009), "Particle size distribution.

American Journal of Engineering Research (AJER)
e-ISSN : 2320-0847 p-ISSN : 2320-0936
Volume-02, Issue-10, pp-86-91
www.ajer.org

Research Paper Open Access

Common Fixed Point Theorems for Sequence Of Mappings Under Contractive Conditions In Symmetric Spaces

T.R.Vijayan,
Department of Mathematics, Pavai College of Technology, Namakkal - 637018, India.

Abstract: - The main purpose of this paper is to obtain common fixed point theorems for sequence of mappings under contractive conditions which generalizes theorem of Aamri [1].

Keywords And Phrases: *- Fixed point, Coincidence point, Compatible maps, weakly compatible maps, NonCompatible maps Property (E.A).*

I. INTRODUCTION

It is well known that the Banach contraction principle is a fundamental result in fixed point theory, which has been used and extended in many different directions. Hicks [2] established some common fixed point theorems in symmetric spaces and proved that very general probabilistic structures admit a compatible symmetric or semi-metric. Recall that a symmetric on a set X is a nonnegative real valued function d on X × X such that (i) d(x, y) = 0 if, and only if, x = y, and (ii) d(x, y) = d(y, x). Let d be a symmetric on a set X and for r > 0 and any x ∈ X, let B(x, r) ={y ∈ X: d(x, y) < r}. A topology t (d) on X is given by U ∈ t (d) if, and only if, for each x ∈ U, B(x, r) ⊂ U for some r > 0. A symmetric d is a semi-metric if for each x ∈ X and each r > 0, B(x, r) is a neighbourhood of x in the topology t(d). Note that $\lim_{n\to\infty} d(x_n, x) = 0$ if and only if $x_n \to x$ in the topology t (d).

II. PRELIMINARIES

Before proving our results, we need the following definitions and known results in this sequel.

Definition 2.1([3]) let (X, d) be a symmetric space. (W.3) Given $\{x_n\}$, x and y in X, $\lim_{n\to\infty} d(x_n, x) = 0$ and $\lim_{n\to\infty} d(x_n, y) = 0$ imply x = y. (W.4) Given $\{x_n\}$, $\{y_n\}$ and x in X $\lim_{n\to\infty} d(x_n, x) = 0$ and $\lim_{n\to\infty} d(x_n, y_n) = 0$ imply that $\lim_{n\to\infty} d(y_n, x) = 0$.

Definition 2.2([4]) Two self mappings A and B of a metric space (X, d) are said to be weakly commuting if $d(AB_x, BA_x) \leq d(A_x, B_x)$, ∀x ∈ X.

Definition 2.3([5]) Let A and B be two self mappings of a metric space (X, d). A and B are said to be compatible if $\lim_{n\to\infty} d(ABx_n, BAx_n) = 0$, whenever (x_n) is a sequence in X such that $\lim_{n\to\infty} Ax_n = \lim_{n\to\infty} Bx_n = t$ for some t ∈ X.

Remark 2.4. Two weakly commuting mappings are compatibles but the converse is not true as is shown in [5].

Definition 2.5 ([5]) Two self mapping T and S of a metric space X are said to be weakly compatible if they commute at there coincidence points, i.e., if $T_u = S_u$ for some u ∈ X, then $TS_u = ST_u$.

Note 2.6. Two compatible maps are weakly compatible. M. Aamri [6] introduced the concept property (E.A) in the following way.

Definition 2.7 ([6]). Let S and T be two self mappings of a metric space (X, d). We say that T and S satisfy the property (E.A) if there exists a sequence $\{x_n\}$ such that $\lim_{n\to\infty} Tx_n = \lim_{n\to\infty} Sx_n = t$ for some t ∈ X.

Definition 2.8 ([6]). Two self mappings S and T of a metric space (X, d) will be non-compatible if there exists at least one sequence $\{x_n\}$ in X such that if $\lim_{n\to\infty} d(STx_n, TSx_n)$ is either nonzero or non-existent.

Remark 2.9. Two noncompatible self mappings of a metric space (X, d) satisfy the property (E.A).

In the sequel, we need a function φ: $IR^+ \to IR^+$ satisfying the condition $0 < \varphi(t) < t$ for each t > 0.

Definition 2.10. Let A and B be two self mappings of a symmetric space (X, d).A and B are said to be compatible if $\lim_{n\to\infty} d(ABx_n, BAx_n) = 0$ whenever (x_n) is a sequence in X such that $\lim_{n\to\infty} d(Ax_n, t) = \lim_{n\to\infty} d(Bx_n, t) = 0$ for some t ∈ X.

Definition 2.11. Two self mappings A and B of a symmetric space (X, d) are said to be weakly compatible if they commute at their coincidence points.

Definition 2.12. Let A and B be two self mappings of a symmetric space (X, d). We say that A and B satisfy the property (E.A) if there exists a sequence (x_n) such that $\lim_{n\to\infty} d(Ax_n, t) = \lim_{n\to\infty} d(Bx_n, t) = 0$ for some t ∈ X.

Remark 2.13. It is clear from the above Definition 2.10, that two self mappings S and T of a symmetric space (X, d) will be noncompatible if there exists at least one sequence (x_n) in X such that $\lim_{n\to\infty} d(Sx_n, t) = \lim_{n\to\infty} d(Tx_n, t) = 0$ for some t ∈ X. but $\lim_{n\to\infty} d(STx_n, TSx_n)$ is either non-zero or does not exist. Therefore, two noncompatible self mappings of a symmetric space (X, d) satisfy the property (E.A).

Definition 2.14. Let (X, d) be a symmetric space. We say that (X, d) satisfies the property (H_E) if given $\{x_n\}$, $\{y_n\}$ and x in X, and $\lim_{n\to\infty} d(x_n, x) = 0$ *and* $\lim_{n\to\infty} d(y_n, x) = 0$ imply $\lim_{n\to\infty} d(y_n, x_n) = 0$

Note that (X,d) is not a metric space.

Aamri [1] prove the following theorems.

Theorem 2.15 (Aamri [1]). Let d be a symmetric for X that satisfies (W.3) and (H_E). Let A and B be two weakly compatible self mappings of (X, d) such that (1) $d(A_x,A_y) \le \varphi(\max\{d(B_x,B_y), d(B_x,A_y), d(A_y,B_y)\})$ for all (x, y) ∈ X^2, (2) A and B satisfy the property (E.A), and (3) AX ⊂ BX. If the range of A or B is a complete subspace of X, then A and B have a unique common fixed point.

Theorem 2.16 (Aamri [1]). Let d be a symmetric for X that satisfies (W.3), (W.4) and (H_E). Let A, B, T and S be self mappings of (X, d) such that (1) $d(A_x,B_y) \le \varphi(\max\{d(S_x, T_y), d(S_x,B_y), d(T_y,B_y)\})$ for all (x, y) ∈ X^2,
(2) (A, T) and (B,S) are weakly compatibles, (3) (A, S) or (B, T) satisfies the property (E.A), and
(4) AX ⊂ TX and BX ⊂ SX. If the range of the one of the mappings A, B, T or S is a complete subspace of X, then A, B, T and S have a unique common fixed point.

III. MAIN RESULTS

In this section we prove common fixed point theorem for sequence of mappings that generalizes Theorem 2.16.

Theorem 3.1. Let d be a symmetric for X that satisfies (W.3) (W.4) and (H_E). Let $\{A_i\}$, $\{A_j\}$, S and T be self maps of a metric space (X, d) such that
(1) $d(A_ix,A_jy) < \max\{d(S_xT_y), d(A_ix,S_x), d(A_jy,T_y), d(A_ix,T_y), d(A_jy, S_x)\}$ for all $(x,y) \in X^2, (i\neq j)$,
(2) (A_i,S) or (A_k,T) are weakly compatibles. (3) (A_i, S) or (A_jT) ,$(i\neq j)$ satisfies the property(E.A) and
(4) $A_iX \subset TX$ and $A_jX \subset SX$ for $(i\neq j)$
If the range of the one of the mappings $\{A_i\}$, $\{A_j\}$, S or T is a complete subspace of X,
then (I) A_i and S have a common fixed point, ∀ i (II) A_j,$(i\neq j)$ and T have a common fixed point provided that (A_k, T) for some k > 1 is weakly compatible. (III) A_i,A_j, S $(i\neq j)$ and T have a unique common fixed point provided that (I) and (II) are true.

Proof. Suppose that (A_j,T) $(i\neq j)$ satisfies the property (E.A.).
=>There exists a sequence $\{x_n\}$ in X such that $\lim_{n\to\infty} d(A_J x_n, t) = \lim_{n\to\infty} d(Tx_n, t) = 0$ for $(i\neq j)$ and for some t∈X. Since $A_jX \subset SX$ $(i\neq j)$, there exists a sequence $\{y_n\}$ in X such that $A_jx_n = Sy_n$.
Hence, $\lim_{n\to\infty} d(Sy_n, t) = 0$ $(\text{since}, \lim_{n\to\infty} d(A_j x_n, t) = 0)$
Let us prove that $\lim_{n\to\infty} d(A_i y_n, t) = 0$
It is enough to prove that $A_iy_n = A_jx_n$, $(i\neq j)$ and for sufficiently large n.
Suppose not, then using (1)
$d(A_iy_n,A_jx_n) < \max\{d(Sy_n,Tx_n), d(A_iy_n,Sy_n), d(A_jx_n,Tx_n), d(A_iy_n,Tx_n), d(A_jx_n,Sy_n)\}$ for all $(x,y) \in X^2$, $(i\neq j)$
$d(A_iy_n,A_jx_n) < \max\{d(A_jx_n,Tx_n), d(A_iy_n,A_jx_n), d(A_jx_n,Tx_n), d(A_iy_n,Tx_n)\}$ for all $(x,y) \in X^2$,$(i\neq j)$,
For sufficiently large n, { since, $A_jx_n=Sy_n$}
$d(A_iy_n,A_jx_n) < \max\{d(A_iy_n,A_jx_n), d(A_iy_n,A_jx_n)\} < d(A_iy_n,A_jx_n)$ {Since, $A_jx_n = Tx_n$ as n→∞}(By H_E)
=><= $A_iy_n \neq A_jx_n$ for $(i\neq j)$
$\lim_{n\to\infty} d(A_iy_n,A_jx_n)=0$ By(W.2),we deduce that $\lim_{n\to\infty} d(A_iy_n, t)=0$.
Suppose SX is a complete subspace of X.Then t = Su for some u∈X.
Therefore, $\lim_{n\to\infty} d(A_iy_n, S_u) = \lim_{n\to\infty} d(A_jx_n, S_u) = \lim_{n\to\infty} d(Tx_n,S_u)$
$= \lim_{n\to\infty} d(Sy_n,S_u)=0$ $(i\neq j)$
Using (1),it follows $d(A_iu,A_jx_n) < \max\{d(S_u,Tx_n), d(A_iu,S_u), d(A_jx_n,Tx_n), d(A_iu,Tx_n), d(A_jx_n,S_u)\}$ for sufficiently large n, $(i\neq j)$
$d(A_iu,S_u) < \max\{d(A_iu,S_u), d(A_iu,S_u)\}(i\neq j)$,
$<d(A_iu,S_u)$ ∀ i =><= when $A_iu\neq S_u$ ∀ i
Therefore, $A_iu=S_u$ ∀ i
This means that A_i and S have coincidence point. But (A_i, S) ∀ i is weakly compatible.

$SA_iu = A_iS_u \ \forall$ i and then $A_iA_iu = A_iS_u = SA_iu = SS_u. \ \forall$ i
Suppose $A_iX \subset TX \ \forall$ i
=>There exists $v \in X$ such that $A_iu=T_v \ \forall$ i
=> $A_iu=S_u=T_v \ \forall$ i
To prove that $T_v= A_jv$, (i≠j)
Suppose $T_v \neq A_jv$,then
(1)=> $d(A_iu,A_jv) < \max\{d(S_u,T_v), d(A_iu, S_u), d(A_jv,T_v), d(A_iu,T_v), d(A_jv,S_u)\}$
$= \max\{d(T_v,T_v), d(S_u, S_u), d(A_jv,T_v), d(T_v,T_v), d(A_jv,T_v)\}$ (i≠j)
$= \max\{d(A_jv,T_v), d(A_jv,T_v)\}$ (i≠j)
$= d(A_jv,T_v) = d(A_jv,A_iu)$, (i≠j)
Therefore $(A_iu,A_jv)<d(A_jv,A_iu)$ (i≠j)
=><= Therefore $A_iu=A_jv$ (i≠j)
=>$A_jv=A_iu=T_v$ Therefore,$A_jv=T_v$ for i≠j
=>$A_iu=S_u=T_v=A_jv$, i≠j
But (A_k,T) is weakly compatible for some k>1
$A_kT_v=TA_kv$ for some k>1 and $TT_v=TA_kv=A_kT_v=A_kA_kv$, for some k>1
We shall prove that A_iu is a common fixed point of A_i and S $\forall$ i
Suppose $A_iu \neq A_iA_iu \ \forall$ i
$d(A_iu,A_iA_iu) = d(A_jv,A_iA_iu)$ (since, $A_jv=A_iu$) (i≠j)
$d(A_iA_iu,A_jv) < \max\{d(SA_iu,T_v), d(A_iA_iu, SA_iu), d(A_jv,T_v), d(A_iA_iu,T_v), d(A_jv,SA_iu)\}$ (i≠j)
$= \max\{d(A_iA_iu,A_jv), 0,0, d(A_iA_iu,A_jv), d(A_jv,A_iA_iu)\}$ (i≠j)
$= d(A_iA_iu,A_jv)$ Therefore, $d(A_jv,A_iA_iu) < d(A_iA_iu\ A_jv)$
=><=
Therefore, $A_iA_iu =A_jv$ (i≠j)
=> $A_iA_iu =A_iu=SA_iu$ (since, $A_iA_iu =SA_iu$)
=> A_iu is a common fixed point of A_i and S. $\forall$ i This proves (I).
To prove that $A_kv = A_iu$ for some k>1 is a common fixed point of A_j (i≠j) and T
Suppose $A_kv \neq A_jA_kv$, then
$d(A_kv,A_jA_kv) = d(A_iu,A_jA_kv)$
$< \max\{d(S_u,TA_kv), d(A_iu,S_u), d(A_jA_kv ,TA_kv), d(A_iu,TA_kv), d(A_jA_kv,S_u)\}$
$= \max\{d(A_iu,A_jA_kv),0, d(A_jA_kv,A_jA_kv), d(A_iu, A_jA_kv), d(A_jA_kv\ A_iu)\}$ (since,$A_jv=T_v$)
$= \max\{d(A_iu,A_jA_kv),0,0, d(A_iu, A_jA_kv), d(A_jA_kv ,A_iu)\}$
Therefore, $d(A_kv,A_jA_kv) < d(A_iu,A_jA_kv)$.
=><= (since,$A_iu=A_kv$)
Therefore, $A_iu=A_jA_kv$ ie., $A_kv=A_jA_kv=TA_kv$ (since,$A_jv=T_v$)
=>A_kv is the common fixed point of A_j and T. This proves (II)
Now,A_iu is a common fixed point of A_i and S. $\forall$ i
$A_kv=A_iu$ is the common fixed point of $A_j$and T for i≠j
Therefore, A_iu is the common fixed point of A_j,Tand S for all j (i≠j)
The proof is similar when TX is assumed to be complete subspace of X.
The cases in which A_iX or A_jX (i ≠j) is a complete subspace of X are similar to
the cases in which SX or TX respectively is a complete space because $A_iX \subset TX$ and $A_jX \subset SX$ (i≠j).
Uniqueness. Suppose u, v are two fixed points of A_i, A_j (i≠j), TandS.
Then $A_iu = S_u = A_ju = T_u = u$, (i≠j) and $A_iv = A_jv = T_v = S_v = v$, (i≠j).Then
$d(u,v) = d(A_iu,A_jv)$ (i≠j)
$< \max\{d(S_u,T_v),d(A_iu,S_u), d(A_jv,T_v), d(A_iu,T_v), d(A_jv, S_u)\}$
$= \max\{d(u,v),0,0,d(u,v), d(u,v)\}$
$=d(u,v)$.
Therefore, $d(u,v)=d(u,v)$
==><== when u≠v.
Therefore, u=v.
ie., A_i, A_j,T and S have unique common fixed point for all i and j.
The following result due to Aamri [1] is a special case of the previous theorem 3.1.
Corollary 3.1. Let d be a symmetric for X that satisfies (W.3) (W.4) and (H_E).Let A_1, A_2, S and T be self mappings of a metric space (X,d) such that
(i) $d(A_1x,A_2y) < \max\{d(S_x,T_y), d(A_1x, S_x),d(A_1x,T_y),d(A_2,T_y), d(A_2y,S_x)\}$ for all $(x,y) \in X^2$,
(ii) (A_1, S) and (A_2, T) are weakly compatibles.
(iii)(A_1, S) or (A_2, T) satisfies the property (E.A.) and

(iv) $A_1X \subset TX$ and $A_2X \subset SX$. If the range of one of the mappings A_1, A_2, S or T is a complete subspace of X, then A_1, A_2, S and T have a unique common fixed point.

Proof. The proof of Corollary 3.1 follows from Theorem 3.1 by putting i = 1 and j=2.

Corollary 3.2. Let d be a symmetric for X that satisfies (W. 3), (W.4) of Wilson and (H_E).
Let A, B and T be self mappings of a metric space (X,d) such that
(i)AX, BX ⊂ TX.
(ii) (A, T) is weakly compatible,
(iii) (A,T) or (B,T) satisfies the property (E.A.),
(iv) $d(A_x,B_y) < \max \{d(T_x,T_y),d(A_x,T_x),d(B_y,T_y), d(A_x,T_y),d(B_y,T_x)\}$
If the range of one of the mappings A, B or T is a complete subspace of X, then
(I) A and T have a common fixed point,
(II) B and T have a common fixed point provided that (B, T) is weakly compatible.
(III) A, B, S and T have a unique common fixed point provided that (I) and (II) are true.

Corollary 3.3. .Let d be a symmetric for X that satisfies (W.3),(W.4)and(H_E).Let G, T be self mappings of a metric space (X,d) such that (i) $d(T_x,T_y) \leq \phi(\max\{d(G_x,G_y),$
$d(G_x, T_y),d(G_y,T_y),1/2[d(G_x,T_y)+ d(G_y,T_y)\}$ for all (x,y) ε X^2,
(ii)G and T are weakly compatibles, (iii)T and G satisfy the property (E.A), and
(iv)TX ⊂GX .If the range of one of the mappings G or T is a complete subspace of X,
then G and T have a unique common fixed point.

Corollary 3.4. Let d be a symmetric for X that satisfies (W.1) of Wilson and (H_E).
Let S and T be two weakly compatible self mappings of a metric space (X,d) such that
(i) $d(T_x,T_y) \leq \phi$ $(\max\{d(S_x,S_y),d(S_x,T_y),d(S_y,T_y),1/2[d(S_x,T_y)+d(S_y,T_y)]\}$ for all (x,y) ε X^2,
(ii) Sand T satisfy the property (E.A.) and
(iii) SX ⊂ TX. If the range of S or T is a complete subspace of X, then S and T have a unique common fixed point.

Theorem 3.2. Let d be a symmetric for X that satisfies (W.3),(W.4) and (H_E). Let A, B, T and S be self mappings of a metric space (X,d) such that (i) $d(A_x,B_y) < \alpha\, d(B_y,T_y)\{ [1 + d(A_x ,S_x)]/1 + d(S_x ,T_y)\} + \beta[d(B_y,T_y)+ d(A_x,S_x)]+ \gamma[d(B_y,S_x)+ d(A_x,T_y)]+\delta\, d(S_x,T_y)$ for all (x,y) x∈ X^2 with α, β, γ, δ≥0 and α + β + 2γ + δ < 1 (ii) (A,S) and (B,T) are weakly compatibles. (iii) (A, S) or (B, T) satisfies the property (E.A.) (iv) AX⊂TX and BX⊂SX. If the range of one of the mappings A, B, S or T is a complete subspace of X, then A, B, S and T have a unique common fixed point.

Proof. Suppose (B, T) satisfies the property (E.A). Then there exists a sequence $\{x_n\}$ in X such that $\lim_{n\to\infty} d(Bx_n,t) = \lim_{n\to\infty} d(Tx_n,t) = 0$ for some t ∈ X. Since BX ⊂SX, there exists in X a sequence (y_n) in X such that $Bx_n = Sy_n$. Hence $\lim_{n\to\infty} d(Sy_n,t) = 0$.
Let us show that $\lim_{n\to\infty} d(Ay_n,t) = 0$
It is enough to prove that $Ay_n = Bx_n$. Suppose not, by (1), we get
$d(Ay_n,Bx_n) < \alpha\, d(Bx_n,Tx_n)\{ [1 + d(Ay_n ,Sy_n)]/1 + d(Sy_n ,Tx_n)\}+\beta[d(Bx_nTx_n)+$
$d(Ay_n,Sy_n)]+\gamma[d(Bx_n,Sy_n)+ d(Ay_n,Tx_n)]+\delta\, d(Sy_n,Tx_n)$,
$<\alpha d(Bx_n,Tx_n)\{[1 + d(Ay_n, Bx_n)]/1 + d(Bx_n ,Tx_n)\}+\beta[d(Bx_n,Tx_n)+d(Ay_n,Bx_n)]+\gamma[d(Bx_n,Sy_n)+d(Ay_n,Tx_n)$
$] + \delta\, d(Bx_n,Tx_n)$
For sufficiently large n,
$d(Ay_n,Bx_n)<0+ \beta[0+d(Ay_n,Bx_n)]+ \gamma[0+d(Ay_n,Tx_n) < \beta d(Ay_n,Bx_n)+ \gamma d(Ay_n,Tx_n)$
$= (\beta+ \gamma)\, d(Ay_n,Bx_n)$ (since, $\lim_{n\to\infty} d(Bx_n,t) = \lim_{n\to\infty} d(Tx_n,t) = 0$)
This is a contradiction, $\lim_{n\to\infty} d(Ay_n,Bx_n) = 0$
By (W.3), we deduce that $\lim_{n\to\infty} d(Ay_n,t) = 0$
Suppose that SX is a complete subspace of X. Then t = Su for some u∈ X
Subsequently, we have $\lim_{n\to\infty} d(Ay_n,S_u) = \lim_{n\to\infty} d(Bx_n,S_u)=\lim_{n\to\infty} d(Tx_n,S_u)=\lim_{n\to\infty} d(Sy_n ,S_u) =0$
Using (1),
$d(A_u,Bx_n) < \alpha\, d(Bx_n,Tx_n)\{ [1 + d(A_u ,S_u)]/1 + d(S_u ,Tx_n)\}+\beta[d(Bx_n,Tx_n)+(d(A_u,S_u)]+\gamma[d(Bx_n,S_u)+$
$d(A_u,Tx_n)]+\delta\, d(S_u,Tx_n)$
Letting $n \to \infty$, we have$\lim_{n\to\infty} d(A_u,Bx_n) < \beta d(A_u,S_u) +\gamma d(A_u,S_u)$
$d(A_u,S_u)< (\beta+ \gamma)d(A_u,S_u)$.
This is a contradiction for $A_u \neq S_u$.
The weakly compatibility of A and S implies that
$AS_u = SA_u$and then $AA_u = AS_u = SA_u = SS_u$.
Since AX ⊂TX, there exists v∈ X such that $A_u = T_v$. Therefore $A_u = S_u = T_v$.
We claim that $T_v = B_v$. If not condition (1) gives

$d(A_u,B_v) < \alpha\, d(B_v,T_v)\{[1 + d(A_u,S_u)]/1 + d(S_u,T_v)\} + \beta[d(B_v,T_v) + d(A_u,S_u)] + \gamma[d(B_v,S_u) + d(A_u,T_v)] + \delta\, d(S_u,T_v) < \alpha\, d(B_v,A_u)\{[1 + 0]/(1 + 0)\} + \beta[d(B_v,T_v) + 0] + \gamma[d(B_v,A_u) + 0] + \delta(0)$
$d(A_u,B_v) < \alpha\, d(B_v,A_u) + \beta d(B_v,A_u) + \gamma d(B_v,A_u)$.
$d(A_u,B_v) < (\alpha+\beta+\gamma) d(B_v,A_u)$.
This is a contradiction for $A_u \neq B_v$.
Therefore $A_u = B_v$ and then $B_v = A_u = T_v$.
This implies that $A_u = S_u = T_v = B_v$.
But (B, T) is weakly compatible implies $BT_v = TB_v$ and $TT_v = TB_v = BT_v = BB_v$.
We shall prove that A_u is a common fixed point of A and S.
Suppose that $AA_u \neq A_u$.
$d(A_u,AA_u) = d(AA_u,B_v)$
$< \alpha\, d(B_v,T_v)\{[1 + d(AA_u,SA_u)]/1 + d(SA_u,T_v)\} + \beta[d(B_v,T_v) + d(AA_u,SA_u)] + \gamma[d(B_v,SA_u) + d(AA_u,T_v)] + \delta\, d(SA_u,T_v)$
$= \gamma[d(B_v,AA_u) + d(AA_u,B_v)] + \delta\, d(AA_u,B_v)$
$= (2\gamma + \delta) d(AA_u,B_v)$
This is a contradiction for $AA_u \neq B_v$.
Therefore $AA_u = B_v$ and then $AA_u = A_u = SA_u$ (since $AA_u = SA_u$)
Therefore A_u is a common fixed point of A and S.
To prove that $B_v = A_u$ is a common fixed point of B and T.
Suppose $B_v \neq BB_v$.
$d(B_v,BB_v) = d(A_u,BB_v)$
$< \alpha\, d(BB_v,TB_v)\{[1 + d(A_u,S_u)]/1 + d(S_u,TB_v)\} + \beta[d(BB_v,TB_v) + d(A_u,S_u)] + \gamma[d(BB_v,S_u) + d(A_u,TB_v)] + \delta\, d(S_u,TB_v)$
$= \gamma[d(BB_v,A_u) + d(A_u,BB_v)] + \delta\, d(A_u,BB_v)$
$= (2\gamma + \delta) d(A_u,BB_v) = (2\gamma + \delta) d(B_v,BB_v)$
which is a contradiction for $B_v \neq BB_v$.
Therefore $B_v = A_u = BB_v = TB_v$.
This means that B_v is a common fixed point of B and T.
Therefore, A_u is the common fixed point of A and S.
$B_v = A_u$ is the common fixed point of B and T.
Therefore, A_u is the common fixed point of A, B, T and S.
The proof is similar when TX is assumed to be a complete subspace of X.
The cases in which AX or BX is a complete subspace of X are similar to the cases in which SX or TX respectively is a complete space because $AX \subset TX$ and $BX \subset SX$.

Uniqueness. Suppose u, v are two fixed points of A, B, T and S.
Then $A_u = S_u = B_u = T_u = u$.
and $A_v = B_v = T_v = S_v = v$. Then for $u \neq v$, and then (1) gives $d(u,v) = d(A_u,B_v)$
$< \alpha\, d(B_v,T_v)\{[1 + d(A_u,S_u)]/1 + d(S_u,T_v)\} + \beta[d(B_v,T_v) + (d(A_u,S_u)] + \gamma[d(B_v,S_u) + d(A_u,T_v)] + \delta\, d(S_u,T_v) = \gamma[d(B_v,A_u) + d(A_u,B_v)] + \delta\, d(A_u,B_v)$
$= (2\gamma + \delta) d(A_u,B_v) = (2\gamma + \delta) d(u,v)$.
This is a contradiction for $u \neq v$. Therefore $u = v$.
This means that A, B, T and S have unique common fixed point.
For three maps, we have the following result by altering the condition (i) in theorem 3.2.

Corollary 3.3. Let d be a symmetric for X that satisfies (W.3), (W.4) of Wilson and (H_E). Let A, B and S be self mappings of a metric space (X,d) such that
(i) AX, $BX \subset SX$,
(ii) (A, S) is weakly compatible.,
(iii)(A, S) or (B, S) satisfies the property (E.A.),
(iv) $d(A_x,B_y) < \alpha\, d(B_y,S_y)\{[1 + d(A_x,S_x)]/1 + d(S_x,S_y)\} + \beta[d(B_y,S_y) + d(A_x,S_x)] + \gamma[d(B_y,S_x) + d(A_x,S_y)] + \delta\, d(S_x,S_y)$ for all $(x,y)\ x \in X^2$ with $\alpha, \beta, \gamma, \delta \geq 0$ and $\alpha + \beta + \gamma + \delta < 1$. If the range of one of the mappings A, B or S is a complete subspace of X, then A, B and S have a unique common fixed point.
For two maps, we have the following result by altering the condition (i) in theorem of Aamri [1].

Theorem 3.3. . Let d be a symmetric for X that satisfies (W.3) of Wilson and (H_E).
Let S and T be weakly compatible self mappings of a metric space (X,d) such that
(i) $d(T_x,T_y) < \alpha\{d(T_x,S_x)/1 + d(S_x,T_y)\} + \beta d(T_x,S_x) + \gamma[d(T_y,S_x) + d(T_x,T_y)] + \delta\, d(S_x,T_y)$ for all $(x,y)\ x \in X^2$ with $\alpha, \beta, \gamma, \delta \geq 0$ and $\alpha + \beta + 2\gamma + \delta < 1$. (ii)T and S satisfy the property (E.A.), (iii) $TX \subset SX$, If SX or TX is a complete subspace of X, then T and S have a unique common fixed-point.

Proof. Since T and S satisfy the property (E.A). Then there exists a sequence $(x_{n)}$ in X such that $\lim_{n\to\infty} d(Sx_n, t) = \lim_{n\to\infty} d(Tx_n, t) = 0$ for some t∈ X.
Therefore, by (H_E), we have $\lim_{n\to\infty} d(Tx_n, Sx_n) = 0$
Suppose that SX is a complete subspace of X.
Then $t=S_u$ for some u∈ X.
We claim that $T_u=S_u$
By (1) we have $d(Tx_n, T_u) < \alpha\{d(Tx_n, Sx_n)/1 + d(Sx_n, T_u)\} + \beta(d(Tx_n,Sx_n)) + \gamma[d(T_u,Sx_n) + d(Tx_n,T_u)] + \delta\, d(Sx_n,T_u)$. Letting n->∞, we have
$\lim_{n\to\infty} d(Tx_n, T_u) < \lim_{n\to\infty}\{\gamma[d(T_u, Sx_n) + d(Tx_n,T_u)] + \delta\, d(Sx_n,T_u)\}$
$d(S_u,T_u) < 2\gamma\, d(S_u,T_u) + \delta d(S_u,T_u) = (2\gamma + \delta)\, d(S_u,T_u)$
This is a contradiction $S_u \neq T_u$. Therefore, $S_u = T_u$.
Since S and T are weakly compatible, $ST_u = TS_u$ and therefore $TT_u = TS_u = ST_u = SS_u$.
Let us prove that T_u is a common fixed point of T and S. Suppose $T_u \neq TT_u$,
Then $d(T_u, TT_u) < \alpha\{d(T_u, S_u)/1 + d(S_u, TT_u)\} + \beta(d(T_u,S_u)) + \gamma[d(TT_u,S_u) + d(T_u,TT_u)] + \delta\, d(S_u,TT_u)$
$< (2\gamma + \delta) d(T_u,TT_u)$
This is a contradiction for $T_u \neq TT_u$.
Therefore, $T_u = TT_u$ and $ST_u = TT_u = T_u$.
The proof is similar when TX is assumed to be a complete subspace of X since TX ⊂ SX.
Uniqueness. Suppose T_u, T_v are two fixed points of T and S with $T_u \neq T_v$. Then
$d(T_u, T_v) < \alpha\{d(T_u, S_u)/1 + d(S_u, T_v)\} + \beta(d(T_u,S_u)) + \gamma[d(T_v,S_u) + d(T_u,T_v)] + \delta\, d(T_u,T_v)$
Therefore $d(T_u,T_v) < (2\gamma + \delta) d(T_u,T_v)$.
This is a contradiction for $T_u \neq T_v$
Therefore, $T_u = T_v$ and hence, T and S have unique common fixed point.

REFERENCES

[1] M. Aamri and D. El. Moutawakil, common fixed point theorems under contractive conditions in symmetric spaces Appl.Math, 3 (2003) 156-162.
[2] T. L. Hicks, Fixed point theory in symmetric spaces with applications to probabilistic spaces, Nonlinear Analysis, 36(1999), 331—344.
[3] W. A. Wilson, on semi-metric spaces, Amer. J. Math., 53(1931), 361—373.
[4] S. Sessa, on a weak commutativity condition of mappings in fixed point considerations, Publ. Inst. Math. (Beograd), 32(46) (1982), 149—153.
[5] G. Jungck, Compatible mappings and common fixed points, Intl. J. Math. Sci., 9 (1986), 771-779.
[6] M. Aamri and D. El. Moutawakil, Some new common fixed point theorems under strict contractive conditions, J. Math. Theory and App., 270 (2002) 181-188.

American Journal of Engineering Research (AJER)
e-ISSN : 2320-0847 p-ISSN : 2320-0936
Volume-02, Issue-10, pp-92-99
www.ajer.org

Research Paper Open Access

Internet of Car: Accident Sensing, Indication and Safety with Alert system

Md. Maminul Islam, Md. Rabiul Hasan, Imran Chowdhury,
Md. Towhid Chowdhury
[1](EEE, AIUB, Bangladesh) [2](EEE, AIUB, Bangladesh) [3](EEE, AIUB, Bangladesh) [4](EEE, AIUB, Bangladesh)

Abstract: - Detecting an accident before occurring it can save human life. To do this, advance accurate human detection and accident detection capability is needed. Several researches are going on regarding pre-crash detection & avoidance system from obstacle. To implement this system, priorities crash is essential for human or animal compared to obstacle. How the system will operate when it faces a situation to between human and obstacle? Differentiating human or animals and obstacles is more important by detecting them. If the system is unable to detect human then there will be a possibility to hit human rather than obstacle. Driver when drive a car in high speed may bypass humans, animals, or any obstacle for a few inches and the measurement is done by his own eyes which may occur an accident. Moreover, risk increases in foggy weather to see further that any animals, human or any obstacle is present in front of the car or any car is coming from opposite direction. Giving the priorities to human or animal, this paper work is done. By this system, a car will try to avoid obstacle after avoiding human or animal if there is any. Driver will also be notified with red lights indicating that obstacles are in front. However, if the system would not be able to avoid accident then our system will automatically generate a tweet in tweeter. For further safety, this system also contains relay and buzzer where relay will protect the car from battery ignition and buzzer will make noise to inform people surrounded.

Keywords: - *Accident Avoidance, Accident detection, Obstacles detection, Wi-Fi, vehicle tracking.*

I. INTRODUCTION

According To The Who 2013 Global Status Report On Road Safety [1], Road Traffic Deaths Would Become The Fifth Leading Cause Of Death. The Report Showed That There Had Been No Overall Reduction In The Number Of People Killed On The World's Roads: About 1.24 Million Deaths Occur Annually. Among Them Cyclist, Motorcyclists, Car Occupants & Unspecified Road Users Are High. Number Of Animals Die In Road Accident Is Also Quite Good. Even In Several Countries The Number Is Pretty High. In Order To Reduce The Number Of Car Crash Charles Birdsong, Ph.D., Peter Schuster, Ph.D., John Carlin, Daniel Kawano, William Thompson Has Designed Pre-Crash Detection System Using Ultrasonic, Laser Range Finder And Radar Sensors [2]. Accident Avoidance And Detection On Highways Is Designed By S.P. Bhumkar, V.V. Deotare, R.V.Babar [3]. These Systems Have The Ability To Detect Obstacles But The Most Important To Detect Human Being Or Animals And Avoid Them Are Missing. This Sensing Technology Can Reduce A Large Number Of Bikers, Cyclist And Passerby Death. There Are Also Lots Of Research Work Is Available On Accident Avoidance, Crash Detection And Alarm System. Megalingam, Rajesh Kannan & Their Group Mate Have Developed "Wireless Vehicular Accident Detection And Reporting System" [4]. Automatic Accident Detection Via Embedded Gsm Message Interface With Sensor Technology Is Developed By C.Vidya Lakshmi, J.R.Balakrishnan [5]. These Methods Uses Break System, Windows Close, Seat Belt Stiffen To Save Life From The Accident But If The Obstacle Is Human Or Animal Then Our System Uses Avoidance System Also. It Also Indicates The Driver That Obstacles Are Ahead. So The Driver Can Turn Left Or Right According To The Indication. If Avoidance Is Not Possible And Accident Happens Then This System Detects The Accident. Beside That It Will Also Generate A Tweet To Tweeter Through Wi-Fi System. It Is Also Possible To Coordinate Location Through Gps System Which Is Not The Main Concern Of Our Project.

Fig. 1:- Human and obstacle detection before 5m distance

II. MAIN TECHNOLOGY USED

1.1 Obstacle detection & indication sensor

This is one of the photoelectric sensors which is a set of transmitter and receiver. Detection distance can be adjusted as it is required. The sensor can detect distance by visible light interference which is small, cheap, and easy to assemble, easy to use, and other characteristics are given bellow:-

1, output current DC / SCR / Relay Control output: 100mA/5V powered
2, DC current consumption < 25mA
3, response time < 2ms
4, point angle: 15 °, effective distance 3-50CM adjustable
5, detection of objects: transparent or opaque body
6, working environment temperature: 25 °C ~ 55 °C
7, standard sensing object: sunlight 10000LX The following incandescent 3000LX

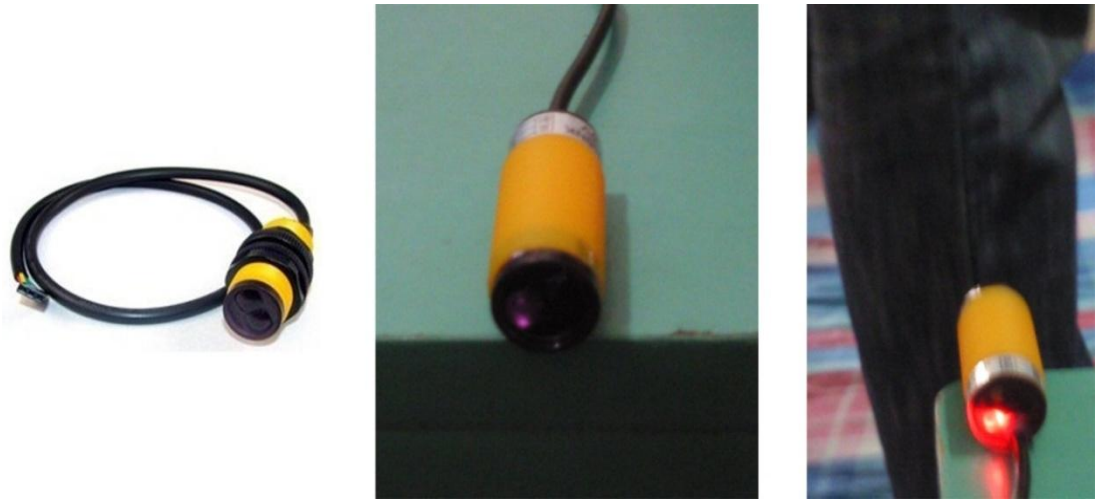

Fig. 2:- Obstacle detection and Indication

In both side of the car two IR obstacles sensors are placed. Anyone coming from the left side of the car or any obstacle found at the left side can be detected by left sensor and right sensor also work in same manner. The presence of an obstacle or human is indicated through red light when it detects human or obstacle. When human detection sensor detects human at the right side of the car and obstacle sensor detects an obstacle at the left side of the car then car will be moved toward left side to save human. As obstacles in both side of the car are detected thus both indication lights will be turned on.

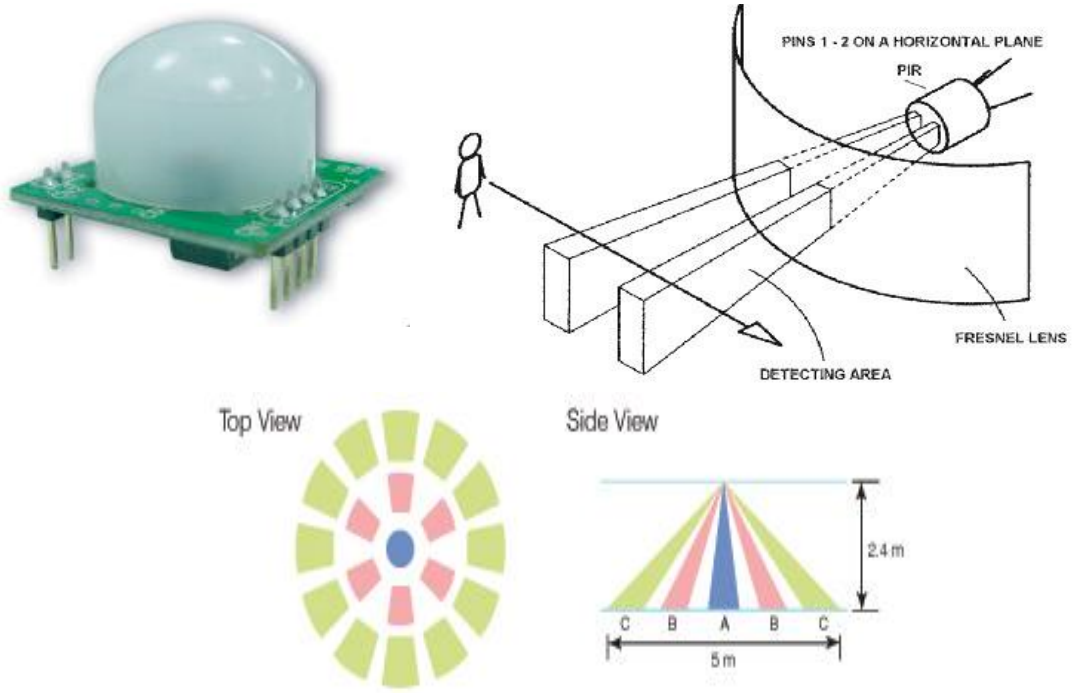

Fig. 3:- Fresnel lens, increase sensitivity and range of PIR sensor

1.2 Passive Infra Red sensor

The key of this project is Human sensing technology. In this project passive infra red sensor has been used to detect human. Infrared radiation exists in the electromagnetic spectrum at a wavelength which is longer than visible light. It can be detected though it cannot be seen. Objects that generate heat also generate infrared radiation and those objects include animals and the human body whose radiation is strongest at a wavelength of 9.4um [5]. PIR sensor is able to detect the change of radiation of this infra red radiation. A picture of working principle of PIR sensor is given below.

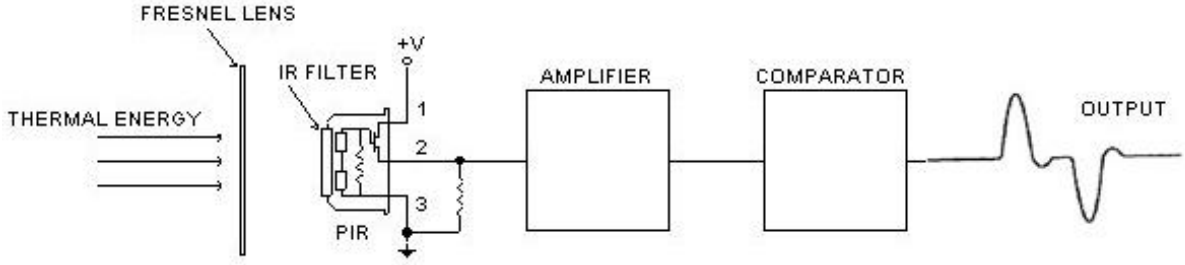

Fig. 4:- Typical configuration of PIR

PIR sensor generates +5v and -5v sine signal when any human or animal passes in front of the sensor or any movement is detected of human or animal in front of this. A breakout board is used to detect this signal and convert it into a longer digital signal. The output of PIR sensor can be adjusted. For max it can create an output signal for approximately 1.2 seconds [6]. This is more than enough to detect the signal.

2.3 Fresnel lenses

FL65 Fresnel lens is made of an infra red transmitting material that has an IR transmission range of 8 to 14um which is most sensitive to human body radiation. It is designed to have its grooves facing the IR sensing element so that a smooth surface is presented to the subject side of the lens which is usually the outside of an enclosure that houses the sensor. The lens element is round with a diameter of 1 inch and has a flange that is 1.5 inches square. This flange is used for mounting the lens in a suitable frame or enclosure. Mounting can best and most easily be done with strips of Scotch tape.

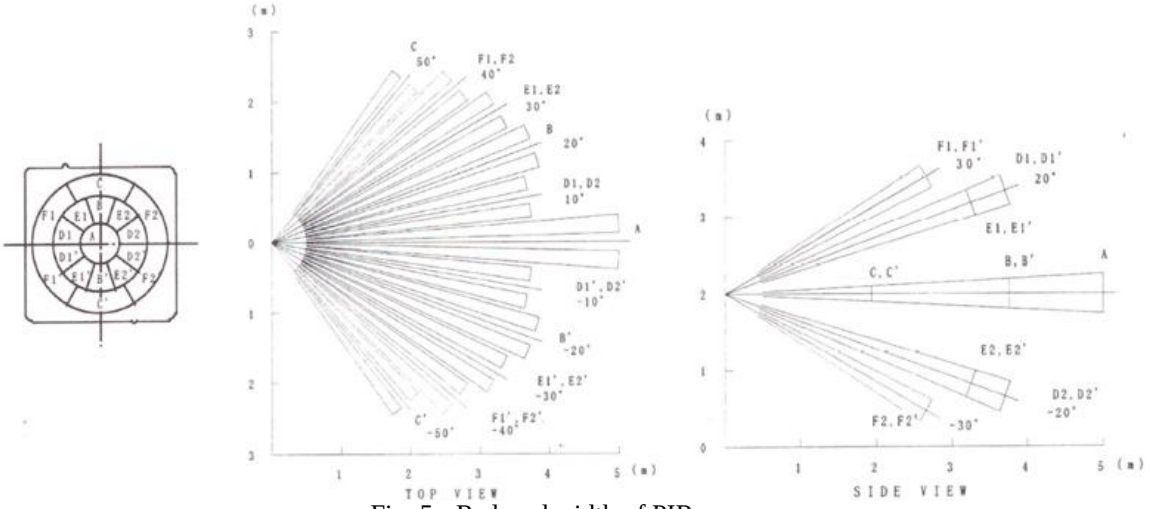

Fig. 5:- Reduced width of PIR sensor

Detection area of a PIR sensor is 3m in width, 5m in length & 3m in height. But on average the width of any car is around 1.5m. We have to detect humans or animals within this width. So, we have covered the lens area to reduce the width to 1.5m. Here is a picture below:-

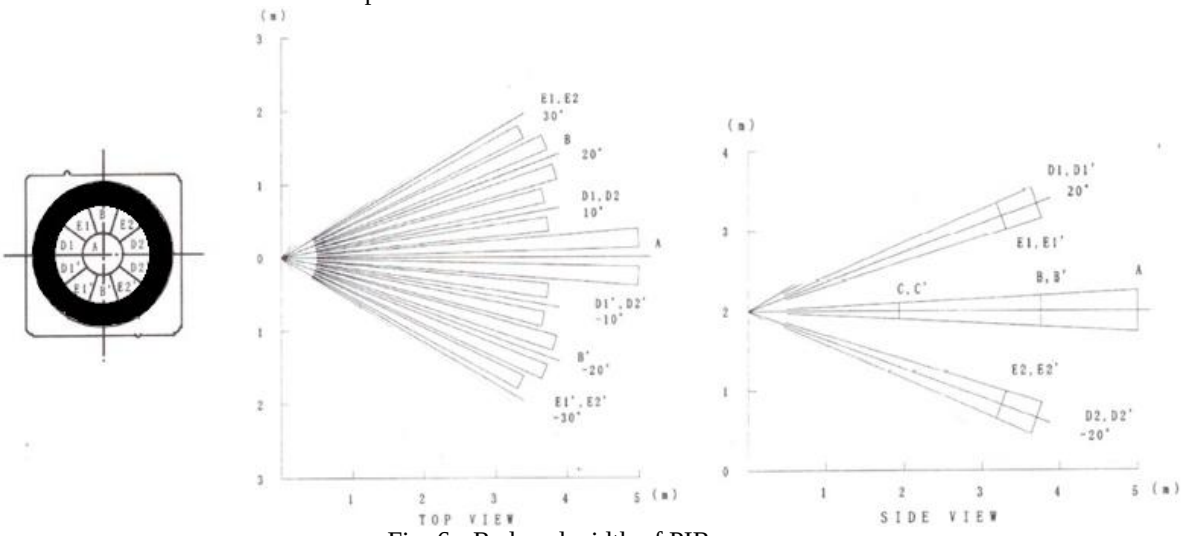

Fig. 6:- Reduced width of PIR sensor

In order to identify the position of the human being we need two sensors. Their detection area will overlap each other at the center. If both the sensor detect human means human is at the center. If left PIR only detect means the person is at the left side of the car and same for the right side. With the help of distance sensor this system [2] is also able to find out the distance of the human. Here is a figure describing the covered area.

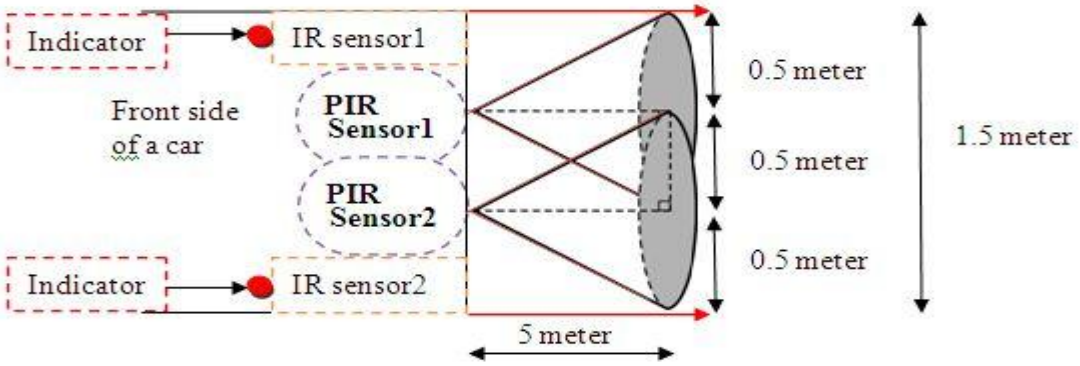

Fig. 7:- Area covered by PIR & IR sensors, human position detection & indication

2.4 Accident avoidance system

An advance pre-crash system is also capable to avoid accident by sensing human and their distance from vehicle. For example an automated braking force can be executed in this system. Moreover, the system can handle the steering by determining the position of human or obstacle. If driver forgets to press horn then the system can also generate an auto horn to indicate the person in front of the car.

2.5 Accident Detection

Most of the accident detection system uses complex 3 axis accelerometer, gravity sensor or costly android mobile phones with complex circuitry. In this system the accident detection method is also cheap and simple. We have used a tilt sensor to detect accident. Whenever any major accidents happens car jump or even flip over. We are detecting the amount of angle it rotated from ground. Tilt sensor can measure a rotation of minimum +15degree or -15 degree [7].

Fig. 8:- Accident Detection using tilt sensor

2.6 Wi-Fi shield

The RN-171 module has been used here as Wi-Fi shield which is a complete TCP/IP wireless networking module. This module is perfect for mobile wireless applications for mobile wireless applications for its small form factor and low power consumption. It incorporates a 2.4 GHz radio, 32-bit SPARC processor, TCP/IP stack, real time clock, crypto accelerator, power management and analog sensor interfaces. It also contains 8 Mbit flash memory and 128 KB RAM, UART and SPI slave hardware interfaces, 10 general purpose digital I/O and 8 analog inputs (14 bit,400mv). It accepts 3.3v regulated power supply or 3v battery.

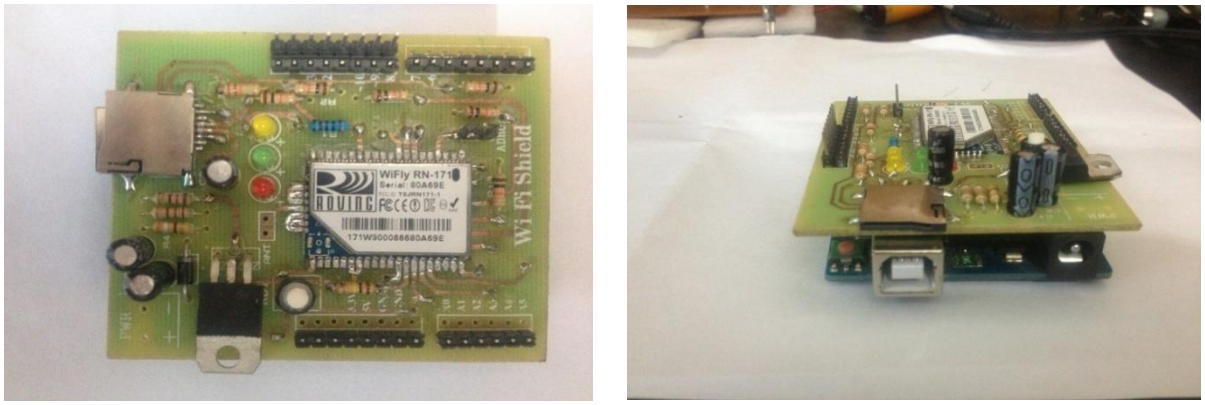

Fig. 9:- Wi-Fi Shield top and side view

2.7 Arduino

The Brain of this project is Arduino uno which is a microcontroller board based on the Atmega328. It has14 digital input/output pins, 6 analog inputs, a 16 MHz ceramic resonator, a USB connection, a power jack, an ICSP header, and a reset button. It contains everything needed to support the microcontroller. To get started it is just needed to connect it to a computer with a USB or power it with an AC to DC adapter. The board can operate on an external supply 6 to 20v. The recommended voltage is 7-12v, otherwise 5v pin may supply less than 5v if supply is less than 7v and the voltage regulator may overheat and damage the board for supplying more than 12v.

Fig. 10:- Arduino uno board

2.8 Relay and Buzzer

In this project 12A/220vAC relay has been used to protect the car from battery ignition when an accident occurs. If any accident occurs then the relay will trip its coil to avoid battery sparking. Buzzer has been used to make noise thus it can inform peoples surrounded when any accident occurs.

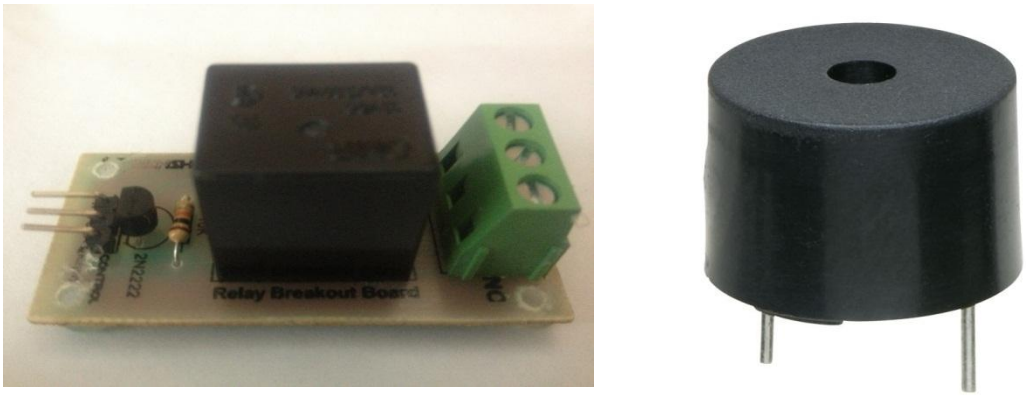

Fig. 11:- Relay and Buzzer

III. CIRCUIT DESCRIPTION

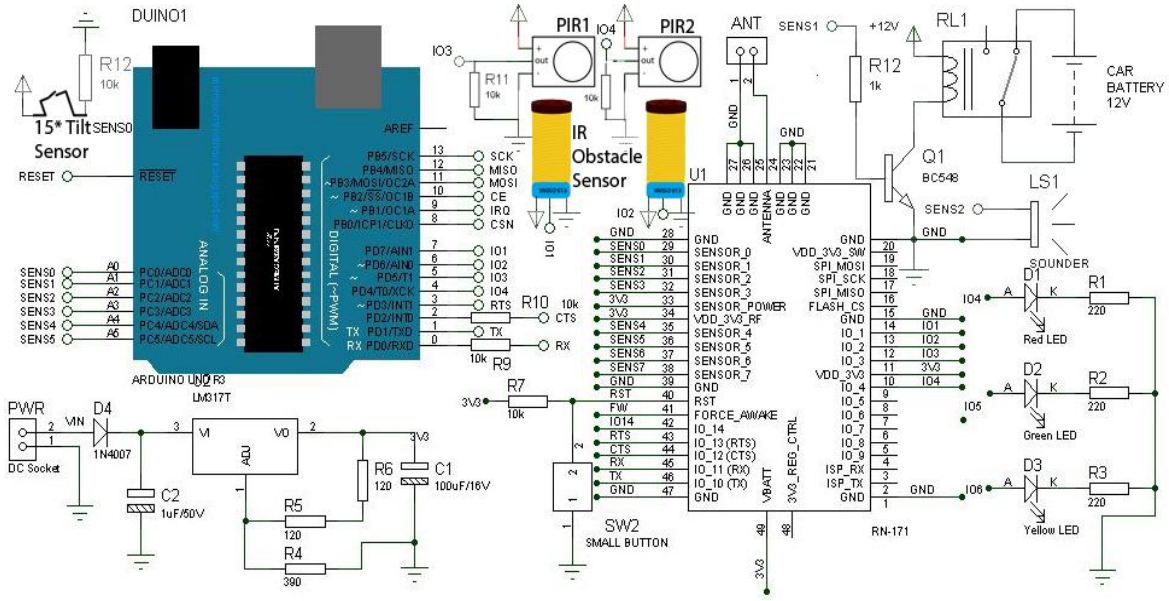

Fig. 12:- Schematic diagram

The controller used in this project is Arduino Uno. Two PIR sensors are connected to IO3 & IO4 bit. One tilt sensor is connected to sens0 bit. All these sensors give digital input that's why all these 3 pins are pulled down by 10K resistors. Here all the VCC are +5v. IR sensors also consume +5v and both sensors are connected to IO0, IO1 bit. Wi-Fi module communicates with microcontroller through serial communication. Other pins are used to control the Wi-Fi modem. Relay is connected to Sens1 no pin. And Buzzer is connected with sens2 no pin. Here LM317T IC is used to generate 3.3v which powers the Wi-Fi module. Power of Arduino comes from USB.

Circuit operation is simple. First step is to detect human. There are three possibilities, human is at left side of the car, at the middle of the car or at right side of the car. If human is at left side only PIR1 will generate a high signal, if human is at the center both the PIR will generate high signal & if the person is at right side only PIR2 will generate a signal. According to the PIR a signal will be sent to turn the staring to avoid the human. If avoidance of obstacle is not possible then the tilt sensor will be get shorted and a +5v will go through sens2 pin. When microcontroller gets this signal it initiates an alarm and sends a tweet to internet through Wi-Fi module. We did not included GPS module for location tracking as there are several Wi-Fi modules are available in market to know the pin point location of car. Relay is used to disconnect the battery of the car while accident occurs. Lots of time spark from batteries ignite fire and cause severe damage. To avoid spark from battery relay is used to disconnect the positive terminal of battery. And buzzer also continuously indicates that accident has occurred and need emergency help. Tilt sensor measure any angle rotation around +15degre of -15degree which confirms the indication of accident.

This module tweets to owners account. Owners tweet account is previously saved in Arduino and Also connecting IP of Wi-Fi module. There are others alert systems can be also implemented like mailing to GMAIL, post in facebook, etc. Bellow showing the output of tweet once accident occurred.

Fig. 13:- Tweet from car indication of accident

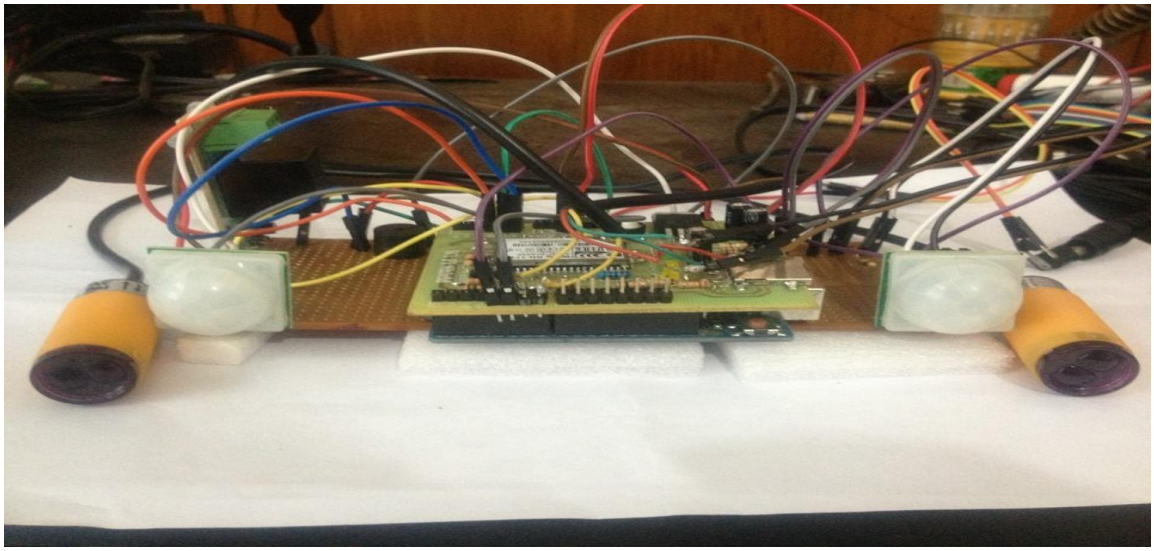

Fig. 14: - Front view of the hardware

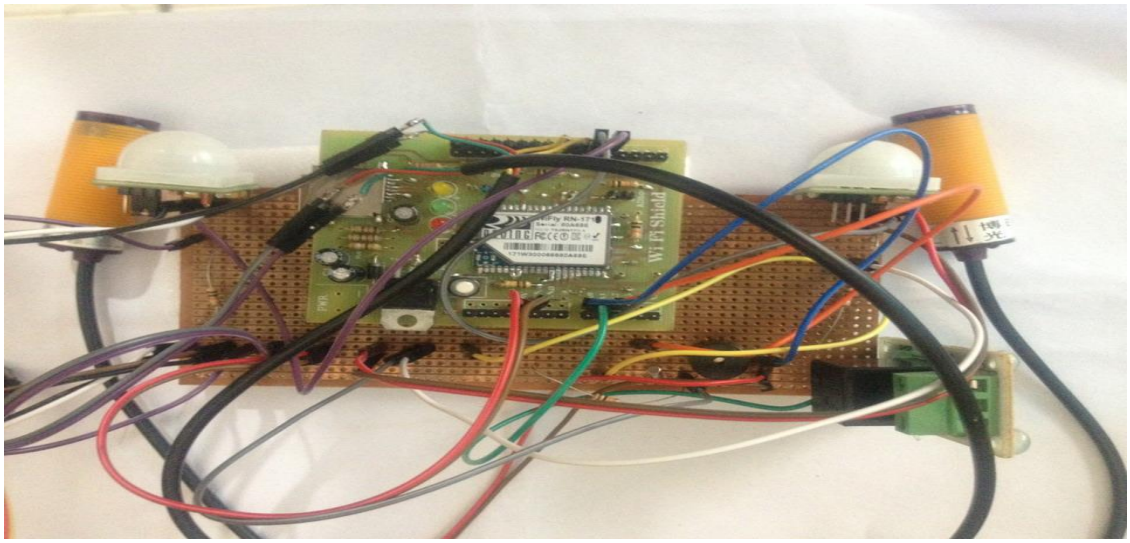

Fig. 15: - Top view of the hardware

IV. FURTHER APPLICATION

1. Avoiding Helicopter or Air plane collision with birds.
2. Robots will be able to identify humans & animals.
3. In NASA robot to detect presence of life using sensor.
4. Earthquake survival finding inside buildings.
5. Fire survival finding inside buildings.

V. CONCLUSION

Passive Infra red sensor is a reliable solution for detecting human or animals and this technique certainly can save lots of life. Human lives are most valuable. Pre-crash detection system must be equipped with combination of different sensors. Detecting humans or animals including obstacles will certainly give us a better solution to reduce the death of humans in road crash.

REFERENCES

[1] Global Status Report on Road safety 2013 by World Health Organization (WHO).
[2] Charles Birdsong, Ph.D., Peter Schuster, Ph.D., John Carlin, Daniel Kawano, William Thompson,"Test Methods and Results for Sensors in a Pre-Crash Detection System"in California Polytechnic State University, San Luis Obispo, California, Paper Number 06AE-19.
[3] S.P. Bhumkar , V.V. Deotare , R.V.Babar, "ACCIDENT AVOIDANCE AND DETECTION ON HIGHWAYS"in International Journal of Engineering Trends and Technology- Volume3 Issue2- 2012.
[4] Megalingam, Rajesh Kannan ; Amrita Vishwa Vidyapeetham, Kollam, India ; Nair, Ramesh Nammily ; Prakhya, Sai Manoj, "Wireless vehicular Accident Detection and Reporting System"in Mechanical and Electrical Technology (ICMET), 2010 2nd International Conference on 10-12 Sept. 2010.
[5] For fig.2 and information about PIR sensor http://www.glolab.com/pirparts/infrared.html
[6] For Figure .3 , figure.4 and information of PIR and lens http://www.ladyada.net/learn/sensors/pir.html
[7] http://learn.adafruit.com/tilt-sensor/overview
[8] http://en.wikipedia.org/wiki/Mobile_Network_Code

American Journal of Engineering Research (AJER)
e-ISSN : 2320-0847 p-ISSN : 2320-0936
Volume-02, Issue-10, pp-100-106
www.ajer.org

Research Paper Open Access

Fault Tree-Based Reliability Assessment of a 132-kV Transmission Line Protection Scheme

Isaac A. Samuel[1], Ayokunle A. Awelewa [1], James Katende[2], and Ishioma A. Odigwe[1]

[1]*Department of Electrical and Information Engineering, College of Science and Technology, Covenant University, P. M. B. 1023, Ota, Ogun State, Nigeria.*

[2]*The Founding Dean of College of Technology, Botswana International University of Science & Technology, Gaborone*

Abstract: - The reliability of a power system network depends greatly on the performance of the protection system. Improving the reliability of the protection scheme of the transmission lines will enhance the overall reliability of the power system network. The focus of this paper is the improvement of the reliability of a power system transmission line using fault tree analysis (FTA). The paper considers the development of fault tree diagrams for the protection scheme of the 150km-long 132-kV transmission line in Northern Nigeria. The existing protection scheme is analyzed and compared with a proposed scheme equipped with a redundancy arrangement. And the result shows that the new scheme offers significant improvement (about 51%) in the availability of the line.

Keywords: *- failure rate, fault tree analysis, mean time before failure, power system reliability, component unavailability*

I. INTRODUCTION

The ability of an electric power system to supply electricity constantly and reliability has a direct effect on the social, economic and industrial development of any nation. The power system is vulnerable to system abnormalities such as control failures, protection and / or communication system failure, and disturbances which include lightning, human operational errors, etc. Therefore, maintaining a reliable power system is an important issue for power system design, operation and maintenance. Reliability study helps system operators in making engineering decisions in planning, designing and operating the entire system, and it is the probability that an item or system will perform a required function without failure under stated conditions for a stated period of time [1]. It is always desirable that an electric power system satisfies the system load requirement with a reasonable assurance of continuity and quality. This concept of power system reliability is extremely broad and covers all aspects of the ability of the system to satisfy consumer requirements. The IEEE Power Engineering Task Force on Bulk Power System Reliability describes a proper level of electric utility system reliability as that which meets customer load demands and energy at the lowest possible cost while maintaining acceptable levels of service quality [2]. In addition, power system reliability has to do with system adequacy and system security. Adequacy relates to the existence of sufficient facilities within the system to satisfy the consumer's load demand, while system security relates to the ability of the system to respond to disturbances arising within the power system [3]. Vitally important to power system reliability are protection systems. And it can be said that a power system is as reliable as its protection systems, which are collections of devices that detect defective power system elements or conditions of an abnormal or dangerous nature, initiate the appropriate control action, and isolate the appropriate power system components [4]. Meanwhile, a fault is any condition that causes abnormal operation of the power system or equipment serving the power system. This fault includes but is not limited to short or low impedance circuits, open circuits, power swings, over voltages, elevated temperatures and off-normal system frequency. Although the function of the protection system (which uses electronics or electromechanical relays) is not to prevent faults, it must be able to take immediate action upon fault

recognition, which is to protect equipment and limit injury caused by electrical failure. This function suggests that the system must have an appreciably high level of reliability. Therefore, the aim of this work is to employ a graphical approach to assess the reliability of a protection scheme of the 150km-long 132-kV transmission line in Northern Nigeria with a view to improving it.

II. FAULT TREE ANALYSIS (FTA): A REVIEW AND PROCEDURE

Fault tree analysis (FTA) was developed in 1962 for the US Air Force by A. H. Watson of the Bell Telephone Laboratories for use with the Minuteman control system, was later adopted and extensively applied by the Boeing Company. FTA is one of many symbolic logic analytical techniques found in the operations research discipline [1]. Following the Aerospace Industry, the nuclear power industry discovered the virtues and benefits of deploying it for nuclear power plants. Many key individuals in the nuclear power industry contributed to advancing fault tree theory and fault tree software. This method used and refined over the years is attractive because it is a practical tool any engineer can learn to use while computer programs are available to assist in developing and analyzing complex fault tree [2]. Fault Tree analysis is a model that graphically and logically represents the major faults or critical failures associated with a product or system, the causes for the faults, and potential countermeasures [6]. In this respect, FTA is a systematic deductive technique, which allows the development of the causal relations leading to a given undesired event. It is deductive in the sense that it starts from a defined system failure event and unfolds backward its causes, down to the primary (basic) independent faults. The method focuses on single failure mode and can provide quantitative information on how a particular event can occur, to what consequences it leads, while at the same time allowing the identification of those components, which play a major role in determining the defined system failure. Moreover, it can be solved in quantitative terms to provide the probability of events of interest starting from knowledge of the probability of occurrence of the basic events, which cause them [7]. In fault tree analysis, a desirable event (which generally represents a system failure mode or hazard for which predicted reliability data are required) is called a top event. And the lower events in each branch of a fault tree are called basic events. These basic events are linked via logic gates symbols to one or more undesirable top events [8], and represent hardware, software, and human failures for which the probability of failure is given based on historical data. Most FTA can be carried out using four basic components: 1) the rectangular boxes used for top and intermediate events. The top event is the foreseeable, undesired event towards which all fault tree logic flows, while the intermediate event describes a system state that is generated by antecedent events, 2) the 'OR' gate, which produces an output if any of its inputs exists, 3) the 'AND' gate, which produces an output if all its inputs co-exist, and 4) the circular boxes used to represent the basic events, which are events initiating fault/failure. The basic events mark the limit of resolution of the analysis. Normally, when analyzing a protection scheme using the FTA method, the scheme failure of concern is designated as the top event, and the probability that the scheme fails for the top event is a combination of the failure probabilities of the components in the scheme. Whereas for an OR gate, in which any input can contribute to scheme failure, the total probability is the sum of the input events, for an AND gate, in which all inputs to that gate must fail together to cause scheme failure, the upper level probability for scheme failure is the product of input probabilities.

To quantify the probability of the top event in a fault tree, the probability of each basic event must be provided. These basic event probabilities are then propagated upward to the top event using the Boolean relationships for the fault tree. The input data that must be supplied for a basic event is usually a component failure probability in some time interval, event occurrence probability in some time interval, pure event probability, or component unavailability [4]. The component unavailability is used for the assessment in this paper and is provided for the basic event to be able to generate the overall unavailability of the top event. This information is provided for a component that is repairable or checkable, i.e., a component which is out of service and unavailable if called upon to operate [7]. And this is exactly the situation with protective schemes.

To estimate the failure probability for each device in the scheme, the device failure rate can be used. One industry practice is to provide failure rates as Mean Time Between Failures (MTBF), which could be based on field failure data or on assumptions about complexity and exposure of equipment. To use this information to estimate probability, the fraction of time that a device cannot perform is assumed [10]. Equation (1) gives the unavailability, q, in terms of MTBF [9]

$$q \cong \lambda T = T / MTBF \quad (1)$$

where λ is the failure rate, and T the average down time per failure. Because each failure causes down time T, then the system is unavailable for time T, and the fraction of time the system is not available is depicted in eqn. (1).

III. THE CASE STUDY: 132-KV KANO – KANKIA POWER TRANSMISSION LINE

The case study, 132-kV Kano – Kankia transmission line is supplied via two parallel 132-kV bus bars. This is to allow for operational flexibility and redundancy of the system. These buses are with their associated isolators and circuit breakers to allow for operational flexibility. The132-kV Kano – Kankia transmission line is a very important line as it supplies the Katsina Steel Rolling Mill and other consumers. More importantly, it is an inter-country transmission line, as it also takes power to Gazaoua at Niger Republic. It is a radial transmission line and its length is about 180km with a load of about 30MVA, including the Gazaoua load in Niger Republic.

The protection scheme used on the 132-kV transmission line is the non-pilot three-zone distance protection scheme. The distance protection zones offer backup protection and take care of phase to phase, phase to phase to ground, and phase to ground faults, operating independently of each other. This scheme uses the Siemens' type electromechanical relay and has a reach setting that is up to 80% of the protected line for instantaneous zone 1 protection (based on the line impedance). Zone 2 setting covers the remaining 20% of the line impedance. The minimum setting of the protected line is 120%. Zone 3 setting is delayed beyond all other protection within its reach and is determined for maximum fault in-feed. Its reach is set to at least 1.2 times the impedance presented to the relay for a fault at the remote end of the second line section. Additionally, breaker failure protection provides backup protection for the primary circuit breaker if it fails to clear a system fault.

The data used in this work are the Kumbotso 330/132/33-kV transmission station single-line diagram and the single-line schematic of the principle of protection and measuring diagram. This information was made available by Power Holding Company Nig. Plc., Kano transmission station, Kano. The data (MTBF) required for the reliability assessment of the protective scheme were obtained from field experience as given in [10]. The protection components on this line are as listed below:

- Distance protection relay 1 piece
- Over Load Relay 2 pieces
- Current transformer 12 pieces
- Voltage transformer 3 pieces
- Circuit Breaker 7 pieces
- Bus differential Relay 2 pieces
- Breaker failure relay 1 piece
- DC battery bank (110V) 1 piece

IV. CONSTRUCTION AND ASSESSMENT OF THE FAULT TREE

FT for the protection scheme used on the 132-kV Kano – Kankia transmission line is now developed from the system schematic diagram. The scope of this assessment is limited to the Kaduna downstream of the line. The resolution is the level or extent to which the failure causes for the top event will be developed. Here the top event is given as general protection failure (Main and Back-up). And the immediate faults and or failures that could lead to the top events are:

- 132-kV protection failure (Main & back up)
- 110-V battery bank failure
- Kumbotso 330-kV backup failure
- Kaduna 330-kV circuit breaker failure.

These four events can lead to the occurrence of the top event. They are linked to the top event via an 'OR' gate showing that any of them that occur can cause the top event. These events are broken down until the basic event is finally reached. In addition, the gates relating one level of events to another were duly selected based on the relationship between the events.

Now the unavailability of the basic event components is calculated for the protective relays, instrument transformers, DC power supply and circuit breakers as highlighted below.

- **Protective relays:**

The distance protection, bus differential, and the overload relays used for this protective scheme are the electromechanical type. Based on field experience, they require routine testing for proper operation, so their reliability is dependent on their regular testing and maintenance. Failure of these relays could go unnoticed until the next maintenance period or until their operation is required. Failure could occur the day following a maintenance test or a day before the next period, which is an average time of six months. T is always large because of lack of automatic supervision. Therefore, from field experience an MTBF of this relay is assumed as 200 years. Hence, unavailability q = (6 x 30) / (200 x 365) = 0.002465. ≈ 2465 x 10^{-6}.

- **Instrument Transformers:**

These include both Current Transformer (CT) and Capacitor Voltage Transformer (CVT). Based on field experience, an MTBF of 500 years and an average protection down time of 2 days are assumed. Therefore, unavailability q = 2 / (500 x 365) = 1.095890411 x 10^{-5} ≈ 10 x 10^{-6}.

- **DC Power Supply:**

The dc power bank is 110V and it consists of battery, charger and distribution circuit. The loss of dc alarm is monitored and responded to promptly in less than a day, say 0.5 day. MTBF is 27 years. Hence, unavailability q = 0.5 / (27 x 365) = 5.073566717 x 10^{-5} ≈ 50 x 10^{-6} .

- **Circuit Breaker:**

The circuit breaker used is the oil type circuit breaker. The unavailability of 300 x 10^{-6} is assumed.

V. PRESENTATION OF RESULTS

The unavailability of the basic events and component unavailability are tabulated as in Table 1 below to allow for quick inspection.

Table 1: Unavailability of the Several Protection Components.

S/no	Component	MTBF	T	Unavailability 10^{-6}
1	Over Load Relay	200	6months	2465
2	Current transformer	500	2days	10
3	Voltage transformer	500	2days	10
4	Circuit Breaker	-	-	300
5	Bus differential Relay	200	6months	2465
6	Distance protection relay	200	6months	2465
7	Breaker failure relay	200	6months	2465
8	Wiring	-	-	1000
9	DC battery bank (110)	27	0.5day	50

.

The fault tree (shown in Appendix 2) illustrates the unavailability of the basic events inserted and propagated upward. Using the rare event approximation, the unavailability associated with each event expressed with the OR gates is summed up and the ones associated with AND gates are multiplied. The unavailability of this protection system, i.e., general protection failure on the 132kV Kano-Kankia transmission line is 5085.023 x 10^{-6}. From the assessment, it could be seen that the relays are the most vulnerable components in this protective scheme because they lack automatic supervision. And this implies that the principal weakness of this scheme is its dependency on several electromechanical relays.

This protection scheme, however, can be improved upon by adding redundant relays to the existing system. The relays could be added as shown in Figure A3 in Appendix 3. The unavailability of the top event (general protection failure) with this redundancy arrangement is 2616 x10^{-6} as against the unavailability of 5085 x10^{-6} of the protection scheme without redundancy. Therefore, the percentage improvement is 51.45%.

VI. CONCLUSION

The fault tree approach to reliability assessment of the 132-kV Kano-Kankia transmission line protective scheme has been successfully carried out. The reliability index used for this assessment is the unavailability. The unavailability of the existing protection scheme of the 132-kV Kano-Kankia has been found to be 5085 x10^{-6}. With a redundancy arrangement of relays, a percentage improvement of 51.45% has been realized. The FTA is a very useful tool for design and operation of complex systems. It helps to identify critical components and enhance system understanding. As a diagnostic tool, it can be used to predict the most likely causes of system failure in the event of break down. As design tool, it helps in eliminating costly design changes and retrofits. In order to improve the reliability of the system, however, electro-mechanical relays should be replaced with modern digital self-test relays and pilot distance protection should be adopted as pilot communications between relays have an added advantage of discrimination and isolation of fault in good and reasonable time.

VII. ACKNOWLEDGEMENTS

Profound gratitude is due to Engineer Shehu Abba of the Power Holding Company of Nigeria Plc., Kumbotso Transmission Station, Kano for the immeasurable assistance he gave during this research work.

REFERENCES

[1] http://www.slideshare.net/ASQwebinars/verview-of-reliability-engineering Overview of reliability engineering, 18th August, 2012.

[2] s.pangonilo.com/index.php?.../Introduction_To_Practical_Power_Systems: Introduction to practical power system protection.

[3] www.ornl.gov/info/reports/1992/3445603649149.pdf Steven L. Purucker et al., Feasibility Study: Application of RCM Techniques for Substation Maintenance at the Bonneville Power Administration.

[4] Don Zhu: "Power System Reliability Analysis with Distributed Generator", M.Sc. Thesis, Virgina Polytechnic Institute and State University, Blacksburg, VA., May 2003.

[5] C. R. Bayliss, Transmission and Distribution Electrical Engineering, Second Edition, Newnes, New Delhi, 1999.

[6] Clint T Summers: "Distance Protection Aspects of Transmission Lines Equipped With Series Compensation Capacitors", M.Sc. Thesis, Virgina Polytechnic Institute and State University, Blacksburg, VA. 1999.

[7] Michael Stamatelatos and William Vesely, SAIC Fault Tree *Handbook with Aerospace Applications*, August 2002.

[8] www.itemsoftware.com/faulttree.html Itemsoftware Demo CD.

[9] E.O. Schweitzer, B. Fleming, T. J. Lee, and P. M Anderson, "Reliability Analysis of Transmission Protection Scheme Using Fault Tree Methods'', *51st Annual Conference for Protection Relay Engineers*, Texas A&M University, College Station, TX, 6th-8th April, 1998.

[10] Jean Leon Eternod, and AntulioJarquin, Reliability Analysis for Generation Shedding Scheme on the CFE Maim Transmission Line, *29th Annual Western Protective Relay Conference*, Spokane, Washington, 22nd - 24th October, 2002.

APPENDIX 1

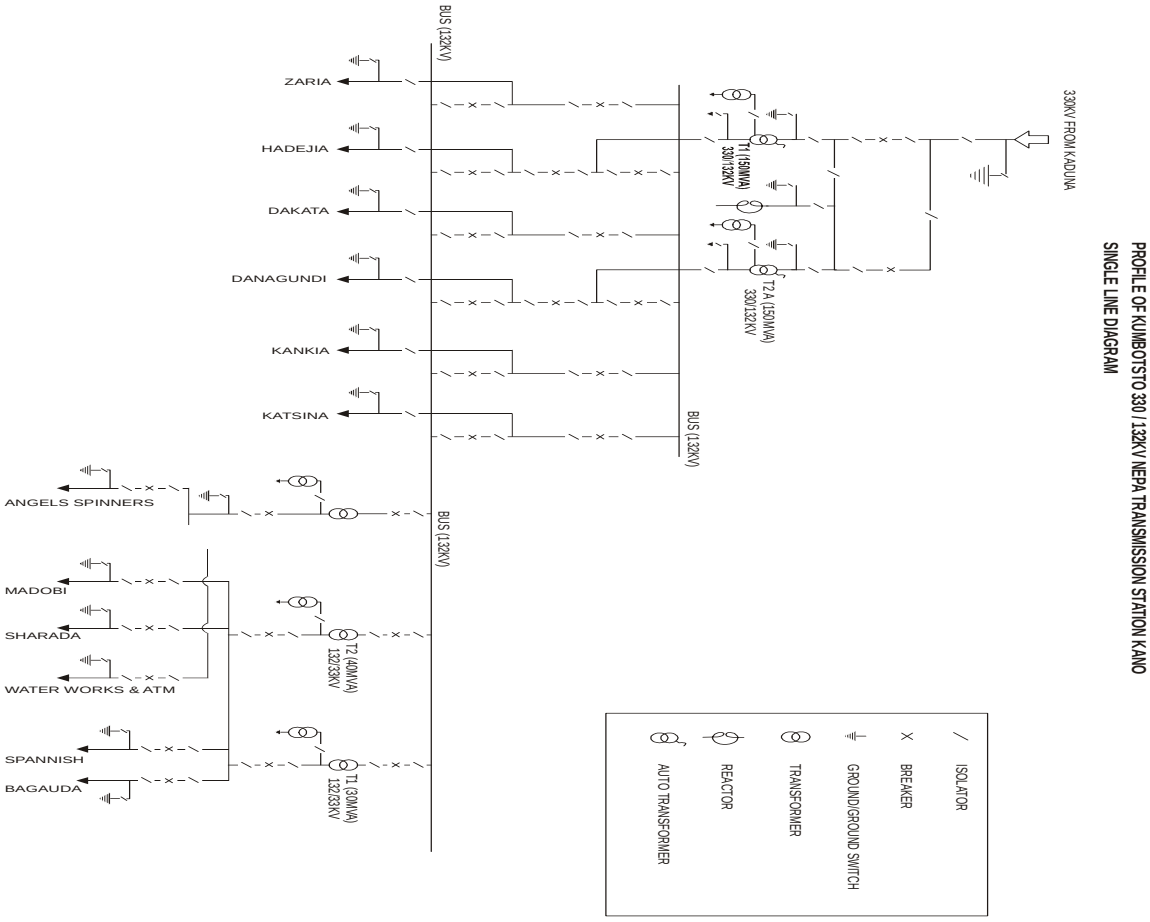

Fig. A1. Single Line Diagram of the132-kV Kano – Kankia transmission

APPENDIX 2

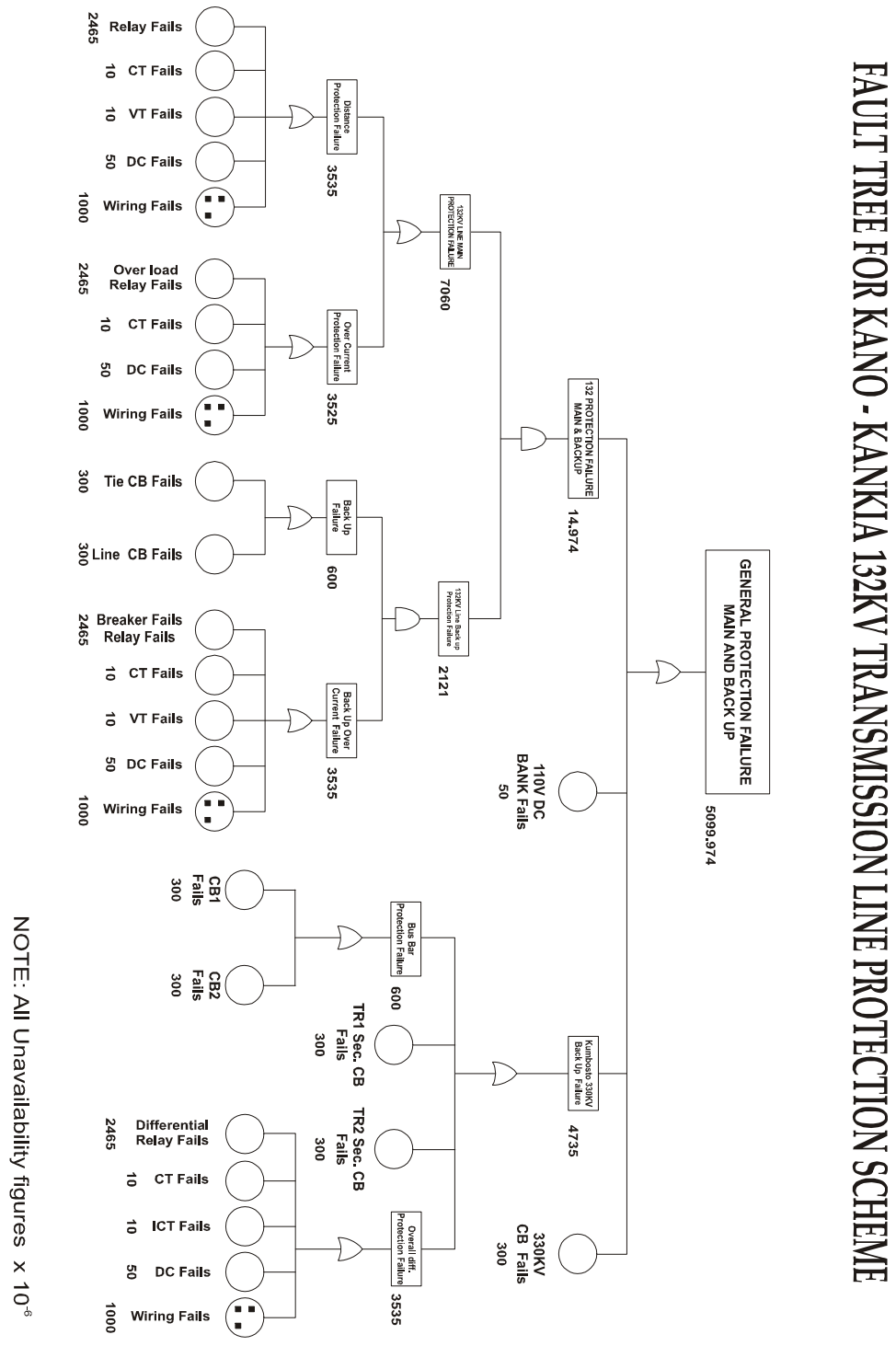

Fig. A2. Fault Tree with unavailability values inserted

APPENDIX 3

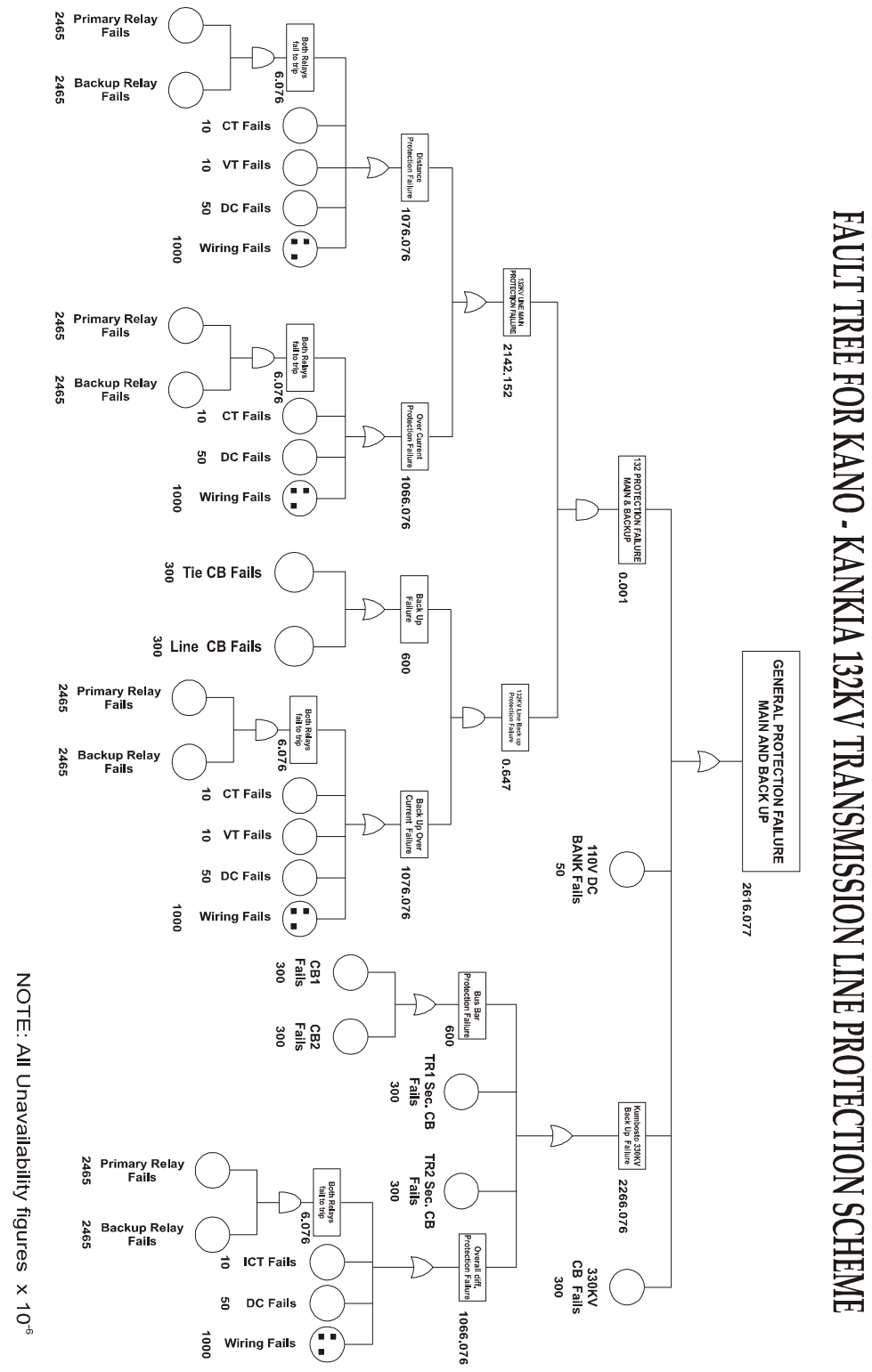

Fig. A3. Fault Tree of the Protection scheme with Redundant Relays

American Journal of Engineering Research (AJER)
e-ISSN : 2320-0847 p-ISSN : 2320-0936
Volume-02, Issue-10, pp-107-111
www.ajer.org

Research Paper Open Access

Robot Selection Using Analytic Hierarchy Process and System Of Equations of Matrices

R. Naveen kumar[1], A. Sreenivasulu Reddy[2], and G. Padmanabhan[3]
[1, 2&3]Department of Mechanical Engineering, Sri Venkateswara University, Tirupati, India

Abstract: - The problem of robot selection plays an important key role concern to various fields of different applications since three decades. This problem has become more difficult in recent years due to increasing complexity of applications of the environment, features and specifications, and facilities offered by various manufactures. The primary objective of this paper is to select the suitable type of robot based on various factors such as type of application, payload, working environment, accuracy, lifespan, weight, purchasing cost etc. The selection procedure is developed for selection of particular type of robot based evaluating the various alternative selection factors using AHP technique and systems of equations of the matrices i.e. Eigen values and Eigen vectors. The ranking evolution will provide a good guidance for the robot selection to the end user. The concept of this work is an attempt has been made to create exhaustive database for identifying maximum possible number of attributes.

Keywords: - *AHP, Robotics, Payload, Cost, System of Equations of matrices*

I. INTRODUCTION

A Robot selection is one of the critical issues, while designing of work cells in the fields of manufacturing environment related to various types of products. Robot selection for a particular type of application is generally described based on experience, manufacturing institution and kinematic considerations like workspace, manipulability, etc. Therefore selection problem has become more difficult in recent years due to increasing complexity, available features, and facilities offered by different robotic manufactures. Systematic procedures were developed for selection of robot manipulator based on their different attributes.

II. METHODOLOGY

The objectives of this work is to develop AHP method for robot selection. The methodology of this work has been adopted from Yahya and Kingsman (1999), Tam and Tummala (2001) and Yu and Jing (2004). In order to comply with collecting quantitative and qualitative data for AHP robot selection model that could be applied by a six steps approach was performed to insure successful implementation

2.1 Robot Selection Criteria

Robots are being used increasingly in industrial workstations to enhance firm's performance. Robots are employed to perform repetitive production jobs, hazardous jobs, multi-shift operations etc., so that it helps to reduce the delivery time, improve the work environment, lower the production cost and even increase the product range to suit market demand from time to time. When a choice must be made among several robots for a given application, it is necessary to compare their performance characteristics in a proper fashion. Some of the main performance criteria of an industrial robot are drive systems, geometrical dexterity, path measuring systems, material of robot, load-carrying capacity, velocity, weight of the robot, programming flexibility, size of the robot and accuracy of the robot. The importance of these criteria is commonly known and thus not elaborated.

2.2 AHP Method

Analytical Hierarchy Process (AHP) is one of Multi Criteria decision making method that was originally developed by Prof. Thomas L. Saaty. In short, it is a method to derive ratio scales from paired comparisons. The input can be obtained from actual measurement such as Weight, Payload, Precision, Cost, Life of robot, Process

etc., or from subjective opinion such as satisfaction feelings and preference. AHP allow some small inconsistency in judgement because human is not always consistent. The ratio scales are derived from the principal Eigen vectors and the consistency index is derived from the principal Eigen value.

2.3 System of Equation of Matrices

The eigenvalue problem is a problem of considerable theoretical interest and wide-ranging application. For example, this problem is crucial in solving systems of differential equations, analyzing population growth models, and calculating powers of matrices (in order to define the exponential matrix). Other areas such as physics, sociology, biology, economics and statistics have focused considerable attention on "eigenvalues" and "eigenvectors"-their applications and their computations. Before we give the formal definition, let us introduce these concepts

III. FIGURES AND TABLES

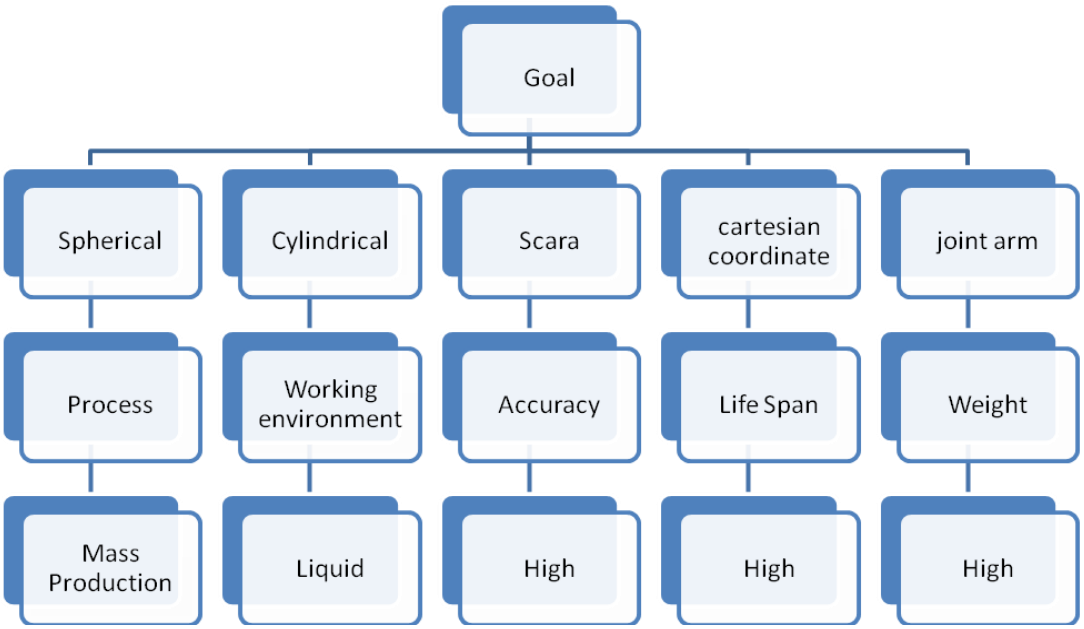

Fig 1: selection criteria

Table 2: pair wise comparison in AHP preference [8]

Verbal judgment preference	Numerical rating
Extremely preferred	9
Very strongly preferred	7
Strongly preferred	5
Moderate preferred	3
Equally preferred	1

Table 3: Pair-wise comparison matrix

Factors	Spherical	Cylindrical	Sacra	Cartesian coordinate	Joint arm
Spherical	1	7	3	1	1
Cylindrical	1/7	1	0.14	0.2	0.2
Sacra	1/3	1/0.14	1	1	1
Cartesian coordinate	1	1/0.2	1	1	1
Joint arm	1	1/0.2	1	1	1

Table 4: Criterion weights obtained in AHP

Factors	Spherical	Cylindrical	Sacra	Cartesian coordinate	Joint arm	Average
Spherical	0.29	0.28	0.48	0.23	0.23	0.31
Cylindrical	0.041	0.04	0.02	0.04	0.04	0.04
Sacra	0.09	0.1	0.16	0.23	0.23	0.20
Cartesian coordinate	0.29	0.2	0.16	0.23	0.23	0.23

Table 5: random inconsistency indices (RI) for N=10[8]

Sample Size(N)	1	2	3	4	5	6	7	8	9
Random Index(RI)	0	0	0.58	0.9	1.12	1.24	1.32	1.41	1.45

3.2. Equations

Step 1: An overall summation of the product of sum of each vector column for both the decision matrix and pair wise comparison matrices with the PV values of each row is carried out to obtain the principal Eigen value λ_{max} i.e.,

$$\lambda_{max} = \sum_{i,j=1}^{K} C_j PV_i$$

Where C_j is the sum of each column vector

Step 2: Comparison of Eigen values and Eigen vectors

Eigen Value

$$A - \lambda_i = 0$$

Eigen Vector

$$(A - \lambda_i)X = 0$$

Step 3: The level of inconsistency in both decision and pair wise compression matrix is checked using the following equation.

$$I.I = \frac{\lambda - N}{N - 1}$$

Where I.I is the inconsistency index, N is the number of element of each of matrix.

Step 4: Prof. saaty proved that for consistent reciprocal matrix, the largest Eigen value is equal to the number of comparisons, or $\boldsymbol{\lambda_{max}}$**=n.** then he gave a measure of consistency, called consistency index as deviation or degree of consistency using the following formula

$$C.I = \frac{\lambda_{max} - n}{n - 1}$$

Step 5: Random inconsistency indices (R.I) are then determined for each of the square matrices equation

$$R.I = \frac{1.98(N - 2)}{N}$$

Step 6: consistency ratio (C.I) which is a comparison between consistency index and random consistency index, or in formula

$$C.R = \frac{C.I}{R.I}$$

IV. RESULTS

AHP Technique

λ_{max} = (3.48*0.31) + (25*0.04) + (6.14*0.20) + (4.20*0.23) + (4.20*0.23)

λ_{max}=5.23

Having a comparison matrix, now compute priority vector, which is the normalized Eigen vector of the matrix. To know what are Eigen vector, Eigen values and how to compute manually. The following method will give a detailed explanation of getting an approximation of Eigen vector (and Eigen value) of reciprocal matrix. This approximation is actually worked well for small matrix and there is no guarantee that the rank will not reverse because of the approximation error. Nevertheless it is easy to compute because all we need to do is just to normalize each column of matrix.

System of Equation of Matrices

Eigen value

λ= **[5.17, 0.93, 0.93, 0.07, 0]**

Eigen Vector

0.6433	0.8065	0.8065	0.5556	0.0000
0.0793	0.0487	0.0487	0.1608	0.0000
0.4057	0.4417	0.4417	0.2010	0.0000
0.4557	0.2758	0.2758	0.5590	0.7071
0.4557	0.2758	0.2758	0.5590	0.7071

The largest Eigen value is called the principal Eigen value, that is λ_{max} **=5.17**
Which is very close to our approximation λ_{max} **=5.23.** The principal Eigen vector is the Eigen vector that corresponds to the highest Eigen value.

Thus in the previous example, we have $\boldsymbol{\lambda_{max}}$ **=5.23** for five comparisons, or n=5, thus the consistency index is

$$C.I = \frac{5.23 - 5}{5 - 1}$$

C.I=0.05

Knowing the consistency index, prof. saaty, T. (1980) proposed that consistency index by comparing it with the appropriate one. The appropriate consistency index is called Random Consistency Index (R.I)

Then, proposed what is called consistency ratio, which is a comparison between consistency index and random consistency index, or in formula

$$C.R = \frac{0.057}{1.12}$$

C.R=0.5

If the value of consistency ratio is smaller or equal to 10%, the inconsistency is acceptable. If the consistency ratio is greater than 10%, we need to revise the subjective judgment.

1.1 GRAPHS

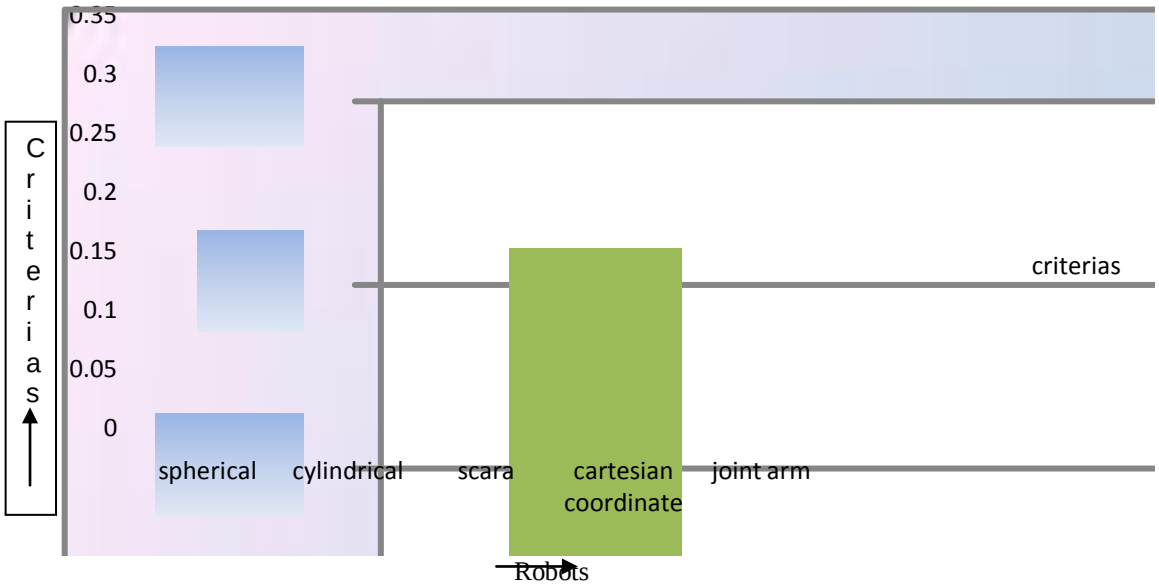

Fig 2: Final criterion weight obtained via AHP.

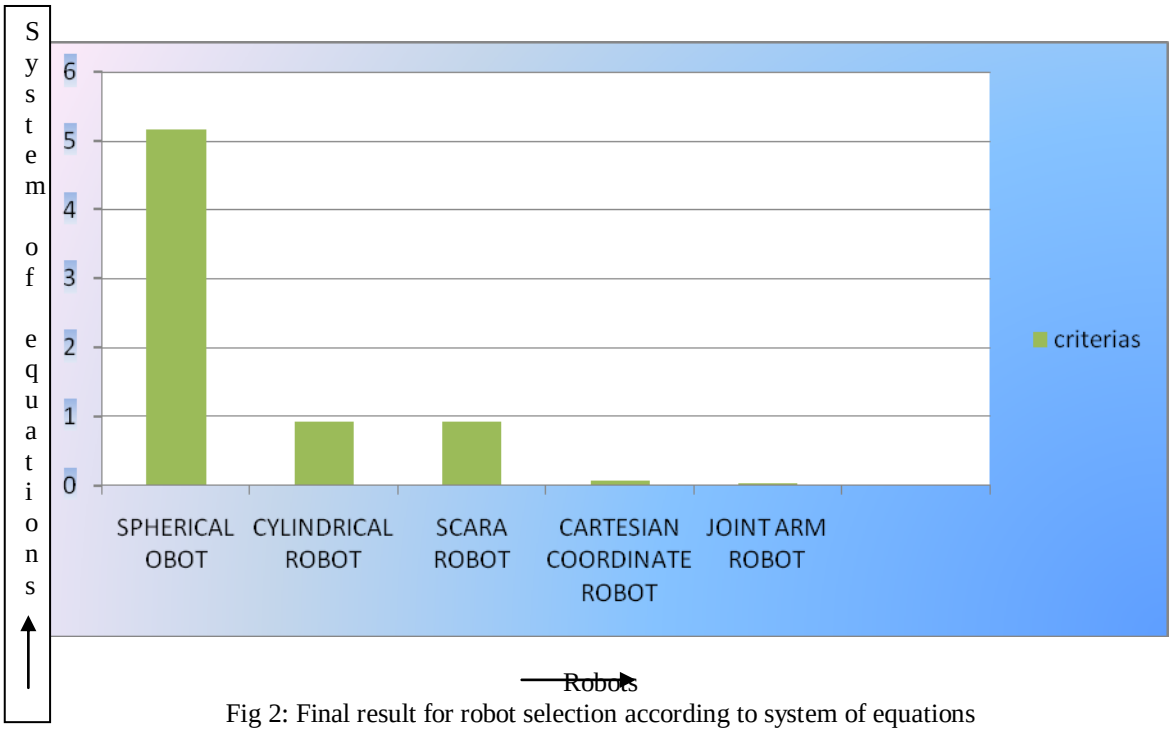

Fig 2: Final result for robot selection according to system of equations

V. CONCLUSION

The priorities obtained from the group decision makers' judgments are depicted. It shows that reliability of robot. the best robot selection criterion, followed by quality of product, life time of the robot, process, work environment, accuracy, life span, weight and cost of product. Thus, suggesting that the decision makers in the case of manufacturing firms should integrate the preceding criteria into robot selection decision. The inconsistency referred as Consistency Ratio is 0.5 < 10 reported by the Mat lab Software. This implies that the group decision maker's evaluation is consistent.

VI. REFERENCES

[1] Agrawal, V.P., Kohil, V. and Gupta. A., computer aided robot selection: the 'multiple attributed decision making' approach. Int. j. Prod. Res., 1991, 29(8), 1629-1644.
[2] Booth, D.E., Kouja, M. and Hu, M., A robust multivariative statistical procedure for evaluation and selection of industrial robots. Int. j. operat. Prod. Manage., 1992, 12, 15-24.
[3] Satty, T. (1980) The Analytical Hierarchy Process: Planning, Priority Setting. New York: McGraw-Hill
[4] Sharma M.J., Moon I., Bae H.: Analytic hierarchy process to assess and optimize distribution network, Applied Mathematics and Computation, 202, 256-265, 2008.
[5] Yahya, S. & B. Kingsman. (1999). Vendor rating for an entrepreneur development programme: a case study using the analytic hierarchy process method. Journal of the operational research society 50: 916-930.
[6] Tam, M.C.Y. & V.M.R. Tummala. (2001). An Application of the AHP in vendor selection of telecommunications system. Omega 29(2): 171-182.

American Journal of Engineering Research (AJER)
e-ISSN : 2320-0847 p-ISSN : 2320-0936
Volume-02, Issue-10, pp-112-116
www.ajer.org

Research Paper Open Access

A Study on Physico-Chemical Characteristics of Groundwater in the Industrial Zone of Visakhapatnam, Andhra Pradesh.

Dr. Yerramsetty Abbulu, Dr. G.V.R.Srinivasa Rao

Abstract: - An attempt is made in the present study to assess the groundwater quality in the industrial zone of Visakhapatnam, a port city. Groundwater samples collected from 114 sampling locations covering uniformly the entire industrial zone of the city are analysed for various physico-chemical characteristics to assess the groundwater quality. From the analysis, it is observed that the port area is found to have high concentrations of hardness, sulphates and calcium. The groundwater in Duvvada, a region surrounded by special economic zone and steel plant is found have more fluoride concentrations. Since, the study is conducted only for one year period, it is suggested to extend the study for more number of years continuously, with due consideration to various hydrological features, so that an authentic conclusion on the quality of groundwater can be made.

Key words: *- Groundwater quality, Physico-chemical characteristics, Hydrological features.*

I. INTRODUCTION

Water is an essential element of nature for the sustenance of life on the planet earth. It is available in the forms as surface water and sub-surface water or groundwater. Surface water is predominantly used for public water supply systems. However, the rapid growth of population and the resultant increased demand of water, necessitated for the usage of groundwater to augment the existing water supply systems, in most of the cities in the country. Secondly, the growing urbanization and industrialization and the consequent pollution of surface water sources, also increased the necessity of using groundwater for various domestic and industrial purposes.

Since, groundwater is occupying a major portion of water supply for both domestic and industrial purposes nowadays, it is highly essential that, its quality should match the domestic water standards. But in most of the industrial cities, the indiscriminate disposal of industrial wastes on to the land is resulting in the deterioration of groundwater quality due to the leachates from these wastes[1] [2][3][5]. However, due to the paucity of sufficient surface waters, invariably the people are thriving upon the groundwater sources to meet their water requirements. Hence, if groundwater sources are to be suggested for various uses, its quality should be assessed [6][4].

Visakhapatnam, the fastest developing industrial city of Andhra Pradesh, is no exception w.r.t. to the increased usage of groundwater for domestic and industrial purposes as well as the degradation of its quality due to the improper disposal of industrial wastes. Hence, an attempt is made in the present work to assess the groundwater quality in the industrial zone of Visakhapatnam city, keeping in view of the increased usage of groundwater in the recent times.

II. METHODOLOGY

A reconnaissance survey is conducted in the industrial area of the Visakhapatnam city with the help of a layout plan of the region, obtained from Greater Visakhapatnam Municipal Corporation (GVMC) in order to fix up the study area. The study area comprised of different parts of Visakhapatnam city spreading from ward numbers 40 to 72, where almost all large and small scale industries are located. The sampling points are located in such a way that, they are uniformly distributed in all the wards of the study area. 114 sampling locations are fixed up for sampling. Mostly, bore wells are considered for sampling. At certain places a few open wells and hand pumps are also considered for the sampling. Water samples are collected from each sampling point and are analysed for the parameters Viz., pH, Conductivity, Turbidity, Alkalinity, Hardness, Chlorides, Fluorides, TDS, Dissolved Oxygen, Iron, Sulphates, Calcium and Nitrogen as per the standard procedures.

III. RESULTS AND DISCUSSIONS

The results of the study are presented in the following table no.1. The following observations are made from the results.

1. The pH of the samples is found to be varying from a minimum value of 6.2 to a maximum value of 9.2. The maximum values are found in ward nos. 67, 68 and 70.
2. Conductivity is found to be more in the wards 45, 49, and 58 indicating high TDS concentration in groundwater of these areas. Conductivity varied from a minimum of 260 micro-seimans to a maximum of 2200 micio-seimans.
3. Turbidity is found to vary from 0.5. NTU to 0.79 NTU with an average value of 0.62 NTU.
4. Alkalinity is found to be more in the wards 67, 68 and 70 and varying from a minimum of 352 mg/l to a maximum of 892 mg/l.
5. Hardness is found to be more in the ward 25 which covers port areas. The maximum and minimum values are found to be 1398mg/l and 92mg/l.
6. Chloride concentration is varied from a minimum of 11mg/l to a maximum of 332mg/l.
7. Fluoride concentration is varied from a minimum of 1.02mg/l to a maximum of 1.65mg/l and it is found to be more in ward no. 57 and 58 covering Duvvada and Steel plant regions.
8. TDS is found to vary from 600mg/l to 1920mg/l with maximum values appearing in wards 45, 49 and 58.
9. D.O levels are found to be in the permissible limits and they varied from a minimum of 4.02mg/l to maximum of 8.2mg/l.
10. Iron is found to vary from a minimum of 0.31mg/l to a maximum of 0.76mg/l.
11. Sulphates are found to be more in the port area. They varied from a minimum of 12mg/l to a maximum of 144mg/l.
12. Calcium is also found to be more in port area and steel plant. It varied from 4.9mg/l to 164mg/l.
13. Nitrates, the analysis of which is done keeping in view of large scale industries dealing with organics, are found to vary from a minimum of 10mg/l to a maximum of 68.5mg/l.

IV. CONCLUSIONS AND SUGGESTIONS

1. pH, Conductivity, Alkalinity and Turbidity are found to be within the permissible limits, over the entire study area.
2. Chlorides and Iron are also found to be in acceptable limits.
3. Hardness, Calcium and Sulphates are found to be more than the permissible limits in the wards covering the entire port area.
4. Nitrates are found to be in permissible limits except in ward no. 45.
5. Fluoride is found to be exceeding the permissible limit of 1.5 mg/l in the region surrounding steel plant.
6. Since the study is conducted for a period of one year only, it is suggested to extend the study for more number of years and covering all seasons, in order to make more authentic conclusions.

REFERENCES

[1] **A.K. Sinha and Kamala Kant** "Underground water quality and its impact on the health of its users in Sarani Block of Rae Bareli" IJEP, 23(9):pp.1017-1024(2003)

[2] **Anuraag Mohan, Kinty Pandey, R.K. Singh and Vineet Kumar.** "Assessment of Underground water quality in industrial area of Bareilly" IJEP, 26(2):pp.153-158(2006)

[3] **D. Buddhi, Punam Tyagi, R.L.Sawhnay and Richa Kothani.** "Groundwater Quality of Pithampur Industrial area: Opinion survey of the residents" IJEP, 24(3):pp.167-172(2004)

[4] **G.R.Chaudhari , Deepali Sohani and V.S. Shrivastava** "Groundwater Quality Index near Industrial Area"

[5] IJEP, 24(1):pp.29-32(2004)

[6] **G.V.Pandian , N. Kannan, K. Paulraj and S. Paulrajan** "Effect of Industrial Pollution on ground water in Madurai Suburban Area" IJEP, 26(10):pp.939-945(2006)

[7] **K. Karunakaran , A. Samoon Nesaraj, S. Manjunatha, A.Doorty, M. Raja and D. Srividhya.** "A study on the Physico-chemical characteristics of groundwater in Salem Corporation. IJEP, 25(6):pp.510-512(2005)

S.No.	Parameter / Sample No.	pH	Conductivity (µs)	Turbidity (N.T.U.)	Alkalinity (mg/las $CaCO_3$)	Hardness (mg/las $CaCO_3$)	Chlorides (mg/l)	Fluorides (mg/l)	TDS(mg/l)	D.O. (mg/l)	Iron (mg/l)	Sulphates (mg/l)	Calcium (mg/l)	Nitrates (mg/l)
1	25/S1(B-2)	7.30	673	0.62	492.0	1064	262	1.25	872.2	4.02	1.146	109.2	136.98	68.5
2	25/S2(B-4)	7.20	1043	0.79	482.0	1398	164	1.29	1132.0	6.93	0.564	142.6	166.54	11.27
3	25/S3(B-7)	7.16	892	0.60	476.0	983	173	1.27	1030.6	6.24	0.702	101.1	129.19	37.44
4	41/S1(B-18)	6.84	920	0.51	443.2	320	137	1.15	1049.1	7.34	0.480	34.8	69.52	22.04
5	41/S2(B-09)	6.81	1083	0.73	437.0	393	193	1.21	1152.0	6.02	0.740	42.1	76.09	40.52
6	41/S3(B-14)	6.62	983	0.64	423.0	415	144	1.16	1062.3	7.94	0.360	44.3	78.07	13.64
7	42/S1(BW2)	6.70	1310	0.58	431.0	600	106	1.34	1356.1	8.20	0.310	62.8	94.72	10.00
8	42/S2(W-1)	6.40	1134	0.57	429.7	312	83	1.29	1293.0	6.30	0.380	34.0	68.80	36.60
9	42/S3(BW1)	6.90	1340	0.59	469.2	448	164	1.28	1368.3	7.30	0.490	47.6	81.04	22.60
10	42/S4(B-02)	6.72	1234	0.58	443.0	372	89	1.31	1298.3	7.90	0.370	40.0	74.20	14.20
11	42/S5(W25)	8.88	1140	0.54	673.40	470	109	1.35	1178.3	5.72	0.80	49.8	83.0	45.0
12	42/S6(W-2)	7.23	1100	0.63	491.30	401	72	1.26	1171.6	8.00	0.35	42.9	76.8	12.8
13	42/S7(W24)	6.20	1000	0.59	373.60	360	92	1.37	1103.5	6.30	0.69	38.8	73.1	36.6
14	43/S1(W-6)	7.10	914	0.57	485.40	334	143	1.29	1046.3	6.45	0.66	36.2	70.7	33.8
15	43/S2(B-21)	7.09	973	0.66	480.30	372	153	1.45	1058.3	6.93	0.56	40.0	74.2	28.2
16	44/S1(W-7)	7.03	934	0.73	478.92	401	167	1.16	1058.3	7.45	0.46	42.9	76.8	19.8
17	44/S2(B-25)	7.03	1083	0.62	478.92	412	274	1.35	1152.0	6.34	0.68	44.0	77.8	36.6
18	45/S1(BW2)	7.20	1400	0.52	492.30	456	192	1.29	1421.9	4.20	1.11	48.4	81.7	66.0
19	45/S2(BW3)	6.96	1100	0.65	469.32	482	127	1.46	1171.6	470	1.01	51.0	84.1	59.0
20	45/S3(BW9)	7.67	110	0.68	812.83	416	157	1.39	1171.6	4.90	0.97	44.4	78.1	56.2
21	45/S4(B-11)	7.60	980	0.62	573.3	436	178	1.26	1090.0	4.8	0.99	64.8	79.9	57.6
22	45/S5(B48)	6.87	1010	0.67	452.3	476	124	1.17	1110.3	4.9	0.97	50.4	83.5	56.2
23	45/S6(B56)	7.28	2000	0.54	493.4	644	210	1.32	1784.0	4.8	0.99	67.2	98.6	57.6
24	45/S7(B57)	7.19	2010	0.61	484.3	652	215	1.19	1790.8	4.7	1.01	68.0	99.4	59.0
25	45/S8(B60)	6.90	900	0.54	471.0	440	180	1.34	1035.5	4.4	1.07	46.8	80.3	63.2
26	45/S9(B65)	6.94	1000	0.57	476.3	484	118	1.16	1103.6	5.3	0.81	51.2	84.2	50.6
27	45/S10-B73	6.96	1010	0.58	478.1	448	126	1.17	1110.3	4.9	0.94	47.6	81.1	56.2
28	46/S1(B85)	7.10	1040	0.66	481.3	356	105	1.22	1130.8	5.4	0.87	48.4	72.7	49.2
29	46/S2(B93)	7.08	1030	0.61	480.5	504	165	1.25	1123.9	5.3	0.89	53.2	86.1	50.6
30	46/S3(BW-103)	6.83	1560	0.64	471.3	444	152	1.16	1484.6	5.2	0.91	47.2	80.6	52.0
31	46/S4(BW-104)	7.12	1040	0.57	483.4	472	123	1.18	1130.8	5.5	0.85	50.0	83.2	47.8
32	46/S5(BW-126)	7.02	1290	0.69	480.4	484	195	1.15	1301.0	4.9	0.97	51.2	84.2	56.2
33	46/S6(BW-128)	7.14	1090	0.71	484.5	456	172	1.24	1165.0	5.6	0.83	48.4	81.7	46.4
34	46/S7(BW-131)	7.18	960	0.52	486.7	356	110	1.36	1076.0	4.4	1.07	38.4	72.7	63.2
35	46/S7(BW-135)	6.92	1070	0.66	477.5	408	155	1.27	1151.0	5.8	0.79	43.6	77.4	43.6
36	46/S9(BW-136)	6.98	1220	0.68	478.1	456	165	1.36	1253.3	5.3	0.89	48.4	81.7	50.6
37	47/S1(BW-100)	6.90	1010	0.62	477.9	480	187	1.24	1110.3	5.6	0.83	50.8	83.9	46.4
38	47/S2(BW-101)	7.01	940	0.52	480.3	408	164	1.36	1062.5	5.4	0.87	43.6	77.7	49.2
39	47/S3(BW-110)	7.09	990	0.61	480.1	488	190	1.45	1096.7	4.2	1.11	51.6	84.6	66.0
40	47/S4(BW-118)	6.84	1100	0.58	464.3	424	182	1.38	1171.6	4.6	1.03	45.2	78.8	60.4
41	47/S5(BW-123)	6.89	1180	0.64	414.5	396	140	1.37	1249	5.2	0.91	42.4	76.3	52.0
42	48/S1(BW-78)	6.84	900	0.62	384.4	484	110	1.26	1034	5.3	0.89	51.2	84.3	50.6
43	48/S2(BW-81)	6.92	1100	0.64	419.7	564	180	1.31	1171	5.6	0.83	59.2	91.4	46.4

44	48/S3(BW-88)	6.89	980	0.62	414.5	432	125	1.25	1086	5.8	0.79	46.0	79.6	43.6
45	48/S4(BW-91)	7.12	970	0.70	453.9	456	134	1.32	1081	5.9	0.77	48.4	81.7	42.2
46	48/S1(BW6)	7.14	2200	0.57	477.4	423	135	14.2	1920	5.3	0.89	45.1	78.8	50.6
47	49/S2(BW-15)	6.90	2000	0.58	416.2	420	162	1.34	1783	5.1	0.93	44.8	78.5	53.4
48	49/S3(BW-22)	7.01	2200	0.56	435.1	436	181	1.19	1920	4.6	1.03	46.4	79.9	60.4
49	49/S4(BW-24)	7.07	2010	0.59	445.4	435	139	1.27	1790	5.1	0.93	46.3	79.8	53.4
50	49/S5(BW-35)	7.06	2080	0.61	443.7	442	145	1.29	1825	5.6	0.83	47.0	80.5	50.6
51	49/S6(BW-41)	7.11	2110	0.56	482.7	429	131	1.26	1858	5.5	0.85	45.7	79.3	47.8
52	49/S7(BW-76)	7.04	1040	0.59	476.8	436	130	1.31	1130	5.2	0.91	46.4	79.9	52.1
53	53/S1(BW5)	6.74	841	0.66	451.7	436	86	1.28	995	5.3	0.89	46.4	79.9	50.6
54	57/S1(BW-19)	6.8	1320	0.56	464.1	240	124	1.6	1321	5.6	0.83	26.8	62.3	46.4
55	57/S2(BW-13)	6.80	1232	0.69	464.1	434	20	1.52	1261	6.4	0.67	46.4	79.7	35.2
56	57/S3(BW-17)	7.0	1060	0.59	478.3	235	141	1.49	1144	5.5	0.85	26.3	61.8	47.8
57	57/S3(T-2)	7.0	1120	0.62	478.3	260	106	1.35	1185	5.4	0.87	28.8	64.1	49.2
58	58/S1(DW)	7.05	1156	0.61	478.9	256	121	1.62	1209	5.6	0.83	28.4	63.7	46.4
59	58/S2(B-02)	6.9	1420	0.58	478.1	230	135	1.54	1389	5.2	0.91	25.8	61.4	52.0
60	58/S3(BW4)	7.0	940	0.68	478.3	290	98	1.49	1062	5.6	0.83	31.8	66.8	46.4
61	58/S4(BW7)	7.00	1340	0.62	478.3	285	154	1.65	1368.3	5.8	0.79	31.3	63.3	43.6
62	58/S5(BW8)	6.90	900	0.59	478.1	270	174	1.59	1039.3	5.7	0.81	29.8	65.0	45.0
63	58/S6(BW9)	6.80	1540	0.58	464.1	265	86	1.61	1513.4	5.4	0.87	29.3	64.5	49.2
64	58/S7(W-1)	6.70	920	0.62	463.3	400	106	1.57	1049.3	6.1	0.73	42.8	76.7	39.4
65	58/S8(W-3)	6.90	2100	0.59	478.1	245	110	1.49	1851.9	5.2	0.91	27.3	62.8	52.0
66	59/S1(BW-12)	7.03	1010	0.56	476.2	576	58	1.23	1110.3	7.6	0.43	60.4	72.5	18.4
67	59/S2(BW-24)	6.80	1230	0.62	464.1	408	70	1.34	1262.5	8.1	0.33	43.6	77.4	11.4
68	59/S3(BW-25)	6.90	830	0.64	478.1	392	306	1.24	998.6	6.6	0.63	42.0	76.0	32.4
69	60/S1(B-1)	7.41	1062	0.56	492.3	368	77	1.02	1155.3	5.1	0.93	39.6	75.4	53.4
70	60/S2(B-3)	7.36	1035	0.53	488.9	356	74	0.99	1136.9	5.0	0.95	38.4	72.7	54.8
71	60/S3(B-5)	7.32	998	0.57	487.8	456	80	1.08	1102.2	5.3	0.89	48.4	81.7	50.6
72	61/S1(B-9)	7.32	1015	0.53	487.8	436	92	1.15	1113.7	5.4	0.87	46.4	79.9	49.2
73	61/S2(B-12)	7.43	1146	0.56	492.7	430	87	1.29	1203.0	6.5	0.65	45.8	79.4	33.8
74	61/S3(B-13)	7.40	1106	0.55	492.8	436	84	1.34	1175.7	6.2	0.71	46.4	79.9	38.0
75	61/S4(B-15)	7.39	1099	0.54	492.6	416	89	1.19	1171.0	5.9	0.77	44.4	78.1	42.2
76	61/S5(B-17)	7.45	1210	0.57	493.0	456	96	1.36	1246.7	7.0	0.55	48.4	81.7	26.8
77	61/S6(B-19)	7.42	1123	0.55	492.9	448	92	1.49	1157.3	6.8	0.59	47.6	81.0	29.8

78	63/S1(BW-16)	7.20	890	0.59	479.9	520	84	1.17	1028.7	6.4	0.67	54.8	87.5	35.2
79	63/S2(BW-26)	7.01	930	0.68	478.8	488	184	1.08	1056.0	5.9	0.77	51.6	92.7	42.2
80	64/S1(BW-142)	7.1	956	0.69	479.0	471	159	1.29	1073.6	6.2	0.71	49.9	83.1	38.0
81	64/S2(BW138)	7.12	941	0.65	479.3	479	141	1.37	1042	6.4	0.67	50.7	83.8	35.2
82	65/S1(BW18)	6.90	1190	0.59	478.1	480	110	1.29	1280	6.8	0.59	50.8	83.9	29.6
83	65/S2(BW-6)	6.72	1010	0.54	463.9	520	109	1.46	1125	6.9	0.57	54.8	87.5	28.2
84	65/S3(BW-7)	7.14	1090	0.62	479.5	680	258	1.05	1153	7.6	0.43	70.8	102.2	18.4
85	65/S4(BW-9)	6.96	1140	0.71	478.9	600	182	1.31	1178	7.4	0.47	62.8	94.7	21.2
86	65/S5(B11)	7.19	1200	0.59	479.0	424	256	1.08	1286	7.2	0.51	40.2	68.9	24.0
87	67/S1(W-04)	7.32	600	0.72	487.8	412	251	1.06	856	6.20	0.71	44.0	78..8	38.0
88	67/S2(W-07)	8.45	220	0.53	676.3	372	78	1.24	572	5.03	0.94	40.0	74.2	54.8
89	67/S3(W-11)	8.65	630	0.50	684.0	92	43	1.50	851	6.90	0.57	12.0	49.0	28.2
90	67/S4(W-14)	8.22	744	0.53	651.6	120	38	1.05	929	5.70	0.81	14.8	51.0	17.0
91	67/S5(W-39)	8.22	1080	0.53	653.3	216	55	1.14	1179	5.70	0.81	24.4	60.2	45
92	67/S6(W-21)	7.32	600	0.72	487.8	412	251	1.25	856	6.20	0.71	44.0	77.8	38
93	67/S1(W-18)	6.72	983	0.63	463.9	176	46	1.19	1062	5.40	0.87	20.4	64.6	49
94	68/S2(BW2)	7.45	804	0.66	489.0	510	138	1.34	1008	7.30	0.49	53.8	86.6	22
95	68/S3(W-36)	8.48	710	0.69	680.9	336	74	1.26	906	7.40	0.47	36.4	70.9	21
96	68/S4(W-19)	9.22	860	0.67	898.0	256	43	1.35	1015	5.10	0.93	28.4	63.7	53
97	68/S5(W22)	8.35	260	0.65	674.0	292	80	1.14	600	4.90	0.92	32.0	67.0	56
98	69/S1(W-33)	7.41	1210	0.58	589.3	248	20	1.15	1291	6.20	0.71	27.6	63.0	38
99	69/S2(W-34)	7.85	1520	0.59	616.3	96	11	1.24	1503	5.70	0.81	12.4	49.3	45
100	70/S1(W2)	9.13	670	0.56	906.3	248	75	1.26	870	5.60	0.83	27.6	63.0	46
101	70/S2(W1)	9.62	460	0.57	953.0	180	17	1.41	736	6.44	0.66	20.8	56.9	35.2
102	70/S3(W-14)	9.44	1790	0.59	937.3	344	39	1.29	1641	6.20	0.71	37.2	71.6	38.0
103	71/S1(W-31)	8.30	1083	0.63	664.8	348	56	1.28	1160	5.70	0.81	45.9	72.0	45.0
104	71/S2(W-30)	8.30	1080	0.71	664.7	160	23	1.19	1158	6.30	0.69	18.8	51.1	36.6
105	1-3/S1(W1)	7.06	1010	0.58	475.3	440	332	1.46	1110	5.20	0.91	46.8	80.3	52.0
106	1-3/S2(W2)	6.79	1220	0.79	463.0	436	184	1.32	1253	5.30	0.89	46.4	79.9	50.6
107	1-3/S3(B5)	6.89	1310	0.62	466.3	480	152	1.16	1314	5.60	0.83	50.8	83.9	46.4
108	1-3/S4(B6)	6.94	960	0.64	479.9	360	192	1.24	1076	5.40	0.87	38.8	73.1	49.2
109	1-3/S5(B7)	6.84	990	0.62	465.9	356	306	1.32	1096	5.80	0.79	38.4	72.7	43.6
110	1-3/S6(B9)	6.79	1210	0.69	477.4	356	164	1.26	1246	5.90	0.77	38.4	72.7	42.2
111	1-3/S8(W7)	7.00	1090	0.68	478.3	316	110	1.19	1070	5.3	0.89	34.4	69.7	50.6
112	1-3/S9(B15)	6.90	1010	0.58	477.9	356	106	1.08	1110	5.6	0.83	38.4	72.7	46.4
113	1-3/S10(B23)	6.82	1290	0.56	438.9	400	56	1.07	1300	5.4	0.87	42.8	76.7	49.2
114	1-3/S11(W11)	6.85	980	0.54	443.7	360	78	1.27	1091	5.2	0.91	38.8	73.1	52.0
	AVERAGE	**7.01**	**1190**	**0.62**	**490**	**460**	**135**	**1.30**	**1130**	**5.8**	**0.76**	**45.0**	**82.5**	**43.0**

American Journal of Engineering Research (AJER)
e-ISSN : 2320-0847 p-ISSN : 2320-0936
Volume-02, Issue-10, pp-117-127
www.ajer.org

Research Paper Open Access

Component Cost of Fuel Oil of Waste Transportation Cost

Burhamtoro, Achmad Wicaksono, M. Bisri, Soemarno
[1)] *Ph.d Candidate on Environment and Development Studies, Graduate School, University of Brawijaya, Malang, East Java, Indonesia*
[2)] *Department of Civil Engineering, Polytechnic of Malang, Indonesia*
[3)] *Department of Civil Engineering, Faculity of Engineering, University of Brawijaya, Indonesia*
[4)] *Department of Water Resources Engineering, Faculity of Engineering, University of Brawijaya, Indonesia*
[5)] *Laboratory of Remote Sensing, Faculity of Agriculture, University of Brawijaya, Indonesia*

Abstract: - The success of the transportation system can be measured based on four things, namely the efficiency of time, energy and fuel efficiency, environmental impact, and safety. Efficiency of energy and fuel is often stated as part of vehicle operating costs (VOC). So need to know the amount of the percentage of the fuel cost component of vehicle operating costs. The purpose of this study was to determine the percentage of the fuel cost component of the total cost of transportation. Research object is a dump truck or on the SCS transport system that serves the city of Malang. Stages of research begins with getting the data needed to analyze the cost of transporting waste. Furthermore, the analysis performed to determine the percentage of each component of transport costs. Results of the analysis showed that the greatest percentage of the cost of each component of the cost of transporting waste is a component of the fuel, while the smallest percentage of the cost of the mechanical components. For the percentage of fuel costs by 28.90% of the variable cost per kilometer, while the percentage of fuel costs by 27.45% of the total cost of transporting waste on his m^3 each.

Keywords**:** - *Fuel Oil, Vehicle Operating Costs, Costs of transporting waste, percentage, Stationery Container System (SCS)*

I. INTRODUCTION

Calculation of vehicle operating cost (VOC) involves several components, such as fuel, oil, spare parts, tires, mechanic and driver wages. Components are calculated using a specific formula obtained from previous studies. Analysis conducted by descriptive approach, based on quantitative data as a result of calculation of the cost of operating the vehicle. The entire cost of the data collected from the survey activities, will be converted into rupiah per 1000 km mileage (Bina Marga, 1995).

The success of the transportation system can be measured based on four things, namely the efficiency of time, the efficiency of energy and fuel, environmental impact, and safety. The efficiency of energy and fuel are often poured as part of the vehicle operation cost (VOC) (Sugiyanto, 2012). So need to know the amount of the percentage of the fuel cost component of vehicle operating costs.

Rise in world oil prices also affected in Indonesia. As a result, vehicle operating costs also increased. But the effect of fuel price increase on vehicle operating costs (VOC) are yet to be in percentage, due to unknown percentage of the cost components of fuel oil to the vehicle operating costs. So that the necessary analysis of the percentage of the cost components of fuel oil to the vehicle operating costs.

Waste transport vehicle operating costs assessed by the volume of waste transported. In the calculation of the transport vehicle operating costs also need to consider the cost of waste fuel used for transporting the waste. Calculation of percentage of fuel cost function of the cost of transporting waste to determine the amount of the percentage of the cost of fuel needed in the services, waste transportation.

II. LITERATURE

2. 1 Garbage Collection Pattern

According to SNI 19-2454-2002 (Indonesia Standart) pattern of garbage collection in Indonesia consists of: individual patterns of direct, indirect individual pattern, the pattern of communal direct, indirect communal pattern, and the pattern of street sweeping. Determination of the pattern of collection of each area is determined by the condition of each region.

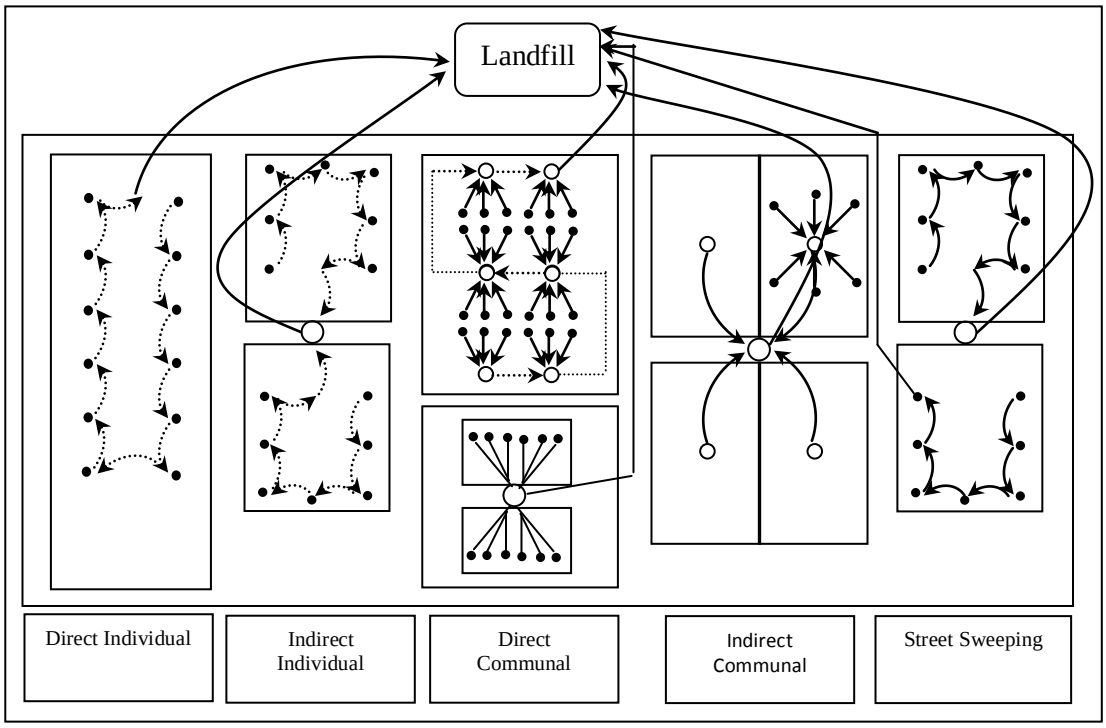

Sour ce: SNI 19-2454-2002

Figure 1. Garbage Collection Pattern

2. 2 Waste Transportation System

Based on the mode of operation and equipment used, known 2 system is the system of transporting waste container lift / hauled container system (HCS) and container system fixed / stationary container system (SCS).

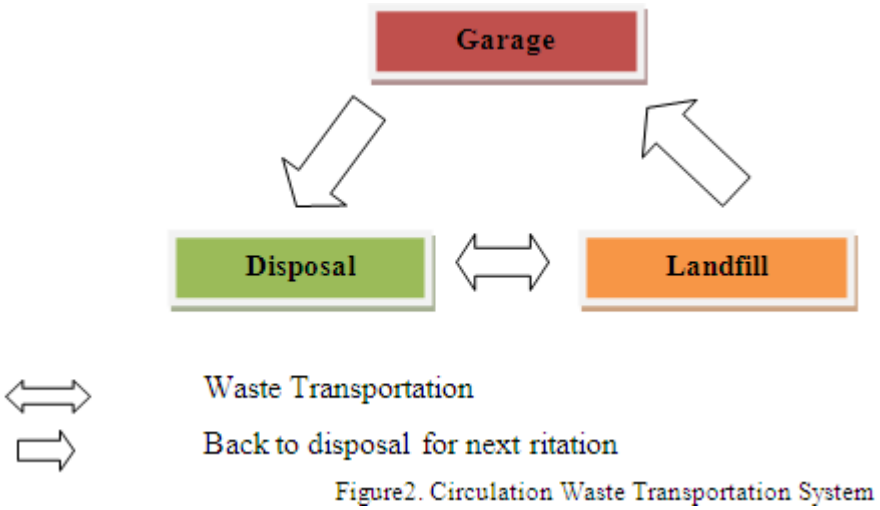

Figure2. Circulation Waste Transportation System

2. 3 Hauled Container System (HCS)

Hauled Container System (HCS) is a system of waste collection by way of container with its contents transported to the landfill, emptied and then returned to its original location (garage) or to a location of the next waste collection (SNI T-13-1990-F).

HCS is suitable for transferring waste from a source with a high level of waste containers used for relatively large size. The use of large containers reduce the handling time so that no unsightly and unhealthy conditions associated with the use of a number of small containers can be prevented. Another advantage of the HCS is their flexibility: containers with different sizes and shapes can be provided for the collection of all types of waste.

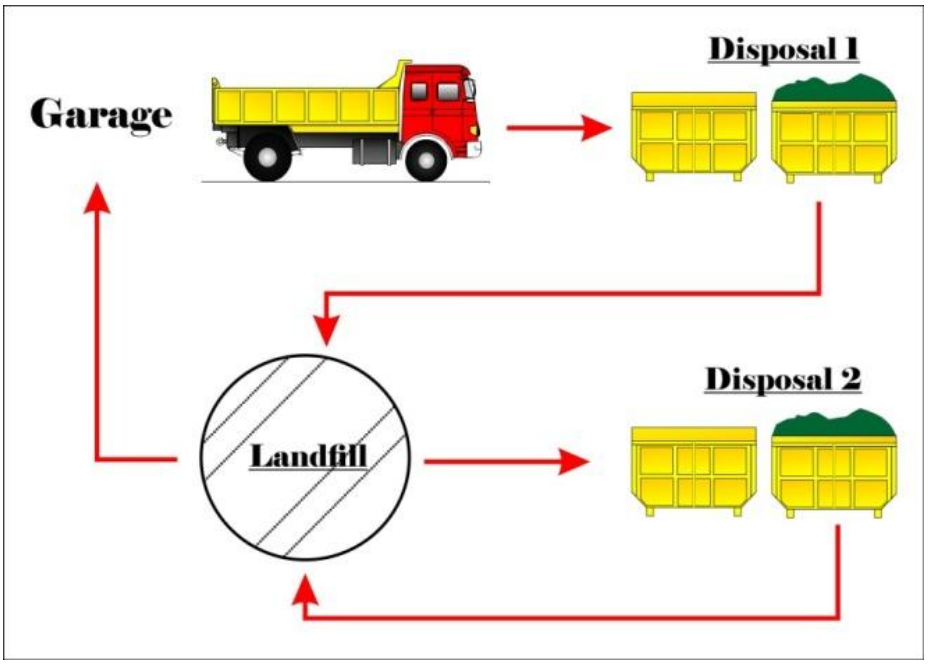

Figure 3. Hauled Container System

Caption:
a. Empty containers taken from the garage to the disposal 1.
b. Containers that have been filled from Disposal 1, was taken to the landfill to be emptied.
c. Containers that have been brought in to replace the empty container in TPS 2.
d. Filled containers of Disposal 2, was taken to the landfill to be emptied, and so on.
e. Truck back to the garage.

2. 4 Stationary Container System (SCS)
Stationery Container System is the waste collection system in a way, the container is left at the point of decision (a). Waste that is transferred into the trucks manually or assisted by mechanical equipment on the trucks (b), and then transported to the landfill.

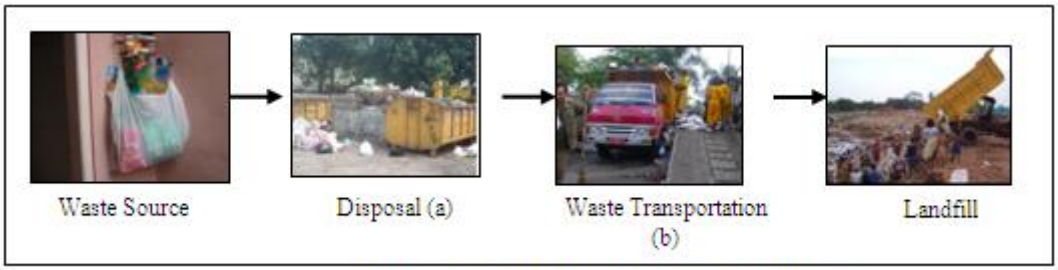

Figure 4. Stationary Container System (SCS)

Collection system at SCS has two main types:
a) Where compaction charging system (self-toading compactor) is used.
b) Where the vehicle charging system manual (manually loaded) is used

2. 5 Vehicle Operation Cost (VOC)
Vehicle operating cost is defined as the cost of all the factors associated with the operation of the vehicle under normal conditions for a particular purpose. Based on economic considerations, the necessary compatibility between the tariff (revenue) (Rahman, 2012). Several methods were attempted to calculate the

VOC component is Transport and Research Laboratory (TRRL) based on research in Kenya, for the calculation of VOC in the road outside the city (rural road) countries - Developing countries, Method Road User Cost Manual, (1992) (RUCM), Methods the Highway Design and Maintenance Standards Model - Vehicle Speeds and Operating Costs, (1987) (HDM-III VOC), Pacific Consultants Internasiona method (PCI) (1990), a method developed by LAPI-ITB (1997) and many more.

Calculation of vehicle operation cost (VOC) are costs that occur with the economical operation of a vehicle under normal conditions for a specific purpose (G Hamidi, 2013). In Indonesia there are two ways commonly used in the calculation of vehicle operating cost (VOC) that are PCI and LAPI-ITB. In the calculation of vehicle operating cost (VOC) is a factor that affects the speed of the vehicle (Levinsion, 2005).
VOC component consists of fixed costs, variable costs and other expenses. Fixed costs include: depreciation expenses, administrative expenses and allowances bus crew salaries, capital interest, vehicle insurance, vehicle crews and employees than management. Variable costs include: the cost of fuel, engine oil costs, tire costs, maintenance costs and the cost of mechanics. VOC component calculation method of PCI is still in units per 1000 km so as to obtain the unit value per km required distance from the road traversed, for speed (running speed) in km / h (Burhamtoro, 2013).

Model PCI (Musashi, 1990), which is used to calculate the VOC is a regression equation with speed as the independent variable. The equation is as follow:

Table 1. Calculation Vehicle Operation Cost (truck)

No.	Parameter Cost	Equations	Informations
1	Fuel Cost	$(0,06427V^2 - 7,0613V + 318,3326)$ x Fuel cost	Fuel Cost (liter/1000km)
2	Oil cost	$(0,00048V^2 - 0,05608V + 3,07383)$ x Oil Cost	Oil Cost (liter/1000km)
3	Tire cost	(0,0011553V - 0,0059333) x Tire cost x n Tire	Tire Cost (1 Tire/1000km)
4	Spare part cost	(0,0000191V + 0,00154) x Vehicle price	Spare part cost (Spare part/1000km)
5	Service cost	(0,01511V + 1,212) x Mechanic wages per hour	Service Cost (Mechanic/1000km)
6	Depreciation	(1/(6,129V + 245)) x Vehicle price	Depreciation cost (Depreciation/1000km)
7	Interest rate	((0,12 x 1000)/(1750V)) x Vehicle price	Interest rate (interest rate/1000km)
8	Insurance	((0,06x1000x0,5)/(1750V)) x Vehicle price	Insurance (Insurance/1000km)
9	Drive wages	(1000/V) x Driver wages	Driver Wages (Wage/1000km)
10	Overhead	Total Cost x 10%	

Information: V = Speed (km/hour)
Source: Yanagiya, 1990

III. RESEARCH METHODOLOGY

Stages of research begins with getting the data needed for the analysis of vehicle operating cost (VOC), including fuel prices, oil prices, tire prices, the price of the vehicle as well as the costs required. The data was obtained through field surveys or primary data. Prices are used as the data is generally accepted price in 2012 in the city of Malang.

The study was conducted on waste transport serving the transport in the city of Malang, in this peneletian research object in dump trucks or vehicles transporting the SCS system. SCS Transportation systems serve 16 temporary shelters (disposal) and spread over 4 districts. The type of vehicle used consisted of four types of brands, that is Cold Diesel, Toyota Dyna By 43 Long, "Toyota Dyna BU 343R" and Toyota New WU 342 R.

Once the data has been obtained, the next step is to conduct an analysis to determine the vehicle operating cost and transportation cost of each vehicle. Next calculate the percentage of each component of the variable costs and freight costs.

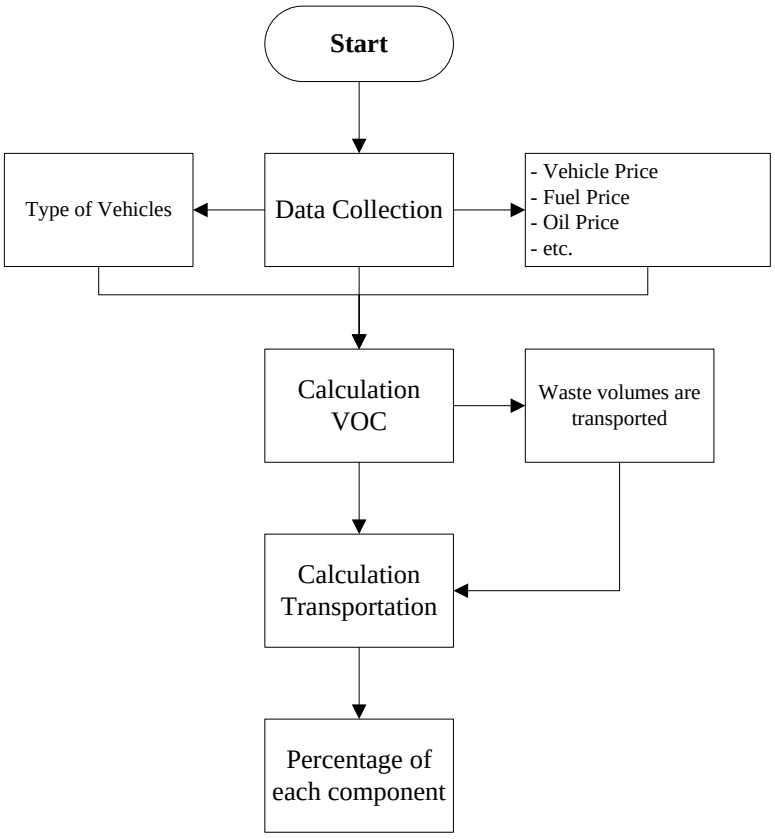

Figure 5. Flow Chart of Research

IV. ANALYSIS AND DISCUSSION

4. 1 Dump Truck vehicle transporting waste

Transporting waste type "Stationery Container System (SCS) in Malang, served 15 fleet serving four districts, that is Lowokwaru, Blimbing, Klojen and Sukun. District Kedungkandang services using system hauled Container System (HCS) with Arm Roll Truck. Initial analysis performed on the movement of the fleet to get the speed of each vehicle. Velocity data obtained by the data in the distance and the travel time for the vehicles transporting. Data distance, time and speed can be seen in Table 2.

Table 2. Distance, travel time and speed of Dump Truck

No	Temporary Disposal	Vehicle	Distance (km)	Time (minute)	Speed (km/h)
1	2	3	4	5	6
1	Cianjur (TMP)	Dump Truck Cold Diesel 1992	40,63	97,73	24,94
2	Sumbersari	Dump Truck Cold Diesel 1992	35,57	84,03	25,40
3	Asahan 1	Dump Truck Cold Diesel 1992	50,79	131,84	23,11
4	Stadin Blimbing	Dump Truck Cold Diesel 1992	38,39	104,59	22,02
5	Rampal Celaket	Dump Truck Cold Diesel 1992	24,88	71,11	20,99
6	Manyar	Dump Truck Cold Diesel 1992	25,41	79,62	19,15
7	Seram	Dump Truck T. New WU 342 R TKMQ AD3 2007	28,87	94,93	18,25
8	Muharto	Dump Truck T. New WU 342 R TKMQ AD3 2007	34,33	93,33	22,07
9	Raya Langsep	Dump Truck T. New WU 342 R TKMQ AD3 2007	34,33	99,43	20,72
10	Borobudur	Toyota Dyna BU 343R 2006	52,46	174,88	18,00
11	Sulfat	Toyota Dyna BU 343R 2006	39,62	141,72	16,77
12	Kartini	Toyota Dyna BU 343R 2005	19,53	42,82	27,37
13	Tawangmangu	Toyota Dyna BY 43 Long/490061 2002	45,84	130,25	21,12
14	Bentoel	Toyota Dyna BY 43 Long/490061 2002	20,79	68,55	18,20
15	Asahan 2	Toyota Dyna BY 43 Long/490061 2002	46,61	147,71	18,93
16	Oro-oro Dowo	Toyota Dyna BY 43 Long/490061 2002	21,87	71,01	18,48

Once known the type and brand of vehicle used, the next is to find the price of fuel, engine oil, tires, vehicle, mechanic wages, salaries and fixed costs of vehicles. Price and cost are used based on the market price in the city of Malang, and the data taken in 2012.

Table 3. List price and the cost of each type of vehicle

No	*Type of Vehicle*	*Price(IDR)*				
		Fuel	*Oil*	*Tire*	*Mechanic*	*Driver*
1	Dump Truck Cold Diesel	4.500	22.500	1.355.000	18.750	10.900
2	Toyota Dyna BY 43 Long	4.500	22.500	1.355.000	18.750	10.900
3	Toyota Dyna BU 343R	4.500	22.500	1.355.000	18.750	10.900
4	Dump Truck Toyota New WU 342 R TKMQ AD3	4.500	22.500	1.355.000	18.750	10.900

Continuation...

No	*Type of Vehicle*	*Price (IDR)*	*Fixed Cost (IDR)*		
		Vehicle	*STNK*	*SWJDKLLJ*	*KIR*
1	Dump Truck Cold Diesel	95.400.000	992.200	163.000	200.000
2	Toyota Dyna BY 43 Long	93.600.000	973.400	163.000	200.000
3	Toyota Dyna BU 343R	110.800.000	1.152.300	163.000	200.000
4	Dump Truck Toyota New WU 342 R TKMQ AD3	112.900.000	1.174.200	163.000	200.000

4. 2 Calculation VOC

The next analysis is to calculate vehicle operating costs (VOC).

Calculation of vehicle operating cost (VOC) can be seen in the following table:

Table 4. Vehicle Operating Cost Calculations (VOC)

Temporary Disposal	Volume (m^3)	Fuel (IDR/1000Km)	Oil (IDR/1000Km)	Tire (IDR/1000Km)	Spare Part (IDR/1000Km)
Cianjur (TMP)	17,30	639.886	44.406,77	186.049,13	192.367
Sumbersari	16,52	625.454	44.080,61	190.315,25	193.195
Asahan 1	11,27	698.007	45.765,37	168.869,15	189.034
Stadion Blimbing	14,82	732.688	46.610,45	158.618,08	187.046
Rampal Celaket	11,15	765.458	47.432,64	148.931,50	185.166
Manyar	23,61	824.053	48.960,00	131.611,57	181.806
Seram	21,80	852.708	49.733,70	123.141,33	213.212
Muharto	9,21	731.204	46.573,77	159.056,71	221.458
Raya Langsep	7,92	774.241	47.656,90	146.335,39	218.537
Borobudur	16,91	860.566	49.948,94	120.818,54	208.723
Sulfat	16,73	899.479	51.034,24	109.316,38	206.131
Kartini	24,37	562.865	42.717,71	208.815,83	228.550
Tawangmangu	21,28	761.508	47.332,33	150.099,00	181.895
Bentoel	12,71	854.278	49.776,59	122.677,33	176.676
Asahan 2	24,19	830.869	49.142,44	129.596,85	177.993
Oro-oro Dowo	11,15	845.279	49.531,42	125.337,32	177.182

Continuation...

Temporary Disposal	Mechanic (IDR/1000Km)	Depreciation (IDR/1000Km)	Interest Rate (IDR/1000Km)	Insurance (IDR/1000Km)	Wage (IDR/1000Km)
Cianjur (TMP)	29.791,89	239.770,45	262.258,13	65.564,53	436.982,34
Sumbersari	29.920,57	238.104,54	257.568,09	64.392,02	429.167,65
Asahan 1	29.273,68	246.722,01	283.011,00	70.752,75	471.561,39
Stadion Blimbing	28.964,48	251.065,31	297.036,06	74.259,02	494.930,37
Rampal Celaket	28.672,30	255.312,34	311.628,92	77.907,23	519.245,43
Manyar	28.149,87	263.275,48	341.639,56	85.409,89	569.250,05
Seram	27.894,38	316.396,31	424.291,87	106.072,97	597.384,66
Muharto	28.977,71	296.896,63	350.779,99	87.695,00	493.883,10
Raya Langsep	28.593,99	303.522,44	373.714,22	93.428,55	526.173,51
Borobudur	27.824,31	311.835,75	422.121,03	105.530,26	605.592,56
Sulfat	27.477,37	318.565,02	452.937,78	113.234,45	649.803,57
Kartini	30.478,61	268.452,06	277.616,11	69.404,03	398.279,72
Tawangmangu	28.707,51	249.985,44	303.949,35	75.987,34	516.188,92
Bentoel	27.880,38	262.531,84	352.715,08	88.178,77	599.006,42
Asahan 2	28.089,10	259.248,60	338.990,98	84.747,74	575.699,16
Oro-oro Dowo	27.960,62	261.259,91	347.309,83	86.827,46	589.826,84

Continuation...

Temporary Disposal	Overhead	VOC (PCI)		Variable
	(IDR/1000Km)	(IDR/1000Km)	(IDR/Km)	Cost
Cianjur (TMP)	209.707,66	2.306.784,25	2.306,78	93.724,64
Sumbersari	207.219,71	2.279.416,81	2.279,42	81.078,86
Asahan 1	220.299,70	2.423.296,73	2.423,30	123.079,24
Stadion Blimbing	227.121,69	2.498.338,62	2.498,34	95.911,22
Rampal Celaket	233.975,48	2.573.730,25	2.573,73	64.034,41
Manyar	247.415,55	2.721.571,03	2.721,57	69.155,12
Seram	271.083,53	2.981.918,85	2.981,92	86.088,00
Muharto	241.652,41	2.658.176,52	2.658,18	91.255,20
Raya Langsep	251.220,28	2.763.423,10	2.763,42	94.868,31
Borobudur	271.296,05	2.984.256,51	2.984,26	156.554,10
Sulfat	282.797,90	3.110.776,88	3.110,78	123.248,98
Kartini	208.717,86	2.295.896,41	2.295,90	44.838,86
Tawangmangu	231.565,31	2.547.218,39	2.547,22	116.764,49
Bentoel	253.371,98	2.787.091,81	2.787,09	57.943,64
Asahan 2	247.437,61	2.721.813,68	2.721,81	126.863,74
Oro-oro Dowo	251.051,42	2.761.565,61	2.761,57	60.395,44

Continuation ...

Temporary Disposal	STNK	SWJDKLLJ	KIR	Fixed	Transportation Cost	
				Cost	IDR/day	IDR/m^3
Cianjur (TMP)	992.200	163.000	200.000	4.706	98.430,20	5.689,61
Sumbersari	992.200	163.000	200.000	4.706	85.784,41	5.193,28
Asahan 1	992.200	163.000	200.000	4.706	127.784,80	11.335,47
Stadion Blimbing	992.200	163.000	200.000	4.706	100.616,77	6.790,78
Rampal Celaket	992.200	163.000	200.000	4.706	68.739,96	6.167,79
Manyar	992.200	163.000	200.000	4.706	73.860,68	3.128,14
Seram	1.174.200	163.000	200.000	5.338	91.425,50	4.193,83
Muharto	1.174.200	163.000	200.000	5.338	96.592,70	10.487,81
Raya Langsep	1.174.200	163.000	200.000	5.338	100.205,81	12.652,25
Borobudur	1.152.300	163.000	200.000	5.261	161.815,55	9.569,22
Sulfat	1.152.300	163.000	200.000	5.261	128.510,44	7.681,44
Kartini	1.152.300	163.000	200.000	5.261	50.100,32	2.056,10
Tawangmangu	973.400	163.000	200.000	4.640	121.404,77	5.705,11
Bentoel	973.400	163.000	200.000	4.640	62.583,92	4.923,99
Asahan 2	973.400	163.000	200.000	4.640	131.504,01	5.436,30
Oro-oro Dowo	973.400	163.000	200.000	4.640	65.035,72	5.832,80

Results of calculation vehicle operating costs, can be described as follows;

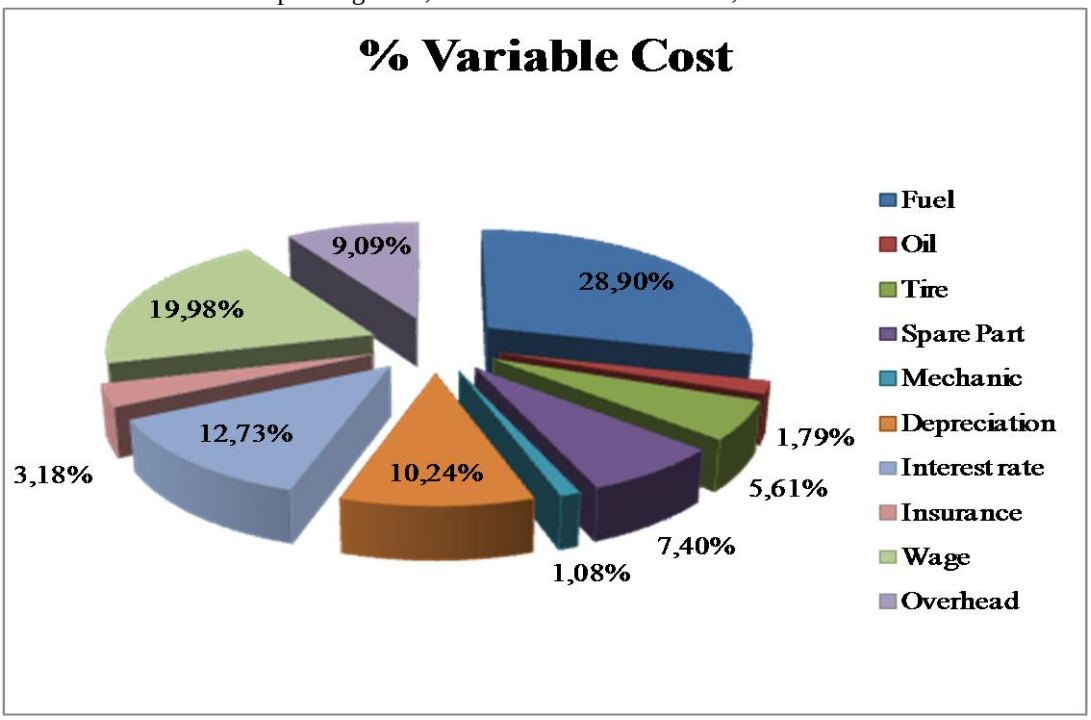

Figure 6. Percentage of the variable cost component of VOC

VOC component percentage is calculated based on the value of the variable cost component of each 1000 km are used as cost per km multiplied by the distance traveled. So as to know the percentage of each component of the variable cost incurred from each vehicle.

On Figure 6, it can be seen that the percentage of fuel (BBM) has the greatest percentage of 28.90% while the smallest percentage was 1.08% for mechanical components. The order of the percentage of each component can be seen as follows;

Component	Percentage
Fuel	28,90%
Wage	19,98%
Interest rate	12,73%
Depreciation	10,24%
Overhead	9,09%
Spare part	7,40%
Tire	5,61%
Insurance	3,18%
Oil	1,79%
Mechanic	1,08%
	100,00%

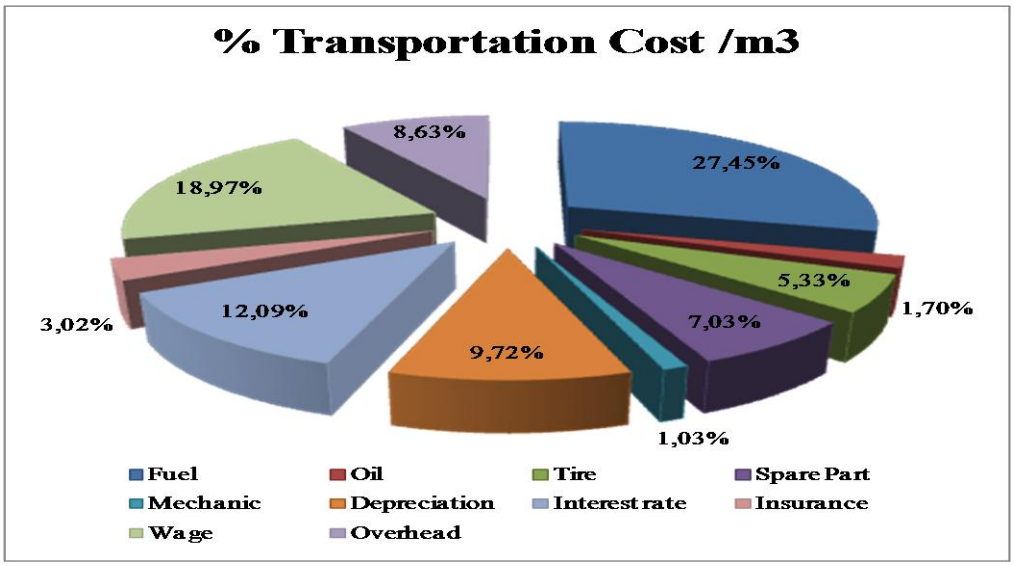

Figure 7. Percentage of the cost of transporting the components VOC

Percentage component of the cost of transporting waste VOC is calculated based on the value of each component of 1000 km which is used as the cost per km to the distance traveled multiplied and divided by the volume of waste transported. So as to know the percentage of each component of the cost of transporting waste. In the calculation of the percentage of components VOC biay waste transportation, it can be seen that the percentage of the cost of fuel oil (BBM) is also the largest that is 27.45%, while the smallest percentage of the mechanical componentsthat is 1.03%. The order of the percentage of each component can be seen as follows;

Component	Percentages
Fuel	27,45%
Wage	18,97%
Interest rate	12,09%
Depreciation	9,72%
Overhead	8,63%
Spare Part	7,03%
Tire	5,33%
Insurance	3,02%
Oil	1,70%
Mechanic	1,03%
Total	94,97%
Fixed cost	5,03%
	100,00%

Based on the analysis of the two can be seen that the fuel component has the largest percentage. Percentage of fuel oil to the calculation of transport costs approximately 27% - 29% of the total cost of transportation.

V. CONCLUSION

Based on the research conducted, it found several conclusions that can be drawn, among others:

1. Percentage of the cost of each component of the cost of transporting waste is the largest component of the fuel, while the smallest percentage of the cost of mechanical components
2. Percentage of the cost of fuel for 28.90% of the variable costs per kilometer.
3. Percentage of the cost of fuel for 27.45% of the total cost of transporting waste on his m^3 each.

VI. REFERENCES

[1] Bina Marga. *Biaya Operasional Kendaraan untuk Jalan Perkotaan di Indonesia*. Departemen Pekerjaan Umum. 1995.

[2] Burhamtoro. Optimizing of Transportation Municipal Solid Waste at Malang City. *Interdisciplinay Research in Natural Resources and Environmental Management, Post Graduate Progam University of Brawijaya*. 2012, pp.77-78.
[3] Burhamtoro. Model of Municipal Solid Wastes Transportation Costs Type Dump Truck (Case Study at The Malang City, Indonesia)**.** *International Journal of Engineering & Technology IJET-IJENS* Vol: 13 No: 03. 2013.
[4] Departemen Pekerjaan Umum. SNI 19-2454-2002 tentang Tata Cara Teknik Operasional Pengelolaan Sampah Perkotaan. 2002**.**
[5] Hamidi Gede Wajib. Analisis Biaya Perjalanan Akibat Tundaan Lalu Lintas**.** *Jurnal Ilmiah Elektronik Infrastruktur Teknik Sipil*, Volume 2, No. 1. 2013.
[6] LAPI. *Metode Pacific Consultants Internasional (PCI)*. Institut Teknologi Bandung, 1997.
[7] Lavinson, D. *Operating Costs for Trucks*. Twin Cities: Department of Civil Engineering University of Minnesota. 2005.
[8] Rahman, Rahmatang. Analisa Biaya Operasi Kendaraan (BOK) Angkutan Umum Antar Kota Dalam Propinsi Rute Palu – Poso**.** *Jurnal Rekayasa dan Manajemen Transportasi* Volume II No. 1. 2012. pp 8 – 21.
[9] Sofyan, M. Saleh, Ade Sjafruddin, Ofyar Z. Tamin and Ruzz Bona Frazila, Pengaruh Muatan Truk Berlebihan Terhadap Biaya Pemeliharaan Jalan, *Jurnal Transportasi*, Volume 9 (1). 2009. pp 85-96.
[10] Sugiyanto, Gito. Permodelan Biaya Kemacetan Pengguna Mobil Pribadi Dengan Variasi Nilai Kecepatan Aktual Kendaraan**.** *Jurnal Transportasi* Vol. 12 No. 2. 2012. pp 123-132.
[11] Yanagiya, Kensuke. *Feasibility Study on The Cikampek-Cirebon Toolway Project***.** Japan International Coorporation Agency. 1990.
[12] Peraturan Menteri Pekerjaan Umum No.21/PRT/M/2006 tentang Kebijakan dan Strategi Nasional Pengembangan Sistem Pengelolaan Sampah (KNSP-SPP).

American Journal of Engineering Research (AJER)
e-ISSN : 2320-0847 p-ISSN : 2320-0936
Volume-02, Issue-10, pp-128-135
www.ajer.org

Research Paper Open Access

Prioritization of sub-watersheds in semi arid region, Western Maharashtra, India using Geographical Information System

Abhijit M.Zende, R. Nagarajan, K. R. Atal
**Research scholar, [@]Associate Professor, [#]Lecturer (SG)*
**Center for Studies in Resource Engineering,*
Indian Institute Of Technology, Bombay
[#] Pune Institute of Computer Technology, Pune

Abstract: - The study area is one of the sub-river basin of Krishna river, covering an area of 3035 km² and lies in west part of Maharashtra state bounded by Latitude 16^0 55' to 17^0 28' N and Longitude 74^0 20' to 74^0 40' E. Poor soil cover, sparse vegetation, erratic rainfall and lack of soil moisture characterize the study area for most part of the year. Due to unavailability/poor managed of surface water storage structures, more than 50% area depends upon groundwater for their daily needs. Recurring drought coupled with increase in ground water exploitation results in decline in the ground water level. So the entire study area has been further divided into 9 sub-watersheds named SWS1 to SWS9, ranging in geographical area from 76 km² to 492 km² and has been taken up for prioritization based on morphometric analysis using Geographical information system (GIS) and remote sensing techniques. The drainage density of sub-watersheds varies between 2.07 to 3.26 km/km² and low drainage density values of sub-watershed SWS5 indicates that it has highly resistant, impermeable subsoil material with dense vegetative cover and low relief. The elongation ratio varies from 0.2 to 0.35 which indicates low relief and gentle ground slope. The high value of circularity ratio for SWS 8 sub-watershed 0.6 indicates the late maturity stage of topography. This anomaly is due to diversity of slope, relief and structural conditions prevailing in this sub-watershed. The compound parameter values are calculated and the sub-watershed with the lowest compound parameter is given the highest priority. The sub-watershed SWS3 has a minimum compound parameter value of 1.68 and SWS 8 has a maximum compound parameter 3.08. Hence it should be provided with immediate soil conservation measures because sedimentation is the major problem for surface water storage structures.

Keywords: - *Morphometric analysis, GIS, prioritization, remote sensing, sub-watersheds, soil conservation, compound parameters*

I. INTRODUCTION

The available surface and ground water resources are inadequate to meet the growing water demands due to rapid urbanization and increasing population. The demand for water has increased over the years, due to which the assessment of quantity and quality of water for its optimal utilization has become essential.

Identification and outlining of various ground features such as geological structures, geomorphic features and their hydraulic characteristics may serve as direct or indirect indicators of the presence of ground and surface water. The geomorphic conditions are essential pre-requisites in understanding the water bearing characteristics of hard rocks. The role of rocks types and geologic structure in the development of stream networks can be better understood by studying the nature and type of drainage pattern and by a quantitative morphometric analysis. The morphometric parameters of a watershed are reflective of its hydrological response to a considerable extent and can be helpful in synthesizing its hydrological behaviour. A quantitative morphometric characterization of a drainage basin is considered to be the most satisfactory method for the proper planning of watershed management because it enables us to understand the relationship among different aspects of the drainage pattern of the basin, and also to make a comparative evaluation of different drainage basins developed in various geologic and climatic regimes.

Krishna basin is located at 73^0 E to 78^0 E and 15^0 N to 19^0 N of Maharashtra covering total area about 90,000 sq km. In Maharashtra it covers an area of 15116sq km in the district of Satara, Sangli, Kolhapur. It is the fourth largest river basin in India. It has an average rainfalls ranging between 600 mm to 1900 mm per annum. The origin of the river is located at Mahabaleshwar having the height of 4500 ft above MSL. The Krishna basin running across Maharashtra, Karnataka, Andhra Pradesh and has an area of 2, 58,948 sq km i.e.7.9 % of India's surface area. The length of the Krishna River within Maharashtra is 304 kms. The term morphometry is the measurement and mathematical analysis of configuration of earth's surface, shape and dimension of its landform (Clark 1966). In the present study, Geographic Information System technique has been used to assessing various terrain and morphometric parameter of drainage basins and watershed. Linear, relief and aerial morphometric parameters are evaluated for development planning of sub watershed in Krishna Basin. Linear parameter analyzed includes stream order (u), stream length (L_u), mean stream length (L_{sm}) and bifurcation ratio (R_b).

Relief parameter analyzed includes Basin Relief (B_h) and Ruggedness number (R_n). Relief aspect of watersheds plays an important role for computing, surface and subsurface water flow, permeability, landform development, Drainage density (D_d), stream frequency (F_s), Texture ratio(T), Form factor (R_f), circulatory ratio(R_c) and Constant Channel Maintenance (C) which helps for drainage development. Drainage density is one of the important indicators of the landform element. It provides a numerical measurement of landscape dissection and runoff potential. The drainage pattern differs a lot in linear, relief and areal morphometric parameters due to difference in geological structure, land form configuration, slope, vegetation and rainfall distribution.

II. STUDY AREA

The study area lies in west part of Maharashtra state bounded by Latitude 16^0 55' to 17^0 28' N and Longitude 74^0 20' to 74^0 40' E. falling in part survey of India topographical sheet no 47 K – 5, 6, 7, 8, 10, 11, 12 and 47 L - 9 on the scale 1:50,000 it covers total area of 3035 km^2 includes two districts (Satara and Sangli) in Maharashtra.

The average annual rainfall increases from 1200 mm in the western side to 300 mm in the east side. Geology of the area is dominantly covered by basaltic rock. The area has suffered a lot by tectonic movement in the past as evidenced by varying fold, fault and lineament association with hills located in the western side of study area (Figure 1).

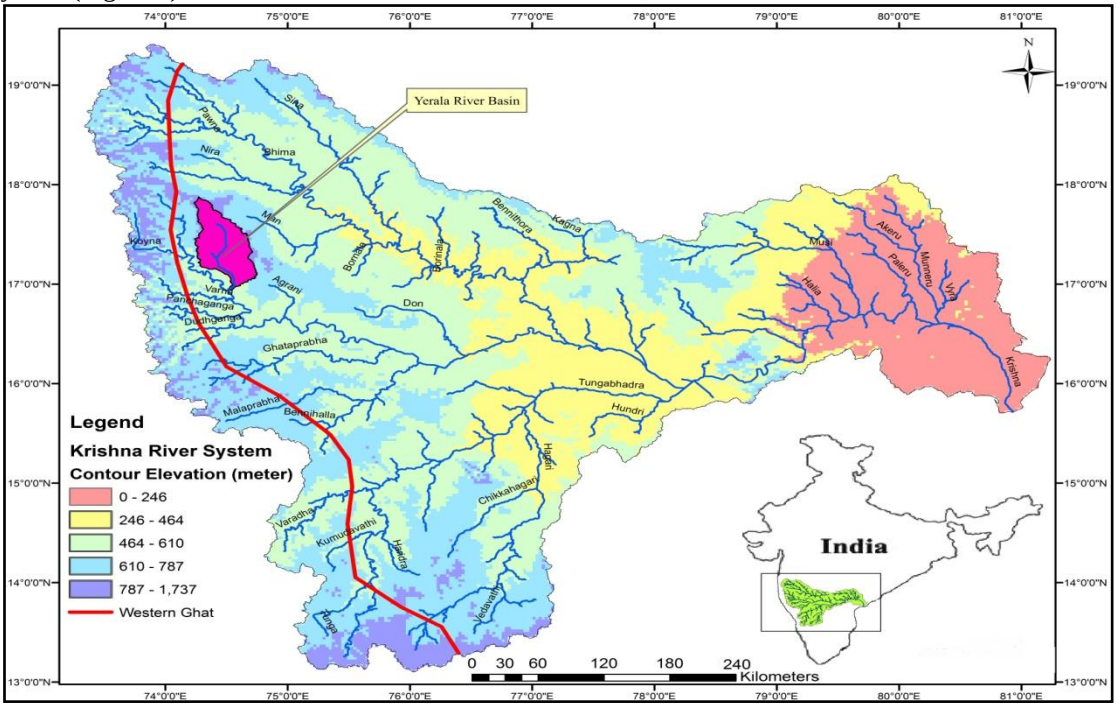

Fig. 1 Index map of Yerala river basin

III. METHODOLOGY

In the present study, the parameters considered for prioritization of sub-watersheds are from the natural resources thematic data, including drainage density, groundwater prospects, irrigated area, forest cover and wastelands derived from satellite imagery and socioeconomic data. The thematic maps are derived from SOI

topographic maps on 1:50000 scale. For better accuracy of the thematic map, ground truth check is done for verification and necessary modifications are made in thematic maps during post interpretation.

The digitization of sub-dendritic drainage pattern was carried out in GIS environment (Figure 2). The stream ordering is carried out using Horton's law. The fundamental parameters namely: stream length, area, perimeter, number of streams and basin length are derived from the drainage layer. The morphometric parameters for the delineated watershed area are calculated based on the formula suggested by (Horton, 1945), (Strahler, 1964), (Schumm, 1956), (Nookaratnam et al., 2005) and (Miller, 1953) given in table 1. Morphometric parameters like stream order, stream length, bifurcation ratio, drainage density, drainage frequency, relief ratio, elongation ratio, circularity ratio and compactness constant are calculated. Prioritization rating of all the nine sub-watersheds of Yerala watershed is carried out by calculating the compound parameter values. The sub-watershed with the lowest compound parameter value is given the highest priority.

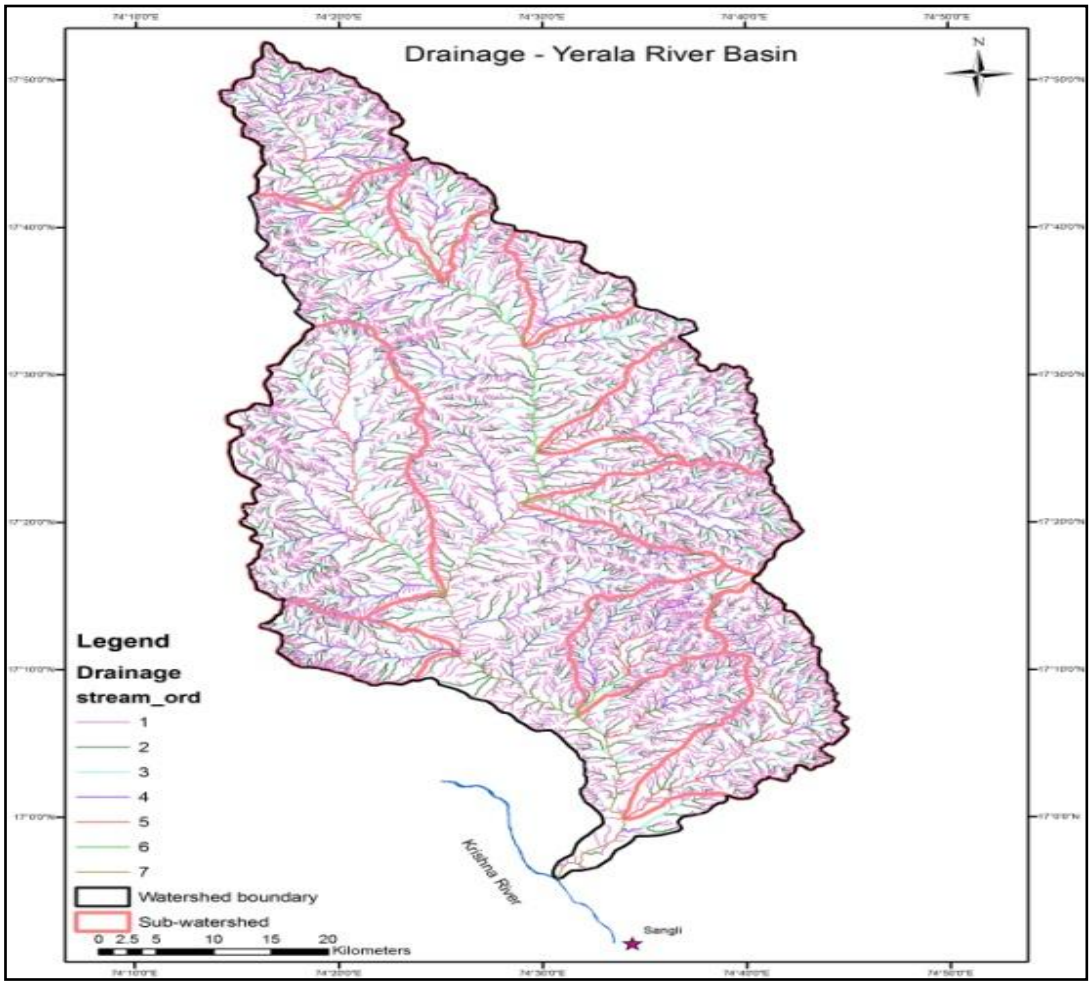

Figure 2 Driange network of Yerala river basin

IV. RESULTS AND DISCUSSION

Drainage pattern is characterized by irregular branching of tributaries in many directions with an angle less than 90º. The watershed is divided into nine sub-watersheds with codes SWS1 to SWS9.

4.1. Linear Aspect

The linear aspects of the channel system are stream order (U), stream length (Lu) and stream frequency (Fs). ***Stream order (U):*** The Yerala River is a 7th order stream covering an area of 3035 km². The sub-watershed SWS9 (Sonhira Odha) is having 4th order streams covering an area of 99 km². The sub-watersheds SWS1, SWS3, SWS4, SWS5 and SWS8 (Dargoba Odha, Darjai Odha, Kapur Nala, Krishnabai Odha and Ner Doha) is having 5th order streams covering an area of 175 km², 76 km², 242 km², 86 km² and 157 km² respectively. The variation in order and size of the sub-watersheds is largely due to physiographic and structural conditions of the region.

Table - 1 Formulae adopted for computation of morphometric parameters

SN	Morphometric	Formula	Reference
1	Stream order (u)	Hierarchical rank	Strahler (1964)
2	Stream length (Lu)	Length of the stream	Horton (1945)
3	Mean stream length (L_{sm})	$L_{sm} = L_u / N_u$ Where, L_{sm} = Mean stream length L_u = Total stream length of order 'u' N_u = Total no. of stream segments of order 'u'	Strahler (1964)
4	Stream length ratio (R_L)	$R_L = L_u / L_u - 1$ Where, R_L = Stream length ratio L_u = Total stream length of the order 'u' $L_u - 1$ = Total stream length of next lower order	Horton (1945)
5	Bifurcation ratio (R_b)	$R_b = N_u / N_u + 1$ Where, R_b = Bifurcation ratio N_u = Total no. of stream segments of order 'u' N_u+1 = No. of segments of the next higher order	Schumn (1956)
6	Mean bifurcation ratio	R_{bm} = Average of bifurcation ratios of all orders	Strahler (1957)
7	Relief ratio (R_h)	$R_h = H / L_b$ Where, R_h = Relief ratio H = Total relief (Relative relief) of the basin (km) L_b = Basin length	Schumm (1956)
8	Drainage density (D_d)	$D_d = L_u / A$ Where, D_d = Drainage density L_u = Total stream length of all orders A = Area of the basin (km2)	Horton (1932)
9	Stream frequency (F_s)	$F_s = N_u / A$ Where, F_s = Stream frequency N_u = Total no. of streams of all orders A = Area of the basin (km2)	Horton (1932)
10	Drainage texture (R_t)	$R_t = N_u / P$ Where, R_t = Drainage texture N_u = Total no. of streams of all orders P = Perimeter (km)	Horton (1945)
11	Form factor (R_f)	$R_f = A / L_{b^2}$ Where, R_f = Form factor A = Area of the basin (km2) L_{b^2} = Square of basin length	Horton (1932)
12	Circularity ratio (R_c)	$R_c = 4 * Pi * A / P^2$ Where, R_c = Circularity ratio Pi = 'Pi' value i.e., 3.14 A = Area of the basin (km2) P^2 = Square of the perimeter (km)	Miller (1953)
13	Elongation ratio (R_e)	$R_e = 2 / L_b$ Where, Re = Elongation ratio A = Area of the basin (km2) Pi = 'Pi' value i.e., 3.14 L_b = Basin length	Schumn (1956)
14	Length of overland flow (L_g)	$L_g = 1 / D * 2$ Where, L_g = Length of overland flow D = Drainage density	Horton (1945)

Stream length (Lu): The stream length was computed on the basis of the law proposed by (Horton, 1945), for all the 9 sub-watersheds. Generally, the total length of stream segments decrease as the stream order increase. In 9 sub-watersheds the stream length followed Horton's law (Table 2).

Table 2 Stream Analysis

Sub Watershed		Stream numbers						Stream Length						Length ratio				
		1	2	3	4	5	6	1	2	3	4	5	6	2/1	3/2	4/3	5/4	6/5
SWS 1	Chand Nadi	397	101	29	7	1	-	242.94	73.9	54.38	29.12	1.15	-	0.30	0.73	0.53	0.03	0.00
SWS 2	Dargoba Odha	309	70	26	8	3	1	176.42	48.54	28.15	12.15	13.82	4.05	0.27	0.57	0.43	1.13	0.29
SWS 3	Darjai Odha	114	35	14	3	1	-	91.67	31.19	25.65	6.9	8.8	-	0.34	0.82	0.26	1.27	0.00
SWS 4	Kapur Nala	543	145	37	11	1	-	362.15	117.18	66.59	21.77	9.94	-	0.32	0.56	0.32	0.45	0.00
SWS 5	Krishna Odha	144	48	11	5	1	-	102.22	36.78	25.69	9.94	3.4	-	0.35	0.69	0.38	0.34	0.00
SWS 6	Mahadev Odha	464	136	31	10	2	1	267.48	103.54	46.91	20.16	9.95	7.93	0.38	0.45	0.42	0.49	0.79
SWS 7	Nani Nadi	826	226	71	19	4	1	593.36	234.06	115.3	63.11	10.12	9.19	0.39	0.49	0.54	0.16	0.90
SWS 8	Ner Odha	490	179	56	21	3	1	299.99	114.32	51.81	28.54	9.33	8.25	0.38	0.45	0.55	0.32	0.88
SWS 9	Sonhira Odha	226	62	22	2	0	-	147.7	72.08	28.04	5.8	-	-	0.48	0.38	0.20	0.00	0.00

Stream Length ratio (Rl): Horton's law of stream length states that mean stream length segments of each of the successive orders of a basin tends to approximate a direct geometric series with stream length increasing towards higher order of streams. The stream length ratio between different sub-watersheds showed an increasing and decreasing trend in the length ratio from lower order to higher order and in the sub-watersheds SWS1, 2, 3, 4, 5, 7, 9 there was a change from one order to another order indicating the late youth stage of geomorphic development of streams in the inter basin area.

Stream frequency (Fs): The stream frequencies of all the sub-watersheds are mentioned in Table 3. Generally if the sub watersheds having large area under dense forest have low drainage frequency and the area having more agricultural land have high drainage frequency. High value of drainage frequency in SWS 8 and SWS 2 produces more runoff in comparison to others.

4.2. Dimensionless factors

Form factor (Rf):

The form factor for all sub-watersheds varies from 0.10 – 0.31 (Table3). This observation shows that the sub-watersheds are more or less elongated. The elongated watershed with low value of Rf indicates that the basin will have a flatter peak flow for longer duration. Flood flows of such elongated basins are easier to manage than from the circular basin.

Elongation Ratio (Re):

The elongation ratio for all sub-watersheds varies from 0.2 – 0.35 which indicates normal relief and gentle ground slope (Table3). The sub-watersheds SWS 2 and SWS 5 has ratio 0.2 and 0.35 respectively.

Circularity Ratio (Rc):

It is influenced by the length and frequency of streams, geological structures, land use/ land cover, climate, relief and slope of the watershed. In the present study (Table 3), the Rc value for all sub-watersheds varies from 0.35 to 0.60 which shows that the sub-watersheds are almost elongated. The high value of circularity ratio for SWS 8 indicates the late maturity stage of topography. This anomaly is due to diversity of slope, relief and structural conditions prevailing in this sub-watershed.

4.3. Measurement of intensity of dissection

Drainage density (Dd):

(Horton, 1932) has introduced drainage density (Dd) as an expression to indicate the closeness of spacing of channels. Drainage density in all the sub-watersheds varies from 2.07 to 3.26 respectively (Table 4). In general it has been observed over a wide range of geologic and climatic types, that low drainage density is more likely to occur in regions of highly permeable subsoil material under dense vegetative cover, and where relief is low. In contrast, high Dd is favored in regions of weak or impermeable subsurface materials, sparse vegetation and mountainous relief (Nag, 1998). Hence in this study in order to find out the correlation of Dd

with land use/cover, spatial distribution of land use/cover was studied. Low Dd value for sub-watershed SWS 5 indicates that it has highly resistant, impermeable subsoil material with dense vegetative cover and low relief.

Table 3 Morphometric Parameters of Yerala River

Sub Watershed	Area (Km^2)	Stream Frequency (Km/Km^2)	Basin Length (Km)	Form Factor	Elongation ratio	Circulatory ratio
SWS 1	172.00	3.11	26.87	0.24	0.30	0.48
SWS 2	98.00	4.26	30.64	0.1	0.20	0.44
SWS 3	76.00	2.19	18.23	0.22	0.30	0.56
SWS 4	242.00	3.05	47.55	0.1	0.20	0.35
SWS 5	86.00	2.43	16.6	0.31	0.35	0.53
SWS 6	183.00	3.51	33.48	0.16	0.25	0.57
SWS 7	492.00	2.33	44.47	0.24	0.31	0.55
SWS 8	157.00	4.79	24.07	0.27	0.33	0.6
SWS 9	99.00	3.15	22.04	0.2	0.28	0.56

Table 4 Values of drainage density, texture and bifurcation ratios for Yerala River Sub- watershed

Sub Watershed	Perimeter	Drainage Density	Drainage texture	Bifurcation ration Rb					Mean Bifurcation ratio
				1/2	2/3	3/4	4/5	5/6	
SWS 1	67	2.330	7.99	3.93	3.48	4.14	7.00	0.00	3.71
SWS 2	53	2.890	7.87	4.41	2.69	3.25	2.67	3.00	3.20
SWS 3	41	2.160	4.07	3.26	2.50	4.67	3.00	0.00	2.68
SWS 4	92	2.380	8.03	3.74	3.92	3.36	3.67	0.00	2.94
SWS 5	45	2.070	4.64	3.00	4.36	2.20	5.00	0.00	2.91
SWS 6	63	2.490	10.22	3.41	4.39	3.10	5.00	2.00	3.58
SWS 7	106	2.080	10.82	3.65	3.18	3.74	4.75	4.00	3.86
SWS 8	57	3.260	13.21	2.74	3.20	2.67	7.00	0.75	3.27
SWS 9	47	2.560	6.63	3.65	2.82	11.00	0.00	0.00	3.49

The compound parameter values of all nine sub-watersheds of Yerala watershed are calculated and prioritization rating is shown in Table 5. The sub-watershed SWS 3 with a compound parameter value of 1.68 receives the highest priority followed by SWS 5 and SWS 4. Highest priority indicates the greater degree of erosion in the particular micro-watershed and it becomes potential candidate for applying soil conservation measures. Thus soil conservation measures can first be applied to sub-watershed SWS3 and then to the other sub-watersheds depending upon their priority. The final prioritized map of the study area and prioritization ranks of sub-watersheds is shown in Figure 3.

Table 5 Prioritization Results of Morphometric Analysis

Sub Watershed	Dd	Fs	T	Rf	Rc	C	Rb	Rt	Compound parameter	Final Priority
SWS 1	2.33	3.11	5.93	0.24	0.48	0.43	3.71	7.99	2.69	7
SWS 2	2.89	4.26	5.83	0.10	0.44	0.35	3.20	7.87	2.77	8
SWS 3	2.16	2.19	2.78	0.22	0.56	0.46	2.68	4.07	1.68	1
SWS 4	2.38	3.05	1.23	0.10	0.35	0.41	2.93	8.03	2.05	3
SWS 5	2.07	2.43	2.53	0.31	0.53	0.48	2.91	4.64	1.77	2
SWS 6	2.49	3.51	1.80	0.16	0.57	0.40	3.58	10.22	2.53	6
SWS 7	2.08	2.33	1.07	0.24	0.55	0.47	3.86	10.82	2.38	5
SWS 8	3.26	4.79	2.00	0.27	0.60	0.30	3.27	13.21	3.08	9
SWS 9	2.56	3.15	2.42	0.20	0.56	0.39	3.49	6.63	2.16	4

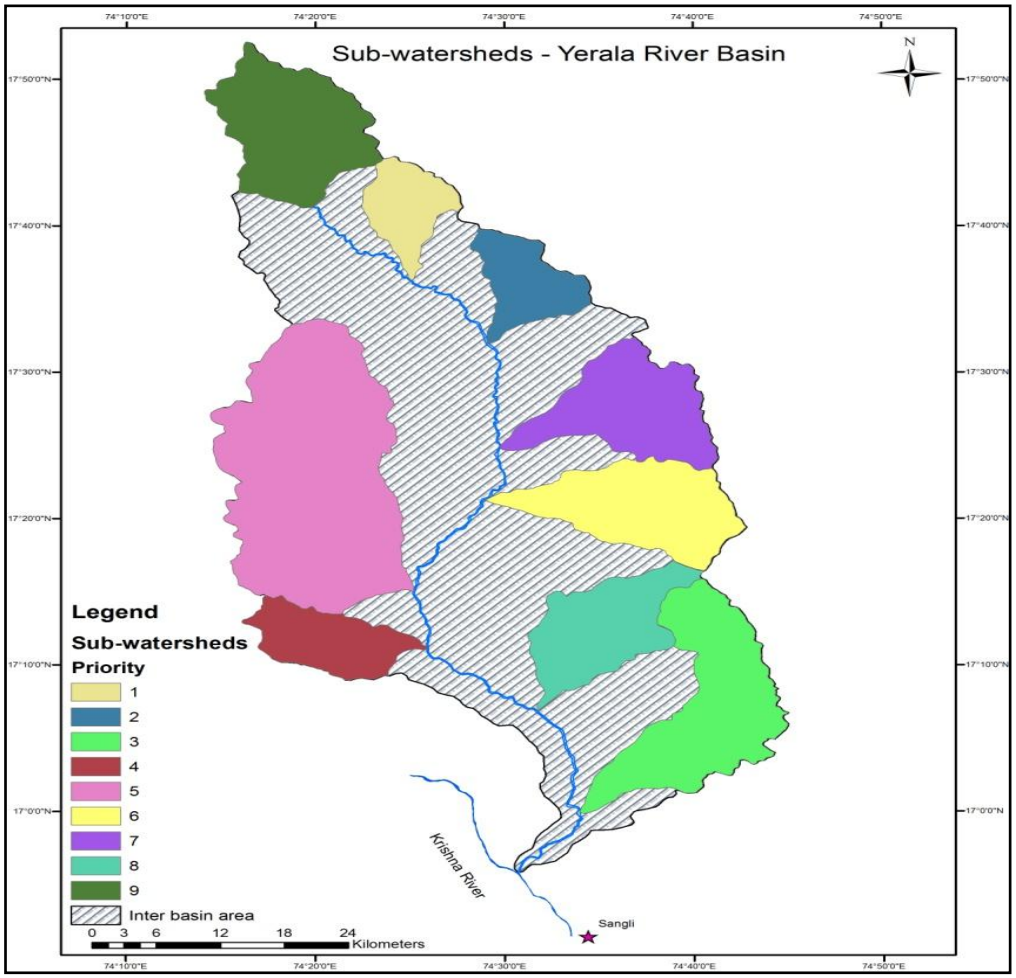

Figure 3 Prioritized sub-watershed map of Yerala watershed

V. CONCLUSION

Watershed prioritization is one of the most important aspects of planning for implementation of its development and management programmes. The present study demonstrates the usefulness of GIS for morphometric analysis and prioritization of the sub-watersheds of Yerala watershed of Western Maharashtra, India. The morphometric characteristics of different sub-watersheds show their relative characteristics with respect to hydrologic response of the watershed. Morphometric parameters coupled with integrated thematic map of drainage density land use can help in decision making process for water resources management. Results of prioritization of sub-watersheds show that sub-watersheds SWS 3 and SWS 5 are more susceptible to soil erosion. Therefore, immediate attention towards soil conservation measures is required in these sub-watersheds to preserve the land from further erosion and to alleviate natural hazards.

REFERENCES

[1] Biswas, S., Sudhakar, S. and Desai, V. R., 1999, Prioritisation of sub-watersheds based on morphometric analysis of drainage basin: A Remote Sensing and GIS approach, Journal of Indian Society of Remote Sensing, 27(3), pp 155166.

[2] CEE, Prioritization of micro watersheds for management in Bijapur district of Karnataka, Centre for Environment Education, Bangalore, 20, p. 89.

[3] Chopra, R., Dhiman, R., and Sharma, P. K., 2005, Morphometric analysis of sub-watersheds in Gurdaspur District, Punjab using Remote Sensing and GIS techniques, Journal of Indian Society of Remote Sensing, 33(4), pp 531539.

[4] Horton, R. E., 1945, Erosional development of streams and their drainage basins; Hydrological approach to quantitative morphology, Geological Society of American Bulletin, 56, pp 275370.

[5] Khan, M.A., Gupta, V.P. and Moharana, P.C., 2001, Watershed prioritization using remote sensing and geographical information system: a case study from Guhiya, India, Journal of Arid Environments, 49, pp 465475.
[6] Miller, V. C., 1953, A quantitative geomorphic study of drainage basin characteristics in the clinch mountain area, Technical report3, Department of Geology, Columbia University.
[7] Nag, S. K., 1998, Morphometric analysis using remote sensing techniques in the Chaka subbasin, Purulia district, West Bengal, Journal of Indian Society of Remote Sensing, 26, 12, pp 6976.
[8] Nookaratnam, K., Srivastava, Y. K., Venkateswarao, V., Amminedu, E. and Murthy, K.S.R., 2005, Check dam positioning by prioritization of micro-watersheds using SYI model and morphometric analysis – Remote sensing and GIS perspective, Journal of the Indian Society of Remote Sensing, 33(1), pp 2528.
[9] Sangita Mishra., R. Nagarajan 2010, Morphometric analysis and prioritization of using GIS and Remote Sensing: a case study of Odisha, India, International Journal of Geomatics and Geosciences Vol – 1, No.2 pp 501-510.
[10] Schumm, S. A., 1956, Evolution of drainage systems and slopes in Badlands at Perth Amboy, New Jersey, Geological Society of America, Bulletin**,** 67, pp 597646.
[11] Shrimali, S.S., Aggarwal, S. P. and Samra, J. S.,2001, Prioritizing erosion-prone areas in hills using remote sensing and GIS – a case study of the Sukhna Lake catchment, Northern India, JAG, 3(1), pp 5460.
[12] Srinivasa, V. S., Govindaonah, S. and Home Gowda, H., 2004, Morphometric analysis of sub-watersheds in the Pawagada area of Tumkur district South India using remote sensing and GIS techniques, Journal of Indian Society of Remote Sensing, 32(4) pp 351362.
[13] Strahler, A. N. (1964), Quantitative geomorphology of drainage basins and channel networks, section 4II, In: Handbook of Applied Hydrology, edited by V.T. Chow, McGraw-Hill, pp 439.
[14] Thakkar, A. K. and Dhiman S. D., 2007, Morphometric analysis and prioritization on mini-watersheds in Mohr watershed, Gujarat using remote sensing and GIS techniques, Journal of Indian Society of Remote Sensing, 35(4) pp 313321.

American Journal of Engineering Research (AJER)
e-ISSN : 2320-0847 p-ISSN : 2320-0936
Volume-02, Issue-10, pp-136-145
www.ajer.org

Research Paper Open Access

VLSI Architecture for Fast Computation of 2D-Discrete Wavelet Transform and Low Power Feed Forward Neural Network Architecture for Image Compression

[1]Mr. Murali Mohan. S, [2] Dr. P.Satyanarayana
[1](Associate Professor, Dept. of ECE, Sri Venkateswara College of Engineering & Technology, Chittoor, A.P., INDIA,
[2](Professor, Dept. of ECE, College of Engineering, S.V.University, Tirupati, A.P.,INDIA,

Abstract: - Artificial Neural Networks (ANN) is significantly used in signal and image processing techniques for pattern recognition and template matching. Discrete Wavelet Transform (DWT) is combined with neural network to achieve higher compression if 2D data such as image. Image compression using neural network and DWT have shown superior results over classical techniques, with 70% higher compression and 20% improvement in Mean Square Error (MSE). Hardware complexity and power dissipation are the major challenges that have been addressed in this work for VLSI implementation. In this work VLSI architecture for neural network and DWT is designed to operate at frequency of 250 MHz and low power techniques are adopted to reduce power dissipation to less than 100mW. Daubechies wavelet filter and Haar wavelet filters are used for DWT, input layer with one hidden layer and output layer consisting of tansig and purelin function used for compression. Low power techniques and low power library in 65nm technology is used for VLSI implementation.

Key words: - *DWT, Neural Network, Image Compression, VLSI Implementation, High Speed, Low Power*

I. INTRODUCTION

Image compression is one of the most promising subjects in image processing. Images captured need to be stored or transmitted over long distances. Raw image occupies memory and hence need to be compressed. With the demand for high quality video on mobile platforms there is a need to compress raw images and reproduce the images without any degradation. Several standards such as JPEG200, MPEG-2/4 recommend use of Discrete Wavelet Transforms (DWT) for image transformation [1] which leads to compression, when encoded. Wavelets are a mathematical tool for hierarchically decomposing functions in multiple hierarchical sub bands with time scale resolutions. Image compression using Wavelet Transforms is a powerful method that is preferred by scientists to get the compressed images at higher compression ratios with higher PSNR values [2]. It is a popular transform used for some of the image compression standards in lossy compression methods. Unlike the discrete cosine transform, the wavelet transform is not Fourier-based and therefore wavelets do a better job of handling discontinuities in data.

On the other hand, Artificial Neural Networks (ANN) for image compression applications has marginally increased in recent years. Neural networks are inherent adaptive systems [3][4][5][6]; they are suitable for handling nonstationaries in image data. Artificial neural network can be employed with success to image compression. Image Compression using Neural Networks by Ivan Vilovic [7] reveals a direct solution method for image compression using the neural networks. An experience of using multilayer perceptron for image compression is also presented. The multilayer perceptron is used for transform coding of the image. Image compression with neural networks by J. Jiang [8] presents an extensive survey on the development of neural networks for image compression which covers three categories: direct image compression by neural networks; neural network implementation of existing techniques, and neural network based technology which provide improvement over traditional algorithms. Neural Networks-based Image Compression System by H. Nait Charif and Fathi. M. Salam [9] describes a practical and effective image compression system based on

multilayer neural networks. The system consists of two multilayer neural networks that compress the image in two stages. The algorithms and architectures reported in these papers sub divided the images into sub blocks and the sub blocks are reorganized for processing. Reordering of sub blocks leads to blocking artifacts. Hence it is required to avoid reorganization of sub blocks. One of the methods was to combine neural networks with wavelets for image compression. Image compression using wavelet transform and a neural network was suggested previously [10]. Wavelet networks (WNs) were introduced by Zhang and Benveniste [11], [12] in 1992 as a combination of artificial neural networks and wavelet decomposition. Since then, however, WNs have received only little attention. In the wavelet networks, the basis radial functions in some RBF-networks are replaced by wavelets. Szu et al. [13], [14] have shown usage of WNs for signals representation and classification. They have explained how a set of WN, "a super wavelet", can be produced and the original ideas presented can be used for the assortment of model. Besides, they have mentioned the big compression of data achieved by such a representation of WN's. Zhang [15] has proved that the WN's can manipulate the non-linear regression of the moderately big dimension of entry with the data of training. Ramanaiah and Cyril [16] in their paper have reported the use of neural networks and wavelets for image compression. Murali and Dr. Satyanarayana [17] reports use of neural networks with DWT improves compression ratio by 70% and MSE by 20%. The complexities of hardware implementation on VLSI platform are not discussed in this paper. Murali andDr. Satyanarayana [18] reports the use of FPGA for implementation of neural network and DWT architecture, the design operates are 127 MHz and consumes 0.45 mW on Virtex-5 FPGAs. ASIC implementation of the algorithm proposed is reported as scope for future work. In this paper ASIC implementation of 2D-DWT architecture with ANN architecture is designed and implemented on ASIC platform using 65nm CMOS technology optimizing area, timing and power. Section II presents theoretical background on neural networks and DWT. Section III discusses the image compression architecture using DWT and ANN technique, section IV presents ASIC implementation of DWT-ANN, section V presents results and discussions and followed with conclusion in section VI.

II. NEURAL NETWORKS AND DWT

In this section, neural network architecture for image compression is discussed. Feed forward neural network architecture and back propagation algorithm for training is presented. DWT based image transformation and compression is also presented in this section. Compression is one of the major subject of research, the need for compression is discussed as follows [17]: Uncompressed video of size 640 x 480 resolution, with each pixel of 8 bit (1 bytes), with 24 fps occupies 307.2 Kbytes per image (frame) or 7.37 Mbytes per second or 442 Mbytes per minute or 26.5 Gbytes per hour. If the frame rate is increased from 24 fps to 30 fps, then for 640 x 480 resolution, 24 bit (3 bytes) colour, 30 fps occupies 921.6 Kbytes per image (frame) or 27.6 Mbytes per second or 1.66 Gbytes per minute or 99.5 Gbytes per hour. Given a 100 Gigabyte disk can store about 1-4 hours of high quality video, with channel data rate of 64Kbits/sec – 40 – 438 secs/per frame transmission. For HDTV with 720 x 1280 pixels/frame, progressive scanning at 60 frames/s: 1.3Gb/s – with 20Mb/s available – 70% compression required – 0.35bpp. In this work we propose a novel architecture based on neural network and DWT [18].

2.1 Feed Forward Neural Network Architecture for Image Compression

An Artificial Neural Network (ANN) is an information- processing paradigm that is inspired by the way biological nervous systems, such as the Brian, process information [16]. The key element of this paradigm is the novel structure of the information processing system. The basic architecture for image compression using neural network is shown in figure 1. The network has input layer, hidden layer and output layer. Inputs from the image are fed into the network, which are passed through the multi layered neural network. The input to the network is the original image and the output obtained is the reconstructed image. The output obtained at the hidden layer is the compressed image. The network is used for image compression by breaking it in two parts as shown in the Figure 1. The transmitter encodes and then transmits the output of the hidden layer (only 16 values as compared to the 64 values of the original image). The receiver receives and decodes the 16 hidden outputs and generates the 64 outputs. Since the network is implementing an identity map, the output at the receiver is an exact reconstruction of the original image.

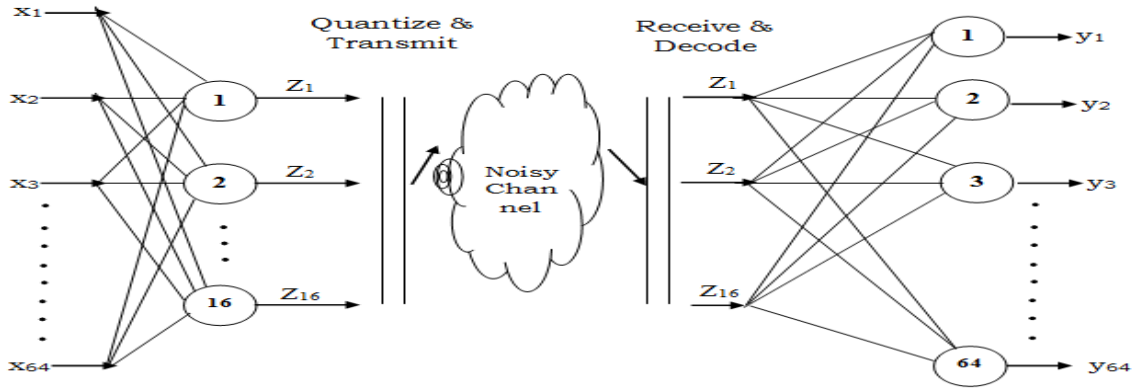

Figure 1: Feed forward multilayered neural network architecture

Three layers, one input layer, one output layer and one hidden layer, are designed. The input layer and output layer are fully connected to the hidden layer. Compression is achieved by designing the network such that the number of neurons at the hidden layer is less than that of neurons at both input and the output layers. The input image is split up into blocks or vectors of 8 X8, 4 X 4 or 16 X 16 pixels. Back-propagation is one of the neural networks which are directly applied to image compression coding [20][21][22]. In the previous sections theory on the basic structure of the neuron was considered. The essence of the neural networks lies in the way the weights are updated. The updating of the weights is through a definite algorithm. In this paper Back Propagation (BP) algorithm is studied and implemented.

2.2 DWT architecture for image compression

The DWT represents the signal in dynamic sub-band decomposition. Generation of the DWT in a wavelet packet allows sub-band analysis without the constraint of dynamic decomposition. The discrete wavelet packet transform (DWPT) performs an adaptive decomposition of frequency axis. The specific decomposition will be selected according to an optimization criterion. The Discrete Wavelet Transform (DWT), based on time-scale representation, provides efficient multi-resolution sub-band decomposition of signals. It has become a powerful tool for signal processing and finds numerous applications in various fields such as audio compression, pattern recognition, texture discrimination, computer graphics [24][25][26] etc. Specifically the 2-D DWT and its counterpart 2-D Inverse DWT (IDWT) play a significant role in many image/video coding applications. Figure 2 shows the DWT architecture, the input image is decomposed into high pass and low pass components using HPF and LPF filters giving rise to the first level of hierarchy. The process is continued until multiple hierarchies are obtained. A1 and D1 are the approximation and detail filters.

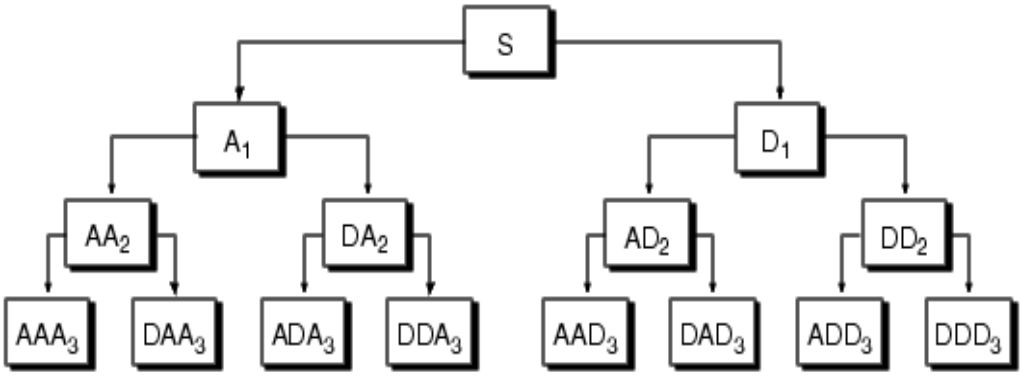

Figure 2: DWT decomposition

Figure 3 shows the decomposition results. The barbera image is first decomposed into four sub bands of LL, LH, HL and HH. Further the LL sub band is decomposed into four more sub bands as shown in the figure. The LL component has the maximum information content as shown in figure 3, the other higher order sub bands contain the edges in the vertical, horizontal and diagonal directions. An image of size N X N is decomposed to N/2 X N/2 of four sub bands. Choosing the LL sub band and rejecting the other sub bands at the first level compresses the image by 75%. Thus DWT assists in compression. Furhter encoding increases compression ratio.

Figure 3 DWT decomposition of barbera image into hierarchical sub bands

III. ANN WITH DWT FOR IMAGE COMPRESSION

Basic architecture for image compression using neural network is shown in the above figure 4. The input image of size 64 x 1 is multiplied by 4 x 64 weight matrixes to obtain the compressed output of 4 x 1, at the receiver 4 x 1 is decompressed to 64 x 1 by multiplying the compressed matrix by 64 x 4. The table in figure 4 shows the compression ratio that can be achieved by choosing the sizes of hidden layer.

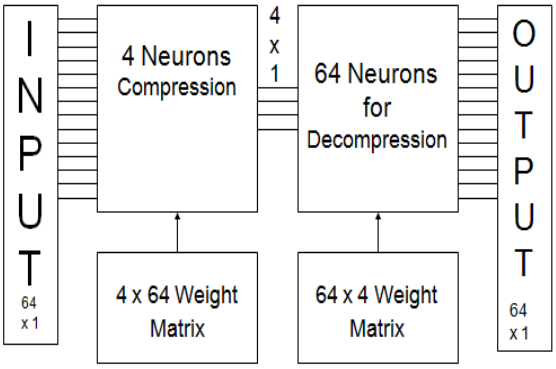

Network size	Size of hidden layer	Compression ratio
64-64-64	64	0%
64-32-64	32	50%
64-16-64	16	75%
64-08-64	08	87.5%
64-04-64	04	93.75%
64-01-64	01	98.5%

Figure 4: Neural network based image compression

Prior to use of NN for compression it is required to perform training of the network, in this work we have used back propagation training algorithm for obtaining the optimum weights and biases for the NN architecture. Based on the training, barbera image is compressed and decompressed; Figure 5 shows the input image, compressed image and decompressed image.

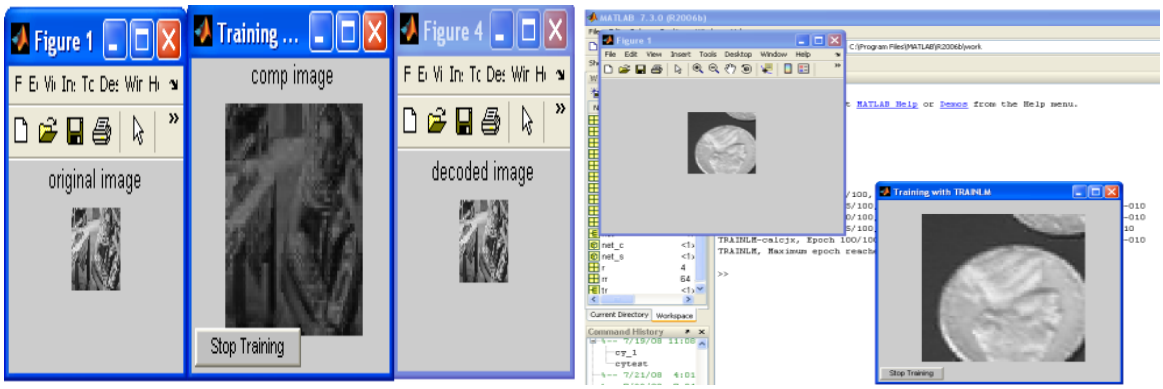

Figure 5: NN based image compression and decompression

Figure 5 also shows the input image and the decompressed image of coins image using neural network architecture. From the decompressed results shown, we find the checker blocks error, which exists on the decompressed image. As the input image is sub divided into 8 x 8 blocks and rearranged to 64 x 1 input matrixes, the checker block arises. This is one of the limitations of NN based compression. Another major limitation is the maximum compression ration which is less than 100%, in order to achieve compression more

than 100% and to eliminate checker box errors or blocking artifacts we proposed DWT combined with NN architecture for image compression.

3.1 Image Compression using DWT-ANN

Most of the image compression techniques use either neural networks for compression or DWT (Discrete wavelet Transform) based transformation for compression. In order to overcome the limitations of NN architecture in this work, DWT is used for image decomposition and an N X N image is decomposed using DWT into hierarchical blocks the decomposition is carried out until the sub block is of size 8 x 8. For a image of size 64 x 64, first level decomposition gives rise to 32 x 32 (four sub bands) of sub blocks, further decomposition leads to 16 x 16 (sixteen sub bands), which can further decamped to 8 x 8 at the third hierarchy. The third level of hierarchy there are 64 sub blocks each of size 8 x 8. Figure 6 shows the decomposition levels of input image of size 64 x 64.

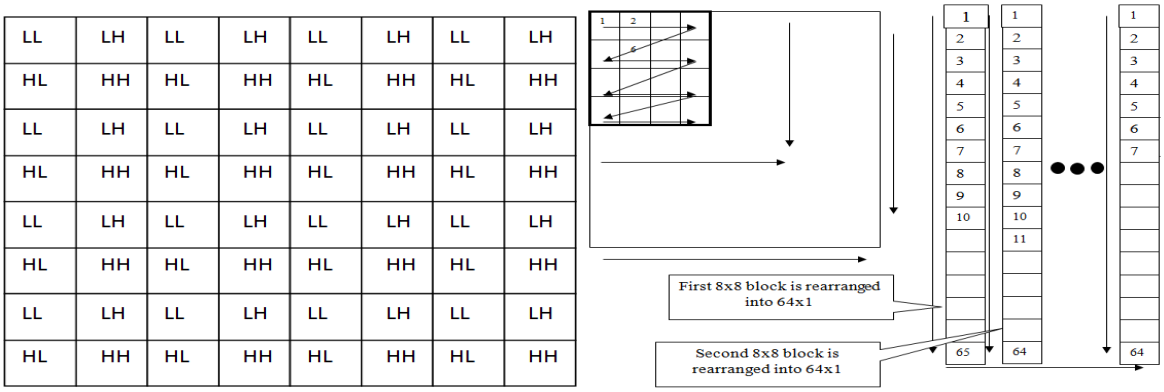

Figure 6: Decomposition of image into sub blocks using DWT

Sub blocks of 8 x 8 are rearranged to 64 x 1 block are combined together into a rearranged matrix size as shown in figure 6. The rearranged matrix is used to train the NN architecture based on back propagation algorithm. In order to train the NN architecture and to obtain optimum weights it is required to select appropriate images [17][18]. The training vectors play a vital role in NN architecture for image compression. The NN architecture consisting of input layer, hidden layer and output layer. The network functions such as tansig and purelin are used to realize feed forward neural network architecture [18]. In this work, hybrid neural network architecture is realized using DWT combined with ANN. The hybrid architecture is discussed in the research paper [Ramanaiah and Cyril]. The NN based compression using analog VLSI is presented in the research paper [Cyril and Pinjare]. Based on the two different papers neural network architecture is developed and is trained to compress and decompress multiple images. The DWT based image compression algorithm is combined with neural network architecture. There are several wavelet filters and neural network functions. It is required to choose appropriate wavelets and appropriate neural network functions. In this work an experimental setup is modeled using Matlab to choose appropriate wavelet and appropriate neural network function. Based on the above parameters chosen the Hybrid Compression Algorithm is developed and is shown in Figure 7.

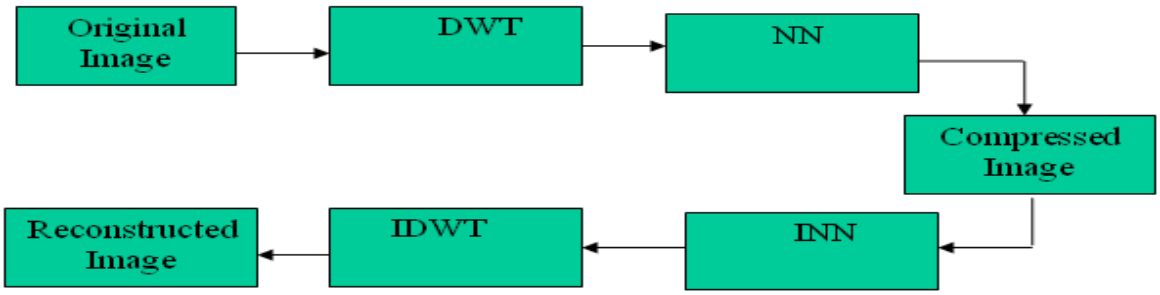

Figure 7: Proposed hybrid algorithms for image compression

Several images are considered for training the network, the input image is resized to 256 x 256, the resized image is transformed using DWT, 2D DWT function is used for the transformation. There is several wavelet functions, in this work Haar and dB4 wavelet functions are used. The input image is decomposed to obtain the sub band components using several stages of DWT. The DWT process is stopped until the sub band

size is 8 x 8. The decomposed sub band components are rearranged to column vectors; the rearranged vectors are concatenated to matrix and are set at the input to the neural network. The hidden layer is realized using 4 neurons and tansig function. The weights are biases obtained after training are used to compress the input to the required size and is further processed using weights and biases in the output layer to decompress. The decompressed is further converted from vector to blocks of sub bands. The sub band components are grouped together and are transformed using inverse DWT. The transformation is done using multiple hierarchies and the original image is reconstructed. The input image and the output image is used to compute MSE, PSNR. The selection of network parameters and performances are discussed in the next section.

IV. ASIC IMPLEMENTATION OF DWT-ANN ARCHITECTURE

Synthesis is a complex task consisting of many phases and requires various inputs in order to produce a functionally correct netlist. Synthesis includes the following main tasks: reading in the design, setting constraints, optimizing the design, analyzing the results and saving the design database. The first task in synthesis is to read the design into Design Compiler memory. Reading in an HDL design description consists of two tasks: *analyzing* and *elaborating* the description. The next task is to set the design constraints. Constraints are the instructions that the designer gives to Design Compiler. They define, the synthesis tool can or cannot do with the design or how the tool behaves. Usually this information can be derived from the design specifications (*e.g.* from *timing specification*). There are basically two types of design constraints: Design Rule Constraints and Optimization Constraints. Optimization constraints are explicit constraints (set by the designer). They describe the design goals (area, timing, power and so on) the designer has set for the design and work as instructions to perform synthesis. The top level model is constrained with the following parameters: clock master_clock (rise edge) of 4.00ns, library setup of -0.05ns, data required time of 3.95ns, data arrival time of -3.95 ns, the slack is found to be 0.00 indicating that the design is able to meet timing constraints. The area report obtained using 65nm low power library from TSMC indicates that the number of ports is 2, number of nets is 714, number of cells is 16, number of references is16, Combinational area occupied by the design is 870596.656057 um^2, Non-combinational area occupied by the design is 329587.191422 um^2 and the total design area occupied is 1200183.847480 um^2. The power report obtained after synthesis indicates that the total dynamic power is 86.8380 mW, cell internal power is 85.6360 mW, net switching power is 1.2021 mW and cell leakage power is 362.3151 uW at load capacitance of 1pF and operating voltage of 1.08V. The synthesized netlist for the compressor unit is shown in Figure 8 (below).

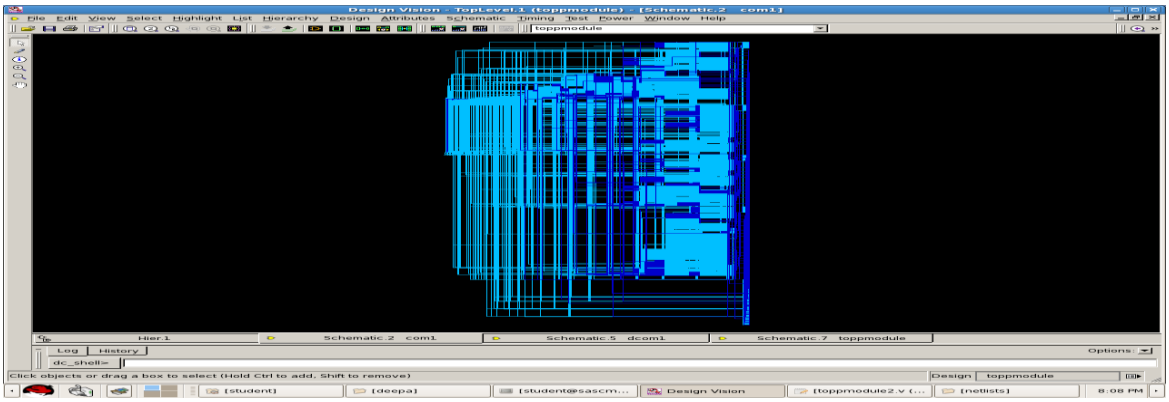

Figure 8: Synthesized netlist for compressor unit

Figure 9 (below) shows the synthesized netlist for the decompressor unit.

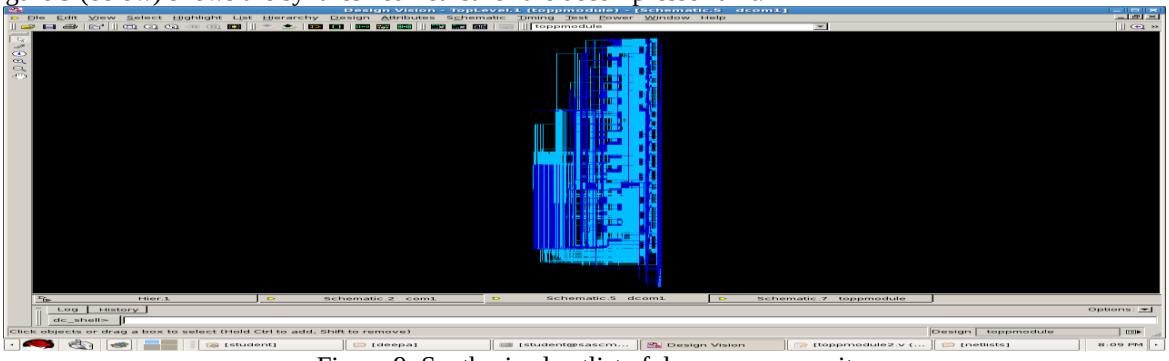

Figure 9: Synthesized netlist of decompressor unit

Figure 10 (below) shows the synthesized netlist of adder circuits used in the design to realize the compressor and decompressor unit.

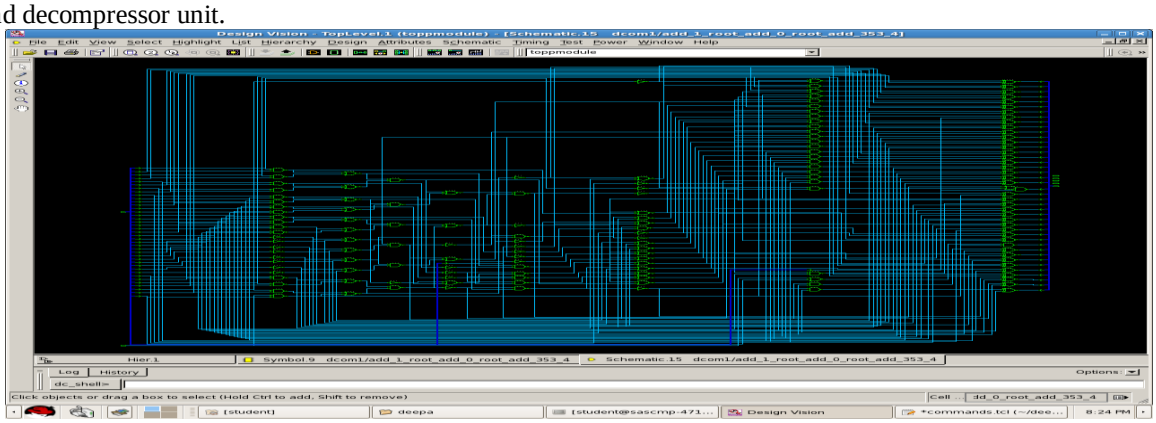

Figure 10: Synthesized netlist of 14-bit Carry Save Adder

Figure 11 (below) shows the synthesized netlist of Wallace tree multiplier used for design of compressor and decompressor unit.

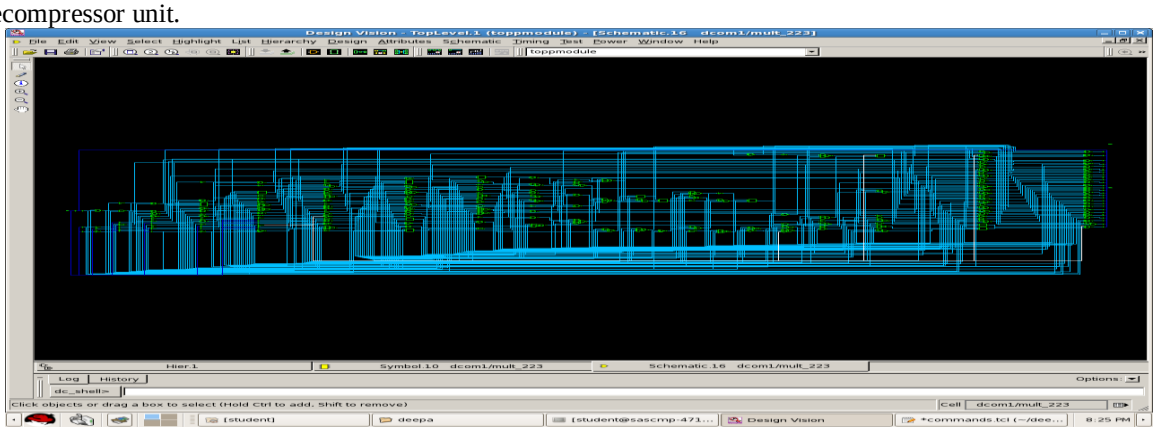

Figure 11: Synthesized netlist of Wallace tree multiplier

V. RESULTS AND DISCUSSION

Figure 12 shows the results of image compression and decompression using the proposed hybrid architecture model. The input image is transformed into four sub bands in the first level decomposition, further is decomposed to second level of hierarchy and is shown in figure 12. The decomposed image is rearranged into column matrix, and is shown in figure 12. The compressed data using NN architecture is decompressed using output layer. The output obtained is further rearranged to sub blocks and is inverse transformed using inverse DWT. The output obtained is shown in figure 13, along with the reconstructed image.

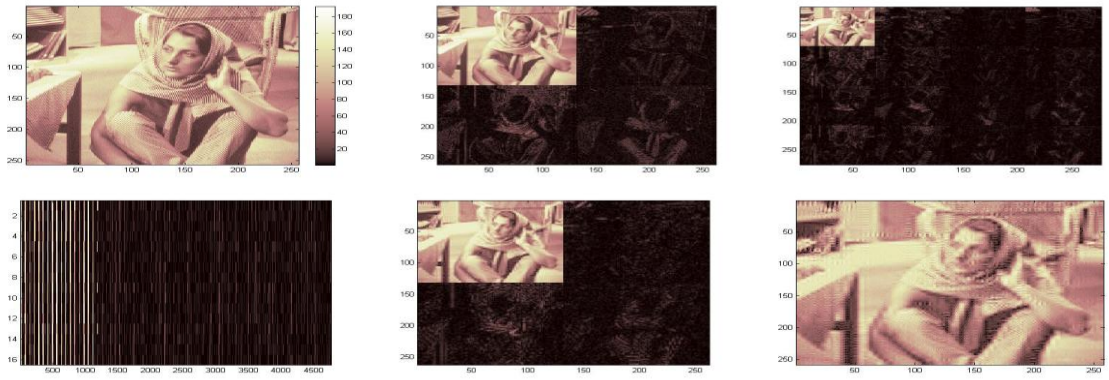

Figure 12: Results of hybrid Neural Network Architecture

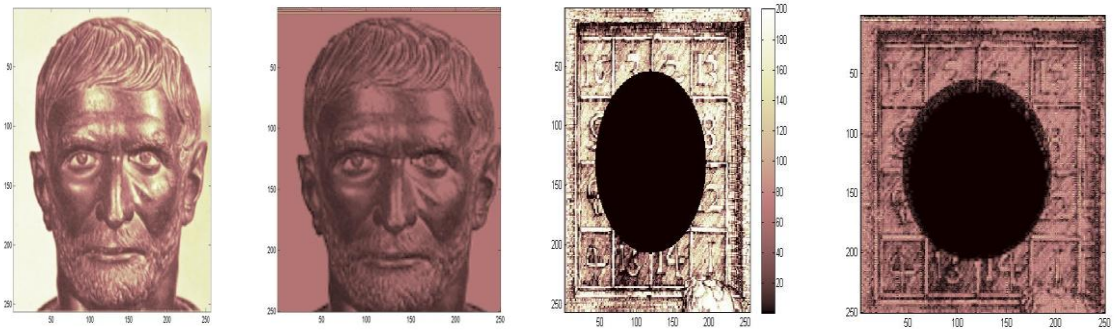

Figure 13: Input Image and Reconstructed Image

The following table summarizes the MSE results for various test images using the hybrid architecture. The results compare the performances of NN architecture, reference design and the present work. With the choice of appropriate wavelet filters (Haar, db4), choice of decomposition levels, number of hidden layers and network function the proposed architecture is superior compared with all the other architectures.

Sl. No.	*Test Image*	*Image MSE (With NN only)*	*Reference*	*Image MSE (With NN and DWT)*
1	Camera man	321	301	262
2	Board	1590	1289	958
3	Cell	39	34	26
4	Circuit	24	21	14
5	Lena	201	190	100
6	Sun	278	149	115
7	Girl	67	51	42
8	Blue hills	38	31	22
9	Sunset	51	47	39
10	Water lilies	56	42	31
11	Winter	89	52	47
12	Drawing	260	232	170
13	College	180	126	97
14	Garden	163	145	87
15	My photo	320	234	197
16	Holi	289	256	175
17	Bhagavad geetha	98	78	65
18	Devine couple	143	101	80
19	Krishna	29	19	7
20	Goddess	76	53	45

Table 1: MSE results for various test images and comparison

From the results presented in table for all the 20 images considered proposed network achieves less MSE compared with the reference design. The input image is decomposed using DWT and is compressed using NN architecture, this introduces delay and hence high speed architectures are required to implement for real time applications.

VI. CONCLUSION

Use of NN for image compression has superior advantage compared with classical techniques; however the NN architecture requires image to be decomposed to several blocks of each 8 x 8, and hence introduces blocking artifact errors and checker box errors in the reconstructed image. In order to overcome the checker errors in this work, we have used DWT for image decomposition prior to image compression using NN

architecture. In this work, we proposed a hybrid architecture that combines NN with DWT and the input image is used to train the network. The network architecture is used to compress and decompress several images and it is proven to achieve better MSE compared with reference design. The hybrid technique uses hidden layer consisting of tansig function and output layer with purelin function to achieve better MSE. The proposed architecture is suitable for real time application of image compression and decompression.

VII. ACKNOWLEDGMENTS

The authors would like to acknowledge Dr. Cyril Prasanna Raj P. for his valuable support during this work. The authors also acknowledge Sundaramoorthy G from NXG Semiconductor Technologies for his support.

REFERENCES

[1] Q. Zang, Wavelet Network in Nonparametric Estimation, *IEEE Trans. Neural Networks*, 8(2):227- 236, 1997.
[2] Q. Zang and A. Benveniste, Wavelet networks, *IEEE Trans. Neural Networks*, vol. 3, pp. 889-898, 1992.
[3] A. Grossmann and B. Torrésani, Les ondelettes, Encyclopedia Universalis, 1998.
[4] R. Ben Abdennour, M. Ltaïef and M. Ksouri. uncoefficient d'apprentissage flou pour les réseaux deneurones artificiels, *Journal Européen des Systèmes Automatisés*, Janvier 2002.
[5] M. Chtourou. Les réseaux de neurones, Support de cours DEA A-II, Année Universitaire 2002/2003.
[6] Y. Oussar. Réseaux d'ondelettes et réseaux de neurones pour la modélisation statique et dynamique de processus, Thèse de doctorat, Université Pierre et Marie Curie, juillet 1998.
[7] R. Baron. Contribution à l'étude des réseaux d'ondelettes, Thèse de doctorat, Ecole Normale Supérieure de Lyon, Février 1997.
[8] C. Foucher and G. Vaucher. Compression d'images et réseaux de neurones, revue Valgo n°01-02, 17-19 octobre 2001, Ardèche.
[9] J. Jiang. Image compressing with neural networks – A survey, Signal processing: Image communication, ELSEVIER, vol. 14, n°9, 1999, p. 737-760.
[10] S. Kulkarni, B. Verma and M. Blumenstein. Image Compression Using a Direct Solution Method Based Neural Network, *The Tenth Australian Joint Conference on Artificial Intelligence*, Perth, Australia, 1997, pp. 114-119.
[11] G. Lekutai. Adaptive Self-tuning Neuro Wavelet Network Controllers, Thèse de Doctorat, Blacksburg-Virgina, Mars 1997.
[12] R.D. Dony and S. Haykin. Neural network approaches to image compression, *Proceedings of the IEEE*, V83, N°2, Février, 1995, p. 288-303.
[13] A. D'souza Winston and Tim Spracklen. Application of Artificial Neural Networks for real time Data Compression, *8th International Conference On Neural Processing*, Shanghai, Chine, 14-18 Novembre 2001.
[14] Ch. Bernard, S. Mallat and J-J Slotine. Wavelet Interpolation Networks, *International Workshop on CAGD and wavelet methods for Reconstructing Functions*, Montecatini, 15-17 Juin 1998.
[15] D. Charalampidis. Novel Adaptive Image Compression, *Workshop on Information and Systems Technology*, Room 101, TRAC Building, University of New Orleans, 16 Mai 2003.
[16] M. J. Nadenau, J. Reichel, and M. Kunt, Wavelet Based Color Image Compression: Exploiting the Contrast Sensitivity Function, *IEEE Transactions Image Processing*, vol. 12, no.1, 2003, pp. 58-70.
[17] K. Ratakonda and N. Ahuja, Lossless Image Compression with Multiscale Segmentation, *IEEE Transactions Image Processing*, vol. 11, no.11, 2002, pp. 1228-1237.
[18] Murali Mohan.S and Dr. P.Satyanarayana, FPGA Implementation of Hybrid Architecture for Image Compression Optimized for Low Power and High Speed applications, *International Journal of Scientific & Engineering Research, (ISSN 2229-5518),*Volume 4, Issue 5, May 2013, pp 1931-40 .
[19] Bo-Luen Lai and Long-Wen Chang, Adaptive Data Hiding for Images Based on Haar Discrete Wavelet Transform, *Lecture Notes in Computer Science*, Springer-Verlag, vol. 4319, 2006, pp. 1085-1093.
[20] S. Minasyan, J. Astola and D. Guevorkian, An Image Compression Scheme Based on Parametric Haar-like Transform, *ISCAS 2005. IEEE International Symposium on Circuits and Systems*, 2005, pp. 2088-2091.
[21] Z. Ye, H. Mohamadian and Y.Ye, Information Measures for Biometric Identification via 2D Discrete Wavelet Transform, *Proceedings of the 3rd Annual IEEE Conference on Automation Science and Engineering, CASE'2007*, 2007, pp. 835-840.

[22] S. Osowski, R. Waszczuk, P. Bojarczak, Image compression using feed forward neural networks — Hierarchical approach, *Lecture Notes in Computer Science*, Book Chapter, Springer-Verlag, vol. 3497, 2006, pp. 1009- 1015.
[23] M. Liying and K. Khashayar, Adaptive Constructive Neural Networks Using Hermite Polynomials for Image Compression, *Lecture Notes in Computer Science*, Springer-Verlag, vol. 3497, 2005, pp. 713-722.
[24] R. Cierniak, Image Compression Algorithm Based on Soft Computing Techniques, *Lecture Notes in Computer Science*, Springer-Verlag, vol. 3019, 2004, pp. 609-617.
[25] B. Northan, and R.D. Dony, Image Compression with a multi-resolution neural network, *Canadian Journal of Electrical and Computer Engineering*, Vol. 31, No. 1, 2006, pp. 49-58.
[26] S. Veisi and M. Jamzad, Image Compression with Neural Networks Using Complexity Level of Images, *Proceedings of the 5th International Symposium on image and Signal Processing and Analysis, ISPA07*, IEEE, 2007, pp. 282-287.
[27] I. Vilovic, An Experience in Image Compression Using Neural Networks, *48th International Symposium ELMAR-2006 focused on Multimedia Signal Processing and Communications*, IEEE, 2006, pp. 95-98.
[28] J. Mi, D. Huang, Image Compression using Principal Component Neural Network, *8th International Conference on Control, Automation, Robotics and Vision*, IEEE, 2004,pp. 698-701.
[29] R. Ashraf and M. Akbar, Absolutely lossless compression of medical images, *27th Annual*
[30] *Conference Proceedings of the 2005 IEEE Engineering in Medicine and Biology*, IEEE, 2005, pp. 4006-4009.
[31] A. Khashman and K. Dimililer, Neural Networks Arbitration for Optimum DCT Image Compression, Proceeding *of the IEEE International Conference on 'Computer as a Tool' EUROCON'07*, 2007, pp. 151-156.
[32] A. Khashman and K. Dimililer, Intelligent System for Image Compression, *Proceeding of 9th International Conference on Enterprise Information Systems, ICEIS 2007*, 2007, pp. 451-454.
[33] A. Khashman and K. Dimililer, Comparison Criteria for Optimum Image Compression, *Proceeding of the IEEE International Conference on 'Computer as a Tool' EUROCON'05*, vol. 2, 2005, pp. 935-938.
[34] A. Khashman and K. Dimililer, Haar Image Compression Using a Neural Network, *Proceedings of the WSEAS Int. Applied Computing Conference (ACC'08)*, Istanbul, Turkey, 27-29 May 2008.
[35] A. Khashman, B. Sekeroglu, and K. Dimililer, Intelligent Identification System for Deformed
[36] Banknotes, *WSEAS Transactions on Signal Processing, ISSN 1790-5022, Issue 3, Vol. 1*, 2005.
[37] Murali Mohan.S and Dr. P.Satyanarayana, Performance Analysis of Neural Network Architecture Combined with DWT for Image Compression, *International Journal of Computer Applications (ISSN:0975 – 8887)*,Volume 58– No.11, November 2012,pp 13-20.
[38] K. H. Talukder and K. Harada, Haar Wavelet Based Approach for Image Compression and Quality Assessment of Compressed Image, *IAENG International Journal of Applied Mathematics*, 2007.

American Journal of Engineering Research (AJER)
e-ISSN : 2320-0847 p-ISSN : 2320-0936
Volume-02, Issue-10, pp-146-153
www.ajer.org

Research Paper Open Access

Design, Load Analysis and Optimization of Compound Epicyclic Gear Trains

Syed Ibrahim Dilawer[1], Md. Abdul Raheem Junaidi[2], Dr.S.Nawazish Mehdi[3]
[1]*Dept. of Mechanical Engineering, Muffakham jah college of engineering and Technology, Hyderabad, 500034.*
[2]*Dept. of Mechanical Engineering, Muffakham jah college of engineering and Technology, Hyderabad, 500034.*
[3]*Dept. of Mechanical Engineering, Muffakham jah college of engineering and Technology, Hyderabad, 500034.*

Abstract: - Gears in the Epicyclic gear trains are one of the most critical components in the mechanical power transmission system in which failure of one gear will affect the whole transmission system, thus it is very necessary to determine the causes of failure in an attempt to reduce them. The different modes of failure of gears and their possible remedies to avoid the failure are mentioned in J.R. Davis (2005) [17], Khurmi & Gupta (2006) [19], P. Kannaiah (2006) [18] [20] as bending failure (load failure), Pitting (contact stresses), scoring and abrasive wear, in any case it is related to the loads acting on the gear and this research deals with the Optimization of the gear design leading to the reduction in the load failure of the gears. Further, table.1 explains the different areas of research carried out by different authors on Epicyclic gear trains. This study carried out in this research shows the optimization analysis of the epicyclic gear train in INDIA to reduce load failure. The analysis is restricted to the optimization of gear train through load analysis of the gears, pinions and annulus including the sun and plant gears, and finding out the optimal load conditions for the gear train to perform effectively without leading to load failure. Epicyclic Gear Trains have been used in Industry for their many advantages which includes high torque capacity, comparatively smaller size, lower weight, improved efficiency and highly compact package, however there has not been a comprehensive study of its load bearing performance with respect to different parameters such as module, material, and power of the epicyclic gear trains [16] [17]. This research paper provides an attempt in filling that gap in aiming to get the epicyclic gear trains load performance on different parameters. This process helps in finding the optimized design for the epicyclic gear trains in which it has the best performance without any failure and with minimum Loads acting on the gears. The main aim of this research investigation is to optimize the epicyclic gear train through load analysis, to prevent load failure from happening in the future.

Keywords: - *Optimization, Planetary Gear Trains, Tangential Tooth load, Wear tooth load, Dynamic tooth load, Static tooth load*

I. INTRODUCTION

A Planetary or Epicyclic Gear Trains comprises of one or more planet gears revolving around a sun gear. Usually, an epicyclical gearing systems are employed to achieve high reduction ratio in a small and power dense package. It is examined that load sharing capability is not equal in the planetary gear train. These Gear Trains are extensively used for the transmission and are the most critical component in a mechanical power transmission system. They play a very vital role in all the industrial areas, any failure in the gear train leads to a total system failure, thus identifying the causes and optimizing to get the best performance is very necessary. The advantages of epicyclic gear trains are higher torque capacity, lower weight, small size and improved efficiency of the planetary design. As the weigh is 60%, and half the size of a conventional gear box, it is very likely to have a misconception that it is not as strong. Thus the loads have to be minimum to reduce the stresses in the gear train. The epicyclic gear train model is taken from BHEL, and some of its parameters have been modified to optimize its performance. The gear train consists of five external gears and 4 internal annulus gears, including sun and planet gears forming an epicyclic gear train. The present work on epicyclic gear trains carries out the design of all the gears, Shafts, keys and the loads are calculated for individual gears in the epicyclic gear train system. The analysis is divided into three parts, in which the first

part, the power of 10HP is taken for the whole epicyclic gear train with four different modules (3, 4, 5, 6) for four different loads Tangential Tooth Load (Wt), Dynamic Tooth Load (Wd), Static Tooth Load (Ws) and Wear Tooth Load (Ww) with Cast Iron as the base material. The same process was conducted for the Power 15 HP and 20 HP while keeping the other parameters (material/module-3, 4, 5, 6) as constant. As the condition was stated that for preventing Gear failure the Static Tooth Load (Ws) and the dynamic Tooth Load (Wd) should be greater than the Wear Tooth Load (Ww) [15] [19], This condition is analyzed for the entire gear train and optimized for to get the least loads on the gears. As these Gear trains are subjected to high loads during their operation they are subjected to high stresses in the process which may cause failure, thus calculating the loads for different modules and for different power levels will show us the best optimized design of the gear train. This paper shows the optimization of gear trains with varying the modules and power of the entire gear train.

Table.1 shows the prominent authors who contributed to the analysis of Gears

Author	**Description of the work carried out**
S. Avinash [1]	Load Sharing behavior in epicyclic gear trains
P. Sunyoung [17]	Failure analysis of a planetary gear train
A. kiril [12]	Alternative method for analysis of complex compound planetary gear train
C. Yuksel [7]	Dynamis tooth load of planetary gear sets
M. Rameshkumar [16]	Load Sharing analysis of High-Contract-Ratio in Spur Gear
B. Gupta [15]	Contact stress analysis of spur gear
A.R. Hassan [14]	Contact stress analysis of spur gear teeth pair

II. COMPUTATIONAL METHODOLOGY

The Compound Epicyclic Gear train in Fig.1 is taken from BHEL and the parameters are altered for the optimization purposes. The Gears, arms, keys and annulus are designed in Solidworks which is shown in Fig.1 (a). Fig.1 (b) shows the general diagram showing all the positions of gears, annulus, shafts and arms. This model of the epicyclic gear train failed due to the high loads acting on the gears. As we know that the gear is one of the most critical components of the power transmission system, failure in the gear will affect the whole transmission system and thus it is necessary to optimize the gear for low load operation and its effective delivery of power transmission.

Loads in an epicyclic gear train are divided into four parts: Tangential Tooth Load (Wt), Static Tooth Load (Ws), Dynamic Tooth Load (Wd) and Wear Tooth Load (Ww).

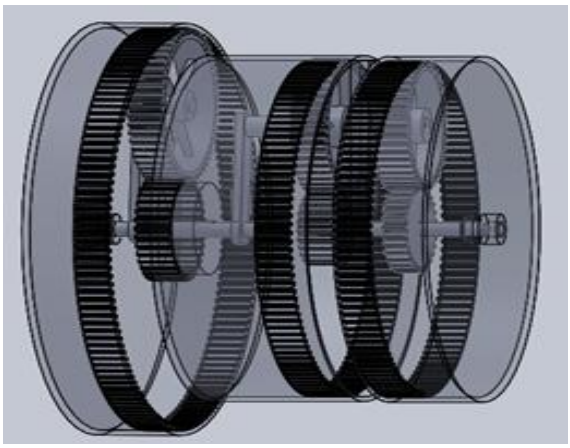

Fig.1(a)

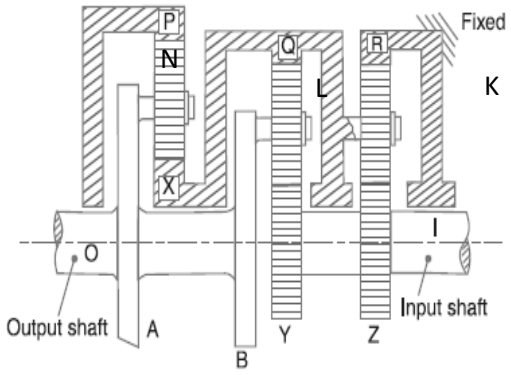

Fig.1(b)

Fig.1 Figure shows the positions of all the internal and external gears including Sun and Plant Gears, (a) Figure shows the Design made in Solidworks software after theoretical calculations, (b) Shows the 2D representation of the Epicyclic gear trains showing all the Gears, Pinion, Annulus including sun and planet gears

Module:-It is the ratio of the pitch circle diameter (in millimeters) to the number of teeth. It is usually denoted by *m*, where $m = D / T$ D=Pitch Circle Diameter, T= Number of Teeth

The recommended series of modules in Indian Standard are 1, 1.25, 1.5, 2, 2.5, 3, 4, 5, 6, 8, 10, 12, 16, 20, 25,

32, 40 and 50. The modules 1.125, 1.375, 1.75, 2.25, 2.75, 3.5, 4.5, 5.5, 7, 9, 11, 14, 18, 22, 28, 36 and 45 are of second choice, from which modules 3, 4, 5 and 6 were selected for the design optimization of gears [18] [20].
Systems of Gear Teeth:-The following four systems of gear teeth are commonly used in practice. 14 ½° Composite systems, 14 ½° Full depth involute systems, 20° Full depth involute system and 20° Stub involute system. The tooth profile of the 20° full depth involute system may be cut by hobs. The increase of the pressure angle from 14 ½° to 20° results in a stronger tooth, because the tooth acting as a beam is wider at the base. The 20° stub involute system has a strong tooth to take heavy loads, thus was selected [16] [15] [18].

Gear Material:-The materials which are used for the gears depend upon the service factor and strength like wear or noise conditions etc, and they come in metallic and non-metallic form. For industrial purposes metallic gears are used, commercially can be obtained in steel, cast iron and bronze. Among these Cast iron is widely used because of its excellent wearing properties, in which Cast Iron with UTS 480 Mpa, Elongation 6-16% was selected because of its long service life, high wear resistance, low production cost, high stability and surface finish [17][13]

Table.2 Shows all the parameters of Epicyclic Gear Train from Gears Z to Gear P (9 Gears) for module 4

Parameters (mm)	Gear Z	Gear k	Gear R	Gear Y	Gear L	Gear Q	Gear X	Gear N	Gear P
No. of Teeth (T)	30	45	120	24	48	120	36	54	114
Pitch Diameter (D)	120	180	480	96	192	480	144	216	576
Circular Pitch (Pc)	12.56	12.56	12.56	12.56	12.56	12.56	12.56	12.56	12.56
Face Width (b)	26.11	40	40	40	40	40	60	40	40
Module (m)	4	4	4	4	4	4	4	4	4
Steady Load (Wt)	795.78	795.78	795.78	994.76	994.76	994.76	3315.7	452.14	452.14
Pressure angle (∅)	20	20	20	20	20	20	20	20	20
Increment Load (Wi)	2897.9	3936.1	3936.1	3763	3796.4	3796.4	3229.2	4206.1	4206.1

Table.3 Shows the parameters of Gear modeling for modules 3, 4, 5, 6

Parameters (mm)	M=3	M=4	M=5	M=6
Addendum (1× m)	3	4	5	6
Dedendum (1.25× m)	3.75	5	6.25	7.5
Working depth (2× m)	6	8	10	12
Total depth (2.25× m)	6.75	9	11.2	13.5
Tooth thickness (1.507× m)	4.52	6.28	7.535	9.04
Clearance (0.25× m)	0.75	1	1.25	1.5
Fillet radius (0.4× m)	1.2	1.6	2	2.4

Table.4 Shows all the Gears, Annulus, Sun and Planet Gears in the Gear Train

S.no	Gear	Annulus	Sun	Planet
1	Z	R	Z	K
2	K	Q	X	L
3	Y	X	Y	N
4	L	P		
5	N			

III. DESIGN AND LOAD OPTIMIZATION OF GEARS

The following are the sample design and load calculations for analysis of Gear-Z having module 4 and power 10 HP, from the Epicyclic Gear train, in which the calculations of the four loads acting on the gears (Tangential Tooth Load (Wt), Static Tooth Load (Ws), Dynamic Tooth Load (Wd) and Wear Tooth Load (Ww)) are calculated, for the module-(4). The parameters for the gears are mentioned in Tables 2, 3 and 4. As the below calculations are performed, similarly the calculations are done for the rest of the eight gears for modules 3, 4, 5 and 6. Now this process is repeated for Power 10HP, 15 HP, 20 HP. All the results are tabulated for Table.6 to Table.14, and the Graphs are plotted from Graph.1 to Graph.9, showing the Load variance on the different modules at different power levels.

DESIGN OF Z -GEAR (pinion):

Teeth of Gear Z(T_Z)=30; Diameter of Gear Z (D_Z)=120 mm = 0.12 m; Speed of Gear Z (N_Z)=1500 r.p.m

Pitch Line Velocity $V = \frac{\pi D_Z N_Z}{60}$ = (πx 0.12 x 1500) / 60 = 9.4247 m/s

Tangential Load(W_T):- Tangential tooth load is also called the beam strength of the tooth. It is the load acting perpendicular to the radial tooth load (Wr) and normal tooth load (Wn) [16] [18] as shown in the fig.3

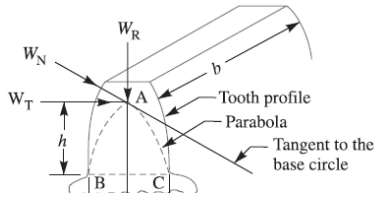

Fig.2 Shows the tangential tooth load direction on the gear tooth profile

$W_T = \frac{P}{V} \times CS = (\frac{7500}{9.4247})$ x 1.5 = 1193.671 N

Where W_T = Permissible tangential tooth load in N, P = Power transmitted in watts, v = Pitch line velocity in m/s; $\frac{\pi DN}{60}$, D = Pitch circle diameter in m, N = Speed in r.p.m., and C_S = Service factor (Cs is taken from the Table.5)

Table.5 Shows Service Factor (Cs) for different loads

Type of load	Type of service		
	Intermittent or 3 hours / day	8 – 10 hours per day	Continuous 24 hours per day
Steady	0.8	1.00	1.25
Light Shock	1.00	1.25	1.54
Medium Shock	1.25	1.54	1.80
Heavy Shock	1.54	1.80	2.00

Applying Lewis Equation [15] [16] [18]
$W_T = \sigma_W \times b \times P_c \times y$ Where σ_W=Permissible working stress, b=Gear tooth face width,
Pc=Circular Pitch = π× m (module), y=Lewis form factor
$\sigma_W = \sigma_O$ x C_V Where σ_O=Allowable Static Stress, Cv= Velocity Factor, σ_O = 90 N/mm^2 as material was nodular Cast iron)
C_V = (4.58) / (4.58+V) = 0.327 Where V= Pitch Line Velocity (9.4247 m/s)
y = 0.154 - (0.912 / T_Z) = 0.1236 Where Tz = Teeth of Gear Z
P_C = πx m = πx 4
Substituting the values in the equation
⇒ 1193.671 = 90 x 0.327 x b x π x 4 x 0.1236
⇒ b = 26.11 mm

Dynamic Tooth Load (W_D):- The dynamic tooth loads act due to inaccuracies in tooth spacing, tooth profiles and deflection of tooth under loads [18]. The formulae for (W_D) is given below as
$W_D = W_T + W_I$ Where W_D=Total Dynamic Tooth Load, W_T =Steady Load due to transmitted torque, W_I=Increment Load due to dynamic action.
W_T = (P / V) = (7500 / 9.4247) = 795.781 N Where P=Power, V= Pitch line velocity
$W_I = \frac{K_3 \times V(b \times C + W_T)}{\sqrt{K_3 \times V + (b \times C + W_T)}}$
Where (K_3 = 20.67), V=Pitch line velocity, b=face width (mm), C=Deformation factor (n/mm) [18]
$C = \frac{e}{K_1[(\frac{1}{Ep})+(\frac{1}{Eg})]}$ Where e=Tooth error (mm), K_1= Factor of Gear Teeth for 20 ^{0} full involute system, E_p=Module of elasticity of Pinion, E_g= Module of elasticity of Gear, (K_1=9; E_P= E_G=164000 N/mm^2) [18]
C = 0.127 / {9 [(1/ 164000) + (1/ 164000)]} C = 115.711 N/ mm Subtituting all the results in W_I
$W_I = \frac{\{20.67 \text{x } 9.4247 \ (26.11 \text{ x } 115.711 + 795.781)\}}{20.67 \text{x } 9.4247 + \sqrt{(26.11 \text{ x } 115.711 + 795.781)}}$ = 2897.939 N Substituting W_T, W_I in W_D
⇒ W_D = 795.781 + 2897.939 = 3693.72 N
Static Tooth Load (W_S):- The static tooth load (beam strength or endurance strength of the tooth) is derived from lewis formula with the substitution of elastic limit stress (σ_e) instead of Permissible working stress (σ_w). It is said that for preventing tooth breakage (Ws) should be greater than Dynamic tooth load (Wd).
$W_S = \sigma_e \times b \times P_C \times y$ Where σ_e = Elastic limit stress (σ_e = 175 N/mm^2), b= Face width, P_C= Circular pitch (πx 4) y=Lewis form factor [18]

W_S = 175 x 26.11 x (πx 4) x 0.1236 = 7096.974 N

Wear Tooth Load (W_W):- It is maximum load that a gear tooth can carry without premature wear. It depends upon the curvature of tooth profile, elasticity and surface fatigue limit of the gear material. It uses Buckingham equation [18] [16].

$W_W = D_Z . b .Q .K$ Where D_Z = Pitch circle diameter of Gear Z, b= Face width, Q = Ratio factor for external or internal gears, K = Load stress factor or material combination factor T_G= Teeth of Gear, T_P = Teeth of pinion

$Q = (2T_G) / (T_G + T_P)$ = (2 x 45) / (45 + 30) = 1.2

$K = \sigma^2_{es}$ x sin∅ / 1.4 [(1/E_P) + (1/E_G)] Where σ = Surface endurance limit, ∅=Pressure angle, E_P= Young modulus of elasticity of Pinion, E_G= Young modulus of elasticity of Gear

$K = 630^2$ x sin 20 / 1.4[(1/164000) + (1/164000)] = 1.1824 N/mm^2 Substituting the values in W_W

$\Rightarrow W_W$ = 120 x 26.11 x 1.2 x 1.1824 = 4445.634 N

The results of the four loads derived for the Gear–Z can be seen in Table.6 and Graph.1, in power 10HP for module4. Similarly the loads for rest of the eight gears for module 3, 4, 5 and 6 for the power 10 HP, 15 HP and 20 HP respectively can be inferred from Tables 6 to 14 and Graphs 1 to 9.

IV. RESULTS AND DISCUSSION

As the resulting loads are calculated for the Gear-Z of Epicyclic Gear Train having module 4, similarly the four loads W_T, W_D, W_S, W_W are calculated for all the rest of the eight Gears and Annulus including sun and planet gears. This process is repeated for different modules (3, 4, 5, 6) with all the 9 Gears in the Epicyclic Gear Train. Now this whole procedure is conducted for three different power levels (10 HP, 15 HP, 20 HP). All the results are tabulated and graphs are plotted accordingly from Table.6 to Table.14 and from Graph.1 to Graph.9. Where the condition is that'' For safety against tooth breakage, the Static Tooth Load (Ws) should always be greater than Dynamic tooth load (Wd), also the Dynamic tooth load (Wd) should not be more than the wear tooth load (Ww) otherwise the gear will fail [18], also the least loads are observed for all the Gears to get the optimized design in the Epicyclic Gear Train. Below are the graphs plotted for the loads where

P=Power (HP); M=Module; Loads (N) Wt = Tangential Tooth Load; Wd = Dynamic Tooth Load; Ws = Static Tooth Load; Ww = Wear tooth Load

Table.6 Shows the different parameters of Gear-Z

P		Wt	Wd	Ws	Ww
10	3	1591.68	5454.16	10267.1	6431.44
10	4	1193.67	3693.72	7096.97	4445.63
10	5	954.93	3310.22	6633.53	4155.33
10	6	797.784	2668.02	5133.143	3215.46
15	3	2372.6	7645.2	15303.6	9586.3
15	4	1779.3	5288.3	10578.8	6626.7
15	5	1423.4	4772.6	9887.11	6193.4
15	6	935.56	3218.55	7952.45	5812.36
20	3	3162.13	7601.9	16365.26	12776.3
20	4	2371.4	6823.6	14098.83	8831.6
20	5	1897.1	6049.8	13148.83	8236.22
20	6	935.56	3218.55	7952.45	5812.36

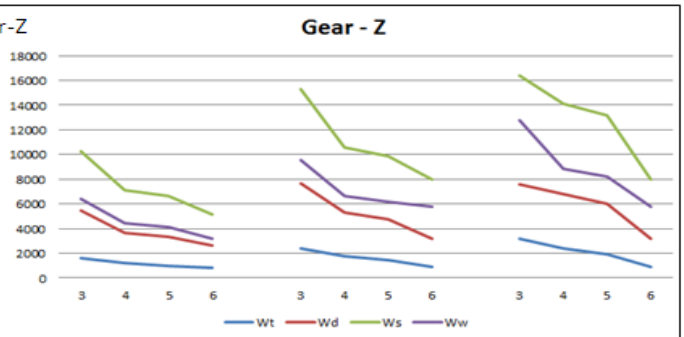

Graph.1 Shows the different parameters of Gear-Z with three different power levels (10 HP, 15 HP, 20 HP) for modules 3, 4, 5 and 6.

Table.7 Shows the different parameters of Gear-K

P	M	Wt	Wd	Ws	Ww
10	3	1591.68	4163.799	5615.487	4746.464
10	4	1193.67	4731.909	10760.87	9215.94
10	5	954.93	6149.585	17376.35	14962.4
10	6	795.784	7937.417	25461.95	21985.5
15	3	2372.6	4982	6615.48	5746.46
15	4	1779.3	5228.1	11760.8	10215.9
15	5	1423.49	6661.7	18376.87	15962.8
15	6	1285.3	7725.69	26461.95	22985.6
20	3	3162.21	3693.2	7615.5	6746.2
20	4	2371.2	6002.2	12760.8	11215.2
20	5	1897.1	5912.2	19376.3	16962.4
20	6	1285.3	7725.7	27461.9	23985.6

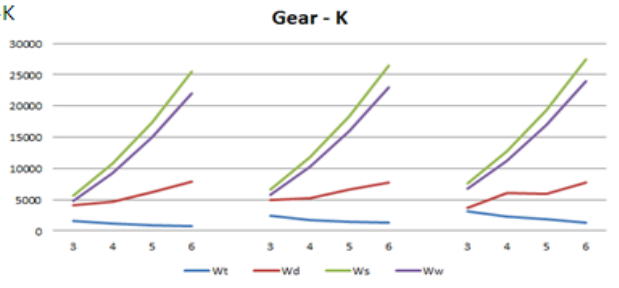

Graph.2 Shows the different parameters of Gear-K with three different power levels (10 HP, 15 HP, 20 HP) for modules 3, 4, 5 and 6.

Table.8 Shows the different parameters of Gear-R

P	M	Wt	Wd	Ws	Ww
10	3	1591.6	4163.7	7243.8	13044.61
10	4	1193.6	4131.9	12878	40523.75
10	5	954.9	6149.5	20121.9	60568.35
10	6	796.1	6256.6	28975.5	66785.6
15	3	2372.6	4980	6615.48	9746.4
15	4	1779.3	5228.8	11878	25486.8
15	5	1423	6661.8	19121	51652.2
15	6	1318.65	6256.6	27975.5	60785.6
20	3	3162.2	3693.3	7443.8	14044.6
20	4	2371.4	6002.2	15878.2	30523.7
20	5	1897.2	5912.6	22121.2	54568.2
20	6	1318.6	6256.6	29975.5	61785.6

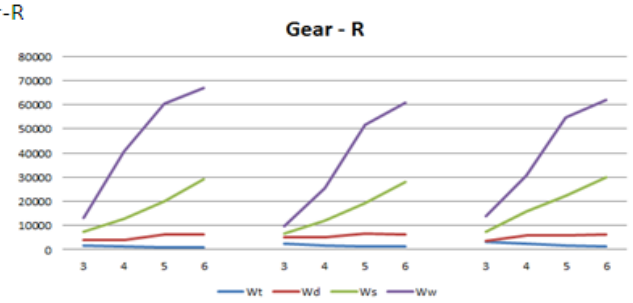

Graph.3 Shows the different parameters of Gear-R with three different power levels (10 HP, 15 HP, 20 HP) for modules 3, 4, 5 and 6.

Table.9 Shows the different parameters of Gear-Y

P	M	Wt	Wd	Ws	Ww
10	3	1989.7	5860.1	11041.4	6534.4
10	4	1492	4757.7	10073.7	5961.7
10	5	1193.6	3707.5	7097.7	4200.5
10	6	930.9	3038.2	5521.5	3276.7
15	3	2966	8144.5	16457.6	8787.1
15	4	2224.1	6718.03	15015	8086.2
15	5	1779.3	5307.5	11273.3	6049.4
15	6	943.4	4038.2	9521.5	4567.7
20	3	3952.9	10283.2	21092.6	13195.4
20	4	2964.2	8630.1	20012.8	10843.8
20	5	2371.4	5618.4	11237.4	6775
20	6	994.7	4038.2	5921.5	4567.7

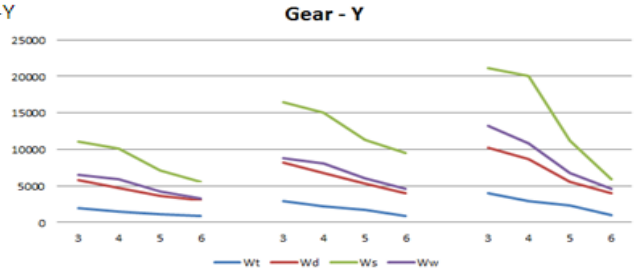

Graph.4 Shows the different parameters of Gear-Y with three different power levels (10 HP, 15 HP, 20 HP) for modules 3, 4, 5 and 6.

Table.10 Shows the different parameters of Gear-L

P	M	Wt	Wd	Ws	Ww
10	3	1989.7	4338.9	7126.3	8652.1
10	4	1492	4791.1	12857.3	14265.3
10	5	1193.6	6020.9	19365.6	21365.3
10	6	994.7	7706.17	22958.7	25174.4
15	3	2966	5318.2	6679.8	9356.2
15	4	2224.1	5549.3	11875.2	14562.3
15	5	1793.3	6063.9	18555	20145.3
15	6	994.78	7706.1	22958.7	26174.4
20	3	3952.9	6294.8	6679.8	8365.3
20	4	2946.2	6317.3	11875.2	13256.3
20	5	2371.4	7301.8	20158	22365.3
20	6	994.7	7706.1	22958.7	27174.4

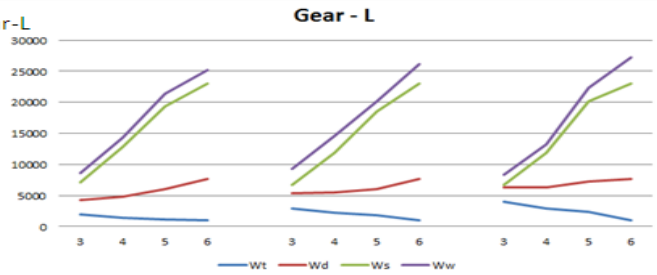

Graph.5 Shows the different parameters of Gear-L with three different power levels (10 HP, 15 HP, 20 HP) for modules 3, 4, 5 and 6.

Table.11 Shows the different parameters of Gear-Q

P	M	Wt	Wd	Ws	Ww
10	3	1992.3	4341.2	7243.8	18924.8
10	4	1502.2	4802.1	12878	56577.2
10	5	1195.6	6022.6	20121	80680.3
10	6	998.3	6203.6	28975.5	85123.8
15	3	2966	5318.2	8443.8	21924.3
15	4	2224.1	5559.1	13478	56755.2
15	5	1779.6	6070.2	24521.9	78680
15	6	994.78	6203.6	30954.5	86132.8
20	3	3953.2	6296.1	9258.1	31927.4
20	4	2949.5	6319.4	14768	56759.7
20	5	2369.1	7303.8	29121.6	80681.2
20	6	993.1	7709.9	33902.5	89133.3

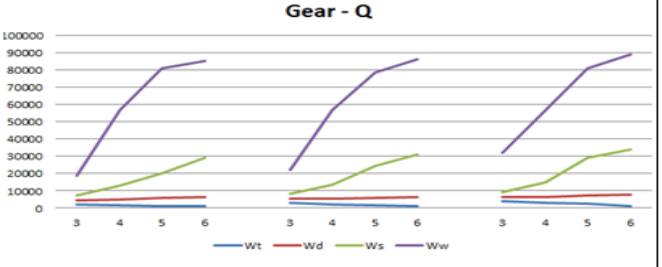

Graph.6 Shows the different parameters of Gear-Q with three different power levels (10 HP, 15 HP, 20 HP) for modules 3, 4, 5 and 6.

Table.12 Shows the different parameters of Gear-X

P	M	Wt	Wd	Ws	Ww
10	3	6631.6	7809.8	20069.3	12566.1
10	4	4973.6	6545	16843.9	10546.6
10	5	3979.4	5928.2	14912	9337
10	6	3316.6	4906.4	12272.3	7684.2
15	3	9885.6	10901.4	28764.3	21622.02
15	4	7414.1	9125.1	25110.23	18635.21
15	5	5932	8256.2	21136.21	14365.21
15	6	3316.6	4906.4	12272.3	7684.2
20	3	13174.9	15689.6	41452.6	36007.3
20	4	9881	11600.3	34559	22325.32
20	5	7905.9	10482.2	20472.1	16325.32
20	6	3316.62	4906.42	12272.3	7684.2

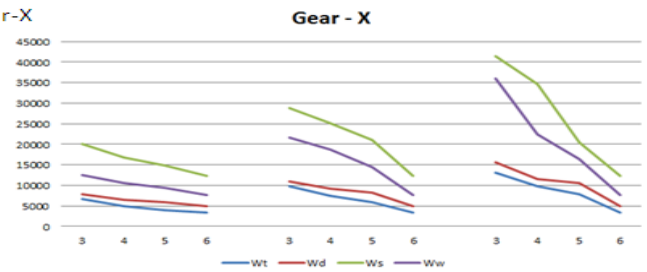

Graph.7 Shows the different parameters of Gear-X with three different power levels (10 HP, 15 HP, 20 HP) for modules 3, 4, 5 and 6.

Table.13 Shows the different parameters of Gear-N

P	M	Wt	Wd	Ws	Ww
10	3	904.34	3866.88	7658.32	6895.76
10	4	678.21	4658.31	13256.3	12259.12
10	5	542.587	6367.75	21654.3	19154.88
10	6	442.11	6524.52	27164.8	19879
15	3	1348.22	4375.21	7783.21	7593.21
15	4	1011.45	5045.21	14059.9	13297.87
15	5	808.15	6632.221	23280.1	20111.32
15	6	442.11	6524.5	29834.9	20776.6
20	3	1523.12	2842.19	8783.7	9223.2
20	4	1347.4	5440.25	16000.2	13997.1
20	5	1077.13	5669.9	24945.2	21777.6
20	6	442.11	6524.52	31974.9	21988.6

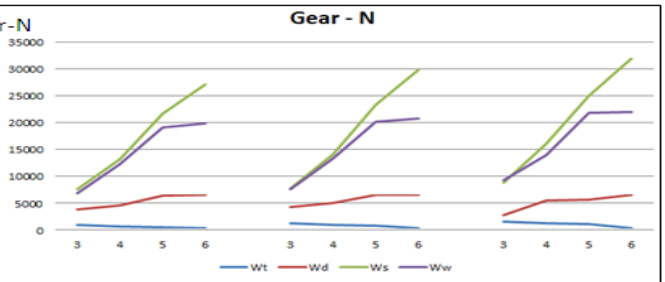

Graph.8 Shows the different parameters of Gear-N with three different power levels (10 HP, 15 HP, 20 HP) for modules 3, 4, 5 and 6.

Table.14 Shows the different parameters of Gear-P

P	M	Wt	Wd	Ws	Ww
10	3	904.34	3866.8	7303.2	30864.8
10	4	678.2	4658.3	12983	72628.4
10	5	542.5	6367.7	19286	85511.8
10	6	452.1	6517.7	29213	98942.7
15	3	1348.07	4375.21	7956.43	30053.4
15	4	1011.45	5048.16	14073.4	73578.4
15	5	808.81	6632.08	24836.7	90361.8
15	6	452.17	6517.7	31947.6	108942.7
20	3	1523.1	2842.2	8194.3	40864.3
20	4	1347.4	5440.3	12059.9	75478.3
20	5	1077.9	5669.9	20286.8	97294.7
20	6	452.2	6517.7	34213	110065.3

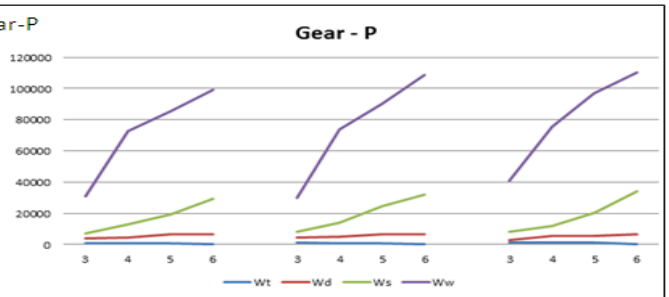

Graph.9 Shows the different parameters of Gear-P with three different power levels (10 HP, 15 HP, 20 HP) for modules 3, 4, 5 and 6.

As all the loads (Wt, Wd, Ws and Ww) were calculated for the gears it was seen that static tooth load (Ws) and wear tooth load (Ww) were greater than dynamic tooth load (Wd) for all the gears and thus the design of the Gear train is safe. It is observed that in the Sun Gears (Z, X, Y), the least loads can be seen at the module 6, but of the plant gears and annuluses the least loads were observed at module 3.

V. CONCLUSION

The purpose of this research paper is to determine the optimal design of the gear train with the load analysis carried out in the gear trains by varying the module (3, 4, 5, 6) for all the gears for three different power levels 10 HP, 15 HP and 20HP. On further examination of the loads for the gears which were plotted from Table 6 to 14 and Graphs 1 to 9, we can notice that the Wear tooth load (Ww) for all the gears in the gear train is higher than the Dynamic tooth load (Wd), and the Dynamic Tooth load (Wd) is less than Static tooth load (Ws) for all the gears in the system. As this condition has to be true for safety against tooth failure, thus we can state that the design is safe. We can observe in Graphs Z, Y and X that the loads are decreasing as the module is increasing and the least load is observed on module 6, as those are the sun gears in the gear train. Also it is observed that the rest of the gears and annulus in graphs K, R, L, Q, N and P that the loads are increasing as the module increases and the lease load is observed on module 3. This was seen consistent with the power level 10HP, 15 HP and 20 HP. Furthermore it is also observed that in Graphs Q, P and R, the wear tooth load is greater than the static tooth load which is why the teeth of the annuls should be of a higher wear resistant

material like cast iron as was suggested in section II of this research paper. Thus as the design satisfy the condition that Static Tooth Load (Ws) should always be greater than the Dynamic Tooth Load (Wd) also the Wear tooth load (Ww) should not be less than the Dynamic tooth load (Wd), the proposed design is safe and the least load conditions being at the least module (3, in this condition) is preferred for the annulus design and the planet gears where as a higher module (6, in this condition) is preferred for the sun gears design for all power levels.

VI. ACKNOWLEDGEMENT

We are thankful to BHEL for their constant support and encouragement in carrying out this research on Epicyclic Gear Trains.

VII. FUTURE SCOPE

The Research could be further extended through further optimization by varying different materials, also taking into consideration the working conditions and different gears (helical, worm etc.). The loads with different materials could be further analyzed and compared with the practical loads and stresses derived on the site.

REFERENCES

[1] S. Avinash, Load sharing behavior in epicyclic gears: Physical explanation and generalized formulation, *Mechanism and Machine Theory*, 45(3), 2010, 511-530.
[2] G. Cockerham, D. Waite, Computer- aided Design of Spur or Helical Gear Trains, *Computer-Aided Design*, 8(2), 1976, 84-88.
[3] Chinwal Lee, Fred B. Oswald, Dennis P. Townsend and Hsiang His Lin, Influence of Linear Profile Modification and Loading Conditions on The Dynamic Tooth Load and Stress of High-Contact-Ratio Spur Gears, *Journal Of Mechanical Design*, 133(4), 1990, 473-480.
[4] V. Daniele, Tooth contact analysis of misaligned isostatic planetary gear train, *Mechanism and Machine Theory*, 41(6), 2006, 617-631.
[5] Y. Hong-Sen, L. Ta-Shi, Geometry design of an elementary planetary gear train with cylindrical tooth profiles, *Mechanisma and Machine Theory*, 37(8), 2002, 757-767.
[6] D. Mundo, Geometric Design of a planetary gear train with non-circular gears, *Mechanism and Machine Theory*, 41(4), 2006, 456-472.
[7] C. Yuksel, A. Kahraman, Dynamic tooth loads of planetary gear sets having tooth profile wear, *Mechanism and Machine Theory*, 39(7), 2004, 697-715.
[8] B. Cheon-Jae, P. G. Robert, Analytical investigation of tooth profile modification effects on planetary gear dynamics, *Mechanism and Machine Theory*, 70(1), 2013, 298-319.
[9] M. Roland, R. Yves, Kinematic and Dynamic simulation of epicyclic gear trains, *Mechanisa and Machine Theory*, 44(2), 209, 412-424.
[10] S. Avinash, Epicyclic Load Sharing Map – Development and Validation, *Mechanism and Machine Theory*, 46(5), 2011, 632-646.
[11] L. Jinming, P.Huei, A Systamatic Design Approach for two planetary gear split hybrid vehicles, *International journal of Vehicle Mechanics and Mobility*, 48(1), 2010, 1395-1412.
[12] A. Kiril, K. Dimitar, Alternative Method for analysis of complex compound planetary gear trains: Essence and possibilities, *Mechanisms and Machine Science*, 13(1), 2013, 3-20.
[13] G. Madhusudhan, C.R. Vijayasimha, Approach to spur gear design, Computer-Aided Design, 19(10), 1987, 555-559.
[14] A. Hassan, Contact stress analysis of spur gear teeth pair, World Academy of Science, *Engineering and Technology*, 58(1), 2009, 611-616.
[15] B. Gupta, A. Choubey, V. Gautam, Contract Stress analysis of Spur gear, *International Journal of Engineering Research & Technology*, 1(4), 2012, 2278-0181.
[16] M. RameshKumar, P. Sivakumar, S. Sundaresh, K. Gopinath, Load sharing Analysis of High-Contact-Ratio spur Gear in Military Tracked Vehicle Applications, *Gear Technology*, 1(3), 2010, 43-50.
[17] P. Sunyoung, J. Lee, U. Moon, D. Kim, Failure analysis of planetary gear carrier of 1200 HP transmission, *Engineering Failure Analysis*, 17(1), 2010, 521-529.
[18] M.M. Gitin, *Handbook of Gear Design* (Tata Mc Graw-Hill Education, 1994)
[19] M.W. Herbert, *Epicyclic Drive trains: Analysis, Synthesis, and Applications* (Wayne State University Press, 1982)
[20] R. August, *Dynamics of early planetary gear trains* (National Aeronautics and Space Administration-NASA, 2010)
[21] J.R. Davis, *Gear Materials, Properties, and Manufacture* (ASM International, 2005)
[22] P. Kannaiah, *Design of Machine Elements* (Scitech Publications Pvt Ltd, 2006)
[23] R.S Khurmi, J.K. Gupta, *Machine Design* (Eurasia Plublications Pvt Ltd, 2006)
[24] P. Kannaiah, N. Sidheswar, V.V.S. Sastry, *Machine Drawing* (Tata McGraw-Hill, 2009)
[25] J.A. Collins, H.R. Busby, G.H. Staab, *Mechanical Design of Machine Elements and Machines* (John Wiley & Sons, 2010)

American Journal of Engineering Research (AJER)
e-ISSN : 2320-0847 p-ISSN : 2320-0936
Volume-02, Issue-10, pp-154-159
www.ajer.org

Research Paper Open Access

Inrush Current Limitation in Wind Generators by SCR Based Soft-starter during grid connection

Sanjay Mishra[1], Prof. S Debdas[2] ,Prof. Y Kashyap[3]
[1](M.Tech-EEE, DIMAT Raipur/CSVTU Bhilai, ,India)
[2](HOD & Prof.-EEE, DIMAT Raipur/CSVTU Bhilai, ,India)
[3](Prof.-EEE, DIMAT Raipur/CSVTU Bhilai, ,India)

Abstract: *-High Inrush current & harmonics is a generic problem wind generators during grid connection. The designed SCR based soft-starter successfully limits the high inrush current during the connection of the wind-turbine system to the grid. The proposed SCR based soft starter using will be simulating in PSCAD on a three-phase induction generator. Expected results will show a significant reduction in high inrush current and smooth connection of the three phase induction generator to the grid with small impact on the power quality. A small-scale wind turbine coupled three phase induction generator is an attractive choice for an isolated grid hybrid power system in remote areas because of its low cost, compactness, ruggedness, high reliability, low inertia and ease in control. In this work, a SCR based soft starter for limiting the high inrush current during the connection of the small-scale wind turbine coupled three phase induction generator to an isolated weak grid has been proposed. Soft-starter is designed to reduce inrush current or surge in current while achieving a proper synchronism between the generator and the grid.*

Keywords: *- Control system, Grid, PSCAD, SCR, Soft starter, Wind Turbine.*

I. INTRODUCTION

The vast majority of the wind turbines in the world are equipped with grid-connected induction generators. Single phase or three-phase squirrel cage rotor type induction generators are preferred rather than synchronous generators because of their cost-effectiveness, robustness, compactness, ruggedness, low inertia and the need of little maintenance [1]. For large scale distributed power supply three-phase induction generators are extensively used. Directly connected induction generator based wind turbines of more than 800 KW are normally equipped with soft-starter to limit massive inrush current to the supply and to connect the system smoothly to the grid without massive mechanical shocks or vibrations that could damage the gear box, bearings and the couplings [2]. In paper [1-5, 7] a few techniques for the soft starter of induction generator has proposed and implemented. Soft-starters based on semiconductor devices such as thyristors, triacs, IGBTs and power resistors have been described in paper [2-5]. All of the soft-connection strategies are done for either three phase large induction machines or for single phase motors. Past research indicates that soft-starters are widely used during the start up of induction motors/AC motors in industrial drives applications [8], [9], [10], [11], [12] to reduce mechanical stresses on the drive system and electrical stresses on the electrical supply. In wind power applications, directly connected squirrel cage induction generator needs to be equipped with soft-starter to minimize the effect on wind turbine generation system during the process of connecting of the wind turbine system to the grid [13], [14], [15], [16]. As the self-excited induction generator of a fixed-speed wind turbine is directly connected to the grid, a soft-starter is used to reduce the inrush current during connection. There are few techniques have been found in the literature which are extensively used as a soft-starter in wind power generation system. A 20 kW Gazelle wind turbine [21] has been commercialized by Gazelle Wind Turbines Ltd which uses SCR based soft-starter to reduce the inrush current during synchronism. The above recommended soft-connection strategies have been used for 15kW or more rated wind energy conversion system. However further research and development is needed to be extended on soft-connection strategy for 3kW or less rated wind turbine system to provide the quality power to the grid and also to reduce the electrical and mechanical stresses on the entire

system. Direct connection of the induction generator to the grid results in high inrush currents, which are undesirable particularly in the case of weak grids and can also cause severe torque pulsations and probably damage to the gearbox, High inrush current during grid connection with induction generator,Massive mechanical shocks or vibrations during interfacing of induction generator Development of transient & Harmonics. Connection and disconnection of electrical equipment in general and induction generators/motors especially, gives rise to so called transients, that is short duration very high inrush currents causing both disturbances to the grid and high torque spikes in the drive train of a WT with a directly connected induction generator. Its disturbances to the grid during switching operations and exerted Load on the gearbox. The voltage changes due to the inrush current of a switching and the flicker effect of the switching.

II. SOFT STARTING TECHNIQUE

Design of Soft Starter

A soft-starter is a device used with AC electric motors/generators to temporarily reduce the load and torque in the power train of the machine during start up. It decreases the mechanical stress on the motor and the shaft, as well as the electro dynamic stresses on the attached power cables and electrical distribution network. Thus it helps in extending the life span of the system. In figure, a typical connection circuit of a small scale variable speed wind turbine with three phase induction generator to an isolated grid is presented. The main purpose of the soft-starter is to create electrical isolation between the wind turbine system and the grid for a very short time to limit the starting high inrush current of the induction generator during the transient period. After that transient period, the wind turbine system is directly connected to the grid through the bypass switch.

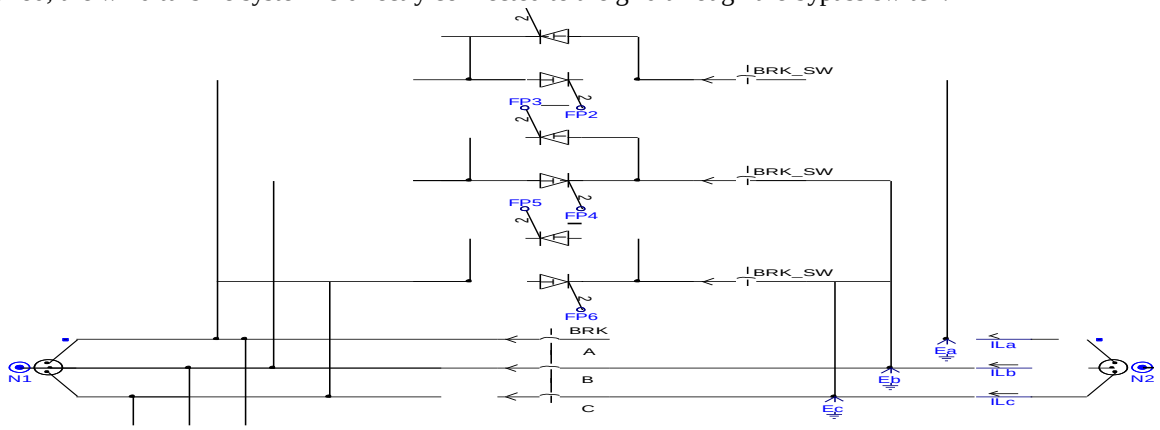

Fig.1 SCR Based soft starter-Model in PSCAD.

The soft starter has a limited thermal capacity and is short circuited by a contactor able to carry the full load current when connection to the grid has been completed. In addition to reducing the impact on the grid, the soft starter also effectively dampens the torque peaks in the air gap of the generator associated with the peak currents and hence reduces the loads on the gearbox.

Developing the model in PSCAD simulating tool

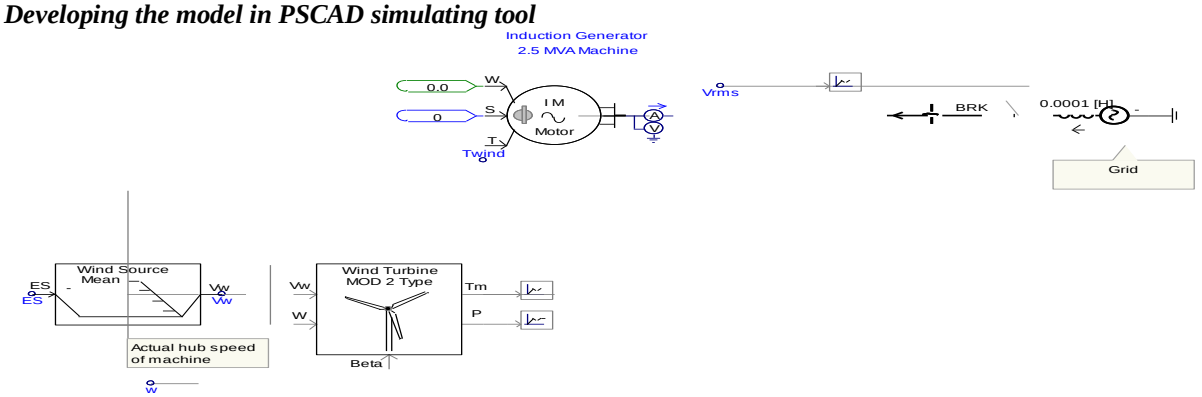

Fig.2 Wind mill with grid-Model in PSCAD.

Wind Turbine & soft starter model in PSCAD simulating tool

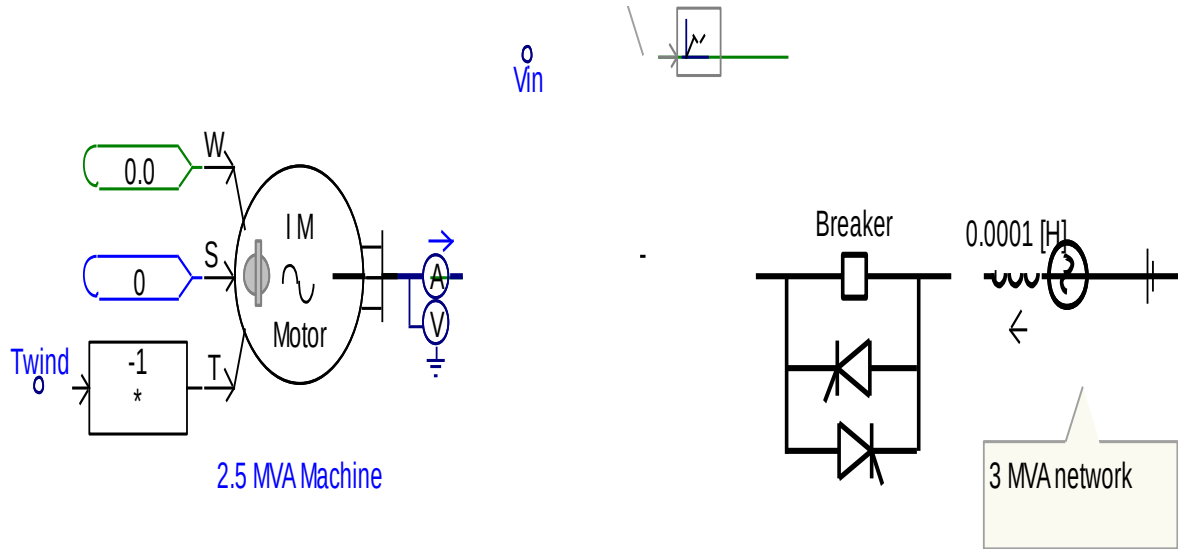

Fig.3 Wind mill & soft Starter with grid-Model in PSCAD.

Inrush current without soft starter

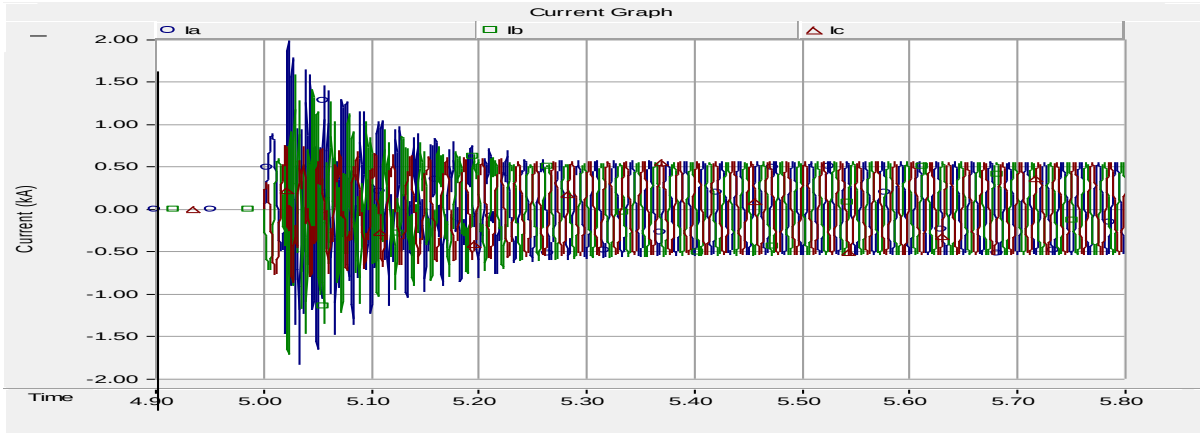

Fig.4 Inrush Current without soft starter

Control of firing angle of SCR in soft starter

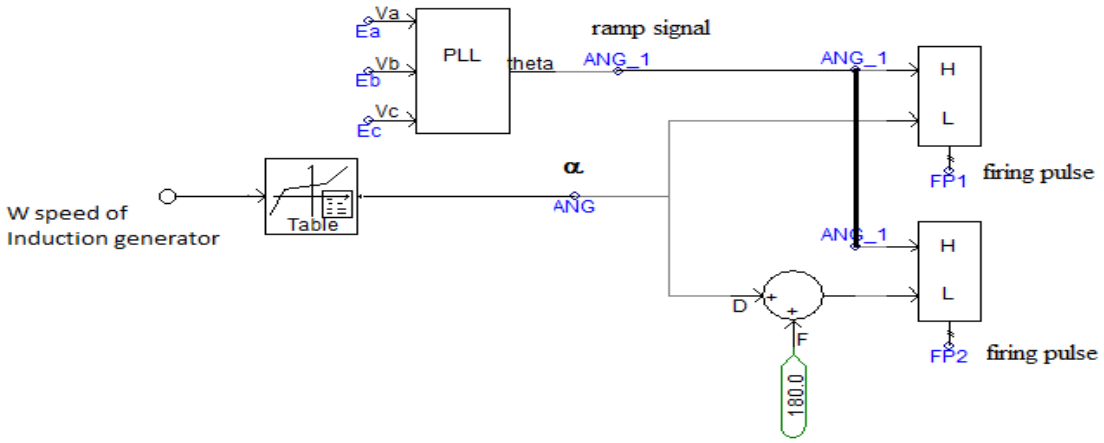

Gate Pulses of SCRs in soft starter

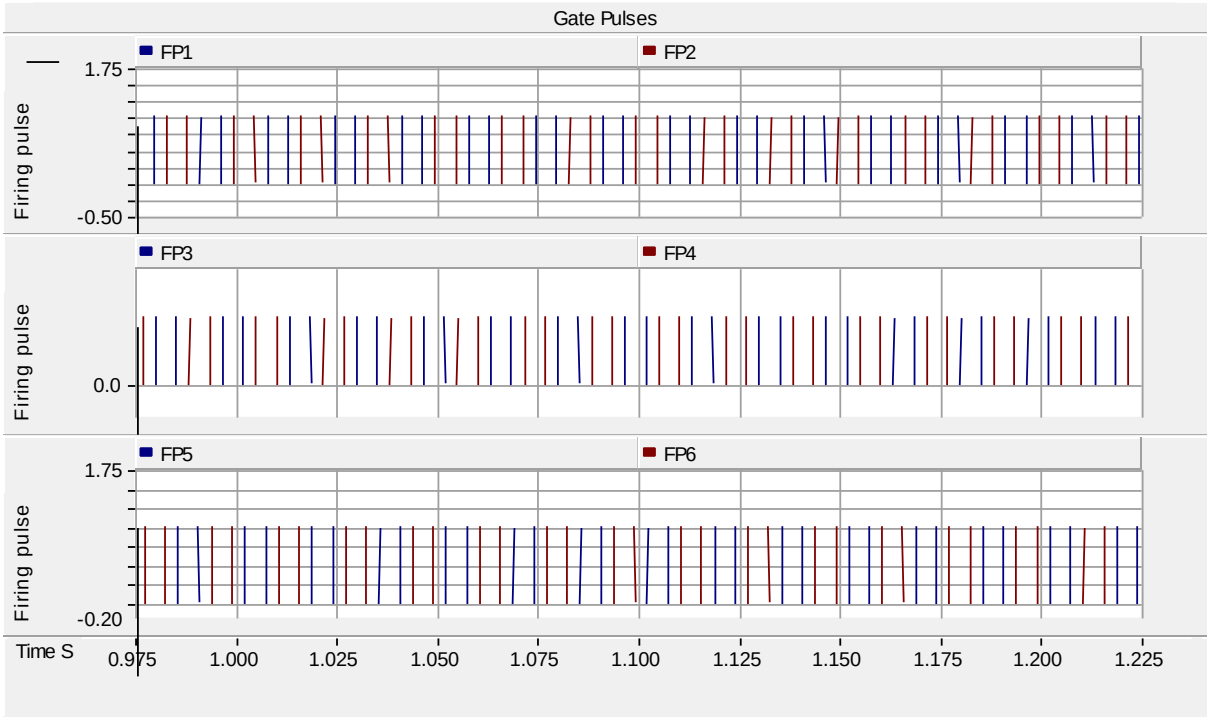

Fig.5 Gate Pulses of SCRs in soft starter

Voltage Graph with soft starter

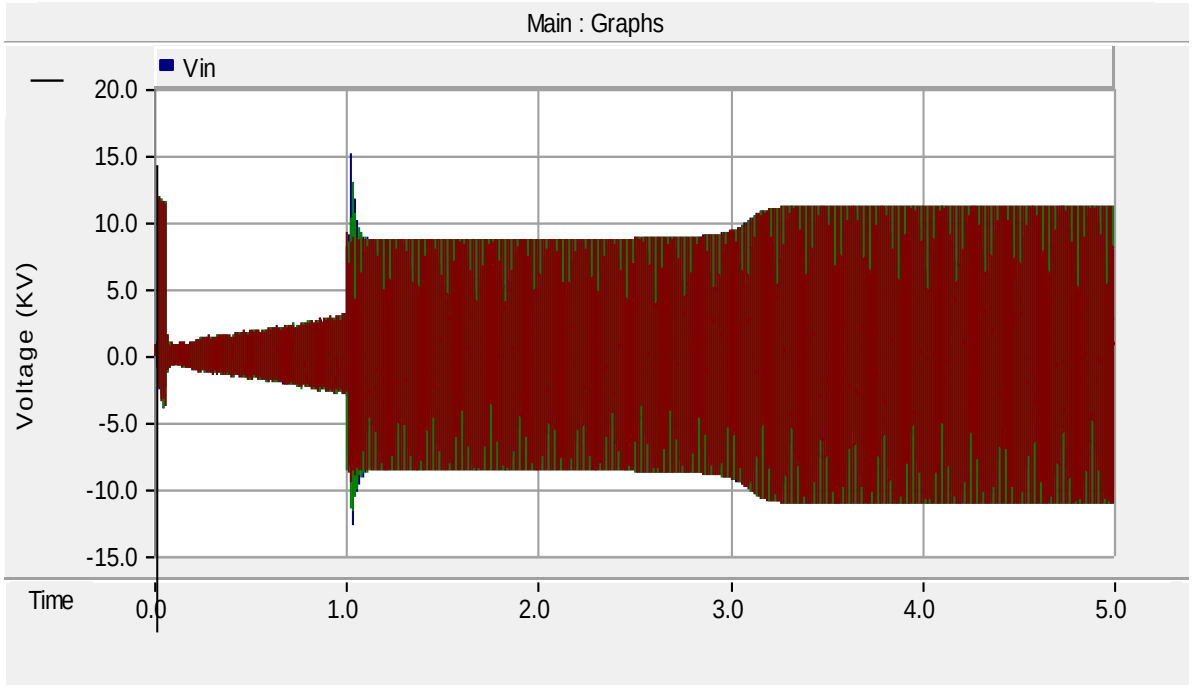

Fig. 6 Voltage Graph with soft starter

Inrush Current with soft starter

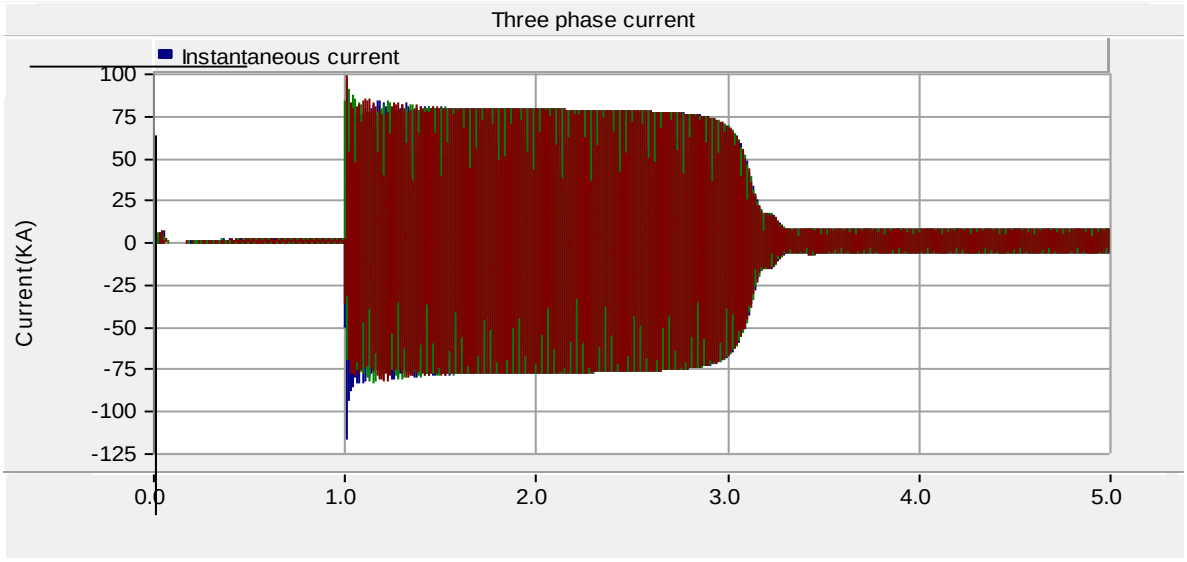

Fig.7 Inrush Current limited with SCR soft starter

Real Power, Reactive Power & Speed – Toruqe Characteristics of Wind Poly phase Generator

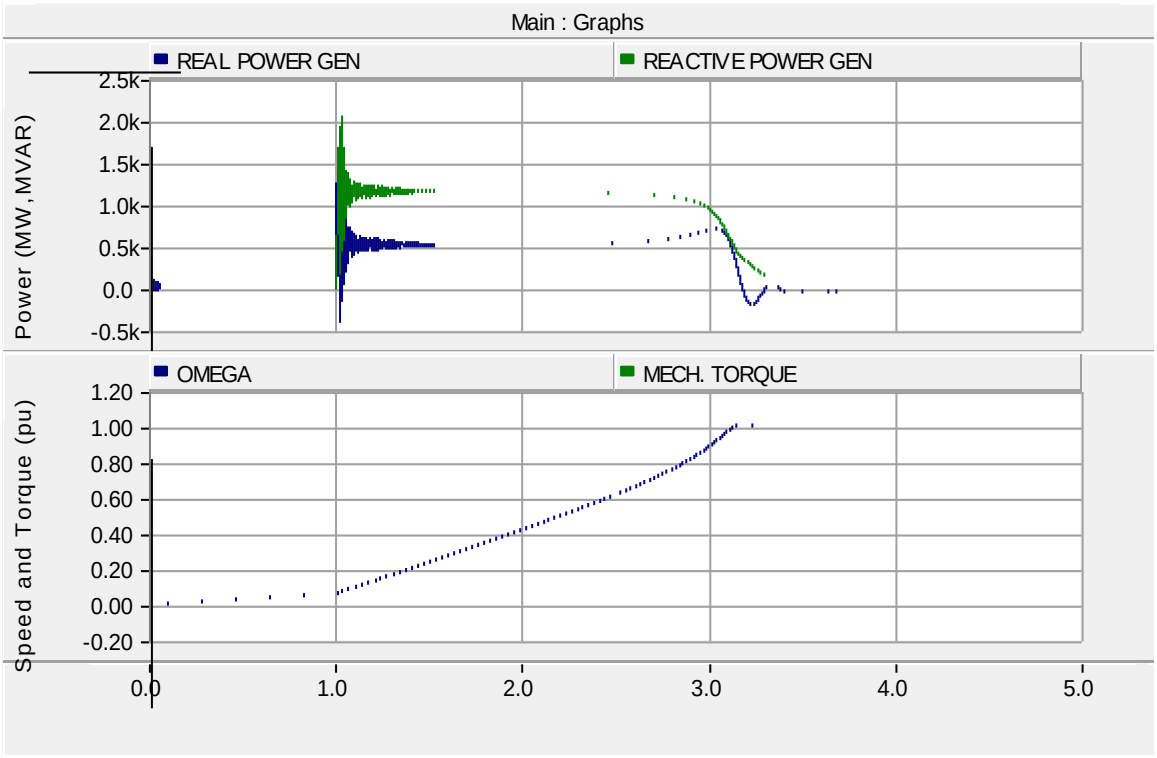

Fig. 8 Real Power, Reactive Power, Speed & Torque Graphs in PSCAD.

III. CONCLUSIONS

This paper describes the design, selection strategy, operation and some test results of a SCR based soft starter for a polyphase induction-generator based grid connected wind turbine with graphical representation of Voltage, Current Power & Speed & Torque of Poly phase induction generator, The Modelling has been done in PSCAD simulation tool. The data has been collected from wind farms & Tech. Specifications of Suzlons. The soft-starter setup is much cheaper which is a good technical benefit for small induction generator based wind turbines.

IV. AKNOWLEDGEMENT

I hereby declare this research paper is totally genuine & is being done by me under supervision & kind support by Prof.. S Debdas, Prof. Yashwant Kashyap & Prof. Shankar Warathe and my parents.

REFERENCES

[1] R. Ahshan, M.T. Iqbal, George K. I. Mann, "Power resistors based softstarter for a small grid connected induction generator based wind turbine" Procedings, the 17th Annual IEEE Newfoundland Electrical and Computer Engineering Conference, November 8, 2007 St. John's, NL

[2] S.F. Rabbi, K. Islam, R. Ahshan and M.A. Rahman,Faculty of Engineering & Applied Science Memorial University of Newfoundland, St. John's, NL, Canada, A1B-3X5.

[3] F. Gharedaghi, 2M. Deysi, 3H. Jamali and 4A khalili, Department of Electrical Engineering, Genaveh [4] Thiringer, T. Author Affiliation: Chalmers University of Technology, Goteborg. Sweden

[4] Florin Iov, Frede Blaabjerg, Zhe Chen Aalborg University, Institute of Energy Technology Pontoppidanstraede 101, DK-9220 Aalborg East, Denmark

[5] Adel Gastli, Senior Member, IEEE, and Mohamed Magdy Ahmed, Member, IEEE

[6] L. Mihet-Popa and I. Filip "Modeling and Sinulation of a sof-starter for large wind turbine induction generator," in Computational Cybernetics and Technical Informatics (ICCC-CONTI), 2010, pp. 465 – 470

[7] G Torbjorn Thiringer, "Grid-friendly connecting of constant speed wind turbines using external resistors", IEEE transactions on energy conversion,Vol. 17, No. 4, December 2002..

[8] F. Iov, Hansen, F. Blaabjerg, Remus Teodorescu, "Modeling of softstarters for wind turbine applications", Power quality 3rd ed., proceedings,May 2003, pp. 179-182..

[9] F. Iov, F. Blaabjerg, Zhe Chen, Hansen, et. al., "A new simulation platform to Model, Optimize and Design Wind Turbines",0-7803-7474- 6/02 IEEE, 2002, pp. 561-566.

[10] Gastli and M.M. Ahmed, "ANN-based soft starting of voltage controlled fed IM drive system", IEEE Trans. Energy Convers, vol. 20, no. 3, pp. 497-503, Sept. 2005. T. Ahmed, K. Ogura, K. Soshin, E. Hiraki and M. Nakaoka, "Smallscale wind turbine coupled single-phase self-excited induction generator with svc for isolated renewable energy utilization", PEDS 2003, vol. 1, pp 781-786

[11] A. Gastli and M.M. Ahmed, "ANN-based soft starting of voltage controlled fed IM drive system", *IEEE Trans. Energy Convers*, vol. 20, no. 3, pp. 497-503, Sept. 2005.

[12] T. Ahmed, K. Ogura, K. Soshin, E. Hiraki and M. Nakaoka, "Smallscale wind turbine coupled single-phase self-excited induction generator with svc for isolated renewable energy utilization", *PEDS* 2003, vol. 1, pp 781-786

[13] Wei Gu, Jianxin Chu, Shihong Gan, "Starting Performance Research of a High-power Middle-voltage Induction Motor Soft Starter Based on the On-off Transformer", *IEEE ISIE 2006*, July 9-12, 2006,Montreal, Quebec, Canada.

[14] M. Ayyub, "ANFIS based soft-starting and speed control of AC voltage controller fed Induction motor", *IEEE Power India Conference*, 10-12 April, 2006.

[15] J. Wu, R. Zhao, Z. Shang, "The design of soft starter for AC motors based on single neuron PI regulator", *Intelligent Control and Automation*, WCICA 2006, Vol. 1, pp. 3009-3013, 21-23 June,2006.

[16] A. Gastli and M.M. Ahmed, "ANN-based soft starting of voltage controlled fed IM drive system", *IEEE Trans. Energy Convers*, vol. 20, no. 3, pp. 497-503, Sept. 2005..

[17] D. Gritter, D. Wang and Habetler, "Soft starter inside delta motor modeling and its control", *IEEE Industry Applications Conference*, vol. 2, pp. 1137 - 1141, 8-12 Oct. 2000.

[18] B. Lemstrm, J. Rkklinen, and E. Peltola, "A wind farm's impact on the quality of electricity in a weak network", *In Proc. Eur. Wind Energy Conf.*, Nice, France, Mar. 1-5, 1999, pp. 747-749.

[19] G. Gerdes, F. Santjer, and R. Klosse, "Overview and development of procedures on power quality measurements of wind turbines", *in Proc. Eur. Wind Energy Conf.*, , Dublin, Ireland, Oct. 1997, pp. 716-721.

[20] A. Larsson, "Guidelines for grid connection of wind turbines", *in Proc. 15th Int. Conf. Electricity Dist.*, Nice, France, June 1-4, 1999.

American Journal of Engineering Research (AJER)
e-ISSN : 2320-0847 p-ISSN : 2320-0936
Volume-02, Issue-10, pp-160-172
www.ajer.org

Research Paper Open Access

Multi performance characteristic optimization of shot peening process for AISI 304 austenitic stainless steel using grey relational analysis with principal component analysis and Taguchi method

Dr. Lakhwinder Singh[1], Dr. RA Khan[2] and Dr. ML Aggarwal[3]
[1] *Associate Professor, Department of Mechanical Engineering, YMCA University of Science & Technology, Faridabad -121006, Haryana , India.*
[2] *Retd. Professor, Department of Mechanical Engineering, Jamia Millia Islamia, New Delhi-110025*
[3]*Professor, Department of Mechanical Engineering, YMCA University of Science & Technology, Faridabad - 121006, Haryana , India.*

Abstract: - Shot peening is a cold working process. It impact on thin surface layer of the material and is used to enhance the mechanical and surface properties. The manufacturer is in demand to reduce the cost and improve the process productivity. He is always in search of an optimization technique which involves multiple performance characteristics. From this work, an optimal combination of shot peening parameters is generated by using a Grey relational analysis (GRA) with Principal component analysis (PCA) and Taguchi method. The present study shows that there are many factors that affect the properties of the AISI 304 austenitic stainless steel. Mechanisms to compensate for surface tractions and further enhancement of mechanical properties are described. The shot peening is discussed to enhance the mechanical and surface properties of AISI 304 austenitic stainless steel. The optimization of shot pening process is done by including multi performance characteristics i.e. tensile strength, surface hardness an fatigue strengths. The analysis includes pressure, shot size, exposure time, nozzle distance and nozzle angle as process parameters. The complete analysis will be helpful to the manufacturer in deciding the shot peening parameters for required performance characteristics.

Keywords: - *ANOVA, Austenitic stainless steel, Gray relational analysis (GRA), optimization, shot peening.*

I. INTRODUCTION

The austenitic stainless steel is used in verity of applications due to its corrosion resistance, ductility, good weldability and resistance to high and low operating temperatures [1].The main constituents for austenitic stainless steel are chromium, nickel, molybdenum, and aluminium. Chromium makes the surface passive by forming a surface oxide film [2, 3], which protects the underlying metal from corrosion. This is because when the metal is scratched; the oxide layer re-forms quickly, hence protecting it from corrosion. However, chromium is a ferrite stabilizer. To counteract this, nickel is added as an austenite stabilizer, so that the microstructure at ambient temperature remains as austenitic [4].The heat treatment processes make austenitic stainless steel soften. Further the addition of carbon results in sensitization. Austenitic stainless steel is usually cold worked to enhance the mechanical properties [5, 6, 7]. Kirk and Payne [5] concluded in their work that martensite formation was easily induced by plastic deformation in austenitic stainless steel.

Many researchers found that shot peening can improve the mechanical properties the material [6, 7]. Shot peening is one of the most versatile tool to strengthen the metal parts against tensile strength, impact strength, surface hardness, compressive residual stress, damping, surface roughness, fatigue failure and corrosion. The induction of compressive residual stress in the thin skin layer of the surface results in the improvement of mechanical and surface properties. Shot peening is used now days in hundreds of different components of automobiles, aircraft and marine industries like railway and automobile leaf spring, helical spring, gears, axle bearing, crankshafts, milling cutters, connecting rod, cylinder block, valve springs, washers etc.

The controlled shot peening parameters helps in enhancing the surface and mechanical properties of the material. T. Dorr et. al. and M. Obata et. al. discussed the increase in surface hardness and surface roughness with increase in shot size and the peening intensity [8, 9]. K.B. Prakash et. al. have made study on shot peening for precision-machined steels with high strength to weight ratio [10]. As per the guidelines given by Champaine [11], the exposure time is an important factor to achieve desired peening coverage for the material. Sharma and Mubeen [12] investigated the effect of shot size on peening intensity. They guided the selection of correct size for shots to obtain desired intensity of shot peening. Sharma et. al. [13] presented a detailed discussion on development of various methods of controlling shot peening parameters. Schulze [14] discussed the characteristics of surface layer produced by shot peening.

Only a few authors have used the design of experiment (DoE) technique with a specialized single-ball controlled shot peening machine. The Taguchi method [15, 16] is a systematic tool for designing and analyzing the experiments for improving product quality. However, it is found that with Taguchi Method only a single performance characteristic is optimized. Phadke et. al. [17] suggested that the optimization of multi performance characteristics became difficult by Taguchi method. Deng [18, 19] proposed that grey relational analysis (GRA) is a part of grey system theory for the optimization of multi performance characteristics. Jeyapaul et al. suggested several modifications to the original Taguchi method for multi performance characteristic's optimization such as principal component analysis (PCA), data envelopment analysis (DEA) and GRA [20]. In recent years, GRA has become a powerful tool to analyze the processes with multiple performance characteristics. Chen et. al. [21], Bin et. al. [22] and Hsiao et. al. [23] are making use of GRA in many applications. Hence in view of all, it is necessary to perform a comprehensive investigations using GRA so as to evaluate the effect of shot peening parameters on surface integrity aspects such as tensile strength, surface hardness and fatigue strength of the material.

This paper proposes a novel design concept evaluation method based on GRA including Taguchi analysis and PCA to optimize the shot peening process for AISI 304 austenitic stainless steel. Effects of process parameters such as pressure, shot size, exposure time, nozzle distance and nozzle angle on tensile strength, surface hardness and fatigue strength were investigated and then process is optimized by using the approach. The performance characteristics considered for material are as tensile strength, surface hardness, and fatigue strength. The investigation is helpful to the manufacturers for reduction of cost, performance variation and scrap to increase productivity.

II. EXPERIMENTAL SET UP

The material AISI 304 austenitic stainless steel was used for various tests. The composition of the material is shown in Table 1. A flat plate having thickness of 10mm was used for making the specimens for various tests. The mechanical properties of the material were: tensile strength 617MPa, fatigue strength 228MPa and surface hardness 271VHN.

Table 1: Chemical composition (wt %) of AISI 304 austenitic stainless steel.

Austenitic stainless steel	C	Si	Mn	P	S	Ni	Cr	Mo	V
AISI 304	0.08	0.57	1.6	0.021	0.02	9.83	18.78	0.25	0.07

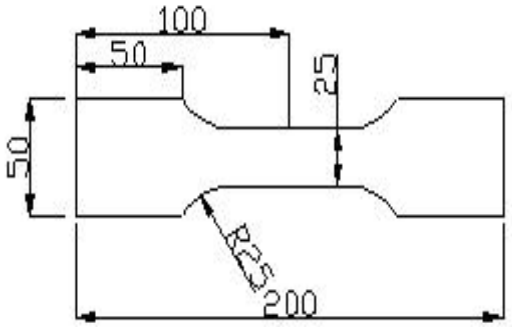

Fig. 1: Specimen for tensile test (all dimensions in mm).

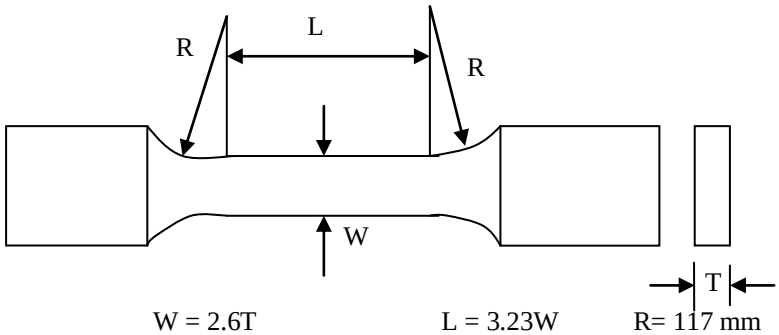

T = 5mm W = 2.6T L = 3.23W R= 117 mm

Fig. 2: ASTM flat specimen for fatigue strength.

The dimension of specimen for tensile strength test is shown in Fig. 1. These specimens were required to perform the tensile test at different process parameter levels. Tensile testing was carried out at room temperature using a universal testing machine of type HEICO HL 590.15 having capacity 400kN with 5mm/min cross-head speed.

Vickers hardness test was carried on the surface of specimens. The hardness measurements were performed on specimens of 20mm by 60mm by 10mm thickness using WOLPERT universal hardness testing machine dia tester – 2, model 2RC. The average values of three readings of surface hardness were taken for different peening parameters.

The fatigue life of the shot peened specimens was tested by an axial fatigue-testing machine. Stress ratio (R) equal to 0.1 was used during fatigue testing. The dimension of specimen for plotting S-N curve is shown in Fig. 2. The dimensions of the specimens were according to the ASTM standards. Fifteen specimens were tested in order to plot an S/N curve. Only the average points were presented for each level. The specimens were testing in axial fatigue testing machine MTS model 810, at a frequency 30Hz, at room temperature. The other specifications of the machine are:

Type : Servo hydraulic system
Force Capacity : $\pm$ 285 kN
Column space : 460 mm
Test space : 978 mm

III. ANALYSIS PROCEDURE

In modern industry the goal of an engineer is to manufacture low cost, high quality products in short duration of time. It is always necessary to produce a component with higher stress to weight ratio. Shot peening is a low cost cold working process used to enhance the mechanical and surface properties of AISI 304 austenitic stainless steel. Moreover, in order to produce any product with desired performance characteristics by shot peening process, the shot peening parameters should be selected properly.

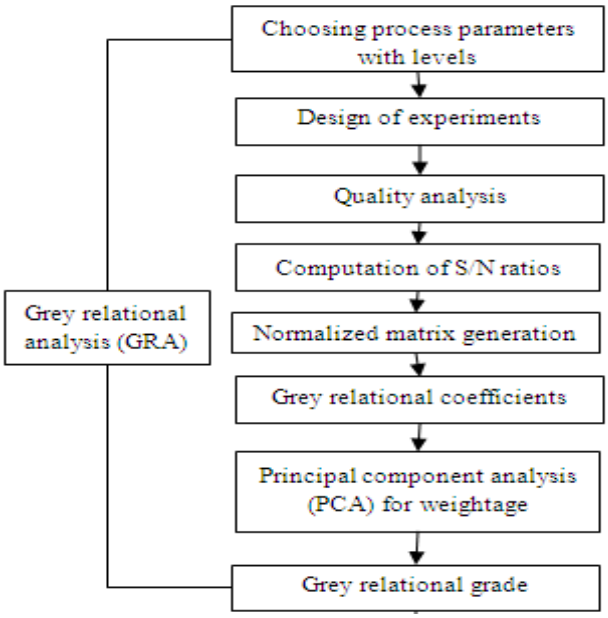

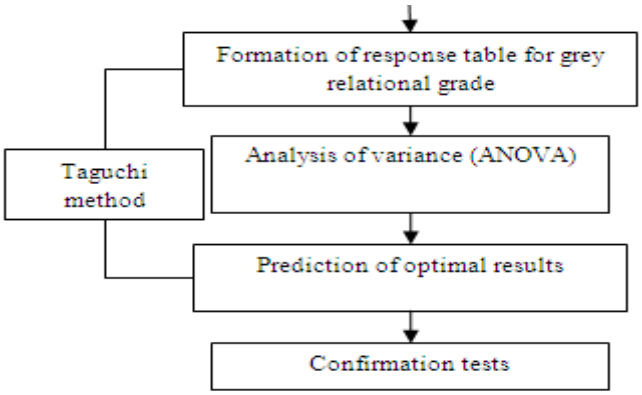

Fig. 3: Flow chart for analyzing process parameters of shot peening process for multi performance characteristics.

The present analysis proposes a novel design method based on GRA with PCA and Taguchi method to select the best combination of shot peening parameters to optimize the performance characteristics of AISI 304 austenitic stainless steel. The optimization of process parameters such as pressure, shot size, exposure time, nozzle distance and nozzle angle for performance characteristics are investigated by using the approach. The flow chart for analyzing and modeling of performance characteristics is shown in Fig. 3. The results of this analysis can be used by the engineers who are willing to search for an optimal solution of shot peening process of AISI 304 austenitic stainless steel.

IV. SELECTION OF SHOT PEENING PARAMETERS

It is viewed that the parameters like coverage, shot velocity, shot intensity etc. are controlled by the air pressure, type of nozzle, exposure time, nozzle distance and feed rate. Therefore with reference to literature [24] and basic experimental results the present investigation involves pressure, shot size, exposure time, nozzle distance and nozzle angle the process parameters which are considerably affecting the shot peening process. In shot peening process the parameters are divided into two categories one is controlled before the start of the process i.e. shot size and nozzle angle and the remaining are evaluated after shot peening process i.e. intensity, saturation, coverage etc. The desired magnitude of intensity, saturation, velocity and coverage are controlled by the air pressure, shot mass flow rate, nozzle type, feed rate of the nozzle along the work piece, nozzle distance from the work piece, and the work piece table speed. Therefore in the present investigation pressure, shot size, exposure time, nozzle distance and nozzle angle are the controllable influential process parameters under consideration. These shot peening parameters along with their levels are shown in Table 2.

Table 2: Process parameter and their levels.

Process Parameter	Parameter Designation	Levels		
		L1	L2	L3
Pressure (MPa)	P	0.196	0.392	0.588
Shot Size (mm)	S	0.85	1.00	1.85
Exposure Time (Sec)	T	80	120	160
Nozzle Distance (mm)	D	80	100	120
Nozzle Angle	E	60^0	75^0	90^0

An air-blast shot peening machine was used for shot peening of the specimens. Spherical cast steel shots were used as a shot peening media. The hardness of shots was 56HRC to 60HRC.

Design of experiments (DoE)

The design of experiment was based on full factorial design considering five factors each at three levels. An orthogonal array is a fractional factorial matrix that ensures a balanced comparison of levels of any parameter. In the present analysis a L27 orthogonal array is used. For three levels of each five factors there are 27 runs. The experimental results for tensile strength (TS), surface hardness (VHN) and fatigue strength (FS) are depicted in Table 3 for different 27 runs.

Signal-to-noise (S/N) ratio

Taguchi method is used to determine signal-to-noise (S/N) ratio. It is used to represent a performance characteristic and the largest value of S/N ratio is always desired. In this method, there are three types of S/N ratios i.e. the lower-the-better, the higher-the-better, and the nominal-the-better.
In the present analysis S/N ratio with a higher-the-better characteristic is used, that can be expressed as:

$$(S/N)_{HB} = -10 \text{ Log} \frac{1}{r}\left[\sum_{i=1}^{r} \frac{1}{y_i^2}\right] \quad (1)$$

where:
y_i = value of the performance characteristic in observation i
r = number of repetitions in a trial
The results of S/N ratios for different performance characteristics are shown in Table 4.

Grey relational analysis (GRA) with Principal component analysis (PCA)

7.1 Grey relational coefficients

The GRA is employed to analyze the complicated inter-relationships between the S/N ratios of performance characteristics. A linear normalization of the S/N ratio is performed in the range between zero and unity. The normalized S/N ratio y_{ij} for the i^{th} performance characteristic in the j^{th} experiment can be expressed by equation (2). The normalized matrix is represented in Table 5.

Table 3: Experimental results for different shot peening parameters.

Exp. No.	P	S	T	D	E	TS	VHN	FS
1	1	1	1	1	1	760.8	361.2	270.5
2	1	1	1	1	2	778.4	381.4	281.3
3	1	1	1	1	3	793.5	390.6	295.6
4	1	2	2	2	1	790.4	370.1	292.4
5	1	2	2	2	2	802.5	382.7	301.8
6	1	2	2	2	3	815.6	395.4	315.2
7	1	3	3	3	1	799.1	360.4	282.6
8	1	3	3	3	2	825.1	381.1	291.3
9	1	3	3	3	3	840.7	395.7	305.1
10	2	1	2	3	1	722.5	370.5	267.3
11	2	1	2	3	2	738.3	386.4	278.2
12	2	1	2	3	3	750.4	397.6	289.6
13	2	2	3	1	1	805.7	391.2	295.6
14	2	2	3	1	2	815.8	403.1	318.2
15	2	2	3	1	3	826.9	415.2	310.3
16	2	3	1	2	1	685.8	355.9	245.7
17	2	3	1	2	2	698.3	375.8	258.4
18	2	3	1	2	3	720.6	381.3	264.6
19	3	1	3	2	1	788.6	390.8	280.8
20	3	1	3	2	2	800.1	412.3	320.5
21	3	1	3	2	3	835.7	419.8	308.2
22	3	2	1	3	1	670.5	362.4	239.1
23	3	2	1	3	2	681.4	377.2	252.4
24	3	2	1	3	3	695.3	389.7	261.3
25	3	3	2	1	1	740.8	399.1	258.1
26	3	3	2	1	2	750.3	416.2	272.6
27	3	3	2	1	3	758.8	426.8	283.8

Larger-the-better $$x'_i(j) = \frac{y_{ij} - \min_j y_{ij}}{\max_j y_{ij} - \min_j y_{ij}} \quad (2)$$

Now from the normalized matrix a reference value is determined as the largest value of normalized value for each criterion.

$$x'_0(j) = \max_{i=1}^{n} x'_i(j) \quad (3)$$

The next step is to construct the difference matrix by taking the difference between the normalized entity and reference value.

$$\Delta_{oi}(j) = | x'_o(j) - x'_i(j) | \quad (4)$$

Afterwards the grey relational coefficients are determined by using equation (5) and they are presented in Table 6. It represents the relationship between the desired and actual experimental results.

$$\delta_{oi}(j) = \frac{\min_{i=1}^{n} \min_{j=1}^{m} \Delta_{oi}(j) + \zeta \times \max_{i=1}^{n} \max_{j=1}^{m} \Delta_{oi}(j)}{\Delta_{oi}(j) + \zeta \times \max_{i=1}^{n} \max_{j=1}^{m} \Delta_{oi}(j)} \quad (5)$$

where ζ ($0 \le \zeta \le 1$) is the distinguishing coefficient or the index for distinguishability and ζ takes the value of 0.5 because this value usually provides moderate distinguishing effects and good stability.

Table 4: Data for S/N ratios of performance characteristics.

Exp. No.	S/N_{TS}	S/N_{VHV}	S/N_{FS}
1	57.6254	51.1550	48.6433
2	57.8241	51.6276	48.9834
3	57.9909	51.8346	49.4141
4	57.9569	51.3664	49.3195
5	58.0889	51.6572	49.5944
6	58.2295	51.9407	49.9717
7	58.0520	51.1357	49.0234
8	58.3301	51.6208	49.2868
9	58.4928	51.9473	49.6888
10	57.1768	51.3758	48.5400
11	57.3647	51.7407	48.8871
12	57.5059	51.9889	49.2360
13	58.1235	51.8480	49.4141
14	58.2317	52.1083	50.0540
15	58.3491	52.3651	49.8356
16	56.7239	51.0266	47.8081
17	56.8808	51.4991	48.2459
18	57.1539	51.6253	48.4518
19	57.9371	51.8391	48.9679
20	58.0629	52.3043	50.1166
21	58.4410	52.4608	49.7767
22	56.5280	51.1838	47.5716
23	56.6680	51.5314	48.0418
24	56.8434	51.8146	48.3428
25	57.3940	52.0216	48.2358
26	57.5047	52.3860	48.7105
27	57.6025	52.6045	49.0602

7.2 Principal component analysis (PCA)

In the next stage a weightage method is used to analyze the weightage of each performance characteristic. The weightage assigned to the performance characteristics is either decided by the manufacturer or determined by using PCA.

The elements of Table 6 represent the grey relational coefficients for the multi performance characteristics of shot peened AISI 304 austenitic stainless steel. This data is used to evaluate the correlation coefficient matrix and further it is used to evaluate the corresponding eigenvalues and eigenvectors from the following equation:

$$[(CC)_{jk} - \beta_l I_m]\, E_{il} = 0 \qquad (6)$$

where β_l represents the eigenvalues; $\sum_{l=1}^{n} \beta_l = n$, l = 1, 2, 3,……..n; and

$E_{il} = [a_{li}\ a_{l2}\ a_{l3}\ \ldots\ldots a_{ln}]^T$ is the eigenvector corresponding to the eigenvalue β_l.

The eigenvalues are shown in Table 7 and the eigenvector corresponding to each eigenvalue is listed in Table 8. The results are obtained by using statistical software MINITAB 14. Hence, for this study, the squares of corresponding eigenvector of first principal component is selected as the weighting values of the related performance characteristic, represented by ω_{TS}, ω_{VHN} and ω_{FS} in Table 9.

Table 5: Normalized matrix elements.

Exp. No.	TS	VHN	FS
1	0.5585	0.0814	0.4211
2	0.6597	0.3809	0.5547
3	0.7446	0.5121	0.7240
4	0.7272	0.2153	0.6868
5	0.7944	0.3996	0.7948
6	0.8660	0.5793	0.9431
7	0.7757	0.0691	0.5705
8	0.9172	0.3766	0.6739
9	1.0000	0.5835	0.8319
10	0.3302	0.2213	0.3805
11	0.4258	0.4526	0.5169
12	0.4977	0.6099	0.6540
13	0.8120	0.5206	0.7240
14	0.8671	0.6855	0.9754
15	0.9269	0.8483	0.8896
16	0.0997	0.0000	0.0929
17	0.1796	0.2994	0.2650
18	0.3186	0.3794	0.3459
19	0.7172	0.5149	0.5486
20	0.7812	0.8097	1.0000
21	0.9736	0.9089	0.8664
22	0.0000	0.0996	0.0000
23	0.0713	0.3199	0.1848
24	0.1605	0.4994	0.3030
25	0.4408	0.6306	0.2610
26	0.4971	0.8615	0.4475
27	0.5469	1.0000	0.5849

7.3 Grey relational grade

In the next step grey relational grades are calculated based on equation (7) from data listed in Table 6. Thus, the optimization design is performed with respect to a single grey relational grade rather than complicated performance characteristics. This grey relational grade is a single numerical value which represents the optimization of multi performance characteristics. The grey relational grade is determined from following equation:

$$\gamma_{oi} = \sum_{i=1}^{m} \delta_{oi}(j)\omega_i \qquad (7)$$

The grey relational grade is calculated by using equation (7). In this equation m is the number of performance characteristics, $\delta_{oi}(j)$ are the grey relational coefficients and ω_i is the weightage assigned to the performance characteristics. The results of grey relational grade are represented in Table 10. Table 10 and Fig. 4 shows the shot peening parameters setting of experiment no. 21 has the highest grey relational grade (0.8590). Thus, the experiment no. 21 gives the best combination of process parameters among the twenty seven experiments for shot peened AISI 304 austenitic stainless steel.

V. ANALYSIS OF EXPERIMENTAL RESULTS

Further ANOVA and Taguchi method are performed on grey relational grade by using statistical software MINITAB 14 to determine the significant process parameter. They help in predicting the best combination of process parameters for optimal performance characteristics.

8.1 Taguchi analysis

Taguchi analysis is performed to generate the response table i.e. the average grey relational grade for each factor level, by using statistical software MINITAB 14. It helps to determine the significant process parameter. The procedure was to group the grey relational grades firstly by factor level for each column in the orthogonal array,

Table 6: Grey relational coefficients for performance characteristics.

Exp. No.	□oi(TS)	□oi(VHN)	□oi(FS)
1	0.5311	0.3525	0.4634
2	0.5950	0.4468	0.5290
3	0.6619	0.5061	0.6443
4	0.6470	0.3892	0.6149
5	0.7086	0.4544	0.7090
6	0.7886	0.5431	0.8978
7	0.6903	0.3494	0.5379
8	0.8579	0.4451	0.6053
9	1.0000	0.5456	0.7484
10	0.4274	0.3910	0.4466
11	0.4655	0.4774	0.5086
12	0.4989	0.5617	0.5910
13	0.7268	0.5105	0.6443
14	0.7900	0.6139	0.9531
15	0.8724	0.7672	0.8191
16	0.3571	0.3333	0.3553
17	0.3787	0.4165	0.4048
18	0.4232	0.4462	0.4332
19	0.6387	0.5076	0.5256
20	0.6956	0.7244	1.0000
21	0.9499	0.8459	0.7892
22	0.3333	0.3570	0.3333
23	0.3500	0.4237	0.3802
24	0.3733	0.4997	0.4177
25	0.4720	0.5751	0.4035
26	0.4986	0.7831	0.4751
27	0.5246	1.0000	0.5464

Table 7: The eigenvalues and proportions for principal components.

Principal Component	Eigenvalue	Proportion (%)
First	2.1202	70.7
Second	0.7004	23.3
Third	0.1794	06.0

Table 8: The Eigenvectors for principal components.

Performance characteristics	First principal component	Second principal component	Third principal component
TS	-0.613	0.419	0.670
VHN	-0.465	-0.877	0.123
FS	-0.639	0.236	-0.732

Table 9: The weightage of each performance characteristic.

Performance Characteristics	Weightage
ω_{TS}	0.3758
ω_{VHN}	0.2162
ω_{IS}	0.4083

Table 10: Grey relational grade.

Exp. No.	Grey relational grade
1	0.4637
2	0.5346
3	0.6194
4	0.5769
5	0.6524
6	0.7784
7	0.5533
8	0.6642
9	0.7974
10	0.4261
11	0.4841
12	0.5482
13	0.6447
14	0.8166
15	0.8254
16	0.3501
17	0.3961
18	0.4308
19	0.5625
20	0.8237
21	0.8590
22	0.3373
23	0.3768
24	0.4171
25	0.4644
26	0.5478
27	0.6328

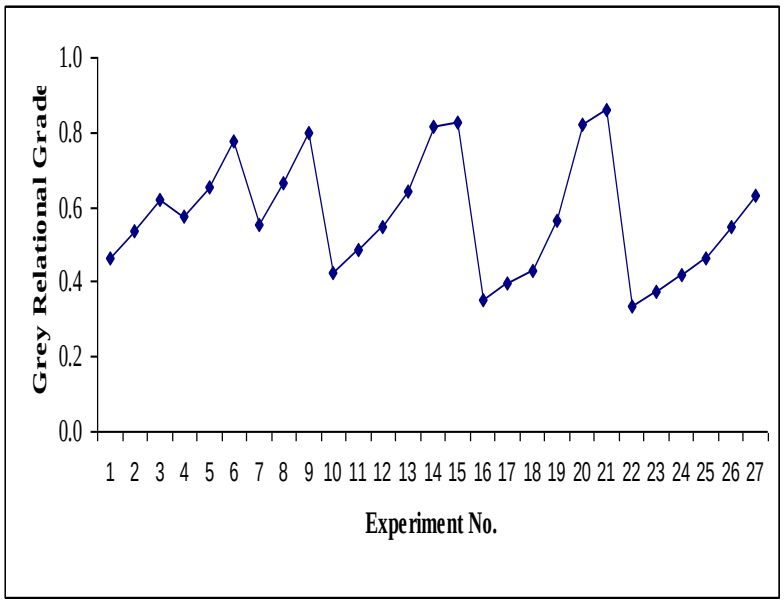

Fig. 4: Graph of grey relational grade.

Table 11: Response table for the grey relational grade.

Level	P	S	T	D	E
1	0.6267	0.5913	0.4362	0.6166	0.4866
2	0.5469	0.6028	0.5679	0.6033	0.5885
3	0.5579	0.5374	0.7274	0.5116	0.6565
Delta	0.0798	0.0654	0.2912	0.1050	0.1699
Rank	4	5	1	3	2

and then to average them. For example, the grey relational grades for factors P at level 1 and 2 can be calculated as follows:

$$P1 = \frac{1}{9}(0.4637 + 0.5346 + 0.6194 + 0.5769 + 0.6542 + 0.7784 + 0.5533 + 0.6642 + 0.7974)$$

$$= 0.6267$$

$$P2 = \frac{1}{9}(0.4261 + 0.4841 + 0.5482 + 0.6447 + 0.8166 + 0.8254 + 0.3501 + 0.3961 + 0.4308)$$

$$= 0.5469$$

The generated response tables are shown in Table 11 for each factor level. The grey relational grades represent the level of correlation between the reference and the comparability sequences. Larger value of grey relational grade shows that the comparability sequence exhibits a stronger correlation with the reference sequence. On the bases of this statement this analysis helps to select the level of process parameters that provides the largest performance characteristics. In Table 11, P1, S2, T3, D1 and E3 have largest value of average grey relational grade for factors P, S, T, D and E respectively. Hence P1S2T3D1E3 is the best combination of shot peening parameters for optimal performance characteristics of AISI 304 austenitic stainless steel. It is restated that for AISI 304 austenitic stainless steel the best combination of shot peening process are as: pressure 0.196 MPa, shot size 1mm, exposure time 160 sec, nozzle distance 80 mm and nozzle angle is 90^0. The impact of each shot peening parameter can be presented clearly by means of the response graphs. These graphs shows the change in the response, when the parameters changes their level from 1 to level 3. The response graphs for shot peening parameters are presented in Fig. 5. In these figures, the higher value of response gives the high value of performance characteristics.

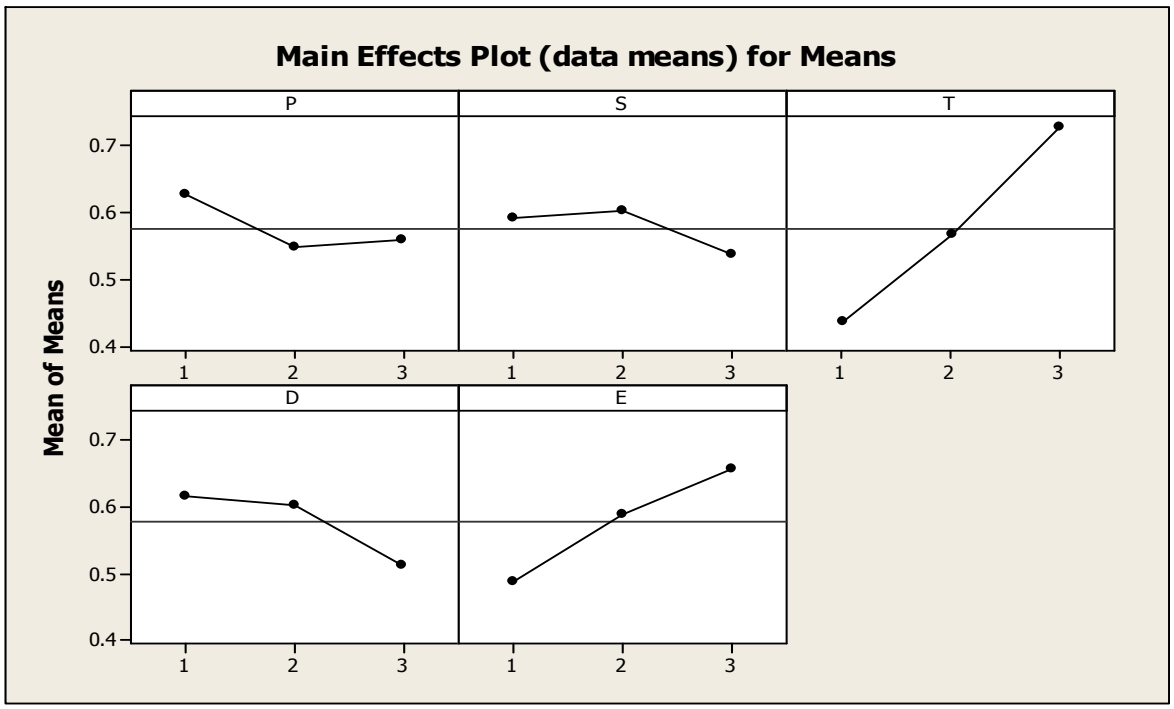

Fig. 5: Response graphs of shot peening parameters.

The order of importance is also observed from Table 11 i.e. by calculating the difference between the maximum and minimum value of the average grey relational grade for each factor. The last row of response tables indicates that the exposure time has stronger effect on the multi-performance characteristics than other parameters.

8.2 ANOVA

The purpose of the ANOVA is to investigate which parameters of shot peening process affect significantly the performance characteristics. This is achieved by separating the total variability of the grey relational grades. To evaluate the impact of each process parameters on performance characteristics, the total sum of the squared deviations can be utilized. Table 12 gives the results of the ANOVA for performance characteristic using the calculated values of grey relational grade in Table 10. According to Table 12, the exposure time with 57.88% of contribution, is the most significant controlled parameters. It is also found that the p-value of all the factors is less than 0.05 that represents significant effect on the performance characteristics.

Table 12: ANOVA results of grey relational grade.

Source	DF	Seq SS	Adj MS	P	Contribution (%)
P	2	0.033656	0.016828	0.003	5.09
S	2	0.021929	0.010965	0.016	3.32
T	2	0.382780	0.191390	0.000	57.88
D	2	0.058830	0.029415	0.000	8.90
E	2	0.131689	0.065844	0.000	19.91
Error	16	0.032389	0.002024		4.89
Total	26	0.661272			
S = 0.0449923 R-Sq = 95.10% R-Sq(adj) = 92.04%					

VI. CONFIRMING EXPERIMENTAL DESIGN

After identifying the most of influential parameters, the final phase is to verify the performance characteristics by conducting the confirmation experiments. The GRA with PCA and Taguchi method gives the optimal parameters combination as P1S2T3D1E3 for shot peening process of AISI 304 austenitic stainless steel. Hence this combination of shot peening parameters is used for confirmation tests. With these optimal settings for AISI 304 austenitic stainless steel, the specimens give the tensile strength of 832.8 MPa, surface hardness of 403.8 VHN and fatigue strength of 318.6 MPa. The optimal grey relational grade (γ_{opt}) is predicted by using the following equation:

$$\gamma_{opt} = \gamma_m + \sum_{i=1}^{n} (\gamma_i - \gamma_m) \quad (8)$$

Where γ_m is the average of grey relational grade, γ_i is the average of grey relational grade at optimum level and n is the number of significantly affecting process parameters. Pressure, shot size, exposure time, nozzle distance and nozzle angle are all the significant parameters used for predicting the optimal grey relational grade. The predicted value of optimal grey relational grade is expressed as:

$$\gamma_{opt} = \gamma_m + \sum_{i=1}^{5} (\gamma_i - \gamma_m)$$

The predicted value of optimal grey relational grade is calculated as:

= 0.5772+(0.7274-0.5772)+(0.6565-0.5772)+(0.6166-0.5772)+(0.6267-0.5772)+(0.6028-0.5772) = 0.9212

Table 13: Experimental and predicted values of grey relational grade.

Performance characteristics	Predicted value	Experimental value
Optimal parameters	P1S2T3D1E3	P1S2T3D1E3
Tensile Strength		832.8 MPa
Surface Hardness		403.8 VHN
Fatigue Strength		318.6 MPa
Grey relational grade	0.9212	0.8713

It is found that calculated grey relational grade for these optimal values of performance characteristics is higher from the grey relational grade among the 27 experiments as shown in Table 13. This table also represents that the grey relational grade for optimal parameters is near to the predicted value of optimal grey relational grade. Hence using the present approach, shot peening of AISI 304 austenitic stainless steel is successfully optimized.

VII. CONCLUSION

The response table and ANOVA presented in Table 11 and 12 shows that pressure, shot size, exposure time, nozzle distance and nozzle angle are the process parameters which significantly affecting the performance characteristics. All parameters affecting the performance characteristics are at 95% confidence level. The GRA with PCA and Taguchi analysis gives the optimal process parameters as P1S2T3D1E3. At this optimal condition the process parameters are set as: pressure 0.196 MPa, shot size 1.00 mm, exposure time 160 sec, nozzle distance 80 mm and nozzle angle 90^0. At this condition of process parameters the confirmatory experiments are performed and the average value of tensile strength, surface hardness and fatigue strength are as 832.8 MPa, 403.8 VHN and 318.6MPa respectively. Hence these are the proposed process parameter levels for the optimal performance characteristics of shot peened AISI 304 austenitic stainless steel.

The maximum grey relational grade for the material is 0.8590 among the 27 experiments. The conformation experiments at optimal process parameters give a grey relation grade of 0.8713. It is higher than the grey relational grade among 27 experiments and near to the predicted value of optimal grey relational grade i.e. 0.9212. Hence it optimizes the shot peening process for AISI 304 austenitic stainless steel. It seems that GRA with PCA and Taguchi analysis is a straight forwarded method for optimizing multi performance characteristic problems in shot peening.

REFERENCES

[1] A. Kyröläinen, M. Vilpas and H. Hänninen, Use of stainless steels in bus coach structures, *Journal of Materials Engineering and Performance. Vol. 9(6)*, 2000, 669-677.

[2] R.W.K. Honeycombe and H.K.D.H. Bhadeshia, *Steels - Microstructure and Properties*, (Second Edition, Edward Arnold, 1995).

[3] P.J. Cunat, A New Structural Material for Passenger Cars: Stainless Steel, *Auto Technology*, 2002, 40-42.

[4] T. Oshima, Y. Habarai and K. Kuroda, Efforts to save nickel in austenitic stainless steels, *ISIJ International. Vol. 47, No. 3*, 2007, 359-364.

[5] D. Kirk and N.J. Payne, Transformation induced in austenitic stainless steels by shot peening, *ICSP-7, Warsaw, Poland*, 1999, 15-22.

[6] M. Milad, N. Zreiba, F. Elhalouani and C. Baradai, The effect of cold work on structure and properties of AISI 304 stainless steel, *Journal of Materials Processing Technolog,. 203*, 2008, 80-85.

[7] A. Hedayati, A. Najafizadeh, A. Kermanpur and F. Forouzan, The effect of cold rolling regime on microstructure and mechanical properties of AISI 304L stainless steel, *Journal of Materials Processing Technology, 210*, 2010, 1017-1022.

[8] T. Dorr, M. Hilpert, P. Beckmerhagan, A. Kiefer and L. Wagner, Influence of shot peening on fatigue performance of high-strength aluminum-and magnesium alloys, *Proceedings of the ICSP-7 conference, Warsaw, Poland*, 1999.
[9] M. Obata and A. Sudo, Effect of shot peening on residual stress and stress corrosion cracking for cold worked austenitic stainless steel, *Proceedings of the ICSP-5 conference, Oxford, UK*, 1993.
[10] K.B. Prakash, B.M. Sunil and Y.S. Chandrakant, Shot peening: state of-the-art, *Proceedings of the ICAMMP Conference, IIT Kharagpur*, 2006, pp 296–303.
[11] J. Champaigne, *Controlled shot peening*, (2nd ed., The Shot Peener, Mishawaka, USA, 1989).
[12] M.C. Sharma and A. Mubeen, Effect of shot size on peening intensity for local peening, *Journal of Mechanical Working Technology, 8*, 1983, 155-160.
[13] M.C. Sharma, H. Deo, S.C. Modi and R.G. Bosshard, *Virtues & limitations of Almen round shot peening*, (Wiley-VCH Verlag GmbH & Co. KgaA, 2006).
[14] V. Schulze, Characteristics of surface layers produced by shot peening, *ICSP-8, Garmisch-Partenkirchen, Germany*, 2002, 145-160.
[15] P.J. Ross, *Taguchi Techniques for Quality Engineering*, (McGraw-Hill, New York, 1988).
[16] R.K. Roy, Design of Experiments using the Taguchi approach: 16 steps to Product and Process, Improvement, *Wiley-Inter science, New York*, 2001, 179-186.
[17] S.M. Phadke, *Quality Engineering Using Robust Design*, (Englewood Cliffs, NJ: Prentice Hall, 1989).
[18] J.L. Deng, *Basic methods of Grey System*, (1st edition Press of Huazhong University of Science and Technology, Wuhan, China, 1987).
[19] J.L. Deng, Introduction to grey system theory, *Journal of Grey Syst., 1*, 1989, 1-24.
[20] R. Jeyapaul, P. Shahabudeen and K. Krishnaiah, Quality management research by considering multi-response problems in the Taguchi method-a review, *International Journal of Advance Manufacturing Technology, 26*, 2005, 1331–1337.
[21] F.S. Chen, T.C. Chang and H.H. Liao, The application of grey relation analysis on teacher appraisa, *IE Times New Roman EE International conference on Systems Man and Cybernetics, 5*, 2000, 6-10.
[22] S. Bin, Y. Ping, L. Yunbai and W. Xishan, Study on the fault diagnosis of transformer based on the grey relation analysis, *International Conference Power System Technology, China, 4*, 2002, 2231-2234.
[23] Y.F. Hsiao, Y.S. Tarng and W.J. Huang, Optimization of plasma arc welding parameters by using the Taguchi method with grey relational analysis, *Material and Manufacturing Processes, 23*,2008, 51-58.
[24] Lakhwinder Singh, R.A. Khan and M.L. Aggarwal, Empirical modeling of shot peening parameters for welded austenitic stainless steel using grey relational analysis, *Journal of Mechanical Science and Technology, 26(6)*, 2012, 1731-1739.

American Journal of Engineering Research (AJER)
e-ISSN : 2320-0847 p-ISSN : 2320-0936
Volume-02, Issue-10, pp-173-179
www.ajer.org

Research Paper Open Access

Design of Automobile Driveshaft using Carbon/Epoxy and Kevlar/Epoxy Composites

R. Srinivasa Moorthy, Yonas Mitiku & K. Sridhar
School of Mechanical and Industrial Engineering, IoT, Bahir Dar University, Bahir Dar, Ethiopia.

Abstract: - Use of advanced composites has resulted in remarkable achievements in many fields including aviation, marine and automobile engineering, medicine, prosthetics and sports, in terms of improved fatigue and corrosion resistances, high specific strength and specific modulus and reduction in energy requirements owing to reduction in weight. The aim of this work is to replace the conventional steel driveshaft of automobiles with an appropriate composite driveshaft. The conventional driveshafts are made in two pieces for reducing the bending natural frequency, whereas the composite shafts can be made as single-piece shafts, thus reducing the overall weight. Carbon/Epoxy and Kevlar/Epoxy composites were designed and analysed for their appropriateness in terms of torsional strength, bending natural frequency and torsional buckling by comparing them with the conventional steel driveshaft under the same grounds of design constraints and the best-suited composite was recommended. Light has been thrown upon the aspects like mass saving, number of plies and ply distribution.

Keywords: - *Carbon/Epoxy, Composite driveshaft, Kevlar/Epoxy, ply distribution.*

I. INTRODUCTION

A composite is a structural material consisting of two or more combined constituents that are combined at a macroscopic level, not soluble in each other. One constituent called *reinforcing* phase in the form of fibres, flakes or particles, is embedded in a continuous *matrix* phase. The inability of monolithic metals and their alloys to meet the complex functional requirements of advanced technologies lead to the use of composites more and more [1]. Generally composite materials have very high specific strength and specific modulus. The strength of graphite epoxy may be the same, but its specific strength is thrice as that of steel. This translates into reduced material and energy costs. Though the material cost is 10-15 times that of steel, manufacturing techniques such as SMC (Sheet Moulding Compound) and SRIM (Structural Reinforcement Injection Moulding) are substantially lowering the cost and production time in manufacturing automobile parts. Unlike metals, composite materials are not isotropic - their properties are not the same in all directions, thus necessitating more material parameters. Nine stiffness and strength constants are needed to conduct mechanical analysis for a single layer of a composite as against four stiffness and strength constants in the case of monolithic materials like steel. Such complexities render structural analysis computationally and experimentally more complicated and highly intensive.

An automotive driveshaft is a rotating shaft that transmits power from the engine to the differential gear of rear wheel drive (RWD) vehicles. Conventional steel driveshafts are usually manufactured in two pieces to increase the fundamental bending natural frequency because the bending natural frequency of a shaft is inversely proportional to the square of the span length. But the two-piece steel driveshaft involves three universal joints, an intermediary thrust bearing and a supporting bracket in its assemblage, which increases the total weight of the vehicle [2].

Since one-piece composite driveshaft will suffice in the place of a two-piece steel driveshaft, it substantially reduces the inertial mass. Moreover, a composite driveshaft can be perfectly designed to effectively meet the strength and stiffness requirements. Since composite materials generally have a lower elasticity modulus, during torque peaks in the driveline, the driveshaft can act as a shock absorber. Moreover, the breakage of composite a driveshaft (particularly in SUV's) is less-risky, since it results in splitting up of the fine fibres as compared to the scattering of broken steel parts in various directions [3].

II. DESIGN SPECIFICATIONS

The following specifications were assumed suitably, based on the literature and available standards of automobile driveshafts:

1. The torque transmission capacity of the driveshaft (**T**) = 2000 N-m.
2. The shaft needs to withstand torsional buckling ($\mathbf{T_b}$) such that $T_b > T$.
3. The minimum bending natural frequency of the shaft ($f_{nb\,(min)}$) = 80 Hz.
4. Outside radius of the driveshaft ($\mathbf{r_o}$)= 60 mm.
5. Length of the driveshaft = 1.8 m.

III. DESIGN OF CONVENTIONAL STEEL DRIVESHAFT

First, the conventional steel shaft was designed to facilitate comparison in terms of mass savings. Be it the conventional driveshaft or the composite one, the design should be based on the following criteria:

- Torsional strength
- Torsional buckling and
- Bending natural frequency.

SM45C steel was selected, since it is widely being used for the design of conventional steel shaft. The properties of SM45C steel are:

Young's modulus (E)	=	207 GPa
Shear modulus (G)	=	80 GPa
Poisson's ratio (ν)	=	0.3
Density of steel (ρ)	=	7600 kg/m^3
Yield strength (σ_y)	=	370 MPa.

3.1 Torsional strength

Since the primary load on a driveshaft is torsion, the maximum shear stress ($\boldsymbol{\tau_{max}}$) at the outer radius ($\mathbf{r_o}$) of the shaft is given by:

$$\frac{\tau_{max}}{F.S.} = \frac{Tr_o}{J} \quad (1)$$

Substituting for **J**:

$$\frac{\tau_{max}}{F.S.} = \frac{32Tr_o}{\pi\left[d_0^4 - d_i^4\right]} \quad (2)$$

where,

T is the maximum torque applied in N-m

J is the polar area moment of inertia in m^4 and

$\mathbf{d_0}$ **and** $\mathbf{d_i}$ are outer and inner diameters of the shaft in m.

Assuming $\tau_{max} = 80$ MPa and a factor of safety (**F. S.**) of 3,

$$d_i = 0.112735\ m.$$

Hence, the inner radius is, $r_i = 0.056368\ m.$

Thus the wall thickness of the hollow steel shaft:

$$t = r_0 - r_i = 3.6325 \times 10^{-3}\ \text{m} \quad (3)$$

3.2 Torsional buckling

A shaft is considered as a long shaft, if [4]:

$$\left(\frac{1}{\sqrt{(1-\vartheta^2)}}\right)\frac{L^2 t}{(2r)^3} > 5.5 \quad (4)$$

where, **r** is the mean radius, such that:

$$r = \left(\frac{r_i + r_o}{2}\right) = 0.058184\ m. \quad (5)$$

Substituting,

$$\left(\frac{1}{\sqrt{(1-0.3^2)}}\right)\frac{(1.8)^2(0.0036325)}{(2\times 0.058184)^3} = 7.8294\ (> 5.5)$$

For a long shaft, the torsional buckling capacity:

$$T_b = \tau_{cr}(2\pi r^2 t) \quad (6)$$

where, the critical stress ($\boldsymbol{\tau_{cr}}$) is given by,

$$\tau_{cr} = \left[\frac{E}{3\sqrt{2}(1-\vartheta^2)^{3/4}}\right]\left(t/r\right)^{3/2} \quad (7)$$

Substituting,

$$\tau_{cr} = 81.6875 \times 10^7 \text{N/m}^2 \text{ and}$$
$$T_b = 63.11735 \times 10^3 \text{N} - \text{m}.$$

Thus,

$$T_b > T.$$

3.3 Bending Natural Frequency

According to Bernoulli-Euler beam theory, by neglecting shear deformation and rotational inertia effects, the bending natural frequency of a rotating shaft is given by:

$$\mathbf{f_{nb} = \frac{\pi p^2}{2L^2}\sqrt{\frac{EI_x}{m'}}} \quad \textbf{(8)}$$

where,

$\mathbf{m'}$ is mass per unit length in kg/m

$\mathbf{I_x}$ is area moment of inertia in x-direction (longitudinal) in m^4.

$$\mathbf{I_x = \frac{\pi}{64}(d_0^4 - d_i^4)} \quad \textbf{(9)}$$
$$= 2.25 \text{ x } 10^{-6} \text{ m}^4.$$
$$\mathbf{m' = \rho(\pi/4)[d_0^2 - d_i^2]} \quad \textbf{(10)}$$
$$= 10.0925\ kg/m.$$

Substituting these values,

$$f_{nb} = 104.148 \text{ Hz}.$$

Thus,

$$f_{nb} > f_{nb\,(min)}.$$

Thus the designed SMC45 steel driveshaft meets all the requirements.

The total mass of the shaft is:

$$\mathbf{m = m'L} \quad \textbf{(11)}$$

Thus,

$$m = 18.1665 \text{ kg}.$$

IV. DESIGN OF COMPOSITE DRIVESHAFTS

Only $0°, \pm 45°$ *and* $90°$ were considered for the composite ply orientations, owing to their specific advantages.

4.1 Design of Carbon/Epoxy Driveshaft

60% fibre volume fraction Carbon/Epoxy shaft ($V_f = 60\%$) with standard ply thickness of 0.13 mm was selected.

4.1.1 Torsional strength

$$\mathbf{\frac{\tau_{max}}{F.S.} = \frac{T}{2\pi r^2 t}} \quad \textbf{(12)}$$

where,

$\mathbf{r}$ is the mean radius of the shaft.

Since the nature of loading is pure shear, 70% of the plies can be set at $\pm 45°$ and the remaining 30% at 0º and 90º orientations.

From Fig. 1,

$$\tau_{max} = 293 \text{ MPa}$$

For a factor of safety **(F. S.)** of 6,

$$r^2 t = 6.5183 \times 10^{-6} \text{m}^3.$$

Thus,

$$t \geq 1.8106 \times 10^{-3} \text{m}.$$

Since the thickness of each ply is 0.13 mm,

$$n = 1.8106 \times 10^{-3}/0.13 \times 10^{-3}$$
$$= 13.93 \cong 14.$$

Hence the corrected values are:

$$t = 1.82 \text{ x } 10^{-3} \text{ m}$$
$$r_i = 0.05818 \text{ m and}$$
$$r = 0.05909 \text{ m}.$$

4.1.2 Torsional buckling

Considering the hollow composite shaft as an isotropic cylindrical shell, the buckling torque is given by:

$$\mathbf{T_b = 2\pi r^2 t(0.272)(E_x E_y^3)^{1/4}\left(\frac{t}{r}\right)^{3/2}} \quad \textbf{(13)}$$

where,

$\mathbf{E_x}$ and $\mathbf{E_y}$ are the Young's modulii in 'x' and 'y' directions respectively.

From Fig. 2,

$$E_x = 38709.5 \text{ MPa.}$$

By permuting (interchanging the percentages of 0° and 90° plies),

$$E_y = 38709.5 \text{ MPa.}$$

Upon substitution,

$$T_b = 2272.49 \text{ N} - \text{m. (> T)}$$

4.1.3 Bending natural frequency

$$\mathbf{f_{nb}} = \frac{\pi}{2L^2}\sqrt{\frac{E_x I_x}{m'}} \qquad \textbf{(14)}$$

From TABLE I, the density of Carbon/Epoxy laminate (ρ) = 1530 kg/m^3.

Hence,

$$I_x = 1.179957 \times 10^{-6} \text{ m}^4 \text{ and}$$
$$m' = 1.03385\ kg/m.$$

Upon substitution,

$$f_{nb} = 101.903 \text{ Hz (> 80 Hz).}$$

The total mass of Carbon/Epoxy composite shaft is,

$$m = 1.86093 \text{ kg.}$$

The ply distribution for the Carbon/Epoxy driveshaft is shown in Fig. 3.

Accordingly, the ply orientation is,

$$[0°/\pm45_2^\circ/90°/\pm45°/90°/\pm45_2^\circ/0°]\,.$$

4.2 Design of Kevlar/Epoxy Driveshaft

Setting 70% of the plies in ±45° and the remaining 30% in 0º and 90º, similar to the previous approach, from the respective figures [5],

$$\tau_{max} = 95 \text{ MPa}$$
$$E_x = 23900 \text{ MPa and}$$
$$E_y = 23900 \text{ MPa.}$$

Using a factor of safety (F.S.) of 6, for $V_f = 60\%$ and ply thickness = 0.13 mm,

$$t \geq 5.5844 \times 10^{-3} \text{m.}$$
$$n = 42.96 \cong 44.$$

The corrected values are:

$$t = 0.00572 \text{ m}$$
$$r_i = 0.05428 \text{ m and}$$
$$r = 0.05714 \text{ m.}$$

The calculated values of buckling torque, bending natural frequency and the total mass are:

$$T_b = 24161 \text{ N} - \text{m}$$
$$f_{nb} = 101.903 \text{ Hz and}$$
$$m = 4.99 \text{ kg.}$$

The ply distribution for the Kevlar/Epoxy driveshaft is shown in Fig. 4.

Accordingly, the ply orientation with mid-plane symmetry is,

$$[0_2^\circ/90_2^\circ/\pm45_6^\circ/90_2^\circ/0_2^\circ/-45^\circ/+45^\circ]_s\,.$$

V. RESULTS AND DISCUSSION

From the detailed analysis, the key results of wall thickness, torsional buckling capacity, bending natural frequency, number of plies and total mass for SM45C steel (as applicable), Carbon/Epoxy and Kevlar/Epoxy driveshafts were extracted and summarized in TABLE II.

TABLE II reveals that use of Carbon/Epoxy results in a mass saving of 89.756% when compared to the conventional SM45C steel driveshaft, whereas Kevlar/Epoxy results in 72.53%. Obviously, the number of plies needed for Carbon/Epoxy is 14 with 1.82 mm wall thickness as compared to 44 plies with 5.72 mm wall thickness in the case of Kevlar/Epoxy. Moreover, the torsional buckling capacity and bending natural frequency are adequate enough to meet the design requirements in the case of Carbon/Epoxy driveshaft.

VI. CONCLUSION

Precisely, for the specifications chosen, using Carbon/Epoxy driveshaft in the place of conventional driveshaft will lead to an appreciable mass saving of 89.756% with barely half of the wall thickness of conventional steel shaft. Though the mass saving is substantial in both the composites considered, making either

of the composites a better choice for the conventional high quality SM45C steel, using Carbon/Epoxy for making automotive driveshaft has multiple advantages as mentioned above.

This work relies purely upon analytical calculations and use of ply distribution tables/graphs pertaining to 60% volume fraction and 0.13 mm ply thickness. The approach can be extended to other widely used composites like Glass/Epoxy and Boron/Epoxy to check their suitability. This approach throws light upon ply distribution in standard orientations of 0º, 90º, +45º and -45º for the composite considered. The effect of varying ply staking sequence on the performance of composites can be found by using computational softwares. Moreover, considering the material and manufacturing cost will give better grounds to compare the overall efficacy, thus resulting in an appropriate selection of the best fibre/matrix combination for making automotive driveshafts.

REFERENCES

[1] Autar K. Kaw, *Mechanics of Composite Materias* (Second edn., CRC Press, 2006).

[2] R.P.Kumar Rompicharla and Co., Design and Optimization of Driveshaft with Composite Materials, *International Journal of Engineering Research & Technology, Vol. 1, Issue 7, September 2012, ISSN: 2278-0181.*

[3] Mohammad Reza Khoshravan et al., Design and Modal Analysis of Composite Driveshaft for Automotive Application, *International Journal of Engineering Science and Technology, Vol. 3, No. 4, April 2011, ISSN : 0975-5462.*

[4] Gummadi Sanjay & Co., Optimum Design and Analysis of a Composite Driveshaft for an Automobile, Department of Mechanical Engineering, Blekinge Institute of Technology, Karlskrona, Sweden, 2007, ISRN: BTH-AMT-EX--2007/D-09--SE.

[5] Daniel Gay, et al, *Composite Materials – Design and Applications* (CRC Press, 2003).

FIGURES AND TABLES

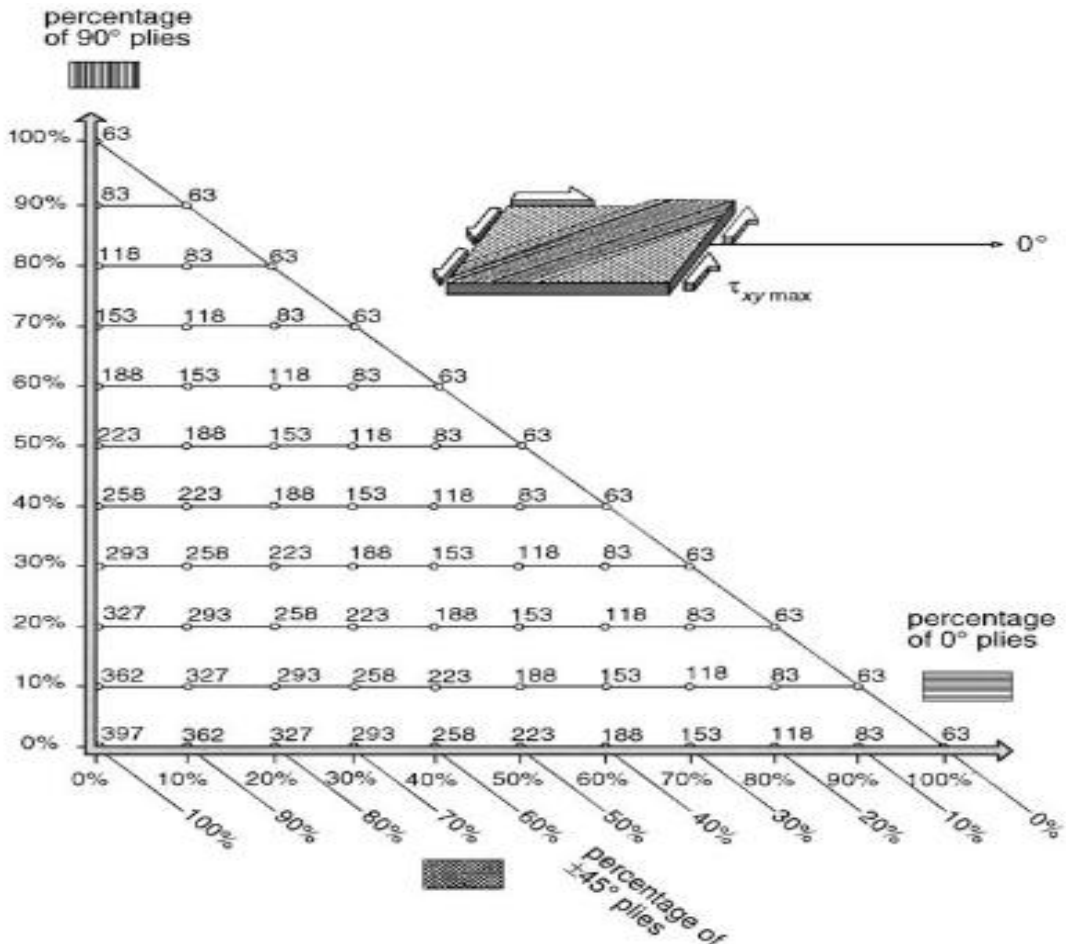

Figure 1: Maximum shear stress (τ_{max}) as a function of ply percentages for Carbon/Epoxy Laminate (V_f = 60%; Ply thickness = 0.13 mm) [5]

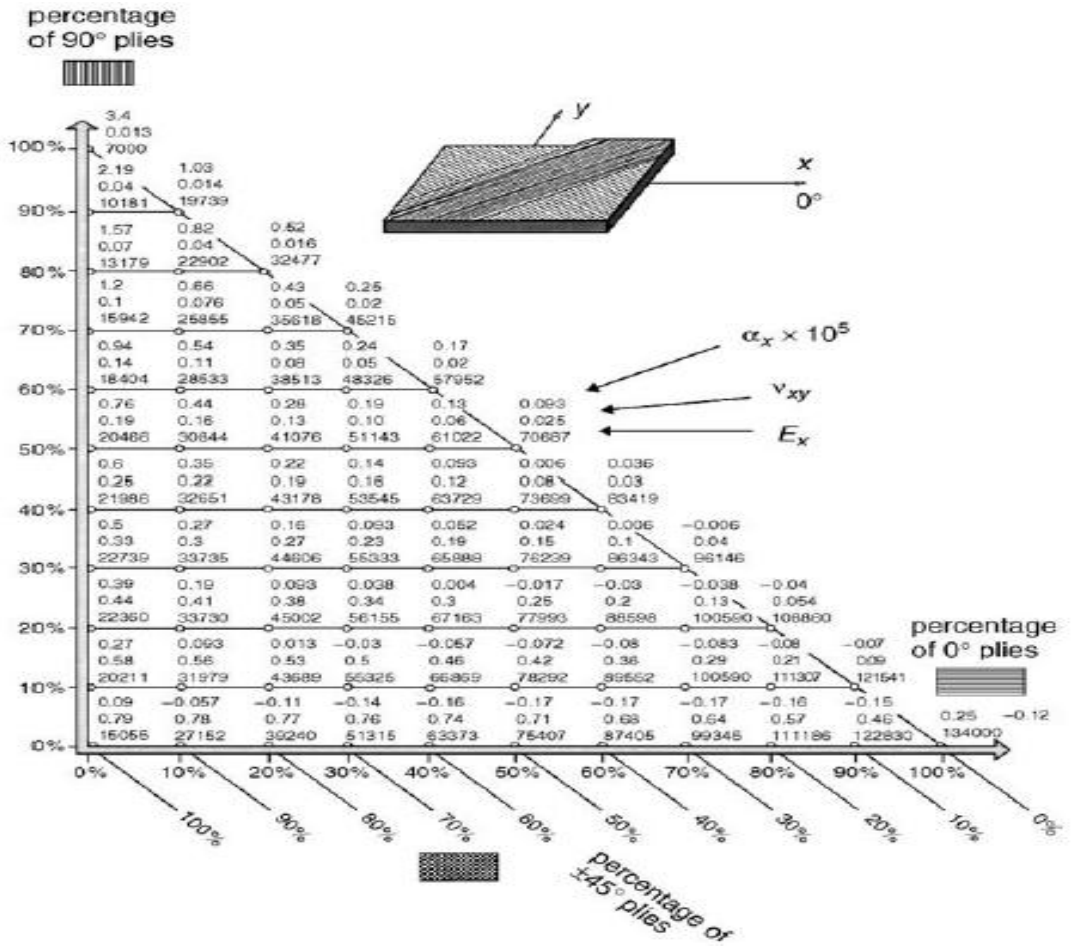

Figure 2: Young's Modulus (E_x in MPa), Poisson's ratio (υ_{xy}) and Co-efficient of thermal expansion (α) as functions of ply percentages for Carbon / Epoxy Laminate (V_f = 60%; Ply thickness = 0.13 mm) [5]

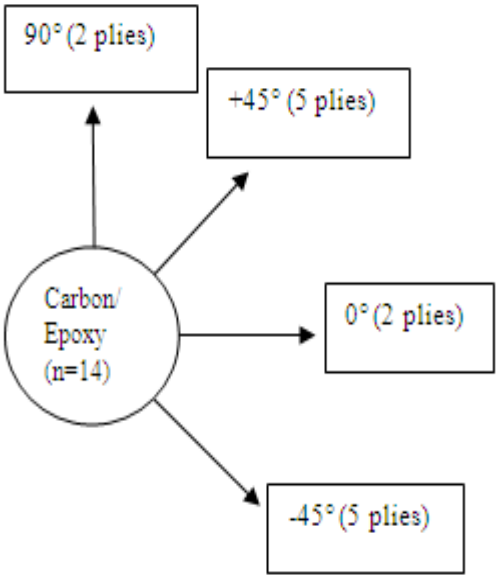

Figure 3: Ply distribution for Carbon/Epoxy driveshaft

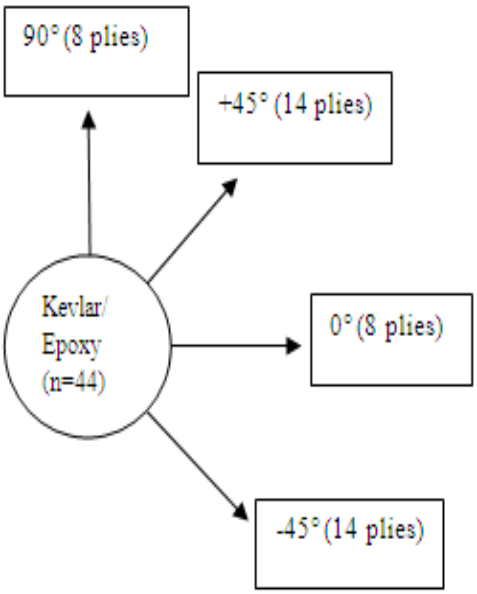

Figure 4: Ply distribution for Kevlar/Epoxy driveshaft

TABLE I: Properties of Fibre/Epoxy Laminates (V_f = 60%)

Property	*Carbon*	*Kevlar*
Specific mass (kg/m^3)	1530	1350
Longitudinal tensile fracture strength (MPa)	1270	1410
Longitudinal compressive fracture strength (MPa)	1130	280
Transverse tensile fracture strength (MPa)	42	28
Transverse compressive fracture strength (MPa)	141	141
Poisson's ratio	0.25	0.34

TABLE II: Comparison of SM45C steel, Carbon/Epoxy and Kevlar/Epoxy driveshafts

S. No.	*Material*	*t (mm)*	*T_b (N-m)*	*f_{nb} (Hz)*	*n*	*m (kg)*
1	SM45C steel	3.63	63117.35	104.148	-	18.1665
2	Carbon/Epoxy	1.82	2272.49	101.903	14	1.86093
3	Kevlar/Epoxy	5.72	24161	267.370	44	4.99

AUTHORS' BIBLIOGRAPHY

R. Srinivasa Moorthy obtained his Masters degree in Mechanical Engineering Design from Kongu Engineering College, Perundurai, Tamilnadu, India; has 17 + years of teaching experience; worked in Erode Sengunthar Engineering College, Erode, Tamilnadu, India, for 10 + years; worked in Eritrea Institute of Technology, Eritrea, North-East Africa, for 4 years; currently working as a Lecturer in School of Mechanical and Industrial Engineering, Institute of Technology, Bahir Dar University, Bahir Dar, Ethiopia.

Yonas Mitiku Degu received his B.Sc. in Mechanical Engineering from Bahir Dar University, Bahir Dar, Ethiopia in 2005; pursued M.Sc. in Applied Mechanics (Mechanical Design) in Addis Ababa University, Addis Ababa, Ethiopia in 2008; currently working as Assistant Professor and Director of School of Mechanical and Industrial Engineering, Institute of Technology, Bahir Dar University, Bahir Dar, Ethiopia.

K. Sridhar received his B.E. degree in Mechanical Engineering from Anna University, Chennai, India and M.E. from Anna University, Coimbatore, India; worked as a Lecturer/Senior Lecturer in S.S.M. College of Engineering, Komarapalayam, Tamilnadu, India for 4 years; currently working as a Lecturer in School of Mechanical and Industrial Engineering, Institute of Technology, Bahir Dar University, Bahir Dar, Ethiopia, from October 2011.

American Journal of Engineering Research (AJER)
e-ISSN : 2320-0847 p-ISSN : 2320-0936
Volume-02, Issue-10, pp-180-190
www.ajer.org

Research Paper Open Access

Enhancing E-Voting Systems By Leveraging Biometric Key Generation (Bkg)

*V. C. Ossai[1], I.C. Okoro, E.O. Alagbu, A.O. Agbonghae and I.N. Okafor
[1]*Electronics Development Institute, Awka. National Agency for Science and Engineering Infrastructure.*

Abstract: - The adoption of e-voting methods in electioneering processes will effectively reduce cost as well as enhance election activities. What makes an e-voting model reliable and acceptable is its ability to properly authenticate voters and provide a secure means through which a voter can express his/her franchise. This paper therefore proposes a design of an e-voting system that leverages a Biometric Encryption scheme known as Biometric key Generation (BKG) which is a secured strategy that entails using of biometrics to generate secure cryptographic keys. The main objective of this research is to improve on the already existing E-voting systems adopting a secured bio-cryptographic technique vis Biometric key Generation (BKG) as well as using a secure transmission channel for confidential datasets of a voting process. This work develops a simulation model of an E-voting system which adopts relevant algorithms with emphasis on biometric key generation schemes. The simulation of a prototype model of the electronic voting system is developed using Proteus 7.6 application software. The prototype model would consist of electronic kiosk polling booths that are all networked to the state electoral collection center and collection centers that are networked to the national electoral collection center via a VPN backbone. The proposed e-voting system uses a Virtual Private Network (VPN) as the means of communication between the various polling booths and collection points. The results of validation show that the proposed model facilitates the adoption of E-governance in the developing countries.

***Keywords*: -** *Biometric Key Generation, Cryptography, E-voting Booths, Privacy, Security.*

I. INTRODUCTION

Election is a process by which members of an organization or a society select people to hold positions of authority [1].

The term "e-voting" encompasses all voting techniques involving the use of electronic voting equipment including voting over the internet, using booths in polling stations (e-booths) and sometimes even from remote sites (e.g. via SMS). According to [2] e-voting is any voting method where the voter's intention is expressed or collected by electronic means. The following e-voting approaches have being identified by this literature viz;

- Kiosk voting (e-booths)
- Remote electronic voting
- Internet voting (I-voting)

Basically, this work uses the term e-voting with the specific emphasis on kiosk voting (e-booth) over the internet (through a secured public network infrastructure). An Electronic Voting System has as its main components [2]:

i. The Electronic Voters Register.
ii. Authentication- which is done prior to balloting.
iii. Voting, Collation and Transmission.

Owing to the fact that there are a lot of vulnerabilities in the current voting schemes currently used in e-voting systems, there is a need to develop a secure, reliable and trusted means of voting so as to reduce the vulnerabilities associated with voting, increase flexibility and security as well as reducing the cost of elections.

In this work, the use of some of Direct Recording Balloting Machines (DREs) connected over a VPN (secure internet facility) is adopted and characterized. This will completely eliminate the cost associated with the printing of several million ballot papers.

This work leverages Biometric Key Generation (BKG) technique and a secured communication channel to transmit voting results which is being characterized in this simulation model. This would help reduce to the barest minimum the fraud and irregularities associated with elections. Worthy of note is that BKG has not yet been adopted in E-voting systems.

II. LITERATURE REVIEW

2.1 Related Works

The work in [3] presented e-voting Schemes and explained that e-voting is a promising application of cryptography, which can have positive impact on democratic process. The work discussed cryptographic aspects of constructing e-voting schemes and tried to generate a preliminary framework on the notion of choice. The author added that on the internet, implementing cryptographic protocols like digital encryption and signature has been widely accepted.

The authors in [4] described the theory behind a practical voting scheme based on homomorphic encryption which entails the application of arithmetic operation like addition to encrypted numbers without previously decrypting them. The resulting encrypted sum can then be revealed with a private decryption key. The homomorphic encryption scheme ensures that individual numbers cannot be decrypted with the private decryption key alone. The major drawback is that homomorphic approaches do not allow complex multi-candidate elections. Most of them are restricted to simple yes/no votes which are easy to count. The work presented the most important goals for electronic voting schemes viz: Privacy, Robustness, Universal verifiability and freeness.

Other Fundamental approaches to electronic voting are known in the literature include the use of blind signatures and anonymous channels [5]

In Anonymous channels on the other hand messages to be sent anonymously, i.e. such that a recipient cannot trace the received messages back to the senders. The most prominent technique for building anonymous channels is mix nets and onions [6], [7]. They are comprised of a collection of anonymization servers whose task is to shuffle a given input sequence of encrypted messages. To ensure that mix-servers or onion routers do not drop or substitute messages, it is necessary that the servers provide proofs of correct operation. The resulting anonymous channel is then called verifiable. Although most existing verifiable anonymous channels are relatively inefficient, progress has been reported recently.

The authors in [8] propose a secure electronic voting protocol that is suitable for large scale voting over the Internet. In their work, the protocol allows a voter to cast his or her ballot anonymously by exchanging untraceable yet authentic messages. The protocol ensures that (i) only eligible voters are able to cast votes, (ii) a voter is able to cast only one vote, (iii) a voter is able to verify that his or her vote is counted in the final tally, (iv) nobody, other than the voter, is able to link a cast vote with a voter, and (v) if a voter decides not to cast a vote, nobody is able to cast a fraudulent vote in place of the voter. The following assumptions were made in the context of this protocol viz [8]:

i. Hard-to-invert permutations
ii. Blind Signature on messages
iii. Secure Transit

In their final analysis, the work concludes that the protocol is suitable for large scale voting over the Internet and that satisfies the core properties of secure voting systems – namely accuracy, democracy, privacy and verifiability.

The idea of blind signatures is to apply a blinding function to a message before sending it to a signing party. Based on a simple RSA-like scheme, this can be done such that the blinding function can be inverted on the blinded signature to finally obtain a regular RSA-based digital signature. At the end of this process, in which the content of the message has been entirely disguised from the signer, the signature is ordinarily verifiable using the signer's public key [4]. The idea in such a scheme is that a voter prepares a ballot in clear text, i.e. a message stating for whom he votes [4]. He then interacts with an authority that can verify that he is eligible to vote and has not already voted. If this is the case, the authority issues a blind signature on the ballot. Informally, this means that the voter obtains the authority's digital signature on the ballot, without the authority learning any information about the contents of the ballot. On the other hand, a voter cannot obtain such a signature without interacting with the authority, and is therefore prevented from voting several times [4]. A major drawback of the protocol is that voters need to be active in at least two phases to ensure verifiability and fairness, which restricts its usability intrinsically.

The work in [9] presents an evaluation of e-Voting systems equipped with voter-Verified Paper Records. The work stated that owing to the need to increase public confidence, various states are increasingly considering electronic voting systems that provide voter verified paper records. In the work, an analysis and evaluation of New Jersey's criteria against several different e-voting machine types revealed potential threats and possible solutions on privacy, security, and performance issues.

The authors in [10], observed that the traditional methods of electioneering is characterized by long period of preparation, fake voting, faulty voting, mistakes made in counting the votes, long period of counting and high cost of voting process, in order to avoid these limitations; the system applied biometric fingerprint authentication. In the work, a biometric based e-voting system is designed for providing a secure election on electronic environment for the electors. Technologies such as XSL language which is compatible with Asp.Net, Framework 2.0, Java Script, Xml is used but can be deployed in Microsoft Windows operating system [10]. Again, the, biometric based software libraries are also used for integrating the fingerprint control to the system. In this regard, the elector identification system is programmed with C# language and equipped with an optical fingerprint scanner SDK (Suprema Inc®) to accept a scan, recognize the elector, and open the correct elector record in the database and verify system (Suprema, 2010). This module uses a dynamic link library (DLL) that can be displayed in a web application. Attacks are indispensible in biometric based systems, hence besides privacy issues, the major identified limitations of the works discussed above is presented. Applying texture-based feature extraction techniques to fingerprint authentication is very vulnerable. In this case, its security properties considering biometric integration is very vulnerable as attackers, Trojan horses, etc. Biometric technologies may add a new level of authentication and identification to applications, but are not, however, without their risks and challenges. There are important technological challenges such as accuracy, reliability, data security, user acceptance, cost, and interoperability, as well as challenges associated with ensuring effective privacy protections. Some common security vulnerabilities of biometric systems include: spoofing; replay attacks; substitution attacks; tampering; masquerade attacks, trojan horse attacks and overriding Yes/No response [11]. All feature extraction e-voting models are weak. A traditional biometric system will store the original templates in a database, for use in authentication/identification comparisons. If an attacker can gain access to the database (despite its security measures) then all template data (X) can be compromised [11].

III. DESIGN METHODOLOGY

In this research, an acceptability Index score was obtained from primary data sources (from local electoral regulatory bodies). Consequently PROTEUS ISIS version 7.6 was used to develop a real time simulation that characterizes the voting scenario using program description language which later was coded with Assembly language. The implementation was characterized with various components to realize the expected simulation behaviour. Also, the control program of the chips was encrypted. The algorithm was captured in the codes and simulated modules/classes include: the Fingerprints Processing Unit (FPU), the Remote Polling Booths (RPB), State Collection Centers (SCC) and the National Collection Center (NCC), all linked via a VPN communication backbone. The methodology used here has embedded in it a certain degree of gate level oriented design in the sense that gate level components are logically connected together and used to characterize various components in this system and programmable VLSI (Very Large Scale Integration) techniques (due to the fact that very complex designs where embedded on chips throughout this design). Also programmable microcontroller chips were embedded in this design to serve as the CPUs of the various blocks in the model, hence conceptualized as *HYBRID MODELING AND SIMULATION METHODOLOGY*. All the logical components characterized or modeled to describe the real life scenarios. After the configurations, the model was run in a simulation environment depicting a contextual voting scenario.

3.1 Multi-Protocol Label Switch -Open Virtual Private Network

This work identifies MPLS-VPN as an important solution to security threats surrounding the use of public networks. It offers a secure network connection between a sender and a receiver over a public non- secure network. A VPN transforms the characteristics of a public network into those of a private secure network and provides the means to securely transmit data between two networked devices over an insecure transport medium [12]. A VPN creates a secure virtual links between their co-operate headquarters and remote sites via the internet. When compared to other solutions e.g. leased lines, VPNs are relatively inexpensive.

In the characterization of the proposed e-voting system, the polling booths at the various wards would be characterized as the remote INEC offices, the state INEC collection centers would be characterized as the branch offices while the INEC headquarters is characterized as the co-operate office.

VPN makes use of many security mechanisms e.g. encryption, the use of digital signature to ensure that data cannot be modified without detection. It uses tunneling process to transport the encrypted data over the internet. Tunneling is mechanism for encapsulating one protocol in another protocol [12]. The VPN architecture consists of the VPN client, Network Access Server (NAS), A Tunnel terminating device (VPN sever), and a VPN protocol.

3.1.1 Open VPN Solution

OpenVPN is a VPN solution adopted in this work. Characterization of tunneling, encapsulation and transfer of data is also enshrined in the simulation of this work. The OpenVPN makes use of VNI (Virtual

Network Interface) for capturing in coming traffic before encryption and sending outgoing traffic after decryption. The VNI appears as the actual network interface to all applications and users.
Essentially, an OpenVPN performs the following viz:

1) Receives packets of data (votes) from the polling booths using after receiving the packets, it compresses the packets.
2) After compression, it encrypts the packets.
3) It tunnels the packet to the receiving end.
4) On receiving the encrypted traffic, the OpenVPN performs the reverse of cryptographic operations to verify its integrity and authenticity.
5) It then decompresses the packets.
6) The decompressed data is passed by the VNI to the user interface.

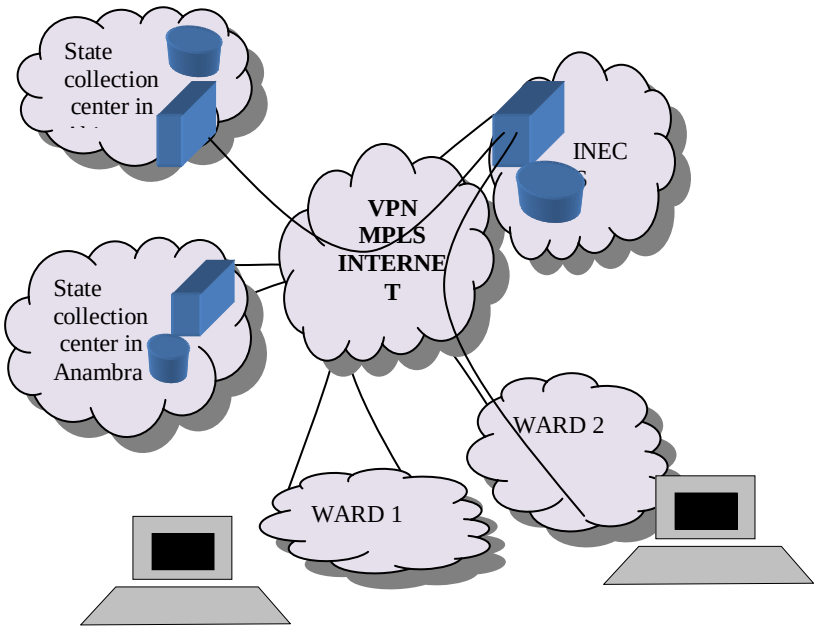

Figure 1: The Communication link diagram of MPLS -VPN backbone for the proposed E-voting system

Fig 1 shows the flow diagram of information between the various polling booths in different wards, the state and national collection centers as characterized in this work

3.2 Biometric Encryption (BE) Adopted in the Proposed Model

The concept of Biometric Encryption (BE) was first introduced in the mid-'90s by [13] and is adopted in this proposed E-voting model. BE is a process that securely binds a key to, or extracts a key from, a biometric, such that neither the key nor the biometric can be retrieved from the "helper data" (also called a "private template") created by this process and stored by the application, except upon presentation of the correct live biometric sample for verification. In essence, the key is "encrypted" with the biometric — a 'fuzzy' process due to the natural variability of biometric samples. It securely binds a digital key to a biometric or generates a digital key from the biometric, so that no biometric image or template is stored. What is stored is the BE template otherwise known as a ''bio-metrically encrypted key'' or ''helper data''. Neither the digital key nor the biometric can be retrieved from the stored BE template which stored [14].

3.2.1 Adopted BE Operational Models

A system and method for generating an encryption key using physical characteristics of a biometric sample is adopted. In this method for generating key using biometric features, the biometric feature from a sample is analyzed to generate a feature vector. After discretizing the features, the resultant feature vector is translated into a bit vector. The bit vector is the secure biometric key that results from the biometrics. The secure biometric key is used to generate at least one cryptographic key. A similar process is used to access the cryptographic key secured by the secure biometric key [15]. If the access biometric key matches the secure biometric key, the cryptographic key is revealed and access is allowed providing a method and apparatus for generating cryptographic keys using biometric data [15]. This technique adopted by the proposed E-Voting

system provides a method for generating a cryptographic key using biometric data. The method includes segmenting an image of a biometric into at least two quadrants, detecting at least one biometric feature associated with the biometric, determining which of the at least two quadrants the feature is located in, generating a subkey value from a quadrant location value derived from the quadrant the at least one feature is located in and a biometric feature type, and generating a cryptographic biometric key by concatenating the subkey value with a predetermined number of other subkey values derived from other quadrant location values and other feature types associated with other biometric features of the biometric [15]. These steps are characterized in the Simulation for the proposed E-Voting system.

3.2.2 Proposed E-Voting Model

An innovative technique for securing a key using a biometrics i.e. biometric key generator is adopted in this E-Voting system. The digital cryptographic key is generated from a biometric trait during enrollment, and this key is later regenerated using the same biometric trait during verification.

A fingerprint images are received from the user. The fingerprints are protected with a time and date stamp which is included in the encrypted fingerprint to assure that the fingerprint was not generated previously and resent. If the fingerprint is encrypted it is decrypted a digital fingerprint image is generated. The features of the fingerprint are then extracted. These features may include one or more of the following: minutiae, including location and orientation; spatial frequency; curvature; ridge count; ridge distance/curvature between points; relation to global features; code words generated by vector quantization to encode subunit spatial characteristics; etc.

A template is created for the user. A template includes at least some of the features extracted from the fingerprint. After the features are extracted, they may be jiggled slightly, to generate different hashes. That is, the features may be moved incrementally, to compensate for a user not placing his or her finger in exactly the same location as when generating the original cryptographic key (Error Correction Codes). The initial features extracted are an initial condition for the cryptographic key. The hash generated from the initial features is used to search the local key space.

The template is hashed. This hash is the cryptographic key. This cryptographic key is identified with the specific fingerprint, and thus with a specific user. For this public key encryption, a private key is generated based on the hash. A public key is generated to correspond to the cryptographic key. Methods of generating a public key which corresponds to a private key include Standard Hashing Algorithms (SHA). Public key/private key pairs are used to authenticate documents, encrypt documents, etc.

The cryptographic key is used. The cryptographic key is generated in order to do something specific. The template is stored. The cryptographic key itself is not stored anywhere on the system. The template is stored with the file for which it was used. The initial use of the key is now complete. A file may have been encrypted. Such a file may be stored on the system, sent, or otherwise disposed of by the user. If the user wishes to decrypt an encrypted document, or otherwise use the cryptographic key again.

The fingerprint is received from the user. The features of the fingerprint are extracted.

The fingerprint features, newly extracted, are compared to the template. The template includes some or all of the features previously extracted from the fingerprint. The comparison tests whether the fingerprint received belongs to the same user as the template.

A comparison is done to see if the features match the template. If the features do not match the template, it jumps back to obtain a new set of fingerprints. The template is again hashed to create a cryptographic key. Since the template was used to generate the first cryptographic key, the same key is generated. The key can then be used in the above described manner. . It is this cryptographic key obtained that now allows the verified voter, access to the e-voting system.

After the voter cast his vote for the party of his choice, the votes is split into packets of data, which is encapsulated another packet with headers and then tunneled over a secured network facility (a VPN for this model). At the receiving end (collection centers), the encapsulated packets is de-encapsulated (the encapsulation and de-encapsulation is done via AES 128 encryption standards). The votes are now tallied at the respective collection centers and the final tally is done at the INEC national headquarters in Abuja.

Fig 2 which shows an analytical representation of the Biometric Key Generation (BKG) technique adopted and characterized in the proposed E-Voting system**.**

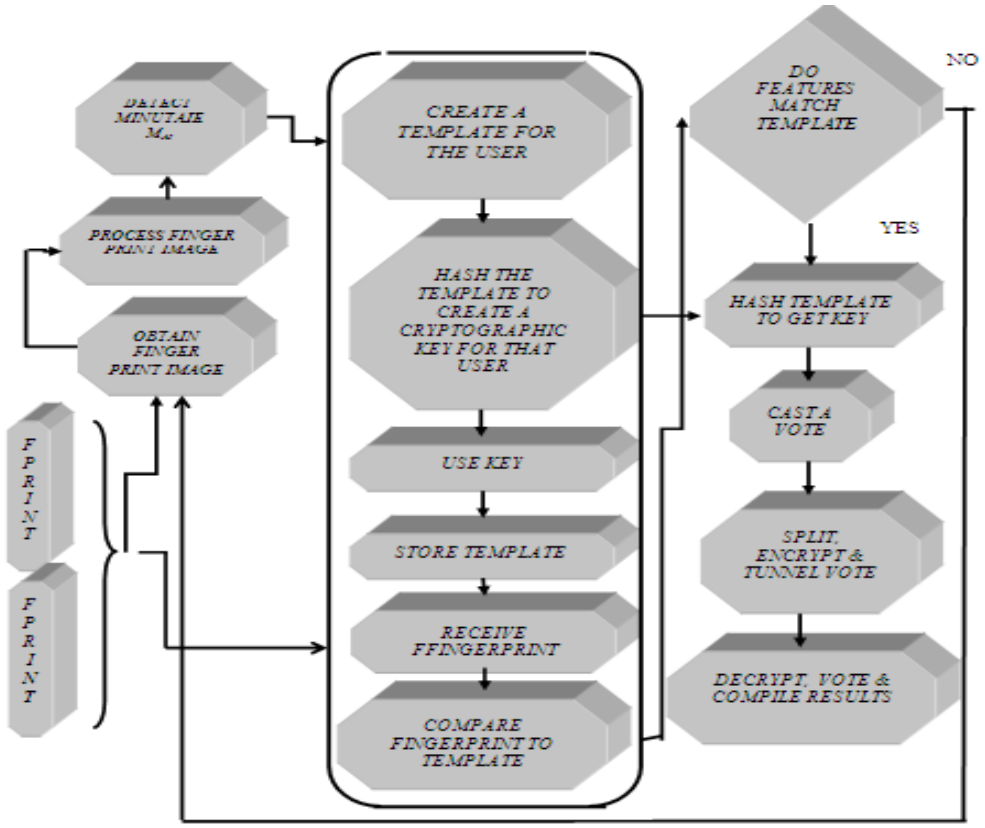

Figure 2 an analytical model for enrollment and verification in a biometrically encrypted E-voting system vis BKG.

3.3 Modeling Assumptions

In this research, the proposed E-voting system is assumed to fit into the Nigerian environment which has 36 states as independent remote blocks. The BKG algorithm, we assume that multiple fingerprint samples F_0 are collected during the enrollment exercise and processed. The fingerprint samples collected from the individuals during the enrollment or registration process are processed and from the processed fingerprints, cryptographic keys *Nk* which are going to be used to encrypt the votes would be generated. *Nk* would be regenerated on representation of the same fingerprint sample *F1* of which $F1 \approx F0'$.

In this security and privacy based algorithm for the proposed E-voting system, the communication link used between the various polling modules {*pm1, pm2,……, pmn*} and collection points {*cp1,cp2,…Σcp*} in this model is the Open VPN backbone given as O*VPNx* where encrypted data (individual votes) *En* is tunneled via a secure and private network *VPNx* that is built on top of existing physical network in context of VPN Multi-Protocol Label Switching(MPLS).

It is assumed that *VPNx* maintains data privacy through the use of a tunneling protocol, AES 128 encryption protocol and other security procedures.

This work assumes the use of two most common types of VPN setups; Remote access VPN and site-to-site VPN. The Remote Access VPN configuration is used to allow the individual polling booths located at remote sites to be able to communicate in a secure manner with the state collection centers while the site-to-site VPN allows for creation of dedicated, secure connections between the various INEC state collection centers and the national collection center across the open Internet or public connection.

Fig 3 gives a block diagram representation of the flow of information from the Remote Polling booth units (RPBU) to the INEC State Collection Centers (SCC) and the INEC National Collection Center (NCC) i.e. the end to end flow of information in the proposed E-voting system.

Each polling booth has these modules:

- Function keypad buttons
- Visual Display Unit
- The finger print module
- Secure Crypto-processor:
- Virtual Network Interface.

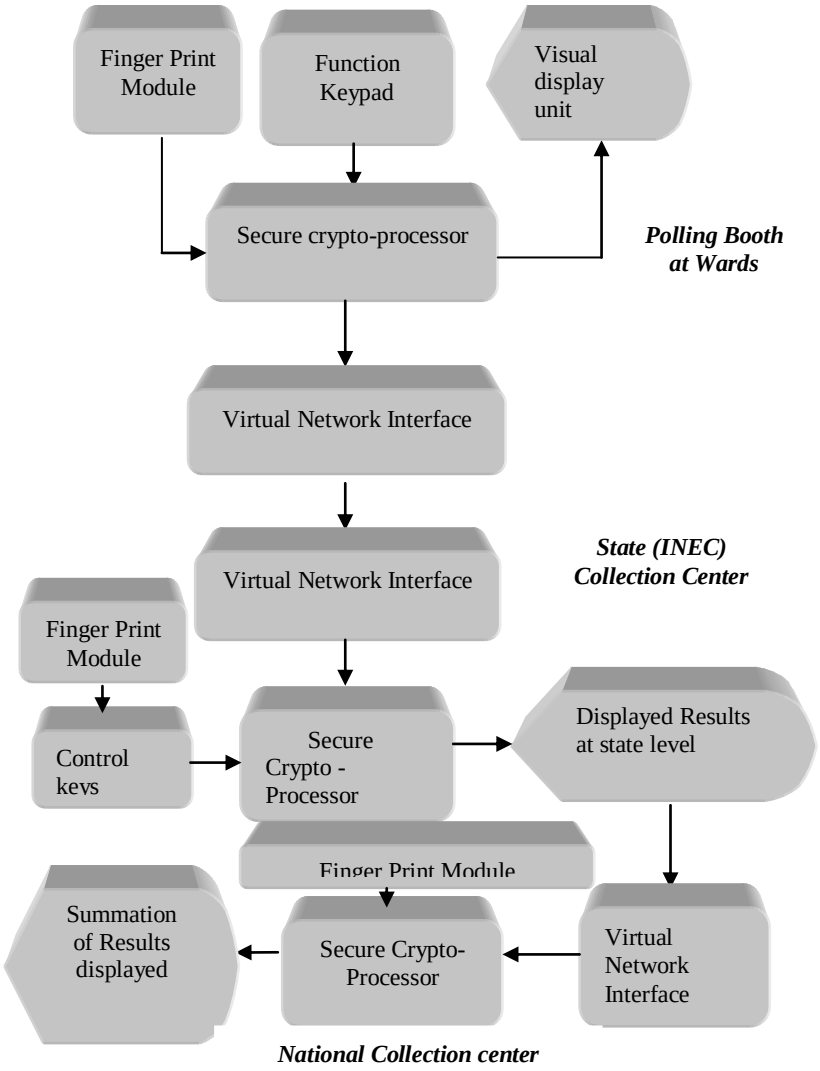

Figure 3: Flow diagram for the proposed E-voting

Each states collection centers and the national collection center will have the following:

- Control keypad
- The finger print module
- Secure Crypto-processor
- Virtual Network Interface

IV. IMPLEMENTATION& EVALUATION

4.1 Simulation Design with Proteus 7.6

In the proposed the proposed E-voting system, Proteus 7.6 ISIS was used to characterize the individual E-polling booths and collection centers. It provides the platform through which the various voting processes were characterized. Typical applications of Proteus 7.6 ISIS include standard-based electronic and logical component feature characterization. The Proteus 7.6 ISIS environment is organized into; probe/simulation environment, component editor, sub circuit editor with a comprehensive collection of work tools that were used to characterize the proposed E-voting system The Proteus 7.6 ISIS environment provides several modules for the simulation comprising a vast enterprise of digital and analog tools which with friendly graphical user interface that can be manipulated to achieve desired results.

3.3 Program Description Language (PDL) for the proposed E-voting system that leverages BKG

A) Polling booths PDL

START

Generate Hashed Key from Finger Print

IF Hashed Finger Print = 1 THEN

DO UNTIL Keypad = 1

Display Chosen Party

```
                    Transmit Vote
                END DO
        ELSE
Display "Voter not allowed"
        END IF
END
```

B) Collection Centers PDL

```
START
        Generate Hashed Key from Finger Print
        IF Hashed Finger Print = 1 THEN

                DO UNTIL Control Keypad = 1
                        Select Polling booth
                        Tally Votes
                END DO
        ELSE
                Do not grant access
        END IF
END
```

The PDL shown above is a summary of the lengthy code used in the characterization of the proposed E-Voting system that leverages BKG.

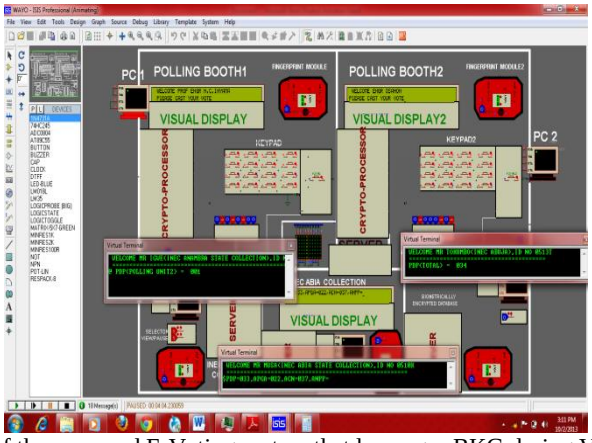

Figure 4: Proteus snapshots of the proposed E-Voting system that leverages BKG during Voting and Collection of total results

Fig 4 presents a Proteus simulation snapshot of proposed E-voting system with the administrators of the state and national collection centers having access to election results as the coming from the various polling booths. It also shows two voters at different polling booths. An MPLS-VPN backbone for the proposed E-Voting system that leverages BKG was characterized based on the parameters in Table 1.

OPNET modeler generates Trace files which are event scripts generated by the OPNET engine after a successful compilation. The OPNET modeler has object palettes with block sets that are configurable with real time or production values. It is these values fed into the OPNET engine that was used to characterize and configure the VPN communication link and it is on that basis that the graphs in fig 7 a-d where generated

4.3 Results and Analysis

The results obtained from the simulation model test bed are presented. The tallied election results are illustrated in pictorial capture on Proteus in the figure 5. The results were obtained from the proposed E-voting system. OPNET was used to evaluate the communication metrics; latency, throughput, stability margin and resource utilization.

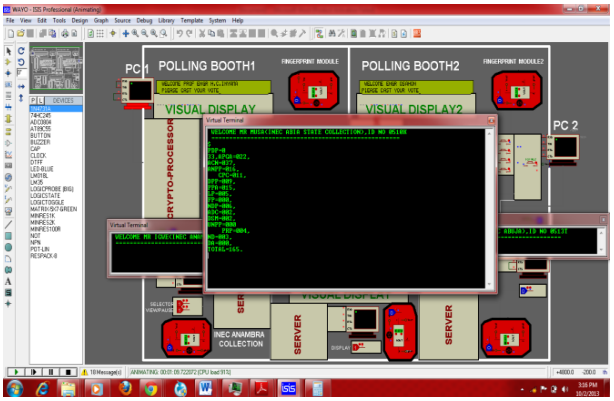

Figure 5 Proteus snapshot capture of proposed E-Voting system that leverages BKG at the national collection center displaying total results on Proteus 7.6

4.4 Validation of Model's Communication Link

For the purpose of validation of the proposed E-voting system communication link, OPNET modeler was used to validate the traffic engineering in the system. OPNET was used to evaluate the end to end latency between the polling modules and the collection centers, its throughput and its network resource utilization. It is seen from the graphs that the VPNMPLS communication backbone for the proposed E-voting system would have low end to end latency, high throughput and efficient resource utilization considering the design layout for deployment of the proposed E-voting system

Table 1: VPN-MPLS Parameters

LDP Configurations	Values
Status	Enabled
No. of Tunnel Sources with Names	[2]-Anambra Polling Booth 1&2
No. of Destination centers with Name	[1]-Headquarter.Network Server
Encryption delay	0.05sec
Decryption delay	0.05sec
Advertisement Policy	No Delay
Signaling DSCP	CS6/NC1
Reoptimization Timer(sec)	3600
Delay (sec)	20
Retry Timer (sec)	120
Propagation TTL	Enabled
Traffic Engineering	BGP
Fast Reroute Status	LSP Config
Revert Timer (Sec)	LSP Config
Label Space Allocation	Global GLA
CSPF Optimization Metric	TE Link Cost
Number of Shortest path	5

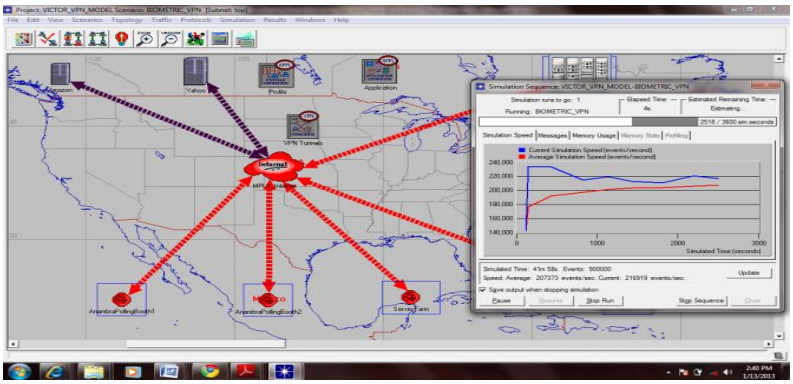

Figure 6: Snapshots capture of the OPNET modeler, showing how tunnels are created from end to end links in the MPLS VPN communication channel.

4.5 Discussion of Results

OPNET was be used to evaluate the end to end latency between the polling modules and the collection centers, its throughput and its network resource utilization. This formed the basis for validation of the proposed E-Voting model that leverages BKG.

It is seen from the graphs in fig 7a, 7b, 7c; the MPLSVPN communication backbone for the proposed E-voting system had high throughput, low end to end latency, and efficient resource utilization considering the design layout for deployment of the proposed E-voting system.

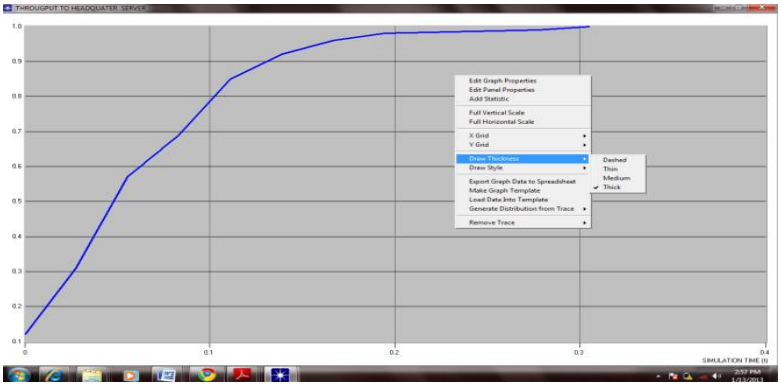

Fig 7a Average Network Throughput Response

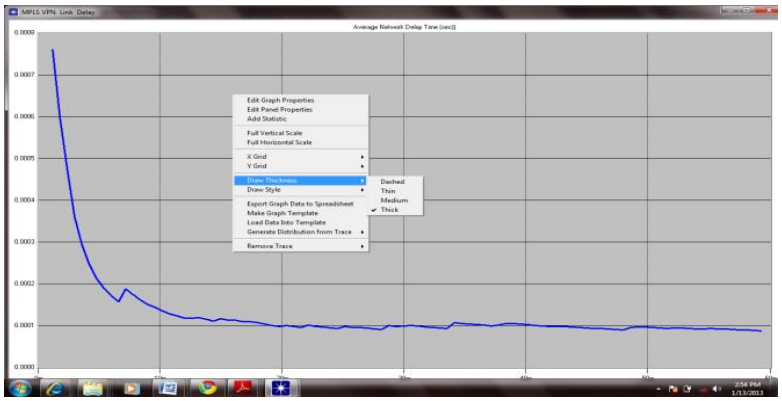

Fig 7b Average Network Delay Response

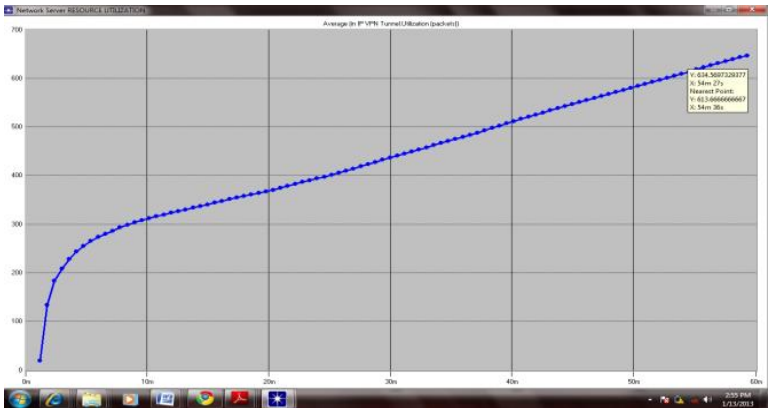

Fig 7c Average Resource Utilization

V. CONCLUSIONS

A simulation model of an e-voting system leveraging on Biometric Encryption viz Biometric Key Generation (BKG) technique for the proposed E-Voting system has been adopted and characterized. An MPLS VPN backbone as its communication link has been successfully adopted and characterized. The communication link has also been validated using metrics like end to end latency, Throughput, Network Stability and Tunnel resource utilization. Worthy of mention is the fact that Biometric Key Generation (BKG) technique has not yet been adopted in any E-voting system.

VI. REFERENCES

[1] Shane, P. (2004) Democracy Online: The Prospects for Political Renewal through the Internet. New York: Routledge

[2] Cramer, R. Franklin M. Schoenmakers B. and Yung M. (2006) Multi-authority secret ballot elections with linear work. *In: Advances in Cryptology,EUROCRYPT'96, Lecture Notes in Computer Science*, pp.72-83.

[3] Oleg Murk,Electronic Voting Schemes, M.Sc term paper,2000

[4] Ivan Damgard, Jens Groth and Gorm Salomonsen, The Theory and Implementation of an Electronic,Voting System, July 31, 2002. Fujioka, T. Okamoto & K. Otha: A practical secret voting scheme for large scale elections, Advances in Cryptology - AusCrypt '92, pp.244-251.

[5] Ohkubo and Abe: A Length-Invariant Hybrid Mix Proceedings of Asia Crypt 00, Springer Verlag LNCS.

[6] Abe: Universally verifiable MIX net with verification work independent of the number of MIX centers; proceedings of Euro Crypt 98, Springer Verlag LNCS.

[7] Indrajit Ray, Indrakshi Ray, Natarajan Narasimhamurthi, ―An Anonymous Electronic Voting Protocol for Voting Over The Internet‖.

[8] www.computer.org/security: Evaluating Electronic Voting Systems Equipped with Voter-Verified Paper Records. IEEE Security & Privacy, 2008.

[9] Adem Alpaslan ALTUN and Metin BĐLGĐN, ― Web based secure e-voting system with fingerprint Authentication‖ In Scientific Research and Essays Vol. 6(12), pp. 2494-2500, 18 June, 2011

[10] Available online at http://www.academicjournals.org/SRE.

[11] J.L, Wayman, ―fundamentals of biometric authentication technologies‖ *Int. Image graphics*, vol.1, no.1, pp. 93-113, 2001.
[12] Cranor L. and Cytron R. (2007) Sensus: a security-conscious electronic polling system for the Internet. *In: Proceedings of the Thirtieth Hawaii International Conference on System Sciences*, Vol.3, pp.561-570.
[13] G.J. Tomko, C. Soutar, and G.J. Schmidt. **"**Fingerprint controlled public key cryptographic system‖. U.S. Patent 5541994, July 30, 1996 (Priority date: Sept. 7, 1994).
[14] Uludag U, Pankanti S, Prabhakar S, Jain AK: Biometric cryptosystems: issues and challenges. Proc IEEE 2004, 92(6):948 960.
[15] DIGITALPERSONA, INC., CALIFORNIA "Cryptographic key generation using biometric data" U.S. Patent 6035398 A, November 14, 1997 (Priority date: November 14, 1997).

PROFILE OF AUTHORS

Ossai Victor is an Engineer at Electronics Development Institute (ELDI), a research institute of the National Agency for Science and Engineering Infrastructure (NASENI). He has his research interest in Encrypted Biometrics Securities and Embedded system designs/Simulations; he is currently pursuing his M.Eng. in Electronics / Computer Engineering (Computer and Control option)at Nnamdi Azikiwe University Awka.

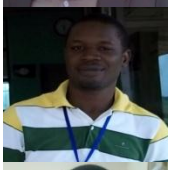

Israel Okoro is a Scientific Officer at Electronics development institute, a research institute of the national agency for science and engineering infrastructure (NASENI), He has his research interest in power electronics and embedded systems, he is currently doing a masters degree in physics electronics at Nnamdi Azikiwe University Awka.

Alagbu Ekene is an Engineer at Electronics Development Institute (ELDI), a research institute of the national agency for science and engineering infrastructure (NASENI). He has his research interest in Artificial Intelligence and Neural Systems; he is currently pursuing his M.Eng. in Electronics / Computer Engineering (Computer and Control option)at Nnamdi Azikiwe University Awka.

Agbonghae Andrew is an Engineer at Electronics Development Institute (ELDI), a research institute of the national agency for science and engineering infrastructure (NASENI). He has his research interest in advanced embedded system designs /controls, Digital System Processing and; he is currently pursuing his M.Eng. in Electronics / Computer Engineering (Computer and Control option)at Nnamdi Azikiwe University Awka.

Nneka Ifeyinwa. Okafor holds B.Eng. in Computer Engineering from Enugu State University of Science and technology, (ESUT) while currently pursuing her M.Sc in Digital Electronics and Computer Engineering from University of Nigeria Nsukka,(UNN). She has Oracle 10g Expert Certification. Currently, she works as a Research Engineer in Electronics Development Institute, Awka under National Agency for Science and Engineering Infrastructure, Nigeria. She is a graduate Member of Nigerian Society of Engineers, Awka Chapter and a member of IAENG. Her research interests are on Software Graphics, Animation Modelling, Database Management and System Analysis. Conact:

American Journal of Engineering Research (AJER)
e-ISSN : 2320-0847 p-ISSN : 2320-0936
Volume-02, Issue-10, pp-191-199
www.ajer.org

Research Paper Open Access

Shear Reinforcements in the Reinforced Concrete Beams

Moayyad M. Al-Nasra[1], Naiem M Asha[2]
[1](*Department of Engineering Technology, West Virginia University Institute of Technology, Montgomery, West Virginia 25136, USA)*
[2](*Department of Civil Engineering, University of Jordan, Amman Jordan)*

Abstract: - This study focuses on the use of different types of shear reinforcement in the reinforced concrete beams. Four different types of shear reinforcement are investigated; traditional stirrups, welded swimmer bars, bolted swimmer bars, and u-link bolted swimmer bars. Beam shear strength as well as beam deflection are the main two factors considered in this study. Shear failure in reinforced concrete beams is one of the most undesirable modes of failure due to its rapid progression. This sudden type of failure made it necessary to explore more effective ways to design these beams for shear. The reinforced concrete beams show different behavior at the failure stage in shear compare to the bending, which is considered to be unsafe mode of failure. The diagonal cracks that develop due to excess shear forces are considerably wider than the flexural cracks. The cost and safety of shear reinforcement in reinforced concrete beams led to the study of other alternatives. Swimmer bar system is a new type of shear reinforcement. It is a small inclined bars, with its both ends bent horizontally for a short distance and welded or bolted to both top and bottom flexural steel reinforcement. Regardless of the number of swimmer bars used in each inclined plane, the swimmer bars form plane-crack interceptor system instead of bar-crack interceptor system when stirrups are used. Several reinforced concrete beams were carefully prepared and tested in the lab. The results of these tests will be presented and discussed. The deflection of each beam is also measured at incrementally increased applied load.

Keywords: *– Concrete cracks, Deflection, Shear, Stirrups, Swimmer bars*

I. INTRODUCTION

One of the main objectives of the design of reinforced concrete beams is safety. Sudden failure due to shear low strength is not desirable mode of failure. The reinforced concrete beams are designed primarily for flexural strength and shear strength. Beams are structural members used to carry loads primarily by internal moments and shears. In the design of a reinforced concrete member, flexure is usually considered first, leading to the size of the section and the arrangement of reinforcement to provide the necessary resistance for moments. For safety reasons, limits are placed on the amounts of flexural reinforcement to ensure ductile type of failure. Beams are then designed for shear. Since shear failure is frequently sudden with little or no advanced warning, the design for shear must ensure that the shear strength for every member in the structure exceeds the flexural strength. The shear failure mechanism varies depending upon the cross-sectional dimensions, the geometry, the types of loading, and the properties of the member.

Reinforced concrete beams must have an adequate safety margin against bending and shear forces, so that it will perform effectively during its service life. At the ultimate limit state, the combined effects of bending and shear may exceed the resistance capacity of the beam causing tensile cracks. The shear failure is difficult to predict accurately despite extensive experimental research. Retrofitting of reinforced concrete beams with multiple shear cracks is not considered an option [1].

Diagonal cracks are the main mode of shear failure in reinforced concrete beams located near the supports and caused by excess applied shear forces. Beams fail immediately upon formation of critical cracks in the high-shear region near the beam supports. Whenever the value of actual shear stress exceeds the permissible shear stress of the concrete used, the shear reinforcement must be provided. The purpose of shear reinforcement is to prevent failure in shear, and to increase beam ductility and subsequently the likelihood of sudden failure will be reduced.

Normally, the inclined shear cracks start at the middle height of the beam near support at approximately 45^0 and extend toward the compression zone. Any form of effectively anchored reinforcement that intersects these diagonal cracks will be able to resist the shear forces to a certain extent. In practice, shear reinforcement is provided in three forms; stirrups, inclined bent-up bars and combination system of stirrups and bent-up bars.

In reinforced concrete building construction, stirrups are most commonly used as shear reinforcement, for their simplicity in fabrication and installation. Stirrups are spaced closely at the high shear region. Congestion near the support of the reinforced concrete beams due to the presence of the closely spaced stirrups increase the cost and time required for installation.

Bent up bars are also used along with stirrups in the past to carry some of the applied shear forces. In case where all the tensile reinforcement is not needed to resist bending moment, some of the tensile bars where bent-up in the region of high shear to form the inclined legs of shear reinforcement. The use of bent-up bars is not preferred nowadays. Due to difficulties in construction, bent-up bars are rarely used. In beams with small number of bars provided, the bent-up bar system is not suitable due to insufficient amount of straight bars left to be extended to the support as required by the code of practice.

In this study, three reinforced concrete beams were tested using the new shear reinforcement swimmer bar system and the traditional stirrups system. Several shapes of swimmer bars are used to study the effect of swimmer bar configuration on the shear load carrying capacity of the beams. Only three beams will be presented in this study. The first beam, BC, is used as a reference control beam where stirrups are used as shear reinforcement. The other two beams were reinforced by swimmer bars. Beam, BW is the beam which is reinforced by two swimmer bars welded to the longitudinal top and bottom bars. Beam, BU is the beam which is reinforced by U-link bars which are bolted to the top and bottom longitudinal bars along with two swimmer bars. Extra stirrups were used to make sure that beam will fail by shear in the swimmer bars side. In this investigation, all of the beams are supposed to fail solely in shear, so adequate amount of tension reinforcement were provided to give sufficient bending moment strength. This study aims at investigating a new approach of design of shear reinforcement through the use of swimmer bars provided in the high shear region. The main advantages of this type of shear reinforcement system are: flexibility, simplicity, efficiency, and speed of construction.

Piyamahant (2002) showed that the existing reinforced concrete structures should have stirrup reinforcement equal to the minimum requirement specified the code. The theoretical analysis shows that the amount of stirrup of 0.2% is appropriate. The paper concluded that small amount of web reinforcement is sufficient to improve the shear carrying capacity. The study focused on the applicability of the superposition method that used in predicting shear carrying capacity of reinforced concrete beam with a small amount of web reinforcement at the shear span ratio of 3. Also the failure mechanisms were considered when small amount of stirrup used [2].

Sneed, and Julio (2008) discussed the results of experimental research performed to test the hypothesis that the effective depth does not influence the shear strength of reinforced concrete flexural members that do not contain web reinforcement. The results of eight simply supported reinforced concrete beam tests without shear and skin reinforcement were investigated. The beams were designed such that the effective depth is the variable while the values of other traditionally-considered parameters proven to influence the shear strength (such as the compressive strength of concrete, longitudinal reinforcement ratio, shear span-to-depth ratio, and maximum aggregate size) were held constant. The values selected for the parameters held constant were chosen in an attempt to minimize the concrete shear strength [3].

Noor (2005) presented several results of experimental investigation on six reinforced concrete beams in which their structural behavior in shear was studied. The research conducted was about the use of additional horizontal and independent bent- up bars to increase the beam resistance against shear forces. The main objectives of that study were studying the effectiveness of adding horizontal bars on shear strength in rectangular beams, the effectiveness of shear reinforcement, and determining the optimum amount of both types of shear reinforcement to achieve a shear capacity similar to that of a normal links system. From experimental investigation of the system it was found that, the use of independent horizontal and bent-up bars as shear reinforcement were stronger than conventional shear reinforcement system [4].

II. SWIMMER BARS

A swimmer bar is a small inclined bar, with its both ends bent horizontally for a short distance, welded or bolted at the top and the bottom of the longitudinal bars. There are three major standard shapes; single swimmers, rectangular shape, and rectangular shape with cross bracings. Several additions to these standard shapes can be explored, such as addition of horizontal stiffener bars in the rectangular shapes, dividing the large rectangle horizontally into smaller rectangles. Additional swimmer bars can also be used. By adding one more

swimmer bar to the rectangular shape, the large rectangular shape will be divided vertically into two rectangles. Addition of two more swimmer bars will divide the large rectangle vertically into four small rectangles. A combination of horizontal bars and additional swimmer bars may also be explored. This swimmer bar system is integrated fully with the longitudinal steel bars. Several options of the swimmer bar systems are used in order to improve the shear performance of the reinforced concrete beams, reduce the amount of cracks, reduce the width and the length of cracks and reduce overall beam deflection. Different bar diameters can be used in order to add stiffness to the steel cage, and increase shear strength of the reinforced concrete beam.

III. ACI CODE PROVISION FOR SHEAR DESIGN

According to the ACI Code [5], the design of beams for shear is to be based on the following relation:

$$V_u \leq \phi V_n \quad (1)$$

Where: V_u is the total shear force applied at a given section of the beam due to factored loads and $V_n = V_c + V_s$ is the nominal shear strength, equal to the sum of the contribution of the concrete and the web steel if present. Thus for vertical stirrups

$$V_u \leq \phi V_c + \frac{\phi A_v f_{yt} d}{s} \quad (2)$$

and for inclined bars

$$V_u \leq \phi V_c + \frac{\phi A_v f_{yt} d(\sin\alpha + \cos\alpha)}{s} \quad (3)$$

Where: A_v is the area of one stirrup, α is the angle of the stirrup with the horizontal, and S is the stirrup spacing. The nominal shear strength contribution of the concrete (including the contributions from aggregate interlock, dowel action of the main reinforcing bars, and that of the un-cracked concrete) can be simplified as shown in Eq. 4.

$$V_c = 0.17\lambda\sqrt{f'_c}\, b_w d \quad (4)$$

Where: b_w and d are the section dimensions, and for normal weight concrete, $\lambda = 1.0$. This simplified formula is permitted by the ACI code expressed in metric units [6].

IV. TESTED BEAMS

This study focused on investigating the shear strength of four different types of reinforced concrete beams; beam reinforced with regular stirrups, beam reinforced with welded swimmer bars, beam with bolted swimmer bars, and beam reinforced with U-link bolted swimmer bar. All specimens were of the same size and reinforced with identical amount of longitudinal steel. The amount of longitudinal steel used in this study is, by design, selected to make sure that the failure will be dictated only by shear and not by bending. The beams were tested to fail due to two point loads by shear given the ratio of a shear span to effective depth of 2.5. The compressive strength of concrete is measured according to ASTM C 192-57. Nine concrete samples were prepared. The compressive strength of concrete is measured at the 28th day. The concrete compressive strength results range between 27.4 N/mm^2 to 30.2 N.mm^2. The variables in these specimens are the shear reinforcement systems.

Four reinforced concrete beams were prepared for the test, BS which the beam with regular stirrups, BW which is the beam with welded swimmer bars, BB beam with bolted swimmer bars, and BU which is the beam with U-link bolted swimmer bars. All of the beams are of the same dimension 2000 mm length, 200 mm width and 250 mm depth. The effective length was also kept at constant value of 1800 mm. Summary of shear reinforcement system for each specimen is given in Table 1. All tested beams were designed with 3ø14 top steel and 4ø16 bottom steel reinforcement. The reference beam, BC, was designed with 10ø8 mm at 600 mm spacing

vertical stirrup at either side without any stirrups at the high moment zone between the two concentrated loads. New type of shear reinforcement called welded swimmer bars 'BW', bolted swimmer bars 'BB', and U-link bolted swimmer bars 'BU' were used in this experiment. The swimmer bars were used as independent bent-up bars and welded/bolted with ø10 mm steel piece. The swimmer bars used in beams BW, BB, BU are of ø10 mm and spaced of 275 mm apart as shown in Figure 1. The weight of each steel cage is also listed in Table 1. The weight of each steel cage is almost the same.

Figure (2) shows the steel cage used in beam BW, the welded swimmer bars, and Figure 3 shows the steel cage used in BB, bolted swimmer bars, and Figure 4 shows the steel cage used in beam BU, the U-link bolted swimmer bars. The weights of these two cages were intentionally designed to be very close in numbers. The erection and assembling time of the bolted beam is relatively less than the erection and assembling time of the welded beam.

Table 1: Summary of steel reinforcement used in the tested beams

Beam No.	**Shear Reinforcement** Vertical stirrup	Bent-up Bars	**Steel Cage Weight (N)**
BC	10ø 8 mm @ 600mm at shear sides	-	255
BW	-	Two welded swimmers, ø10 mm @ 275 mm	250
BB	-	Two bolted swimmers, ø10 mm @ 275 mm	258
BU	-	Two U-link Bolted swimmers, ø10 mm @ 275 mm	255

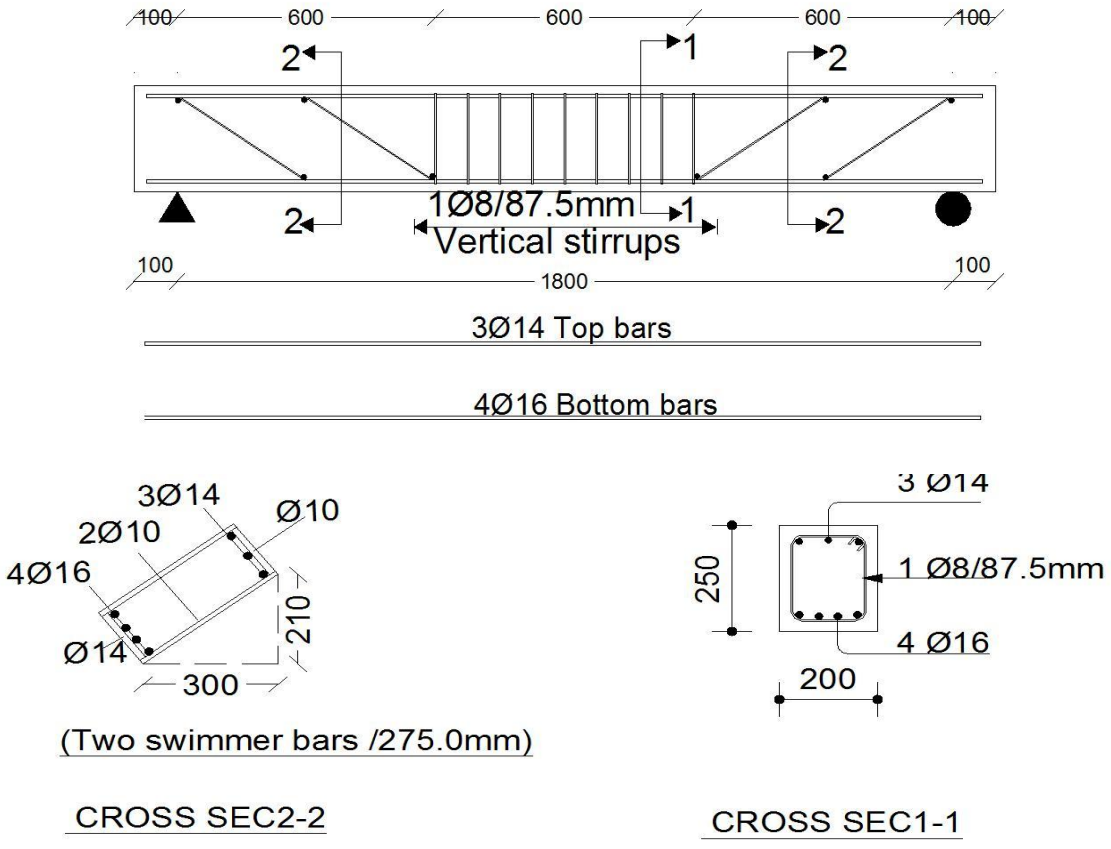

Figure 1: Reinforcement details of BW, BB, and BU.

Figure 2**:** Steel cage reinforcement of the beam BW, welded swimmer bars.

Figure 3: Steel cage reinforcement of beam BB bolted swimmer bars.

Figure 4: Steel cage reinforcement of the beam, BU, U-link bolted swimmer bars.

V. TEST PROCEDURE

Prior to testing, the surface of the specimens was painted with white emulsion for the purpose of making the cracks more visible and easy to track. At age 28 days reinforced concrete beams were prepared for testing. Marking lines were used to show the location of the point loads, supports and the mid-span of the beam in order to make it easier to install the beams on the testing machine. The test was carried out with the specimen placed horizontally in a simple loading arrangement. The beams were supported by solid round steel on their two edges that can be considered as simply supported beam member. All the beams were designed to ensure the beams will only fail in shear rather than in flexure.

To ensure that shear cracks will occur near the support, two point loads were applied symmetrically to the beam with a_v less than 2.5d. In this testing, $a_v \approx 550$ mm, where a_v is shear span (the distance from the point of the applied load to the support), and d is the effective depth of a beam.

A loading jack was placed at the mid-span position above the beam. The load was applied by jacking the beam against the rig base member at a constant rate until the ultimate load capacity of the beam was reached. A universal column section was used to transfer the load to the beam at two point loads via transfer girder. A reasonable time interval was allowed in between each 20.0 kN load increments for measuring deflections, marking cracks, measuring the shear reinforcement strain and recording the ultimate load. Each beam took about two hours to complete the test. The cracks were monitored at each load increment. Figure 5 shows the experimental set up.

Figure 5: Experimental set up and crack monitoring

VI. TEST RESULTS

The beam BC showed typical mode of failure by shear at the ultimate load of 180 kN. Beam BW, BB, and BU showed quite similar mode of failure. Several micro-cracks appeared early in the loading process. These cracks were extended and widened as the load increases. These cracks became visible at the load of about 100 kN. As the loading was increased more cracks developed. The cracks migrate towards the top corners as the load increases. More flexure cracks appeared at a load of 100 kN in the moment region. These cracks increased by increasing the applied load, and new cracks developed but at relatively slower paste. Figure 6 shows the beam BU at failure stage which identical to the mode of failure of the beams BC, and BB. Figure 7 shows the mode of failure of the welded beam BW.

Figure 6: Beam BU at failure stage

Figure 7: The mode of failure of the welded beam BW.

Figure 8 shows the maximum applied load the beam carried just before failure. All of the tested beams in this study failed by shear. The beam of welded swimmer bars exhibit similar strength as the beam of U-link bolted swimmer bars, and the bolted swimmer bars BB. This proves that welding can be avoided when dealing with swimmer bars. The welding process is of a major concern when it comes to the quality control of the welds.

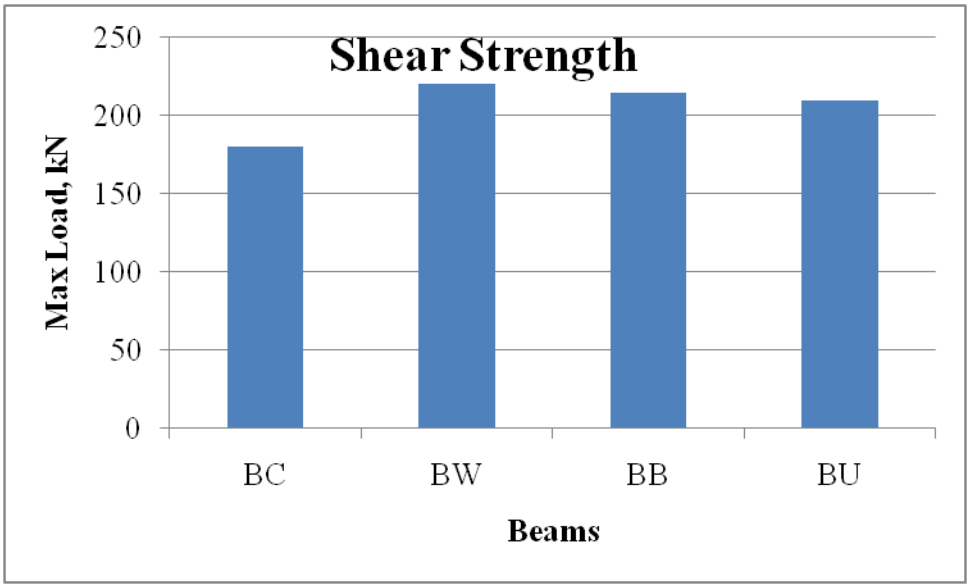

Figure 8: Shear strength of the three tested beams

Figure 9 shows the maximum recorded deflection just before failure. No major difference in the load deflection relationship was observed in the tested beams. Beams deflection increased with the increase in load up to the failure load.

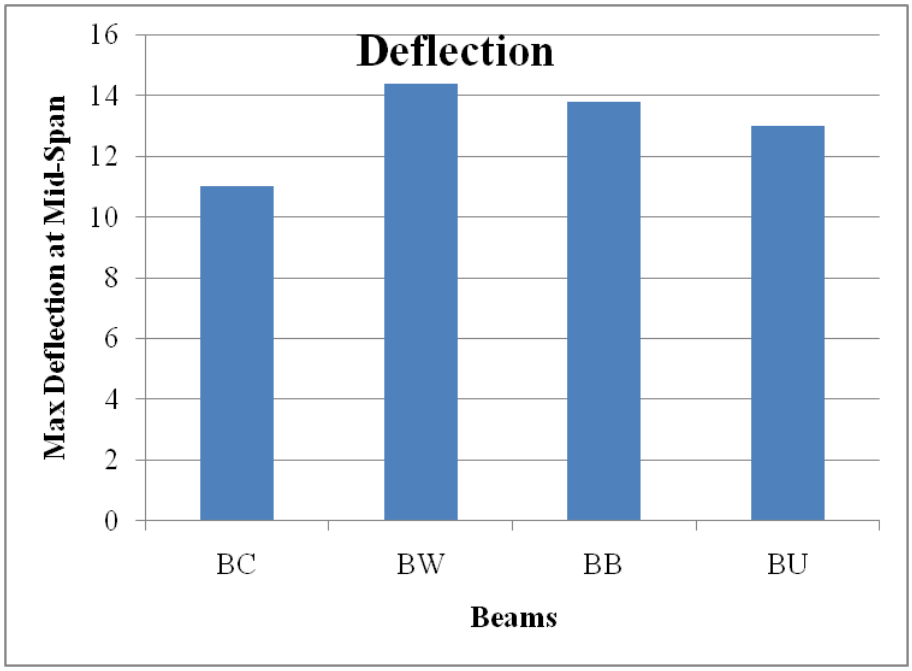

Figure 9: Maximum deflection at mid-span of tested beams just before failure.

VII. CONCLUSION

This study presented four different types of shear reinforcement that can be used in reinforced concrete beams. New type of shear reinforcement system was used, which is swimmer bars system either bolted or welded to the longitudinal bars. There is improvement in shear strength of reinforced concrete beams by using swimmer bars in general. The bolted swimmers bars through U-links showed similar results as the welded. The width and length of the cracks were observed to be less using swimmer bars compared to the traditional stirrups system. The bolted swimmers bars as well as the u-link bolted swimmer bars exhibit similar behavior under load compared to the traditional stirrups system.

REFERENCES

[1] Al-Nasra, M.M., and Wang, L.R.L., 1994, Parametric Study of Slab-On-Grade Problems: Due to Initial Warping and Point Loads. ACI Structural Journal, Vol. 91 No. 2. http://www.concrete.org/PUBS/JOURNALS/OLJDetails.asp?Home=SJ&ID=4596

[2] Piyamahant, (2002) , Shear behavior of reinforced concrete beams with small amount of web reinforcement, M. Eng. Dissertation, Kochi University of Technology, Japan

[3] Lesley H. Sneed and Julio A. 2008, Effect of Depth on the Shear Strength of Concrete Beams without Shear Reinforcement, USA Portland and cement Association. http://www.cement.org/exec2/11-03-08.htm

[4] Noor Hamid (2005). The Use of Horizontal and Inclined Bars as Shear Reinforcement , Master Thesis, University of Technology , Malaysia, http://sunzi.lib.hku.hk/hkuto/record/B26643352.

[5] ACI 318-11, 2011. Building Code Requirements for Structural Concrete Commentary. http://www.concrete.org/pubs/newpubs/31811.htm

[6] Edward G.Nawy, 2009. Reinforced Concrete: A Fundamental Approach, Prentice Hall International, US, PP 120-315, ISBN 0132417030, 9780132417037

American Journal of Engineering Research (AJER)
e-ISSN : 2320-0847 p-ISSN : 2320-0936
Volume-02, Issue-10, pp-200-204
www.ajer.org

Research Paper Open Access

Water Quality Assessment of Ake Stream, Near College of Advanced and Professional Studies Makurdi, Nigeria.

Dr. Aho, I.M., Gbayan, N.T. and Engr. Lagasi J.E.
[1,2]*Department of Civil Engineering, University of Agriculture Makurdi, Nigeria*
[3]*Department of Agric Engineering, Federal Polytechnic, Bauchi, Nigeria*

Abstract: - Analysis of the physico-chemical and biological quality of Ake stream located near College of Advanced and Professional Studies Makurdi, Benue State Nigeria was examined over duration of 7 months. The survey was conducted in the period between April and September based on random sampling with a view to ascertaining the impurity level of the stream. The physico-chemical analysis gave average results for Temperature, Turbidity, Iron, Chromium and Sulphate as 28.7^{0}C, 200.5NTU, 2.0, 0.2 and 44.3mg/l respectively. The Bacterial load per 100ml of water ranged between 978 – 1800 giving average value of 1389. The overall results revealed that the stream is heavily stagnated, especially in terms of microbial load, which is an indication of human and feacal contamination. Most of the physical and chemical perimeters were above the maximum permissible levels, indicating that treatment is required before water from the source can be used for domestic applications.

Keywords*: - Analysis, Ake stream, Examined, Impurity, Domestic application.*

I. INTRODUCTION

Water is undoubtedly one of the most precious natural (divine) resources that exist in our planet, (Karthikeyan and others, 2007). The public health significance of water quality cannot be over emphasized since many infectious diseases are transmitted by water through the fecal-oral route.

It is thus, important that drinking water should be safe and portable. The bacterial qualities of surface water, pipe borne water and other natural water supplies in Nigeria have been reported to be unsatisfactory, with coliform counts far exceeding the level recommended by the World Health Organization (Edema et al 2001).

Ake stream, which is located in *Myade Asta* community of Makurdi local Government area of Benue State lies on undulating plain of River Benue, about 50m from the College of Advanced and Professional Studies Makurdi. The stream flows to River Benue.

Makurdi the headquarter of Benue State, lies within Longitude 70 45 ^{o}E and 80 00 ^{o}E and Latitude 70 45 ^{o}N and 80 15 ^{o}N. The area is located within the hot humid climate belt, with fairly high temperatures, especially between April and October, with the heaviest rainfall usually between July and September. It is however warm and humid during the rainy season with a mean temperature range of 26^{0}C to 30^{0}C, and mean rainfall of 1300mm.

The geological formation of Makurdi is underlain essentially by sand stones. Though in some areas one finds thin bed of clay, shale and limestone. The geology of the area influences the quality of water to be obtained. Streams on steep slopes flow swiftly; they often have better water quality than streams on gentler slopes. Streams on steep slopes also experiences more turbulence as water cascades over rocks and logs, adding oxygen to the water by mixing with the air. Streams located on mild slopes do not have the benefit of turbulent mixing to aerate the water. Swift-flowing streams, however, have greater energy for causing erosion.

The dwellers of this community face serious threats to the quality of life and safety with urbanization resulting into high degree of population densities and concentration of socio-economic activities. It has become increasingly difficult to meet the entire water requirement both in quantity and quality. The public water supply is generally inadequate and in most cases inaccessible, the supply is intermitted and unreliable thus resulting into high dependency on unsafe supplementary sources such as streams, and ponds which are harmful to human health (Kakulu Osibanjo,1992; Olajire and Imeppeoria, 2001; Nnodu and llo,2002). There is therefore the need

to determine the quality status of Ake stream which is one of the major sources of water supply in the community.

II. MATERIALS AND METHODS

Sample Collection

Stream samples were carefully collected in very clean disinfected containers. The samplings were done upstream, midstream and downstream at 10m apart by dipping at approximately 20-30cm below the water surface, projecting the mouth of the container against the flow direction. Samplings were done three (3) times a month, namely, beginning, middle and the end. A total of fifty four (54) samples were collected.

Sample Analysis

Samples were collected from April to October 2012. The laboratory analysis was done at the Benue State water board laboratory in Makurdi. The physical, chemical and bacteriological properties of the samples were analyzed immediately they were taken to the laboratory following standard procedures as described by (PEPA, 1991).

The equipment used for the determination of these parameters include: Hach direct reading spectrophotometer model DR/200 for turbidity, fluoride, suspended solids and colour. Mercury thermometer was used for temperature measurement conductivity meter model 50150 was used for determination of electrical conductivity. pH was obtained by colometric technique and chloride by mercuric nitrate method. Similarly, titrimetric and pillow methods were used for total hardness and total iron respectively. Sulphate and phosphate were determined by sulfaver 4 and phosver – 3 methods respectively. 1,5 – diphenlycarbohydrazide method was adopted for chromium determination and MPN-multiple technique was for coliform enumeration.

3.1 RESULTS AND DISCUSSION

The results from the seven months experimental analysis are as shown in figures 1 – 14. The properties and findings are as discussed below.

Physical Parameters

Apart from total dissolved solids (TDS) with average value of 52.9mg/l, colour and turbidity values were far above the acceptable limits specified by world Health organization. The distribution as seen in figures 1 – 4 shows maximum pollution between the rainy months of April and May. The average temperature of the stream as indicated in figure 2 agrees with the ambient temperature range of Makurdi and its environs.

Chemical Parameters

The pH of the water changed from being slightly basic (7.5) in July to slightly acidic (6.4) in August. This may be attributed to the geological formation of the area as shown in figure 5. The concentration of iron in the stream especially in the months of May to August indicates maximum levels between 0.27 and 5.74mg/l (figure 6); far above the recommended 0.05mg/l by WHO (1993). The same trend was observed for sulphate and chromium as indicated in figures 10 and 11 respectively. And so largely, only total hardness (figure 9) was found within acceptable limit as specified by World Health Organization (1993) of the assessed chemical parameters.

The chemical oxygen demand of the stream varied from 147 to 207mg/l and Biological oxygen demand (BOD) varied from 73 to 87mg/l throughout the study period (figures 12 & 13). Higher levels of COD were observed middle stream and downstream of the discharge points. This is considered undesirable since continuous effluent discharge is already impacting negatively on the quality of the freshwater, and capable of causing harm to the aquatic life downstream.

Biological Parameter

The result of the coliform count was high ranging from 978 to 1800MPN/100ml of water (see figure 14). The high limit is indicative of gross contamination which may be due to disposal of fecal waste in the stream. It may also be due to time of the study (April – October, 2012) which are months of rainy season usually associated with seepage due to runoff that contaminates surface waters (Isikwue and others, 2011).

III. CONCLUSION

The water quality assessment has revealed the negative impact on the physio-chemical and biological parameters of the stream. This is likely to pose health risk to the rural Ake community that rely on it as their main source of domestic water supply.

While measures should be put in place by relevant agencies in the state to create awareness on the dangers associated with the use of Ake stream for domestic consumption, government of Benue State is requested to

render assistance by providing portable water supply to the community. Meanwhile, boiling of water from the stream before domestic application by the community is recommended

REFERENCES

[1] Edema, S.A., Ekiye, E. O. and Zejiao, L.O. (2001). "Water Quality Monitoring in Nigeria". *Journal of American Science* Vol. 6(2):22-28.
[2] Isikwue, O.O, Ahmed, K. and Tanko, A. I. (2011). Assessment of Water Quality Changes for Irrigation in the River
[3] Hadeja Catchment. *Journal of Arid Agriculture* Vol. 10(2): 89 – 84.
[4] Kakulu, O. O. Anna, E. O. and Adedipe, N. O. (1992). *Water Quality Monitoring and Environmental Status in*
[5] *Nigeria.* FEPA Monograph 6, Abuja, Nigeria pp. 239 – 242.
[6] Karthikeyan, S. T., Katsuro, A. and Hayao, S. (2007). *Heavy Metal Distribution in River Waters and Sediment a*
[7] *firefly Village*. Analytical Science Vol. 20. Pp. 79 – 84.
[8] Nnodu, K.K. and 110, A.C. (2002). *Quality Evaluation of Portable Water and Waste Water in Imo State*.
[9] Unpublished Ph.D Thesis.
[10] PEPA (1991). *Guidelines and Standards for Environmental Pollution Control in Nigeria*. Environmental Standards
[11] Parts 2 and 3, Lagos Nigeria.
[12] WHO (1993). *International Quality Standard for Drinking Water.* World Health Organization Geneva.
[13] WHO (2002). *Water and Health in Europe; WHO Regional Publication;* European Series Number 93.

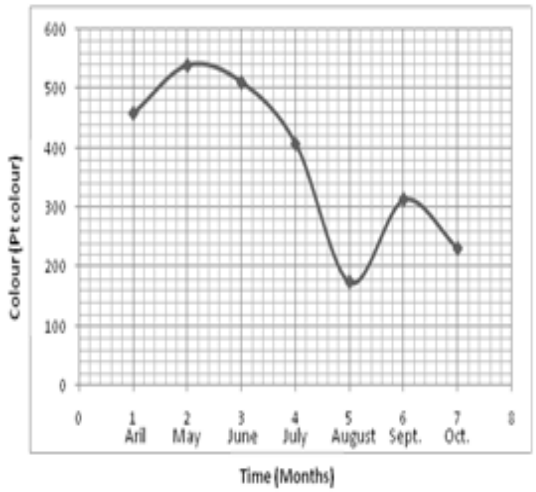

Fig 1: *Colour of water samples*

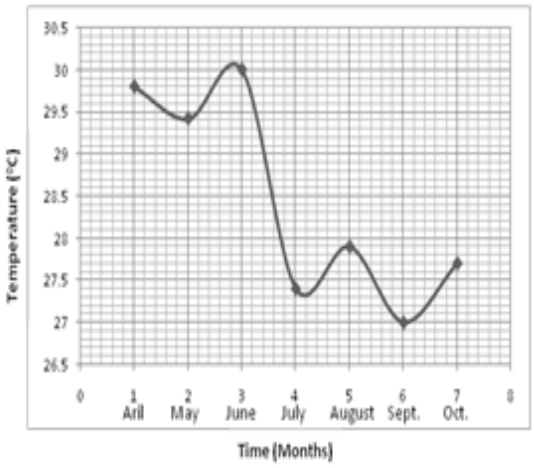

Fig 2: *Temperature of water samples*

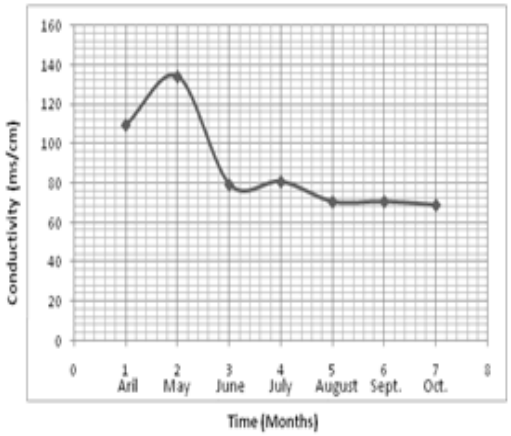

Fig 3: *Conductivity of water samples*

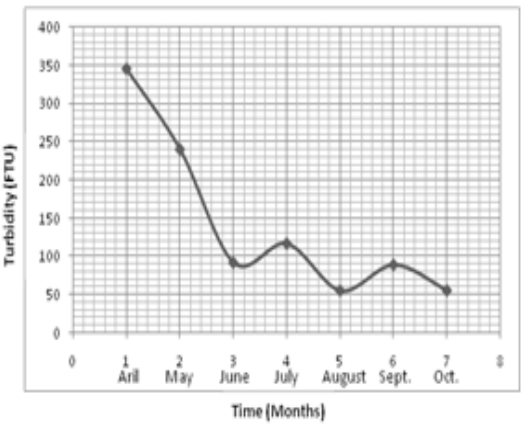

Fig 4: *Turbidity of water samples*

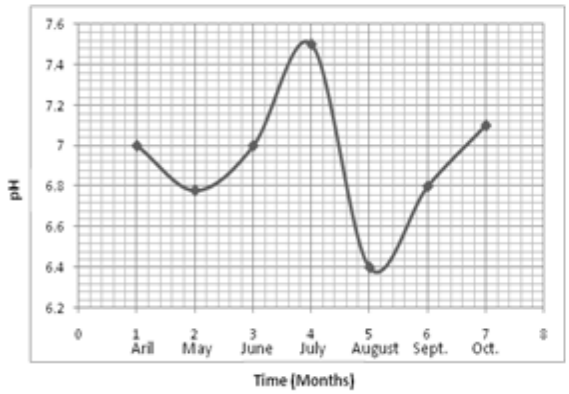

Fig 5: *pH of water samples*

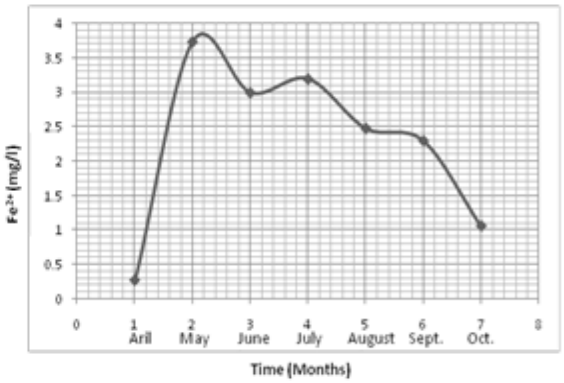

Fig 6: *Iron of water samples*

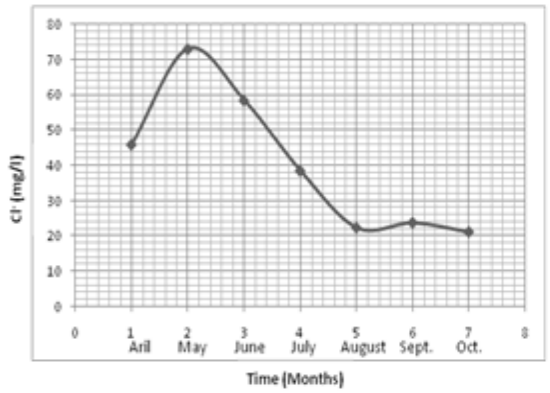

Fig 7: *Chloride of water samples*

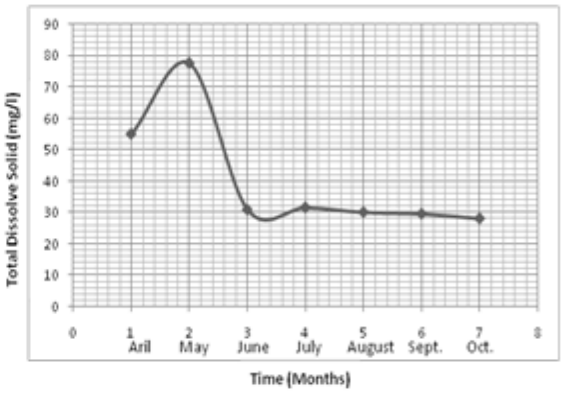

Fig 8: *TDS of water samples*

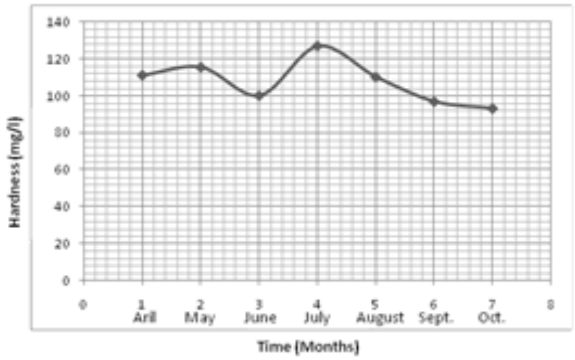

Fig 9: *Total hardness of water samples*

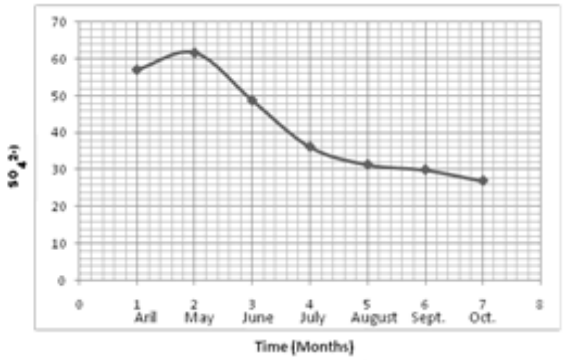

Fig 10: *Sulphate of water samples*

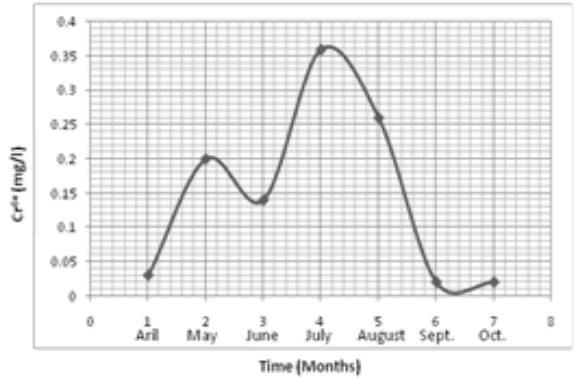

Fig 11: *Chromium of water samples*

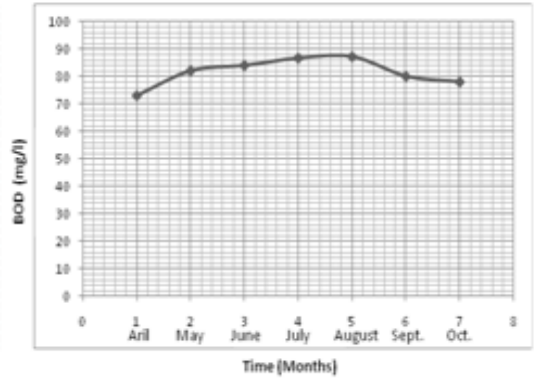

Fig 12: *BOD of water samples*

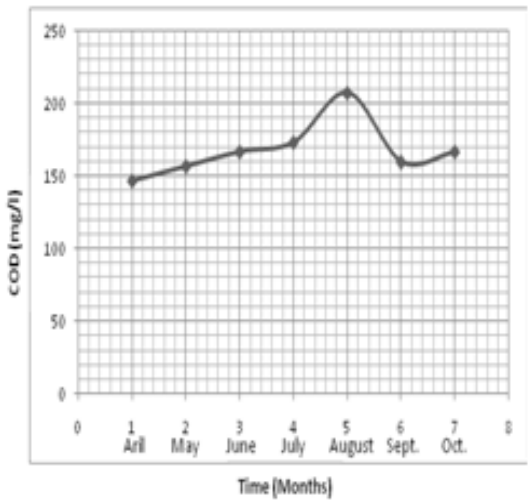

Fig 13: *COD of water samples*

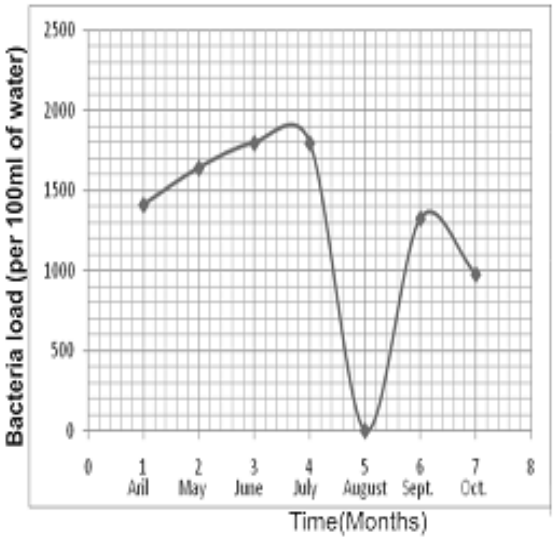

Fig 14: *Bacterial load of water*

American Journal of Engineering Research (AJER)
e-ISSN : 2320-0847 p-ISSN : 2320-0936
Volume-02, Issue-10, pp-205-213
www.ajer.org

Research Paper Open Access

Detection of Hazardous Elements in Foundation Layers in Carbonate Coastal plain, Port-Sudan – Suakin, Red Sea, Sudan

Al-Imam, O. A. O.; Elzien, S. M.; Mohammed A. A.; Elkrail, A.B.; & Mustafa A.A.
Faculty of Petroleum & Minerals, Al-Neelain University, Khartoum, Sudan

Abstract: - The area between Port-Sudan and Suakin is a carbonate coastal plain affected by climatic and environmental factors. Boreholes and trial pits were drilled to expose subsurface sediments and bore water samples from deferent depths. The samples were obtained for geochemical analyses which show interaction as ionic exchange in a complex process with sea water. The area has been subjected to both weathering and deposition process due to combination of factors. Sea water interaction, rainfall, evaporation rate and material supply by the drainage pattern.The Hydrochemical of the groundwater indicates dominance of the Cl^- and SO^{-2}_4, whereas, that of cation indicates the dominance of Na^+ and Mg^{2+} ions. Consequently, four types of groundwater can be chemically distinguished: Na-Cl -facies; Mg-Na-Cl- facies, Na-Ca- Cl-faciesCa-Mg-Na-Cl –facies and Na-Ca-Cl - Facies. The dominance of Na^+, Cl^- and SO_4^{-2} ions with very high concentrations reflect an existence of sea water intrusion phenomenon.
The hazardous constituent of the foundation layer had been detected by weathering – deposition companion model.

Keywords: - *Port-Sudan and Suakin, carbonate coastal plain, sea water,subsurface sediments,and ionic exchange*

I. INTRODUCTION

The construction engineers are face real problems to decide the foundation layer in the Sudanese coastal plain, due seasonal and inter-seasonal subsurface characteristics changes. The rainfall, Evaporation, Sea water interaction with the subsurface and drainage pattern has significant influences in the foundation layers characteristics. Weathering and depositional products subjected to chemical change during transportation as ion exchange which were take place in pore water and subsurface sediments. The prevailing subsurface condition (Alkaline and Acidity environment) assists in form of activities and sinkholes in suchformation **(Al-Imam, 2005)**. Geological investigations were provided that several locations in Sudanese coastal plain characterized by different size of cavities and sinkholes filled by loose fine sediments **(Al-Imam, 2005)**.
Coastal reef limestone covered the area at depth (more than 60m) and mainly geologically formed of Aragonite, Calcite, Mg-Calcite and Dolomite. These carbonate minerals mostly refer to organic origin. The nature of carbonate distribution reflects the coral of carbonate mineralogy by the balance between the organic carbonate (mainly coarse grained constituents composed of aragonite and high Mg-Calcite) and terrigenous carbonate contribution (Calcite and Dolomite) **(Al-Zain& Al-Imam, 2002, 2004; Al-Zain, Al-Imam and AlShafie, 2005)**.

Sabkha along the coast between Port-Sudan and Suakin are super tidal surface which has been developed as result of sedimentation. **Al-Amoudi (1993)** reported that the Sabkha deposits appear to be cemented and the process of cementation are selective and varies with depth. At the present, the red sea has marks rainfall deficit (an excess of evaporation over precipitation personal communication), (Metrological Department-Port-Sudan office). The depth of ground water level in our Sabkha isaffected by continuous water evaporation process and chemically stable (dehydration of Gypsum ($CaSO_4.2H_2O$) to ($CaSO_4$).
Previous studies and literature is very scanty even. Managed realignment is one of several “soft” engineering options which may reduce the cost of coastal defense, providing a more natural response on the problem of

rising sea level and at the same time deliver environmental especially natural conservation benefit **(Flemming and Delafonlaina, 2000: Watts et al., 2000 and Zheuhan et al., 2004)**. However, coastal geotechnical engineering as a field of investigation causing a lack of information so that engineering properties of coral reef limestone was ignored.

II. LOCATION AND SAMPLING

The area of study extends about 60Km from Port-Sudan to Suakin harbor bounded by coordinate lat. (19º 00′ ; 19º 50′ N) and long (37º 00′ ; 37º 30′ E) **Fig (1).**

Five sites were selected for sampling there are:

1- Tahlyia site: seven boreholes were drilled adjacent KhorSalalab of 40m depth in average to obtained subsurface sediments and pore water plus sea water sample.
2- DamaDama: about 7.0 km southern Port-Sudan. Two exploration boreholes of 40m depth for sediments and pore water samples plus surface and from 5.0m depth sea water samples.
3- Green area: (Southern Port) one trial pit of 0.6m on the back shore for sediments and pore water plus surface and one from 5.0m depth sea water samples.
4- Free Zone: about 37km from Port-Sudan toward Suakin. Two trial pits of 3m and 4m for sediments and pore water and one surface sea water samples.
5- Suakin: one trial pit of 1.0m on Sabkha flat and one surface sea water samples.

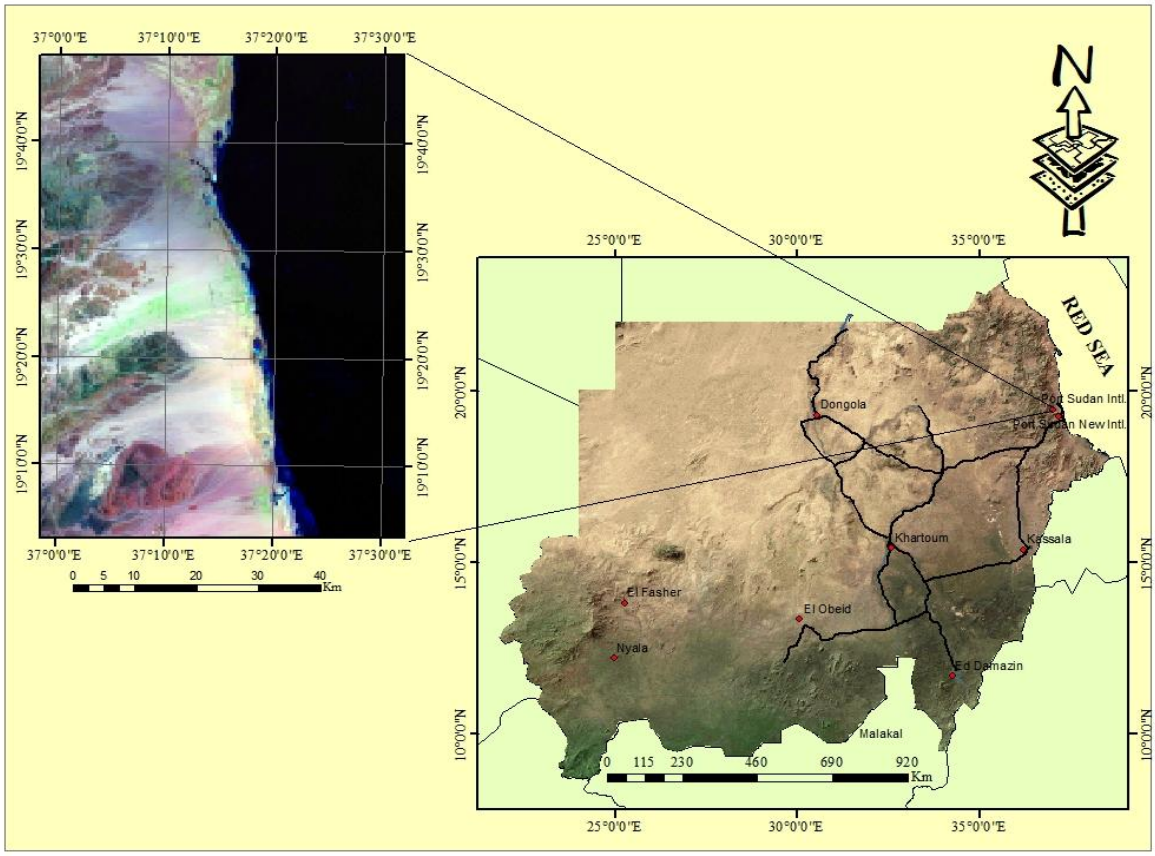

Fig. 1: Location Map of the Study area

III. GEOLOGY

The coastal plain of the red sea, Sudan, is located between the shore line and the Red sea hills. The basement rock occur over a large area in North- West Sudan of Pre- Nubian sand stone age which exhibit variable degree of metamorphism including sediments incorporate into complex sequence of igneous intrusive and extrusive suite **(Gass, 1981: Babikir, 1977: Vail, 1979: El-Nadi, 1984)**.

The igneous rocks cover a large area with unknown thickness of foliated and un-foliated granite and diorite **(El-Nadi, 1984)**. The meta-sedimentary inliers reaching the amphibolite metamorphic facies crop out in the Northern and Southern Red Sea Hills and West of Port-Sudan included a continental origin of the sediments **(El-Tom, 2002; Al-Imam, 2005)**. Volcanic sedimentary unit and green Schist assemblage's crop out NW Port-

Sudan and Suakin. However, the shield in the Red sea hills region had been more stable during most of lower and upper Paleozoic eras. Nubian sandstone is widely and in different continental environmentsdeposition of cretaceous. In the coastal plain, these Nubian form a wide part with other continental material reach the coastline particularly in the near shore zone **(Cowell et al., 2005; Punter, 1989)**.The widely spread Pre-Cambrian Afro-Arabian shield which had been available uplifted and eroded in the Red Sea region to produce three successive sequence of mixed carbonate and clastic sediments. The ultimate sedimentary phase was succeeded by period of large scale intrusion variously called the ring complexes are injection and red granite **(Krö ner, 1993)**.

The Quaternary and Recent formation are classified as marine and continental sediments. The drainage system (Khors and Wadis) is filled by Quaternary continental sediments such as gravel, sand and silt varying in thickness. These depositions are alluvial deposits controlled by the configuration of the basement complex bed rock. Generally, Quaternary and Recent marine sediments are mainly composed of reef and reefal sand. Sabkha deposits and salt rocks mostly covered the back shore area **(Fig. 2).**

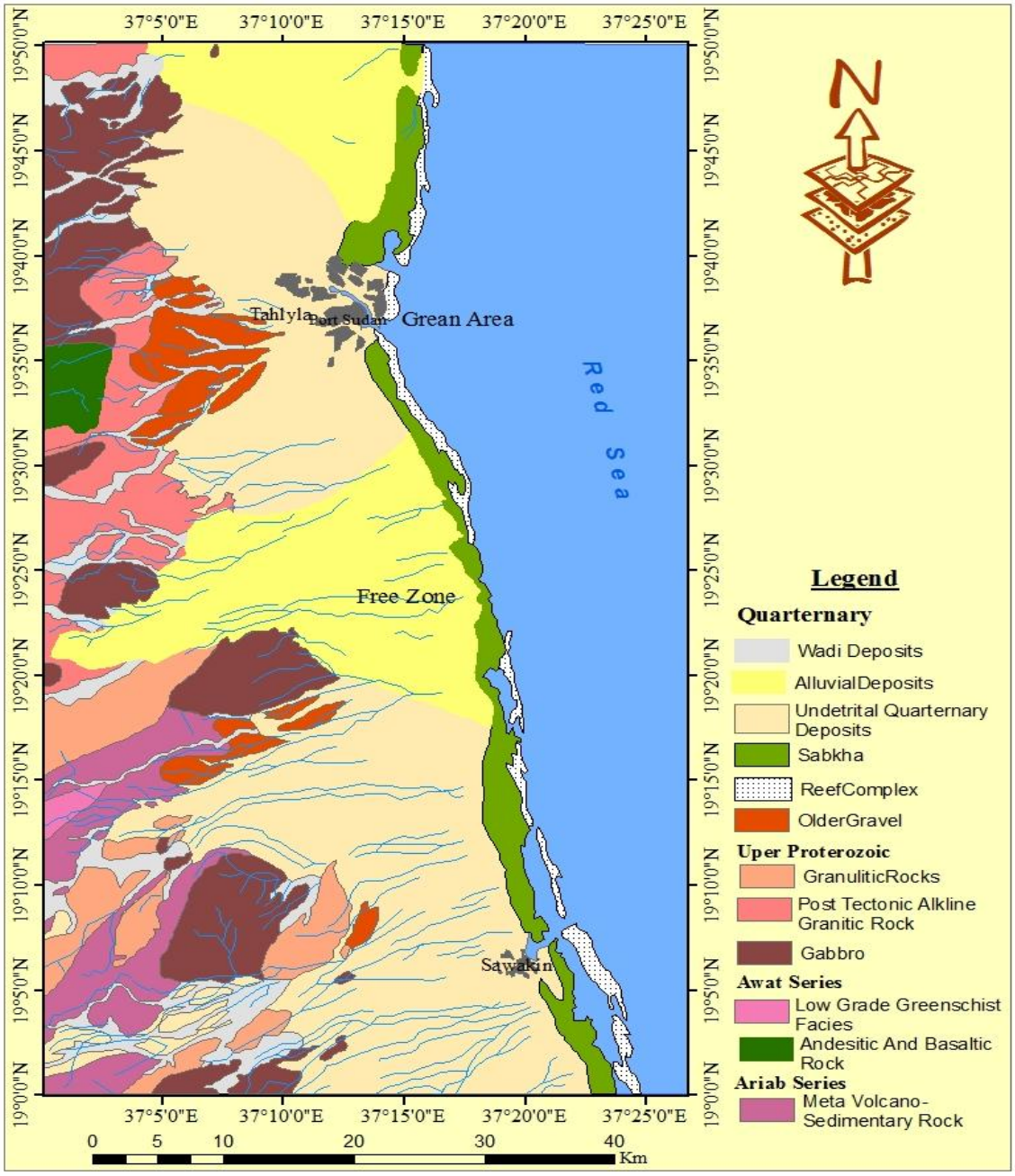

Fig. 2: Geological Map around the Study area

IV. REGIONAL TECTONICS AND SEDIMENTATION

Carbonate builds up on both tectonically passive active margins. Both were available in Sudanese coastal plain which had been subjected to tow different movements: vertically uplift and lateral displacement. However, reef complex may have originated grown over the uplift block resulting from faulting in the Pre-Pleistocene. Coral reef limestone terrace between Port-Sudan and Suakin has been uplifted 2.5m by vertical movement of the submerged coral bed rock. The lateral distribution of different facies in the Sabkha and reef flat has the same constituent and trend. Lateral shifting and depositional setting was frequent and could lead to lateral discontinuous shallowing upward **(Al-Zain and Al-Imam, 2002, 2004,Al-Zain; Al-Imam, and AlShafie 2005)**.

The onshore Pleistocene sediments are largely coarse graver and sand thought to have been derived from the basement complex. They reflect primarily rapid lateral attenuation siliciclastic deposits which may replace as such as in Green area. Back shore or any later overlain by carbonate as in Khor Salalab (Tahlyia site).Two separate groups of evidence that are related to deposition of alluvial wadi deposits and that to marine succession are involved. Marine sequence in particular are built up of sediments accumulations (mostly after reef), formed when sea level was higher than the highest point within the deposition. These are punctuated by erosion surface which may represent sea level or sub aerial surface. In Free zone, the coral reef assemblage height about 2.5m referring to sea-level while had with drawl simultaneously with uplift process. In contrast, compensation of these processes is represented in Suakin region at the entrance of main harbor which uplifted up to 3.0m.

The coastal plain on which the drainage system run through have varied view of alluvial terrains deposits such as fan of Pleistocene debris spreading seaward a cross the coastal plain and have been dissected by more recent streams activity. In general, alluvial deposits are correlated with period of high rainfall. Recent sands, commonly coarse and arkosic are associated with heterogonous gravels. These are lateral gradation from unsorted screes to stratified and current-bedded sands and more grounded gravel. However, some of these alluvial deposits are resting on coral reefs, while others are laterally equivalent to carbonate.

V. HYDROGEOLOGICAL ANALYSIS

Sea water, pore water and trial pit sediments samples have been analyzed to measure the hazardous cations and anions using **HASH (1989)** method. Results of different waters are compared with sea water which used as standard content

Table 1: Hydrochemical Facies of the Water from Port Sudan-Suakin area

Sample No.	unit	Na+	K	Ca	Mg	Cl	F	SO4	HCO3	NO2	NO3	NH3	pH	W. Facies
TBw-1	Ppm	13616	1953.5	96	97.2	24850	2.4	5956.6	597.8	6.6	30.8	NA	6.74	Na-Cl water Facies
TBw-2	Ppm	14490	1531.5	14	17.1	21655	3.2	3259.08	143.6	13.2	28.6	NA	7.22	Na-Cl water Facies
TBw-3	Ppm	23000	2429.5	19.2	23.13	40115	3.2	3885	533.8	3.3	39.6	NA	7,17	Na-Cl water Facies
TBw-4	Ppm	22599	2130.5	18.4	28.2	33015	3.2	3212.6	512.4	0	16.5	NA	7.33	Na-Cl water Facies
TBw-5	Ppm	24150	1870	18.4	27.7	33015	5	5077.7	439.2	3.3	28.6	NA	7.35	Na-Cl water Facies
TBw-6	Ppm	23000	1943	15	30.1	37275	3.2	5205.7	463.6	3.3	29	NA	7.42	Na-Cl water Facies
TBw-7	Ppm	18400	2090.5	16	29.2	31595	3.2	4964	916	3.3	23.1	NA	7.35	Na-Cl water Facies
Tsw-1	Ppm	11040	1999.5	480	1044	21535	2	3188.7	158	N.A.	8.36	NA	7.45	Na-Cl water Facies
DBw-1	Ppm	23654	2368	1240	2056.5	41712.5	5	7778.5	170.8	3.3	7.9	NA	6.8	Na-Cl water Facies
DBw-2	Ppm	32500	2160	1080	1992.5	60350	5	7375.6	170.8	16.5	10.56	NA	6.9	Na-Cl water Facies
DPw-1	Ppm	15318	1985.5	500	466.4	25602.5	2	4430	97	0	14.5	NA	7.45	Na-Cl water Facies
Dsw-1	Ppm	15318	1833	480	1020.6	31950	2	3424.9	170.8	Na	4	NA	7.98	Na-Cl water Facies
Dsw-2	Ppm	11500	1438	480	874.8	22035	2	3831.1	119.56	3.3	8.36	NA	8.05	Na-Cl water Facies
Gpw-1	Ppm	30015	2325.5	640	1142.1	51475	3	5280	195.2	NA	16.2	NA	7.76	Na-Cl water Facies
Gsw-1	Ppm	227.6	5	40	777.8	300.3	2	34.5	73.2	NA	6.16	NA	7.86	Mg-Na-Cl water facies
Fpw-1	Ppm	1.695	1009.5	6080	1625.4	3342.5	2	1499.7	73.2	NA	24.6	NA	6.7	ca-mg-na-cl -water facies
Fpw-2	Ppm	5750	880.5	4160	777.8	18825	3	1959.6	73.2	NA	26.8	NA	6.86	Na-Ca-Cl water Facies
Spw-1	Ppm	20700	2156.5	880	1069.2	38870	4	5606	134.2	6.6	12.76	NA	7.48	Na-Cl water Facies
Ssw-1	Ppm	15571	1810.5	480	899.1	27475	2	3404.9	219.6	3.3	7.48	NA	8.02	Na-Cl water Facies

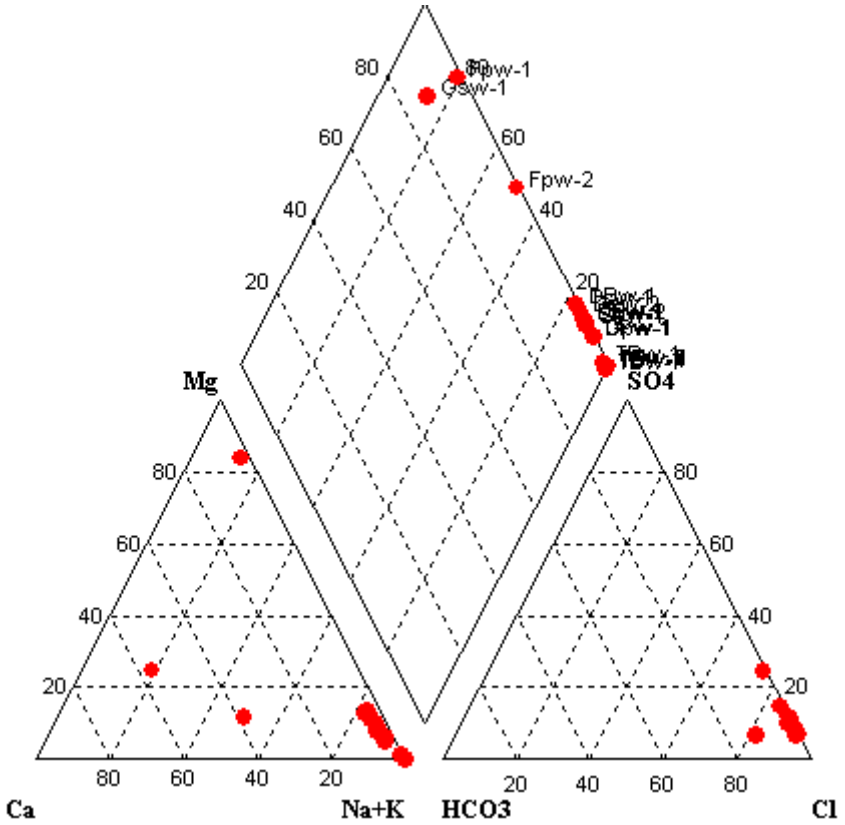

Fig.3: Piper Diagram for Coastal groundwater from Port Sudan to Suakin (Piper, 1953)

The results of the chemical analyses of the total wells in the study area were plotted on Piper diagram **(Fig. 3)** for hydrochemical facies. As results, groundwater is significantly dominated by Na^+, and Cl^- , ions**(Table 1).** The content of cations and anions give an indication of increasing salinity of pore water.
However, the sub surface stratigraphic facies, geomorphological feature, structural and tectonic provide that the area is well developed karsts formation. Such formation consist of carbonate minerals e.g. Calcite $CaCO_3$ and Dolomite Ca Mg $(CO_3)_2$.

In Tahalyia, pore water, Na^+ has excess content in range of 10.58% - 16.85% where K^+ (2.57% - 6.95%), Ca^{2+} (1.34 % - 3.21%) and Mg^{2+} (0.97% - 7.08%) are less in average values. In contrast, a complexity in the distribution of the anions concentration reflects the inland interaction. NH_3^- is completely absent; where NO_2exceed by 0.01% to 0.13% in content than that of the sea water, but there is not recorded in boreholes numberTBw–4;TBw–5 and TBw–7. The distribution of content of NO_3 is approximately similar to that of NO_2. Bicarbonate (HCO_3) and sulphate (SO_4^{2-}) recorded more concentration than sea water by 0.45% to 1.8% and 4.11% to 3.46% respectively. Cl^- has regular distribution with less concentration, except in borehole No. TBw–3 and TBw–6 where is associated with high concentration of SO_4^{2-} (3.47% and 0.21% respectively). Most of pore water have the same content of fluorite but generally reflected as high content.

In Dama Dama, generally, K^+ has less concentration by 1.99% than sea waters where other cations are increasing. The difference between DBw-1and DBw-2 in Na^+ concentration is 5.67% but in DBw-2 K^+, Ca^{2+} and Mg^{2+} recorded more than these in DBw-1. Although these boreholes are located in the same environment, Cl^- is decreasing in DBw-1 by 0.78 % and increase by 5.09% in DBw-2 with reverse content of SO_4^{2-}.
Very wide variation in concentration of both cations and anions in Green area (GPw-1) compared with sea water, where Na^+contents is 17.1% and K^+ is 3.44% respectively increasing, while, Ca^{2+} 10.57% and Mg^{2+} 4.78% decrease. All anions have excess concentration in different percentage: 18.2% Cl^-, 0.98% SO_4^{2+}, 0.43% F, 17.25% HCO_3 and No_3 1.45%.

The result of (FPW-1) pore water shore that all anions and cations have less content than sea water, except Cl^- which approximately equal of that of sea water. The coastal (SPw-1) in Suakin is characterized by high concentration of Na^+ and Ca^{2+} compared to sea water. They have 0.45% and 0.99% while K^+ and Mg^{2+} decrease by 0.96% and 0.48% respectively.

The pH values of sea water and most of pore water are in ranges 7.0 to8.0 where some other pore waters are less by (6.7-6.9). Although Na^+ is high concentration in pore water, the pH values are less than sea

water referring to the anions balance between them (sea water and pore water). SO_4^{2+}, HCO_3 and Na^+ cause the acidity in some pore water.

VI. GEOCHEMISTRY OF SUBSURFACE SEDIMENTS

Result of chemical analyses of samples of water obtained using atomic absorption spectrophotometer (A.A.S) as shown in **(Table 2).**Cl^- and SO_4^{2-}content in Tahalyia subsurface sediments varies between (1.26%-1.86%) and (0.43%-2.7%) respectively. It is very low content when compared with pore water. Although the trial pits consist of different types of sediments, they have more or less the same content of Tahalyia subsurface sediments. However, any consist in content of anions in the sediments is due to the leaching from pore water certainly in Sabkha deposits (GPs-1), FPs-1, FPs-2 and SPs-1). In deeper depths where clastic deposits occur, the content in percentage of Cl^- is more than carbonate (TBs-1, TBs-2 and TBs-4). In Sabkha deposits, where pits are located, Cl^- is high indicating the nature of Sabkha and salt marshes.

The content of anions generally, decreasing in pore water than in sediments. Clastic deposits are richer in Na^+ than in carbonate. This high concentration of Na^+ as well as K+ in the first sample of DBs-1 as a resultant of mixture with alluvial deposits on the surface in which Na^+ and K^+ have the same behavior of content disruption. Subsurface clastic deposits facies process, mostly rich in Na^+ and K^+ as sodic and alkaline sediments where other elements predicated in carbonate pore water.

Table 2: Chemistry of subsurface Sediments

Code	No.	Depth (m)	Cr %	So_4^{2-} %	Na^+ %	K^+ %	Ca^{2+} %	Mg^{2+}	Type of Sediments
TBs-1	1	18	1.56	*	1.25	0.61	30.19	0.45	Limestone
	2	41	1.86	*	3.45	1.40	3.25	0.59	Clastic Deposits
TBs-3	1	38	1.52	2.13	4.06	1.63	16.11	1.38	Carbonate sandy
	2	46	1.54	2.00	4.05	1.60	6.41	1.19	Mud
									Clastic Deposits
TBs-6	1	10	1.38	0.59	3.94	0.71	31.92	0.93	Limestone
	2	31	1.79	*	1055	4.21	10.78	2.56	Clastic Deposits
	3	40	1.67	1.66	3.38	1.60	428	9.78	Clastic Deposits
TBs-9	1	14	1.71	*	1.72	0.76	28.30	0.75	Carbonate Sandy
	2	38	1.27	2.77	2.92	1.32	3.92	1.30	Mud Clastic
									Deposits
DBs-1	1	11	1.23	0.44	6.75	1.40	23.29	1.09	Limestone
	2	23	1.60	1.00	3.85	1.10	32.17	0.72	Sandy limestone
	3	48	1.36	0.43	3.85	0.81	32.34	0.81	Limestone
DBs-2	1	26	1.57	0.40	2.57	0.67	33.47	0.70	Limestone
	2	39	0.43	1.72	1.82	0.62	28.79	0.52	Limestone
	3	49	1.41	0.52	2.66	0.79	31.08	0.81	Limestone
DBs-1	1	1.01.5	1.55	0.28	0.94	0.09	32.08	0.53	Coral reef
	2		1.80	0.28	0.92	0.25	42.21	0.45	Coral &clay
GPs-1	1	0.6	1.60	0.52	1.25	0.43	27.93	0.53	Sand,shel
									Fragment
FPs-1	1	2.5	2.48	*	2.50	1.39	5.80	0.56	Sabkha, muddy
									Sand
FPs-2	1	2.0	1.74	1.08	2.57	1.84	4.06	0.45	Sabkha, muddy
	2	3.5	1.87	*	2.54	1.83	4.32	0.48	Sand
SPs-1	1	1.5	1.67	*	1.21	0.72	31.18	0.40	Coral fragment

VII. DISCUSSION

Arid and semi-arid climatic factors have direct effect on different environment processes. Temperature, moisture and humidity are affecting the physical and chemical properties of surface and subsurface sediments. Geology, geomorphology and drainage system patterns play an important role in controlling effective factors and mechanism of reaction. The capability ofdrainage patterns to carry a dense load and a large amount of

clastic material as meta-sediments and meta-volcanics which are deposited over tertiary deposits toward the sea. However, stratigraphy and geophysical studies show deep weathering to depth of 40m **(Al-Imam, 2005)**. As the sea water effected on pore water and surface sediments it is also directly influences directly subsurface layer. These change due to the sea water seepage and interaction cause ionic exchanges with constituents of layers. Carbonate rock and evaporation rate in such regionexceeding increasing content of Na^+ and Cl^- in pore water and/or in the sediments. Clastic clay which is delivered from surrounding highlands and milky white materials which originate from carbonate rock filled joints and fractions in form of kaolinite, bicarbonate, silicic acid and release Na^+, Ca^+ and Mg^{2+}. This condition stimulate the weathering reaction and causes Na^+ to be release with exchange of H^+ due to the excess of Na^+ and high HCO_3 concentration in shallow water table and deep pore water in the subsurface layers. Formation of HCO_3 causes depletion of H^+ and CO_2^{2-} leading to decrease in grade of weathering process which require substantial amount of sea water to convert the alternated terrigenous and clay minerals as biotite and K-feldspar to kaolin, silicic acid and bicarbonate. However, the weathering processes are progressive and proceeds downward erosion through the layers. Newly formed minerals will be transformed into other mineral assemblages by exceeding rate of evaporation **(Salama et al., 1999)**.

As well as sea water sprays, Chlorite content in the rainfall decreases with increasing distance from the sea. Different type of rocks in the Red Sea hills weather by rainfall. In the produce subjected to chemical exchange during transportation through the carbonate coastal plain. Two process of water movement take place in the coastal plain: 1- rain water percolation downward during winter (rainy season) and 2- evaporation by capillary rise of hyper saline pore water during the year. The second process has more influence than of the first one. Hereinafter, the formation of carbonic acid, bicarbonate and carbonate dissolution or precipitation involves equilibrium with setting sequence of carbonate:

$CO_2 + H_2O$ ------ H_2CO_3 ……..... (1)

$HCO_3 + H^+$ ------- H_2CO_3 ……..... (2)

and from weathering:

$H^+ + CO_3$ ---------HCO_3 ……..... (3)

$Ca^{2+} + 2HCO_3$ ----------$CaCO_3 + CO_2 + H_2O$ …….. (4)

As a result of exchange between pore water and subsurface sediments with increasing alkalinity and Mg^{2+} in pore water, dolomite will precipitated.

$Mg^{2+} + 2HCO_3 + CaCO_3$ -------- $CaMg(CO_3)_2 + CO_2 + H_2O$……. (5)

As Ca^{2+} is removing, the Mg/Ca ratio is increases. At ratio of (6) or grater $CaCO_3$ as aragonite in the sediments possibly convert to dolomite conditioning by increasing evaporation and precipitation of Mg^{2+}**(Drever, 1982)**. Similarly, this process in Sabkha and salt marshes environments:

$2CaCO_3 + Mg^{2+}$ ---------- $CaMg(CO_3)_2 + Ca^{2+}$……..…. (6)

The free Ca^{2+} associate with SO_4^{2-}, with increase salinity to form Gypsum:

$Ca^{2+} + SO_4^{2-} + 2H_2O$ ---------$CaSO_4.2H_2O$……..…. (7)

When HCO_3 is more and CO_2 dissolved in water and reacts with Ca^{2+}, Calcite will form (eq. 4). If weathering process is reserved, silicic acid and sepiolite will form and other cations which are produced during weathering process percolate downwards:

$Mg^{2+} + 2HCO_3 + 4H_4SiO_4$ ---------- $Mg_2Si_3O_6(OH)_2 + 2CO_2 + 6H_2O$…… (8)

The clay minerals (Alumino-silicates) are precipitated when degradation takes place in clays:

$K^+ + 2Al^{3+} + 1.5H_4SiO_4 + 5H_2O$ --------- $KAl_2O_3(SiO_2)1.5(H_2O) + 6H^+$…….. (9)

The position of the groundwater samples in the anion triangle indicates dominance of the Cl^- and SO^{-2}_4, whereas, that of cation indicates the dominance of Na^+ and Mg^{2+} ions.Consequently, four types of groundwater can be chemically distinguished: Na-Cl -facies; Mg-Na-Cl- facies, Na-Ca- Cl-facies Ca-Mg-Na-Cl –facies and Na-Ca-Cl - Facies. The dominance of Na^+, Cl^- and SO_4^{-2} ions with very high concentrations reflect an existence of sea water intrusion phenomenon.

VIII. CONCLUSION

The precipitation of clay minerals fills the fissure fractions, cracks, voids and cavities. This process may lead to sliding of buildings which are proposed to be constructing on such foundation layer and may also causing settlement of foundation**(Fig. 4).**

Moreover, carbonic acid and silicic acid are may attack the concentrate and the reinforcing steel of foundation causing corrosion and damage to foundation structures.

The equilibrium between the alkalinity and acidity in such environment is requiring as a factor in subsurface constructions. The sulphate minerals in Sabkha environment such a Sepiolite and Gypsum are directly precipitated in foundation layers associated with carbonic acid. To avoid the hazardous chemical components, the pH value, type of building materials (type of cement, aggregate, brats...…..etc.) and foundation design are very important and care should has been taken.

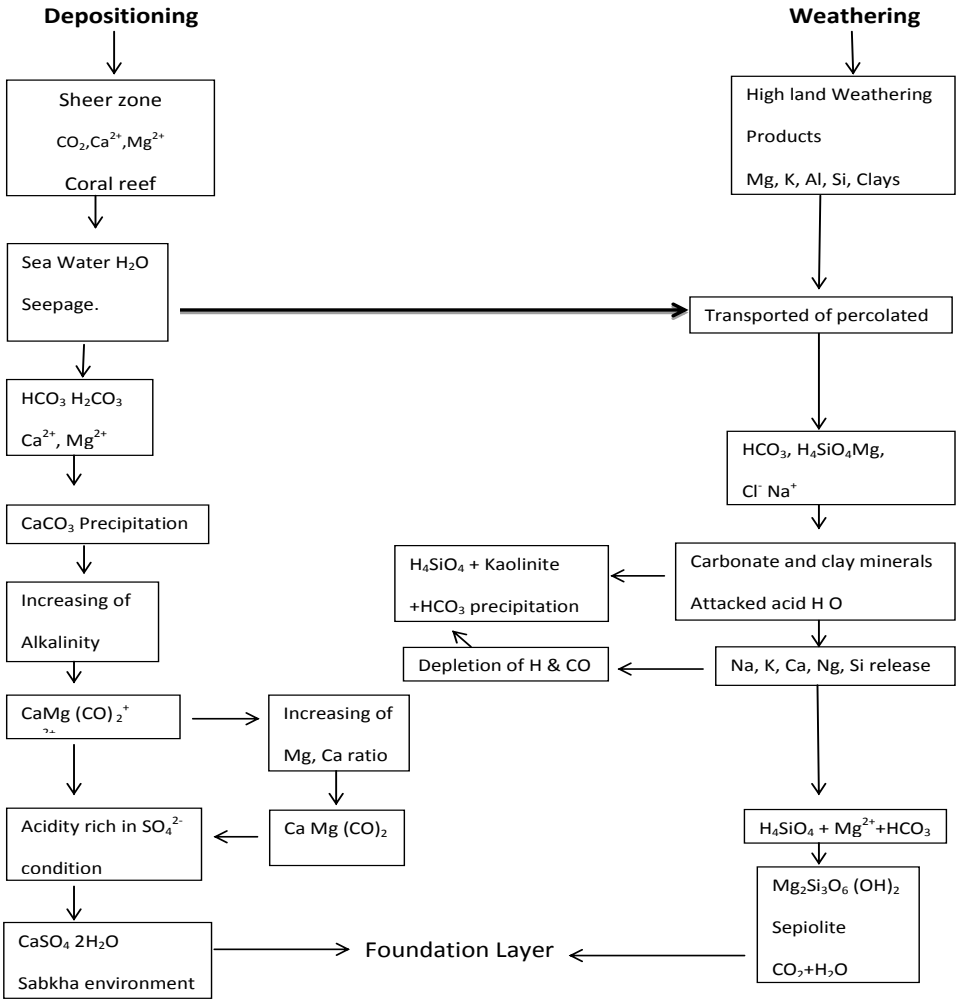

Fig.4: Weathering depositions companion model

REFERENCES

[1] **Al-Imam, O.A.O., (2005).**Coastal Geotechnical Properties and Pilling Foundation Design area between Port Sudan and Suakin, Red Sea, Sudan. Ph.D. Thesis, Alneelain University 300p.

[2] **Al-Zain, S.M.& Al-Imam, O.A.O., (2002).** Carbonate Minerals diagenesis in Towaratit Coastal Plain, south Port-Sudan, Red Sea, Sudan. Nile Basin Research Journal.Alneelain University, Khartoum, Issue No. 4, Vol. II p35 – 58.

[3] **Al-Zain, S.M.& Al-Imam, O.A.O., (2004).**Sea Level Changes and Evolution of Towaratit Coastal Plain south Port-Sudan, Red Sea, Sudan.Nile Basin Research Journal.Alneelain University, Khartoum, Issue No. 6, Vol.III, p 32-54.

[4] **Al-Zain, S.M.; Al-Imam, O.A.O., and AlShafie A.I.,(2005).** Surface Textural Characteristics of the sediments in Towaratit Coastal Plain, south Port-Sudan Red Sea, Sudan, Natural Science Magazine, Higher Education, Khartoum. SJBS (G), 6:149-167.

[5] **Al-Amoudi, O.S.B., (1993).** Chemical Stabilization of Sabkha soils at high moisture contents. Eng. Geol., 36:279-291.

[6] **Babikir, I.M., (1977).**Aspects of the Ore Geology of Sudan. Ph.D. Thesis. University College og Cardiff. U.K.

[7] **Cowell, P.J.; Stive, M.J.F.; Niedoroda, A.W.; De Vriend, H.J.; Swift, D.J.P.; Kaminsky, G.M.; Capobianco, M., (2005).** The coastal tract (Part I): A conceptual approach to aggregated modeling of low-order coastal change. Spec Issue, Jour. Coast.Res.

[8] **Drever, I.J., (1982).**The geochemistry natural waters.Prentice Hall, Englewood, Cliffs, NJ.

[9] **El Nadi, A.H., (1984).**The geology of the Precambrian metavolcanics. Red Sea Hills, NE Sudan. PhD. Thesis. University of Nottingham, England, UK.

[10] **El Tom, A.M., (2002).**Water resources development and management, Red Sea State, Port – Sudan area. Ph.D. Thesis. Alneelain University, Khartoum, Sudan.

[11] **Flemming, B.W.; Delafontaine, M.T., (2000).** Mass physical properties of muddy intertidal sediments: Some applications, misapplications and non-applications. Continental Shelf Research, 20:1179 – 1197.
[12] **Gass, I.G., (1981).**Pan-African (upper Proterozoic) Plate tectonics of the Arabian-Nubian Shield.In: A. Kröner (ed) Precambrian Plate tectonic. 387-405.
[13] **HASH (1989).**Standard methods for the examination of water and waste water. 17th (ed). Rand, M.C. and et al., New York U.S.A.
[14] **Kröner, A., (1993).** The Pan- African Belt of north-eastern and eastern Africa. Madagascar, southern India, Sri Lanka and east Antarctica: Terrane amalgamation during formation of the Gondwana supercontinent. In: Thorweihe, U., and Schandelmeier, H. (ed): Geoscientific Research in northeast Africa, S3-9, Rotterdam (Balkema).
[15] **Piper, A.M., (1953).**A graphic procedure on geochemical interpretation of water analysis.U.S. Geol. Surv.Groundwater, Note 12.
[16] **Putner, Majid (1989).** The Sudanese Red Sea: I, new developments in stratigraphy and petroleum – geological evolution. J. of Pet. Geol. 12 (2): 145-166.
[17] **Salama, R.B., Otto, J., and Fitzpatrick, W., (1999).**Contribution of groundwater conditions to soil water salinization Jour. Of Hydrol. 7: 46-64.
[18] **Vail, J.R., (1979).** Outline of Geology and mineralization of the Nubian shield east of the Nile Valley, Sudan. In: Tahoun, S.A., (ed). Evolution and Mineralization of the Arabian Shield. 1: 97-107.
[19] **Watts, C.W.; Tolhurst, T.J.; Black, H.S., and Whitmore, A.P., (2000).** In situ managements of erosion shear stress and geotechnical shear strength of the intertidal sediments of the experimental managed realignment scheme at Tollesbury, Essex, U.K. Estuarine, Coastal and Shelf Science, 58: 611-620.
[20] **Zhenhan, Wu; Patrick, J.; Daogong Hu; Zhonghai Wu; Xitao Zhao; Peisheng Ye and Wan Jiang (2004).** Hazard posed by active major faults along the Golmud-Lhasa railway route, Tibetan Plateau, China. Eng. Geol., 74: 163-182.

American Journal of Engineering Research (AJER)
e-ISSN : 2320-0847 p-ISSN : 2320-0936
Volume-02, Issue-10, pp-214-220
www.ajer.org

Research Paper Open Access

Analysis of Black Hole Effect and Prevention through IDS in MANET

Nisha[1], Simranjit Kaur[2], Sandeep Kumar Arora[3]
[1](ECE, S.S.C.E.T Badhani/ PTU, India)
[2](ECE, S.S.C.E.T Badhani/ PTU, India)
[3](ECE, LPU Phagwara/LPU, India)

Abstract: - A mobile ad hoc network (MANET) is an autonomous network. It is a collection of mobile nodes that communicate with each other over wireless links. From last few years, the interest in the area of Mobile Ad-hoc Network (MANET) is growing due to its practical applications and requirement of communication in mobile devices. In the comparison to wired or infrastructure-based wireless network, MANET is vulnerable to security attacks due to its fundamental characteristics, e.g., the open medium, dynamic network topology, lack of clear lines of defense, autonomous terminal, lack of centralized monitoring and management. There are various types of attacks in MANET which drops the network performance. Black hole attack is one of them. Ad hoc On-demand Distance Vector routing (AODV) is a popular routing algorithm MANET. In this paper we investigated the effects of Black Hole attacks on the network performance. In our work we simulated black hole attacks in Network Simulator 2 (ns-2) and measured the throughput, PDF and routing load in the network with and without a black hole. We also proposed a solution against black hole attacks using intrusion detection system (IDS).

Keywords: - *MANET, RP-AODV, Black hole attack, IDS.*

I. INTRODUCTION

Wireless network is the combination of mobile computer nodes or stations that are not physically wired. The main advantage of this type of network is communicating with rest of the world while being mobile or wireless. But disadvantage is their limited bandwidth, memory, processing capabilities and open medium [1]. Wireless networks consist two basic system models are fixed backbone wireless system i.e. infrastructure based network and Wireless Mobile Ad hoc Network (MANET) i.e. known as infrastructureless network. The infrastructure based networks uses fixed and wired gateways. The bridges for these networks are known as base stations which are responsible for coordinating communication between the mobile hosts (nodes). The other type of network is infrastructureless mobile network commonly known as an ad-hoc network. In this type of network the mobile nodes communicate with each other without any fixed infrastructure between them. An ad hoc network is a collection of mobile nodes that do not rely on a predefined infrastructure to keep the network connected. So all functioning of networks is dependent on the trust and co-operation between nodes. Nodes are the mobile systems or devices i.e. mobile phone, laptop, PDA (personal digital assistance), MP3 player or personal computer that is participating in the network. They can form arbitrary or dynamic topologies depending on their connectivity with each other in the network. Nodes are very helpful to conveying information about the topology of the network and share the responsibility of managing the network. Hence in addition to acting as hosts, each mobile node does the function of routing as well as relaying messages for other mobile nodes [2]. However, due to its inborn characteristics of dynamic topology, lack of centralized management security and limited physical security, MANET is vulnerable to various kinds of attacks than wired networks. As shown in figure 1, ad hoc network consist several home-computing devices including cellular phones, laptops, PDAs and so on. Communication can be done directly between nodes within its transmission range.

Most important networking operations include routing and network management [3]. There are many routing protocols that provide efficient routing in the network. Routing protocols can be divided into three classes i.e.

proactive, reactive and hybrid protocols, depending on the routing topology. Proactive protocols are basically known as table-driven routing protocol. In this each node maintains predetermined routing information. Examples of this type include DSDV, WRP and CGSR. Reactive protocol also known as source-initiated on-demand protocols, in contrary, do not periodically update the routing information. Whereas in reactive routing protocols, routes are established whenever it is necessary. Example of this type includes DSR, AODV, TORA SSR and ABR. Hybrid protocols have features of both reactive and proactive approaches. Example of this type includes ZRP. Security is a major concern in all kinds of communication networks, but ad hoc networks face the greatest challenge due to their inherent nature. As a result, there exist various kinds of attacks that can be performed on an Ad hoc network. [4]. In this work, we discuss one such attack known as Black Hole Attack on the widely used AODV (Ad -hoc On-demand Distance Vector) routing protocol in MANETs. A mechanism presented shows the method to detect & prevent from black hole attack in Mobile ad hoc network and also protection through black hole attack activity using intrusion detection system (IDS) in AODV routing protocol. Intrusion detection systems (IDS) are mainly used to detect and call attention to suspicious behavior.

The rest of this paper is organized as follows. In section II, we discuss the some related work for security of MANET by routing attacks. Section III, describes overview of AODV protocol. Section IV (A) we discuss Black hole Attack and in IV (B) describe solution to black hole attack. Section V presents the simulation environment. Sections VI discuss important results obtained in simulation. Section VII describes the conclusion of the paper and future work.

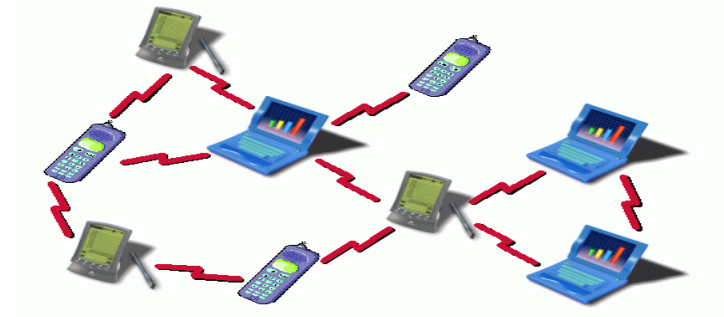

Figure 1: Wireless Ad-Hoc Network

II. LITERATURE REVIEW & RELATED WORK

The first intrusion detection model was developed in 1987 in which Denning proposed a model based on the hypothesis that security violations can be detected by monitoring a system check records for abnormal patterns of system usage [5]. In contrast to securing the routing layer of ad hoc networks, some researchers have also focused on simply detecting and reporting misleading routing misbehavior. In contrast to securing the routing layer of ad hoc networks, some researchers have also focused on simply detecting and reporting misleading routing misbehavior. Researchers have proposed solutions to identify and eliminate a single black hole node [1]. In [6], Marti, Giuli, Lai and Baker describe misbehavior detection and its effects. The paper presents two extensions to the DSR algorithm: the watchdog and the path rater. The watchdog identifies function of misbehaving nodes by listening promiscuously to the next node transmission. This technique is imperfect due to collisions in routes, limited transmission power and partial dropping. In [7], Sen et al. have presented a scheme for detection of malicious packet dropping nodes in a MANET. He provides a mechanism i.e. based on local misbehavior detection and flooding of the detection information in a controlled manner in the network so that the malicious node is detected even if moves out a local neighbourhood. In [8], black hole attack is mitigated by analyzing the destination sequence number in the RREP packet. If the destination sequence number in the RREP packet is higher than the destination sequence number at the source, then the node sent RREP packet is assumed to a malicious node. In [9], he proposes a modified protocol viz. MR-AODV based on our previous finding viz. R-AODV that eliminates limitations of existing mechanisms. MR-AODV isolates Blackhole and Grayhole nodes during route discovery phase as R-AODV and sets up a secure route for data transmission. In his simulation results prove that MR-AODV is a reliable solution which gives significant improvement in PDR with acceptable average end-to-end delay and normalized routing overhead under various network parameters and traffic conditions.

III. AODV-RP

In this paper we use AODV as the routing protocol. AODV is a reactive routing protocol and it is an adaptation of the DSDV protocol for dynamic link conditions [10]. Basically it has combined properties of both DSR and DSDV. It uses on-demand approach to find available routes, i.e. a route is established only when it is

required by a source node to transmit the data packets. AODV protocol operates in two phases: route discovery and route maintenance. It uses three types of control messages namely Route-Request (RREQ), Route-Reply (RREP), Route Error (RERR) are used for establishing and maintaining the routing path from source to destination. Route discovery process is used by node when the packet sender has no route to destination in its Routing Table. When the source node wants to make a connection with the destination node, it broadcasts an RREQ message over the network. This RREQ message received by neighbours or intermediate nodes of the source node. Each node receives a RREQ will check its Routing Table to see whether it has a path to the requested destination. It replies if there is one with RREP packet to source node. Source node receives multiple RREP packets via different paths. Source node selects fresher and shorter path among them to send the application data. If there is no route to destination, the RREQ is forwarded. Before forwarding, it keeps a reverse path to the source node in its routing table. The Routing Table records the route information of the next hop, the distance and the current highest sequence number it has seen. Route maintenance starts when its one hop neighbours go out of its range. Then the node invalidates a cached route. It is used to notify the source node or to trigger a new route discovery.

Sequence numbers are also used in the RREP messages. The sequence number is a 32-b it unsigned integer. When a node sends any type of routing control message, it automatically increases its own sequence number. Higher sequence number indicates more accurate information. When a node sends the highest sequence number, its information is considered most up to date and route is established over this node by the other nodes. So, more the sequence number means more is the freshness. A destination node updates its own sequence number either a node initiates a route discovery process or a destination node responds to RREQ with a RREP.

IV. BLACK HOLE ATTACK

A Black Hole attack [11] is a kind of DoS attack where a malicious node can attract all packets to pretend to have a fresh route to the destination and then absorb the network traffic and block data packets by dropping them. Black Hole nodes are difficult to find if they start using sequence number comparable to the current sequence number of networks. In Figure 2, we assume that Node M is the malicious node (Black Hole Node). Node S is a source node initiates route discovery by broadcast RREQ packet to all nearest neighbour. If this RREQ packet is received by malicious node M, it sends faked RREP packet by inserting high sequence number in the attention of having valid or fresh route. AODV-RP relies on sequence number to check freshness of the route. Then source gets deceived by the faked RREP packet and ignore all other replies from other nodes. The node S sends data packets in that route. The malicious node, instead of forwarding data to destination it simply drops. In this way black hole attack decrease the packet delivery percentage of the network significantly. In this work, to see the effect of an attack on the network we modify RP-AODV to BLACKHOLEAODV. In this we configure blackhole node to perform the attack in the network.

V. INTRUSION DETECTION SYSTEM

Intrusion detection is based in collection and analysis of system and network audit data. Upon detection, intrusion should be reported to security management. It continuously monitors activities like packet traffic. Each mobile node runs IDS independently to observe behaviour of neighbouring nodes, looking signs of intrusion locally, making decision to prevent the system from attack or it can also request for data and actions from neighbouring nodes if needed [12].

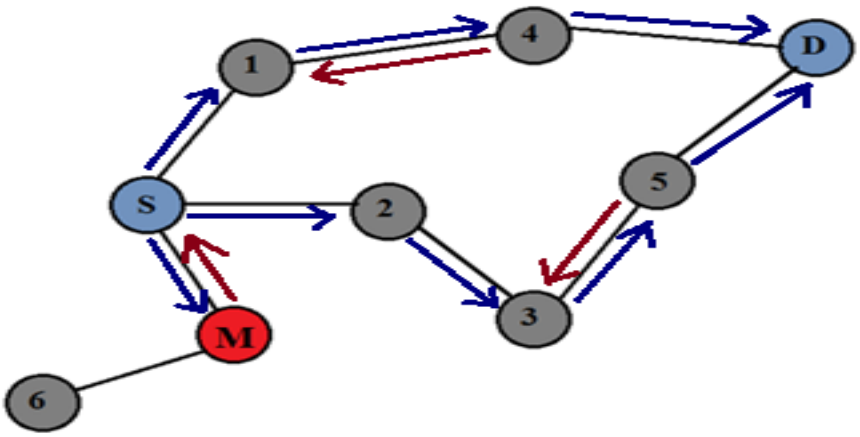

Figure 2: Black Hole Attack scenario

Intrusion detection systems in the Ad Hoc networks are divided into various categories from different viewpoints. The most important IDS systems are network based intrusion detection (NIDS) and host based intrusion detection (HIDS). In NIDS detecting attacks and malicious actions are done with the help of neighbouring nodes by their cooperation between each other. It runs on a gateway of a network and obtained audit data from traffic and then analyzed the data collected. In HIDS data acquires through hope rating system's log files that run on the node. In ad hoc network, a combination of the HIDS and NIDS can be used to discover attacks. This combination makes a powerful and distributed intrusion detection system. In this system, packets are exchanged in the network and also data collected from the network nodes are considered as a basis for intrusion detection.

As we know black hole attack is very difficult to detect than other attacks. To minimize the effect of blackhole node and improve the performance of network we use IDS and also modify RP-AODV to IDSAODV. As we see in III (A), black hole send an RREP message without checking the tables, it is more likely for the first RREP to arrive from the Black Hole. But with the help of IDSAODV Protocol it will check the RREP packet from Black Hole node for minimum path to destination and choose maximum destination sequence number. The IDSAODV Protocol will discard the first RREP packet from Black Hole node and choose second coming RREP packet from destination. The IDSAODV Protocol will also find another path to destination. To see the effect of IDSAODV, we configure the nodes as IDSAODV Protocol in our work and observed various performance parameters. We used same scenarios for IDSAODV as we used for normal RP-AODV and for Black hole attack to do the comparison.

VI. SIMULATION AND RESULTS

In this section, we describe simulation environment and simulation results.

6.1 Simulation Environment

We use NS-2 (v-2.35), a network simulation tool to simulate wireless and wired communication network. NS2 is discrete event simulator developed by the University of California in Berkeley. It provides a good platform for MANET simulation. We simulate our model for 20, 30 and 40 nodes. The random waypoint model is selected as a mobility model in a rectangular field (600 x 600 m^2). RP-AODV is used for simulation at network layer. Nodes send constant bit rate (CBR) traffic at varying rates over UDP connections. Each packet is of size 512 bytes. We have repeated the experiments by changing the number of node 20, 30 and 40 to see the performance of network under attacks. The simulation parameters are given in Table I.

Table I. Network Simulation Parameters

Parameter	Definition
Protocol	AODV, BLACKHOLEAODV, IDSAODV
MAC layer	IEEE 802.11
Simulation duration	500s
Node placement	Random
Simulation area	600m *600m
Size of data packet	512 bytes
Traffic sources	CBR/UDP
Number of nodes	20, 30, 40
Version NS-2	2.35

6.2 Result analysis

A simulation study was carried out to evaluate the performance of MANET in presence of attacks using metrics such as throughput, packet delivery ratio and normalized routing load.

6.2.1 Throughput

It is defined as amount of data transferred from sender to receiver in a given amount of time. It is measured in bits per second or packets per second. Throughput is calculated for the network in normal condition, then in the presence of the black hole attack and in the presence of IDS to improve the performance of network. Throughput values for 20, 30 and 40 nodes for normal AODV, BLACKHOLEAODV and for IDSAODV are plotted in X-graph as shown in figure 3.

6.2.2 Packet delivery function

Packet delivery fraction is calculated by dividing the number of packets received by the destination

through the number of packets originated by the application layer of the source (i.e. CBR source). It specifies the packet loss rate, which limits the maximum throughput of the network. The better the delivery ratio, the more complete and correct is the routing protocol. PDR is calculated by considering number of nodes 20, 30 and 40 for different routing protocols are plotted in graph as shown in figure 4. PDR characterize both correctness and efficiency of network. It is observed from simulation that PDR value of network in normal condition is higher than the network under attack but when we use IDS (intrusion detection system) in the presence of attack, the PDR ratio again rise. PDR values for 20, 30 and 40 nodes for normal AODV, BLACKHOLEAODV and for IDSAODV are plotted in X-graph as shown in figure 4.

6.2.3 Normalized routing load

Normalized routing load is the ratio between the total numbers of packets transmitted from routing layer of the source to the total number of packets received at the application layer of the destination. It characterizes the protocol routing performance under congestion. Normalized routing load values for 20, 30 and 40 nodes for normal AODV, BLACKHOLEAODV and for IDSAODV are plotted in X-graph as shown in figure 5.

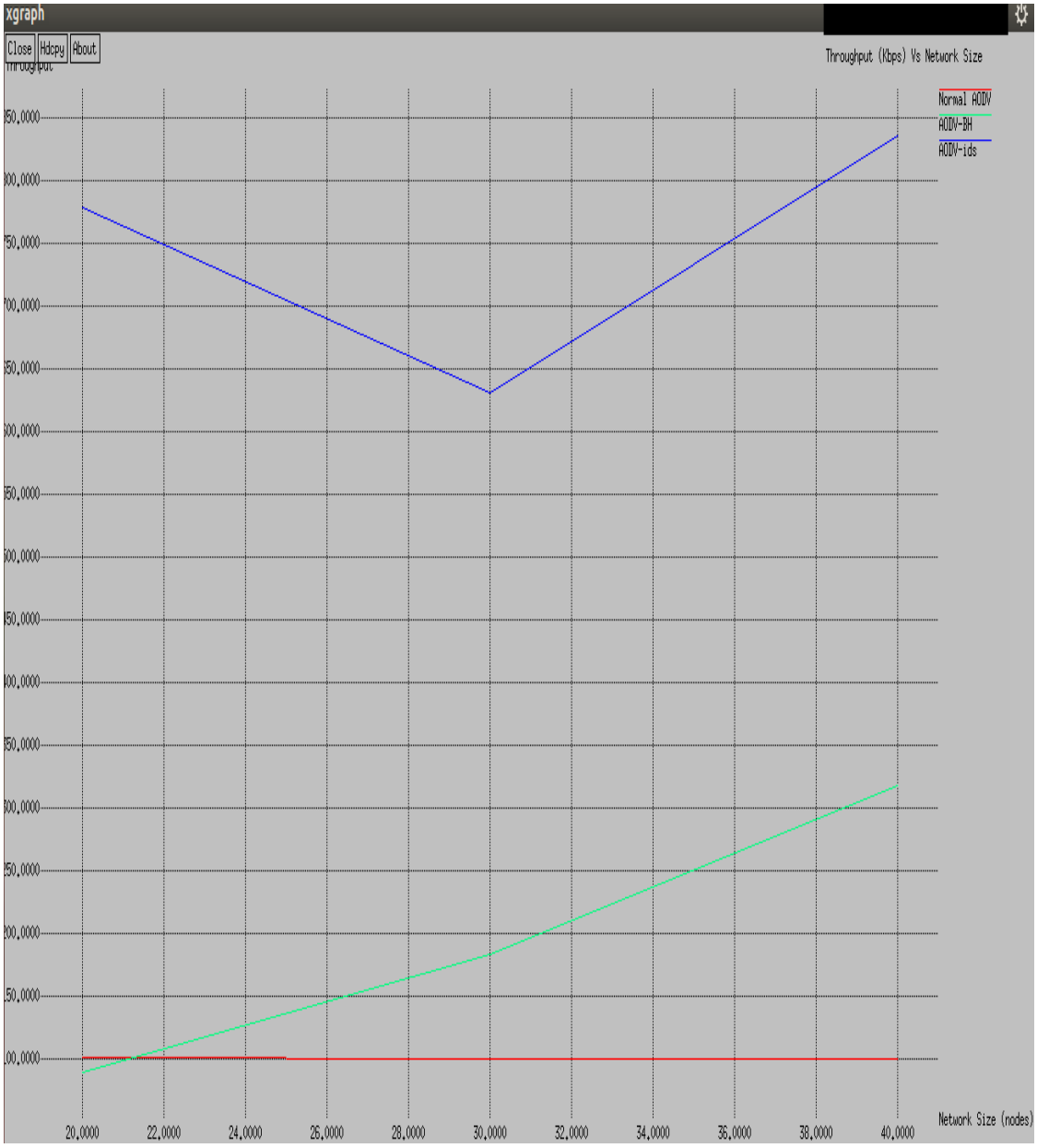

Figure 3: Throughput values for different routing protocols

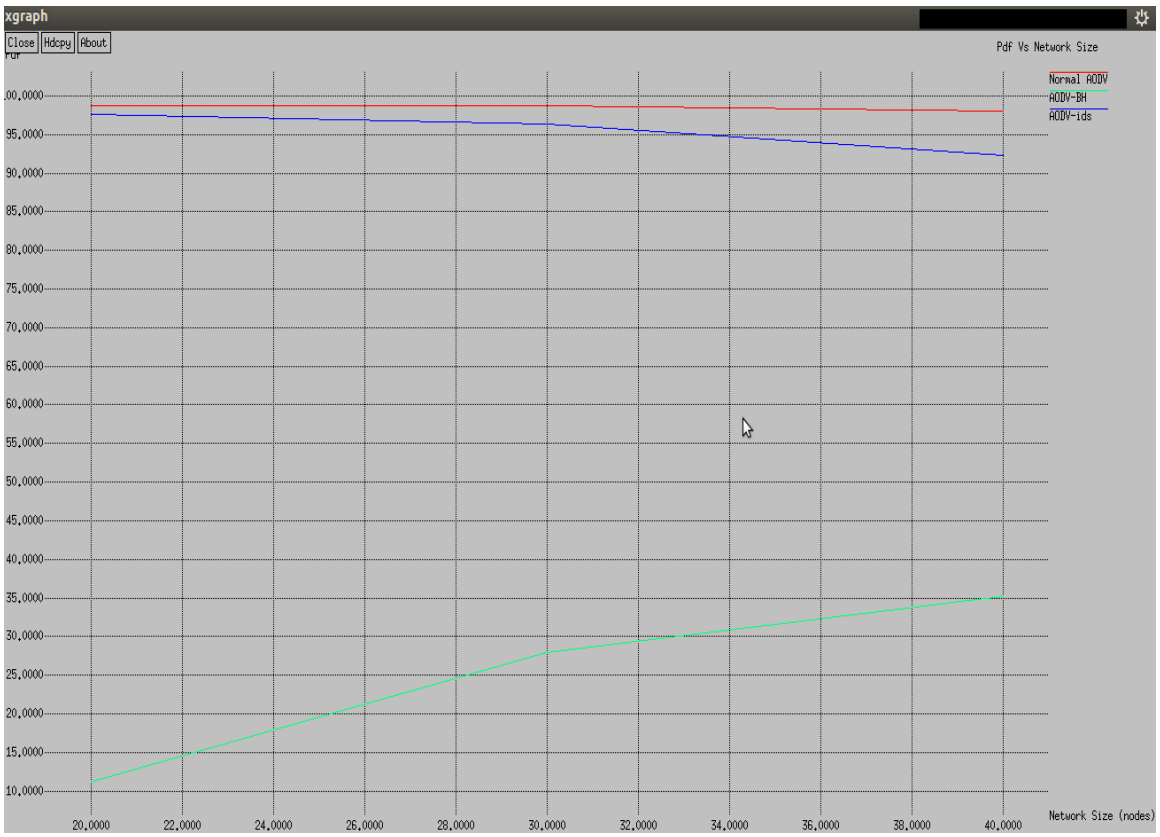

Figure 4: PDR values for different routing protocols

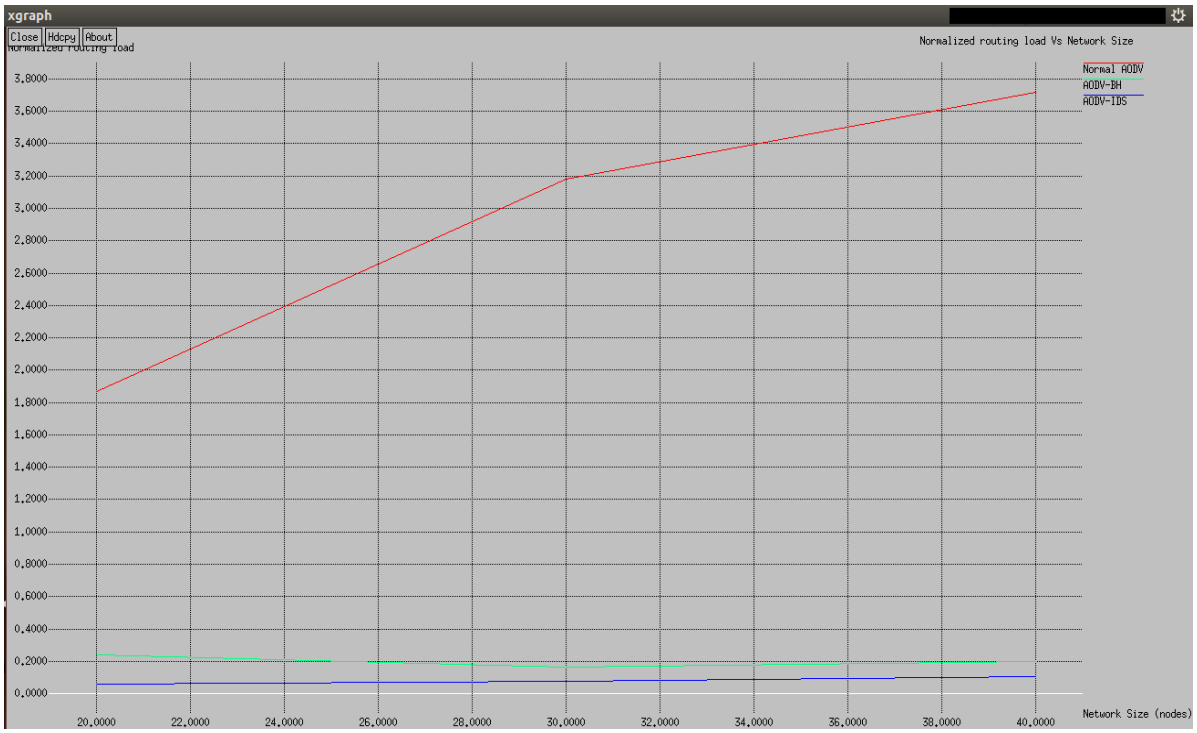

Figure 5: Normalized routing load values for different routing protocols

VII. CONCLUSION

In this paper we are discussed the routing security issues of MANETs. Black hole attack can easily deploy against the MANET. We introduced a black hole in each scenario and compared the performance of the networks with and without a black hole. We also introduced a prevention of black hole attack through IDS. For this we implemented an IDSAODV protocol. The observation and results shows that throughput increases in the presence of IDS. The PDF in the presence of black hole attack varies from 10% to 40% but when we used IDS to prevent the system from attack, the value rises and varies between 90 – 98%. The value for routing load increases in the presence of black hole attack but drops when we applied IDS. The advantage of using this approach is that IDSAODV does not require any additional overhead and require minimum modification in AODV protocol and other one is that it does not make any modifications in the packet format hence can work together with the AODV protocol.

REFERENCES

[1] Hongmei Deng, Wei Li, and Dharma P. Agarwal, "Routing Security in Wireless Ad Hoc Networks", University of Cincinnati, IEEE communication magazine, October 2002

[2] C.Siva S Ram Murthy and B.S.Manoj," Ad hoc Wireless Networks – Architectures and Protocols", Pearson Education, 2007.

[3] V. Karpijoki, "Security in Ad Hoc Networks", Seminar on Net Work Security, HUT TML 2000.

[4] Lidong Zhou, Zygmunt J. Haas, "Securing Ad Hoc Networks", IEEE network, special issue, November/December 1999.

[5] L. Prema Rajeswari, R. Arockia Xavier Annie, A. Kannan, "Enhanced Intrusion Detection Techniques For Mobile Ad Hoc Networks", Uk International Conference on Information and Communication technology in Electrical Sciences (ICTES 2007), Dec. 20-22, 2007. Pp. 1008-101.

[6] S. Marti, T. J. Giuli , K. Lai, and M. Baker mitigating routing Misbehaviour in mobile ad hoc networks. In mobile Computing and Networking (MOBICOM), Pp.255–265, 2000. Available on:citeseer.ist.psu.edu/marti00mitigating.html.

[7] J. Sen, M. Girish Chandra, P. Balamuralidhar, S.G. Harihara, and H. Reddy, "A distributed protocol for detection of packet dropping attack In mobile ad hoc networks", in Proceedings of IEEE International Conference on Telecommunications (ICT'07), May 2007, Penang, Malaysia.

[8] N. Mistry, D. C. Jinwala, and M Z averi, "Improving AODV protocol against black hole attacks, " Proceeding of International Muiti Conference of Engineers and Computer Scientists vol. II, IMECS 2010, pp. 1034-1039, Hong Kong, March 17-19, 2010.

[9] Rutvij H. Jhaveri, "MR-AODV A Solution to Mitigate Blackhole and Grayhole Attacks in AODV Based MANETs", Third International Conference In Advanced Computing & Communication Technologies (ACCT), pp.254 – 260, 6-7 April 2013.

[10] Charles E. Perkins, Elizabeth M. Belding- Royer, Samir R. Das, Mobile Ad Hoc Networking Working Group, Internet Draft, February 2003.

[11] Yi-Chun Hu, Adrian Perrig, "A Survey of Secure Wireless Ad Hoc Routing", IEEE Security and Privacy May/June 2004.

[12] Niyati Shah and Sharada Valiveti, "Intrusion Detection Systems for the Availability Attacks in Ad hoc network", International Journal of Electronics and computer science engineering, Vol.1, pp.1850-1857.

American Journal of Engineering Research (AJER)
e-ISSN : 2320-0847 p-ISSN : 2320-0936
Volume-02, Issue-10, pp-221-228
www.ajer.org

Research Paper Open Access

Design, Construction and Effectiveness Analysis of Hybrid Automatic Solar Tracking System for Amorphous and Crystalline Solar Cells

Bhupendra Gupta[1], Neha Sonkar[2], Brahman Singh Bhalavi[3], Pankaj J Edla[4]
[1] *Assistant Professor, Jabalpur Engineering College, Jabalpur,*
[2,4] *Student, Master of Engineering, Heat Power, JEC, Jabalpur*
[3] *Assistant Professor, School of Energy & Environmental studies, DAVV, Indore, India*

Abstract: - This paper concerns the design and construction of a Hybrid solar tracking system. The constructed device was implemented by integrating it with Amorphous & Crystalline Solar Panel, three dimensional freedom mechanism and microcontroller. The amount of power available from a photovoltaic panel is determined by three parameters, the type of solar tracker, materials of solar panel and the intensity of the sunlight. The objective of this paper is to present analysis on the use of two different material of Solar panel like Amorphous & Crystalline in a Solar tracking system at Stationary, Single Axis, Dual Axis & Hybrid Axis solar tracker to have better performance with minimum losses to the surroundings, as this device ensures maximum intensity of sun rays hitting the surface of the panel from sunrise to sunset.

Keywords: *- Solar Tracker, Three way of rotating freedom mechanism, Amorphous & Crystalline Solar Panel, Microcontroller.*

I. INTRODUCTION

At present, there is a great interest towards solving the energy problems facing the world. This has led to research on alternative energy source that would complement the conventional fossil fuel. The alternatives energy sources include solar, nuclear and wind, but in this research work we focused on solar energy. Solar energy is the energy generated by the power of the solar radiation. It is the cleanest source of energy whose use can contribute to saving exhaustible energy sources. Photovoltaic panels convert the suns radiation to electricity. The amount of power available from a photovoltaic panel is determine by three parameters first, the type of tracking system, material of the solar panel and the intensity of the sunlight. In this research the review in the use of two different material Solar panel like Amorphous & Crystalline in a Solar tracking system at Stationary, Single Axis, Dual Axis & Hybrid Axis solar tracker to have better performance with minimum losses to the surroundings. As this device, solar tracker ensures maximum intensity of sun rays hitting the surface of the panel from sun-rise to sunset.

II. THEORY

A solar panel must be able to follow the suns movement to produce the maximum possible power. This is achieved through the designed and implementation of the tracker system, that maintains the panel orthogonal position with the light source. The device is implemented by integrating it with Amorphous & Crystalline solar panel, three dimensional freedom mechanism and microcontroller connected with the computer to accumulate the data. The construction of the tracker is made up of three segments, the mechanical, computer Science and electronics & electrical part respectively. The mechanical system consists of the DC motors, worm gears and the frame that housed the entire system. The electrical & electronic system consists of PV sensor, a comparator circuit and a microcontroller and at last to connect the complete system with computer by software to accumulate data & data base.

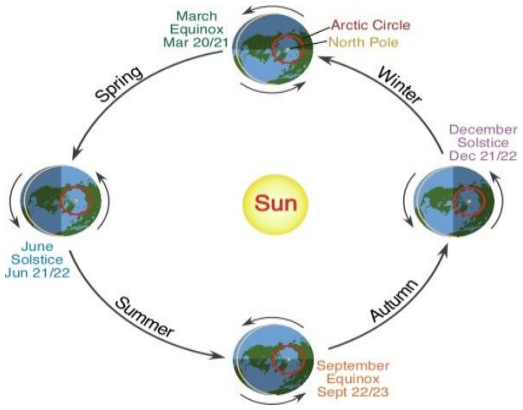

Fig 1 (a) Earth revolution around the Sun.

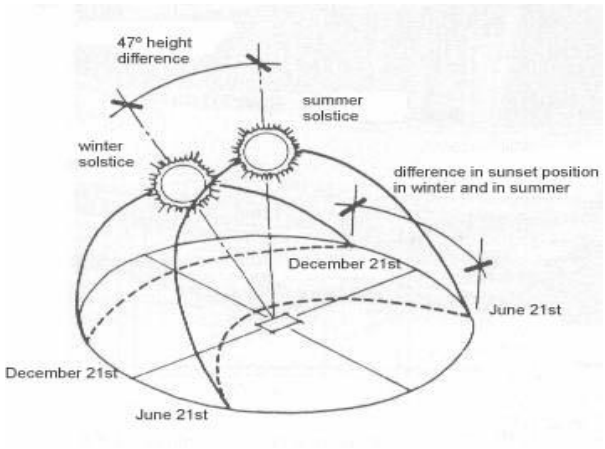

Fig 1 (b) Position of Sun with respect to Earth.

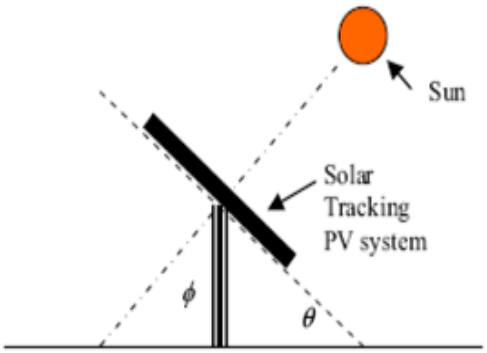

Fig2. Tilt Angle θ of a PV Array.

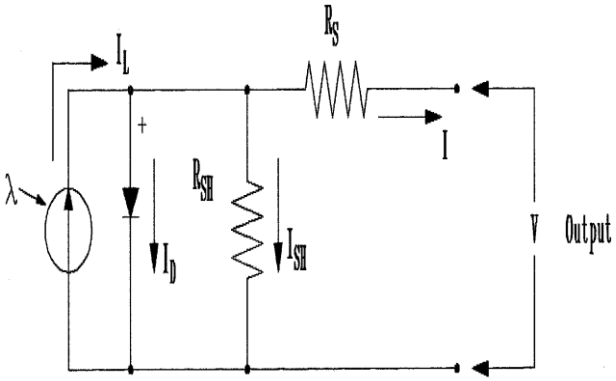

Fig. 3. Equivalent electrical circuit of PV module

For many years, several energy companies and research institutions have been performing solar tracking for improving the efficiency of solar energy production. The current work shows that a comparable system can be designed at a lower cost particularly for academic institutions.

Before the advent of solar tracking, fixed solar panels have been positioned within a reasonable tilt range based on the latitude of the location. A rule of thumb is to select a tilt angle of within ± 15° of the latitude depending on whether a slight winter or summer bias is preferred in the system. The PV array would face "true south" in the northern hemisphere and "true north" in the southern hemisphere. Solar tracking is best achieved when the tilt angle of the tracking PV array system is synchronized with the seasonal changes of the sun's altitude and with the geographical insolation level for optimized solar tracking during the day

As depicted in Fig 1(a), the position of the sun with respect to that of the earth changes in a cyclic manner during the course of a calendar year. Tracking the position of the sun in order to expose a solar panel to maximum radiation at any given time is the main purpose of a solar tracking PV system. The normal to the cell is perpendicular to the cell's exposed face.

Fig2. The sunlight comes in and strikes the panel at an angle. The angle of the sunlight to the normal is the angle of incidence (h). Assuming the sunlight is staying at a constant intensity (k), the available sunlight to the solar cell for power generation (W) can be calculated as-

$$W = A\ k\ \mathrm{Cos}\theta \quad (1)$$

Here, A represents some limiting conversion factor in the design of the panel because they cannot convert 100% of the sunlight absorbed into electrical energy.

Equivalent electrical circuit of pv module, showing the diode and ground leakage currents.

$$Voc = V + I\ R_{sh} \quad (2)$$

The diode current is given by the classical diode current expression:

$$I_d = I_D\ [QV/AKT-1] \quad (3)$$

Where I_D = the saturation current of the diode
Q = electron charge = $1.6 \cdot 10^{-19}$ Coulombs
A = curve fitting constant
K = Boltzmann constant = $1.38 \cdot 10^{-23}$ Joule/°K
T = temperature on absolute scale °K

The load current is therefore given by the expression:

$$I = I_L - I_D [e^{Q\,Voc\,/AKT} - 1] - V_{OC}/R_{sh} \quad (4)$$

PV CELL TECHNOLOGIES

In making comparisons between alternative power technologies, the most important measure is the energy cost per kWh delivered. In PV power, this cost primarily depends on two parameters, the photovoltaic energy conversion efficiency, and the capital cost per watt capacity. The continuing development efforts to produce more efficient low cost cells have resulted in various types of pv technologies available in the market today, in terms of the conversion efficiency and the module cost. The major types are discussed in the following sections:

(a) Single-Crystalline Silicon

The single crystal silicon is the widely available cell material, and has been the workhorse of the industry. In the most common method of producing this material, the silicon raw material is first melted and purified in a crucible. A seed crystal is then placed in the liquid silicon and drawn at a slow constant rate. This results in a solid, single-crystal cylindrical ingot. The wafers are further cut into rectangular cells to maximize the number of cells that can be mounted together on a rectangular panel.

(b) Amorphous Silicon

In this technology, amorphous silicon vapour is deposited on a couple of μm thick amorphous (glassy) films on stainless steel rolls, typically 2,000-feet long and 13-inches wide. Compared to the crystalline silicon, this technology uses only 1 percent of the material. Its efficiency is about one-half of the crystalline silicon at present but the cost per watt generated is projected to be significantly lower.

III. EXPERIMENTAL SETUP

The experimental setup comprises of different element used for three dimensional freedom mechanisms for tracking the maximum intensity of sun rays. Mechanical Arrangement for movement in three direction i.e. Horizontal axis, Vertical Axis & hybrid Axis is mentioned below.

Horizontal Axis

To rotate the panel along with the sun in horizontal Axis is mounted in a shaft of 1x35inches & clamped by aluminium strips.

Gear Arrangement of three Spur Gear of 72, 16 & 36 teeth respectively with Single start Worm gear connected with Stepper Motor 18°/pulse, 12 Volt, 6Ω has been done for rotating the panel to horizontal axis. (Fig 6)

Vertical Axis

Similar as horizontal axis here too the gear arrangement is with Spur Gear of 72 teeth assembled with the Single start Worm gear connected with Stepper motor 18°/pulse, 12 Volt, 6Ω with Simply supported two wheel bearing. (Fig 5)

Hybrid Axis

For moving the panel to hybrid axis a stud of 10 mm is assembled with Spur gear of 42 teeth & Single start worm gear connected with Stepper motor 18°/pulse, 12 Volt, 3.9Ω. (Fig 7)

Micro Controller

The Micro Controller used in the solar tracking system is P1C16F877A (Fig. 8) contains number of element which performs different work to control the panel & to prepare the data base of the analysis the same was connected with the desktop with Terminal Software. The element of microcontroller is listed below

- IRs detects the sunlight intensity. When consume high sunlight intensity resistance is decreased and supply high current trough it.
- The motor controller IC MAX 232 drive the DC motor by the direction of microcontroller
- LCD JHD162AC is mounted on the micro controller to represent the current Voltage & Current for both the material i.e. Amorphous & Crystalline.
- Amplifier T1P122 used to amplify the data of micro controller 7 provide the input to Stepper motor.

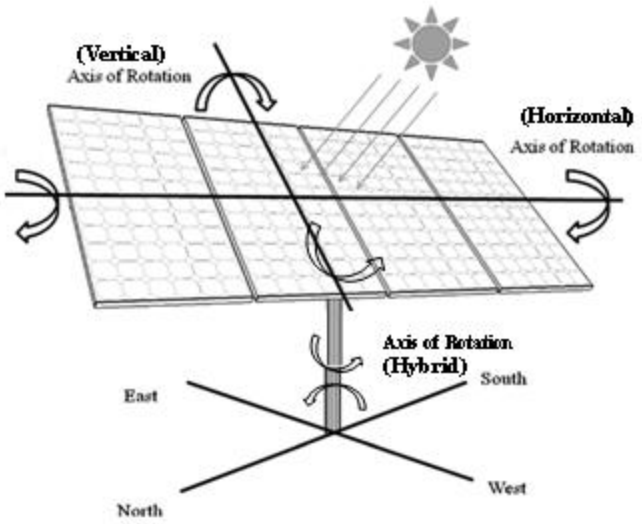

Fig4. Structural view of three ways rotating freedom solar tracker.

In the system shown in Figure 4, a solar panel is mounted over the supporting arm with consisting three direct current motor with gear mechanism, four IR (Infra Red Sensor) sensors and a control box. The light detecting system consists of four Infra Red Sensor (IR) which are IR 1, IR 2, IR 3 and IR4 mounted on the solar panel and placed in an enclosure. The sensors are setup in a way that IR 1 and IR 2 are used to track the sun horizontally for drive the horizontal positioning motor while IR 3 and IR 4 are use to track the sun vertically for drive the vertical positioning motor. The all operations are operated by control box where microcontroller and motor control ICs processes whole detection and control system. So that, all the three motors vertical, horizontal& hybrid movement to ensure proper tracking of the solar panel in any position of the sun with respect to the East-West or North-South.

Solar panel should be directly perpendicular to the sunlight so that radiation of sunlight is highest. But, position of the sun is not same place during the whole day. Therefore, direction of the sun radiation is not same and its changes during the course of the day. So, if we can use solar tracking system it would give maximum solar efficiency.

The dimension of Solar panel used in the setup is 49x15inchs for Amorphous & 30x12inchs for Crystalline. The picture of setup along with the Hybrid Tracking Mechanism is shown in Fig. 9

Fig 5. Gear Mechanism for Vertical Axis

Fig 6. Gear Mechanism for Horizontal Axis

Fig 7. Gear Mechanism for Hybrid Axis

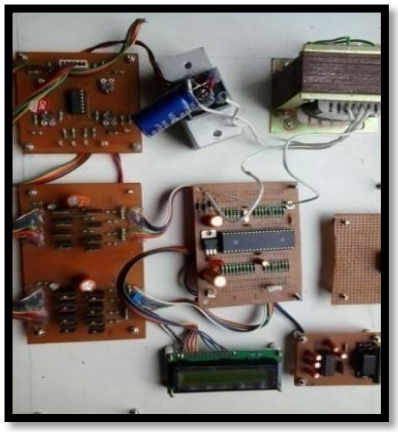

Fig 8. Microcontroller

IV. METHODOLOGY

The complete methodology used in the construction & design of the Hybrid Automatic Solar Tracking system is drawn below (fig. 10) with the help of block diagram. The construction of the tracker is made up of three segments, the mechanical, computer Science and electronics & electrical part respectively.

The key component of the system under above three segments is clearly mentioned in the block diagram used to convert solar energy into electricity.

Here SP1 is Solar Panel 1st for Crystalline,

SP2 is Solar panel 2nd for Amorphous.

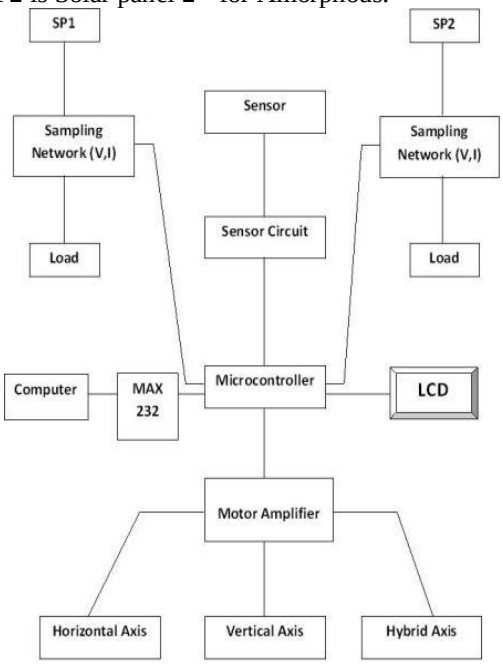

Fig. 9 Schematic view of Hybrid Automatic System.

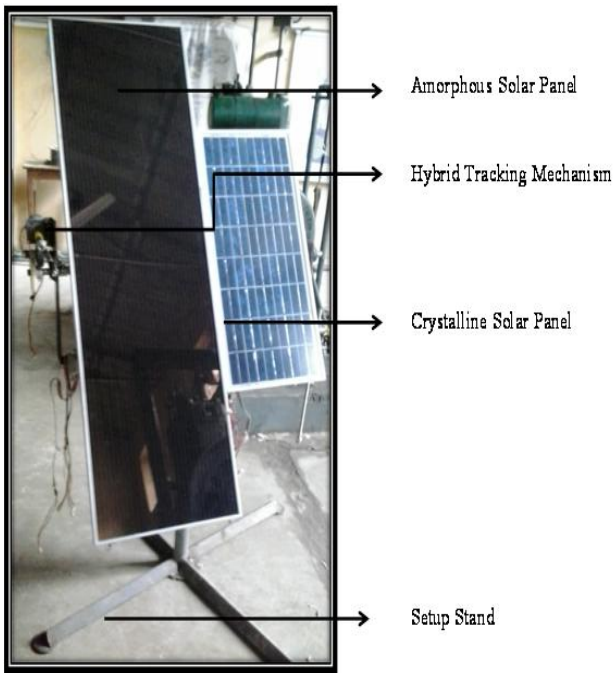

Fig.**10 Block diagram of Hybrid Automatic Solar Tracking Solar Tracking System.**

V. RESULTS & DISCUSSION

The performance assessment of Amorphous & Crystalline Solar panel at different positions are discussed below-

1. Stationary Tracking System.

The power generated by Amorphous & Crystalline Solar Panel at Stationary position that is 23.5°with the horizontal & other two axis are fixed is maximum at 12:00 noon & drop with respect to the time.(Fig 11)

The maximum power generated by Crystalline Solar panel is 13.2W where the power generated by Amorphous Solar panel is 11.9W at 13:00PM

Table1. Amorphous & Crystalline PV Module

Amorphous Solar Panel different position of Solar panel							
Time	Pw of stationary (W)	Pw of single-axis (W)	Pw of dual axis (W)	Pw of hybrid (W)	% difference between St and DA	% difference between SA and DA	% difference between SA and hybrid
10:00	8.85	8.92	8.95	8.98	1.16	0.34	0.66
11:00	10.94	10.96	10.98	12.50	0.44	0.25	14.09
12:00	11.50	14.50	15.90	16.40	38.26	9.66	13.10
13:00	11.90	15.10	16.10	16.10	35.29	6.62	6.62
14:00	10.50	13.84	13.88	16.70	32.14	0.29	20.71
15:00	9.30	12.37	12.39	12.40	33.18	0.15	0.24
16:00	7.90	8.24	8.27	8.29	4.66	0.29	0.55
Average percent difference between 10:00 and 16:00					**21.98**	**3.03**	**8.87**

Crystalline Solar Panel different position of Solar panel							
Time	Pw of stationary (W)	Pw of single-axis (W)	Pw of dual axis (W)	Pw of hybrid (W)	% difference between St and DA	% difference between SA and DA	% difference between SA and hybrid
10:00	9.30	12.30	9.50	9.61	2.15	29.47	21.87
11:00	12.80	12.80	13.70	13.80	7.03	7.03	7.81
12:00	13.20	14.90	17.15	18.50	29.92	15.10	24.16
13:00	12.50	16.20	17.60	18.10	40.80	8.64	11.73
14:00	12.10	15.30	16.15	17.90	33.47	5.56	16.99
15:00	11.10	14.90	15.50	15.90	39.64	4.03	6.71
16:00	10.30	10.90	13.50	13.90	31.07	23.85	27.52
Average percent difference between 10:00 and 16:00					**26.81**	**5.96**	**10.17**

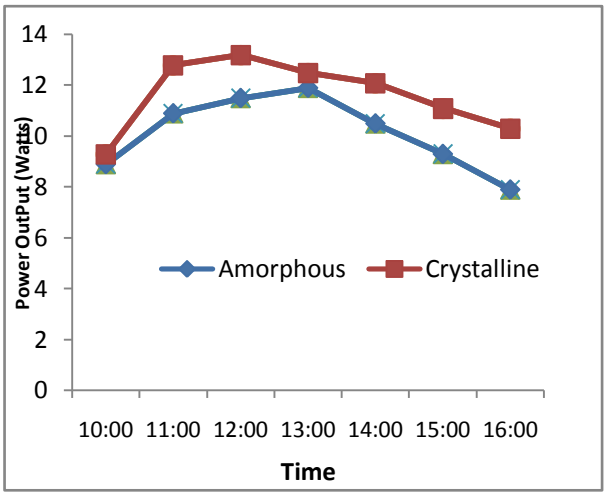

Fig 11.Performance assessment at Stationary Solar Tracking System

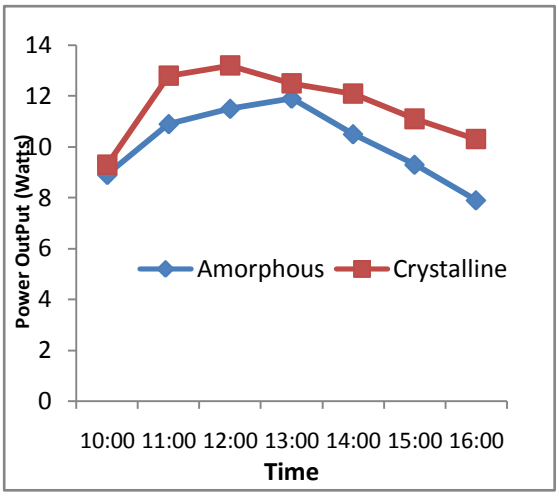

Fig 12.Performance assessment at Single Axis Solar Tracking System

2. Single Axis Tracking system.

As its name implies the panel in single axis tracking system is rotated in one direction that is the horizontal axis to track the sun & ensure maximum sun rays hitting the surface of the panel. The amount of Power generated by the Crystalline Solar Panel is 16.2W & for Amorphous it is 15.1W. (Fig 12)

3. Dual Axis Tracking system.

In dual axis tracking System two of the axis of solar tracker is moving along with the suns direction one is the horizontal axis & second is the vertical axis. The maximum power generated by Crystalline & amorphous in Dual axis tracking system is 17.6 & 16.1 respectively. The curve shows that the maximum power is generated in between 12:00-13:00 PM when the intensity of sunrays is highest. (Fig 13)

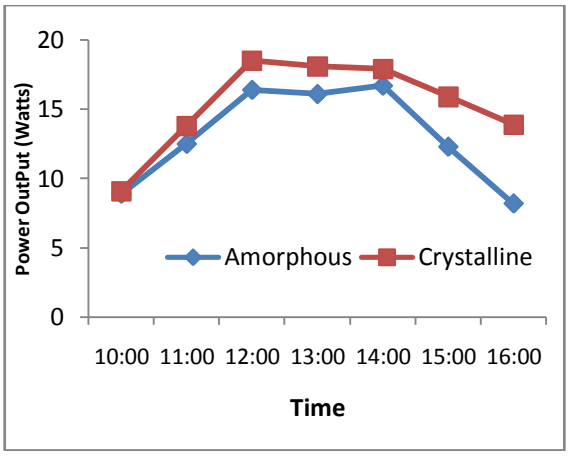

Fig 13.Performance assessment at Stationary Solar Tracking System

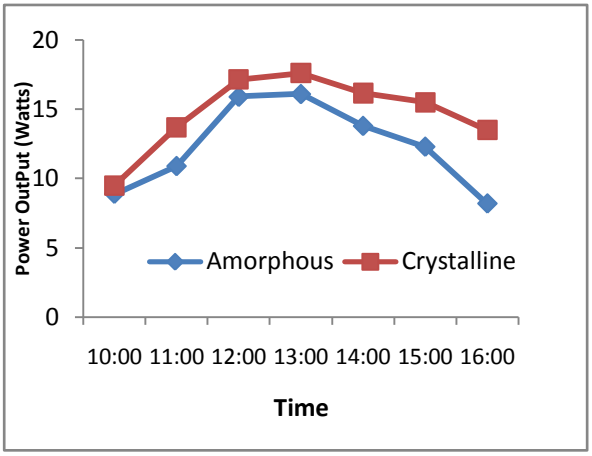

Fig 14.Performance assessment at Hybrid Axis Solar Tracking System

4. Hybrid Tracking System.

In this system the panels are capable to rotate in all the three direction for tracking the sun to have the maximum intensity of solar radiation over the year from sun rise to sun set. The results of hybrid tracking system are as it produces power output 18.5W by Crystalline Solar panel & 16.4W by Amorphous Solar panel. (Fig 14)

VI. CONCLUSION

In this paper, it has been presented a solar-tracking system which is an efficient system. It can be utilize anywhere such as house-hold activities in office even in industrial purposes. Today's world is facing acute power crisis. We need to find new resource and also need to boost efficiency for the production of power from other renewable energy sources.

We also need a better power system to give service to those people who live in remote area. Under this circumstance, this type of project can give a good result when energy crisis is one of the most vital issues in the world.

A comparative analysis was performed using four systems, i.e., hybrid tracking, dual-axis, single-axis, and stationary. The results showed that the use of the dual-axis tracking system produced 17.87% gain of power output, compared with a single-axis tracking system. The gain of output power with the hybrid tracking system was much higher (52%) when compared with a stationary system inclined at 23.5 deg to the horizontal.

REFERENCES

[1] **Asmara hid Ponniran1, Ammar Hashim1, Ariffuddin Joret**A Design of Low Power Single Axis Solar Tracking System Regardless of Motor Speed
[2] International Journal of Integrated Engineering, Vol. 3 No. 3 2011.
[3] **Adrian Catarius, Mario Christiner2010,** Azimuth-Altitude Dual Axis Solar Tracker, A Master Qualifying Project: submitted to the faculty of Worcester Polytechnic Institute.
[4] **Bull, S. R., 2001, "**Renewable Energy Today and Tomorrow," IEEE Proc.89 (8), pp. 1216–1226.
[5] **J. Rizk, and Y. Chaiko2008** Accurate analytical method for the extraction of Solar Cell Model Parameters,University of Singapore Kent Ridge, Singapore 0511
[6] **Jeff Muhs, Oak Ridge National Laboratory 2000,** Design and analysis of hybrid solar lighting and full-spectrum solar energy systems. Oak Ridge National Laboratory, Oak Ridge, Tennessee 37831-8048, Lockheed Martin Energy Research Corp.
[7] **Minor M. Arturo, García P. Alejandro 2010,** High–Precision Solar Tracking System, Proceedings of the World Congress on Engineering 2010 Vol II WCE 2010, June 30 July 2010, London, U.K.
[8] **NurKhuzairy Bin Jamaludin 2008,** Solar Tacking System, University Malaysia Pahang.
[9] **Nur Mohammad, TarequlKarim**, Design and Implementation of Hybrid Automatic Solar-Tracking System Journal of Solar Energy Engineering 2012 by ASME February 2013, Vol. 135.
[10] **Okpeki U.K. otuagoma. S**.O 2007, Design and Construction of a Bi–Directional Solar Tracking System. International Journal Of Engineering And Science Issn: 2278-4721, Vol. 2, (February2013),Pp 32-38
[11] **Rahman, S., 2003, "**Green Power: What Is It and Where Can We Find It?," IEEE Power Energy Mag., 1(1), pp. 30–37.

[12] **Saboj Kumar Ray, Md Abdul Bashar** Global Journal of Research In Engineering, General Engineering Vol 12 Issue 4 Version 1.0 Year 2012, Publisher: Global Journals Inc. (USA) Online Issn 2249-4596 & print Issn: 0975-5861.

Dr. Bhupendra Gupta received B.E.(Mechanical Engineering), M.TECH (Energy Engineering), And Ph.D. (Mechanical Engineering) currently working as Assistant Professor at Jabalpur Engineering College, Jabalpur, India. He has authored 8 textbooks in the field of engineering and published more than 20 papers in International Journals, 4 in international conferences, 05 in national conferences. He is life member of ISTE, SESI and IE (India). His key research area of interest is Solar, Biomass Fuel Cell, Renewable Energy and Thermal Engineering.

Neha Sonkar, Student Master of Engineering, Heat Power, JEC, Jabalpur. Gold Medalist in Industrial & Production Engineering & University Topper in Bachelor of engineering. Chancellor's Scholarship by Governor. Presented 3 papers in National Seminar & achieved 2 Gold & 1 Silver Medal.

American Journal of Engineering Research (AJER)
e-ISSN : 2320-0847 p-ISSN : 2320-0936
Volume-02, Issue-10, pp-229-238
www.ajer.org

Research Paper Open Access

Prospect of Buchanan's Traffic Planning Approach in Small Towns of India: A Case Study in Tezpur Town

Prakash Jyoti Saikia, Dr. Abani Kumar Bhagabati
[1]*Department of Geography, Tezpur College, Assam, India*
[2]*Department of Geography, Gauhati University, Assam, India*

Abstract: - With fast pace of increase in vehicular population, even the small towns in India are facing serious traffic and parking problems. So, traffic planning from modern perspectives becomes the need of the hour. Today, the much-adopted transport planning tool for urban centres has been the simulation models and there are many such models that are available for the purpose. But, while many resources have been devoted to the development of more complex computer modelling tools (e.g., UrbanSim and TRANSIMS etc.), less attention is focused on simpler modelling approaches. In the case of the small towns of India, it is next to impossible to think for a modern and sophisticated method of transportation planning, not only because they are too expensive, time consuming, but also from the view point of expertise and other managerial constraints. So, this paper preferred to take the help of the approach suggested in famous 'Traffic in Towns', 1963 (popularly known as Buchanan Report after Professor Colin Buchanan). To illustrate the role of the adopted approach, the present work uses a descriptive case study of Tezpur town. More specifically, this case study provides a practical study to suggest that this simpler approach can be a cost-effective approach to support certain aspects of the urban planning decision-making process.

Keywords: - *Small town, Transportation planning, Urban master plan*

I. INTRODUCTION

In the towns of India, road transport is the most widespread means of transport. But, the continued growth of traffic on urban roads has led to unwanted traffic congestion as well as noticeable increase in road accident. For the purpose of planning a town, preparation of land-use master plan is a common approach in India. Here, the transport planning process is based on the premise that capacity requirements of urban transport networks should be dimensioned to meet predicted demand resulting from changes in land use and socio-economic factors[1]. In other words, the transport system has been based on the layout of the land use instead of the other way round, where the land use plan should be formulated based on the transport forecast and analysis. This may probably be one of the causes why, despite having master plans, most of the Indian towns face serious traffic and parking problems. So, the central research question of this paper is concerned with the problem of managing moving traffic and parking in the towns of India (particularly the small towns) by an affordable approach that could support the master planning process.

The study of the current state-of-the-art in transportation planning shows that within the transportation planning process, an entire set of transportation forecasting modeling tools has been developed[2]. But, while vast resources have been spent in the development of more complex computer modelling tools, less attention has been focused on simpler approaches[3]. The high cost and large data requirements to run large-scale models have necessitated the use of simpler approaches for the small towns of India and, thus, the present work preferred to take the help of the approach suggested in famous 'Traffic in Towns', 1963 (popularly known as Buchanan Report after Professor Colin Buchanan). To illustrate the role of the adopted approach, the present work uses a descriptive case study of Tezpur town. More specifically, this case study illustrates how this simple approach can be used as a part and parcel of the master plans.

II. METHODOLOGY AND DATABASE

The goal of this research is not to develop a new Transportation and Land use Modelling tool, but to use an existing approach and apply it to the small towns of India. For this purpose the present work mainly resorts to the established work of the steering group and working group appointed by the Ministry of Transport, Her Majesty's Stationary Office (HMSO), London, entitled 'Traffic in Towns'. It is the pioneer study on the long-term problems of traffic in urban areas, published by HMSO in 1963. The present work finds this approach as an example of a simpler modelling approach that could be used to support urban planning decision-making. For the small and medium sized towns of India, such an approach can be beneficial for two basic reasons – firstly, it involves the collection of a very modest data and secondly, it is operational. Here, question may arise as to whether the approach taken by Buchanan in 1960s may be considered as a modern approach or not? But it is worth to mention that, in majority of the Indian towns (especially in the small towns), most of the variables for the traffic problems are almost the same as they were in the 60s in England and though the number and magnitude of some of them may show some change, they can be treated as those affected the traffic of London in 1960s.

The methods for working on the Buchanan's approach and modifying it as per the local conditions include a practical case study on the master plan area of Tezpur town, Assam (Fig. 1) and surveys for the purpose. For instance, a random survey with survey schedule method was taken as means to collect data on economic condition of the residents of the town, number of vehicles they have and the places of their work and market. As the population is very large, this survey covered only 2 to 3 per cent households of the municipal area and each of the villages forming the master plan area of the town. The information from this survey was then used to obtain the basic catchment area of the major nodes in the town and used for further analysis.

Besides the above, 2 municipality wards and 14 villages from the master plan area were chosen randomly to collect detail information. It is noteworthy that for this selection, the master plan area was first divided into well defined population density zones as per 2001 Census and then the proportionate representation from each of the density zones was maintained as far as possible. Information from these selected wards and villages are then collected by means of a schedule, covering at least 50% of the residential households for the wards and 70 - 100% households in the case of the villages.

The primary data regarding traffic volume were collected at all the 8 major entry points into the town. It was done manually by counting and classifying traffic, flowing past the selected fixed lines on the road. To know the hourly pattern of traffic volume in the central area of the town, the traffic on the roads in the central area of the town were also counted at 13 different locations.

The carriageway widths as well as the shoulder widths of roads within the master plan area were measured manually at 104 cross sections on different roads. While taking the measurement, the condition of the road was also observed and recorded. The conditions were evaluated on the basis of black toped, graveled or *kutcha* road and the physical condition of the road.

In order to gather an understanding of the parking situation in the town, a parking survey was done by the 'walked petrol' method[4]. Here, a frequency of half an hour was taken for recording the on-street parking. Accident data were generated from the secondary source, i.e. from the police records. For this, month wise total number of accidents, place of having maximum number of casualties, hour of the day having maximum number of accidents and the days of the week having maximum case of accidents for the period from 2004 to 2008 were collected.

To address the specific need of the work, the surrogate variable of transportation structure indices viz. Cyclomatic number (μ), Alpha index (α), Beta index (β) and Gamma index (γ) for assessing the transport network were used[5]. Similarly, the population projection is done by arithmetic projection (the horizon year is taken as 2025) method with formula-

$Pn = Po + n(Po - Pm)/m$, Where, Pn = Projected population in n year later from the year, Po = Present population and Pm = Population at a date m years earlier from the present

The numbers of vehicles at present (2011) as well as at the horizon year are projected with the same above formula, as has been used for projecting the population. Again, with the help of the per capita trip generation (as obtained from the household survey of the aforementioned 14 villages and wards), the number of daily trips for different population density zones and catchment areas of major nodes are estimated.

Last but not the least, it may be mentioned that, due to lack of reliable statistics, the observations are a vital part in the investigation. The necessary secondary data were collected from Public Works Department, District Transport Office, Municipal office, Office of the Town and Country Planning, Census office etc. To know the planning procedure, the Town and Country Planning Officer and two of the engineers were interviewed.

III. APPROACH OF BUCHANAN

In 1963, Professor Colin Buchanan in the 'Traffic in Towns' had explained the traffic planning in such a way that it has received appropriate treatment. It had produced a new design for towns, which was meant for contriving the efficient distribution or accessibility of large number of vehicles to large number of buildings in such a way that a satisfactory standard of environment is achieved[6]. The following few paragraphs highlight the main recommendations of the report, its response and legacy.

The report recommended that the urban redevelopment should look to the long term, and avoid parsimonious short-termism. Further, it stresses that if a town or city is both financially able and willing, it should rebuild itself with modern traffic in mind. However, if circumstances meant that this was not possible, it would have to restrain traffic, perhaps severely. According to this report, planners should set a policy regarding the character being sought for each urban area, and the level of traffic should then be managed to produce the desired effect in a safe manner. The report also emphasised on a lattice of environmentally-planned areas in the town, joined by a road hierarchy, with longer distance traffic being directed around and away from these areas. In the case of small towns, for instance, the report showed the possible way that could be taken to redevelop Newbury town in a pattern with vehicles easily integrating into the urban scenery. The suitability of this approach has been proved when the A34 Newbury Bypass was proposed, alongside extensive pedestrianisation and road changes within the town. The new roads dramatically reduced the impact of motor vehicles on the town and accompanied the reinvigoration of Newbury which had managed to retain its historic core[7].

However, as towns were developed according to the Buchanan's blue print, several issues emerged. For instance, some of the grand plans that were called for have had a poor reputation in their implementation. Another point of criticism was the courage needed to develop the schemes proposed in the report. The recognition of environmental issues was also less well understood in the 1960s. Because, the considerations in the report were more for the human environment, rather than the natural issues which have tended to confound some subsequent road proposals.

IV. CASE STUDY TOWN

Tezpur is the administrative headquarters of Sonitpur district of Assam, a north-eastern state of India. It is located in and around 26º 37´ N latitude and 92º 47´ E longitude and its altitude is about 79 metres above mean sea level[8]. It is located over a slightly undulating topography. While a few low hills (with heights 120 to 160 m) cover the southern part, the northern side of the town is flat. It has also some low-lying areas (locally known as *hollas*) and is dotted with many tanks, *tillas* and *tikas*. The area of its Municipal jurisdiction is 7.10 sq. km, and the Master Plan area is 126.60 sq. km[9].

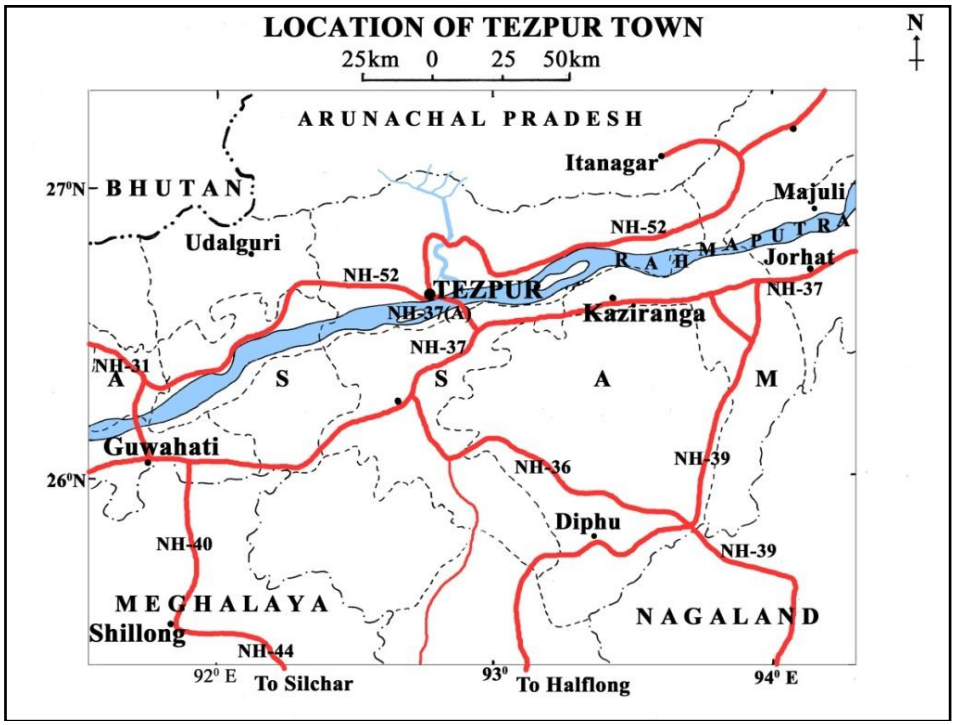

Fig. 1: Location of Tezpur town

History shows that the Chinese aggression of 1962 had a great impact on this town, which had enhanced the importance of the town as a strategic place from defense point of view. Moreover, the Government and Semi-Government establishments that came after this had created employment opportunities to a considerable extent and as a result of this, people from outside were attracted to the town[10]. In 2001, the total population of the town had crossed the one lakh mark (with a population density of 11,349 persons per sq.km.) and became a class-I town of Assam. As far as the whole master plan area is concerned, the 2001 Census put the total population as 2,17,791 (with density 1,720 persons per sq. km).

V. RESULTS AND DISCUSSION

V.1 Provision of road traffic planning

The study reveals that though the master plan of the town has a brief chapter on urban transportation and there is a provision for the formulation of an efficient circulation plan, the plan resort only to short-term programs to cope mainly with the present transport difficulties. But, these schemes are not based on detail study as well as on sound traffic engineering and management measures.

V.2 Present status and estimation

Tezpur is a cosmopolitan town. There are also many Army bases in the northern and the north-western portion just outside its outgrowths. But, the most striking feature regarding the spatial distribution is that while the western part of the master plan area, particularly to the west of the NH-52, is inhabited by Hindu people, the eastern half of it is inhabited mainly by the Muslim Community. As a matter of fact, the spatial pattern of growth of population shows that while the growth has been high in the eastern half of the master plan area, in the western half and in the municipal area, the population growth is relatively low. The spatial pattern of the growth of houses and the workers also conform to the growth of population.

About the road network, the general framework is seen to be composed of four radial roads, interlinking transverse roads and some lower order feather roads, all of which woven intricately to form a pattern of spider web. However, the local physiography causes it to deviate from the general spider web. Similarly, the situation of the town on the river bank also has made the spider web limited to its half. Out of the total roads of this network, above 59% roads are black topped, 23% are gravelled and about 18% are *kutcha*.

The computed connectivity indices for the existing road networks show that in terms of degree of connectivity the town presents a poor picture. For instance, the computed alpha index is 19.15%. The strength of the existing network is further aggravated by the overall condition of the roadways. Most of the roads are narrow. Lack of sidewalks or specified track forces pedestrians, cyclists and other slow movers to use the shoulder or the roadway itself. Uncontrolled on-street parking exacerbates the situation by narrowing further the right of way (R/W) for moving traffic. Many roads are in a dismal state of disrepair, often unpaved and riddled with potholes. It is also observed that there has been a general lack of modern traffic signals, even in situations where they are warranted.

The traffic in the town is of heterogeneous in nature. Modes having maximum speed ranging from 15-100 km per hour and width ranging from 0.5 - 2.6 metre are sharing the same road space. To be mentioned that the carriageway width of the National Highways in the town is 7.10 metre. In the case of the major distributors, the paved portion ranges from 3 to 7.35 metre, with maximum frequency at 5.7 to 5.8 metre category. But, the paved portion is found to be narrow on almost all the local distributors (ranging from 2.7 to 5.8 metre, with maximum frequency to the lower ends). When compared to the peak hour traffic volume (as obtained from the traffic count), the widths of the roads are found inadequate for the existing and growing needs of traffic. It is found that the roads have been carrying up to 2 to 3 times more traffic than their prescribed capacity[11]. The study shows that due to the narrowness of the carriageway, many roads face a good deal of congestion. In these roads, even a stationary vehicle can impede the flow of traffic in the whole road. The accessibility, especially at the time of the peak period, is also found to be significantly low. Moreover, inadequate loading facilities, lack of parking etc. are also observed at several places.

It is found that apart from the town centre, there are five major nodes in the master plan area of Tezpur, where people go for work and shopping. So, the shortest routes from the catchment areas of these nodes form the corridors for movement. Generally the radial roads form these major corridors [(Fig.3 (A)]. However, the transverse road, in the form of NH 37(A) and a part of NH 52, forms another important corridor. Within the central area, the important corridors identified are the road from Tribeni point to Civil Hospital point, road from Murhateteli to Chandmari, the Barahalia road and the road from Dadhara to Dhanwanagar etc.

The roads having basically the intra-master plan area traffic have a peak hour between 8.30 AM to 9.30 AM. On such roads, a sharp decrease in the traffic can be seen after this peak hour. The reason for this is that the traffic on these roads basically consisted of workers, who have to reach the town centre by 9.00 AM to 10.00 AM. On the other hand, the roads, where both long distance and intra-town commuters along with through traffic move, there has been a more or less constant high traffic after 9.00 AM. For example, count points like

Mission Chariali, Haleswar and Murhateteli show such trend, having a peak hour at 10.30 AM to 11.30 AM. In the case of the traffic to the town centre, the peak volume of traffic forms a wave, starting at around 9.00 AM at the periphery and ends at around 10.00 to 10.30 AM at the town centre.

Lack of adequate parking place for motorised vehicles has already created serious problem in the commercial area of the town. The parking survey revealed a shortage of about 230 car parking spaces at the peak hour. The investigation of the cases of accidents shows that places like Mission Chariali, Batamari and Solagaon exhibit high accident proneness not only in terms of number of cases, but also in terms of casualties. The study shows that while majority of cases in and around the municipal area is between light motor vehicles and pedestrians (38.08% during the study period 2004 - 2008), out side the municipal area it is the heavy vehicles that cause most of the accidents with other road users (nearly 54% of the total number of accidents caused by all types of vehicles). The involvement of motor cycles in the accidents is also found to be high (27%). Following are the results of the estimation of the population, number of vehicles, number of daily trips and modal preference in the town:

(a) The projected population at present and at the horizon year for the master plan area is around 26 to 28 and 30 to 36 lakhs respectively.
(b) By 2025 or so, the number of motorised vehicles, especially the motorcycles and cars for the journey to work itself would rise (given an adequate network and suitable parking places) from about 22,449 at present to nearly 33,844 (about 66% increase). On the contrary, the total number of persons travelling for work by all forms of transport would increase by only about 41%.
(c) The number of motorised vehicles seeking to enter the municipality area daily would increase from about 22,000 - 23,000 at present to about 29,000 - 32,000 by 2025. In addition to this, there would be about 50,000 - 55,000 non-motorised vehicles. The total peak hour flow would be of the order of 3,662 motorised vehicles (out of which about 80% would be composed of motor cycles and cars) and about 2,600 - 2,700 non-motorised vehicles. The composition of the non-motorised vehicles would be about 1,750 cycles, about 700 - 800 cycle rickshaws and 200 - 300 *thelas* and animal drawn carts. The ultimate parking demand for this level of traffic would be about 3,000 spaces (as against about 2,000 spaces at present) for the motorised vehicles and above 2,000 spaces to accommodate the non-motorised ones.
(d) The field survey places the per capita trip generation to be 0.57. Again, from the total trips found in the survey, the estimated total trips for the Tezpur master plan area becomes 1,40,498 at present and 1,78,207 at the horizon year. It is to be noted that, the worked out per capita trip generation by different modes for different density zones and the catchment areas (which was done in lieu of the conventional techniques of multi-stage distribution of the trips) also gives the total trips to be about 1,60,000 – 1,65,000 for the horizon year.
(e) The total number of vehicles in the whole master plan area would rise from about 84,484 at present to about 1,07,253 at the horizon year. Out of this, above 50 % will be bicycles and cycle rickshaws, 30% will be motor cycles and 10% will be cars and the remaining 10% will embrace all other types of vehicles. Regarding the spatial pattern, it is seen that while bicycles and motor cycles predominate in the comparatively low income zones of the northern and eastern sides of the study area, the percentage of cars is high in the zone comprising the municipal area and its fringe.

V.3 Future directions

The heterogeneous nature of traffic is likely to continue in less motorised Tezpur town and because of the socio-economic realities and compulsions, pedestrians, bicyclists and motorised two-wheeler riders will remain dominant on the roads of the towns for many decades. So the future traffic planning for the town has to address the following issues:

Various road users have different and often, conflicting requirements. Motorised vehicles need clear pavements and shoulders, while the bicyclists and pedestrians need shaded trees along the pavement. Owners of private transport modes prefer uninterrupted flow and minimum delays, whereas public buses require frequent stops for picking and discharging passengers. Since our infrastructure design does not account for the existing conflicting requirements of different modes, future traffic models must account for the users of these different transport modes. Another cause of concern for the traffic problems in this town is that the sections of National Highways passing through it have to serve multiple purposes. On the one hand they carry through traffic and on the other, the adjacent land use generates cross-traffic and demands multiple space usage like space for parking vehicles or space for informal shopping, etc. The existing design standards do not account for conflicting demand between local traffic and through traffic resulting in long delays for through traffic and safety hazards for both kinds of traffic. So, despite the situation of low per-capita income and low capacity for capital intensive infrastructure compared to that of the advanced nations, road efficiency and safety has to be promoted.

It is found that a large number of road users in the town are bicyclists, pedestrians and other slow moving vehicles. So, the road designs have to address their needs in addition to the needs of motorised vehicles.

Motorised vehicles can use a longer route and over-bridges, but, a pedestrian or bicyclist would prefer not to use an underpass or over-bridge just because it is safer to do so. A major shift, thus, is required in the design principles itself. The quality of roads is perhaps the greatest issue that has to be addressed with high priority. This is important in terms of providing better facilities for the traffic and relief to the road side residents.

VI. DESIRABLE POLICY OBJECTIVES

VI.1 Transport policy objectives

The paper wants to stress on an integrated transportation planning policy, which may consider three policy issues for the overall transport planning of the town. These are (i) Promoting and improving public transportation and to encourage public transport use. It is important because many rural and suburban commuters of the study town are seen to depend on scooters, motor cycles or personal cars due to lack of convenient public transport. Other techniques may include coordinating interdepartmental efforts, shift of work/school hours from peak period to off-peak period, enforcing stricter traffic rules etc., (ii) Policy innovations for managing traffic and travel demand and (iii) Policy for promoting non-motorised modes of transportation, especially the bicycles, increasing education and awareness levels, controlling urban population growth etc.

VI.2 Land use policy objectives

The key land use policy objectives would be land use concentration and mix of uses. These types of spatial structures are described in the planning literature as economical in both transport and land use terms. One may also envisage the development of some of the urban nodes, so as to provide them with self-containment in terms of the proportion of the total trips generated by their hinterlands, having destination within that node. It may also be helpful in terms of purpose and mode of travel.

VI.3 The strategy

The basis for the strategy lies on a vision of the town's future and the position of the transport system in it. Now if one follows Buchanan, this vision should include solutions for allocating urban space and attention for modes of transport. For example, an area within the central location of the town that is accessible for all forms of passenger traffic cannot at the same time be efficiently supplied. Another example may be that the choice for an effective and efficient public transport system cannot be combined with a system in which the passenger car is given all the space it needs. Having analysed the present and future status of different aspects related with traffic, the desired traffic planning for Tezpur town may be seen as a series of choices at different levels. But, by following Buchanan, in this study we seek to consider following principles upon which the traffic problems might be tackled –

(i) Numbers, types and speeds of vehicles to be kept down to a level compatible with environmental standards.
(ii) Circulation of essential traffic to destinations to be contrived, but not necessarily by the shortest route nor even any choice of route.
(iii) Streets and areas which are used predominantly by the pedestrians to be converted for pedestrian use only.
(iv) All through movements to be prevented.
(v) Internal movements to be reorganised to eliminate the conflict of criss-cross journeys.

Thus, in the conditions that are likely to arise in the future, following may be the ideal basis of any transportation planning for the study town: As the first ideal, one could see that what is needed for Tezpur town is an efficient primary network, which is capable of discharging the heavy load of different types of vehicles even at the peak hour. Now, considering the principles on which this primary network could be planned, the present work assumes that the thorough traffic using the road running from Kalia Bhomora Bridge to Mission Chariali and then proceed to Balipara side on the one hand and towards Mangoldoi side on the other would be removed by the provision of suitable by-passes. The location of the by-passes is outside the scope of this paper. However, it may be pointed out that any by-pass should not criss-cross the main line of movement to the town centre. In that sense, the location of one of such by-pass, relieving NH 37(A) from the through traffic to and from Nagaon side, may be thought of running through the bank of the Brahmaputra. Question may arise whether the provision of these by-passes would be a solution to Tezpur's problems. The answer is that if the by-passes could be built now they would certainly bring a measure of relief as far as the movement in the master plan area is concerned. However, regarding the movement into the municipality area, the proposed provision of by-pass would not affect the traffic. Further, our study shows that as the number vehicles increases in the future it is the build up of traffic within the master plan area that really becomes the formidable problem to cope with.

As the second principle, one may consider the environment of the town. For this purpose, the whole town was examined in order to determine the possible arrangement of the town into groups of major environmental areas. These environmental areas are taken as the residential areas, areas of educational

institutions (particularly the schools for small children) and their surroundings, important commercial as well as industrial centres or areas used by other important activities such as by Air Force and Army base etc. (Fig. 2). It is found that a particular environmental difficulty arose on all the four radial roads from the town centre. In the areas away from the municipal area, these roads not only serve to provide direct access to the dwellings, but also function as local distributors (linking with a number of access roads). In the absence of any alternative route there has been some added complication that through traffic to and from the southernmost part of the town has to make use of the radials. Even if the through traffic is disconnected, the volume of traffic in 2025 would build up along these radials. A decision has to be taken, therefore, whether to direct traffic away from the radials or to convert the radial roads into distributors. Here, the present work has opted for the second alternative and will try to treat the radial roads as major distributors.

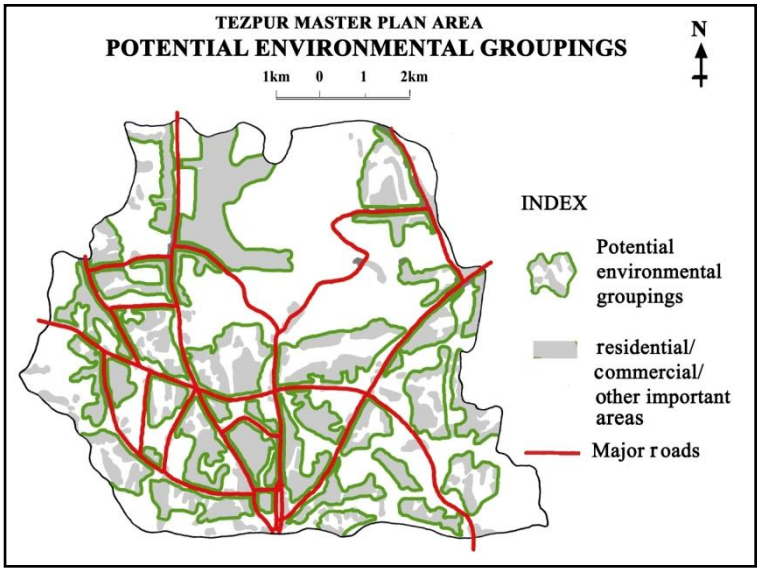

Fig. 2: Tentative grouping of environmental areas

Then the question of cyclists arises. Because, in the analysis of model choice, it is seen that though the car ownership is now growing, it still lags behind the widespread use of bicycles. It is also seen that though the car ownership and use has been increasing, the bicycle has remained popular. Thus, it can be said that bicycle has a good future and its use could still be increased significantly especially in a small town like Tezpur. In this regard, the scope for increasing bicycle use for the trips currently made by car may be considered. This particularly applies to short trips currently made by cars. In the study, it has been found that almost 40% of the short trips are not longer than 5 km, and 67% are not longer than 7.5 km. Motorists themselves admit that a quarter of all car trips could easily be made by motor cycles or bicycles, and another quarter could be made by bicycles. Thus almost up to 50% of car trips within the town could be replaced by bicycle trips. To be noted that from the household survey it was evident that 37.41% of all non-walking urban journeys in the town are made using bicycles and only 9.30% use cars. However, some town planners may see the bicycle as a significant cause of traffic congestion and traffic accidents, and want to discourage its use in the town centre. Others may see the bicycles as a cheap and non-polluting mode of transport that should be further encouraged. But, realising the popularity and possibility for an increase in bicycle use in Tezpur town, present work envisages an urgent need to have a clear policy regarding the use of bicycles. In this context, it should be mentioned that, according to Buchanan cycles should not be admitted on the primary network. It is because of the fact that cycle tracts on the primary network become too complicated to build. At the same time, he also clearly stated that it is really expensive, and probably impracticable, to create and maintain a completely separate system of tracts for cycles. So, the structural change, which is required in the entire transport and traffic system, will be a major challenge. Here, it is to be cleared that, by following Buchanan we may think for the diversion of cycle traffic increasingly to the less busy roads. But such a venture may result in inconvenience to the majority of cyclists in a town like Tezpur, where cycle is one of the prime modes of journey. So, in spite of Buchanan's remark, we may think for at least a network of radial bicycle routes as the first step towards such a change. In future, these radial routes may be added with some ring routes to upgrade the system. On the basis of the road inventory, present paper wants to suggest 2 such cycle routes [(Fig. 4 (B)].

The fast growth of motorcycles becomes the next cause of concern. The household survey reveals that the motorcycle ownership in the town is above 125 vehicles per 1,000 persons (much higher than that of only

about 40 cars per 1,000 persons). As a means of transport, the motorcycle has played two important roles: first, it has replaced a number of bicycles, taking up an increasingly higher share in the total trip modes; second, it becomes the convenient transport means for suburban dwellers to enter the town for work and business, promoting integration of the urban and rural economies. Compared to the automobile, the motorcycle has advantages in price, energy consumption and road occupation and compared to bicycles, it has advantages in speed and comfort. It, therefore, seems to have strong potential for competing against all other kinds of transport means in the town. However, they are also creating certain specific problems. For example, without any control these are growing at a very fast pace and swamping the urban road system causing frequent accidents and also the problem of pollution. Thus, the use of motorcycles should be brought under strict enforcement and covered by the suitable medium of education.

Turning to the design of the primary network for the town, the basis for the design is shown in the diagrams from (A) to (C) in Fig. 3. Here, the first diagram (A) shows the main zones of traffic generations in relation to the main corridors of movements in the master plan area. The second diagram (B) depicts the directions of main movement-desires. The third diagram (C) shows the main nodes, where most of the people work. Figure 4 (A) and (B) presents tow options for the primary network, one at minimum redevelopment and the other at some partial redevelopment.

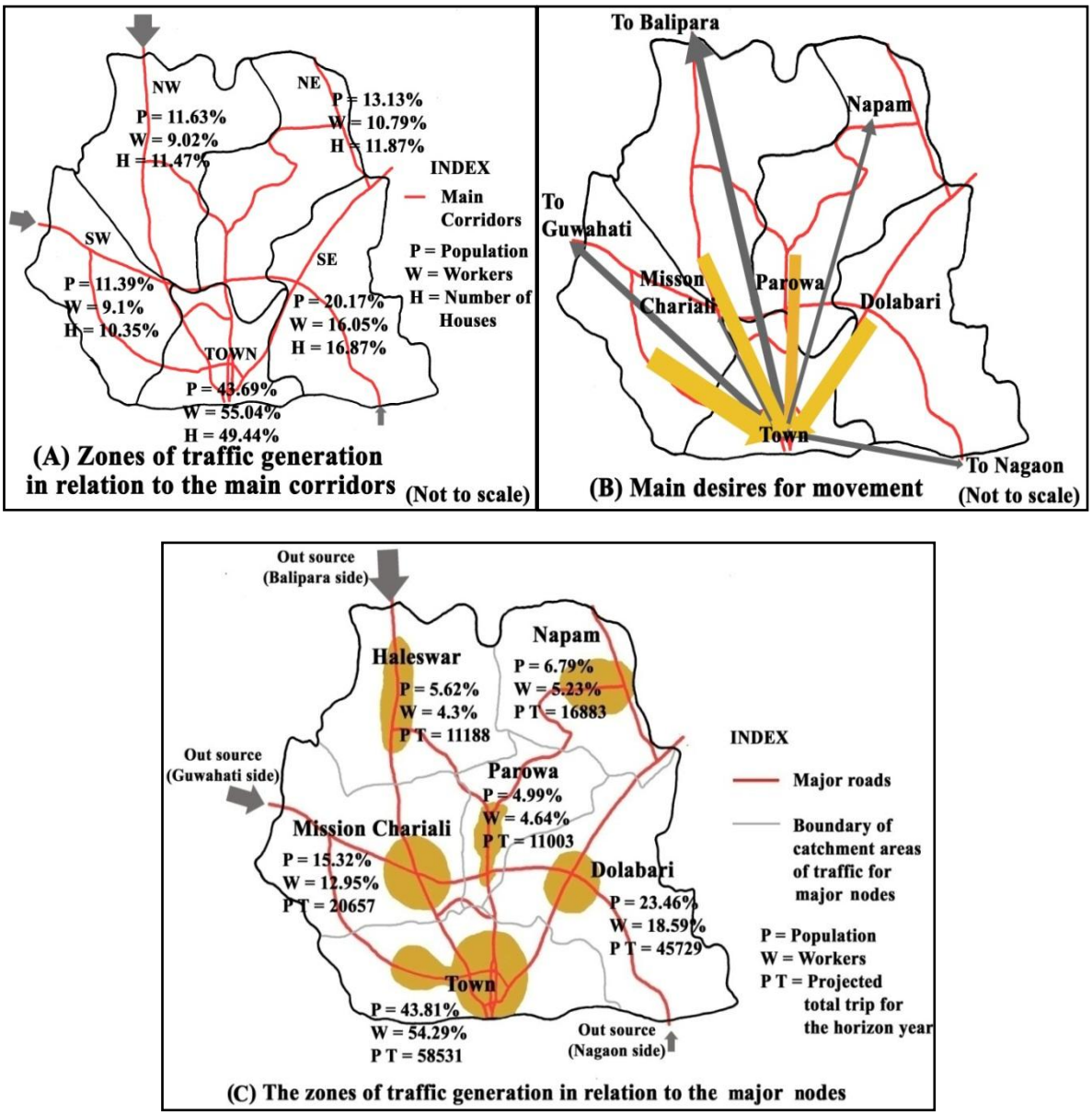

Fig. 3: The sequence of diagrams (A to C), show the basis for the design of the primary network

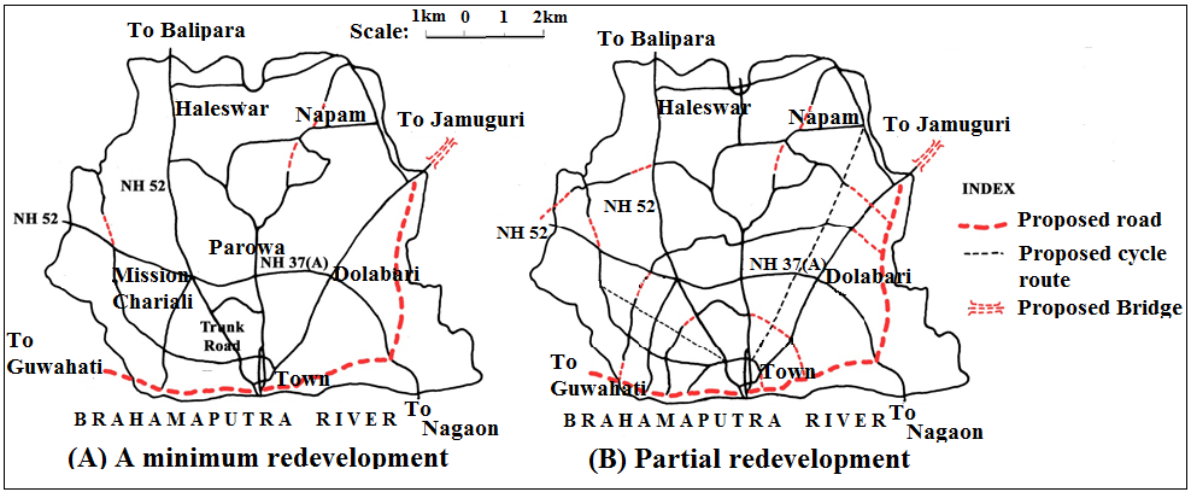

Fig.4: The theoretical network with a minimum redevelopment and with partial redevelopment

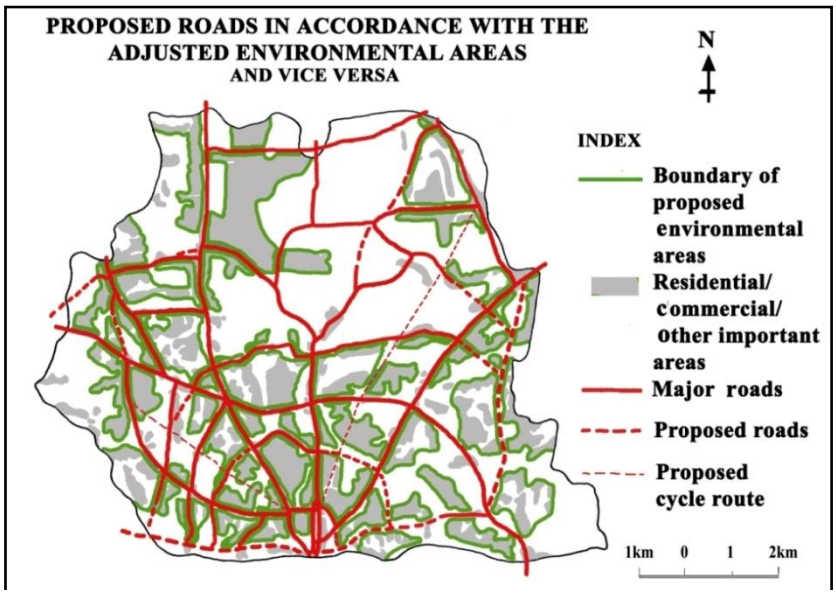

Fig. 5: Proposed roads in accordance with adjusted environmental areas and vice versa.

Besides, the five major nodes (excluding the town centre), where people go for work and market purpose have to be developed with varying socio-economic and land use characteristics. In other words, they should be provided with high degree of self-containment to reduce the travel demand for work, shopping, recreation and other facilities at the town centre.

VII. CONCLUSIONS

The study shows that there would be a very formidable potential build-up of traffic in the study town as vehicular ownership and usage increase to the saturation level. The accommodation of this full potential is beyond any practical possibility of being realised in the foreseeable future. Thus, it is necessary to consider to what extent and by what means this potential is to be managed. Because it may range up to drastic and expensive measures, on a scale, that is seemingly unusual for a town of the size of Tezpur. Here to mention the law propounded by Buchanan that - given a determination to observe a certain worthwhile standard of environment, the amount of traffic that can be admitted depends upon the money that can be invested in physical attraction. Surprisingly, the present situation is that while the estimated capital invested by the people in acquiring the vehicles (based on the information from DTO, Tezpur) is about Rupees 100 -150 crores per year, the amount of money spent by the Government in building or maintaining the roads in and around Tezpur town (as reported by the PWD Office and Municipality Board, Tezpur) is only Rupees 57.78 crores in the last 5 years. So, the choice will be either to match the investment in vehicles with an equivalent investment in road works or to manage the demand for travel.

Turning to the master plan of the study town, it is trying to cope with the steadily increasing volume of traffic by means of minor alteration. But, as per Buchanan, such a venture will lead to both a poor traffic access and a grievously eroded environment. So, while supporting Buchanan, this paper wants to emphasise that the approach used by him seems to provide a reliable base for formulation of suitable plans. Further, in the light of present study, the paper wants to conclude that the most economical course (though at the first instance, it seems to be expensive) and probably the best course for Tezpur town would be to build the primary network along with the by-passes that curtail the load of through traffic. It would be the best choice because it would immediately give the town a relief from the through traffic and also provide a sound framework on which the local traffic would build up.

VIII. GLOSSARY

Hollas - low lying marshy/wet lands. *Tillas* – Low hillocks. *Tikas* – low plateau like small table lands in between hollas. *Lakh* – One lakh means 1, 00,000. *Chowk Bazar* – the central market place. *Kutcha road* – Earthen road. *Thela*- A light two wheeled carrier-vehicle pushed by a person walking.

IX. ACKNOWLEDGEMENT

We take the pleasure to acknowledge the co-operation and advice received in all aspect of this work from Dr. Padma Kanta Borah, renowned professor and retired head of the Department of Civil Engineering, Assam Engineering College, Guwahati.

REFERENCES

[1] D. B. Sarma, *Nagar Jyoti (a special souvenir highlighting the achievements in Urban Sector)*, Urban Development Department, Government of Assam, Dispur, 2004.

[2] Iacono, Michael, David Levinson, and Ahmed El-Geneidy, Models of Transportation and Land Use Change: A Guide to the Territory, *Journal of Planning Literature 22(4)*, 2008, 323-340, available at http://www.jpl.sagepub.com/cgi/collection/topcitedtransport

[3] Hardy, H. Matthew, *Simplified Integrated Transportation and Land Use Modeling to Support Metropolitan Planning Decisions: An Application and Assessment*, doctoral diss., George Mason University, Fairfax, VA, 2011, 4-5, available at ProQuest Dissertations and Theses, http://www.udini.proquest.com/view/simplified-integrated-pqid:2346138251/

[4] L.R. Kadiyali, *Traffic Engineering and Transport Planning* (Khanna Publishers, New Delhi, 2004) 70-71, 529-533

[5] M. H. Yeates, *An introduction to Quantitative Analysis in Economic Geography* (New York: Mc. Graw Hill Book Co., 1968) 115.

[6] Traffic in Towns: A study of the long term problems of traffic in urban areas: *Reports of the Steering Group and working Group appointed by the Minister of Transport*, Her Majesty's Stationary Office, London, 1963, 41-52.

[7] *Historic Newbury fit for the future*, West Berkshire Council, 2006, 17, available at http://www.westberks.gov.uk/media/pdf/h/t/historic_newbury_cs_1.pdf

[8] Kanak Sharma, *Tezpur Nam Eto Nagar Bisesh* (Self publishing, 2001) 26-27.

[9] The Assam Gazette, Extraordinary, *No. 401*, Government of Assam, Dispur, 28th Dec., 2007, 2532-2533.

[10] The Assam Gazette, Extraordinary, *No. 166*, Government of Assam, Dispur, 14th Dec., 1977, 915.

American Journal of Engineering Research (AJER)
e-ISSN : 2320-0847 p-ISSN : 2320-0936
Volume-02, Issue-10, pp-239-252
www.ajer.org

Research Paper Open Access

Pollution Control: How Feasible is Zero Discharge Concepts in Malaysia Palm Oil Mills

Yahaya S. Madaki[1], Lau Seng[2]
[1](Institute of Biodiversity and Environmental Conservation, Universiti Malaysia Sarawak, Malaysia)
[2](Centre for Technology Transfer and Consultancy, Universiti Malaysia Sarawak, Malaysia)

Abstract: - Many palm oil mills in Malaysia still discharged either partially treated or raw palm oil mill effluent (POME) into nearby rivers. Either partially treated or untreated POME depletes a water body of its oxygen and suffocates aquatic life. Vast amounts of biogas are also generated during anaerobic digestion of POME. This paper presented the key findings from the survey mailed to 86 palm oil mills located in Sarawak and Sabah. The survey results provide an overview of the position of the palm oil mills operators on current advance POME treatment technology (PTT) in relation to achieving zero discharge concepts. The survey attempted to identify the key issues about the PTT in respect to feasibility of zero discharge concepts in palm oil mills. The results shows that, although palm oil mills generate a lot of different types of wastes during processing of Fresh Fruit Bunches, according to the operators and available literature, POME is the most difficult waste to manage. The results also shows that, palm oil mills cannot meet up with the new discharge limits of 20ppm of BOD and zero emission using only conventional open or closed pounding system.

Keywords: - *Anaerobic digestion, Biogas, Palm oil mill, Palm oil mill effluent, Zero discharge concept*

I. INTRODUCTION

The global market has become increasingly dependent on palm oil, but major producers like Malaysia and Indonesia are facing tougher operational challenges to cater for the rapidly growing global demand. Among the major challenges faced by palm oil industry especially in developing countries like Malaysia are environmental issues. The processing of oil palm fresh fruit bunches (FFB) primarily for palm oil also results in concomitant production of wastes in the forms of palm oil mill effluent (POME), empty fruit bunches, mesocarp fiber and shell. POME consists of water soluble components of palm fruits as well as suspended materials like palm fiber and oil residues. Despite its biodegradability, POME cannot be discharged without first being treated because it is acidic and contains residual oil that cannot be easily separated using conventional gravity-based systems. Essentially, this oily mix needs a lot of oxygen before it can decompose completely, and this phenomenon is called having a high biochemical oxygen demand (BOD). In the past, when the industry was at its infancy in 1960's, either palm oil mills usually discharged partially treated or raw POME into nearby rivers as this was the easiest and cheapest method for disposal. However, excessive quantities of untreated POME deplete a water body of its oxygen and suffocate aquatic life, and many rivers have been devastated by such discharges. The problem of pollution accruing from a mere 92,000 tonnes production by only 10 mills was not apparent then. The environment could somehow absorb these wastes.

This lackadaisical attitude did not last long. By the 1970's the growth of the industry was literally exponential, bringing along with it pollution which the waterways could no longer handle, so much so that palm oil processing became synonymous with POME pollution. Ton for ton, the oxygen depleting potential of raw POME is 100 times that of domestic sewage. The industry was faced with a major problem, virtually completely lacking in any proven technology to treat POME. Committed to overcome the problem, the government and the industry worked together to source for treatment technologies that are environmentally and economically sound. Bear in mind, none was available anywhere in the world then to specifically treat POME. This government-industry synergy towards common goal-pollution abatement paid off handsomely. Systems for treatment of

organic industrial wastes were successfully adapted for POME treatment. The three most commonly used systems were ponding system, open tank digester and extended aeration system, and closed anaerobic digester and land application systems. [1].

Although particular aspects of environmental control had been the subject of legislation in past decades around the world, for example the Control of Pollution Act 1974, Trade Effluent Regulations 1989, and the Environmental Protection Act 1990 which raised significantly the profile of the environment as an industrial responsibility and which brought many industrial activities under the direct control of the Environment Agency or local authorities in U.K [2]. However, the growing international concern about the environmental sustainability, public awareness and community involvement in the protection of their immediate environment has continue to mount more pressure on manufacturing industries especially palm oil mills in Malaysia to control environmental pollution.

Sporadic research has been performed and new methods and technologies have been developed to find approachable solutions for managing POME, yet palm oil mills are still struggling to meet up with more stringent limits of effluent discharge allowed. By 1984, law on effluent discharge in Malaysia limits the Biological Oxygen Demand (BOD), a measure of effluent strength, to 100 parts per million (PPM). However, in environmentally sensitive areas of Sabah and Sarawak like Kinabatangan River, Department of Environment (DOE) Malaysia had imposed a more stringent condition of 20 ppm since 2006. For example, for new mills, a 20-ppm BOD requirement coupled with land irrigation has been imposed in Sabah. In very sensitive areas, the DOE has even imposed a zero discharge requirement

There are more than 430 palm oil mills in Malaysia, of which 55 mills are in Sarawak and 124 mills in Sabah, making the state the largest crude palm oil (CPO) producer in Malaysia [1]. Based on these new challenges being faced by palm oil mills, there is urgent need for the palm oil mills in Malaysia to explored and take advantage of the current available options or additional alternative to improve their environmental performance. This paper provides the outcome of the preliminary studies carried out on the feasibility and sustainability of the palm oil mills acquiring and adopting the zero discharge technology to achieve zero discharge concepts.

II. WORLD PALM OIL PRODUCTION

Nigeria was the largest exporter of palm oil and palm kernels until 1934 when the country was surpassed by Malaysia. Malaysia and Indonesia had surpassed Africa's total palm oil production. According to oil palm review, published by the Tropical Development and Research Institute (TDRI) in the United Kingdom, over 3 million tonnes of palm oil was produced by Malaysia alone in 1983, compared with about 1.3 million tonnes of Africa production. In 1995, Malaysia was the world's largest producer with a 51% of world share, but since 2007, Indonesia has been the world's largest producer, supplying approximately 50% of world palm oil volume.

Worldwide palm oil production during the 2005-2006 growing season was 39.8 million metric tonnes, of which 4.3 million tonnes was in the form of palm kernel oil. However many economists predict palm oil will be the leading internationally traded edible oil by the year 2012. Table 1.2 is records of 2012 world palm oil production [3]

Table 1.2; 2012 World Palm Oil Production [3]

Rank	Country	Production (1000 MT)
1.	Indonesia	28, 000.00
2.	Malaysia	19, 000.00
3.	Thailand	1,700.00
4.	Colombia	900.00
5.	Nigeria	850.00
6.	Papua New Guinea	530.00
7.	Ecuador	510.00
8.	Cote'd Ivoire	300.00
9.	Brazil	275.00
10.	Honduras	252.00

2.1. Production of Palm Oil and Palm Kernel Oil in Malaysia

Palm oil production in Malaysia has increased over the years, from 4.1 million tonnes in 1985 to 6.1 million tonnes in 1990 and to 16.9 million tonnes in 2010. It reached 18.9 million tonnes in 2011 and in 2012 the production was estimated to be at 19.4 million tonnes [3]. The Malaysian palm oil industry easily meets the

local oils and fats demand, and the excess are exported. Palm kernel oil production in 1999 was 1.3 million tonnes, and reached 4.7 million tonnes in 2011. Prior to 1970, most of the palm kernels produced was exported. Since 1979, they were crushed locally to produce crude palm kernel oil and palm kernel cake. Malaysia currently accounts for 39 % of world palm oil production and 44% of world exports. If taken into account of other oils & fats produced in the country, Malaysia accounts for 12% and 27% of the world's total production and exports of oils and fats. Being one of the biggest producers and exporters of palm oil and palm oil products, Malaysia has an important role to play in fulfilling the growing global need for oils and fats sustainably. [1].

III. GENERATION OF WASTES FROM PALM OIL MILLS

The processing of oil palm fresh fruit bunches (FFB) primarily for palm oil also results in concomitant production of wastes. According to [4], during processing in palm oil mill, more than 70% (by weight) of the processed FFB is usually left over as oil palm wastes. The wastes products from oil palm processing consist of oil palm trunks (OPT), oil palm fronds (OPF), palm oil mill effluent (POME), empty fruit bunches (EFB), palm press fiber (PPF), shell, palm oil mill sludge (POMS), and palm kernel cake (PKC) [5, 6] According to [7] fiber, shell, decanter cake and EFB accounts for 30, 6, 3, and 28.3% of the FFB respectively.

Palm kernel oil (white palm oil) is obtained from the seed known as kernel or endosperm. When oil has been extracted from the kernel, what remains is known as 'palm kernel cake (PKC). This is rich in carbohydrate (48%) and protein (19%) [8]. POME is generated mainly from oil extraction, washing and cleaning processes in the mill and these consists of water soluble components of palm fruits as well as suspended cellulosic materials like palm fiber, fat, grease and oil residues [9]. Among the wastes that are generated from processing of oil palm fruits, POME is considered the most harmful waste for the environment if discharged untreated. [10].

3.1. Records of Generation of Pome by Palm Oil Mills in Malaysia

It has been estimated that about 26.7 million tonnes of solid biomass and an average of 30 million tonnes of POME were generated from 381 palm oil mills in Malaysia in 2004 [11]. Based on palm oil production in 2005 of 14.8 million tonnes, an average of about 53million m^3 POME is being produced per year in Malaysia [12]. However [13], reported that 66.8 million tonnes of POME were generated in 2005. Based on the statistical value of total CPO production in May 2011, the production of 985,063 tonnes of CPO means a total of 1.5 million m^3 of water was used, and 738,797 m^3 was released as POME, in that month alone. [11], in their estimation stated that about 0.5- 0.75 tonnes of POME would be generated from mill for every ton of fresh fruit bunch. However, for a well-run mill with good housekeeping, it is estimated that 2.5 tonnes of POME are generated for every ton of CPO produced. However, the national average is about 3.5 tonnes of POME per ton of CPO. This is an indication of increase in generation of POME in tonnes as production and processing of palm oil continue to rise to meet both domestic and global demand.

3.2. Palm Oil Mill Effluent (POME)

The extraction of palm oil involves a number of steps; fruit bunch sterilization, stripping, digestion, pressing, clarification, purification, and vacuum drying. When these entire steps are added together, a significant amount of water is needed for a palm oil mill's operations. On average, it is estimated that for 1 ton of crude palm oil produced, 5-7.5 tonnes of water are required, and more than 50% of the water will end up as POME [14]. Raw POME is a colloidal suspension containing 95%-96% water, 0.6-0.7% oil and 4-5% total solids including 2-4% suspended solids that are mainly consisted of debris from palm fruit mesocarp generated from three main sources, namely sterilizer condensate (36%), separator sludge or clarification (60%) and hydro cyclone (4%) wastewater [15, 16]. The typical characteristic of individual wastewater streams coming out of palm oil mill from the three main source of generation is given in Table 2.3[17]

Table 2.3: Characteristics of individual wastewater streams [17]

Parameters	Sterilizer condensate	Oil clarification wastewater	Hydro cyclone wastewater
pH	5.0	4.5	-
Oil & Grease	4,000.0	7,000.0	300
BOD; 3-day, 30°C	23,000.0	29,000.0	5,000
COD	47,000.0	64,000.0	15,000
Suspended solid	5,000.0	23,000.0	7,000
Dissolve solid	34,000.0	22,000.0	100
Ammonical Nitrogen	20.0	40.0	-
Total Nitrogen	500.0	1,200.0	100

* All the units are in mg/L except for pH

The raw or partially treated POME has an organic matter, which is due in part to the presence of unrecovered palm oil [14]. This highly polluting wastewater can therefore cause pollution of waterways due to oxygen depletion and other related effects as reported by [14]. The depletion of the oxygen level in rivers leads to anaerobic conditions and the release of noxious gases, particularly hydrogen sulphide. Thus, the natural ecology of the rivers is destroyed, [18]. In Malaysia, POME produces 25 million tonnes per year of chemical oxygen demand (COD), [19].

3.3. Characteristics of POME

POME composition depends mainly on the season, raw material quality and the particular operations being conducted at any given time. POME, when fresh, is a thick brownish colloidal mixture of water, oil and fine suspended solids. It is hot (80-90 0^{C}) and possesses high amounts of total solids (40,500 mg/l), very high Biochemical Oxygen Demand (BOD) (25,000 mg/l), Chemical Oxygen Demand (COD) (50,000 mg/l), oil and grease (4,000 mg/l), [16]. The effluent is non-toxic, as no chemicals are added to the extraction process [18, 20]. Typically, POME is low in P^{H} because of the organic acids produced in the fermentation process; it is acidic with a P^{H} of around 4.5 as it contains organic acids in complex forms that are suitable to be used as carbon sources [21]. POME consists of water soluble components of palm fruits as well as suspended materials like oil residues, short palm fiber, cell walls, organelles, a variety of carbohydrates ranging from cellulose to simple sugars, a range of nitrogenous compounds from proteins to amino acids, free organic acids and assembly of minor organic and mineral constituents [22]. Nutrients contains in POME according to [23] and [24], are nitrogen, phosphorus, potassium, magnesium and calcium, which are the vital nutrient elements for plant growth.

Due to the non-toxic nature and fertilizing properties, POME can be used as fertilizer or animal feed substitute, in terms of providing sufficient mineral requirements.

[24] reported that POME contains high content of A1 as compared to chicken manure and composted sawdust According to [23], toxic metals, such as lead (Pb), can also be found in POME, but [25], reported that Pb concentrations are usually below sub lethal levels (>17.5 ug/g). According to [24], Pb is found in POME as a result of contamination from plastic and metals pipes, tanks and containers where Pb is widely used in paints and glazing materials.

Despite its biodegradability, POME cannot be discharged without first being treated because it is acidic and contains residual oil that cannot be easily separated using conventional gravity-based systems. Essentially, this oily mix needs a lot of oxygen before it can decompose completely, and this phenomenon is called having a high biochemical oxygen demand (BOD), and raw POME can sometimes have a BOD of up to 100 times higher than that of domestic sewage.

POME even when treated, still imposes a demand on the environment as is still contains a significant amount of organic matter. Microbes in water take in dissolved oxygen as they digest organic matter. This demand for oxygen known as biochemical oxygen demand (BOD) is usually measured in milligrams per liter (mg/l) and is widely used as an indication of the organic quality or the degree of organic pollution of water; a higher BOD means poorer quality, and the inverse holds true as well.

Generally, the microbial population increases in proportion to the amount of food available. In such instances, the microbial action will consume dissolved oxygen faster than atmospheric oxygen can dissolve in the water. When that happens, fish and other aquatic life might die because of depleted oxygen. Raw or untreated POME is characterized by high BOD, often in the range of 25,000gm/l or higher as shown in Table 2.3.

3.4. Pollution by POME from Palm Oil Mills

During the last century, a great deal of research and development as well as application has been devoted to pollution control advance technologies for treatment and management of both solid and liquid waste generated from palm oil mills. The major reason for such huge efforts is that waste generation from palm oil mills have been declared as one of the major source of environmental pollution. For every metric ton of palm oil produced, 2.5metric tonnes of effluent (POME) are generated from processing in palm oil in mills. Direct release of this effluent causes freshwater pollution, which can affect downstream biodiversity and people [26]. In Malaysia, the total production of crude palm oil in 2008 was 17,734,441tonnes.

However, the production of this amount of crude palm oil results in even larger amounts of palm oil mill highly polluting effluent that were mostly discharged directly into environment especially by small and medium palm oil mills operators. In 1983, more than 7.5 million metric tonnes of POME was generated in Malaysia and POME has been singled out as the chief contributor to Malaysia's environmental pollution. [27].

Palm oil mills discharged palm oil effluent into environment in its raw form. Studies on the effect of palm oil effluent on soil showed that raw POME is acidic and alters microbiological and physico-chemical properties of soil, which ultimately affects soil fertility. [28]. Anthropogenic release of greenhouse gases (CO_2 and CH_4) from palm oil mills during anaerobic digestion of POME has been recognized as one of the main causes of global warming which contribute to climate change all over the world. Several measures under the Kyoto Protocol 1997 have been drawn up to reduce the greenhouse gases emission. One of the measures is Clean Development Mechanisms (CDM). In Malaysia, palm oil industry particularly from palm oil mill effluent (POME) anaerobic treatment has been identified as an important source of methane. In a research to investigate the actual greenhouse gases emission from Lagoons and open digesting tank in palm oil mills, the result indicated that methane contribution to biogas released from the open digesting tank and lagoon system were 35% and 45% respectively. Also in a study to quantify the actual CH_4 emission from the open digesting tanks in Felda Serting Hilir palm oil mill Malaysia, the CH_4 emission pattern recorded for 52 weeks from 3600 metric tonnes was between 13.5% and 49.0%. The total CH_4 emission per open digesting tank was 518.9kg per day [29]. Consequently, similar situations have been reported in countries like Thailand, Indonesia, and Nigeria that are into large-scale palm oil production.

IV. CHALLENGES FACED BY PALM OIL MILLS

The United Nations Conference on Environment and Development (UNCED) 1992 in chapter 21 of its Agenda 21 observed that environmentally sound management of waste to control environmental pollution was among the environmental issues of major concern in maintaining the quality of Earth's environment and especially in achieving environmentally sustainable development in countries of the world. It went further to say that effective control of generation, storage, treatment, recycling and reuse, transport, recovery and disposal of wastes is of paramount important for health, environmental protection, natural resource management and sustainable development. It therefore becomes imperative for the palm oil mills to have modern, advance, and sustainable technologies to handle and manage its waste in a proper and environmentally sound manner to control environmental pollution. There is no gain in improving the economic and welfare of the people and only for them and their environment to be polluted because of indiscriminate discharge of waste especially POME by palm oil mills.

In the past, when the industry was at its infancy in 1960's, palm oil mills usually discharged either partially treated or raw POME into nearby rivers as this was the easiest and cheapest method for disposal. However, excessive quantities of untreated POME deplete a water body of its oxygen and suffocate aquatic life, and many small rivers have been devastated by such discharges. The problem of pollution accruing from a mere 92,000 tonnes production by only 10 mills was not apparent then. The environment could somehow absorb these wastes.

This lackadaisical attitude did not last long. By the 1970's the growth of the industry was literally exponential, bringing along with it pollution which the waterways could no longer handle, so much so that palm oil processing became synonymous with POME pollution. Tone for ton, the oxygen depleting potential of raw POME is 100 times that of domestic sewage. The industry was faced with a major problem, virtually completely lacking in any proven technology to treat POME. Committed to overcome the problem, the government and the industry worked together to source for treatment technologies that are environmentally and economically sound. Bear in mind, none was available anywhere in the world then to specifically treat POME. This government-industry synergy towards common goal-pollution abatement paid off handsomely. Systems for treatment of organic industrial wastes were successfully adapted for POME treatment. The three most commonly used systems were ponding system, open tank digester and extended aeration system, and closed anaerobic digester and land application systems. [1]. However, the growing international concern about the environmental

sustainability, public awareness and community involvement in the protection of their immediate environment has continue to mount more pressure on manufacturing industries especially palm oil mills in Malaysia to control environmental pollution.

Malaysia has been identified as the country that produces the largest POME pollution load in the river [13]. Due to this fact, the palm oil industry faces the challenge of balancing the environmental protection, its economic viability and sustainable development. Therefore there is urgent necessity to find an approach to preserve the environment while keeping the economy growing.

Sporadic research has been performed and new methods and technologies have been developed to find approachable solutions for managing POME, yet palm oil mills are still struggling to meet up with more stringent limits of effluent discharge allowed. By 1984, law on effluent discharge in Malaysia limits the BOD, a measure of effluent strength, to 100 parts per million (PPM). However, in environmentally sensitive areas of Sabah and Sarawak like Kinabatangan River, Department of Environment (DOE) Malaysia had imposed a more stringent condition of 20 ppm since 2006. For example, for new mills, a 20-ppm BOD requirement coupled with land irrigation has been imposed in Sabah and in very sensitive areas; the DOE has even imposed a zero discharge requirement.

Over the last two decades, several treatment and disposal technologies have been successfully developed and used to treat POME [30]. They were all designed and constructed to meet a discharge limit of 100mg per liter BOD. They consist of conventional biological systems using anaerobic and aerobic or facultative processes. If operated according to design criteria and maintained well, the processes are able to treat POME to the discharge limits set by the DOE Malaysia.

Although, anaerobic digestion is the most suitable method for the treatment of effluents containing high concentration of organic carbon such as POME [31]. Anaerobic digestion according to [32], has been proven unique and the most beneficial stabilization technique as it optimizes cost effectiveness, is environmentally sound, minimizes the amount of final sludge disposal, and has the ability to produce a net energy gain in the form of methane (CH_4). The processes, being biological, rely on suitable bacteria to break down the organic matter (pollutants) and, consequently, reduce the BOD of the effluent. The end- products of anaerobic degradation are biogas (consisting of about 65% methane (CH_4), 35% carbon dioxide (CO_2) and trace amounts of hydrogen sulphide) and sludge. At the mill, POME is collected in a sludge pit and retained for a day or two to allow the residual oil to rise and be skimmed off before being pumped to a treatment plant. It is important to ensure that as little oil as possible gets into the treatment plant as; otherwise, the efficiency of treatment will be compromised. Anaerobic digestion of POME generates vast amounts of biogas, about 28 cubic meters per ton of POME treated. Both CH_4 and CO_2 are greenhouse gases and CH_4 is more potent. Biogas is also corrosive and odorous. Thus its emission to environment is undesirable and this has been seen as the main disadvantage and challenges faced by palm oil mills in the use of anaerobic method for treatment of POME. However, production and recovery of biogas during anaerobic digestion of POME can be turn into economic advantage and means of achieving zero discharge concepts if the palm oil mills would acquire and adopt available current advance technologies that have capacity to harness biogas for heat and electricity generation.

This study, apart from its quest to establish the feasibility of zero discharge concepts in palm oil mills. It also explored the challenges faced by palm oil mills in their effort to meet up with new stringent regulations and growing awareness of need not to pollute. Consequently a reliable and sustainable means of achieving this fits as mentioned earlier is by acquiring and adopting of current advance POME treatment methods or technologies that can harness the biogas that are generated during anaerobic digestion of POME. This has been agreed as one of the best environmental practices that will guaranty zero discharge concepts.

V. POLLUTION CONTROL AND ZERO DISCHARGE CONCEPTS

United States America (USA) congress, the United States Environmental Protection Agency (EPA), and environmental professionals concluded in the 1980s that a new industrial waste management philosophy was needed if the ever-expanding industrial pollution and resource depletion problems were to be solved, [33]. They argued that indiscriminate use of virgin resources in manufacturing and subsequent end-of –pipe treatment of resulting wastes would not provide the resource sustainability and environmental quality demanded by the public. As a result, a new paradigm was developed which emphasized minimizing the use of harmful or overexploited resources and eliminating or minimizing waste production at the source in the industry's product area. This philosophy became known by many names, including waste minimization, source reduction, waste reduction, green engineering, and sustainable engineering, but the name that is most often associated with it is pollution control.

Pollution control is a term used to described production technologies and strategies that result in eliminating or reducing waste streams. The U.S. EPA defines pollution control or prevention as; the use of

materials, processes or practices that reduce or eliminate the creation of pollutants or wastes at the source. It includes practices that reduce the use of hazardous materials, energy, water or other resources and practices that protect natural resources through conservation or use that is more efficient. .
Thus, pollution control includes both the modification of industrial processes to minimize the production of wastes and the implementation of sustainability concepts to conserve valuable resources. However, "zero discharge concepts" is a new idea, strategy, or proposal that involved an industrial processes design, pollution control plan, and or environmental management system to prevent release of any harmful or toxic material to the environment. (Authors). Pollution control activities range from product change to process changes in method of operation. The main premise underlying pollution prevention according to [35], that it makes far more sense for a generator not to produce waste than to develop extensive treatment schemes to ensure that the waste poses no threat to the quality of the environment and this assertion is likened to "zero discharge concept" which this study seeks to establish its possibility in palm oil mill industry in Malaysia that is striving hard to change its present image as environmental polluters.

VI. RESEARCH METHODOLOGY

Data for this research were collected between September 2012 to March 2013 by means of a questionnaire survey mailed to 86 palm oil mills located in both Sarawak and Sabah in Malaysia as a pilot project. The questionnaire explored a range of issues relating to the treatment and management of palm oil mill effluent (POME). In this research, emphasis was placed on the type(s) of technologies palm oil mills are presently using for POME treatment and most importantly focused on the possibility and feasibility of palm oil mills in Malaysia acquiring and adopting the current advance POME treatment technologies to achieve clean production and ultimately zero discharge concepts.
The response rate of 58% was achieved. The questionnaire explored the following aspects of POME treatment and management in palm oil mills;

- Is POME the most difficult waste to handle by palm oil mills?
- Which method(s) or technology does palm oil mills used in treating POME?
- Knowledge of availability of current advance POME treatment technologies by palm oil mills.
- Willingness of the palm oil mills to acquire current advance POME treatment technology as option for clean production and means of achieving zero discharge concepts.

The responses received were coded and entered into the SPSS database and analyzed using mean, ANoVa, t-test and correlation functions since in this research, what [36] referred to as complex research approach (combination of more than one type of research approach) was adopted. However, according to [37], a number of studies have been reported in the literature, including [38], [39], [40], [41], [42], [43], and [44]; all supports the use of means, percentage and frequency to be used as part of analysis especially for descriptive or exploratory studies.

Consequently, review of the case studies, pilot projects on current advance POME treatment technology in Malaysia palm oil mills and analysis of the data obtained from the palm oil mills formed the direction and position of this study on the feasibility or other wise of zero discharge concepts in palm oil mills in Malaysia.

VII. FINDINGS AND DISCUSSION

7.1 POME as a Difficult Waste from Palm Oil Mills

Although, different types of wastes are generated during processing of oil palm fresh bunches (FFB). According to Prasertan and Prasertan (1996), during processing of FFB in the palm oil mills, more than 70% (by weight) of the process FFB is usually left over as oil palm wastes. The wastes products from oil palm processing consists of oil palm trucks (OPT), oil palm fronds (OPF), empty fruit bunches (EFB), palm press fibers (PPF), palm kernel cake (PKC), shell, palm oil mill effluent (POME) and palm oil mill sludge (POMS) [5, 6].
Respondents were asked to provide their response on which of the wastes generated by them is more difficult to handle or manage. From the simple statistic percentage, 100% of the respondents claimed that POME is the most difficult waste to manage by the mill and these are some of the reasons given by the operators.

- The volume by weight of the POME generated per one ton of FFB is enormous.
- During POME treatment to reduce the level or strength of BOD and other parameters, other by products like biogas, sludge etc. are generated.

- It involved a lot of labor, required a lot of time, close monitoring and too expensive to achieve the required BOD level of 20ppm or less before final discharge.

Obviously, these are also some of the reasons why majority of palm oil mills discharged either partially or untreated POME into nearby rivers as reported several times happened at Kinabatangan and Tenaggang rivers all in Kota Kinabalu. In Mukah land District, Oya-Dalat land District and Miri-Bintulu all in Sarawak, various palm oil mills were fined between RM 18,000 (US $ 6000) to RM 25,000 (US $ 8333) and three months imprisonment each after the owners pleaded guilty to the charge framed against them under section 16 (1) of the Environmental Quality Act 1974 and punishable under section 16 (2) of the same act. The operators were found guilty of discharging POME into watercourse. All the liquid wastes discharged into the watercourse were found to contain substances in concentration exceeding the stipulated limits under regulation 12 (4) Environmental Quality (Prescribed Premises) (Crude Palm Oil) Regulations, 1977.
According to the report by Borneo Post online, the mills were prosecuted by the Department Of Environment Officers. [45]

7.2 Methods or Technologies Palm Oil Mills used in treating POME

The cheapest way of discharging POME is to either disposed it on the land inform of land application or release it into the river untreated, since POME is a non-toxic oily waste. Nevertheless, discharging of POME into water bodies cause water depletion and results in aquatic pollution [46]. Over the last two decades, several treatment and disposal technologies have been successfully developed and used to treat POME [30]. They were all designed and constructed to meet a discharge limit of 100mg per liter BOD. These methods or technologies consist of conventional biological systems using aerobic and anaerobic and or facultative processes. If operated according to design criteria and maintained well, the process are able to treat POME to the discharge limit set by Malaysia Department OF Environment (DOE). However, type of method or technology currently implored by mills was reflected in the questionnaire responses. The percentage calculated from the survey responses provided 97% respondents claiming the use of ponding system of aerobic and anaerobic process in treating their POME.

Aerobic and anaerobic processes are biological treatment systems that rely solely on microorganisms to break down pollutants and they need proper maintenance and close monitoring. Microorganisms are very sensitive to change in their environment and hence, great care must be taken to maintain the condition in which they thrive. This requires the attention of skilled operators, and the commitment of management. Unfortunately, the palm oil industry still considers wastewater treatment a burden rather than as part of the production process, let alone a profit opportunity. Undoubtedly, this aspect has the lowest priority in the maintenance budget. As a result, according to [30] most palm oil mills are not always able to comply with the discharge limits. According to [31], anaerobic process is a suitable treatment method due to the organic characteristic of POME. Therefore, ponding system is the most conventional method for treating POME in Malaysia, [18, 47].

The pond system has been applied in Malaysia for POME treatment since 1982 and they are classified as waste stabilization pond [48]. [48], reported that more than 85% of palm oil mills exclusively use ponding systems due to their low cost. Ponding systems are easy operating systems but [48] and [49] argued that they have some disadvantages, such as occupying a vast amount of land mass, relatively long hydraulic retention time (HRT) of 45-60 days for effective performance, bad odor and difficulty in maintaining the liquor distribution and biogas production which results into harmful effect on the environment when allowed into atmosphere. However, production of biogas during anaerobic treatment of the POME has been considered as the main challenge being faced presently by the operators of the palm oil mills. Consequently, the management and utilization of this biogas as a source of renewable energy to control pollution aiming to achieve zero discharge concept is the focus of this study.

7.3 Knowledge of the Availability of the Current Advance POME Treatment Technologies by Palm Oil Mills Operators

Dozens of methods and technologies have been developed to treat and control POME pollution. This implied that, there is availability of various new advance POME treatment technologies that are ready to be acquire and use by palm oil mills. Nevertheless, the question is, does the palm oil mills operators have knowledge of the availability of these technologies? This study explored this question by asking the respondents if they have knowledge about these new advance technologies. A number of new technologies and methods were listed in the questionnaire and multiple responses were allowed. Overall, 86% of the respondents claimed to have knowledge of the new advance technologies and 2% of these respondents also claimed to be involved in research and development of new technology in collaboration with universities and research institution in and

outside Malaysia. On the other hand, 14% of the respondents claimed not to have knowledge about availability of new advance POME treatment technologies.

There have been reports and review of literature on various new advance POME treatment technologies that has been tested and proven effective through a plot projects. Some are however still at the testing stage. A collaboration between Shanghai Jiao tong University and Malaysia's own Ronser Bio-Tech Sdn Bhd offered two proprietary systems called AnaEG and BioAX for evaluation at a pilot plant at Labu Negri Sembilan. The five tons per hour pilot plant at Labu is intended to demonstrate that is possible to achieve a zero emission of POME into environment. The plant is designed to be able to generate biogas at a rate of 150 cu. meters per hour, produce sludge that can be used as fertilizer, and produce wastewater that is good enough for boiler use. The first stage of the plant will see to the recovery of waste oil from POME, before the sludge is treated by the AnaEG or BioAX processes. The biogas that is produced will be captured for power generation by burning them in gas engines, while some solid high-potash fertilizer is also recovered. The final bits involve membrane separation, followed by ultrafiltration, and reverse osmosis, to produce clean water as shown in Fig 1.

Figure1. Pilot project of Ronser Bio-Tech's Zero Discharge POME treatment technology at Labu, Negri Sembilan

A new palm oil mill in Bintulu, Sarawak has also order a turnkey plant for effluent treatment and biogas recovery system. The advance technology is to be referred to as Membrane Bio Reactor (MBR), a wastewater treatment method that combines a membrane and bio treatment (Anaerobic), which the company has confirmed its performance based on the site pilot tests for two years.

Veolia Water Solutions and Technologies officially lunched and announced its Pomethane technology during 2012 POMREQ Conference in Malaysia. Veolia's Pomethane Technology offers affordable, greener solution to treat POME. Pomethane technology has already been implemented by several Southeast Asian companies, including Felda, Malaysia's largest crude palm oil producer. Pomethane, according to the company represents a best practice application for managing palm oil industrial waste through an anaerobic thermophilic digestion process. Some of the important benefits derivable from Pomethane Technology are;

- ✓ Technical solution that meets Clean Development Mechanism (CDM) requirement
- ✓ Economic efficiency
- ✓ In compliance with International Environmental Standards
- ✓ Environmental friendly and
- ✓ Renewable energy product

In addition, the anaerobic digestion of POME by use of thermophilic bacteria in Pomethane Technology provides a number of advantages compared to the conventional mesophilic bacteria;

- The retention time is significantly shorter at thermophilic operating conditions which results in a reduction of the digester tank size and thus capital cost and maintenance
- Thermophilic bacteria are capable of digesting more complex degradable substances, which may not be

degraded by mesophilic bacteria. This results in an increase of the biogas yield.

- At mesophilic temperature range fungi and viral may grow in the substrate thus causing potential health hazard from the effluent. Unwanted Microbiology will not survive in the thermophilic temperature range.
- The effluent from the secondary digester will run through a clarifier system.
- The effluent from the clarifier will be treated in the downstream wastewater treatment system.
- A part of the sludge will be recycled to the digester and the excess sludge can be composted after further decanting or taken straight to the plantation as fertilizer.

Finally, Pomethane Technology has the capacity to remove COD exceeding 90% and final effluent discharge of BOD < 20 PPM.

Other new advance POME treatment technology that has also been reported is Camco Southeast Asia. A regional clean energy company, planned to build a 2-megawatt biogas project in Malaysia that will make use of methane pollutants found in POME from palm oil mills. The US $ 4 million project is part of a 13 years "build-own-operate-transfer" agreement between Camco and the mill owner. Under the terms of agreement, the mill owner will provide adequate POME feedstock free for the entire duration of the contract. The biogas project will use anaerobic digestion technology for breaking down biodegradable material in the absence of oxygen.

In a related development, Alambumi Palm Oil Mill has also entered into collaboration agreement with Konzen Clean Energy Sdn Bhd to develop a CDM project at Alambumi Palm Oil Mill in Miri. Divided into two phases, the first phase would involve building up a closed anaerobic tank digester to capture methane gas costing around RM 7.5 million (US $ 2.5 million) and the second phase would be biogas utilization costing around RM 7 million. (US $ 2.3 million). However, this will be Konzen's second biogas CDM project from palm oil mill effluent in Sarawak after Rinwood Pelita Palm Oil Mill in Mukah.

Professor Abdul Latif Ahmad of Universiti Technologi Malaysia (UTM) and his team invented a system, which he claimed could turn palm oil waste into drinking water. The invention is called the "Novel membrane-based treatment system which turns POME into crystal clear drinking water. According to inventor, the technology required four steps to treat the waste before it became clean enough to drink. The environment-friendly technology is set to reduce water pollution, as it will help ensure zero discharge of palm oil waste into rivers.

7.4 Willingness of the Palm Oil Mills to acquire and adopt the Current Advance POME Treatment Technology

There is no doubt that the current advance POME treatment technologies has been developed and found to be effective by various organizations as clearly mentioned earlier. The target was to help palm oil mills to achieve zero discharge concepts and to maximize the utilization of biogas generated during POME treatment as a source of renewable energy. On records, the technologies are also available in global biogas plants market. As stated earlier 86% of the palm oil mills captured in this study claimed to have knowledge of availability of new advance POME treatment technologies (PTT). However, the willingness of palm oil mills operators to acquire and adopt the new technology was reflected in the questionnaire responses. The respondents were asked to choose either "YES", "NO" or "NOT SURE" to state their willingness of acquiring and adopting the new technology. 36% of the respondents choses "YES" indicating "Willingness". While 41% of the respondents' choses "NO" indicating "Unwillingness" and 23% of the respondents choses "NOT SURE" indicating neither YES or NO. The results of this survey revealed that despite the need for the palm oil mills to meet up with the new stringent condition of 20ppm BOD and imposed zero discharge requirements by Malaysia Department of Environment, many palm oil mills are not still willing and ready to acquire and adopt the new advance POME treatment technology.

This category of the palm oil mill operators clearly advanced the following reasons for their position. In some cases, millers claimed that utilization of biogas for power generation required a high initial capital to acquire a new plant. Many argued that the government call for millers to become green independent power producers (IPPs) is not practical. According to the millers, there are still no clear-cut biomass and biogas policy and sufficient incentives to convince them to go into such projects. The mill operators argued that until the government provide more attractive incentives for palm oil industry. This will encourage the millers to acquire the new advance POME treatment technology that enable them make full use of the biogas to first generate electricity for their mills and gradually selling its electricity to the national power grid where ever possible. One of such attractive incentive according to the millers is to increase the tariff on green energy from $ 0.21 per unit to between $ 0.29 and 0.40 per unit.

VIII. CONCLUSION

This paper has presented the key findings from the survey mailed to 86 palm oil mills located in Sarawak and Sabah in Malaysia. Although this is a pilot project, the survey results provide an overview of the position of the palm oil mills operators on current advance POME treatment technology in relation to achieving zero discharge concepts in their operations. The survey attempted to identify the key issues about the current advance POME treatment technologies in respect to feasibility of zero discharge concepts in palm oil mills in Malaysia.

The results shows that, although palm oil mills generate a lot of different types of wastes during processing of FFB, according to the operators and available literature POME is the most difficult and expensive waste to manage. This is because POME contains large quantity of pollutants that are harmful to the environment. Obviously, palm oil mills cannot meet up with the new discharge limits of 20ppm of BOD and zero emission in some sensitive areas using only conventional open ponding system. Therefore, there is need for paradigm shift from the conventional ponding system that is popular among palm oil mills in Malaysia to the current advance POME treatment technology. The new available technology has been proven effective to guaranty zero emission that improve environmental performance and ultimately curb the industry's environmental footprint. The results also found that majority of the operators generally have knowledge of the availability of the advance and more suitable POME treatment technologies. According to available records and reviewed literatures, some palm oil mills are already collaborating with different research institutions and manufacturing companies in acquiring the new POME treatment plants.

Although, the millers claimed they want to achieve zero emission to improve their environmental performance. The responses from the survey shows that majority of the millers are not willing to acquire and adopt the current technology. This was evident from the reasons they advanced as stated earlier.

Based on the survey, records, reports, and reviewed literatures, the finding of this pilot study can be summarized in the following points;

- Across the globe, current advance POME treatment technologies and or biogas plants are available for palm oil mills to acquire and adopt for clean production.
- Attractive incentives and supports, that were found to be a major factor that will attract the millers to embrace the new technology, are available at both national and international level.
- At the national level, the Malaysia government in her effort to promote green technology development in 2011, provided a found of up 500 million US dollar under the Green Technology Financing Scheme (GTFs). This is to support green technology development in Malaysia, which includes utilization of biomass, and biogas in palm oil industry. Ministry of Science, Technology and Innovation (MOSTI) and Ministry of Higher Education (MOHE) also financially support Malaysia's research and development sector. These ministries provide research grants to qualified institutions to support potential research projects that will promote the utilization of renewable energy sources.

The promotion of utilization of renewable energy sources available in Malaysia was implemented in 2011 under the Small Renewable Energy Program (SREP). Biogas generated from the treatment of POME was identified as one of these potential renewable energy sources. In addition to introduction of the fee-in-tariff (FiT) from US $ 0.09 KW/h onwards. Malaysia government has implemented the promotion of investment Act 1986 (The commissioner of Law Revision, 2006). This Act offers incentives to companies that generate energy from renewable resources that is then either sold to other companies or retained for self-consumption.

The incentives offered include the granting of Pioneer Status (PS), Investment Tax Allowance (ITA), Import Duty, and Sales tax Exemption (ID-STE). PS allows for income tax exemption on statutory income, whereas ITA offers tax allowances on qualified capital expenses. Any palm oil mill that produces biofuel or renewable energy is eligible for the incentive application to encourage the utilization of renewable energy sources. In a related development, commercial banks in Malaysia have also gone into Green Technology Financing (GTF) in view of the potential market for environmental business. Of the foreign commercial bank in Malaysia, Sumitonw Mitsui Banking Corp. of Japan has team up with the Federation of Malaysia Manufacturers (FMM) to provide RM 632 million (USD 200 million) financing for local manufacturers. It was first kind of financing from a commercial bank to be used on green initiatives such as renewable energy, recycling and waste management project. Other banks offering green financing include HSBC, Maybank, and Standard Chartered Bank.

However, during 6th World Islamic Economic Forum, Malaysia Prime Minister has also proposed the setting up of a Clean Energy Development Bank to boost Eco-sustainable efforts by developing countries of the organisation of the Islamic Conference.

- At the international level, the Clean Development Mechanism (CDM) under the Kyoto Protocol (UNFCCC,

1998) is a scheme to promote sustainable development. It introduces carbon credits through which developing countries can gain profit by trading certified emission reductions (CER), while developed countries can achieve their emission reduction targets by purchasing the tradable carbon credits. The palm oil industry is eligible to earn CER through biogas-methane capture released by POME.

More than five CDM projects from the palm oil industry were approved and issued at least 0.5Mt of CO_2 equivalent CER [50]. Recently, Rinwood Pelite palm oil mill in Miri and Alambumi palm oil mill in Mukah are among the few palm oil mills that have utilized this incentive from CDM project of carbon credits and other income generated from biogas utilization. With the worldwide trend in energy generation using RE, the availability of current advance POME treatment technology and attractive incentives at both national and international level. The prospect of zero discharge concepts and its feasibility in palm oil mills in Malaysia is certain.

Finally, more needs to be done in the aspects of incentives and support from Malaysia government. Green Investment Bank (GIB) for renewable energy, carbons capture and storage and energy efficiency measures recently launched in UK can be replicated and adopted by Malaysia government. More research and development that will result into less expensive technology should be encouraged. More collaboration with the stakeholders in palm oil industry. Awareness campaign through organizations like Round Table Sustainable Palm Oil (RSPO) will greatly influence the millers towards embracing the new advance POME treatment technology to achieve zero discharge concepts in Malaysia.

IX. ACKNOWLEDGEMENT

The authors thank the Universiti Malaysia Sarawak, and Institute of Biodiversity and Environmental Conservation (IBEC) for providing fund and facility used for this Study.

REFERENCES

[1] T.Y.Wu, A.W. Mohammad, J. Md. Jahim, N. Anuar, Pollution control technologies for treatment of palm oil mill effluent (POME) through end-of-pipe processes, *Journal of Environmental Management 91, 2010*, 1467-1490

[2] A. K. Edward, B. B. Daniel, *Environmental science, earth as a living planet (*John Willey & Sons, Inc. UK, 1998). (2)

[3] United States Department of Agriculture (USDA) (2012), *2012 World palm oil production*

[4] S. Prasertsan, P. Prasertsan, Biomass residues from palm oil mills in Thailand: an overview on quantity and potential usage. *Biomass Bioenergy, 11(5),* 1996, 87-395.

[5] H. Aziz, B.T. Abdul, *Reactive extraction of sugars from oil palm empty fruit bunch hydro lysate using naphthalene-2-boronic acid,* Masters diss., Universiti Sains Malaysia, KL, 2007. (13)

[6] R. P. Singh, Composting of waste from palm oil mill: a sustainable waste management practice. *Reviews in Environmental Science and Bio/Technology, 9 (4),* 2010, 331–344.

[7] H.S. Pleanjai, G. Shabbir, G. Savitri, Environmental evaluation of biodiesel production from palm oil in a life cycle perspective, *Proc. JIC Conf. on Sustainable Energy and Environment,* Hua Hin, Thailand, 2004, 1-3.

[8] I.C. Onwueme, T.D. Sinha, Field crop production in tropical Africa, *The Technical Centre for Agricultural and Rural Co-operation*, Ede, Netherlands, 1991, 1–480

[9] P. Agamuthu, Palm oil mill effluent and utilization. In*:* C.A. Sastry, M.A. Hashim, P. Agamuthu, (Ed.). *Waste treatment plant.* (New Delhi Narosa Publishing House, 1995), 338-360.

[10] P. F. Rupani, R.P. Singh, M.I. Hakimi, N. Esa, Review of current palm oil mill effluent (POME) reatment methods : vermicomposting as a sustainable practice, *World Applied Sciences Journal, 11(1),* 2010, 70–81.

[11] S.Yacob, M.A. Hassan, Y. Shirai, M. Wakisaka, S. Subash Baseline study of Methane Emission from open digesting tanks of palm oil mill effluent treatment. *Chemosphere, 59 (3)* 2005, 1575–1581.

[12] A.A.Z. Lorestani, *Biological treatment of palm oil effluent (POME) using an up-flow anaerobic sludge fixed film (UASFF) bioreactor,* doctoral diss., Universiti Sains Malaysia, KL, 2006. (899)

[13] C.S .Vairappan, A.M. Yen, Palm oil mill effluent (POME) cultured marine microalgae as supplementary diet for rotifer culture, *Journal of Applied Physics, 20(5),* 2008, 153-158.

[14] A. L. Ahmad, S. Ismail, S. Bhatia, Water Recycling from palm oil mill effluent (POME) using membrane technology. *Desalination, 157*, 2003, 87-95.

[15] R. Borja, C.J. Banks, Anaerobic digestion of palm oil mill effluent using an up-flow anaerobic sludge blanket reactor, *Biomass Bioenergy*, *6*, 1994, 381-389.

[16] A.N. Ma, Environmental Management for the Oil Palm Industry. *Palm Oil Development*, *30*, 2000, 1-10

[17] Department of Environment Malaysia, *Handbook on industrial processes and the environment: crude palm oil industry* (Aslita Sdn Bhd Kuala Lumpur, 1999). (3)

[18] R. Khalid, W.A.W. Mustafa, External benefits of environmental regulations: resource recovery and the utilization of effluents, *The Environmentalist, 12(4)*, 1992, 277-285.

[19] A. N. Ma, Palm oil mill effluent: A survey, *Proc. PORIM Regional Workshop on Palm Oil Mill Technology and Effluent Treatment*, Serdang, Malaysia, 2001, 233-269.

[20] A.N. Ma, S.A. Cheah, M.C. Chow, Current status of palm oil processing waste management in Yeoh B.G (Ed.) *Waste management in Malaysia, current status and prospects for bioremediation*, 1993, 111–136

[21] M.F. Md Din, Storage of polyhydroxyalkanoates (PHA) in fed-batch mixed culture using palm oil mill effluent (POME). *Proc. 4th JSPS-VCC Conf. on Water Management* Johor, Malaysia 2006, 119-127

[22] E.O. Ugoji, Anaerobic digestion of palm oil mill effluent and its utilization as fertilizer for environmental protection, *Renewable Energy, 10*, 1997, 291-294.

[23] M.A.B. Habib, Nutritional values of chironomid larvae grown in palm oil mill effluent and algal culture, *Aquaculture, 158*, 1997, 95-105.

[24] S. Muhrizal, J. Shamshuddin, I. Fauziah, M.HA.H. Husni, Changes in iron-poor acid sulphate soil upon submergence, *Geoderma, 131*, 2006, 10-122

[25] R. James, K. Sampath, S. Alagurathinam, Effects of lead on respiratory enzyme activity, glycogen and blood sugar levels of the teleost Oreochromis mossambicus during accumulation and depuration, *Asian Fisheries science, 9*, 1996, 87-100

[26] Clay, *World Agriculture and the Environment*, 2004, 219

[27] T.Y. Wu, A.W. Mohammad, J.M. Jahim, N. Anuar, A holistic approach to managing palm oil mill effluent (POME): Biotechnological advances in the sustainable reuse of POME, *Biotechnology Advances, 27*, 2009, 40-52

[28] C. Bek-Nielsen, G. Singh, T.S. Toh, Bioremediation of palm oil mill effluent, *Proc. 16th PORIM International Palm Oil Congress*, KL, Malaysia. 1999.

[29] S. Yoshihito, Reduction of methane released from palm oil mill lagoon in Malaysia and its countermeasures; Mitigation and adaptation strategies for global change. *Kluwer Academic Publishers, 8*, 2003, 237-252.

[30] A.N. Ma, Treatment of palm oil mill effluent. In: G. Singh, K.H. Lim, T. Leng and L.K. David, (Ed.), *Oil palm and the environment: a Malaysian perspective*, (Malaysian Oil Palm Growers' Council Kuala Lumpur, 1999,) 113-126

[31] M. Perez, L. I. Romero, D. Sales, Organic matter degradation kinetics in an anaerobic thermophilic fluidized bed bioreactor, *Anaerobe, 7* 2001, 25-35.

[32] L. De Baere, Anaerobic digestion of solid waste: state-of-the-art, *Water Science and Technology, 41* 2000, 283-290.

[33] P. L. Bishop, *Pollution prevention* (New York: McGraw Hill) 2000, (2)

[34] U.S. EPA, *Pollution Prevention, EPA 21P-3003*, Washington, DC: EPA, 1991.

[35] H.M. Freeman, Pollution prevention: The U.S. Experience, *Environmental progress, 14*, 1995, 214-23

[36] J. W. Creswell, *Research design: A qualitative, quantitative and mixed method approaches* (Sage Pub. Inc., California, 2009) (3)

[37] A.Zutshi, A. Sohal, Environmental management system adoption by Australasian organizations: part 1: reasons, benefits and impediments, *Technology, 24, 2004*, 335-357.

[38] D. Davies, Middle managers and quality programs: Preliminary survey results, *proc. 2nd In. and 5th NR Conf. on Quality Management*, Australia, 1997, 19-25

[39] B. Sharma, T. Fisher, Does the application of single or combined generic strategies matter? *proc. 2nd In. and 5th NR Conf. on Quality Management*, Australia, 1997, 187-195

[40] A. Preston, I. Saunders, Matching leadership and quality practices in a hospital setting, *proc. 2nd NR Conf. on Quality Management*, Australia, 1995, 59-72

[41] A. Brown, Industry experience with ISO 9000, *proc. 2nd In. and 5th NR Conf. on Quality Management*, Australia, 1995, 147-159.

[42] S. Davenport, C. Grimes, J. Davis, Managers and research collaboration: the case of TBG. *Proc. Conf. on Technology for Manufacturing*, New Zealand, 1997, 19-25 (1)

[43] A. Brown, R. Millen, T.V. Wiele, An empirical investigation of the use of self-assessment practices in the USA, *proc. 2nd In. and 5th NR Conf. on Quality Management*, Australia, 1997, 14-18

[44] G.A. Vargus, C. Cabanas, Social and organizational aspects of quality implementation: a Spanish experience, *proc. on Conf. Decision Sciences Institute 3rd In. meeting*, 1995, 227-229.

[45] Press, www.theborneopost.com/2011/08/26/oil-palm-mills-fined-for-polluting-waterways/

[46] T. K. Hwang, S.M. Ong. C.C. Seow, H.K. Tan, Chemical composition of palm oil mill effluents, *Planter,*

54, 1978, 749-756.
[47] A.N. Ma, A.S.H. Ong, Pollution control in palm oil mills in Malaysia, *Journal of the American Oil Chemists' Society, 62(2)*, 1985, 261-266
[48] C.O. Onyia, Increasing the fertilizer value of palm oil mill sludge: bio augmentation in nitrification, *Water Science and Technology, 44,* 2001, 157-162.
[49] K.K. Chin, S.W. Lee, H. H. Mohammad, A study of palm oil mill effluent treatment using a pond system, *Water Science and Technology, 34,* 1996, 119-123.
[50] M.B. Wahid, *Biogas utilization in palm oil mills*, (Malaysia Palm Oil Board, Kuala Lumpur, Malaysia, 2009). (2)

American Journal of Engineering Research (AJER)
e-ISSN : 2320-0847 p-ISSN : 2320-0936
Volume-02, Issue-10, pp-253-257
www.ajer.org

Research Paper Open Access

Cyber laws encompassing the Security of E-Quran in Saudi Arabia

Naasir Kamaal Khan
Department of Computer Engineering, Jazan University, Jazan, Kingdom of Saudi Arabia

Abstract: - Past two decades in the world have seen tremendous growth in the use of Information Technology in almost every field of daily life. We have seen abrupt changes in the society and paper world is completely changed to electronic world. The use of electronic format of storing, processing and retrieval of data made ease for the human kind in a multidimensional way which influences the human being in all the aspects of life. The growth of using Holy Quran for reading and learning through electronic mode is increasing day by day. As there are always two faces of a coin, the other side shows the risks and vulnerabilities associated with the use of e-Quran. With over 1.5 billion of Muslim population in the world, several calls were raised in the Islamic countries to establish a law suitable to handle computer crimes which matches the Islamic Shariah law. In this paper threats associated with the use of digital format of Quran and existing cyber laws associated with it, are discussed, both in the Kingdom and worldwide. The author conducted on extensive review of published literature on a number of computer crime laws developed by many countries, which includes Texas Computer Crime Law, Anticrime act 2007 of Saudi Arabia and cyber laws in other countries of Middle East. Lastly author proposes the amendments in the latest version of Cyberlaws for securing the Holy Quran, in the light of present Anticrime act of World especially in Middle East as computer crime is of a global nature and the present penalties associated with Modification and fabrication of electronic data is not enough when we talk about the holy book Quran.

Keywords: - *Piracy; Cyber Laws; Texas Law; Islamic Law; e-Quran.*

I. INTRODUCTION

Information Technology is rapidly growing field in the modern era. The electronic form of data storage, processing and retrivel has completely removed the paper world. The use of data in electronic form facilitates its user to carry it anywhere without any intervention of physical boundry. The compulsion of size and space has also been vanished. But the darker aspect of this technology has also a great impact, which can not be neglected.Tremendous growth in computer and Internet users since last few years increases the problem manyfold. Computer is now not limited to corporate, business or education world, it has been reached to each individual in one form or another which leads to unauthorised access of digital data.

This unauthorized creation and distribution of any software is considered as software piracy. The origin of software piracy lies in the early 1960s, when computer programs were freely distributed with mainframe hardware by hardware manufacturers. In the late 1960s, manufacturers began selling their software separately from the required hardware [1]. Some file sharing programs like ‘bit torrent’ and ‘napster’ are also contributing in software piracy. According to the BSA statistics, the piracy rate is increased from 2% to 43% in short span, just because of the highly demanded PC market in developing countries [2]. People in the world get used to install and download false materials and products and also feel happy to be able to afford these materials without any cost and resulting harm to the individual or masses [3].

II. THREATS TO E-QURAN

Computer crime by definition means where computer is used as a target, tool or both. Threats associated with computer are classified as Interception, Interruption, Modification and Fabrication. Out of which Modification and fabrication is the severe one which attacks on Integrity of data. As transmitting and receiving the data in electronic form does not follow any physical rule due to anonymity of source, it is difficult to track the

malpractice easily. But laws can be incorporated as soon as malpractice is detected and the culprit can be punished. Hackers are continuously identifying new means of stealing information. Unfortunately, the presence of unaware users in an environment surrounded by digital world makes them an easy target for hackers. User education and training is a must to combat computer security threats. This is not a simple task to achieve and not the sole responsibility of the user or the organization. Many groups have to be involved to produce an IT security-aware resident [4].

The electronic use of Quran is common now a days, whether it is through Desktop PC, Tablet or Smart phones. The e-Quran is also vulnerable to various attacks including the most severe one, which is attack on Integrity. There are several threats and vulnerabilities to e-Quran which can be classified broadly in two categories. First, Fabrication of false e-Quran from scratch and secondly Interception and modification in authenticated copy of e-Quran. The first category falls under integrity of the content which closely resemble with the financial and banking data. Spoofing and Masquerading are two types of attack which talks about integrity but usually ignored in cyber crime dictionary and assumed to be less harmful crime. The word spoof means to deceive. In digital world spoofing refers tricking or deceiving computer systems or other computer users. This is typically done by hiding one's identity or faking the identity of another user on the Internet.

The second category falls under confidentiality of data, software piracy is popularly known crime in this category. Term Data diddling is also used for small alteration of data Masquerading is an attack by which a person claims to be another person and takes all the privileges available in that IP-address. Data diddling is a man in the middle attack where the MITM not only intercept the data but also alter the data. Diddle means a small change in setting to bring your system down, like in buffer overflow attacks. [5]

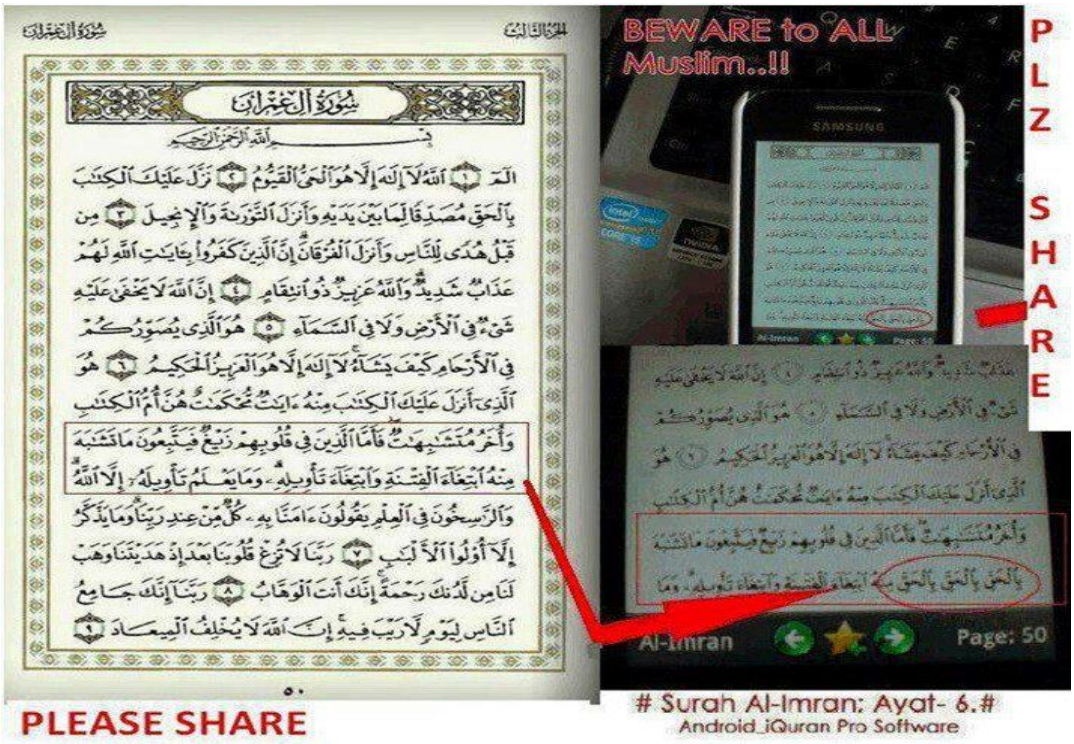

Figure 1 - Integrity Attack (retrieved from Facebook)

III. EXISTING CYBER LAWS

Most the countries across the globe have cyberlaws based on their requirement, culture and ambience. In Islam the basis of law is Quran and hadith and cyberlaws are also replica of the same. In section 33.02 of Texas cyber law [6] breach of computer security is described under several parameters of personal and financial security. U.S cyberlaws [7] states in section 18 U.S.C. § 1028 about Fraud and related activity in connection with identification documents, authentication features, and information, section18 U.S.C. § 1028A about Aggravated identity theft and 18 U.S.C. §§ 2516 about Interception of wire, oral, or electronic communication i.e piracy.

The study of present cyber legislation of all the Economic and Social Commission for Western Asia (ESCWA) members, namely: Bahrain, Egypt, Iraq, Jordan, Kuwait, Lebanon, Oman, Palestine, Qatar, Saudi Arabia, the Syrian Arab Republic, the United Arab Emirates and Yemen shows the flaws and shortcoming in existing laws [8].

In this paper three major countries of Middle East namely Saudi Arab, Oman and UAE are taken into consideration and their laws related to above mentioned two categories are being analyzed.

Country	Data Crimes			Network Crimes		Access Crimes		Related Crimes		
	Data Interception	Data Modification	Data Theft	Network Interference	Network Sabotage	Unauthorized Access	Virus Dissemination	Aiding and Abetting Cyber Crimes	Computer-Related Forgery	Computer-Related Fraud
Australia	✔	✔	✔	✔		✔			✔	✔
Brazil		✔			✔	✔		✔		
Canada	✔	✔	✔	✔	✔	✔	✔			✔
Chile	✔	✔	✔	✔	✔					
China		✔		✔			✔			
Czech Republic		✔	✔		✔	✔				✔
Denmark		✔		✔						✔
Estonia		✔	✔	✔	✔	✔	✔	✔		✔
India		✔	✔	✔	✔	✔	✔	✔		✔
Japan	✔	✔	✔	✔	✔	✔		✔	✔	✔
Malaysia		✔				✔		✔		✔
Mauritius	✔	✔		✔	✔	✔	✔	✔	✔	
Peru	✔	✔	✔	✔	✔	✔				✔
Philippines	✔	✔	✔	✔	✔	✔	✔	✔	✔	✔
Poland		✔	✔	✔				✔		
Spain	✔	✔	✔					✔		✔
Turkey		✔	✔	✔	✔		✔	✔	✔	✔
United Kingdom		✔		✔	✔	✔		✔		
United States	✔	✔	✔	✔	✔	✔	✔	✔		✔

Figure -2. Countries with Updated Law [8]

A. Cyberlaws of United Arab Emirates

Article 10 of UAE cyber laws [9] states that penalty of Impersonation, masquerading or fraud is imprisonment for a term of at least 1 year and fine of at least AED 30,000 or either. Article 15 states that the penalty of imprisonment upto 7 years for following crimes through computers

- Abuse of an Islamic holy shrine or ritual
- Abuse of a holy shrine or ritual of any other religion where such shrine or ritual is protected under Islamic Sharia.
- Defamation of any of the divine religions.
- Glorification, incitement or promotion of wrong doing.

B. Cyberlaws of Oman

Chapter Four of Oman Cyber laws [10] named Forgery & information Fraud states in Article 12 that the penalty with imprisonment for a period not less than one year and not exceeding three years and a fine not less than OMR one thousand and not exceeding OMR three thousands or by either penalty, shall be applied to any person who uses the information technology tools in the commission of informational forgery crimes by changing the nature of such data or the electronic information by addition or deletion or replacement with the intent to use it as proper data or electronic information, acceptable in an informational system legally a matter which might causes personal benefit to him or the other or causes damage to the other. If such data or electronic information is governmental, then the penalty shall be temporary imprisonment for a period not less than three years and not exceeding fifteen years and a fine not less than OMR three thousands and not exceeding OMR fifty thousands. The same punishment provided for in the previous paragraph shall be applied mutatis mutandis to any person who knowingly uses the forged data or electronic information.

In Article 19 The penalty with imprisonment for a period not less than one month and not exceeding three years and a fine not less than OMR one thousand and not exceeding OMR three thousands or by either penalty, shall be applied to any person who uses the informational network or the information technology facilities to produce or publish or distribute or purchase or possess whatsoever that might prejudice the public order or religious values.

C. Cyberlaws of Saudi Arabia

Article 6 of Saudi Arabia Cyber law [11] states that Any person who is involved in Production, preparation, transmission, or storage of material impinging on public order, religious values, public morals, and privacy, through the information network or computers shall be subject to imprisonment for a period not exceeding five years and a fine not exceeding three million riyals or either.

IV. PROPOSED AMENDMENTS TO EXISTING LAW

Existing Cyberlaws all over the world addresses integrity issue of data storage, processing and retrival. It includes software piracy and intellectual property right, but nowhere laws are made specifically against malpractice or fabrication of religious scripture including UAE, Oman and Saudi Arabia.

In Surah Baqarah, from ayat 78 to 81 (2:78 to 2:81) Allah says that **"**Among them are unilletrate ones who do not know the Scripture except in wishful thinking, but they are only assuming. So woe to those who write the

"scripture" with their own hands, then say, "This is from Allah ," in order to exchange it for a small price. Woe to them for what their hands have written and woe to them for what they earn. And they say, "Never will the Fire touch us, except for a few days." Say, "Have you taken a covenant with Allah ? For Allah will never break His covenant. Or do you say about Allah that which you do not know?" Yes, whoever earns evil and his sin has encompassed him - those are the companions of the Fire; they will abide therein eternally." So the penalty of modification and fabrication of Quran should not be less then capital punishment as the intruders not only doing a crime of diddling text whether intentionally or un-intentionally but also spreading mischief to Innocent and unaware computer / smartphone users.

Author advocates that the ammendments should be done in cyber laws as the present laws are insufficient and weak. So more stronger laws should be included at least in arab world to protect integrity of e-Quran. The penalties to the criminal should not be less then the Drug traficking or Cyber Terrorism.

In author's view this crime should come in the category of content crime in present Omani Cyber Laws [10], where the penalty is life imprisonment and a fine of one hundred thousand OMR or as in Article 25 where the punishment is the death penalty or life imprisonment and a fine of twenty five thousand OMR. In Saudi Arabian cyber laws [11] this crime should come under Article 7 where imprisonment is for ten years, and a fine of five million riyals.

In this context Author Proposes following Amenmends in the present Cyberlaws :

1. *A Separate Article in the law should be made against foregery of e-Quran.*
2. *This Article should be subdivided in two categories; Fabrication of e-Quran and Modification of e-Quran.*
3. *For Fabrication the penalty should not be less then life imprisonment.*
4. *For Modification the penalty should not be less then ten years of imprisonment and fine of five million riyal.*
5. *In both the cases criminal should be banned to use computer and Internet for a lifetime.*

V. DISCUSSION

Legislation is the back bone of every society. In Saudi Arabia there is a special case in that the sanctions imposed as punishment are approved as stated in the Qur'aan and Sunnah. There are public sanctions such as theft, murder, adultery for which an Anti-Crime act was introduced in 2007 to combat cyber crimes. It also determines the level of each crime and the resulting harm[12]. In [4] some recommendations were given such as formation of Computer Emergency Response Teams (CERT) to enhance the security awareness among residents. Involvements of Police Departments, Enterprises, Telecommunication companies (ISPs), Media and Users.

In 2008, a new initiative has been proposed to fight cyber terrorism by bringing governments, businesses, and academia together from all over the world. The initiative, known as the International Multilateral Partnership Against Cyber Threats (IMPACT) [13], consists of the international partnership of more than 30 countries to study and respond to high-level cyber security threats.

Apart from the common legislation of cyber crime in Kingdom, it is now important to have a special law to protect integrity of e-Quran. It is observed in the near past that the smart phone users are increasing day by day and several versions of software of e-Quran is now available. So the chance of forgery and fabrication also increases proportionally. A common user can easily be misguided due to unawareness of this fraud. An example of "Musaylimah bin Ḥabīb" alias Kazzab belonged to tribe Banu Hanifa used to compose verses and offer them, as Quranic revelations. Most of his verses extolled the superiority of his tribe, the Bani Hanifa, over the Quraysh [14]. He was killed in the battle of Yamama and later his followers were executed. There are many hidden culprits in cyber world now a day's who intentionally spread mischief in the land so it is necessary to make strong law to protect Holy Scripture in electronic form.

In Figure 3 it is shown that any security system cannot be established until it is supported by three features, viz. Selection of Control policies, Implementation and Monitoring. So to have a strict law it is recommended to have all these features incorporated in the system.

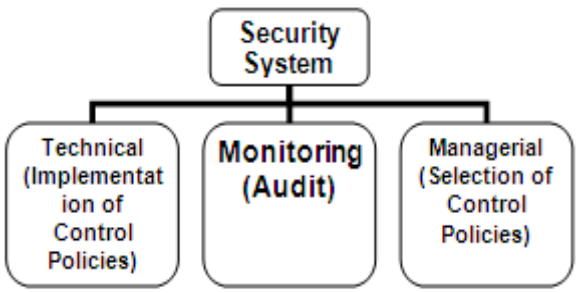

Figure 3 - Security System features

VI. CONCLUSION

In this paper several forms of cybercrime were discussed especially those are connected to piracy and fraud. A correlation has been made of these crimes with the threats of e-Quran and various other threats were also discussed. After analyzing threats to e-Quran they were categorized in two broad fields, modification and fabrication which challenge the integrity of e-Quran. Existing laws related to piracy and forgery were discussed in general and related to e-Quran in particular in the cyber laws of many countries particularly UAE, Oman and Saudi Arabia. It was observed that any of the three does not include any clear law to protect e-Quran. Author proposes some amendments in the existing law and advocated to have stronger law for security of e-Quran as it is matter of faith, religion and moral values. Lastly some case studies were discussed related to this research with managerial, social and technical aspects.

VII. REFERENCES

[1] Business Software Alliance, "Eighth annual BSA global software 2010 piracy study", May 2011.

[2] Ajay Nehra, Rajkiran Meena, Deepak Sohu, and Om Prakash Rishi. "A Robust Approach to Prevent Software Piracy".Students Conference on Engineering and Systems (SCES), IEEE 2012.

[3] Samir N. Hamade. "The Legal and Political Aspects of Software Piracy in the Arab World" Proceedings of the Third International Conference on Information Technology: New Generations (ITNG'06), IEEE 2006.

[4] Fadi A. Aloul."Information Security Awareness in UAE: A Survey Paper". IEEE International Conference for Internet Technology and Secured Transactions (ICITST), London, UK, pp. 1-6, November 2010.

[5] CAPEC; A Community of knowledge resource for building secure software, available online at http://capec.mitre.org/data/definitions/184.html

[6] Texas Computer Crime Law. Available Online: http://www.statutes.legis.state.tx.us/Docs/PE/htm/PE.33.htm

[7] Cybercrime Laws Of The United States. Compiled October 2006 by Al Rees, CCIPS. http://www.qcert.org/sites/default/files/public/documents/us-ecrime-compilation_of_cybercrime_laws-eng-2006.pdf Last accessed on 1/7/2013

[8] Models of Cyber Legislation ESCWA Countries. Available online at http://www.escwa.un.org/information/publications/edit/upload/ictd-07-8-e.pdf.

[9] The Federal Law No. (2) of 2006 on The Prevention of Information Technology Crimes published in the Official Gazette of the United Arab Emirates, Volume 442, 36th year, Muharam 1427 H/ January 2006.

[10] Cybercrime Law Sultan of Oman, Royal Decree No 12/2011; English Version available online http://www.qcert.org/sites/default/files/public/documents/om-ecrime-issuing_the_cyber_crime_law-eng-2011.pdf .

[11] Anti-Cyber Crime Law of Kingdom of Saudi Arabia. Bureau of Experts at the Council of Ministers Official Translation Department Translation of Saudi Laws, 8 Rabi1, 1428 / 26 March 2007.

[12] Naasir Kamaal Khan. "Taxonomy of Cyber Crimes and Legislation in Saudi Arabia" in International Journal of Advanced Research in Computer Engineering & Technology (IJARCET) ISSN: 2278-1323 Volume:1, Issue:8 October 2012, page 207-209.

[13] International Multilateral Partnership Against Cyber Threats (IMPACT), available online at www.impact-alliance.org/

[14] The Life of the Prophet Muhammad: Al-Sira Al-Nabawiyya By Ibn Kathir and Muneer Fareed.

American Journal of Engineering Research (AJER)
e-ISSN : 2320-0847 p-ISSN : 2320-0936
Volume-02, Issue-10, pp-258-263
www.ajer.org

Research Paper Open Access

An Experimental investigation of sea sand as an Abrasive material in vibrating chamber by using Tungsten Carbide Nozzle in Abrasive Jet machining Process.

N. S. Pawar, R.R. Lakhe, R. L. Shrivastava,
**Department of Mechanical Engg, Government Polytechnic , Nagpur, Maharastra state, India*
*** Director, shreyas Quality Management system, Training and consultancy (9001:2000),11, Tulsivihar Abhayakar Nager Road TF-III, Nagpur-10, Maharastra State, India*
**** Professor in Mech Engg Dept.,Yashwanrao chavan college of Engg. Nagpur Maharastra State, India*

Abstract: - A large number of investigation carried out in Abrasive jet machining and water jet machining process with different parameter but no detailed work have been found or carried out by using sea sand as an abrasive in AJM process by using different types of nozzles and variable parameters. The present work gives performance of sand having grain structure of 100-150 micron in the tungsten carbide nozzle. The experimentation in this study give characteristic of sea sand as abrasive material. The parameter like pressure, standoff distance of nozzle from work piece keeping constant and variable. It give the result of material removal rate , powder flow rate, similar to actually abrasive used like Aluminum oxide, silicon oxide etc. The R square value o.97 to 0.996 degree of polynomial equation. It is also notice that width of cut slightly increase with increase of feed rate .The taper cut slot was found to be a higher at greater stand of distance and work feed rate .Tungsten carbide is very hard. It maintain high cutting ability as abrasive strike on work piece.

Keywords: - *sea sand, Vibrating chamber, Abrasive jet machine , abrasives, Nozzles, glass,*

I. INTRODUCTION

Sand Abrasive compressed air is used for surface cutting, holing of surface on the brittle material like glass, this also used for surface cleaning and surface texturing etc. In AJM process fine particles of sea sand having grain size 100-150 micron accelerate in mixing chamber. The sea sand particle directed toward working surface. The Tungsten carbide Nozzle is one of the most useful nozzle in modern AJM engineering process because of its high hardness, high wear resistance, high chemical inertness, high young's module and thermal conductivity. In earlier studies of Deng Jianxin used ceramic based composite have been developed and used in various application.

Nevertheless considering its working condition the AJM process can generate penetration. The acceleration of the sand abrasive in vibrating chamber generate the proper turbulence of particles along with compressed air of pressure varying from 5 kg per cm sq. to 12 kg per cm sq. The cam and follower at lower base side of the gives vibrating motion to chamber. The studies by Dong sam park (1) machining profile of grooves shows U type shape. He also elaborate masking for good result independent of the heating temperature with water abrasive jet machining . By Deng Jianxin (3) he focus on reducing stresses on entrance of ceramic nozzle with apparent increasing in erosion wear resistance. The effect of hardness of nozzle was reported by Jianais Deng (5). The experimental work carried out by Balasubramaniam (7) the effect of particles size on its normalized erosion profile and effect of normalized erosion profile as velocity assumed to be constant. For all stand of distance he conclude that the peripheral velocity of jet is increases it also increases the rate of material removal rate.

The present study set a target of sea sand as abrasive material in vibrating chamber of tungsten carbide nozzle with varying parameter of pressure, standoff distance. The morphology of impacted surface is compared conventional abrasive which used in AJM as well as water abrasive Jet machine process. In fact the quadratic polynomial and cubic polynomial model fit curve gives the R-square vary near to 1 i.e. 0.98 to 0.9918 which result good fitting of curve.

II. EXPERIMENTAL PROCESS AND SET UP

Experimentation were conducted to proposed sea sand as abrasive material with grain size vary from 100-150 micron. The microscopic structure can observed by sedimentation and decontation, sedimentation balance, BET, illustration method. For 1.5 to 2 mm diameter of nozzle 50-150 micron grain size is preferably used. The sieving size range start from 37 micron below this not possible to used for grain size measurement if the size is above 37 micron electronic microscope is used.
The pressure varying from 5 to 12 kg per cm. sq. and standoff distance keeping variable and constant for different powder flow rate throughout the machining process.

Table No.1:Experimental condition

Abrasive----------sea sand
Grain size----------100-150 micron
Pressure----------5 to 12 kg/cm²
Standoff distance ----------constant
Tungsten carbide Nozzle--------2mm dia
Time consider for penetration----variable
Work piece----Glass & Thickness = 4 mm

Fig No:1 Experimental set up

In this work process the material removal rate and powder flow rate were calculated in different condition apply for set up. The high turbulence is created in vibrating chamber with compressed air by which the particle moves with high speed of stream. The impact through nozzle cause severe erosion or material removal gm/sec. the erosion of material surface depends upon velocity of particle direction and brittleness of work piece. Some studies are showed that erosion rate depend upon impact angle.

Table No: 2.when pressure variable and standoff distance constant.

Sr. No	P Kg/cm²	SOD mm	MRR W/T = gm/sec)	PFR Wa/T = gm/sec	DOC mm
1	5	8	0.043	1.10	4.5
2	5.5	8	0.051	1.21	4.7
3	6	8	0.060	1.34	5.0
4	6.5	8	0.065	1.50	5.1
5	7	8	0.075	1.73	5.1
6	7.5	8	0.077	1.73	5.2
7	8	8	0.080	1.74	5.4
8	8.5	8	0.081	1.75	5.6
9	9	8	0.081	1.75	5.4
10	9.5	8	0.080	1.76	5.5

The quadratic and cubic polynomial model fit for MRR v/s pressure shows the R square value are not much more differ and the percentage of difference is 0.5 % which is very less. The graphical representation of material removal rate and pressure show the nature of sand abrasive with different condition. The depth of cut is slightly increase as the SOD is increased. It is observed that sprinkling of abrasive is more then DOC is also more.

Graph No. 1 Effect on MRR v/s Pressure at R-square value is 0.9934

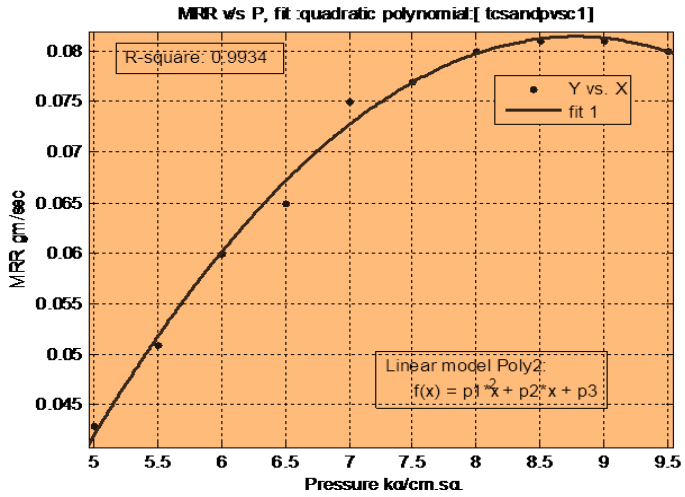

Graph No.2 Effect of MRR v/s Pressure at

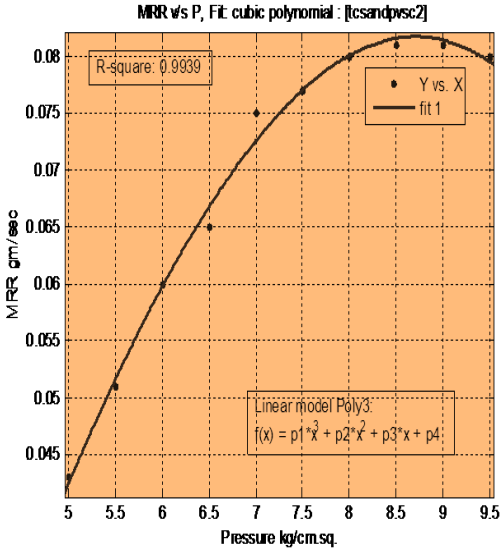

R-square value is 0.9939

Graph No :3 behavior of MRR v/s PFR at quadratic polynomial fit at R-square value 0.9836

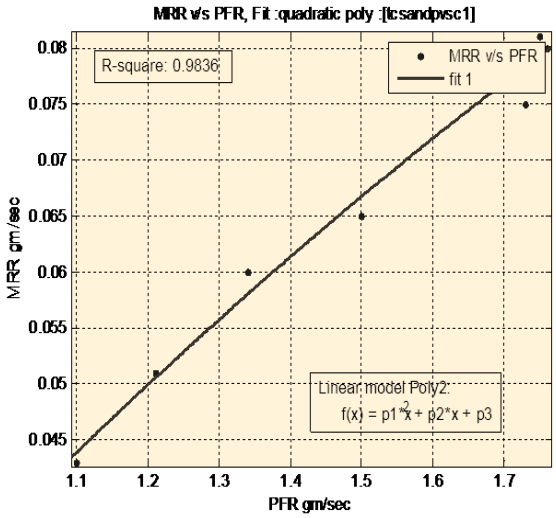

Graph No :4 behavior of MRR v/s PFR at cubic fit at R-square value 0.9903 which is not much differ

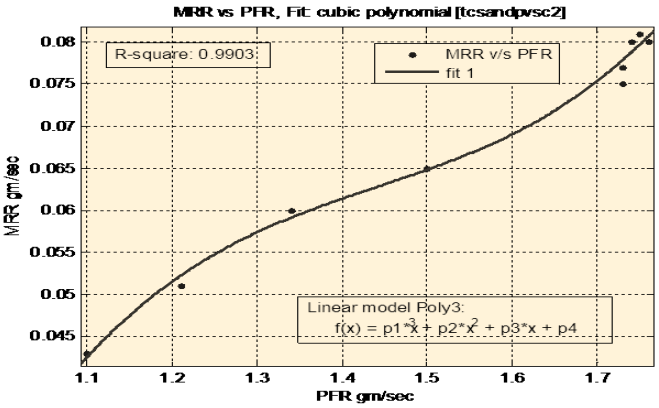

Table no:3 when SOD is constant

Sr. No	P Kg/cm²	SOD mm	MRR W/T = gm/sec)	PFR Wa/T = gm/sec	DOC Mm
1	8	9.5	0.082	1.80	5.1
2	8	9.5	0.082	1.81	5.0
3	8	9.5	0.081	1.81	5.1
4	8	9.5	0.082	1.81	5.1
5	10	9.5	0.081	1.80	5.0

III. ANALYSIS

Analysis is carried out even the effect of some vibration , grain size of sea sand, was properly analysis by good fitting curve. It was tested under different polynomial fit i.e. linear polynomials, quadratic polynomial, cubic polynomial, 4th degree poly fit etc. above all cubic polynomial fit gives their good fitting of curve and R square value is 0.9934 and 0.9939 The linear model equation of polynomials is

F(x)= p1*x^3+p2*x^2+p3*x+p4 and

In this experimental study the assumption were made in present analysis condition and simplifying equation

F(x)= 0.219*x^3-0.947*x^2+1.399*x^1-0.6417

The analysis of MRR v/s PFR of first derivation, second derivation, and first integration are obtained with 95% prediction bond are

Graph No: 5 Analysis for MRR v/s PFR

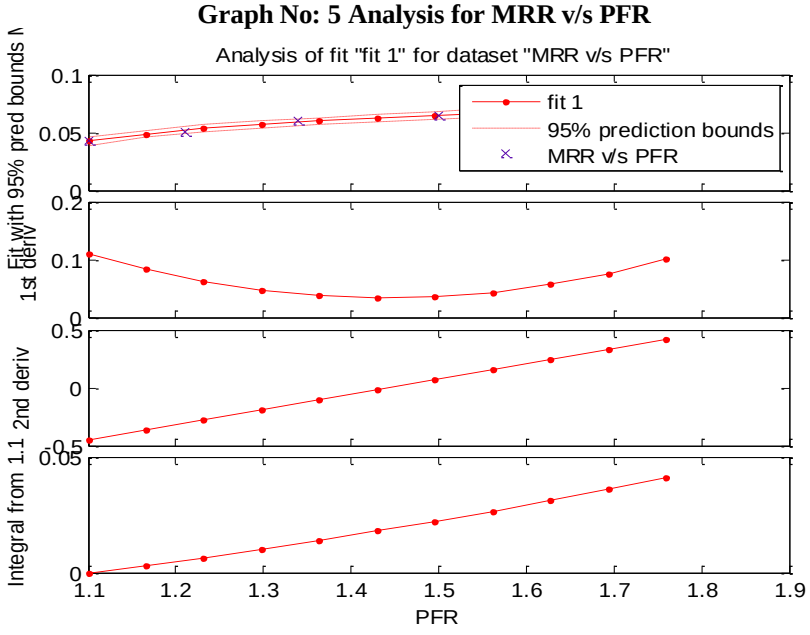

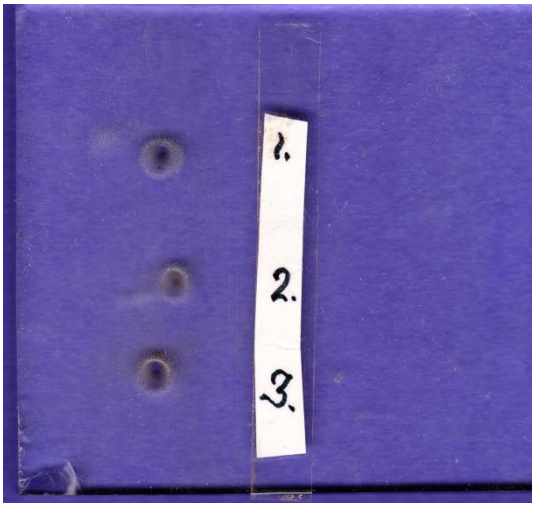

Fig No: 2 photograph of cut section of work piece:

IV. DISCUSSION

Photograph shows the actual diameter of cut of brittle material. The value of material removal rate and powder flow rate were obtained by varying pressure and SOD and constant then after. The observation and all relevant value of MRR and PFR are obtained by cubic polynomial fit for this observational set

V. CONCLUSION

The following conclusion are made at the end of analysis.

a) As the pressure increases the MRR is also changing
b) The value of R-square very near to 1 i.e. 0.9934 and 0.9939.
c) If the SOD is constant there is no more effect on MRR
d) The validation of work i.e. the value of MRR at pressure 5 kg per cm sq. is 0.043 gm/sec by concluding observation and the by using linear polynomial model

F(x)= 0.219*x^3-0.947*x^2+1.399*x-0.6417
F(x)= 0.0421 and the percentage of error is very less

REFERENCES

[1] Dong-Sam Park, Myeong-Woo cho, Honghee Lee, Won-Seung Cho, Micro grooving of Glass using micro –Abrasive jet machining. ELSEVIER, Journal of material processing technology 146 (2004) 234-240 ,Incheon, South Korea
[2] Matthieu Barge, Jeol Rech, Hedi Hamdi, Jean-Michel Bergheau, Experimental study of abrasive process, ELSEVIER , WEAR, Journal of science direct,98156 ,28 Aug 2006,pg 101-107
[3] Deng Jianxin, Liu Lili, Ding Mingwei, Sand erosion performance of SiC/ (W,Ti)C gradient ceramic nozzles by abrasive air-jets, ELSEVIER ,MATERIALS AND DESIGN, Journal of science direct 28 (2007) , pg 2099-2105
[4] Jianxin Deng, Xihua Zhang, Pingzhang Niu, Lili Liu, Jinghai Wang, wear of ceramic nozzles by dry and sand blasting, ELSEVIER, Tribology International 29 (2006), pg 274- 280
[5] Deng Jianxin, Feng Yihua, Ding Zeling, Shi Peiwei, wear bahavier of ceramic nozzles in sand blasting treatments, ELSEVIER, Lournal of European ceramic society 23 (2003), pg 323-329
[6] M. Wakuda, Y. Yamuachi, S. Kanzaki, effect of workpiece properties on machinability in abrasive jet machining of ceramic materials, ELSEVIER, journal of the international societies for precision engineering and nanotechnology 26 (2002), pg 193-198
[7] R. Balasubramaniam, J. Krishanan, N. Ramkrishanan, A study of shape of surface generated by abrasive jet machining, ELSEVIER, the journal of material processing technology 121 (2002), pg 102-106.
[8] Manabu Wakuda, Yukihiko Yamauchi, Shuzo kanzaki, material response to particle impact during abrasive jet machining of alumina ceramics, ELSEVIER, the journal of material processing technology 132, (2033), pg 177-183
[9] A.EI- Domiaty, H.M.Abd EI-Hafez, and M.A.shaker, drilling glass sheet by abrasive jet machining , world academic science engineering and technology 56 (2009), 61-67

[10] S.paul, A.M. Hoogstrate, C.A. van Luttervelt, H.J.J.Kals, an experimental investigation of rectangular pocket milling with abrasive water jet , ELSEVIER, the journal of material processing Technology 73 (1998), pg 179-188.
[11] Adnan Akkurt, the effect of material type and plate thickness on drilling time of abrasive water jet drilling process , ELSEVIER, the journal of material and design 30 (2009), pg 810-815
[12] L. Chen, E. Siores, W.C.K.Wong, optimizing abrasive waterjet cutting of ceramic materials, ELSEVIER, the journal of material processing tech. 74 (1998), pg 251-254
[13] A.A.Khan, M.M. Haque, performance of different abrasive material during abrasive water jet machining of glass, ELSEVIER, the journal of material processing technology 191, (2007), pg 404-407
[14] L.Chen E. Siores, W.C.K.Wong, kerf charecterstics in abrasive waterjet cutting of ceramic materials PEERGAMON, PUBLISHED BY Elsevier science ltd, pg 1201-1206
[15] P.K.Ray, A.K.Paul, some studies on abrasive jet machining, the journal of institution of engineer (India),vol 68,pg 27-30, 2 Nov 1997

American Journal of Engineering Research (AJER)
e-ISSN : 2320-0847 p-ISSN : 2320-0936
Volume-02, Issue-10, pp-264-270
www.ajer.org

Research Paper Open Access

Forming of universal optimal operation model of frame for coil winding with finished yarn according to selected measuring points based on the effect of mechanical oscillations

Professor dr. Slobodan Stefanović[1], Professor dr. Radoje Cvejić[2], Professor dr. Duško Kostić[3], Professor dr. Srbislav Radivojević[4], Professor dr. Imre Kriss[5]

[1]*High School of Applied Professional Studies of Vranje, Serbia*
[2]*Associate Professor, Faculty of strategic and operational management, Belgrade, Serbia*
[3]*HighVocational School for Entrepreneurship, Belgrade, Serbia*
[4]*Visoka strukovna tehnička škola, Zvečan, Serbia*
[5] *Faculty of Engineering, University Politehnica Timisoara, Romania*

Summary: - In order to create a universal optimal model of certitude functioning it is necessary to analytically determine the shape of the transfer functions of the optimal operation model $M_{\xi}(t)_{NK}$ that will define the frequency of the analyzed sklopa.Analiza security model is undertaken stepping and to determine the sub-models according to selected measuring points for determining the mechanical oscillations and then made structures block diagram linking sub-models of transportation mode input processing yarn (carded tape) to the output (cross road).

Keywords: - *model, the transfer function, the system for winding yarn, the algorithm, the monitoring system.*

I. INTRODUCTION-- DESCRIPTION OF A FRAME FOR COIL WINDING WITH FINISHED YARN

Powertrain system of a frame for for coil winding with finished yarn is shown in Figure 1. and consists of the following parts and components which are classified on the basis of spun yarn which is produced by a twist of the rotor (turbine) and on its way to the coil which is wound.

THREAD GUIDE (F1) - used to evenly and safely winding yarn on cone coil. His movement is straight with reciprocating, the number of cycles is 120 cycles/minute. It is made from a special type of ceramic with a metal plate on the occurrence of friction-resistant. Installation and removal are very easy.
CORE HOLDERS (F2) - are used for alignment and uniform circular rotation of the coil winding. Holders are made of special type of polymer, the special shape drawn on holly bearings. When bearing is broke, due to the effects of dust in it, comes to his seizure, but also to break the insert coil holder.
TENSIONER AND LIFTER OF A SPOOL (F3) - a spring lever system which supports the full spools onto the conveyor belt. The spring system is unstrained in coil winding yarn, while at the same full coils are activated and divides the full coil coating in which the coil tighter when reloading.
SPOOL BRAKE (STOP BEFORE THE YARN BREAK) (F4) - is a system that consists of a cylindrical lining of which overlaps coil winding in and of the lever which is activated at the binding of a broken yarn.

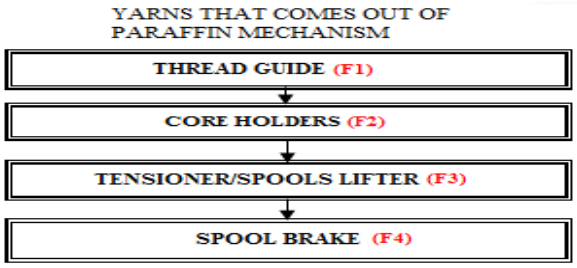

Figure (1). The transmission system of a frame for coil winding with finished yarn

II. RESEARCH INTO THE CAUSES OF DEFECTIVENESS OF THE POWER TRANSMISSION COMPONENTS FRAME OF THE OE SPINNING MACHINES - FAULT SCAPE ANALYSIS

Failures were due to subassemblies OE - spinning on the basis of elevated levels of mechanical oscillations recorded on the basis of the data collection ie. organization of the course of the level of mechanical oscillations measured values of stochastic signals at selected measuring points. Based on all the registered clients of the analyzed complexes formed integral components of the fault tree circuits OE spinning machines.
Failure analysis on the frames of OE – spinning machines included the use of methods fault tree analysis occurring as a result of mechanical oscillations of the analyzed circuits. This analysis will later be used in the analysis of the reliability of the components of the analyzed components.

From the standpoint of functionality and structural characteristics analyzed circuits of OE - spinning labeled R_1 are complex technical circuits in textile technology in terms of operation and maintenance in terms of technology. The structural part of the technical components is derived from the production of components that have a high technological level (very good surface treatment, durability and stability). However, as with all technical components are certain weak points.

The main elements of the transmission circuits are analyzed and their weak points are chosen technical components and are defined as a single weak points where the failures are repeated, and the same can be partly overcome by the introduction of technology proper maintenance on them ie. maintaining the level of mechanical oscillations in the specified bands (within certain limits their their impact). Continuous monitoring of failure occurrence, due to the increased activity of mechanical oscillations, there is the goal of maintaining the condition that. regular preventive maintenance can mitigate the effect of the impact of mechanical oscillations, and thus decrease the number of clients integral components of the analyzed components. Fault tree analysis shows that intensive monitoring of failure leads to the discovery of weakness on the techniques of circuits, which in this part of the analysis done.

Failure analysis is presented deductive technique in which the specification of unintended consequences resulting from the impact of mechanical oscillations (vibrations) that appear in the process of exploitation of the analyzed components OE - spinning. The analysis included the character causes of failure of the main circuit elements (related to the analysis of complex spinning boxing - heart OE spinning machines and assembly of finished coil winding yarn) and the ways in which the cause leads to failure.
The results of the number of poor points failure who receive the service conditions, be used in the safety analysis of the functioning of the analyzed components (determination of the percentage of failures) and to determine their reliability.

In figure 2. are given the reasons for the impact of mechanical oscillations that lead to failure of components and assemblies of components analyzed, based on which one can predict the actions of their preventive maintenance technologies.

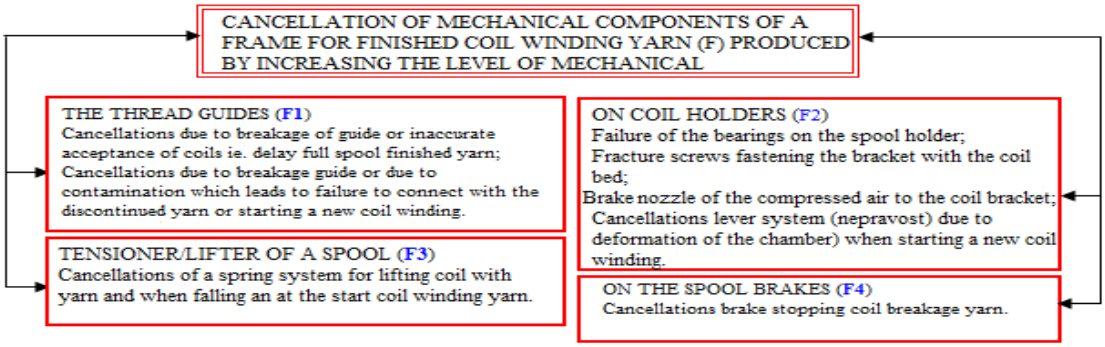

Figure (2). Failures in the constituent assembly components for the finished yarn winding coils due to the increased effects of mechanical oscillations

III. ANALYSIS MODEL

The analysis model included the methodology using an algorithm to determine the security of the constituent components of the clutch system with OE - spinning. The methodology included the construction of the monitoring system (Figure 3.).

IV. ESTABLISHMENT OF A UNIVERSAL OPTIMAL OPERATION MODEL OF A FRAME FOR COIL WINDING WITH FINISHED YARN ACCORDING TO SELECTED MEASURING POINTS BASED ON EFFECT OF MECHANICAL OSCILLATIONS – DETERMINATION OF FREQUENCY CERTITUDE

In this analysis started from the method for determining the sub-models according to selected measuring points for determining the mechanical oscillations and then was made a structural block diagram submodel in the way of movement and its yarn processing delay.
Structural block diagram of transmission on selected sampling points is shown in Figure 4.,

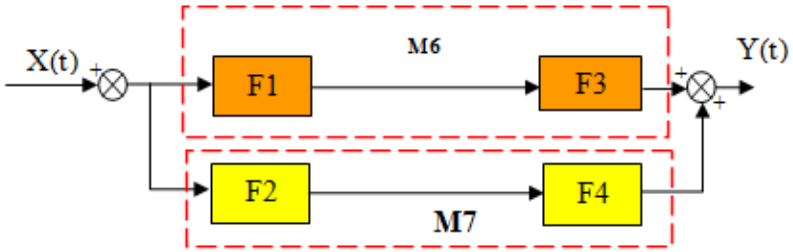

where:
M6 - measuring point level fluctuations on the conductor strands and the cylinder to rotate the spool in his winding the finished yarn,
M7 - measuring point level fluctuations on the tensioner/lifter spool, and the spool holder.

Figure (4). Display of a frame for coil winding with finished yarn through structural blocks

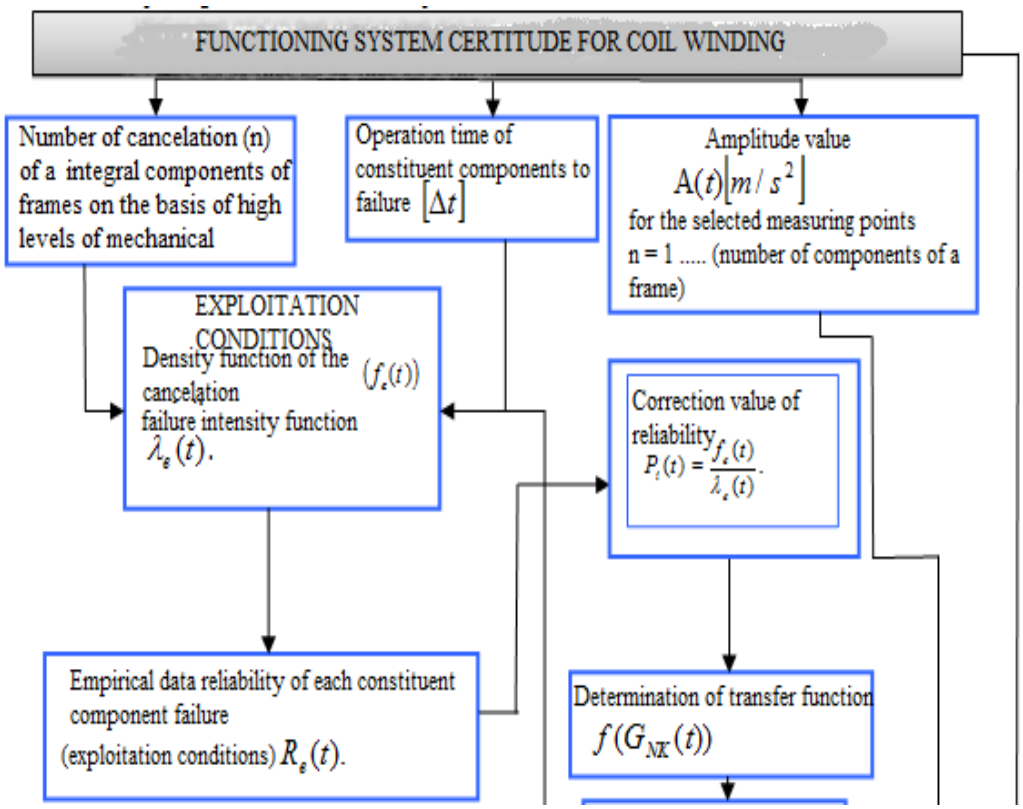

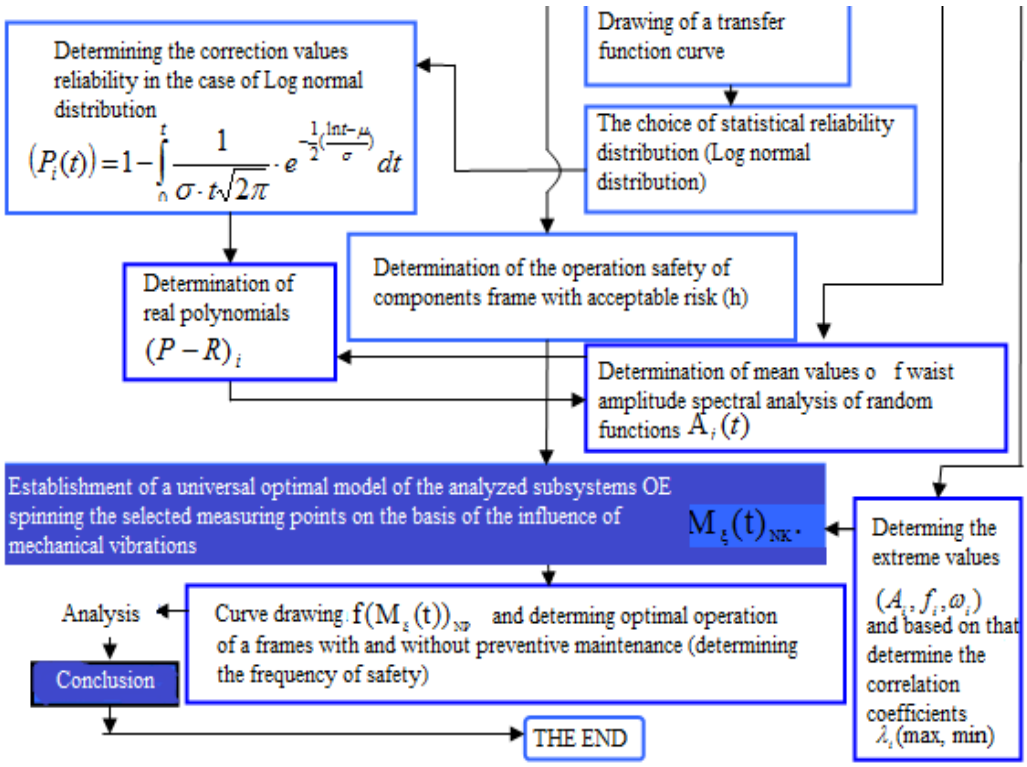

Figure (3). Monitoring system (algorithm) methodology of determing certitude functioning of the analyzed frames - OE spinning machines

NOTE: In the formation of this model started from the block diagram that are different from the block diagram in determining the reliability of the transfer function. The reason is that the measuring point 6 includes the impact of the tensioner and lifter (F3) while another part that makes this subgroup of a brake coils (F4) belongs to the measuring point 7, so it is necessary to distinguish their effects. In determining the reliability of the transfer function that was not of great importance, and models for determining the optimal assembly for winding coils the finished yarn is of great importance, because it determines the measuring points and the influence of each component of the heat caused by the occurrence of mechanical oscillations.
With the introduced labels measuring points (M6 and M7) transformation of the structure of the block diagram is as follows (Figure 5.):

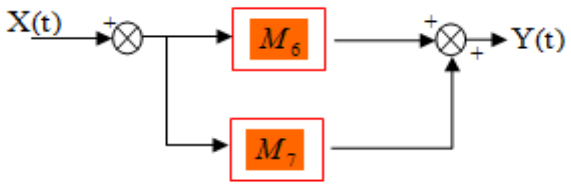

Figure (5). The transformation of the structure of the block diagram of transfer to sub-models for winding coils with the finished yarn

Model analysis was carried out and stepping to determine the sub-models according to selected measuring points for determining the mechanical oscillation (vibration), and then made srtuktura block diagram linking sub-models of transportation mode input processing yarn yarn (thread guide) to the output (cross the road) ie. the final stage (the final winding yarn around a spool).
Note: This block diagram structure will be further used to determine the general form of the transfer function of the optimal model $M_\xi(t)_{NK}$ **to be defined as the frequency of the safety assembly for winding coils the finished yarn.**
To carry out the general form of the transfer function of the optimal model, it is necessary to determine the terms of sub-models (M_i) that are included locations of measuring the level of vibration.

6. Measuring point 6, includes components – threas guide (F1) and spool tensioner/lifter (F3).

Thread quide moving in a straight line - the axial direction and with 60 cycles in one minute (30 cycles in an axial direction, and so in the other) in a way that leads spun yarn from one end to the other end of the coil winding is being carried out. As the authoritative speed takes the speed of one cycle of movement guide:

$$\vartheta_{VODIČ\cdot NITI}(t) = \omega_{F_1}(t) = f\left(A_6(t)_{F_1}\right) \neq \omega_6.$$

Spool tensioner/lifter is activated when the process begins winding the yarn on the bobbin ready and then when fully wound bobbin yarn, which frees it from the rollers to rotate the coil winding is raising up. The relevant angular velocity is the speed of the roller rotation coil (roll is the same shape as the coil and act on it in pairs)

$$\omega_{VALJKA}(t) \neq \omega_6(t).$$

$\omega_6(t)$ - The angular velocity circular assembly at the measuring point 6, as a function of the oscillation amplitude $A_6(t)_{F_1}$, $A_6(t)_{F_3}$.

Equation 6 is a sub-models:

$$\mathrm{M}_6 = \mathrm{M}_6^{'} \cdot \mathrm{M}^{"}{}_6 = \frac{R_{F1}(t)\cdot \mathrm{A}_6(t)_{F1}}{\omega_{F1} = f(\omega_6)} \cdot t_{13} \cdot \frac{R_{F3}(t)\cdot \mathrm{A}_6(t)_{F3}}{\omega_{F3} = f(\omega_6)} \cdot t_{14} = \frac{(P-R)_{F_1}(t)}{\omega_6} \cdot t \cdot \frac{(P-R)_{F_3}(t)}{\omega_6} \cdot t$$

$$\mathrm{M}_6 = \frac{t^2}{\omega_6^2}\left((P-R)_{F_1}(t)\cdot(P-R)_{F_3}(t)\right). \qquad (1)$$

$R_{F1}(t)$ - The reliability of the guide or the useful period of work;

$R_{F3}(t)$ - The reliability of the belt / pickup coil in a useful period of work;

$\mathrm{A}_6(t)_{F_1}\left[m/s^2\right]$ - The amplitude of oscillation in a helpful guide or period of the measuring point 6;

$\mathrm{A}_6(t)_{F_3}\left[m/s^2\right]$ - Amplitude of oscillation belt / pickup coil in a useful period of the measuring point 6;

$t_{13}, t_{14}[s]$ - Uptime components at the measuring point 6;

$(P-R)_{F_1}(t)$ - A polynomial with real coefficients, which gives the dependence of reliability of the component guides in the function or value of the level of mechanical vibrations at the measuring point 6

$(P-R)_{F_3}(t)$ - A polynomial with real coefficients, which gives the dependence of the component reliability tensioner/lifter operational level values of mechanical vibrations at the measuring point 6.

7. Measuring point 7., includes components: coil holder (F2) and the brake coil (F4).

Coil holder has a circular motion and turning over the rolling bearing, over which sits in firmly. Longitudinal rotation speed $(\omega_{LEŽAJA}(t))$, is the speed bearing that is different from the circular velocity at the measuring point 7.

$$\omega_{F_2} = \omega_{LEŽAJA}(t) \neq \omega_{F4}(t) = f\left(A_7(t)_{F_2,F_4}\right) \neq \omega_7.$$

$\omega_7(t)$ - The angular velocity circular assembly at the measuring point 7, as a function of the oscillation amplitude $A_7(t)_{F_2}$, $A_7(t)_{F_4}$.

Equation of a sub-models 7 is:

$$\mathrm{M}_7 = \mathrm{M}_7^{'} \cdot \mathrm{M}^{"}{}_7 = \frac{R_{F2}(t)\cdot \mathrm{A}_7(t)_{F2}}{\omega_{F2} = f(\omega_7)} \cdot t_{15} \cdot \frac{R_{F4}(t)\cdot \mathrm{A}_7(t)_{F4}}{\omega_{F4} = f(\omega_7)} \cdot t_{16} = \frac{(P-R)_{F_2}(t)}{\omega_7} \cdot t \cdot \frac{(P-R)_{F_4}(t)}{\omega_7} \cdot t$$

$$\mathrm{M}_7 = \frac{t^2}{\omega_7^2}\left((P-R)_{F_2}(t)\cdot(P-R)_{F_4}(t)\right). \qquad (2)$$

$R_{F2}(t)$ - The reliability of the coil holder in a useful period of work;

$R_{F4}(t)$ - The reliability of the brake coil in a useful period of work;

$A_7(t)_{F_2}\left[m/s^2\right]$ - The amplitude of the oscillation coil holder in a useful period of the measuring point 7;

$A_7(t)_{F_4}\left[m/s^2\right]$ - Amplitude of oscillation brake coil in a useful period of the measuring point 7;

$t_{15}, t_{16}[s]$ - Uptime components at the measuring point 7;

$(P-R)_{F_2}(t)$ - A polynomial with real coefficients, which gives the dependence of reliability of the component holder coil operational level values of mechanical vibrations at the measuring point 7;

$(P-R)_{F_4}(t)$ - A polynomial with real coefficients, which gives the dependence of the reliability of components brake coil operational level values of mechanical vibrations at the measuring point 7;

V. CONCLUSION

The general form of the universal equation of the optimal model assembly for winding coils the finished yarn is obtained by entering all prior specific factors (the transfer function of the optimal model $M_{\xi}(t)_{NK}$, **which is defined as the frequency of the safety assembly for winding coils the finished yarn**) so that:

$$M_{\xi}(t)_{NK} = M_6 + M_7 = \left(\frac{t^2}{\omega_6^{\,2}}(P-R)_{F1}(t)\cdot(P-R)_{F3}(t)\right)+\left(\frac{t^2}{\omega_7^{\,2}}(P-R)_{F2}(t)\cdot(P-R)_{F4}(t)\right). \quad (3)$$

The introduction of shift:

$$\begin{aligned}(P-R)_{F1}(t)\cdot(P-R)_{F3}(t)&=\xi_{10};\\ (P-R)_{F2}(t)\cdot(P-R)_{F4}(t)&=\xi_{11}.\end{aligned} \quad (4)$$

it is obtained universal equations of the optimal model for the security of the complex coil winding the finished yarn:

$$M_{\xi}(t)_{NK} = \frac{Y(t)}{X(t)} = t^4\left(\left(\frac{\xi_{10}}{\omega_6^{\,2}}\right)+\left(\frac{\xi_{11}}{\omega_7^{\,2}}\right)\right). \quad (5)$$

This equation is a universal equation of the transfer function of the optimal model of assembly of the finished coil winding yarn by selected sampling points from the effect of mechanical oscillations, and it gives the frequency dependence of the safety of operations.

VI. REFERENCES

[1] Adamović Ž., Stefanovic, S., Procedures for the implementationof controlof mechanicalvibrationsand method of collectionof the dataontechnical systems, XVIII Yugoslavconference withinternational participation "Noise and Vibration", Faculty of Occupational Safety, Niš, 2002.

[2] Application of Reliability – centered majnenance to naval aircraft, weapon systems and support equipment, MIL-HDBK-266, DoD, USA, 1981.

[3] Arnold D., Auf dem Weg zum Autonomen Materialfluss, Logistik im Unternehmen, Nov./Dez., 1989.

[4] Barlow, G., Proshan, F., Statistical Theory of Reliability and Life Testing Probability Models, Holt, richard nad Winston Inc., New York, 1975.

[5] Barlow, G.,Proshan, F., Statistical TheoryofReliability andLifeTestingProbabilityModels,Holt, RichardofWinstonInc.., NewYork, 1975.

[6] Callick, E.B., Teretechnology – principles and practice, teretecnology Handbook, HMSO, London, 1978.

[7] Deanzer, W., SystemsEngineering, Verlag industrilOrg., Zurich, 1979.

[8] Fitch, J.C., Proactive Maintenace Can Yield More Than a 10-fold Savings Over Conventional Predictive/ Preventive Maintenance Programs, diagnetics, Inc., 1997.

[9] Prasad, B., "CONCURRENT ENGINEERING-INTEGRATED PRODUCTAN DPROCESS ORGANIZATION", Vol. 1,Prentice-Hill, NewJersey, 1996.

[10] Nakajima, S., "TPM DevelopementINPLEMENTINGPROGRAMTOTALproductivemaintenence" productivitPress,Cambridge, Massachutsetts, Norwalk, Connecticut, 1989.
[11] ROTORSpiner, GMB, RIETERR, 1995.
[12] S. Stefanovic, DETERMINATION OF THE VALUE OF SELECTED OSCILLATION FREQUENCY MEASUREMENT POINT ANALYZED PARTS OE SPINNING - On theboxspinning, PRIYANKA RESEARCH JOURNAL PUBLICATION, International Journal of Mechanical Engineering Research and Development (IJMERD) ISSN 2248-9347, India, 2012.
[13] S. Stefanovic, DETERMINATION OPERATION TIME RISK OF BOX SPINNING COMPONENTS - OE SPINNING MACHINE American Journal of Engineering Research (AJER) e-ISSN : 2320-0847 p-ISSN : 2320-0936, 2013.
[14] S. Stefanovic, THE ANALYSIS OF FUNCTIONING OF BASIC COMPONENTS OF OE - TECHNICAL SYSTEM, INTERNATIONAL JOURNAL OF ENGINEERING, Tome XI (Year 2013). Fascicule 1. str. 237-244, ISSN 1584 – 2665, ANNALS of Faculty Engineering Hunedoara, Romania.
[15] S. Stefanović, RESERCH INTO THE CAUSES OF INACCURACIES OF COMPONENTS OF COMPLEX FOR COIL WINDING WITH FINISHED YERN AT OE. Lucrarea trimisă redacției MetalurgiaInternational a fost acceptată spre publicare în numărul 2013., ISSN 1582 – 2214, "METALURGIA INTERNATIONAL" is introduced in THOMSON SCIENTIFIC MASTER JOURNAL LIST, letter M, position 440.
[16] Stefanovic, S., Ugrenović, M., Productivitymodernspinning machines, depending on the parametersof diagnosticfailureinpower transmission systems, JournalTEHDISno.1/2002., Belgrade.
[17] S. Stefanovic, effects of the appearance of mechanical oscillations TO SAFE OPERATION circuit in fluid power systems and textile machinery, Doctoral dissertation, University of Novi Sad 2006th

American Journal of Engineering Research (AJER)
e-ISSN : 2320-0847 p-ISSN : 2320-0936
Volume-02, Issue-10, pp-271-275
www.ajer.org

Research Paper Open Access

Assessment of energy use pattern in residential buildings of Kano and Kaduna Northern Nigeria

Yohanna Irimiya, Iortyer A. Humphery, Ierve I. Aondover,
[1] *ECWA, Goodnews Katsit, P.O.Box 432. Kafanchan,Kaduna,Nigeria*
[2] *Mechanical Engineering Department Federal University of Agriculture,Makurdi, 2373, Nigeria,*
[3] *Works and Housing Department,Buruku Local Government Council, Buruku, Nigeria,*

Abstract: - The energy consumption end use of some selected residential buildings in Kaduna and Kano in the Northern part of Nigeria was studied by comparing their energy consumption pattern. The energy usage and intensities of the buildings as-built (Coventional) and when retrofitted with green features were studied and the impact of the green retrofits documented. An Analysis of Variance (ANOVA) was conducted at 0.05% which indicates a significant difference in the Energy consumption between the Conventional and Green features in the six study areas. From the study, the annual energy intensity of Kaduna for conventional buildings is 25.24 kwh/m^2. With the introduction of green appliances, a drastic reduction in the buildings annual energy consumption was recorded which stood at 20.57 kwh/m^2 representing about 18.26% reduction in annual energy consumption which indicates a significant energy saving. In Kano VAC consumed the highest energy 12.49 kwh/m^2 of the total consumption of all end-users. When replaced with energy efficient appliances the consumption dropped to 7.95 kwh/m^2 representing 34.14% reduction. The use of energy efficient appliances is recommended.

Keywords: - *Energy use, Residential Buildings, Northern Nigeria*

I. INTRODUCTION

Energy consumption all over the world is growing annually at an alarming rate. It's on this note that electricity utilities in many developing nations need to adopt the energy policy that encourages the efficient usage of limited electricity supply. This has been a grievous issue in many nations (Nigeria inclusive). In line with the recently held conference on Earth summit at Rio, it's believed that for energy to be made available to all, the developing nations need to reconsider their respective energy efficiency policy and strategies. This becomes necessary looking at the critical situation with respect to the energy consumption pattern in most of these nations which has left much to be desired [1].

According to [2] and [3] in collaboration with [4], the world consumes about 7,500Mtoe of energy every year. While primary energy consumption will grow by almost 50% from 2005 to 2030, the shares of different energy sources are not expected to change significantly in the near future. Also, according to [5], about 30-40% of all the primary energy is used in buildings worldwide. While in high and middle-income countries this is mostly achieved from the use of fossil fuels and biomass. This shows that, in the near future, more fossil fuels will be used to meet the energy demands of many nations. [3], also estimated that buildings account for about 30-40% of the word's energy consumption which is equivalent to 2,500 Mtoe every year. It is, therefore, an established fact that the building sector is responsible for a large share of the word's total energy consumption.

Energy consumption patterns in the world today shows that Nigeria and indeed African countries have the lowest rates of consumption. Nevertheless, Nigeria suffers from an inadequate supply of usable energy due to the rapidly increasing demand, which is typical of a developing economy. Paradoxically, the country is potentially endowed with sustainable energy resources. Nigeria is rich in conventional energy resources, which include oil, national gas, lignite, and coal. It is also well endowed with renewable energy sources such as wood, solar, hydropower, and wind [6].

The patterns of energy usage in Nigeria's economy can be divided into industrial, transport, commercial, agricultural, and household sectors [7]. The household sector accounts for the largest share of energy usage in the country - about 65%. The major energy-consuming activities in Nigeria's households are cooking, lighting, and use of electrical appliances. Cooking accounts for a staggering 91% of household energy consumption, lighting uses up to 6%, and the remaining 3% can be attributed to the use of basic electrical appliances such as televisions and pressing irons [8]

Energy consumed by households includes electricity, gas, diesel, kerosene, inverters, candles, lanterns etc. However, consumption is dominated by electricity. The enormity of Nigeria's energy problem creates a greater need for energy efficiency practice to be adopted by residential households as electricity demand in Nigeria far outstrips the supply which is epileptic in nature [9]. Energy efficiency has become the key driver for sustainable development. If we use energy more efficiently it will lead to saving of personal income and reduce the need for more power stations in the country [10], [11]. In the last few years more stringent environmental laws and souring energy prices has increased the need for household to react and participate in energy reduction and housing sustainability [12].

In most Nigerian homes, it is evident that energy efficiency is not factored in the choice of household appliances and electrical fittings. It could therefore be argued that electrical energy utilization in Nigeria is far from being efficient as in most homes; filament bulbs of wattages ranging from 40 watts to 120 watts per hour are still used.

The energy crises the country is facing coupled with population and infrastructural growth and the unrelenting rise of energy prices have stimulated research interest towards finding ways of alleviating or eliminating the unnecessary use of energy. Limited literatures on energy use in residential buildings have been reported:

[13], studied the monthly electric energy consumption of a total of 17 housing units at king Fahd University of petroleum and minerals, Dhahran, Saudi Arabia over a period of about five years. They found the annual average total electric energy consumption for 4.3.2 and 1 bedroom housing units to be 193, 208, 217 and 224 kwh/m^2 respectively. They reported that on average, the air – conditioning energy accounted for about 73% of the total energy consumed in the studied housing units. In another study, which compared energy consumption patterns of low – energy buildings to conventional buildings in Malaysia. The aim of this study is compare the impact of green buildings on efficient energy utilization in Nigeria. The objectives:

1. To identity the green features that can be retrofitted into buildings to enhance energy efficiency and conservation;
2. To highlight several dividends accruable from green buildings;

The importance of this work will among other things include, Identifying energy-saving measures (i.e. green retrofits) in buildings adaptable to the climate of our region, which will help in maximizing the total energy need of the nation; Provide a comprehensive database for identifying and quantifying projected benefits from investment in green building projects.

II. MATERIALS AND METHODS

2.1 Materials

The materials used are the Surveyor tape, Engineering Compass, the single phase *Lanvis* Analogue electric Meter.

2.2 The study area

Kano state is the second largest industrialized State in Nigeria. It is the centre of commerce and economy in Northern Nigeria. It lies between latitudes 12^0 23' and 9^0 33' north and longitudes 9^0 29' and 7^0 43' east. It has a population of 9, 383,682 in 2006. The estimated total land area is 20, 760 square kilometers. It has 44 local government areas. Kaduna State is a State in central Northern Nigeria,. Its capital is Kaduna. It has coordinates 10^0 27'N 7^0 45' and an area of 46,053km^2. It ranks between 3rd out of the 36 States and has a population 6,066.552 in 2006.

2.3 Data collection

The required data for the work were identified and classified as electrical energy-dependent appliances. The appliances were sub-categorized into ventilation and air-conditioning (VAC), lighting, cooking, food preservation, water heating, electronic and laundry. In order to determine the energy consumption of the selected buildings, parameters of household appliances such as energy rating, number of units consumed, hours of operation and the cost were collated as the primary data. Other parameters included the size of building and

building orientations. Summary of the parameters is presented in Table 1. The buildings investigated were 3 bed room flats.

Table 1: Summary Data of Buildings

Building	Location	Type	Area (m^2)	Orientation
Kaduna 1	Afaka, Mando	3-Bedroom	137.5	S75E
Kaduna 2	Ungwan Rimi	3-bedroom	72	S40E
Kaduna 3	NAF BASE	3-Bedroom	160	S30W
Kano 1	AKTH, KANO	3-Bedroom	168	N50E
Kano 2	AKTH, KANO	3-Bed room	168	N50E
Kano 3	Sallari, Kano	3-Bed room	162	East

2.4 Experimental procedure

A data collection form was designed for easy documentation of all the parameters collected from various buildings. The data measured included the size of the building in square meters, the orientation of the buildings and of the windows. The duration, in hours, of the building access to power supply from Power Holding Company of Nigeria (PHCN) was also recorded. The orientations of some of the buildings investigated shade them away from the direct incidence and impact of sunlight when the sun is at its peak. The buildings enjoy power supply from PHCN for 7-18 hours per day on the average. The buildings' household devices depended largely on electricity for their operation.

The physical characteristics (orientations and locations) of the green building were taken to be the same with their conventional counterparts. However, the conventional buildings were retrofitted with green products, which varied from one building to the other depending on the power consumption of the appliance incorporated into the buildings. Some of the green devices retrofitted into the building were lighting, cooking, cooling, ventilation, and electronic devices. These are energy-efficient household appliances such as compact fluorescent lamps, improved fridges, electric fans, air conditioners, and deep freezers. Each of these appliances was connected to an electric power recording meter (Single phase *Lanvis* Analogue Meter) through which the energy consumption of the appliance was observed and recorded. The Conventional Appliances were each connected to a recording meter. The readings were collected for a period of six months after which the buildings were retrofitted with more energy-efficient appliances and readings collected for another period of six months, making one year, the energy intensity was determined from the floor area of building and the energy consumption of each appliance.

2.5 Data Analysis

Monthly consumption for each type of appliance and the percentage breakdown of total consumption were analysed descriptive statistics on Microsoft Exec 2007. The Energy Intensity (EI), which determines the ratio of the energy consumed in kWh to the floor area of building in square meter, was calculated using equation 1. A computer application software (micro soft Excel) was employed in the preparation, interpretation and analysis of the collated data. Analysis of variance (ANOVA) was carried out on the energy intensity data of the conventional and green buildings using sigma Plot 11.0 software version in order to determine if there are significant differences between their means.

$$Energy\ Intensity = \frac{Total\ Energy\ Consumption}{Floor\ Area} \quad (1)$$

III. RESULTS

3.1 Analysis of variance for the conventional and energy efficient appliances for the study area

Then data was subjected to analysis of variance at 5% to test for significant differences. The Anova test shows that, there was significant difference at 95% for the seven appliances (rows) indicating that there was a difference in the energy intensity between the conventional and the energy efficient buildings appliances. The Anova test shows no significant difference at 95% for the study areas (columns), implying that the study was standardized. The mean values for the entire study was then considered for analysis.

Table 2: ANOVA for conventional and energy efficient appliances for the study area

ANOVA

Source of Variation	*SS*	*df*	*MS*	*F*	*P-value*	*F crit*
Rows	175.5414	5	35.10827	4.080773	0.007598	2.602987
Columns	24.99242	5	4.998484	0.580994	0.714171	2.602987
Error	215.0834	25	8.603338			
Total	415.6172	35				

$H_{o:}\ F \leq Fcrit.$ $\propto = 0.05$
$H_{a:}F \geq Fcrit.$

3.2 Energy end use in the study area

Table 3 shows the breakdown of energy consumptions by the various energy end-users in Kaduna. From the Table 3, energy intensities of VAC, lighting, cooking, preservation, water heating, electronic and laundry devices were 4.16kwh/m^2, 5.08 kwh/m^2, 10.19 kwh/m^2, 3.47 kwh /m^2, 0.53 kwh /m^2, 1.09 kwh /m^2, 0.71 kwh /m^2while consumption for the retrofitted building was 3.4 kwh /m^2, 3.16 kwh /m^2, 9.36 kwh /m^2, 2.63 kwh /m^2, 0.48 kwh /m^2, 0.88 kwh /m^2 and 0.65 kwh /m^2 representing 16 %, 32%, 8.39%, 24.25%, 9.43%, 14.93%, 8.45%, reduction respectively of the total energy consumption of the conventional buildings in Kaduna. The least energy was consumed by water heating with 0.53 kwh/m^2 representing 9.43 % savings of the overall energy consumption while the highest was consumed by cooking, 10.19 kwh/m^2. The annual energy intensity of Kaduna for conventional buildings is 25.24 kwh/m^2. With the introduction of green appliances, a drastic reduction in the buildings annual energy consumption was recorded which stood at 20.57 kwh/m^2 representing about 18.26% reduction in annual energy consumption which indicates a significant energy saving.
Energy consumptions pattern in Kano for both conventional and efficient appliances is presented in Table 4. VAC consumed the highest energy 12.49 kwh/m^2 of the total consumption of all end-users. When replaced with energy efficient appliances the consumption dropped to 7.95 kwh/m^2 representing 34.14% reduction. Details of energy consumption in kWh/m^2 in Kano are as shown in Table 4.
Fig. 1 shows the overall energy intensity for the entire study. Lighting and VAC has the highest annual consumption (42.19 kwh/m^2 and 15.92 kwh/m^2) followed by preservation and cooking (3.97 kwh/m^2 and 3.87 kwh/m^2) electronic, laundry and water heating have the lowest consumption of (1.24 kwh/m^2, 0.06 kwh/m^2 and 0.05 kwh/m^2).

Table 3: Energy consumption and savings for conventional and energy efficient buildings in Kaduna

Usage	Conventional kw/m_2	Energy Efficient kw/m^2	Energy savings kw/m^2	Energy savings (%)
VAC	4.16	3.4	0.76	16
Lighting	5.08	3.16	1.85	32
Cooking	10.19	9.36	0.83	8.39
Preservation	3.47	2.63	0.84	24.25
Water heating	0.53	0.48	0.05	9.43
Electronic	1.09	0.88	0.21	14.93
Laundry	0.71	0.65	0.06	8.45
Total	**25.23**	**20.56**	**4.6**	**113.45**

Table 4: Energy consumption and savings for conventional and energy efficient buildings in Kano

Usage	Conventional kw/m^2	Energy efficient kw/m^2	Energy savings kw/m^2	Energy savings %
VAC	12.49	7.95	4.48	34.14
Lighting	3.92	2.48	1.44	40.16
Cooking	1.78	1.77	0.01	1.5
Preservation	1.49	1.01	0.48	21.32
Total	**19.69**	**13.21**	**6.41**	**97.12**

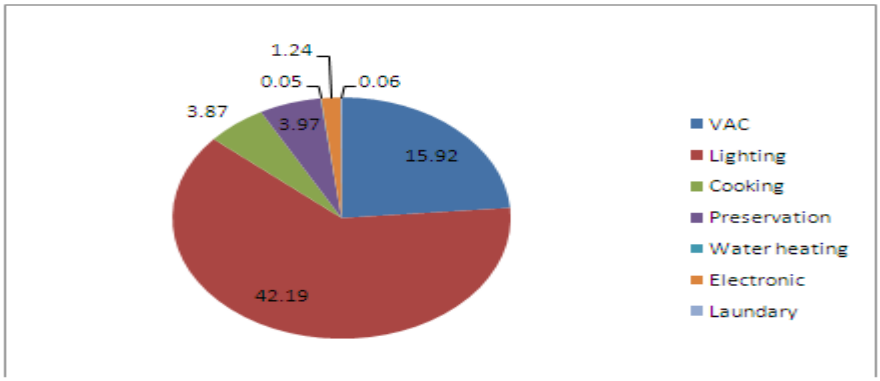

Figure 1: Overall energy intensities of conventional and energy efficient buildings in the study areas

IV. CONCLUSIONS AND RECOMMENDATIONS

The study has shows that overall energy intensity for the entire study was Lighting and VAC has the highest annual consumption (42.19 kwh/m^2 and 15.92 kwh/m^2) followed by preservation and cooking (3.97 kwh/m^2 and 3.87 kwh/m^2) electronic, laundry and water heating have the lowest consumption of (1.24 kwh/m^2, 0.06 kwh/m^2 and 0.05 kwh/m^2).

It can therefore, be concluded that green buildings impacts positively on energy consumptions in residential buildings in Nigeria. This is evident in the low energy consumptions recorded in the green buildings compared to those of the conventional buildings. Hence, the contribution of this research finding will bring about considerable energy savings in conventional buildings in Nigeria. Energy consumptions of residential building in Nigeria should be adequately monitored and data collected on monthly basis. This would give exact representation of residential buildings energy consumptions.

REFERENCES

[1] www.punchng.com/feature/power-talkback/case-for-energy-efficient-appliances/
[2] IEA, World Energy outlook, 5-7, 2002
[3] IEA, Key World Energy Statistics, 25-30, 2005
[4] Energy Information Administration, E1A. World Energy Overview, 1993-2003. Energy information Administration Washington DC 2005 http://www.eia.doe.govr/emeu/overview/htm/.
[5] UNEP, Buildings and Climate Change Status, Challenges and opportunities'' United Nations Environmental programme, 2007
[6] Okafor ECN, Joe-Uzuegbu CKA, Challenges To Development Of Renewable Energy For Electric Power Sector In Nigeria. International Journal Of Academic Research 2(2):211- 216, 2010
[7] Energy Commission of Nigeria (ECN) National Energy Policy. Federal Republic of Nigeria,Abuja. 2003
[8] Energy Commission of Nigeria (ECN), Renewable Energy Master Plan. 2005
[9] Sule, B.F., Ajao, R.K., Ajimotokan, A.H. and Garba, M.K. Compact Fluorescent Lamps and Electricity Consumption Trend in Residential Buildings in Ilorin, Nigeria, International Journal of Energy sector Management,5 (2): 162-168, 2011, Emerald Group Publishing Limited, UK
[10] Otegbulu, A.C. Economics of Green Design and Environmental Sustainability, Journal of Sustainable Development,. 4(2); 240-248, 2011, Canadian
[11] CREDC, Energy Efficiency Survey in Nigeria, *Community Research Development Centre (CREDC)* Benin City, 2009
[12] Eves, C. and Kippen, S. (2010) Public Awareness of Green and Energy Efficient Residential Property: An empirical survey based on data from New-Zealand, Property Management, 28(3), 193-208 2010, Emerald Group Publishing Limited, UK
[13] Elhadidy, M.A and Manzoor-ul-Haq, A.AElectric energy consumption in selected resident ion buildings at King Fahd University of petroleum and Minerals, Dhahran, Saudi Arabia, 2011

American Journal of Engineering Research (AJER)
e-ISSN : 2320-0847 p-ISSN : 2320-0936
Volume-02, Issue-10, pp-276-281
www.ajer.org

Research Paper Open Access

An inverse steady state thermal stresses in a thin clamped circular plate with internal heat generation

C. M. Bhongade[1] and M. H. Durge[2]
[1]Department of Mathematics, Shri. Shivaji College, Rajura, Maharashtra, India
[2] Department of Mathematics, Anand Niketan College, Warora, Maharashtra, India

Abstract: - This paper deals with the determination of temperature, displacement and thermal stresses in a thin clamped circular plate with internal heat generation. A clamped circular plate is subjected to arbitrary known interior temperature. Under steady state, the fixed circular edge and lower surface of circular plate are thermally insulated. Here we modify Kulkarni (2008) and designed most general solution of displacement potential, radial stresses and angular stresses. The governing heat conduction equation has been solved by the method of integral transform technique. The results are obtained in a series form in terms of Bessel's functions. The results for temperature change, displacement and stresses have been computed numerically and illustrated graphically.

Keywords: - *Inverse problem, thin clamped circular plate and internal heat generation.*

I. INTRODUCTION

During the second half of the twentieth century, nonisothermal problems of the theory of elasticity became increasingly important. This is due to their wide application in diverse fields. The high velocities of modern aircraft give rise to aerodynamic heating, which produces intense thermal stresses that reduce the strength of the aircraft structure.

The inverse thermoelastic problem consists of determination of the temperature of the heating medium, the heat flux on the boundary surfaces of the thin clamped circular plate when the conditions of the displacement and stresses are known at the some points of the thin clamped circular plate under consideration. Noda *et al.* (1989) discussed an analytical method for an inverse problem of three dimensional transient thermoelasticity in a transversely isotropic solid by integral transform technique with newly designed potential function and illustrated practical applicability of the method in engineering problem. Sabherwal K. C. (1965) studied an inverse problem of heat conduction. Greysa *et al*. (1989) investigated an inverse temperature field problem of theory of thermal stresses. Deshmukh and Wankhede (1998) studied an inverse transient problem of quasi static thermal deflection of a thin clamped circular plate. Ashida *et al.* (2002) studied the inverse transient thermoelasticity problem for a composite circular disc constructed of transversely isotropic layer. Most recently Bhongade and Durge (2013) considered thick circular plate and discuss, effect of Michell function on steady state behavior of thick circular plate, now here we consider a thin clamped circular plate with internal heat generation subjected to arbitrary known interior temperature. Under steady state, the fixed circular edge and lower surface of circular plate are thermally insulated. Here we modify Kulkarni (2008) and designed most general solution of displacement potential, radial stresses and angular stresses. The governing heat conduction equation has been solved by the method of integral transform technique. The results are obtained in a series form in terms of Bessel's functions. A mathematical model has been constructed for thin clamped circular plate with the help of numerical illustration by considering aluminum (pure) circular plate. No one previously studied such type of problem. This is new contribution to the field.

The inverse problem is very important in view of its relevance to various industrial mechanics subjected to heating such as the main shaft of lathe, turbines and the role of rolling mill.

II. FORMULATION OF THE PROBLEM

Consider a thin clamped circular plate circular plate of thickness $2h$ defined by $0 \leq r \leq a, -h \leq z \leq h$. Let the plate be subjected to arbitrary known interior temperature $f(r)$ within region $-h < z < h$. With lower

surface $z = -h$ and circular surface $r = a$ are thermally insulated. Under these more realistic prescribed conditions, the unknown temperature $g(r)$, which is at upper surface of the plate. Temperature, displacement and stresses in a thin clamped circular plate with internal heat generation are required to be determined.

Following Roy Choudhuri (1972), assume that for small thickness *h* plate is in a plane state of stress. In fact the smaller the thickness of the plate compared to its diameter, the nearer to a plane state of stress is the actual state. Then the displacement equations of thermoelasticity have the form

$$U_{i,kk} + \left(\frac{1+v}{1-v}\right) e_{,i} = 2\left(\frac{1+v}{1-v}\right) a_t T_{,i} \quad (1)$$

$$e = U_{k,k}\ ; k, i = 1,2. \quad (2)$$

where

U_i - displacement component

e - dilatation

T – temperature

and v and a_t are respectively, the Poisson's ratio and the linear coefficient of thermal expansion of the plate material.

Introducing

$$U_i = U_{,i} \qquad i = 1, 2.$$

we have

$$\nabla_1{}^2 U = (1+v) a_t T \quad (3)$$

$$\nabla_1{}^2 = \frac{\partial^2}{\partial k_1{}^2} + \frac{\partial^2}{\partial k_2{}^2}$$

$$\sigma_{ij} = 2\mu\left(U_{,ij} - \delta_{ij} U_{,kk}\right), \quad i, j, k = 1, 2. \quad (4)$$

where μ is the Lames constant and δ_{ij} is the Kronecker symbol.

In the axially-symmetric case

$$U = U(r, z),\ T = T(r, z)$$

and the differential equation governing the displacement potential function $U(r, z)$ is given as

$$\frac{\partial^2 U}{\partial r^2} + \frac{1}{r}\frac{\partial U}{\partial r} = (1+v) a_t T \quad (5)$$

$$U = \frac{\partial U}{\partial r} = 0, \quad r = a \text{ for all time } t. \quad (6)$$

The stress function σ_{rr} and $\sigma_{\theta\theta}$ are given by

$$\sigma_{rr} = \frac{-2\mu}{r}\frac{\partial U}{\partial r} \quad (7)$$

$$\sigma_{\theta\theta} = -2\mu\frac{\partial^2 U}{\partial r^2} \quad (8)$$

In the plane state of stress within the plate

$$\sigma_{rz} = \sigma_{zz} = \sigma_{\theta z} = 0 \quad (9)$$

Temperature $T(r, z)$ of the circular plate satisfying heat conduction equation as follows,

$$\frac{\partial^2 T}{\partial r^2} + \frac{1}{r}\frac{\partial T}{\partial r} + \frac{\partial^2 T}{\partial z^2} + \frac{q}{k} = 0 \quad (10)$$

with the conditions

$$\frac{\partial T}{\partial r} = 0 \ \ at \ \ r = a,\ -h \le z \le h \quad (11)$$

$$\frac{\partial T}{\partial z} = 0 \ \ at\ z = -h,\ 0 \le r \le a \quad (12)$$

$$T = f(r)\ (known)\ at \ \ z = \xi\ ,\ -h \le \xi \le h,\ 0 \le r \le a \quad (13)$$

and

$$T = g(r)\ (unknown)\ at \ \ z = h\ ,\ 0 \le r \le a \quad (14)$$

where *k* is the thermal conductivity of the material of the plate, *q* is the internal heat generation.

Equations (1) to (14) constitute the mathematical formulation of the problem.

III. SOLUTION

To obtain the expression for temperature T (r, z), we introduce the finite Hankel transform over the variable *r* and its inverse transform defined as in Ozisik (1968)

$$\bar{T}(\beta_m, z) = \int_{r'=0}^{a} r' K_0(\beta_m, r)\ T(r, z)\, dr' \quad (15)$$

$$T(r, z) = \sum_{m=1}^{\infty} K_0(\beta_m, r)\ \bar{T}(\beta_m, z) \quad (16)$$

where $K_0(\beta_m, r) = \frac{\sqrt{2}}{a}\frac{J_0(\beta_m r)}{J_0(\beta_m a)}$

and $\beta_1, \beta_2 \ldots\ldots$ are roots of the transcendental equation

$$J_1(\beta_m a) = 0 \tag{17}$$

where $J_n(x)$ is Bessel function of the first kind of order n.

On applying the finite Hankel transform defined in the Eq. (15) and its inverse transform defined in Eq. (16) to the Eq. (10), one obtains the expression for temperature as

$$T(r,z) = \sum_{m=1}^{\infty} \frac{\sqrt{2}}{a}\frac{J_0(\beta_m r)}{J_0(\beta_m a)} \left\{ \begin{array}{c} -[A(\beta_m,\xi) - F(\beta_m)]\frac{\cosh[\beta_m(z+h)]}{\cosh[\beta_m(h+\xi)]} \\ -\frac{1}{\beta_m}\frac{dA(\beta_m,-h)}{dz}\frac{\sinh[\beta_m(z-\xi)]}{\cosh[\beta_m(h+\xi)]} + A(\beta_m,z) \end{array} \right\} \tag{18}$$

where $A(\beta_m, z)$ is particular integral of differential Eq. (10) and $F(\beta_m)$ is Hankel transform of $f(r)$.

The unknown temperature $g(r)$ can be obtained by substituting $z = h$ in Eq. (18) as

$$g(r) = \sum_{m=1}^{\infty} \frac{\sqrt{2}}{a}\frac{J_0(\beta_m r)}{J_0(\beta_m a)} \left\{ \begin{array}{c} -[A(\beta_m,\xi) - F(\beta_m)]\frac{\cosh[2\beta_m h]}{\cosh[\beta_m(h+\xi)]} \\ -\frac{1}{\beta_m}\frac{dA(\beta_m,-h)}{dz}\frac{\sinh[\beta_m(h-\xi)]}{\cosh[\beta_m(h+\xi)]} + A(\beta_m,h) \end{array} \right\} \tag{19}$$

To obtain displacement potential $U(r,z)$ using Eq. (18) and Eq. (5), one obtain,

$$U(r,z) = \frac{\sqrt{2}}{a}(1+v)a_t \sum_{m=1}^{\infty} \frac{[J_0(\beta_m r) - J_0(\beta_m a)]}{{\beta_m}^2 J_0(\beta_m a)} \times \left\{ \begin{array}{c} [A(\beta_m,\xi) - F(\beta_m)]\frac{\cosh[\beta_m(z+h)]}{\cosh[\beta_m(h+\xi)]} \\ -\frac{1}{\beta_m}\frac{dA(\beta_m,-h)}{dz}\frac{\sinh[\beta_m(z-\xi)]}{\cosh[\beta_m(h+\xi)]} + A(\beta_m,z) \end{array} \right\} \tag{20}$$

Now using Eqs. (18) and (20) in Eq. (7) and (8), one obtains the expressions for stresses respectively as

$$\sigma_{rr} = \frac{2\sqrt{2}\mu}{a\,r}(1+v)a_t \sum_{m=1}^{\infty} \frac{{J_0}'(\beta_m r)}{\beta_m J_0(\beta_m a)} \times \left\{ \begin{array}{c} [A(\beta_m,\xi) - F(\beta_m)]\frac{\cosh[\beta_m(z+h)]}{\cosh[\beta_m(h+\xi)]} \\ -\frac{1}{\beta_m}\frac{dA(\beta_m,-h)}{dz}\frac{\sinh[\beta_m(z-\xi)]}{\cosh[\beta_m(h+\xi)]} + A(\beta_m,z) \end{array} \right\} \tag{21}$$

$$\sigma_{\theta\theta} = -\frac{2\sqrt{2}\mu}{a}(1+v)a_t \sum_{m=1}^{\infty} \frac{{J_1}'(\beta_m r)}{J_0(\beta_m a)} \times \left\{ \begin{array}{c} [A(\beta_m,\xi) - F(\beta_m)]\frac{\cosh[\beta_m(z+h)]}{\cosh[\beta_m(h+\xi)]} \\ -\frac{1}{\beta_m}\frac{dA(\beta_m,-h)}{dz}\frac{\sinh[\beta_m(z-\xi)]}{\cosh[\beta_m(h+\xi)]} + A(\beta_m,z) \end{array} \right\} \tag{22}$$

IV. SPECIAL CASE AND NUMERICAL CALCULATIONS

1. $f(r) = r^2$ (23)

applying finite Hankel transform as defined in eq.(15) to the eq.(23), one obtains

$$F(\beta_m) = \frac{\sqrt{2}\,a}{J_0(\beta_m a)}\left[aJ_1(\beta_m a) - 2J_2(\beta_m a)\right]$$

2. $q(r,z) = \delta(r - r_0)\delta(z - z_0)$

$$\bar{q}(\beta_m, z) = \frac{\sqrt{2}}{a} r_0 \delta(z - z_0)\frac{J_0(\beta_m r_0)}{J_0(\beta_m a)}$$

where $\delta(r)$ is well known dirac delta function of argument r.

$a = 1m, h = 0.1m, r_0 = 0.5m$ *and* $z_0 = 0.05m$.

4.1 *Material Properties*

The numerical calculation has been carried out for aluminum (pure) plate with the material properties defined as

Thermal diffusivity α = 84.18× 10^{-6} m^2s^{-1},

Specific heat c_ρ = 896 J/kg,

Thermal conductivity k = 204.2 W/m K,

Shear modulus G = 25.5 G pa,

Poisson ratio ϑ = 0.281,

4.2 *Roots of transcendental equation*

The $\beta_1 = 3.8317$, $\beta_2 = 7.0156$, $\beta_3 = 10.1735$, $\beta_4 = 13.3237$, $\beta_5 = 16.4704$, $\beta_6 = 19.6159$ are the roots of transcendental equation $J_1(\beta_m a) = 0$. The numerical calculation and the graph has been carried out with the help of mathematical software Mat lab.

V. DISCUSSION

In this problem, thin clamped circular plate is considered which is subjected to arbitrary known interior temperature and determined the expressions for unknown temperature, displacement and stresses. As a special case mathematical model is constructed for $f(r) = r^2$ and performed numerical calculations. The thermoelastic behavior is examined such as temperature, displacement and stresses in a thin clamped circular plate with internal heat generation.

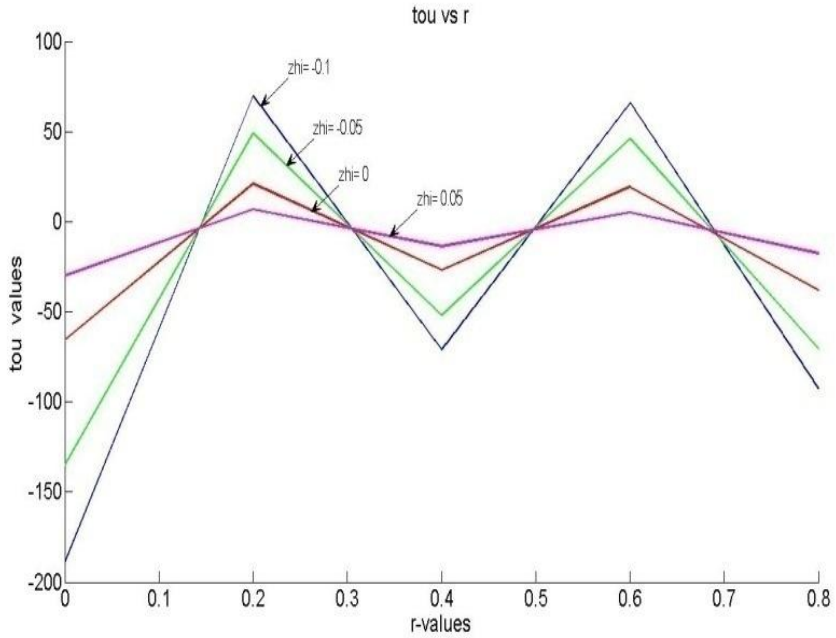

Fig. 1 Temperature $T(r,z)$ in radial direction

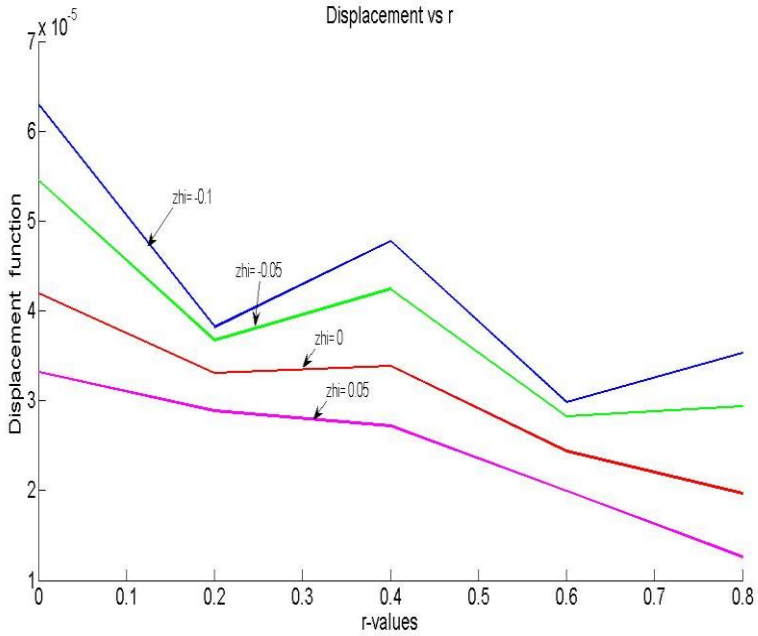

Fig. 2 Displacement $U(r,z)$ in radial direction

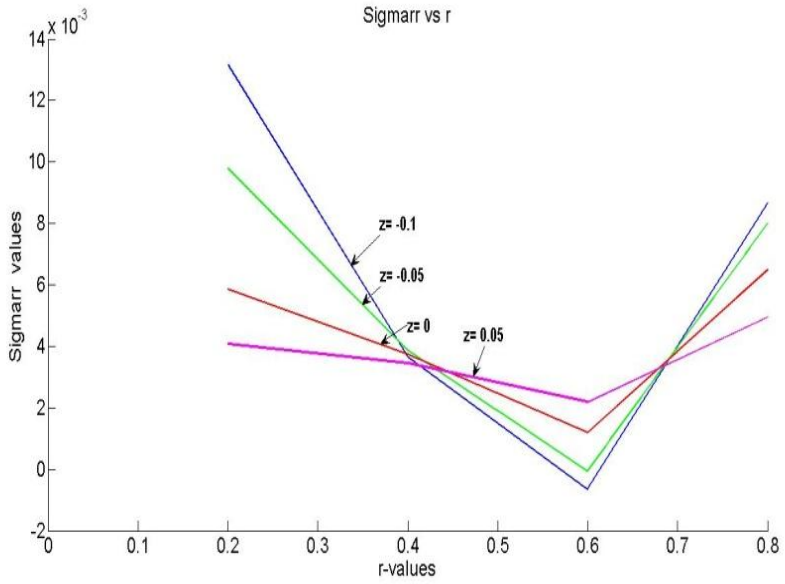

Fig. 3 Radial stress σ_{rr} in radial direction

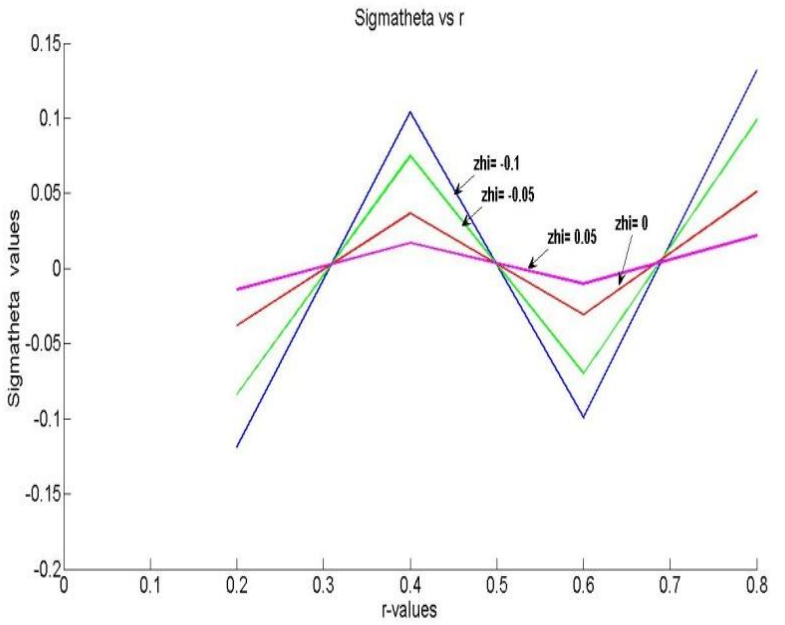

Fig. 4 Angular stress $\sigma_{\theta\theta}$ in radial direction

From Fig. 1 Due to internal heat generation temperature is increasing for $0 \leq r \leq 0.2$, $0.4 \leq r \leq 0.6$ and decreasing for $0.2 \leq r \leq 0.4$, $0.6 \leq r \leq 0.8$ along radial direction. The overall behavior of temperature is decreasing and it is inversely vary with arbitrary known interior temperature along radial direction.
From Fig. 2 Due to internal heat generation displacement is decreasing for $0 \leq r \leq 0.2$, $0.4 \leq r \leq 0.6$ and increasing for $0.2 \leq r \leq 0.4$, $0.6 \leq r \leq 0.8$ along radial direction. The overall behavior of displacement is decreasing and it is inversely vary with arbitrary known interior temperature along radial direction.
From Fig. 3 Due to internal heat generation the radial stress is decreasing for $0.2 \leq r \leq 0.6$ and increasing for $0.6 \leq r \leq 0.8$ along radial direction. The overall behavior of radial stress is compressive and it is inversely vary with arbitrary known interior temperature along radial direction.
From Fig. 4 Due to internal heat generation the angular stress is increasing for $0.2 \leq r \leq 0.4$, $0.6 \leq r \leq 0.8$ and decreasing for $0.4 \leq r \leq 0.6$ along radial direction. The overall behavior of angular stress is tensile and it is inversely vary with arbitrary known interior temperature along radial direction.

VI. CONCLUSION

Due to internal heat generation temperature and displacement are decreasing and it is inversely vary with arbitrary known interior temperature along radial direction. Due to internal heat generation the radial stresses are compressive and the angular stresses are tensile and It is inversely vary with arbitrary known interior temperature along radial direction.

The results obtained here are useful in engineering problems particularly in the determination of state of stress in a thin clamped circular plate, base of furnace of boiler of a thermal power plant and gas power plant.

REFERENCES

[1] Noda N., Ashida F. and Tsuji T, An inverse transient thermoelastic problem of a transeversly isotropic body, *Journal of applied Mechanics, 56(4),* 1989,791-797.

[2] Sabherwal K. C., An inverse problem of transient heat conduction, *Indian Journal of Pure Applied Physics, 3E(10),* 1965, 397-398.

[3] Grysa K., Cialkowski M. J. and Kaminski H., An inverse temperature field problem of theory of thermal stresses, *Nucl. Eng. Des..64*, 1981169-184.

[4] Deshmukh K.C. and Wankhede P. C., An inverse transient problem of quasi-static thermal deflection of a thin clamped circular plate, *Bulletin of pure and applied sciences, 17E(1),* 1998 .

[5] Ashida F. and Sakata S., Tauchert, T. R. and Yamashita Y., Inverse transient thermoelastic problem for a composite circular disc, *Journal of thermal stresses*, *25*, 2002, 431-455.

[6] Bhongade C. M. and Durge M. H., Effect of Michell function on steady state behavior of thick circular plate, *IOSR J. of Mathematics, 8(2),* 2013, 55-60.

[7] Kulkarni V. S., *Study of some thermoelastis problem*, Thesis, R. T. M. Nagpur University, Nagpur, 2008.

[8] Roy Choudhary S. K., A note of quasi static stress in a thin circular plate due to transient temperature applied along the circumference of a circle over the upper face, *Bull Acad Polon Sci, Ser, Scl,Tech, 20,* 1972, 21.

[9] M. N. Ozisik, *Boundary Value Problems of Heat Conduction*, International Text Book Company, Scranton, Pennsylvania, 1968.

American Journal of Engineering Research (AJER)
e-ISSN : 2320-0847 p-ISSN : 2320-0936
Volume-02, Issue-10, pp-282-290
www.ajer.org

Research Paper Open Access

Assessment of the Chemical Characteristics of a Spring Water Source at Ife-Owutu, Ezinihite-Mbaise, Southeastern Nigeria.

Ibeneme, S.I.[1], Ukiwe, L.N.[2], Essien, A.G.[1], Nwagbara, J.O.[1], Nweze, C.A.[2], Chinemelu, E.S.[1] And Ivonye, C.A.[1]

[1]*Department of Geosciences, Federal University of Technology,Owerri, Imo State, Nigeria.*
[2]*Department of Chemistry, Federal University of Technology,Owerri, Imo State, Nigeria.*

Abstract: - The chemical characteristics of the Giri Giri Nwanjoku Spring in Owutu Ezinihitte-Mbaise, South Eastern Nigeria was investigated to carefully determine some basic geochemical constituents of the water source with a view to identifying those constituents whose concentrations are unacceptably high, compared with the maximum permissible level of a regulatory body and as such determine its wholesome portability for diverse usage. The resultant data conform to the Nigerian Industrial Standard (2007) and the World Health Organization (2006) Standard. The water source is generally neutral with an average pH of 6.85. However, the samples gave an average Calcium and Magnesium ion concentrations of 3.205mg/l and 0.82mg/l respectively and an average hardness (as $CaCO_3$) of 11.375mg/l, indicating that the water is relatively soft. The Stiff and Schoeller plots show at a glance the spatial variations of the chemical constituents of the spring with Tri-oxo-carbonate and Calcium dominating. From the Box and Whisker plot, the greater amount of the cations and anions lie within the second quarter of the box ranging from 0.01meq/l to 0.05meq/l indicating similarity in origin. The Piper trilinear diagram reveals an alkaline earth and weak acid group predominantly the Tri-oxo-carbonate and as such classified as Ca-(Mg)-Na-HCO_3 water facies which indicates portability. The Sodium Absorption Ratio (SAR) and Percentage Sodium (%Na) values of 0.27 and 34.20% respectively show that the water is good for Agricultural use. The Pollution Index (PI) value of 0.6 (which is less than the critical value of unity) shows that the spring water is not polluted. For industrial use, the Saturation Index (SI) value of -3.41 reveals that the water may lead to moderate corrosion if not properly treated.

Key Words: - *Eyelet, Hydrogeochemistry, Saturation Index, Spring, Water Facies.*

I. INTRODUCTION

Water is the most abundant molecule on Earth's surface. It can also be the most abundant natural resource on earth. It constitutes about 75% of the Earth's surface. Water is a vital component of life for both plants and animals. It is available in forms of rain and snow thereby making rivers, oceans, streams, lakes, springs etc. A spring can be described as any natural occurrence where water flows on to the surface of the earth from below the surface. Some springs discharge where the water table intersects the land surface, but also they occur where water flows out from caverns or along fractures, fault or rock contacts that come to the surface. Spring may result from karst topography where surface water has infiltrated the earth's surface (recharge area), becoming part of the area's ground water that travels through a network of cracks and fissures/openings ranging from intergranular spaces to large caves. The water eventually emerges from below the surface, in the form of spring. The forcing of the spring to the surface can be the result of a confined aquifer in which the recharge area of the spring water table rests at a higher elevation than that of the outlet. The Giri Giri Nwanjoku spring occurs at the scarp face of the Umuosita-Awaka mini-escarpment. This spring serves as water source for the inhabitants of the area who utilize the water for their daily activities. Hence there arose the need to assess the quality of this spring to make recommendations where necessary.

II. AIMS AND OBJECTIVES OF THE STUDY

The principal aim of the study is to carefully determine some basic geochemical constituents of the water source within the study area with a view to identifying those constituents whose concentrations are unacceptably high and anomalous, compared with the maximum permissible level of a regulatory body and as such determine its wholesome portability for diverse usage.

III. LOCATION, PHYSIOGRAPHY AND GEOLOGY OF THE STUDY AREA

The study area is bounded by longitudes 7^{o} 16'E to 7^{o} 23'E and latitudes 5^{o} 26' N to 5^{o} 32' N (Fig. 1). The area is located within the Anambra/Imo river basin. Ife-Owutu is located within Ezinihitte Mbaise Local Government Area of Imo state, south eastern Nigeria and is accessible through diverse road networks. The study area lies within the tropical rain forest region of Nigeria. The region has four dry months in which precipitation is less than 60mm, while the annual total rainfall ranges between 1800mm and 2600mm. The mean temperature of the area is about 80^{o}F [1]. The vegetative cover of the area is mainly shrub, rain forest and savannah vegetation. It is dominated by grass species. The drainage pattern is dendritic. Geologically, Ife-Owutu area is underlain by a sequence of sedimentary rocks belonging to the Benin Formation of Miocene to Recent age. It comprises of a thick sequence of poorly consolidated to unconsolidated sandstones that are friable with sorting ranging from poorly to fairly sorted [2]. Several grain sizes occur within the unit and the coarse and fine unit alternate along the vertical sequence. The thick sandy units are frequently separated by thin and discontinuous clay streaks and lenses. The clay beds are thin (less than 1m) and sometimes occur as lamination lining the bedding plane of the unconsolidated sandstone beds. The Formation starts as a thin edge at its contact with the Ogwashi/Asaba Formation in the north of the area and thickens southwards [3]. The Formation across the whole Niger Delta is about 90% sandstone with minor shale intercalations.

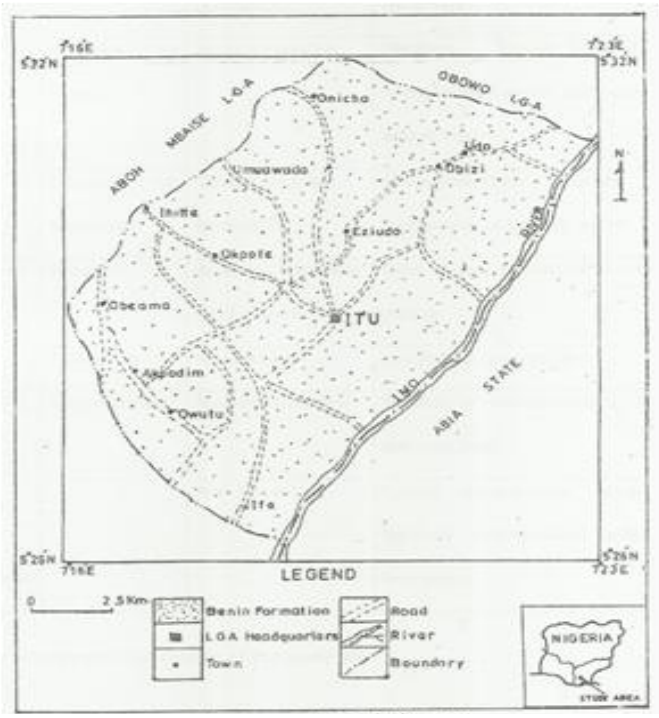

Figure 1. Geological map of the study area.

IV. METHODOLOGY

Water sampling was carried out from two different eyelets (hair-like openings from which water oozes out of a rock) of the spring and labeled GE I and GE II. The location of studied spring was taken with the help of GARMIN GPSmap76CSx. The water samples were collected into 1 L polyethylene bottles which were pre-cleaned with concentrated hydrochloric acid and distilled water. pH and temperature of the water samples were measured on-site with a Thermo electron Corporation Orion 3 Star pH Benchtop. This was also done to avoid unpredictable changes in characteristics as per the standard procedure [4]. Sampling protocols according to [5] and [6] were adopted. Total dissolved solids (TDS), electrical conductivity (EC) or specific conductance and resistivity of collected water samples were measured using Delta Ohm HD 2306.0 conductivity meter. All the water samples were preserved in a refrigerator to exclude microbial activity and unwanted chemical reaction until analysis was completed within 2 days. The determinations of other physico-chemical properties of the

water samples were performed within 2 days of sampling. HACH DR 2800 Spectrophotometer was used in the determination of different hydro geochemical properties such as Na, K, HCO_3, Cl, NO_3, and SO_4. Analytical water test tablets prescribed for HACH DR Spectrophotometer 2800 using procedures outlined in the HACH DR 2800 Spectrophotometer manual were used for the examination of the water quality. Other analyses such as the determination of Mg and Ca concentrations were done by complexometric titration method. The analytical data quality was evaluated by computing the sum of the equivalents of the cations with the sum of the equivalents of the anions [7]. A positive result means that both an excess cations or insufficient anion exists, and a negative result means the opposite. For freshwater, ionic balance is assumed to be good if it lies within the range of ±10% [8]. In this study, ionic balance values ranged from -0.92 to + 0.22%. Table 1 displays the result of the hydro geochemical analysis of the spring water sample, along with the Nigerian Industrial Standard [9] and World Health Organisation Standard [10]. Such drinking water standards are generally based on two main criteria [11]: (1) presence of objectionable taste, odour, and colour and; (2) presence of substances with adverse physiological (health-effect) characteristics.

Table 1. Result of the hydrogeochemical analysis of the spring water samples, compared with the Nigerian Industrial Standards (NIS 2007) and World Health Organization Standard (WHO 2006).

PARAMETER	GE I	GE II	GE MEAN	NIS 2007	WHO 2006	UNDESIRABLE EFFECTS AT HIGHER LEVELS
Temperature	26	24	25	Ambient	25	
pH	6.8	6.9	6.85	6.5-8.5	6.5-8.5	High pH-Corrosion; Low pH-Taste/Soapy feeling.
Colour (TCU)	5.0	5.5	5.25	15	15	Appearance.
Turbidity (NTU)	3.0	5.0	4.0	5	5	Appearance.
Conductivity	50.0	62.0	56.0	1000	100	-
T.D.S (mg/l)	25.5	20.4	22.95	500	500	Taste.
T.S.S(mg/l)	7.0	9.0	8.0	-	-	-
Calcium(mg/l)	3.6	2.81	3.21	100	75	Scale Formation.
Magnesium(mg/l)	0.89	0.75	0.82	0.2	<30	Hardness and Gastrointestinal Irritation.
Potassium(mg/l)	0.95	1.23	1.09	200	200	-
Sodium(mg/l)	2.17	1.98	2.08	200	200	Taste.
Sulphate(mg/l)	0.45	0.37	0.41	100	250	Taste and Corrosion.
Nitrate(mg/l)	0.10	0.08	0.09	50	10	Physiological problems.
Chloride(mg/l)	0.69	0.83	0.76	250	200	Taste and Corrosion.
Bicarbonate(mg/l)	18.74	25.6	22.17	500	500	-
Hardness as CaCO3(mg/l)	12.65	10.10	11.37	150	200	High-Scale deposit and scum formation; Low-Possible corrosion.

Table 2. Concentration of the major Cations and Anions in (meq/l)

PARAMETER	**Concentration (meq/l)**
Calcium(mg/L)	0.1599
Magnesium(mg/L)	0.0675
Potassium(mg/L)	0.0279
Sodium(mg/L)	0.0903
TOTAL	**0.3456**
Sulphate(mg/L)	0.0085
Nitrate(mg/L)	0.0015
Chloride(mg/L)	0.0214
Bicarbonate(mg/L)	0.3633
TOTAL	**0.3947**

V. RESULTS AND INTERPRETATION

The major parameters measured in water samples collected from the study area include hardness, Total Dissolved Solids, Temperature, Colour, Concentration of the major cations and Concentration of the major anions. The mean values were compared against the Nigerian Industrial Standard for Drinking water Quality (2007) and the World Health Organization Standard for drinking water (2006) to determine its potability.

The pH is a parameter that indicates the acidity of a water sample. The operational guidelines [NIS (2007) and WHO (2006)] recommended that drinking water is to maintain pH between the values of 6.5 to 8.5.

The idea behind controlling the pH is to produce water that is neither acidic nor excessively basic. From the results of the analysis carried out, the mean pH value of the water sample is 6.9 which falls within the limit. The mean colour value of the water sample is 5.25 TCU which is within the range of the maximum permitted levels set by the regulatory bodies. Higher concentration affects the appearance of the water. The mean turbidity of the water samples is 4.00 NTU and conforms to the standards. Higher concentrations of turbidity also affect the appearance of water. Total Dissolved Solids (TDS) refers mainly to the inorganic substances dissolved in water. The mean TDS value of 22.95 mg/l lies within the allowable limit. The mean value of Calcium concentration obtained from the water sample is 3.205mg/l while the maximum concentration level set by the WHO 2006 is 75mg/l. This means that the calcium content is minimal though it has the highest concentration among the cations analyzed (Fig. 2). The problem with high concentration of Calcium in water is that it leads to scale formation and hardness. Magnesium has a mean value of 0.82mg/l and it falls within the range of the WHO 2006 standard which is less than 30mg/l. High concentrations of Magnesium leads to water hardness and gastrointestinal irritation. Potassium has a mean concentration value of 1.09mg/l and it falls within the range of 200mg/l set by the regulatory bodies (NIS 2007 and WHO 2006). The presence of Potassium in water may be due to agricultural activities. Sodium has a mean concentration value of 2.075mg/l which falls within the range of 200mg/l set by the NIS 2007. High levels of Sodium in water are noticeable in the taste of the water. The Sulphate content in the water sample gave a mean value of 0.41mg/l which meets the standard set by the NIS 2007 of 100 mg/l. High concentration of Sulphate lead to taste in water and corrosion. A major percentage of Nitrates in water originates from organic sources or from industrial and agricultural chemicals [12]. The Nitrate content in the water samples gave a mean value of 0.09 mg/I which falls within the range set by the regulatory bodies. High concentration of Nitrate leads to physiological problems. Chloride is a common non-toxic material present in small amounts in drinking water and possesses a detectable salty taste. The mean Chloride ion concentration of the water samples is 0.76 mg/l which is within the range set by the regulatory bodies. The Bicarbonate content concentration from the analysis gave a mean value of 22.17 mg/l. This is the most dominant anion in the spring (Fig. 3).

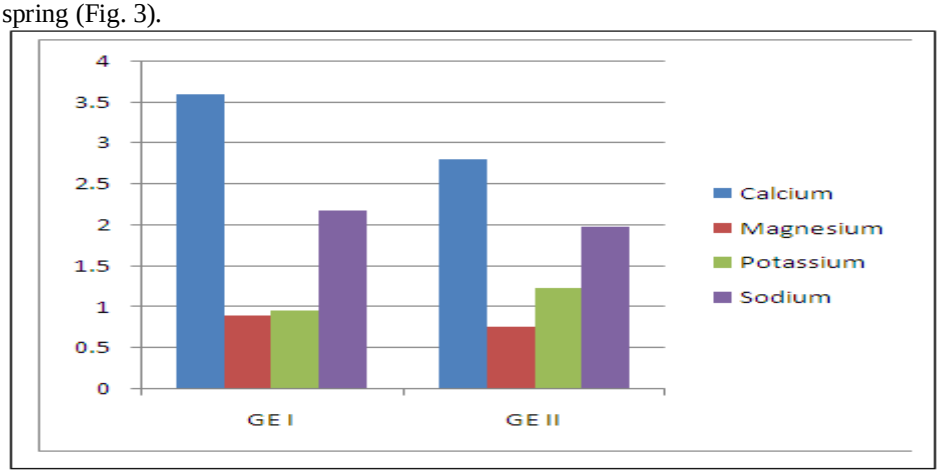

Figure 2. Cation concentration (in Mg/l) of the spring water.

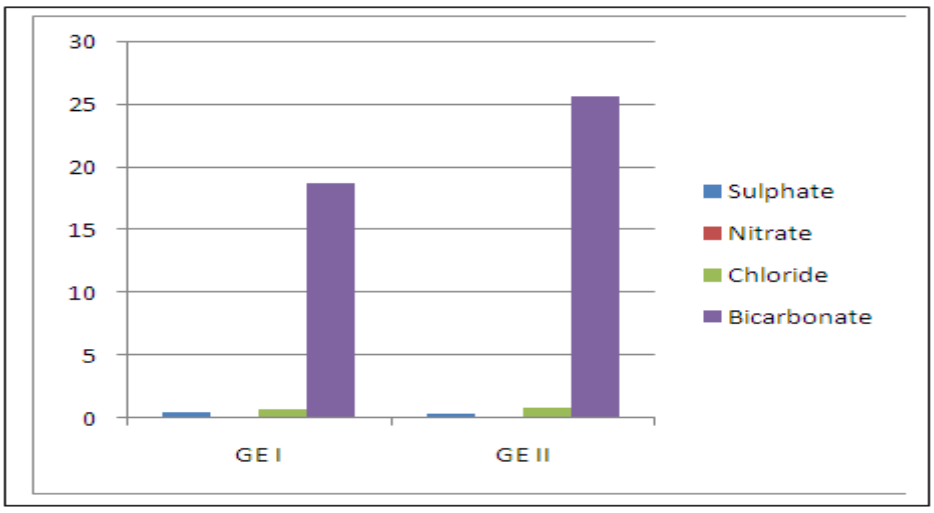

Figure 3. Anion concentration (in Mg/l) of the spring water.

The classification of water for agricultural purposes is based on specific conductance expressed as Total Dissolved Solids (TDS), Sodium content and Boron concentration [13]. The Sodium content can be said to be the most important element used to determine water quality for the basis of agriculture because it is the reaction of sodium with soil that determines soil's permeability.
To determine the Sodium content, a formula called the Sodium Absorption Ration (SAR) is used:

$$SAR = \frac{[Na^+]}{[Ca^{2+} + Mg^{2+}]^{1/2}} \quad \text{……..(1)}$$

After determining the SAR, a table adapted from [13] (Table 3) was used to classify the SAR value so as to determine the water class for agricultural purposes.

Table 3. Water Classification for Agricultural purposes (Adapted from [13]).

SAR	**WATER CLASS (for agricultural purposes)**
0 - 10	Excellent
10 – 18	Good
18 – 26	Fair
➢ 26	Poor

The SAR is 0.27; so from Table 3, the water falls within the excellent range (0-10), indicating that the water is very good for agricultural purposes. The Stiff (Fig. 4) and Schoeller (Fig. 5) plots are generated using the milli equivalents per litre (meq/l) values of the parameters of the samples collected (Table 2). These values are plotted against their various corresponding parameters and show at a glance the distributions of these parameters. A Box and Whisker plot is equally done using the milli equivalent per liter (meq/l) values of the major cations and anions present in the water samples (Fig. 6). It shows the degree of clustering of the dorminant species. The parameters of the spring are observed to concentrate within the second quarter of the box ranging from 0.01meq/l to 0.05meq/l indicating similarity in origin. From the Piper's trilinear diagram, the spring water sample falls within the region that indicates the dominance of alkaline earth and weak acids and the water facies classified as Ca-(Mg)-Na-HCO_3 water (Fig. 7). Water of this facies is generally portable for domestic use.

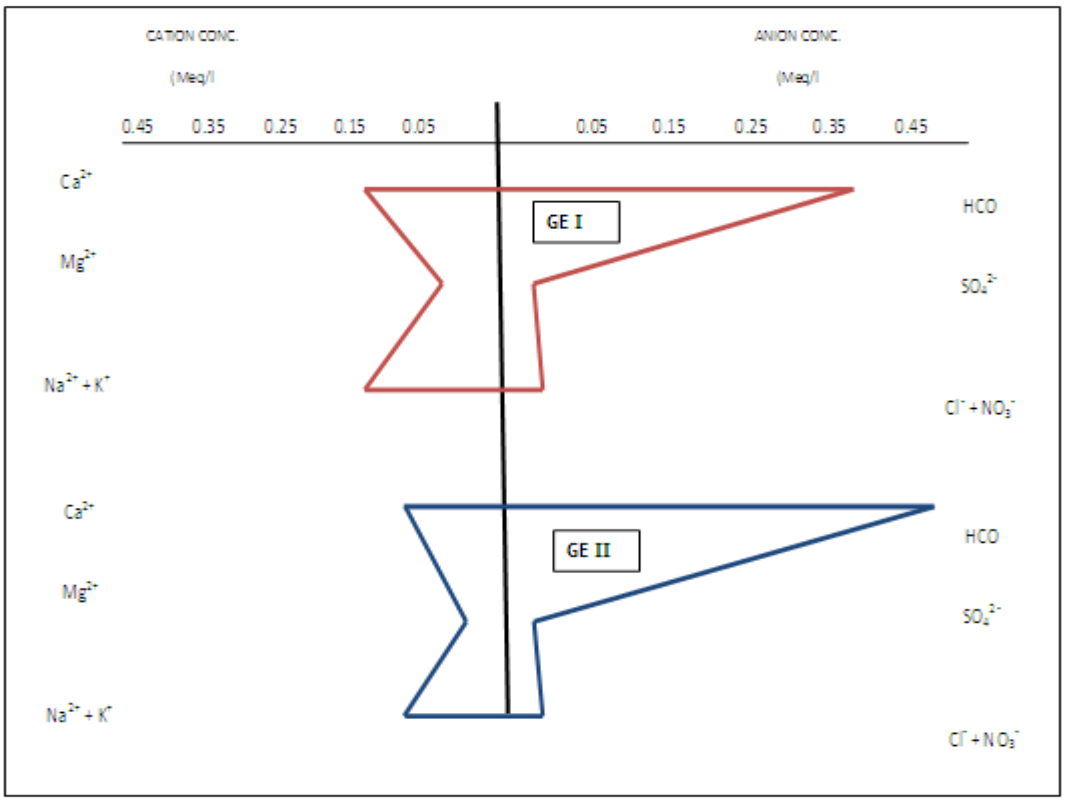

Figure 4. Stiff Diagram displaying the relative concentrations of the Cations and Anions.

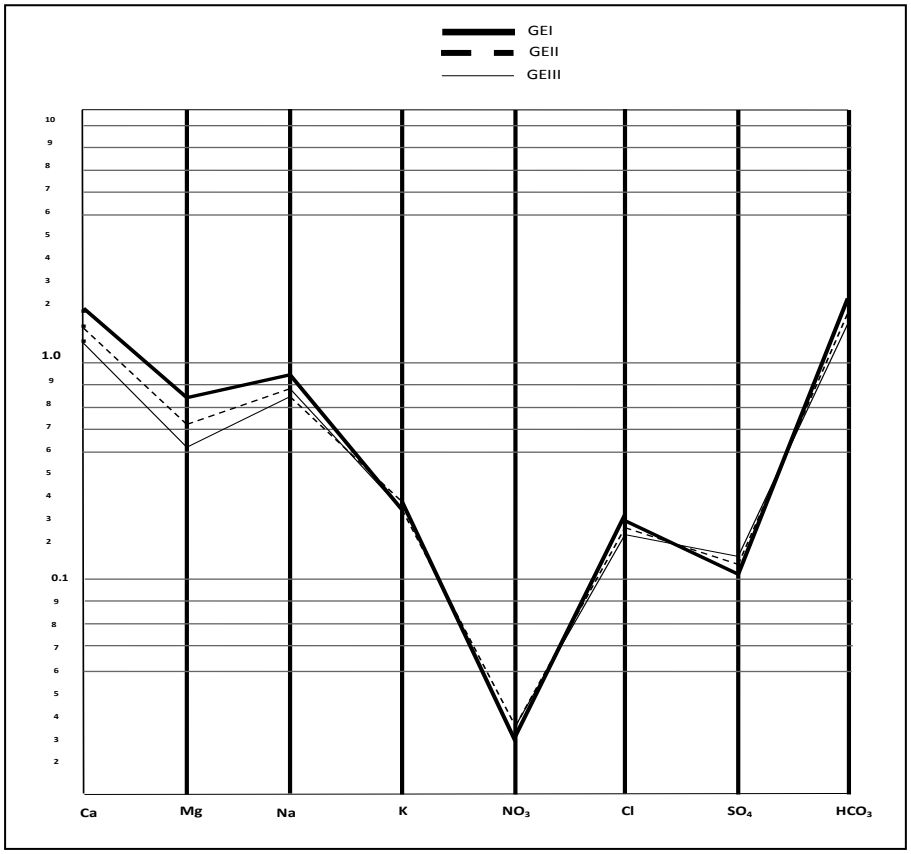

Figure 5. Schoeller Plot showing the relative concentrations of the Cations and Anions.

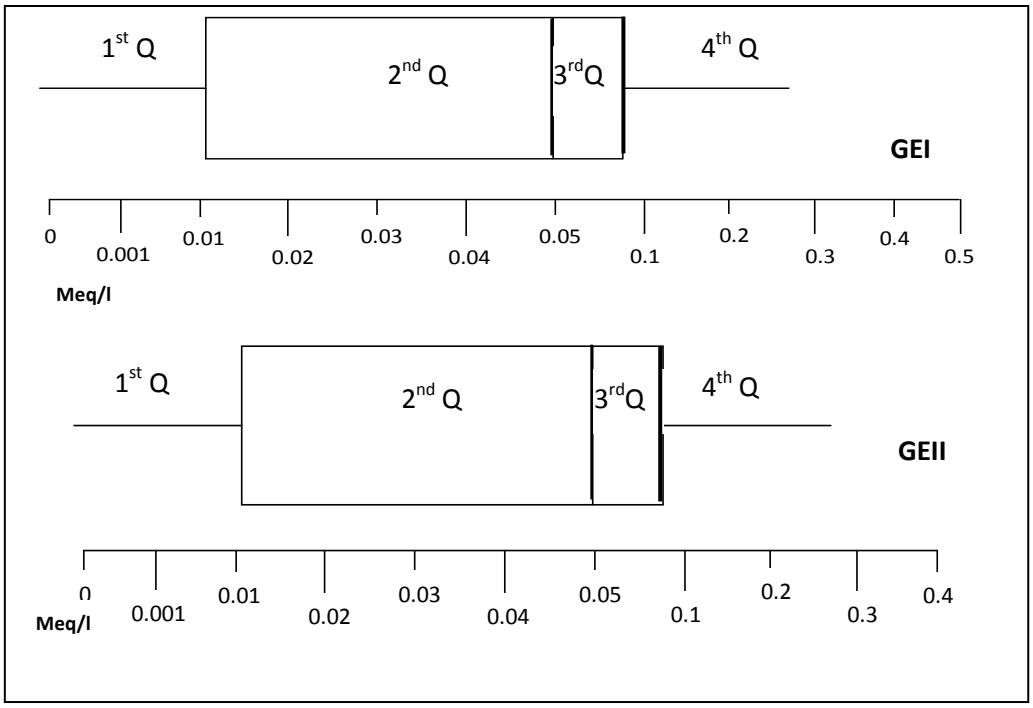

Figure 6. Box and Whisker plot of the spring water parameters.

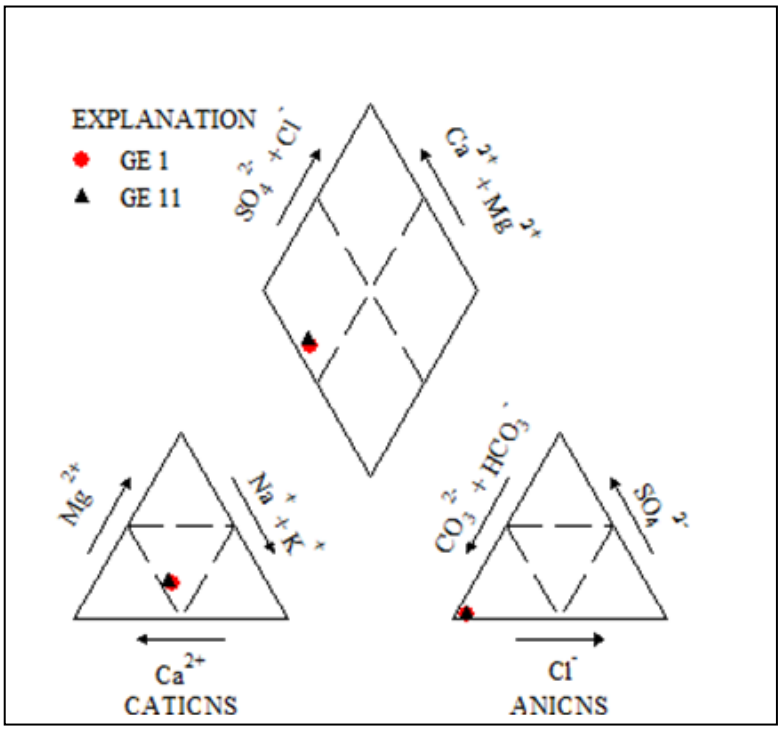

Figure 7. Piper Trilinear Diagram of the spring water samples.

To further assess the portability of the spring water source, the pollution index was determined using the relation proposed by [18]:

$$PI = \frac{\sqrt{IMax(Gij/Wij)]^2 + [Mean(Gij/Wij)]^2}}{2} \quad \ldots\ldots\ldots\ldots\ldots\ldots (2)$$

Table 4. Data for calculating the Pollution Index of the Spring water.

PARAMETER	MEAN VALUE (Gij)	WHO 2006 (Wij)	(Gij/Wij)
P^H	6.58	6.5-8.5	0.810
Turbidity	4.00	5	0.800
Conductivity	56.00	100	0.560
T.D.S	22.95	1000	0.023
Calcium	3.21	75	0.043
Magnesium	0.82	<30	0.027
Potassium	1.09	200	0.005
Sulphate	0.41	400	0.001
Nitrate	0.09	10	0.009
Chloride	0.76	200	0.004
TOTAL			**2.282**
MEAN		2.28/10	**0.228**

The Pollution Index (PI) calculated using (2) above gave a value of 0.6. This value, which is less than the critical value of unity, shows that the spring water is not polluted.

The Langelier Saturation Index (SI) is a means of evaluating water quality data to determine its tendency to form a chemical scale [19].

The Saturation Index is;

$SI = P^H - P^HS$ ……. (3)

Where;

P^H = the actual P^H measured in the water sample

P^H s = the P^H at saturation in Calcite or Calcium Carbonate and is defined as:

$P^HS\ (9.3 + A + B) – (C+D)$ ……. (4)

Where;

$A = (Log_{10}\ [TDS] – 1)/10$ ……. (5)

$B = -13.12 \times Log_{10}\ (Temperature + 273) + 34.55$ ……. (6)

$C = Log_{10}$ [Ca^{2+} as Calcium Carbonate] – 0.4 ……. (7)

$D = Lo_{10}$ [Alkalinity as Calcium Carbonate] ……. (8)

With these relations, and combining (3)-(8), the Saturation Index (SI) was obtained as -3.41. This value is compared against table 5 below.

Table 5. Quality Classification of water for industrial purposes

SATURATION INDEX	DESCRIPTION	GENERAL RECOMMENDATION
-5	Severe Corrosion	Treatment Recommended
-4	Severe Corrosion	Treatment Recommended
-3	Moderate Corrosion	Treatment Recommended
-2	Moderate Corrosion	Treatment may be Needed
-1	Mild Corrosion	Treatment may be Needed
-0.5	None-Mild Corrosion	Probably no Treatment
0	Near Balance	No Treatment
0.5	Some Faint Coating	Probably no Treatment
1	Mild Scale Coating	Treatment may be Needed
2	Mild to Moderate Coating	Treatment may be Needed
3	Moderate Scale Forming	Treatment Advisable
4	Severe Scale Forming	Treatment Advisable

From table 5, the ideal range for the saturation index is -0.5 to 0.5, values below -0.5 are considered corrosive while values higher than +0.5 indicate the formation of scales.

VI. CONCLUSION

From the results obtained, it indicates that the concentrations of the constituents are within the recommended range as provided by the Nigerian Industrial Standard (2007) and WHO (2006) and as such good for domestication. The spring water is excellent for agricultural purposes sequel to the Sodium Absorption Ratio (SAR) value of 0.27 and the Percentage Sodium value of 34.20%. The spring water is not polluted because the pollution index value of 0.6 is less than the critical value of unity (1). The Piper plot indicates that the water samples in the study area belonged to Alkaline Earth group and classified as Ca-(mg)-Na-HCO_3 facies. The Saturation Index of – 3.41 revealed that the spring water needs some sort of treatment before put into industrial use to avoid moderate to severe corrosion.

REFERENCES

[1] P. E. S. Inyang, Climatic Region in Ofomata G.E.K. (ed), *Nigeria in maps, Eastern States* (Benin Nigeria Ethiope 1975) 22-29

[2] A.C. Onyeagocha, Petrography and Depositional Environments of the Benin Formation, *Journal of Mining Geology 17 (2)*, 1980, 147-150.

[3] A. A. Avobovbo, Tertiary Lithostratigraphy of Niger Delta, *Bull. Am. Assoc. Pet. Geol 62*, 1978, 295-306.

[4] APPHA, Standard methods for the examination of water and waste water. *American Water Works Association, Water Environment Federation*, 1995.

[5] M. Barcelona, J.P.Gibb, J.A. Helfrich, E.E. Garske, Practical guide for groundwater sampling. Champaign: *Illinois State Water Survey ISWS Contract Report* 374, 1985.

[6] H. C. Classen, Guidelines and techniques for obtaining water samples that accurately represents the quality of an aquifer, *Lakewood: US Geological survey open file report* 82-1024, 1982, 49.

[7] A.W.Hounslow, *Water Quality data analysis and interpretation* (New York: Lewis, 1995).

[8] L. Celesceri, A.E. Greenberg, A.D. Eaten, Standard method for the examination of water and waste water, *American Public Health Association, Washington*, 1998, 134.

[9] Nigerian Industrial Standard (NIS 554:2007), Nigeria Standard for Drinking water Quality, *ICS 13.060.20*, 2007, 15-19.

[10] WHO, Guide line for Drinking Water Quality. World Health Organization, Geneva, *2nd Edition (2)* 2006, 281-308.

[11] S. N. Davis and R.J.A. Dewiest, *Hydrology* (New York: John Wiley and sons, 1966).

[12] R. Sugisaki, Water supply treatment and distribution (Englewood Cliffs, New Jersey: Prentice-Hall, 1978).

[13] J.O. Etu-Efeotor, Preliminary Hydro geochemical investigation of subsurface waters in parts of the Niger Delta, *Jour. Min. Geol. 18, (1)*, 1981, 103-106.
[14] J.R. Stiff, L. E. Davis, A method for predicting the tendency of oil field water to calcium carbonate, *Pet. Trans. AIME 195*, 213, 1951.
[15] H. Schoeller, Utility of the notion of the basic exchanges for the comparison of the water sources, *Fr. Soc. Geo. Journal 5th Edition*, 1953, 651-657.
[16] G. E Box, D. R Cox, An Analysis of Transformation. *JRSS, B26*, 1964, 221-243
[17] A.M. Piper, A Graphic Procedure in the Geochemical Interpretation of water Analysis. *Washington D.C, US Geol. Survey. ISBN ASIN: B0007H2Z36*, 1953.
[18] R.K. Horton, An Index Number Rating system for rating Water quality, *J. Water pollution control federation 37*, 1965, 300-306.
[19] W. F. Langelier, The Analytical Control of Anticorrosion water Treatment, *Journal of the American water works Association (AWWA) 28 (10)* 1936, 1500-1521.

American Journal of Engineering Research (AJER)
e-ISSN : 2320-0847 p-ISSN : 2320-0936
Volume-02, Issue-10, pp-291-297
www.ajer.org

Research Paper Open Access

Physico-Chemical Properties of Bio-diesel from Wild Grape Seeds Oil and Petro-Diesel Blends

M. U. Kaisan, G. Y. Pam and D. M. Kulla
[1]*Energy Commission of Nigeria, Abuja, Nigeria*
[2] *Department of Mechanical Engineering, Ahmadu Bello University Zaria, Nigeria*
[3]*Department of Mechanical Engineering, Ahmadu Bello University Zaria, Nigeria*

Abstract: - The swiftly depleting conventional fossil fuel resources and increasing environmental distress has considerably popped up research curiosity in renewable energy fuel for internal combustion engines. Accordingly, in this research work, biodiesel from wild grape seed (Lannea Microcarpa) was blended with petro-diesel in a ratio of 5:95, 10:90, 15:85 and 20:80 and pure fossil diesel designated B5, B10, B15, B20 and B0 respectively. The physico chemical properties of the biodiesel/petro diesel blends were determined. The properties are specific gravity, viscosity, flash point, calorific value, sulphur content, copper strip corrosion, colour, diesel index, cetane number, and cloud point. It was observed that, 9 out of the 10 properties determined conform to ASTM standards except for the colour which was dark brown for the oil and biodiesel, and brown for the automotive gasoline oil. The specific gravity and viscosity increase with percentage increase of biodiesel in the blends. The sulphur content, calorific values, cetane number and diesel index decrease with increase in the percentage biodiesel from the blends. The colour of the samples does not conform to the ASTM standards. All the samples have the best ASTM value for copper strip corrosion and as such, they could be run in any diesel engine without any fear of corrosion tendencies. Whence, Wild Grape seed biodiesel is physically okay, chemically stable, environmentally friendly and economically viable for use in compression ignition engine as a blend to partly replace the automotive gasoline oil.

Keywords: *– Biodiesel, Blend, Physico-Chemical Properties, Wild Grape Seeds*

I. INTRODUCTION

Biodiesel means fatty acid methyl ester or mono-alkyl esters derived from vegetable oil or animal fats for use in diesel engines (Nigerian Bio-Fuel Policy and Incentives, 2011). Biodiesel is an alternative for or an additive to diesel fuel, that is derived from the oils and fats of plants, like sunflower, canola, Jatropha, neem seed oil (Ambumani and Sing, 2010). With fuel prices increasing and growing environmental awareness, the need to consider alternative energy and fuel sources are becoming a necessity. One alternative is the use of biodiesel fuel which is becoming more and more popular today (Haresh, 2008).

The physico-chemical properties of fuel are the fuel specifications that define and set the quality standards. For biodiesel, physico-chemical properties are a set of property specifications measured by specific American Society for Testing and Material (ASTM) test methods such as ASTM 6751 – 02 (Gerpen *et al.*, 2004). This specification must be met for a fatty acid ester product to carry the designation "biodiesel fuel" or "B100" or for use in blends with any petroleum-derived diesel fuel (Gerpen *et al.*, 2004). These properties are termed physico-chemical properties which include but not limited to: specific gravity, viscosity, flash point, calorific value, cetane number, acid value, volatility, and saponification value.

There exist in Nigeria, a set of problems due to exploration, refining, transportation and final combustion of the petroleum products in which diesel fuel is not an exception. There are environmental catastrophes like oil spills, acid rains and depletion of the ozone layer. Recently, the Federal Government of Nigeria has removed its subsidy on petroleum products which lead to rise in prices of the products. Therefore, there is need to surmount these challenges and as such, we have to search for alternatives and or additives that will wholly or partially replace the expensive petroleum products. There alternatives are supposed to be locally abundant, environmentally friendly and economically viable. In the light of the above, this work therefore seeks

to evaluate the physical and chemical properties of transesterified wild grapes seeds oil/petro-diesel blends. Result of this study is expected to contribute to the existing database of locally available alternative energy resources with the objective of reforming the global energy and environmental predicaments.

II. MATERIALS AND METHODS

2.1 Materials

2.1.1 Sample Collection

The seeds to be used in this work is botanically called *lannea microcarpa*; it is also referred to as wild grapes in English and "Faru" in Hausa, the main language in Northern Nigeria. The sample was obtained from Kankia local government, Katsina State of North Western Nigeria.

2.1.2 Extraction Procedure and Biodiesel Production

Seed sample was washed and dried, oil was extracted from the sample using the mechanical press engine driven expeller. The oil yield from the sample was initially 12.5% with very high free fatty acid (FFA), and then later increased to 37.5% after the free fatty acid was reduced using acid esterification reactions on the sample. The free fatty acid was 42% but reduced to 2.52 after a repeated esterification reaction. Alkali esterification reaction was carried out on the sample and bio-diesel was produced. The biodiesel was blended with fossil diesel in a ratio of 5:95, 10:90, 15:85 and 20:80 and a pure petro-diesel sample kept for control purpose as B5, B10, B15, B20 and B0 respectively

2.2 Determination of Physico-Chemical Properties

The physico chemical properties of the biodiesel produced were determined as follows:

2.2.1 Measurement of the specific gravity:

The specific gravity of the samples was measured at room temperature of 27 ^{0}C using a Fisher brand hydrometer (size 0.795-0.910, accuracy 0.001). The measurement was performed according to the method adopted by Coronado *et al.* (2009). The hydrometer is a graduated glass tube filled with air and fitted with a weight.

- To measure specific gravity, a hydrometer and a large graduated cylinder were obtained
- The graduated cylinder was filled with the sample and the hydrometer was then dropped into the blend.
- The point at which the hydrometer floats gives the measurement of the specific gravity.
- Hydrometer readings were taken at temperatures between 16 ^{0}C to 30 ^{0}C.

2.2.2 Measurement of viscosity:

The viscosities of the samples were measured with a viscometer at 40 ^{0}C (Siivaramakrishnan *et al.*, 2011). According to Adebayo *et al.* (2011) the viscosity at 40 ^{0}C (313k) is measured following the ASTM D445 method using a calibrated viscometer with a calibration constant of 0.1057. In this research, the determination of viscosity was done following the Institute of Petroleum (IP) method by Milner and Whiteside, (1986).
This involves measuring the time of flow of the sample between two marked points on the Ostwald viscometer (Nafi'u *et al.*, 2012).

2.2.3 Flash point

The flash point of the biodiesel/diesel blends was determined by the method of ASTM D93, using the Pensky-Martens closed cup tester. The determination of the flash point of biodiesel was done in the temperature range of 60 °C to 190 °C by an automated Pensky-Martens closed cup apparatus according to the standard method of testing flash point. The flash point determination was carried out by heating a sample of the fuel in a stirred container and passing a flame over the surface of the liquid. If the temperature was at or above the flash point, the vapour was ignited and an easily detectable flash would be observed. The fire point has produced sufficient vapour to maintain a continuous flame (Babgy et al., 1987).

2.2.4 Cetane number:

The cetane number was determined using a portable cetane/octane metre. The cetane index of the biodiesel-diesel blends was determined by the ASTM D.976 method (Kywe and Oo, 2009).

2.2.5 Cloud point:

The cloud point was determined by visually inspecting for a haze to become visible as the fuel is cooled in a refrigerator.

2.2.6. Calorific value

The calorific values of the biodiesel/diesel blends were measured using a bomb calorimeter. A known amount of fuel was placed in a crucible. The crucible was then placed over a ring and a fine magnesium wire touching the fuel sample is stretched across the electrodes. The lid was tightly screwed and the bomb was filled with oxygen up to 25 atmosphere pressure. The initial temperature was recorded.

The electrodes were then connected to a 6 V battery and the circuit was completed. As soon as the circuit was completed and the current was switched on, the fuel in the crucible burnt with the evolution of heat.

Heat liberated by burning of the fuel increases the temperature of water and the maximum temperature attained was recorded.

2.2.7 Pour point:

The pour point was determined by the ASTM D.97 method (Kywe and Oo, 2009). 3.0 g of the blend was placed into a test tube in which a thermometer was inserted through a cork which was used to cover the mouth of the test tube. The test tube was placed in a refrigerator and observed at 10 minute intervals for a period of two hours. The test tube was removed and tilted to ascertain if the oil flowed or moved, until it showed no movement when the test tube was held horizontally for seconds; it was said to be solidified. The pour point was then taken at the temperature of 5 ^{0}C above the solid point.

2.2.8 Total sulphur Content:

The total sulphur content was determined using X-ray analyses of the fuel samples. This test method covers the determination of total sulphur by monochromatic, wavelength-dispersive X-ray fluorescence (MWDXRF) spectrometry in single-phase biodiesel, diesel fuels, and refinery process streams used to blend bio-diesel and petro-diesel. The precision of this test method was determined by an inter laboratory study using representative samples of the fuels.

2.2.9 Copper strip corrosion

A three inch copper strip was prepared by cleaning and polishing all sides so that no discoloration or blemishes were visible. The strip was then placed in the test samples and held for 3 hours at 100 °C as the typical starting point. At the end of the exposure period, the strip was removed, wiped cleaned and matched with coloured reproduction strips characteristic of the descriptions.

2.2.10 Diesel Index

The diesel index was calculated using the following equation:

$$Diesel\ Index = \frac{aniline\ point(^0F)XDegreesAPI(60^0F)}{100}$$

III. RESULTS

The physico chemical properties of the various biodiesel blends with pure diesel are presented in table 1and illustrated in figures 1 to 7.

Table 1: Physico Chemical Properties of Biodiesel from Wild Grape Seeds/Diesel Blends

Sample	Physico-Chemical Properties									
	Specific Gravity	Sulphur % (wt)	Calorific Value	Flash Point (^{0}C)	Viscosity @ 40^{0}C (mm^2/s)	Cetane Number	Cloud Point (^{0}C)	Colour (ASTM)	Diesel Index	Copper Strip Corrosion
B0	0.8645	0.202	10,831	75	3.93	44	-5	<3.5	47	1a
B5	0.8645	0.191	10,831	60	4.19	44	-15	6.5	47	1a
B10	0.8655	0.181	10,827	45	4.21	41	-12	<8	44	1a
B15	0.8665	0.171	10,823	40	4.28	39	-15	<8	40	1a
B20	0.8675	0.155	10,820	40	4.42	36	-18	>8	37	1a

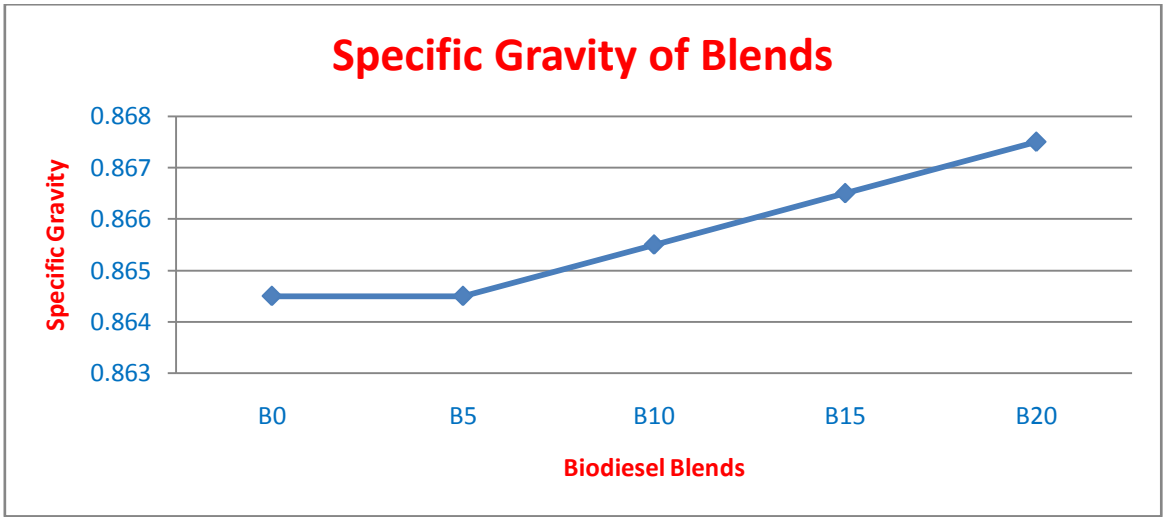

Figure 1: Specific Gravity of Biodiesel Blends

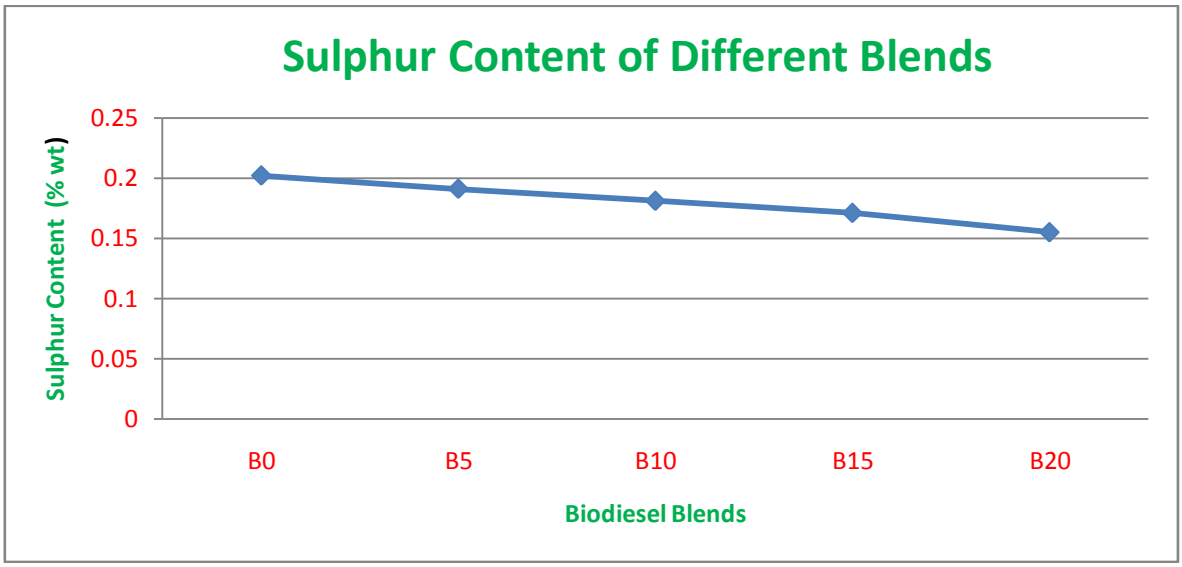

Figure 2: Total Sulphur of Biodiesel Blends

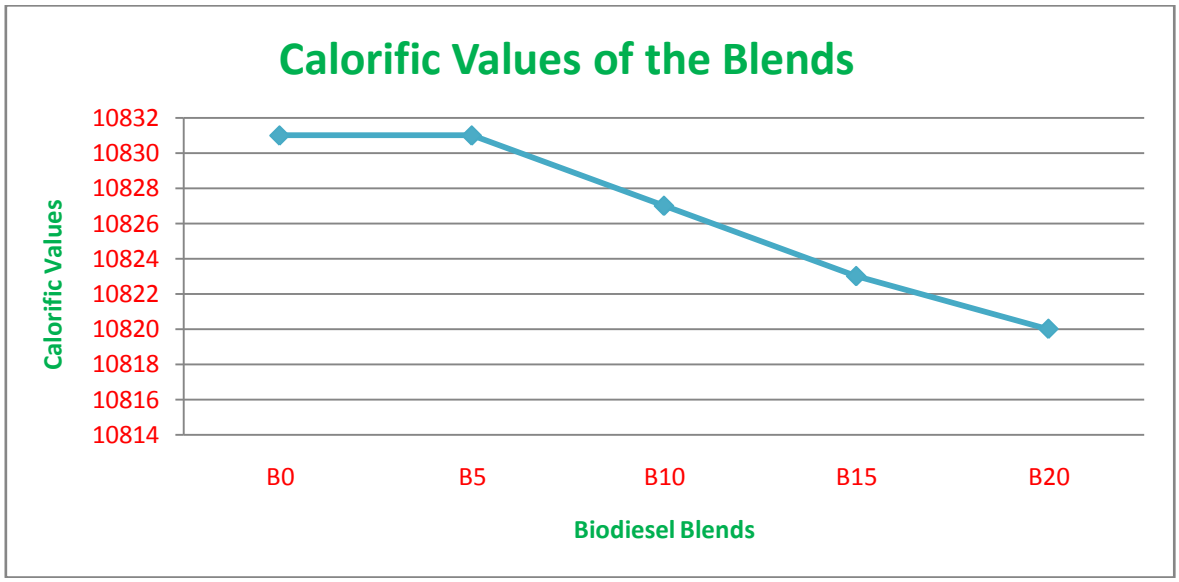

Figure 3: Calorific Values of biodiesel Blends

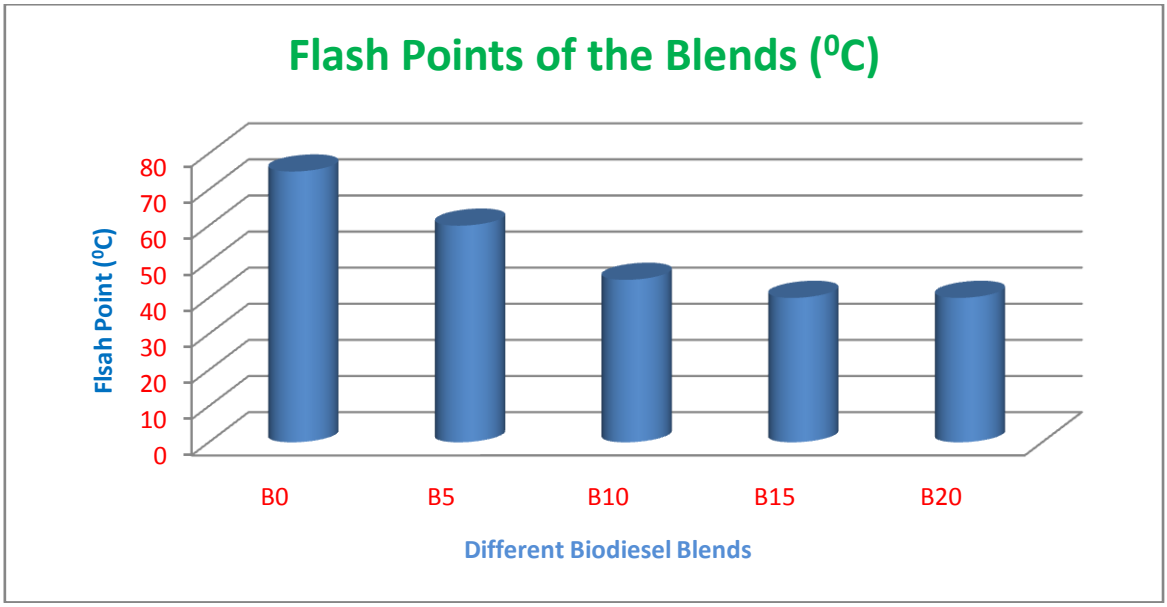

Figure 4: Flash Points of Biodiesel Blends

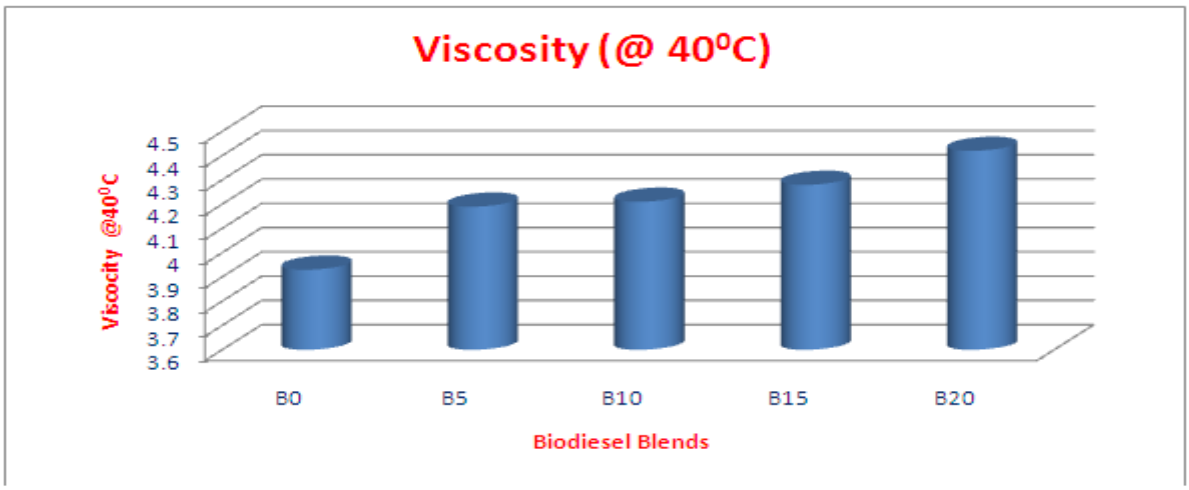

Figure 5: Viscosities of Biodiesel Blends

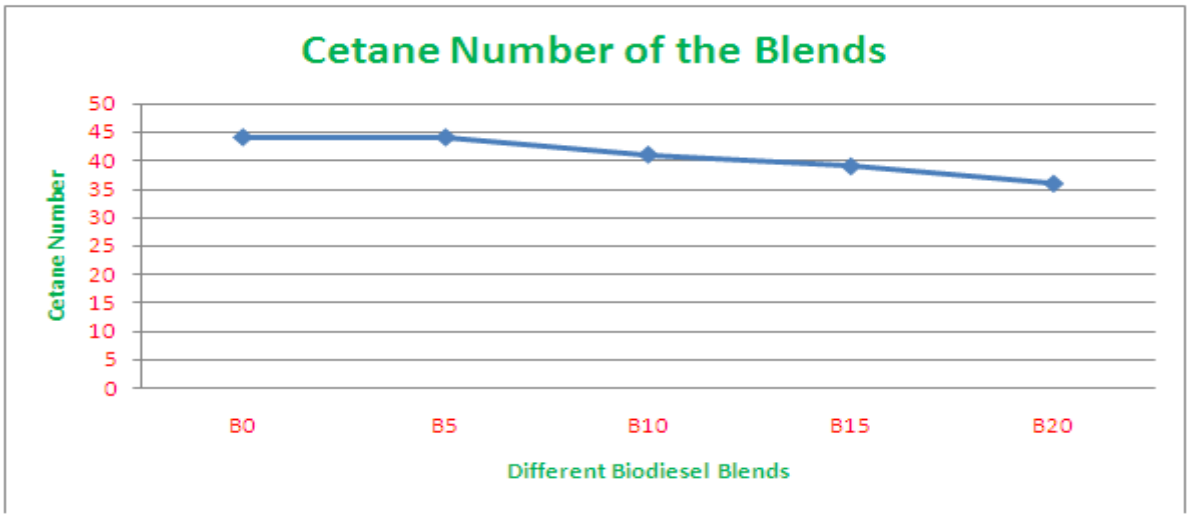

Figure 6: Cetane Values of Biodiesel Blends

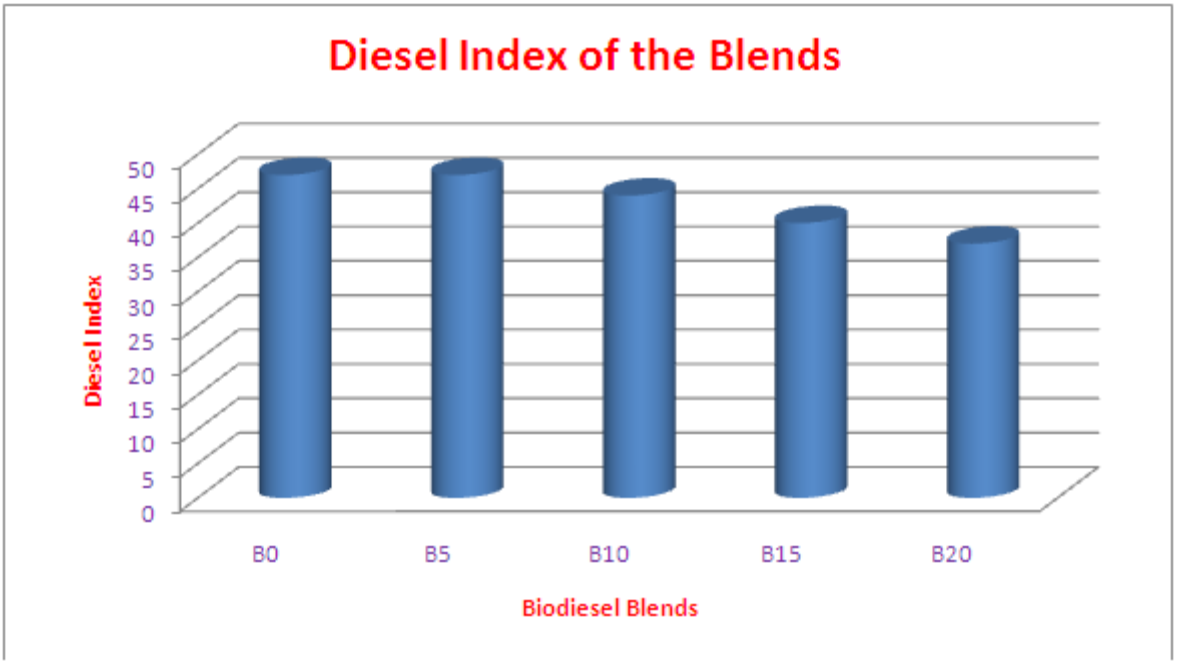

Figure 7: Diesel Indices of Biodiesel Blends

IV. DISCUSSIONS

The graph of specific gravity against blends is presented in figure 1. From the graph, pure diesel (B0) and 5% biodiesel blend (B5) have the lowest specific gravity of 0.8645 each, B10 has 0.8655 with B15 and B20 having 0.8665 and 0.8675 respectively. The ASTM standard for specific gravity for diesel fuels and biodiesels is from 0.8000 to 0.9000, and all the blends fall within this range and hence, conform to the required standard for specific gravity. Therefore, the specific gravities of all the samples B0, B5, B10, B15 and B20 of wild grape seeds biodiesel/diesel blends are within the acceptable limit.

The sulphur content of the biodiesel blends are shown in figure 2. It is seen that, sulphur content decreases with increase in the percentage biodiesel from the blends. The sulphur content of the petro diesel is 0.202 by weight from test. It reduced to 0.191, 0.181, 0.171 and 0.155 with increase in biodiesel content from 5 % through 10% and 15 % up to 20 % respectively. This shows that the wild grape seed biodiesel is capable of reducing the emission of sulphur dioxide into the atmosphere. The sulphur content of the pure biodiesel which was not captured on the table is 0.04 wt %. This is within the standard range of ASTM D5453 which allows a maximum of 0.05 wt % for total sulphur content in a given biodiesel.

The calorific values of the pure diesel as well as the different blends are presented in figure 3. B0 and B5 blends have the same calorific values, while there was decrease in the values with increase percentage of biodiesel in the blends. The calorific value of B20 was the lowest and that of the B0 was the highest. The calorific values are decreasing with percentage increase of biodiesel in the blends. The calorific value of B0 and B5 are the same; this is because, with 5 % of biodiesel in the blend, the quantity of biodiesel in the blend is not enough to alter the calorific value of the blend.

Figure 4 shows the respective flash points of the pure diesel and the biodiesel blends B0, B5, B10, B15 and B20. The minimum flash point for biodiesels according to ASTM 6751-02 D93 test method is 100 ^{0}C and the maximum is 170 ^{0}C. The flash point range for pure diesel is 60 ^{0}C to 80 ^{0}C. While the ones obtained in this test have the highest flash point as 75 ^{0}C of the petro diesel which is within the standard. The lowest was 40 ^{0}C for B15 and B20. From B5 to B10, there was a slight decrease in flash point and further decrease was also observed between B10 and B15.

Figure 5 presents the graphical variation in viscosity of the biodiesel blends. The viscosity of the pure diesel was 3.93 mm^2/s at 40 ^{0}C. There was increase in viscosity with corresponding increase in biodiesel percentage in the blends. B5 has a viscosity of 4.19mm^2/s and B20 has 4.42 mm^2/s. The ASTM range for viscosity is between 1.9mm^2/s and 6.0mm^2/s. The standard for diesel fuel is 1.3mm^2/s to 4.1mm^2/s. Hence, both the petro diesel and the blends have conforming viscosities.

The various cetane numbers are presented in the figure 6. The ASTM standards for cetane number of biodiesel are 48-65. It was observed that, with increase in biodiesel blends, there was a corresponding decrease in cetane number from B10 through B15 to B20.

Therefore, the knocking tendency of the engine increases with an increase in the percentage of the blend. However, at 5 % blend, there was no any change in cetane number; it was same 44 as the petro diesel cetane index, this is because, there is no any significant change with 5 % blend as compared to B0 as it was also observed with specific gravity and calorific value.

The values of the cloud point of the samples are presented in table 2. According to Gerpen *et al*. (2004) there is no any standard limit for cloud point. From the table 3, however, the cloud point of the samples are: -5 ^{0}C, -15 ^{0}C, -12 ^{0}C, -15 ^{0}C and -18 ^{0}C for B0, B5, B10, B15 and B20 respectively. The trend of the curve starts from its highest value for B0, then goes down to the lowest value for B20.

The petro- diesel used in this experiment has a very bad colour likewise the biodiesel produced and the blends. The colour of the biodiesel was dark brown (Coffee Colour), while that of the pure diesel used (B0) was light brown. From table 2, the values of the colours for B0 and B5 were >3.5 and 6.5 respectively, these are the minimum colour codes of the samples produced. The ASTM standards for colour codes of biodiesels is <3. Hence the colour of the samples does not conform to the ASTM standards.

From table 2, the respective values for copper strip corrosion for B0, B5, B10, B15 and B20 were presented as 1a each. This is very interesting, as it shows that all the samples have the best ASTM value for copper strip corrosion and as such, they could be run in any diesel engine without any fear of corrosion tendencies. The ASTM value for copper strip corrosion is 3max (Maximum value of 3).

The diesel indices of the pure diesel and those of the blends are presented in figure 7. The diesel indices of pure diesel and 5 % biodiesel are the same, whereas for B10, B15 and B20 it reduces with increase in the percentage of the biodiesel present in the blends.

V. CONCLUSIONS

The specific gravity and viscosity of the biodiesel blends increase with percentage increase of biodiesel in the blends. With increase in the percentage biodiesel there was corresponding decrease in sulphur content, calorific values flash point, diesel index and cetane numbers.

The pure diesel used in this experiment has a very bad colour likewise the biodiesel produced and the blends. The colour of the biodiesel was dark brown (Coffee Colour), while that of the pure diesel used (B0) was light brown.

The entire blends have the best ASTM value for copper strip corrosion and as such, could be run in any diesel engine without any fear of corrosion tendencies. Besides the colour, all the physico chemical properties of the blends conform with ASTM standards.

REFERENCES

[1] Adebayo, G. B. Ameen, O. M. and Abbas, L. T. (2011). Physico-Chemical Properties of Bio-diesel Produced from Jatropha Curcas Oil and Fossil diesel, *Journal of Microbiology and Biotechnology Research*, Scholars Research Library, J. Micro-biol. Bio-tech, 1(1): 12-16

[2] Anbumani, K. and Sing, A. P. (2010). Performance of Mustard and Neem Oil Blends with Diesel Fuel in C.I. Engine, *ARPN Journal of Engineering and Applied Sciences*, 5(4): 14-21

[3] Bagby, M. O. Freedman, B. and Schwab, A.W. (1987). Seed Oils for Diesel Fuels: Sources and Properties. ASAE Paper No. 87-1583, presented at the *International Winter Meeting of the ASAE*, Chicago

[4] Coronado, M. Yuan, W. Wang, D. and Dowell, F. E. (2009). Predicting the Concentration and Specific Gravity of Biodiesel-Diesel Blends Using Near-Infrared Spectroscopy, Applied Engineering in Agriculture. *American Society of Agricultural and Biological Engineers*, 25(2): 217-221

[5] Garpen, J. V. Shanks, B. Pruszko, R. Clements, D. and Knothe, G. (2004). *Biodiesel Production Technology*, National Renewable Energy Laborotory Press, Cole Boulevard, Golden, Colorado, USA, PP. 1-27

[6] Haresh, K. (2008). Production of Biodiesel. *Transesterification Process.* Retreived on 23rd July, 2012, from http://www.brighthub.com/environment/renewable-energy/articles/6718.aspx.

[7] Kywe, T. T. and Oo, M. M. (2009). Production of Bio-diesel from Jatropha Oil in Pilot Plant. *World Academy of Science, Engineering and Technology*. 50: 477-483

[8] Nafi'u, T. Ike, P.O. Usman, B.B. Malami D. I. and Matholo A. (2012). Trace Elemental Analysis of Nigerian Petroleum Products Using AAS Method, *International Journal of Scientific and engineering Research*, 3(2): 1-5

[9] Nigerian Bio-Fuel Policy and Incentives (2011). Unpublished Policy Document of Nigeria National Petroleum Corporation, PP.4-23. NNPC Approved Ethanol Policy Draft, NNPC Towers, Abuja, Nigeria

[10] Siivaramakrishan, K. and Ravikumar, P. (2011). Determination of Higher Heating Values of bio-diesel. *International Journal of Engineering Science and Technology*, 3(11): 7981-7987.

American Journal of Engineering Research (AJER)
e-ISSN : 2320-0847 p-ISSN : 2320-0936
Volume-02, Issue-10, pp-298-307
www.ajer.org

Research Paper Open Access

Design, Analysis and Implementation of a Robotic Arm- The Animator

Md. Anisur Rahman[1], Alimul Haque Khan[1], Dr. Tofayel Ahmed[3], Md. Mohsin Sajjad[2]

1. *Electrical & Electronic Engineering, Bangladesh University (BU).*
2. *Electrical & Electronic Engineering, Bangladesh University of Engineering & Technology (BUET).*
3. *Cowater, Canadian International Development Agency (CIDA).*

Abstract: - A humanoid robotics is a new challenging field. To co-operate with human beings, humanoid robots not only have to feature human like form and structure, but more importantly, they must prepared human like behavior regarding the motion, communication and intelligence. The model number of this beginner is ASR K-250. This paper we consider the mechanism and mechanical structure of ASR K-250 (Beginner) and its implementation.

Keywords: - *Degrees of freedom, kinematic structure, ellipsoid, redundancy, elbow pitch, Hardware interface, joint speed*

I. SUMMARY

In the field of robotics the beginner can contribute many functional operations in the world. This arm can solve many human's limitations. Many people cannot move from one place to another place for their limitation but they have needed to move for collect something like mug, jog, and so on. For that they require getting help from other persons. When they use this type of robot they can solve their problem easily without help other person for its easy operation system. For an example when a person has needed to carry an object from drawing room to bed room he can use this robot. It can move surround also collect photo and other information. When earthquake will be occurred by using these types of robot people can unseat many weight full objects from destroyed area to a safety place.

Introduction:

The application of robotics field is broadly used in the field of research, laboratory based work, industrial work to automate process and reduce the human errors. This paper is describing the design of mechanical structure of a robotic arm. This robotic arm is often indicated to move an object from one place to another place. One kind of example of this application is in an industrial area where need to move a weighable object like tank or container or other object. The advantage of automated process results is faster completion time with lowest errors. This paper also describes the implementation of a robotic arm with switching controlled. The application of the force controlled function can be seen in the industrial/manufacturing environments.

Overview of the arm:

Degrees of freedom: 5
Payload capacity: 180gm (Experimentally)
Joint speed (approximate):40-60 rpm
Hardware interface: 2 pin connector
Base spin: 180 degrees
Shoulder base spin: 160 degrees
Elbow pitch: 160 degrees
Finger opening (Max): 10cm

II. MECHANICAL STRUCTURE

The mechanical design of a robotic arm is based on a robotic manipulator with similar function like a human arm. In order to establish a generalized operating systems and the technological systems for the analysis, design, integration and implementation of a humanoid robotic arm.

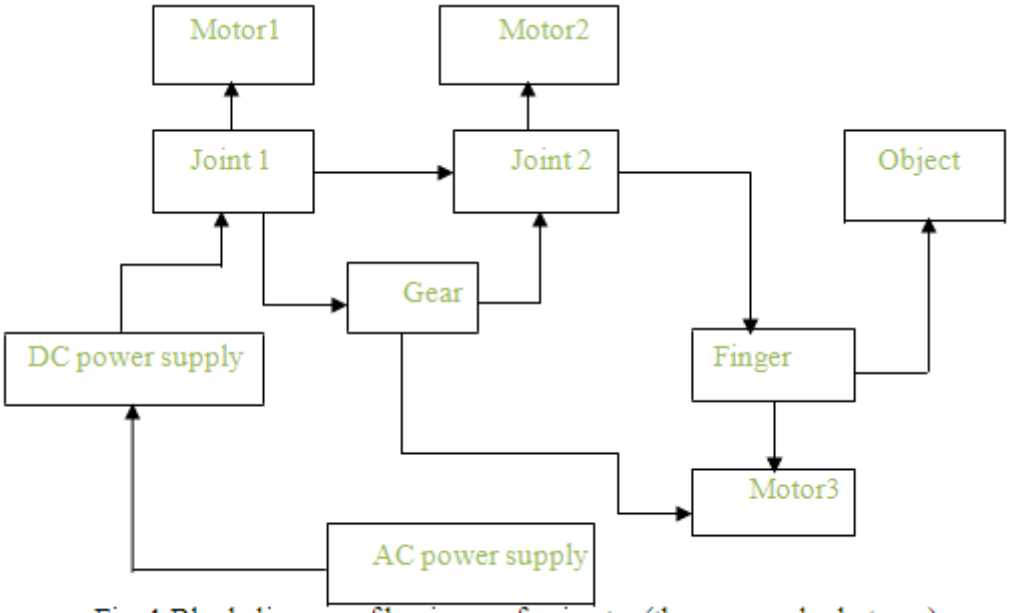

Fig. 1 Block diagram of beginner of animator (the proposed robot arm)

For operating DC motor we need DC power supply that's way we attached an AC to DC converter for getting DC power. This DC power supplies each motor. In this robot arm each and every motor is connected with external gear with external gearbox.

III. CALCULATED TORQUE

Torque means measure of how much force are acting on an object reasons that object to rotate. Torque is denoted by T. Torque (**T**) is defined as a moving "force" and is calculated using the following equation:

$T=F*L$ …….. (1)

Where T is torque F means calculated force and L is denoted the length from a pivot point. The force is accelerating on an object due to gravity (**g** = 9.81m/s^2) multiplied by its mass.

$F=M*g$ …….. (2)

Mass (M) and gravity (g)

The force (F) is also considered of an object's weight (W)

$W = M*g$…….. (3)

The torque required to hold a mass at a given distance from a pivot point is showing therefore

$T = (M*g)*L$…… (4)

The length L is the perpendicular length from a pivot point to the force. This equation can found by similar doing a torque balance about a point.

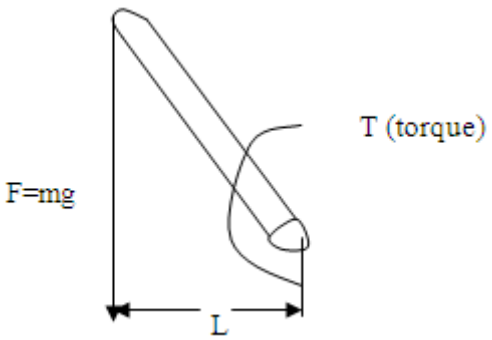

Fig. 2 torque balance

$\sum T = 0 = F*L - T$ ..... (5)
Therefore, replacing the force (F) with mass and gravity (m*g) we can find out the same equation above. This is the more accurate way to find out the torque by using the torque balance.
$M*g*L = T_A$ ..... (6)
In order to estimate the torque required at each joint, we can must chose the worst case scenario.

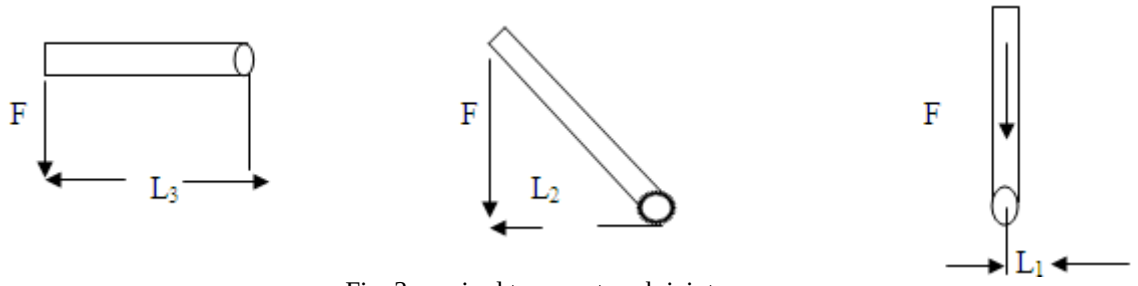

Fig. 3 required torque at each joint

From the above figure we can see a link of required length L is rotate clockwise. Only for perpendicular component of the length (L) between the pivot point and force (F) is taken into account. We can observe that the distance of length (L) is decreasing from length L3 to length L1. Since from the torque equation the length (L) or distance multiplied by the force (F), the greatest value will be obtained by using L3, The force (F) does not change. We can rotate the link counterclockwise similarly and observe the same effect.
The weight of the object (load) being held as Indicated in the Figure 4 by A1, which is multiplied by the distance its center of mass and the pivot point gives the torque required at the pivot. The tool takes into the consideration that the links may have a significant weight (W1, W2……) and its center of mass is located at roughly the center of its length (L).
The torque caused by this difference masses must be added. The torque required at the first joint is therefore.
T1 = L1*A1+L1*W1 ("A" is weight of the actuator or the load.) ……..... (7)
We may consider that the actuator weight A2 which is as shown in the diagram below is not included when calculating the torque at that point. This is because by the length (L) between its center of mass and the pivot point is zero. The torque required at the 2nd joint must be re-calculated with the new lengths, which is as shown in the following figure. (The applied torque shown in green color like T_1 and T_2)

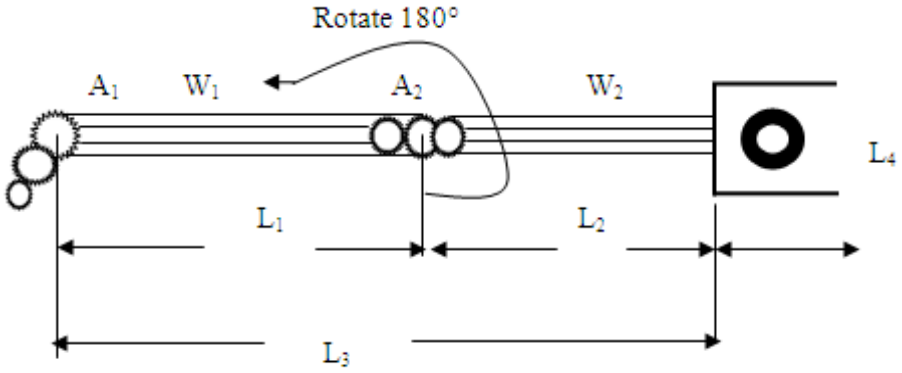

Fig. 4 calculation of applied torque

$T2 = L_3*A_1 + L_1*W_1 + L_2*A_2 + L_4*W_2$ ..... (8)
Knowing that the link weight (W2, W2) are located in the center point of the lengths, and the distance between the actuators (L1 and L3 shown in the diagram above) we can re-write the equation as follows:
$T2 = (L_1+L_2)*A_1 + (L_1+L_3)*W_1 + (L_2)*A_2 + (L_2)*W_2$ ..... (9)
Only for the tool requires that the user enter the lengths (L) of the each link, which would be L1 and L3 above so the equation is showing accordingly. The torques at each subsequent of the joint can be found similarly, by re-calculating the lengths between each new pivot point and each weight.

IV. THE KINEMATIC STRUCTURE OF BEGINNER ARM

The following figure shows the reference and link coordinate systems of 5- DOF arm using the first step of the animator. The values of the kinematic parameters are listed below in the table (I). Where l_u, l_s and l_f are the link lengths of the shoulder, back arm and forearm respectively.

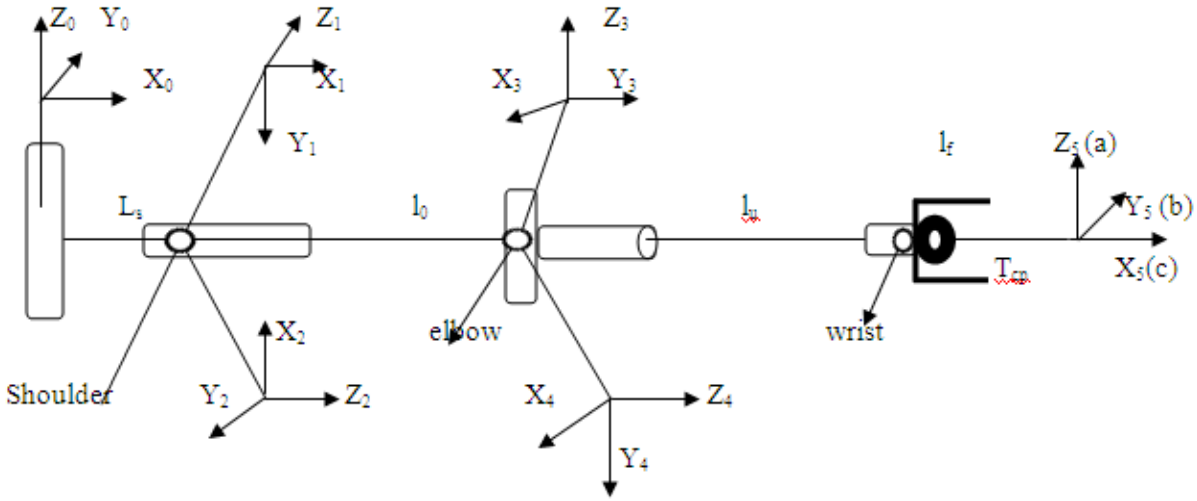

Fig. 5 The coordinate system of the arm

Defined a frame of each link, the coordinate transformation is describing the position and orientation of the end-effectors with respect to (wrt) the base frame is given by

$$T_{tcp}(\theta) = \prod_{i=1}^{5} \left[A_i(\theta_i) \right] = \begin{bmatrix} a & b & c & p \\ 0 & 0 & 0 & 1 \end{bmatrix} \quad \text{..... (10)}$$

Allude the basic construction of the forward kinematics function by composing the coordinate transformations into the one homogeneous transformation matrix. The actual description of the coordinate transformation system between frame i and frame I – 1 is given by homogeneous transformation matrix.

$$A_i = \begin{pmatrix} C\theta_i & -C\alpha_i S\theta_i & S\alpha_i S\theta_i & \alpha_i C\theta_i \\ S\theta_i & C\alpha_i C\theta_i & -S\alpha_i C\theta_i & \alpha_i S\theta_i \\ 0 & S\alpha_i & C\alpha_i & d_i \\ 0 & 0 & 0 & 1 \end{pmatrix} \quad \text{..... (11)}$$

Where $S\theta_i$ and $C\theta_i$ are $S\alpha_i$ and $C\alpha_i$, respectively.

Table 1 the parameters of the arm

i	θ_i	α	a_i(mm)	d_i(mm)	range
1	θ_1	-90°	l_s	0	- 90°…….90°
2	θ_2 - 90°	-90°	0	0	- 90°…….90°
3	θ_3+180°	180°	0	l_u	- 180°…...180°
4	θ_4	-90°	l_h	0	0……180°
5	θ_5	90°	0	l_f	- 45°…….45°

Where θ is denoted by the vector of the joint variables, a, b and c are the unit vectors of the frame attached to the end- effectors.

V. CONSIDERATION OF ELBOW POSITION

The main description is the intersection of the ellipsoid and the sphere mentioned above is analytically difficult. To make this task mathematically tractable, firstly we determine the intersection between the ellipsoid and the sphere at Z = ze. The redundancy curve of the arm can eventually be obtained by combining all such intersections for all values of ze in the interval. (Note that Z_e^{min} and Z_e^{max} are the minimal and the maximal values of the Z coordinate of the elbow for a given position and orientation of the end-effectors.)

Let $Z_e \in [Z_e^{min}, Z_e^{max}]$ are be the coordinator of Z of an elbow position of this arm for a given position of the end-effector. The radius r_1 and center C_1 of this circle are given below:

$$r_1 = l_s + \sqrt{l_u^2 - z_e^2} \quad \ldots\ldots (12)$$

$$C_1 = (0.0.z_e)^T \quad \ldots\ldots (13)$$

The intersection of the sphere with the plane Z = Ze results in a circle. Then the radius r_2 and the center c_2 of this circle can be determined as follows.

Basically there are two points like C_1 and C_2 provided by the intersection of the circles represents two possible positions of the elbow. The unit vectors of the frame (x4, y4 and z4) attached to the elbow position must be established.

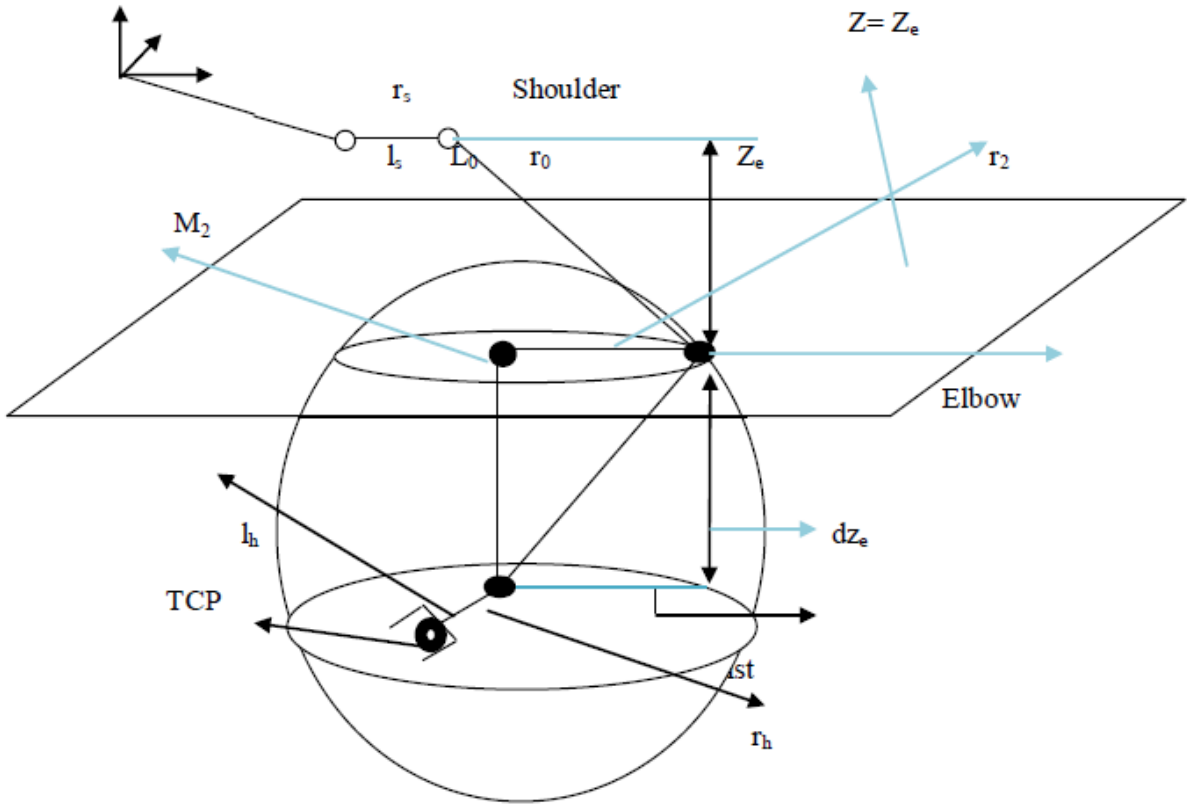

Fig. 6 Plane Z = Ze and ellipsoid

$$r_2 = l_s + \sqrt{l_f^2 - dz_e^2} \quad [dz_e = z_e - z_w] \quad \ldots\ldots (14)$$

And

$$C_2 = (x_w.y_w.z_e)^T \quad \ldots\ldots (15)$$

The vector z4 lies along the forearm and points to the wrist. The vector y4 is perpendicular to the upper arm (r_u) and fore arm (r_f). The vector x4 completes the right handed coordinate.

The redundancy of the arm:

The redundancy of the animator robots' arm can be described by the rotation of the center of the elbow joint about the axis. The base frame (x_0, y0, z0) of the feasible position of the elbow around this axis is defined by the curve. This curve can be described from the ending point of the upper arm which can be describes an ellipsoid. The centered of the origin of the base coordinate system (x_0, y0, z0) and that the starting points of the forearm derived a sphere centered on the wrist position (x_w, y_w, z_w) which corresponds to the origin of the coordinating system (x_s, y_s, z_s) which is as shown in the following figure.

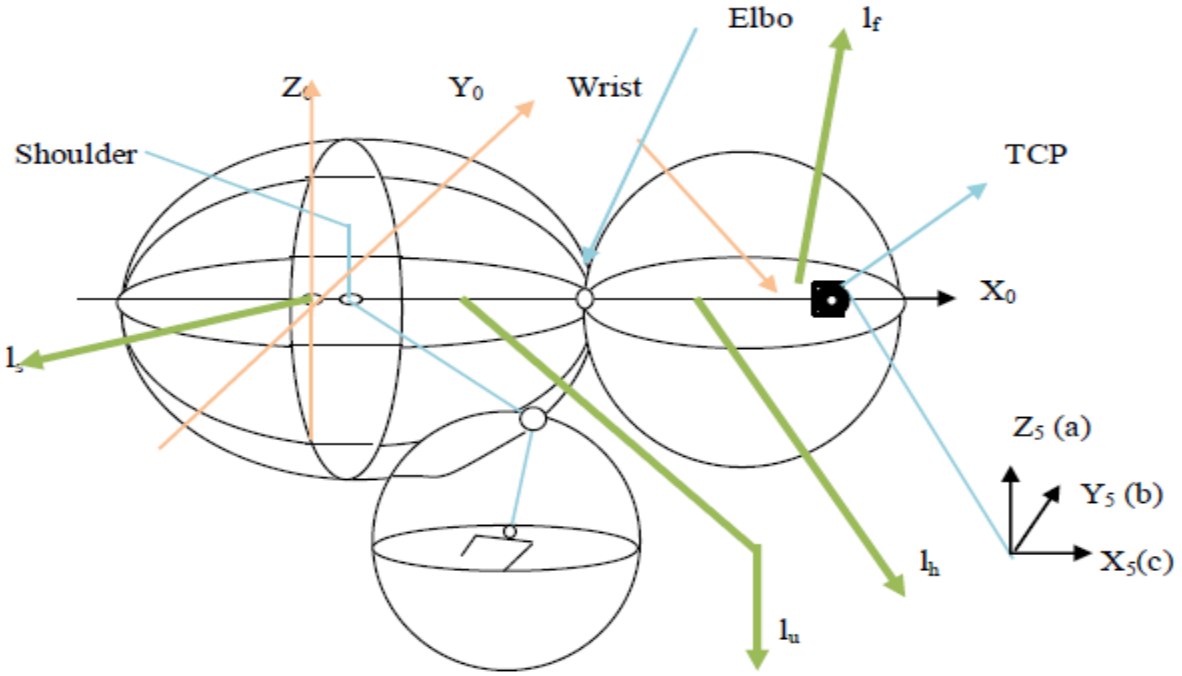

Fig. 7 work space of the upper arm and forearm of this arm

Since this two points have to same to looking the redundancy of the curve results from the intersection of the ellipsoid and the sphere. Mathematical equation is given as follows:

$$\frac{X}{(l_s+l_0)^2} + \frac{y}{(l_s+l_0)^2} + \frac{z}{(l_0)^2} = 1 \quad \ldots\ldots (16)$$

And also

$$W = (x_w, y_w, z_w)^T = \vec{p} - \vec{i_h}.\, c \quad \ldots\ldots (17)$$

Gear:

Gear is a rotating machine part which having cut teeth or cogs, which mesh with another toothed part in order to transmit the torque. A gear can produce a mechanical advantage through a gear ratio and thus may be considered a simple machine. Geared devices can change the speed, torque and direction of a power source.

A particular gear train is made up of two or more gears. Between an input and output shaft; there will be a change in angular velocity and torque. The basic speed relationship of their is given by

Gearboxes:

A gear train is made up of 2 or more gears. In these types of robot there will be a change in the angular velocity and torque between an input and output.

Fig. 8 Attached with another teeth or cogs.

The gear is increased by attaching external gearboxes in this robot arm. The mathematical relationship of speed is given below

$$n = \pm\frac{\omega i}{\omega 0} = \pm\frac{N0}{Ni} + \frac{x^3}{3!} \quad \text{..... (18)}$$

$$n = \pm\frac{\omega in}{\omega 0ut} = \left(-\frac{N2}{N1}\right)\left(-\frac{N3}{N2}\right) = \left(\frac{N3}{N1}\right) \quad \text{..... (19)}$$

Where N_i and N_0 are the number of teeth of the input and output gear. ω_i and ω_0 are the angular velocity of the input and output gear. These types of robot we use spur type gear.

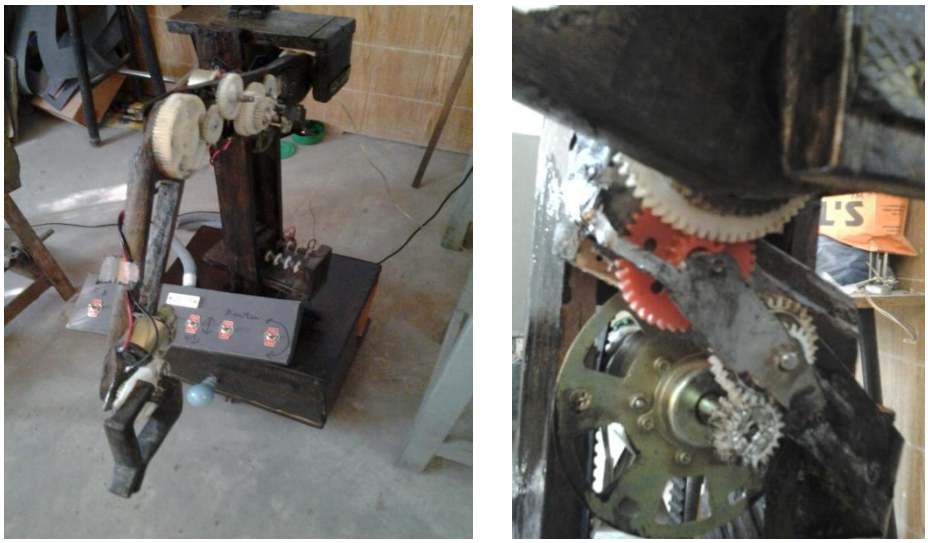
Fig. 9 increasing torque by adding external gear

In general, any two of the three components (like flexspline, circular spline and wave generator) that build up the gearbox can be used as the input to, and also the output from, the gearbox, giving the designer considerable flexibility. The robot need to increasing the gear for his hand work successfully.
This arm the required gear added by using external gear with motor.

Motor:

In these types of robot we consider the DC electric gear motor. Actually a DC motor is designed to run on DC electric power. The AC or DC power electric motor is an electromechanical device that can converts electrical energy into mechanical energy. The moving part of the electric motor is called rotor and the stationary part of the electric motor is known as stator.

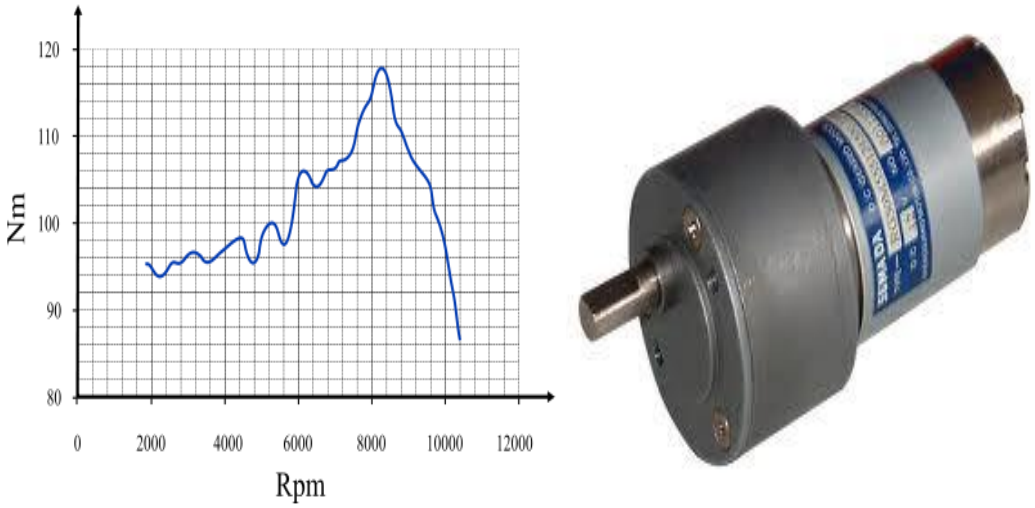

Fig. 10 A DC gear motor and torque related curve.

In order to obtain more torque which is as shown in figure 10? The exact or containing speed of a DC or AC induction motor is influenced by an applied load and the consequences slip. The torque of the motor produces by also a function of the slip. If we can produce more slip ultimately we can produce more torque. Actually a DC electric motor is designed to start on DC electric power.

Series connected and shunt connected DC type motor:

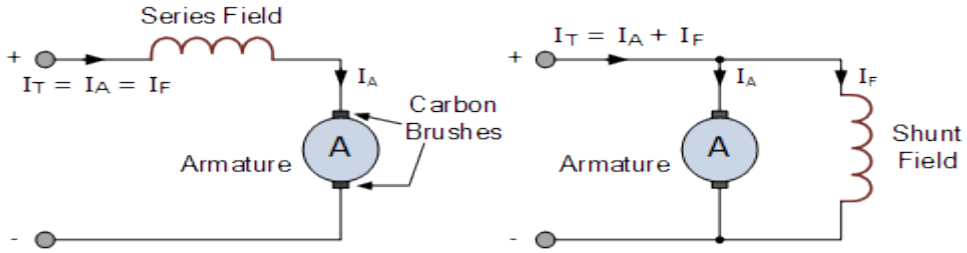

Fig. 11 series and shunt connected DC motor.

Basically there are there basic types of DC motor. Most of them are series motors, shunt motors and compound motors.

Motor Power Rating:

How can we apply high voltage to a motor? All motors are operated to a certain rated voltage. The inefficiency of energy conversion is directly related to heat output. When produce too much heat, the coils of a motor melt will be occurred. So it is highly preferred to maintain a sustainable power for usable motor. We can explain the power rating of a motor by a simple equation. The related equation is given below

Power (in watts) = Voltage * Current

Switch:

These types of robot arm we bonhomie and adjust DPDT switch. It stands double pole and double through. These types of switch can flow electricity both clockwise and anti clockwise. For continuing the work of this arm we need to rotate both ways. For up and down of this arm need to flow current in both ways so that the DPDT switch attached perfectly.

Some function of a DPDT switch is given below:

- A DPDT can be used in any application that requires a NO, that means normally open and NC, that means normally closed wiring system.
- DPDT can be used in such cases for block controlled due to the ease and flexibility of the wiring.

- Block controlled allows the relay coil to be triggered remotely, while another relay is controlling by another block.

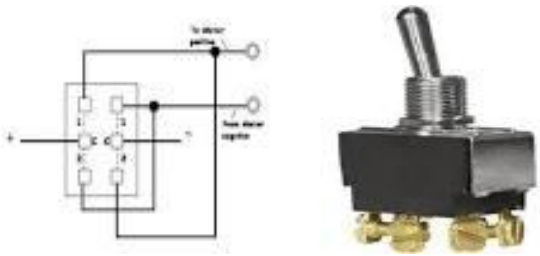

Fig. 12 DPDT switches construction and circuit diagram

Table 2 Switch connection with motor and its mechanism.

Input A	Input B	Motor Function
0	0	Motor Stopped (OFF)
1	0	Motor Rotates Forward
0	1	Motor Rotates Reverse
1	1	Not Allowed

In the table 2 we describe about the operation system of DPDT switch. When input and output will both 0 then the motor speed 0 that means motor is stopped. When input is 1 and output 0 then motor will rotate with forward kinematics or clockwise direction. On the other hand when input is 0 and output 1 then the motor will rotate inverse kinematics or anticlockwise direction.

VI. RESULTS AND CONCLUSIONS

The generation of the human-like manipulation motions has been implemented and also tested successfully for the 4 degrees of freedom (DOF) arm of the humanoid robot. The presented approach does not consider the dynamics of the robot arm. This would be necessary to generate realistic velocity distribution for the manipulation motions. In this paper has reviewed the characteristics of the main mechanical structure and construction of a humanoid robotic arm. From this arm the exploration of afterwards will be a full body which is controlled by body switch. The final step of this robot is auto learner, in this stage this robot can learn automatically. The real/exact position and orientation of the arm can be obtained significantly large modifications of the joints θ_1, θ_2 and θ_3. The assistive robotic arm will must be able to contribute most of the challenges in our daily life. However, the resulting configuration is not guaranteed to be human-like.

VII. ACKNOWLEDGEMENT

Authors are very grateful to Almighty for giving the strength and encourage to completing this project. The authors also would like to acknowledge to contribution for made by the university authors (BU) who give us an environment where we work more time. We are really grateful to Bangladesh University of Engineering & Technology (BUET) for their logistic and technical support. We want to thank to all who have been directly related to this thesis for their support and encouragement. We also thank all the personnel at the general library and reference library for providing us with the books and thesis papers to complete this thesis.

REFERENCES

[1] www.springerlink.com/index/V67J235820033K72.pdf
[2] en.wikipedia.org/wiki/Natural environment
[3] www.societyofrobots.com/robot_arm_tutorial.shtml
[4] ai.stanford.edu/~ang/.../icra11-LowCostCompliantManipulator.pdf
[5] www.societyofrobots.com/robot_arm_tutorial.shtml
[6] en.wikipedia.org/wiki/Cartesian_coordinate_robot
[7] www.allonrobots.com/spherical-robots.html
[8] www.allonrobots.com/cylindrical-robot.html
[9] en.wikipedia.org/wiki/SCARA
[10] www.wisegeek.com/what-is-an-articulated-robot.htm
[11] www.robotshop.com/robot-arm-torque-tutorial.html
[12] www.robotshop.com/robot-arm-torque-tutorial.html
[13] www.mbfys.ru.nl/~stan/gielen-MotorControl-2004.pdf
[14] en.wikipedia.org/wiki/Power_(physics)
[15] en.wikipedia.org/wiki/Energy en.wikipedia.org/wiki/Energy

[16] en.wikipedia.org/wiki/Electric_motoren.wikipedia.org/wiki/Brushed_DC_electric_motor en.wikipedia.org/ wiki/DC_motor www.wisegeek.org/what-is-a-dc-motor.htm en.wikipedia.org/wiki/Electric_motor
[17] en.wikipedia.org/wiki/Torque en.wikipedia.org/wiki/Induction_motor
[18] en.wikipedia.org/wiki/Gear https://www.princeton.edu/~achaney/tmve/wiki100k/docs/Gear.html
[19] en.wikipedia.org/wiki/Caster
[20] en.wikipedia.org/wiki/Electrical_connector whatis.techtarget.com › ... › Networking › Network hardware whatis.techtarget.com › ... › Networking › Network hardware
[21] www.conwire.com/
[22] www.kpsec.freeuk.com/breadb.htm
[23] en.wikipedia.org/wiki/Bearing_(mechanical)
[24] physics.tutorvista.com/.../torque.html -
[25] en.wikipedia.org/wiki/AC_adapter
[26] www.ehow.co.uk › Home wiki.answers.com › ... › Heating Ventilating and Air Conditioning www.diyguitarmods.com/push-pull-potentiometer.php

American Journal of Engineering Research (AJER)
e-ISSN : 2320-0847 p-ISSN : 2320-0936
Volume-02, Issue-10, pp-308-313
www.ajer.org

Research Paper Open Access

Automotive Parking Lot and Theft Detection through Image Processing

Md.Towhid Chowdhury, Ebad Zahir.
[1](EEE, AIUB, Bangladesh)\ [2](Faculty, AIUB, Bangladesh)\

Abstract: - Automotive parking lot and theft detection through image processing is a smart parking lot which will save time for the owner to park his car in a more organized way and also prevent theft of the car. It is a technology to optimize the checkout process by analysing a database of images of number plates of cars. The heart of the project is based on image processing. The images of number plates will be detected by Matlab and a picture of the driver will be saved in a similar database. As soon as both the images are saved, the garage entrance pole will shift 90 degrees upward using a DC MOTOR and will remain in that position for 30 seconds to allow the car to enter. After 30 seconds it will return back to its previous position. When the car exits the earlier steps will be repeated and Matlab will match both the images that were taken during entering and leaving. Meanwhile the seven segment display will show that a car has left the parking lot, by decrementing a number from its display. The cars are controlled by a microcontroller which is also able to detect and display if a vacant parking space is available. If there is no vacancy a red LED lights up, where as a green LED is used to display presence of parking space along with how many parking spots are available. It is applicable to be used in super market car parking lots and also apartment garages.

Keywords: - *Parking Automation, Accident detection and avoidance, Obstacles detection, Vehicle tracking.*

I. INTRODUCTION

With an increasing number of vehicles being used in our country, it is getting difficult to manually accommodate the cars in big parking spaces. Because in a big parking space no one can systematically control the entry and exits of the numerous cars; because this is very difficult to know how many cars and vacant places are available in the parking lot at any given time. But this system shows digitally how many places are vacant and how many cars can enter the parking space. This system also saves the cars' number plates and driver's pictures in a database for security measures. In order to automate the processes and make it more effective, a system is required to easily identify a vehicle. The important question here is how to identify a particular vehicle? The answer to this question is – by using the vehicles' number plate and tagging it to its driver's picture from the database. Vehicles in every country have a unique license number, which is imprinted on its license plate. This number which also includes letters distinguishes one vehicle from the other, which is useful especially when both are of same make and model. In Bangladesh the license plate has numbers and letters imprinted in Bengali.

PARKING SYSTEM WHICH IS NOT THE MAIN CONCERN OF OUR PROJECT.

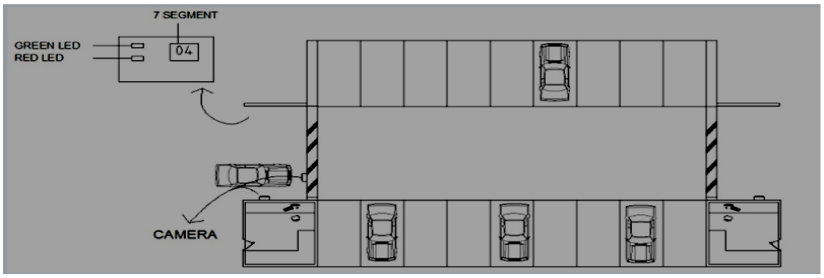

Figure 1: - Parking System

II. MAIN TECHNOLOGY USED

1.1 Obstacle detection & indication sensor

The main objective of this project was to design and develop a model of an automotive car parking lot and theft detection through image processing. The processing is controlled by Matlab which gives the command to the microcontroller to allow Exit or Entry of a car and the save the car's plate number in the database with the driver's picture. When that same car is ready to exit the parking garage, the software will match the number with the one collected earlier at the point of entry. If the number plate does not match, the microcontroller will not raise the gate and therefore the car cannot exit. Automotive car parking lot and theft detection through image processing needs the following components:

1, Atmega16
3, Serial Port RS232
4, IC ULN2003A
5, Adapter (Power Source)
6, Seven segment display
7, Stepper motor, camera and display.

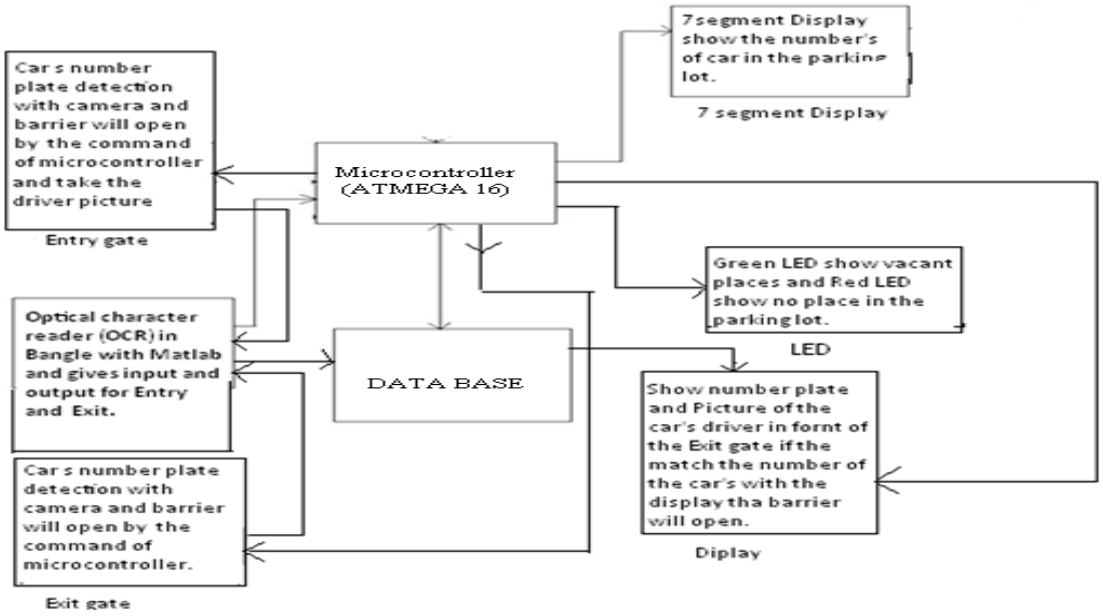

Figure 2:- Block Diagram of the overall project.

1.2 Optical character reader (OCR) in Bengali by Matlab:-

MATLAB is a high-performance language for technical computing created by Math Works in 1984. Matlab uses a high-level language and interactive environment to enable you to perform computationally intensive tasks faster than with traditional programming languages such as C, C++, and FORTRAN. It integrates computation, visualization, and programming in an easy-to-use environment where problems and solutions are expressed in familiar mathematical notation.

1.3 Acquiring the image

After the picture has been taken by the camera, Matlab will import the picture and begin processing the data manipulation.

Figure 3: - Number plate of the car

2.4 Template created:-

To match the number plate at first we have to make a Bengali template database from 0 to 9. These templates will save on the bin box. These templates will match, when the Matlab code calls for the template acquired from the number plate.

Figure 5: - Bengali Template

2.5 Matlab code execution flow:-

Before matching the template with the saved digits, a concatenation process is performed to separate them. After the matching process, the numbers will show in the variable 'id' in lines as 124420. It will show when the templates and numbers on the plates match. If they do not match, it will not show in the monitor. Figure 6 below shows the overall flow of the executed code. If the number plate and the template does not match than the output shows an error. If the template matches with the number plate, then it shows the output digits and the Entry or Exit gate will open; and an additional step will be to save the number in memory which can increase security in future operations.

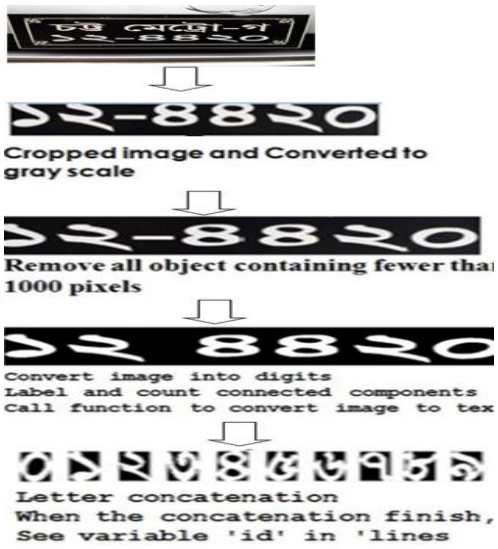

Figure 6: - Matlab steps execution

2.6 Results

Figure 7 below shows the results after a correct execution of the code.

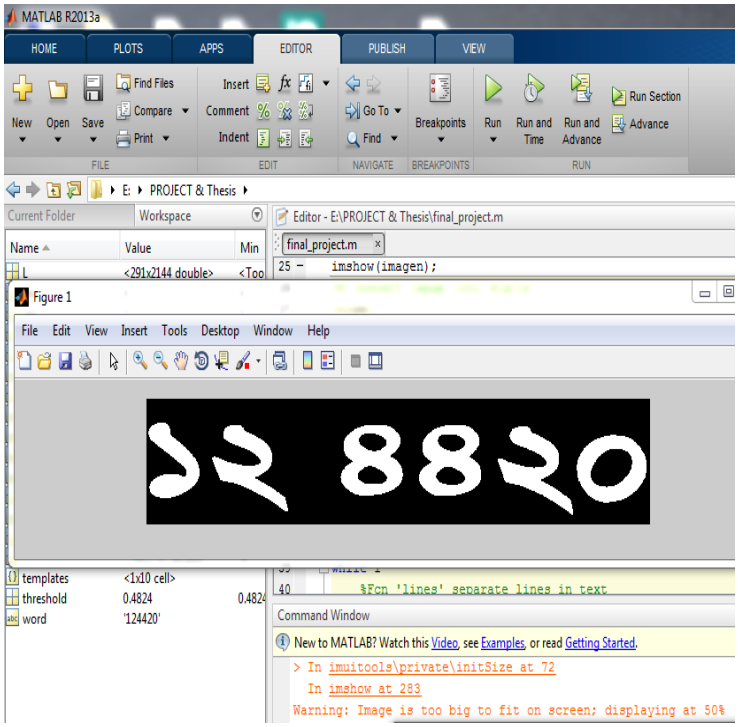

Figure 7: - Matlab execution and display of results

3.1 Circuit Diagram Description

Figure 8 below shows the complete circuit diagram of the automotive parking lot. Here the interfacing of some peripherals and ICs with the microcontroller ATMEGA 16 is shown. The circuit is initially simulated on Proteus, which is basically an electronic circuit simulation tool on windows platform. The camera here monitors the car during entrance and exit to capture the images. After the images are taken and saved to memory, data is transferred to the microcontroller through a serial communication cable. The gate opens and pin no. 40 controls this entrance. The recorded sample is stored in the microcontroller by pin number 14 and 15. Pull-up network resistances of 10KΩ are provide at each port. Since we are not using the LCD display RS (Resister Select), R/W (Read/Write) and E (Enable) are not needed. The Reset switch connects at pin 9 of microcontroller to provide a manual reset of the microcontroller. If any problem occurs or if the system hangs we can push the reset button to reboot the whole system. When any vehicle reaches the parking lot and after the data is transferred to the microcontroller, the systems registers an increase in the number of vehicles and records the count. The Count is for current recording time. Pin no. 22 to 29 controls the seven segment display. After completion of recording interval this count value is saved in the memory. The microcontroller is connected to the computer through a serial communication cable. Matlab instructs the microcontroller to send the recorded data for monitoring. It can also ask the microcontroller to erase previously recorded data after analysis is completed.

The seven segment display will get positive voltages from pins 2 and 3. The green LED is switched on to show that there are spaces available in the parking lot. Pin no. 1 is for the red LED which will turn on when there are no spaces available. Pin no. 12 and 13 have not been used in our project. Pin no. 39 controls the exit. Pin no. 18 to 21 controls the stepper motors. Pin no. 10 is for the Vcc supply and 11 is for ground. Figure 8 below shows the entire circuit for the project. It is operated with a voltage level of 0-5V. It also uses a 0V to 9V transformer to step down the 220V AC supply to 9V AC. It is further filtered through a 1000 uF capacitor and then regulated using IC 7805 to get +5V. To isolate the output voltage of +5V from noise further filtering is done using a 220uF capacitor.

As for the power requirement of the hardware of the system for the microcontroller, we used a supply voltage of +5V w.r.t GND and 12V for the two stepper motors. Matlab transfers the recorded data to the microcontroller by serial communication. This data is used for matching both the images taken during entrance and exit. To interface the UART and PC all 4 outputs are connected through the microcontroller for the signal conversion. A data transfer protocol is implemented through the software. Matlab collects all the recorded data.

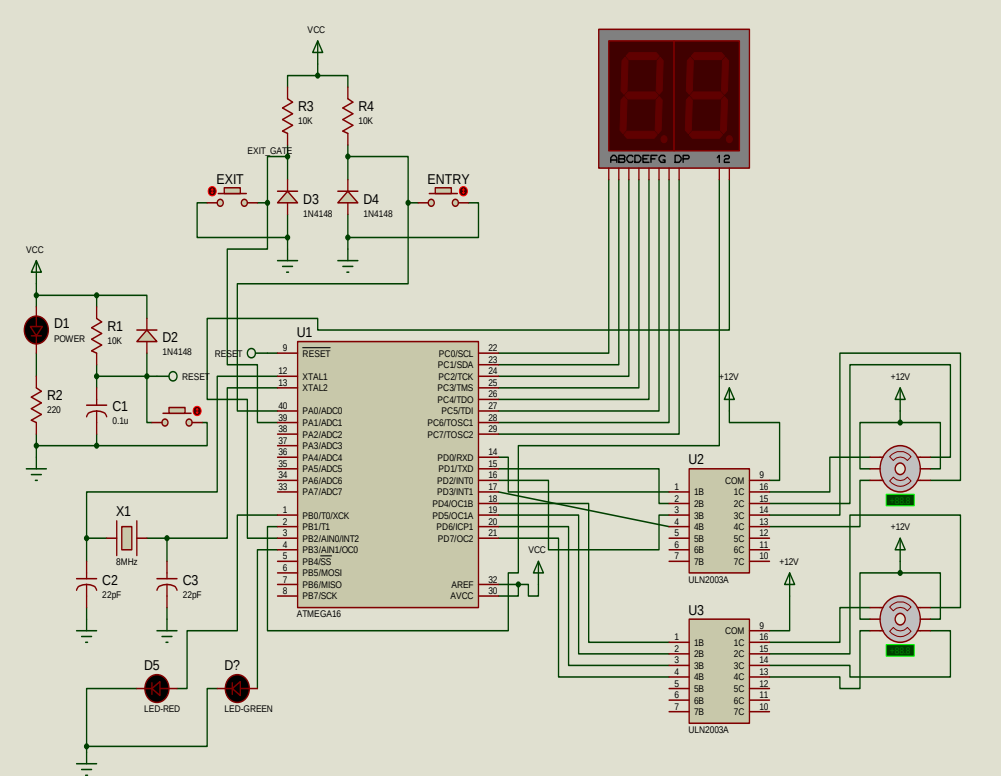

Figure 8: - Schematic of the overall project

3.2 Entry processes

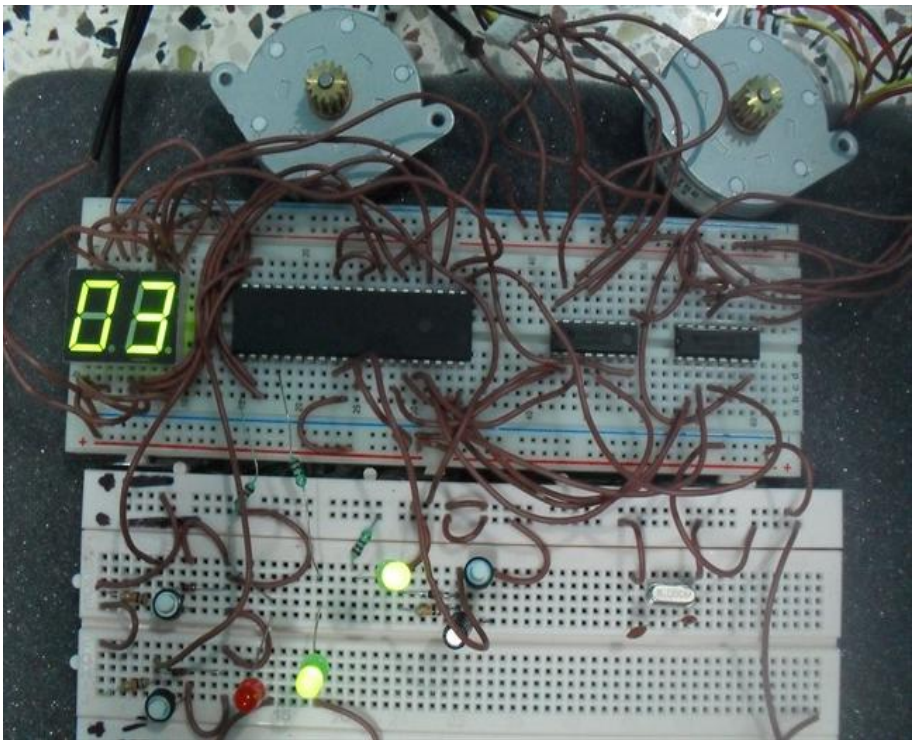

Figure 9: - Hardware implementation showing availability of parking space

Figure 9 above shows two motors for the exit and entry gates and also the 7segment display which will show how many cars are already in the parking lot (as shown by the green display of the number 03). It also means that there are still available places for parking and the green LED indicates this. Another green LED (in the middle) represent that the whole system is running.

3.3 Red light

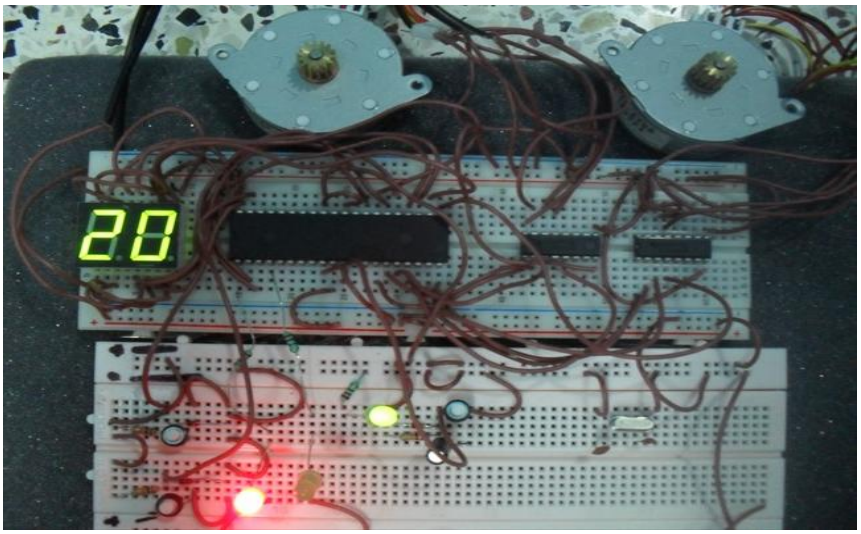

Figure 10: - Hardware implementation showing that the parking lot is full

This project was modeled for only 20 cars. Since the display is showing the number 20, it means there are no more parking places left. The Red LED (at the bottom) is lit to further indicate this. Note that the green LED (in the middle) is representing that the whole system is still running error free.

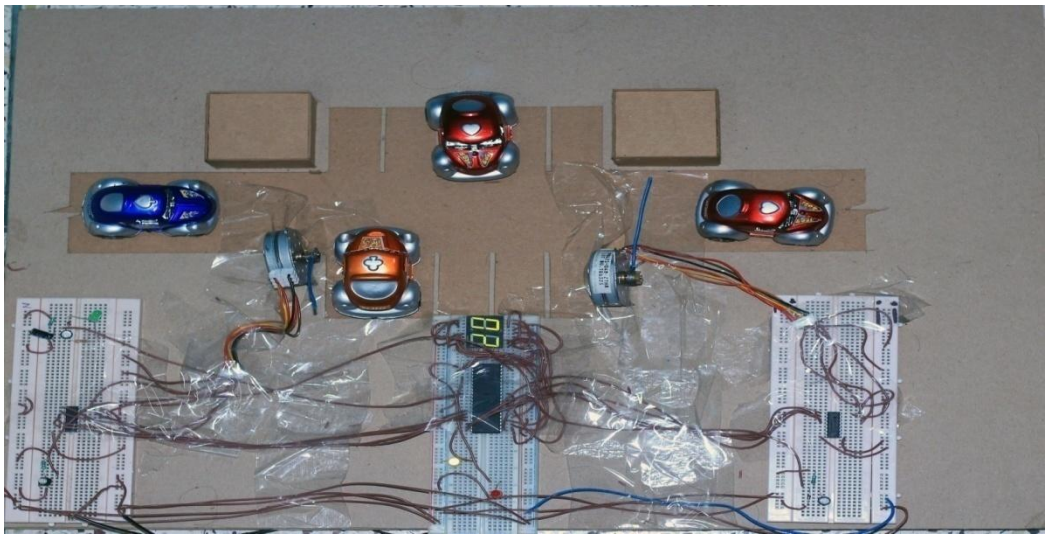

Figure 11: - The Entire Model

III. FURTHER APPLICATION

1. Notifying the owner the exact location of the car inside the parking lot by SMS.
2. Adding a finger print scanning and password option for added security.

IV. CONCLUSION

This project presented a recognition method in which the vehicle plate image is obtained by digital cameras and the image is processed to get the number plate information. The model of the entire system was designed and tested thoroughly. By identifying the car's number plate as a reference on image detection, it makes the process of detecting images as a reference more efficient compared to the use of a moving object. The conceptualization of this project is to establish a sophisticated and smart parking system by using image processing instead of using sensor based security methods. An intelligent parking system is developed using an integrated image processing approach to reduce cost of sensor and wiring hassle. Detecting the number plate and taking a picture is shown as a technique that can save time and manpower while also reducing theft. All these features put together make it a very attractive package.

REFERENCES

[1] (2013) HTS website. [Online]. Available: http://www.htsol.com/

[2] Robertson, Patrick (1974). *The book of firsts*. C. N. Potter : distributed by Crown Publishers. p. 51. Retrieved 13 August 2011.

[3] Friedrich, Markus; Jehlicka, Prokop; Schlaich, Johannes (2008). "Automatic number plate recognition for the observance of travel behavior" Universität Stuttgart Institut für Straßen und Verkehrswesen. Retrieved 2013-07-02.

[4] Road Transport (Permits) Act, CHAPTER 69:03

[5] Friedrich, Markus; Jehlicka, Prokop; Schlaich, Johannes (2008). "Automatic number plate recognition for the observance of travel behavior". *8th International Conference on Survey Methods in Transport: Harmonisation and Data Comparability, May 2008, Annecy, France*. Universität Stuttgart Institut für Straßen und Verkehrswesen. Retrieved 2013-07-02.

[6] Leslie Howard Saunders. *An Orangeman in public life: the memoirs of Leslie Howard Saunders.* Britannia Printers, 1980 pg. 97

[7] Hugh McGee (2003). *NCHRP Synthesis 310*. National Cooperative Highway Research Program. p. 12.

[8] (2012) The IEEE website. [Online]. Available: http://www.ieee.org/

[9] M. Shell. (2002) IEEEtran homepage on CSD. [Online]. Available: http://www.computer.org/csdl/proceedings/icinis/2012/4855/00/4855a009-abs.html

[10] Met given real time c-charge data" *BBC*. 17 July 2007. Archived from the original on 13 September 2007.

[11] "Transport for London". Cclondon.com. 17 July 2011

[12] Speeding tickets can potentially be avoided by changing lanes" *The Daily Mail* (London). 15 October 2006. Retrieved 2012-01-24. "The Home Office admitted last night that drivers can avoid being caught the by hi-tech 'SPECS' cameras which calculate a car's average speed over a long distance."

American Journal of Engineering Research (AJER)
e-ISSN : 2320-0847 p-ISSN : 2320-0936
Volume-02, Issue-10, pp-314-321
www.ajer.org

Research Paper Open Access

Optimal design of two feeder system: simulation studies for techno-economic feasibility

Haider Hussain, Dr. A. I. Khandwawala
[1](*Research Scholar, Bhagwant University Ajmer (Rajasthan), India)*
[2](*Ex. Professor, Mechanical Engineering Department, SGSITS, Indore, India)*

Abstract:- In the casting technology, defect free casting had been the primary goal since the inception of the technology. However in the present casting arena, emphasis on the precise and defect free casting has got greatly increased due to energy saving, environmental and economy considerations apart from the stringent product quality standard requirements. In order to achieve this level, computer simulation is inevitably necessary. FEM based simulation software is used to find solidification related defects specially shrinkage porosity very precisely. In the present work ANSYS, an FEM based versatile software has been used for hot spots identification in a two feeder system. The feeders have been designed and optimized. ANSYS has been used for transient thermal analysis and then optimization process has been performed. Path of two feeder optimization for sand casting on ANSYS have been searched. Conductive and convective heat transfer has been taken in to consideration. The whole process is performed using traditional modulus approach also. The results are compared. The comparison reveals that ANSYS optimizer provides better results for casting having two feeders. It saves material and energy thus resulting into economy and environmental benefits too. Hence it may be recommended as superior over modulus approach for two feeder system in sand casting.

Keywords: - *Feeder design optimization, FEM, Modulus Approach, Sand Casting, Shrinkage porosity.*

I. INTRODUCTION

Sand casting is the most widely used process for both ferrous and non – ferrous metals, and accounts for approximately 90% of all castings produced [1]. In sand casting, sand mixed with binders and water is compacted around wood or metal pattern halves to produce a mould. The mould is removed from the pattern, assembled with cores and metal is poured in to the resultant cavities. After cooling, moulds are broken to remove the casting. After casting is removed from the sand moulds, sand mould is destroyed [2]. This leads to not only the loss of material but also to the loss of energy required for molding and remolding the material again and again. in fact the repeated molding-remolding consumes huge amount of fuel ultimately contributing to the global warming which is the greatest havoc for modern civilization. Hence the optimal design of feeder system must be seen not only from the material saving point of view, it must simultaneously be pursued from the environmental considerations too [16]. The modern casting processes not only require high precision and accuracy, they require energy efficiency and environmental consistency too. The present work is a determined step in this direction.

In sand casting, molten liquid metal is poured into a cavity which takes the negative shape of the object and the mould is made from sands. Heat removal is by heat transfer in sand mould, the governing equations for heat transfer are [3]

$$\frac{\partial T}{\partial t} = \alpha \frac{\partial^2 T}{\partial^2 x} \quad (1)$$

$$T(x, 0) = T_0 \quad (2)$$

$$T(0, t) = T_M \text{ (Temperature at metal end)} \quad (3)$$

$$T(\infty, t) = T_0 \quad (4)$$

Finite Element Method (FEM) is a powerful computational tool that is used to numerically solve many engineering problems. Most of the Research on the area of casting processes modeling uses FEM as a solver to

the casting Process model. The numerical simulation of solidification process using either Finite Difference or Finite Element Methods (FDM/FEM) involves the following steps: [1]

1. Formulating an accurate mathematical model of the solidification process.
2. Specifying accurate values for thermal properties of material involved.
3. Performing the analysis to obtain the temperature history of casting and mould points.
4. Post – processing the results to visualize the solidification pattern and identify defects.

Feeders are designed to compensate the solidification shrinkage of a casting, and make it free of shrinkage porosity. Feeder design parameters include the number, location, shape and dimensions of feeder. Feed path and feeding distance influence the location and number of feeders. The volume of the feeders must be minimized to increase the yield. The criterion is given by for getting feeder yield C_{F3}:

$$C_{F3}=N_c v_c/\left(N_c v_c + \sum_i v_{fi}\right) \quad (5)$$

Finite element analysis based software ANSYS 12.0 has been used. Modal of casting is done in Pro E wild fire and cylindrical feeders have been created in ANSYS modeling. Element selection and material property feeding is done latter. Convective load have been considered after proper meshing. Proper boundary values of temperature have been provided and then transient thermal analyses have been performed. DB log file has been assigned to ANSYS optimizer and then design variable, state variable and objective functions have been provided [5]. They are height of feeder, maximum temperature difference of feeder and respective casting zone, inverse of feeder yield respectively with suitable allowances and factor of safety. First order optimization has been performed through ANSYS 12.0.

In FEM, the field variables are the temperatures at all nodal points that vary with time .Thermal properties like thermal conductivity, density, specific heat also vary with temperature and hence the problem becomes non – linear transient in nature Galerkin's weighted residual approach has been reported[7]. The advantage of using FEM is the ability to handle complex boundaries, the ease in implementing boundary condition. But this method requires much effort for formulation of problem, data preparation and need long processing time [8].

In general, FEM is preferred as it allows a wider choice of element shapes and better accuracy, while FDM based simulation programs are faster and easier to execute. Recent advances have been in the areas of automatic preprocessing (mesh generation), adaptive remeshing for better accuracy in critical regions, heat transfer models for considering the effect of variable air gap and mould coatings, convective and radiation heat transfer and improving the efficiency of computation[9]. Feeder optimization has been performed using topology optimization [10], poison equation approximation [11] and genetic algorithm [12].

P. Prabhakara Rao gives advantages of computer simulation based design enumerated. The procedures thus described have been demonstrated with the above case study of application of Pro CAST simulation at G.S alloy Foundry. It is demonstrated that the foundries can derive mileage by resorting to FEM simulations of the casting process for process development and optimization. [13]

The application of casting simulation softwares in the foundries not only minimizes the wastages of resources required for final castings, but also improves / enhances the quality and yield of castings, which implies higher value addition and lower production cost. The experimental study represents the effect of sizes of risers and necks on the solidification behavior of the aluminum alloy castings. The simulated results are more or less similar with experimental results. [14]

The application of computer aided method, solid modeling, and casting simulation technologies in foundries can able to minimize the bottlenecks and non value added time in casting development, as it reduces the number of trial casting required on the shop floor. In addition, the optimization of riser neck reduces or completely removes the occurrence of shrinkage defect in the casting. The application of casting simulation software based on finite element method and vector element method shows good results and matched with the experimental results.[15]

II. DATA COLLECTION

Multi feeder optimization has been performed on a dumbbell casting of Aluminium-06. Two feeders have been considered.

Volume = 10.87-06 M^3 , Surface Area = 12.98e-2 M^2

Feeders can be optimized by modulus approach. The thickest section has highest value of modulus [1]. The optimization can be performed on ANSYS12. [5]

III. FEEDER OPTIMIZATION

The use of negative of the gradient vector as a direction for minimization was first made by Cauchy in 1847. In this method we start from initial trial point X1 and iteratively move towards the optimum point.[4]

The method of steepest descent may appear to be the best unconstrained minimization technique since each one-dimensional search starts in the best direction. Design optimization works entirely with the ANSYS Parametric Design Language (APDL) and is contained within its own module (/OPT). Design optimization is largely concerned with controlling user-defined, APDL functions/parameters that are to be constrained or minimized using standard optimization methods (e.g., function minimization, gradients, design of experiments).The independent variables in an optimization analysis are the design variables. The vector of design variables is indicated by: [4]

$$X = [X_1 X_2 X_3 \dots X_n] \quad (5)$$

Design variables are subject to n constraints with upper and lower limits, that is,

$$\underline{X_i} \le X_i \le \overline{X_i} \ (i = 1,2,3,\dots,n) \quad (6)$$

Where: n = number of design variables.

The design variable constraints are often referred to as side constraints and define what is commonly called feasible design space. Now, minimize

$$f = f(X) \quad (7)$$

Where: f = objective function

Subject to

$$g_i(X) \le \overline{g_i} \quad (i = 1,2,3,\dots,m_1) \quad (8)$$

$$\underline{h_i} \le h_i(X) \ (i = 1,2,3,\dots,m_2) \quad (9)$$

$$\underline{W_i} \le W_i(X) \le \overline{W_i} \ (i = 1,2,3,\dots,m_3) \quad (10)$$

g_i, h_i, W_i = state variables containing the design, with underbar and overbears representing lower and upper bounds respectively. (input as min, max on OPVAR command) $m_1 + m_2 + m_3$ = number of state variables constraints with various upper and lower limit values. The state variables can also be referred to as dependent variables in that they vary with the vector **x** of design variables. [4]

IV. OPTIMIZATION OF DUMBBELL CASTING WITH MODULUS APPROACH AND ANSYS

For removing shrinkage porosity defect, two feeders are designed here by modulus approach and ANSYS 10.0 design optimizer for dumbbell casting. Dumbbell has been considered in four sections A, B, C, D. First modulus approach has been used and then ANSYS Optimizer applied.

Modulus Approach-

Table 1: Dumbbell casting data (Section wise)

S	Volume M^3	Surface Area M^2 Area M^2	Modulus=V/A M^1
A	8.0×10^{-6}	2.4×10^{-3}	3.33×10^{-3}
B	1.131×10^{-6}	4.90×10^{-4}	2.3×10^{-3}
C	6.4×10^{-5}	9.6×10^{-3}	6.67×10^{-3}
D	1.131×10^{-6}	4.9×10^{-4}	2.3×10^{-3}

Calculation for first feeder-

Diameter of feeder = D_{f1} , Height of Feeder = H_{f1}

$H_f = 1.5\ D_{f1}$, Volume of feeder = V_{f1}

$V_f = 0.375\ \pi\ D_{f1}^3$

Area of feeder $A_f = 1.75\ \pi\ D_{f1}^2$

Modulus of feeder $M_f = \frac{V_{f1}}{A_{f1}}$

Also Modulus of feeder = $0.214\ D_{f1}$

Modulus of feeder = 1.2 × modulus of region around Hot Spot.

$0.214\ D_{f1} = 1.2 \times 3.33\times 10^{-3}$ M

$D_{f1} = 18.6$ MM

Height of Feeder = 27.9 MM

Diameter of Second feeder = D_{f2}

Height of Second Feeder = H_{f2}

$H_{f2} = 1.5\ D_{f2}$

Volume of feeder = V_{f2}

$V_{f2} = 0.375\ \pi\ D_{f2}^3$

Area of feeder $A_{f1} = 1.75\ \pi\ D_{f2}^2$

Modulus of feeder $M_{f1} = \frac{V_{f2}}{A_{f2}}$

Also Modulus of feeder = $0.214\ D_{f2}$

Modulus of feeder = 1.2 × modulus of region around Hot Spot.

0.214 D_{f2} = 1.2 × 6.67× 10^{-3} M

D_{f2} = 37.4 MM

Height of Second Feeder = 56.10 MM

So feeder yield by Modulus method is = 51.77%

The process of analysis of this case with Design optimizer of ANSYS 12.0 (An FEM Based general purpose software) has been search out for two feeders. Here we have taken height of feeders as a design variables, State variable S1 = FT1-CT1 (always positive), State variable S2 = FT2-CT2 (always positive) with suitable allowances and factor of safety so that hot spot must not remain in casted part. It should be in respective feeder. FT= maximum feeder temperature for respective zone, CT= maximum casting temperature of catchment. Following are the graphs as a result of optimization. Figure1 is showing the temperature according to cooling. It can be seen that higher temperature are with feeders as compare to casing. This assures that the shrinkage porosity will be in feeders only.

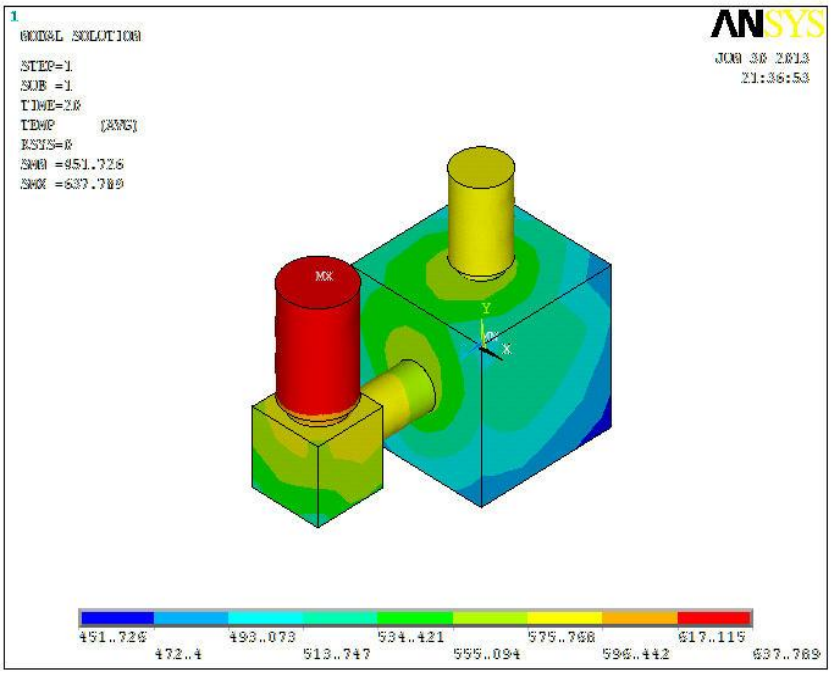

Figure 1: Dumbbell shape casting with optimized feeders

Fig. 1 is showing the temperature variation on the central plane of Casting and Feedeers.

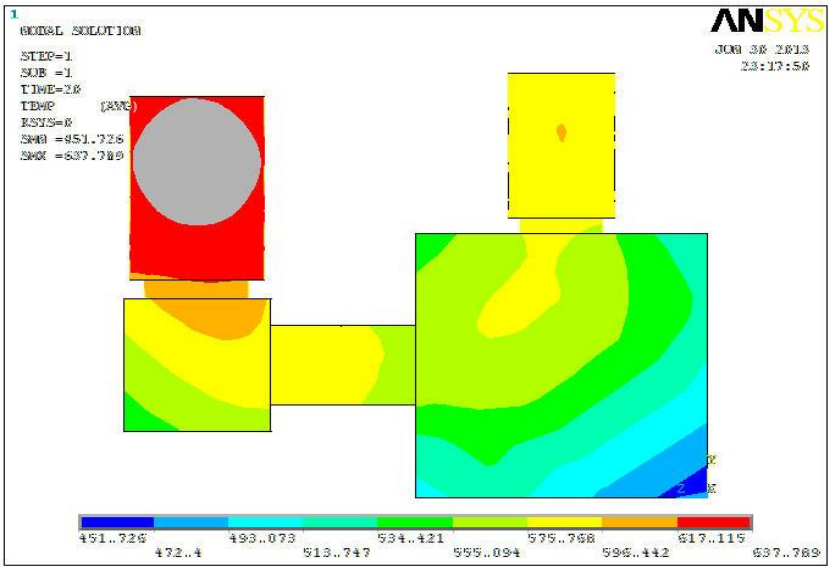

Figure 2: At centre plane of dumbbell shape casting with optimized feeders

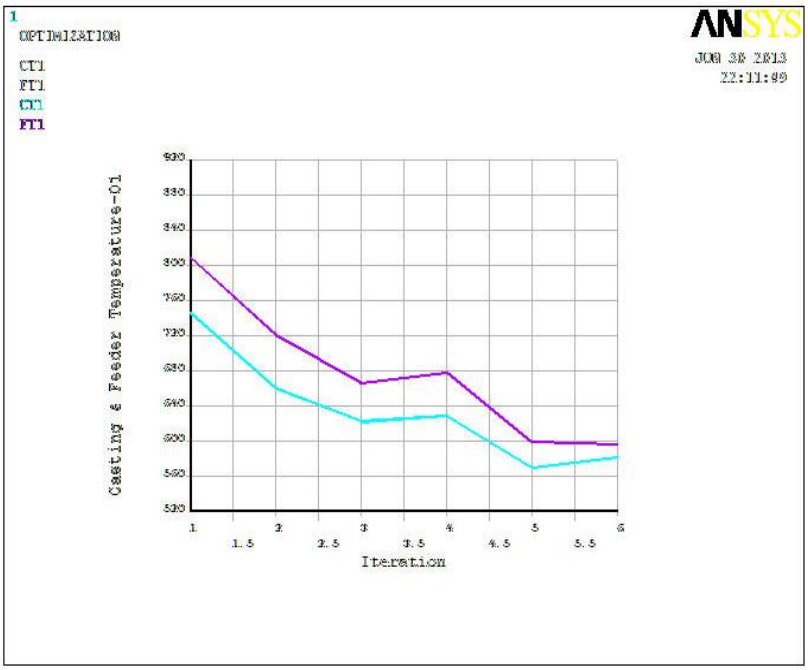

Figure 3: Feeder 01 Temperature remained higher than corresponding casting zone 01 temperature during entire optimization process.

Fig. 3 and Fig. 4 are showing that maximum temperature of Feeder remained higher than respective casting zone temperature.

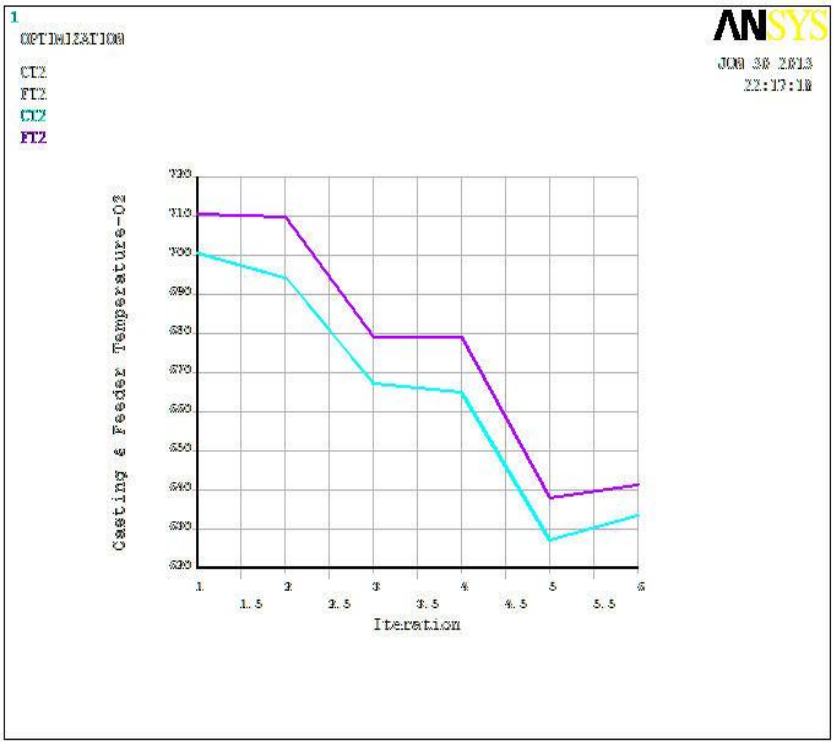

Figure 4: Feeder 02 temperatures remained higher than corresponding casting zone 02 temperature during entire optimization process.

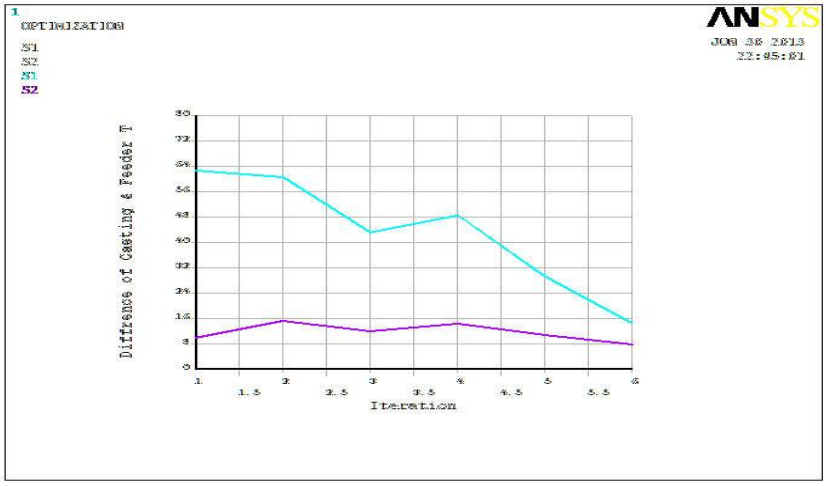

Figure 5: Feeder and corresponding casting deference during entire optimization process

Fig. 5 is showing drop of deference of feeder and casting temperature.

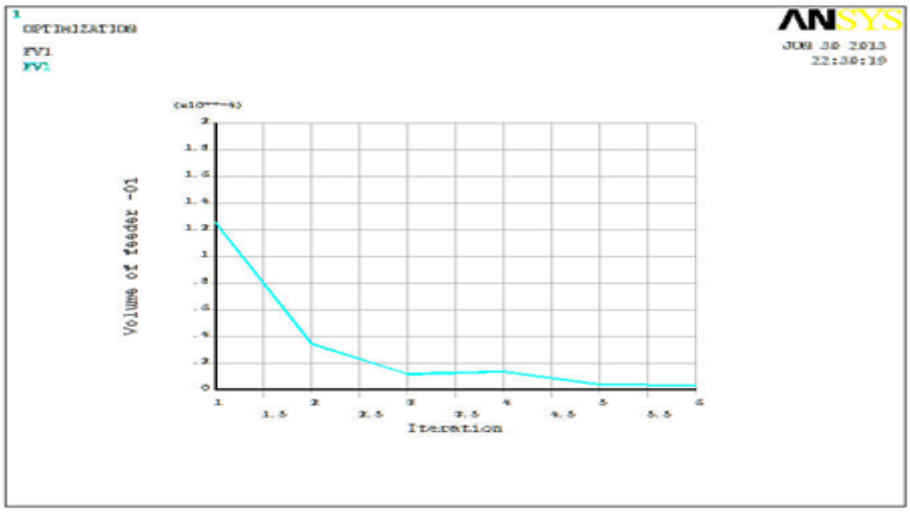

Figure 6: Volume of feeder 01 during entire optimization process

Fig. 6 and fig. 7 are showing drop of volume of feeder 1 and feeder 2 respectively.

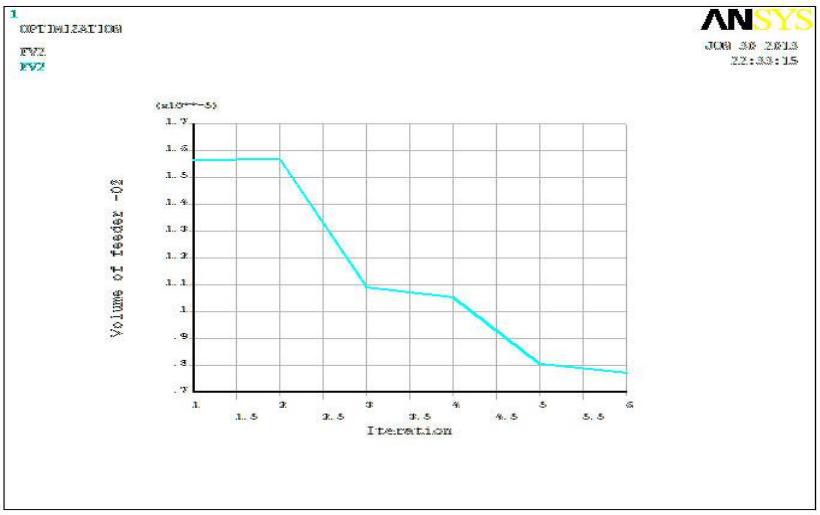

Figure 7: Volume of feeder 02 during entire optimization process

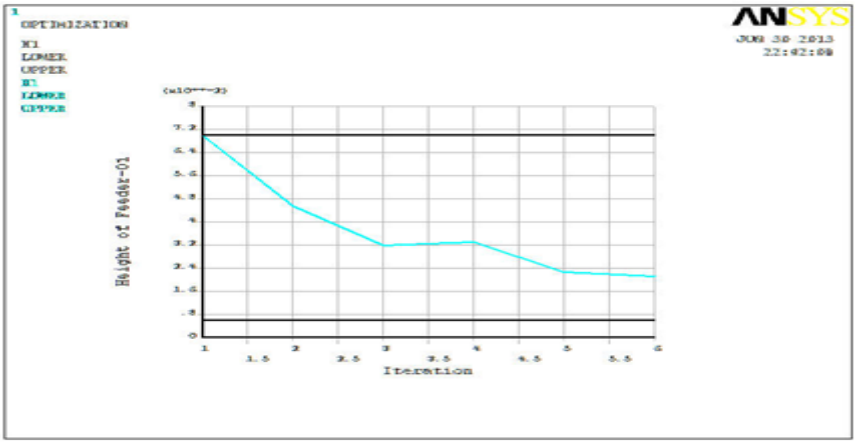

Figure 8: Height of feeder 01 during entire optimization process

Fig. 8 and Fig. 9 are showing the drop of feeder height during optimization process.

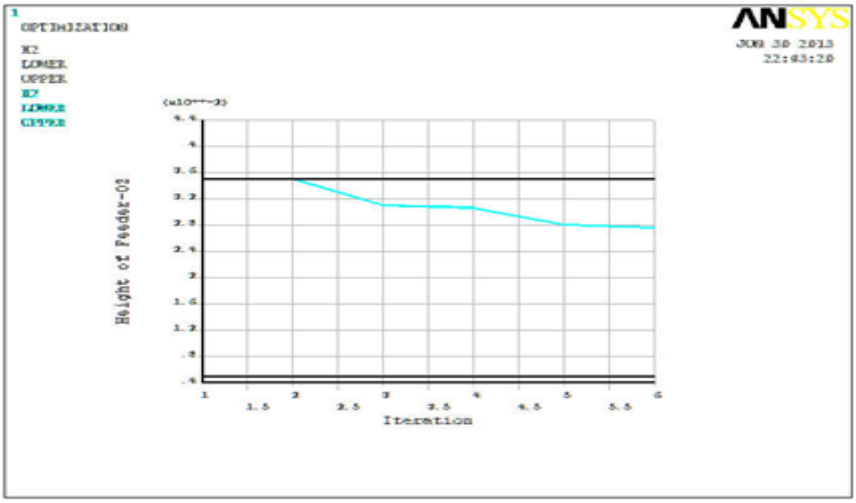

Figure 9: Height of feeder 02 during entire optimization process

Fig. 10 is showing the inverse of feeder yield which is continuously drop during optimization. Here objective is to achieve higher feeder yield.

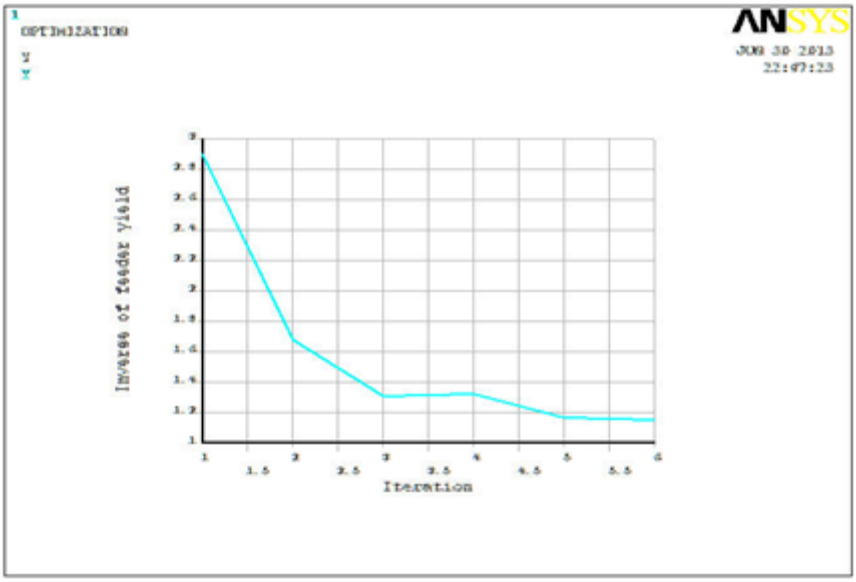

Figure 10: Inverse of feeder yield during entire optimization process

V. CONCLUSION

Feeder yield obtained comes out from modulus method is equal to = 51.77 %. Feeder yield obtained comes out from feeder optimizer is equal to = 86.88 %. So net advantage gained by ANSYS 12.0 design optimizer is 35 %. Optimization on ANSYS works better for small castings. Importing IGES file, Modeling, Meshing, in ANSYS may put forth produce problems for complicated complex shapes. After optimization of feeder design, the suggested value can be checked by animation on the center plane and temperature contour can be plot at every time step. Two feeder design optimization can be performed on ANSYS 12 which is low priced general purpose FEM based software. ANSYS optimizer can produce precise feeder design as compare to modulus approach for design of feeder but optimization process on ANSYS requires more time and skill relatively.

VI. ACKNOWLEDGEMENTS

The authors are thankful to the Bhagwant University for providing the support & facility and Dr Joshi, Prof. in Mechanical Engineering, SGSITS, Indore for useful technical suggestions.

REFERENCES

[1] Ravi B., Metal Casting -computer aided design and analysis PHI, 2005.
[2] Jain R.K., Production Technology, Khanna Publishers, Delhi, 15th Edition Auguest,1995
[3] Qin Rongshan, Workshop: Heat management, Lecturer 7, Graduate Institute of Ferrous Technology, POSTECH computational metallurgy laboratory Korea, lecturer notes, seen on web in dec., 2008.
[4] Rao S.S., Optimization; Theory and Application, Wiley Eastern Limited, 1975.
[5] ANSYS help - Thermal Tutorial, First order optimization, ANSYS Inc.
[6] http://www.mece.ualberta.ca/Tutorials/ANSYS
[7] Joshi Durgesh and Ravi B., comparison of finite element method and vector element method for casting solidification simulation, Indian Foundry Journal,22-23. vol. 54 no.9 September. 22-23, 2008, PP. 21-27.
[8] Venkatesan A., Rajadurai A., Effect of Air-Gap on Casting Solidification, American Foundary Society, 2006, PP.191-199.
[9] Ravi B. and Srinivasan M.N., casting solidification analysis by modulus vector method, International Journal of Cast Metals Res., 1996, PP.1-7.
[10] Tavakoli R. And Davami P., Optimal riser design in sand casting process with evolutionary topology optimization, Struct multidisc optim, accepted on 8 June 2008, DOI 10.1007/s00158-008-0282-z,Springer – Verlag, 2008, PP. 1-10.
[11] Tavakoli Rohalla and Davami Parviz , Optimal riser design in sand casting by topology optimization with SIMP method I : Poisson approximation of nonlinear heat transfer, equation, Struct multidisc optim , accepted on 29 October 2007, Springer – Verlag.2008, PP. 193-202.
[12] Elizabeth Jacob , Roschen Sasikumar , B. Praveen and V. Gopalakrishna , Intelligent design of feeders for castings by augmenting CAD with genetic algorithms, Journal of Intelligent Manufacturing , 15, 2004, PP.299-305.
[13] P. Prabhakara Rao, G.Chakraverthi, A.C.S. Kumar, G. Srinivasa Rao, Modeling and Simulation of Solidification in Alloy Steel Sand Castings, International Journal of Thermal Technologies, Vol.1, No.1 Dec. 2011, PP.121-127.
[14] T. Nandi, R. Behera, A. Chanda and G. Sutradhar, Study on Solidification Behaviour of LM6 Castings by Using Computer -Aided Simulation Software, Indian Foundry Journal, Vol. 57,No. 3, March 2011, PP.44-49.
[15] Behera Rabindra, Kayal.S, Sutradhar. G, Solidification behavior and detection of Hotspots in Aluminium Alloy castings: Computer Aided Analysis and experimental validation, International Journal of Applied Engineering Research, Dindigul, Volume 1, No 4, 2011,PP.715-726 .
[16] Belmira Neto, Carolien Kroeze, Leen Hordijk, Carlos Costad, Modelling the environmental impact of an aluminium pressure die casting plant and options for control, Environmental Modeling & Software, Volume 23, Issue 2, February 2008, PP.147–168

American Journal of Engineering Research (AJER)
e-ISSN : 2320-0847 p-ISSN : 2320-0936
Volume-02, Issue-10, pp-322-329
www.ajer.org

Research Paper Open Access

Performance and Emission Analysis of Diesel Engine Using Fish Oil And Biodiesel Blends With Isobutanol As An Additive

S. Kiran Kumar
Lecturer, Department of Mechanical Engineering Bule hora university, Ethiopia

Abstract: - Biodiesel with fuel additives has been gaining increased attention from engine researchers in view of the energy crisis and increasing environmental problems. The present work is aimed at experimental investigation of Isobutanol as an additive to the diesel- biodiesel blends. Experiments were done on a 4-Stroke single cylinder diesel engine by varying percentage by volume of isobutanol in diesel-biodiesel blends. The effect of isobutanol on brake thermal efficiency, brake specific fuel consumption, cylinder pressure, heat release and exhaust emissions were studied. It was found that brake thermal efficiency is Increased with increase in blend percentage both with 5% and 10% isobutanol. Addition of isobutanol shows negative impact on Brake specific fuel consumption (BSFC) which decreased with blend percentage while it increases with isobutanol percentage.CO emissions and smoke capacity decreased significantly while NO_x emissions decreased marginally with the increase in isobutanol percentage.

Keywords: - *Combustion characteristics, Diesel-Biodiesel blends, Isobutanol, Performance.*

I. INTRODUCTION

Researchers have used different additives to petrol and diesel fuels for efficiency and emission improvement. The addition of alcohol based fuels to petroleum fuels has been increasing due to advantages like better combustion and lower exhaust emissions. Oxygenates like ethanol, I-propanol, I-butanol and I-pentanol improved performance parameters and reduced exhaust emissions [1, 2]. Gasoline-ethanol blends with additives such as cyclooctanol, cycloheptanol increased brake thermal efficiency when compared to gasoline with reduction in CO,CO_2 and NOx while HC and O_2 increased moderately[3]. Gasoline with additives like ethanol and ethanol-isobutanol increased the brake power, volumetric and brake thermal efficiencies and fuel consumption. The CO and HC concentrations in the engine exhaust decreased while the NOx concentration increased. The addition of 5% isobutanol and 10% ethanol to gasoline gave the best results[4]. Bio-additives (matter extracted from palm oil) as gasoline additives at various percentages (0.2%, 0.4% and 0.6%) showed improvement in fuel economy and exhaust emissions of SI engine[5]. Methyl-ester of Jatropha oil diesel blends with Multi-DM-32 diesel additive showed comparable efficiencies, lower smoke, CO_2 and CO [6]. The addition of Di Methyl Carbonate (DMC) to diesel fuel increases efficiency marginally with reductions in NOx emissions while PM and soot emissions were reduced considerably [7,8]. Biodiesel with Di Ethyl Ether in a naturally aspirated and turbocharged, high-pressure, common rail diesel engine reduced NOx emissions with slight improvement in brake thermal efficiency [9,10]. Ethanol addition to diesel-biodiesel blends increased brake thermal efficiency with reduction in carbon monoxide and smoke emissions and at the same time hydrocarbons, oxides of nitrogen and carbon dioxide emissions increased [11]. Some researchers have used cetane improvers and some others have used additives in coated engines. Biodiesel blended fuel, and a cetane improving additive (2-EHN) reduced PM emissions [12]. Addition of di-1-butyl peroxide and the conventional cetane improver, 2-ethylhexyl nitrate additives to diesel fuel reduced all regulated and unregulated emissions including NOx emissions [13].

Present work attempts to investigate performance, combustion and emission characteristics of diesel engine with Isobutanol as an additive to the diesel-biodiesel blends. Isobutanol has higher energy density and lower Reid Vapor Pressure (RVP) which make it as a suitable additive for diesel-biodiesel blends. The properties of Isobutanol are shown in Table.1.

Table.1 Isobutanol properties

Property	Range
Flash Point, Tag Open Cup, °C	37.7
Specific Gravity, 20/20°C	0.8030
Viscosity at 20°C (Centipoise)	3.95
Auto ignition Temperature, °C	440
Surface Tension at 20°C(dynes/cm)	22.94
Heat of Combustion, Kj/kg	36162

II. EXPERIMENTAL SET UP AND PROCEDURE

2.1 EXPERIMENTAL SET UP

The engine shown in plate. 2.1 is a 4 stroke, vertical, single cylinder, water cooled and constant speed diesel engine which is coupled to rope brake drum arrangement to absorb the power produced. The engine crank started. Necessary dead weights and spring balance are included to apply load on brake drum. Suitable cooling water arrangement for the brake drum is provided. Separate cooling water lines fitted with temperature measuring thermocouples are provided for engine cooling. A measuring system for fuel consumption consisting of a fuel tank, burette, and a 3- way cock mounted on stand and stop watch are provided. Air intake is measured using an air tank fitted with an orifice meter and a water U- tube differential manometer. Also digital temperature indicator with selector switch for temperature measurement and a digital rpm indicator for speed measurement are provided on the panel board. A governor is provided to maintain the constant speed.

Plate 2.1 Diesel Engine Test Rig

Table 2 Specifications of the Test Engine

Specifications of the Test Engine	
Particulars	**Specifications**
Make	Kirloskar
Rated Power	3.7 kw(5hp)
Bore	80 mm
Stroke Length	110 mm
Swept volume	562 cc
Compression ratio 16.5:1	Compression ratio 16.5:1

2.2 TEST FUELS

For experimental investigations, biodiesel derived from fish oil was mixed with diesel in varying proportions 10%, 20% and 30% by volume and isobutanol as an additive was added as 5% and 10% by volume respectively to all the blends.

2.3 EXPERIMENTAL PROCEDURE

Calculate full load (W) that can be applied on the engine from the engine specifications. Clean the fuel filter and remove the air lock. Check for fuel, lubricating oil and cooling water supply. Start the engine using decompression lever ensuring that no load on the engine and supply the cooling water allow the engine for 10 minutes on no load to get stabilization. Note down the total dead weight, spring balance reading, time taken for 20cc of fuel consumption and the manometer readings. Repeat the above step for different loads up to full load. Connect the exhaust pipe to the smoke meter and exhaust gas analyzer and corresponding readings are tabulated. Allow the engine to stabilize on every load change and then take the readings. Before stopping the engine remove the loads and make the engine stabilized Stop the engine pulling the governor lever towards the engine cranking side. Check that there is no load on engine while stopping.

III. RESULTS AND DISCUSSION

3.1 PERFORMANCE ANALYSIS USING OPTIMUM BLEND WITH IGNITION IMPROVER

The experiments are conducted on the four stroke single cylinder water cooled diesel engine at constant speed (1500 rpm) with varying loads. Various performance parameters such as, The variation of Brake Thermal efficiency with Brake Power is shown in Fig. 3.1From the plot it is observed as the BP increases there is considerable increase in the BTE. The BTE of diesel at full load is 32.82% while the blends of F30 is 34.01%, B30D69.5I5 is 35.14%, B30D69I10 is 34.01%, among the three the maximum BTE is 35.14% which is obtained for B30D69.5I5. The increment in brake thermal efficiency due to better combustion because of adding ignition improver it effects to decrease the viscosity. The variation of Mechanical efficiency with Brake Power is shown in Fig. 3.2. From the plot it is observed optimum blend and various blends like F300D69.5I5, B30D69I10 slightly increases at full load conditions. The variation of volumetric efficiency with Brake Power is shown in Fig. 3.3. From the plot it is observed optimum blend contains 75.95% at full load condition, but in case of after adding the ignition improver blends slightly variation at compared to optimum blends. The variation of Brake Specific Fuel Consumption with Brake Power is shown in Fig. 3.4. The plot it is observed that as the load increases the fuel consumption decreases, the minimum fuel consumption is for F30D69I10 is 0.25 as to that of F30 is 0.258. The BSFC of after adding ignition improver of Bio-diesel is slightly increases as compared with optimum blend (F30) at full load condition. The variation of Indicated Specific Fuel Consumption with Brake Power is shown in Fig. 3.5. From the plot it is observed that F30D69.5I5 line varies similar with the optimum blend, The ISFC of after adding ignition improver of Bio-diesel is increases slightly as compared with optimal blend at full load condition. The variation of Air-Fuel Ratio with Brake Power is shown in Fig. 3.6. From the plot it is observed that decreases compare with optimum blend at full load condition of F30D69.5I5. As load increases more power is to be developed by the engine to compensate the load. The only way to increase the more power development is to inject the more amount of fuel into the cylinder which tends to reduce the air fuel ratio.

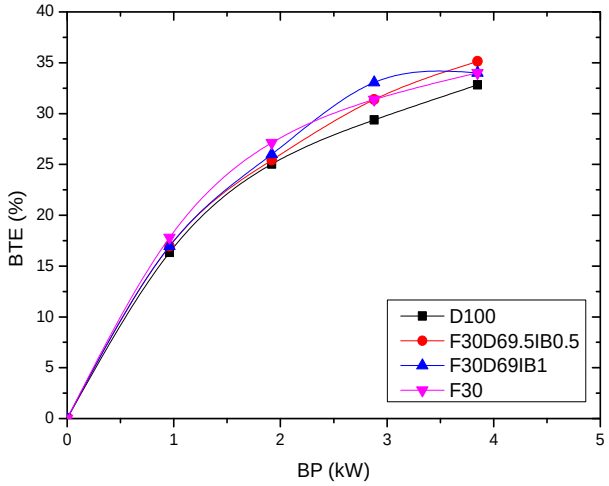

Fig. 3.1 Variation of Brake Thermal Efficiency with Brake Power Using Ignition Improver

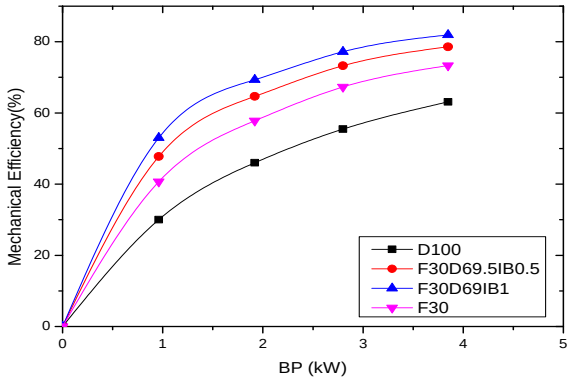

Fig. 3.2 Variation of Mechanical Efficiency with Brake Power Using Ignition Improver

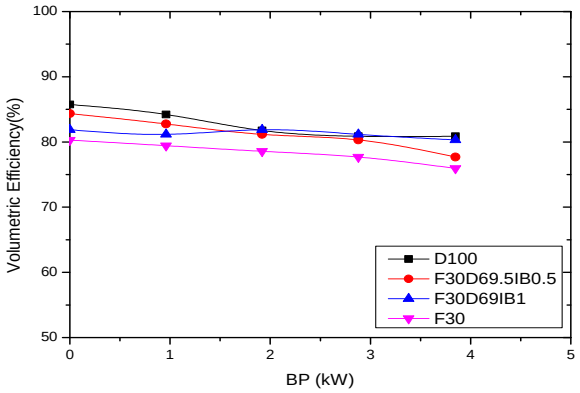

Fig. 3.3 Variation of Volumetric Efficiency with Brake Power Using Ignition Improver

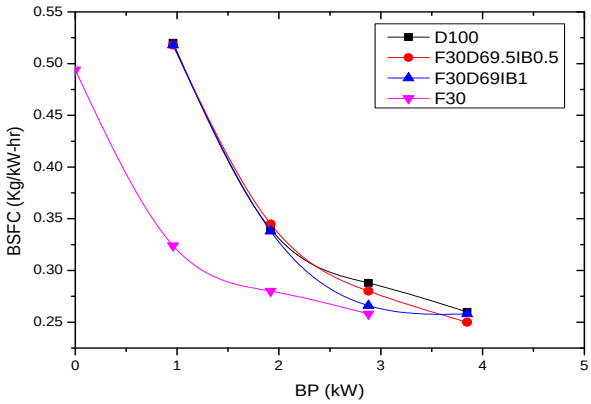

Fig. 3.4 Variation of Brake Specific Fuel Consumption with Brake Power Using Ignition Improver

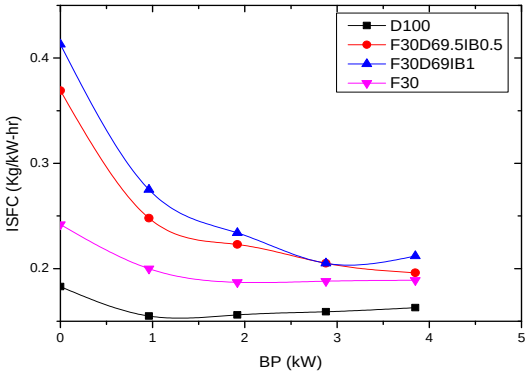

Fig. 3.5 Variation of Indicated Specific Fuel Consumption with Brake Power Using Ignition Improver

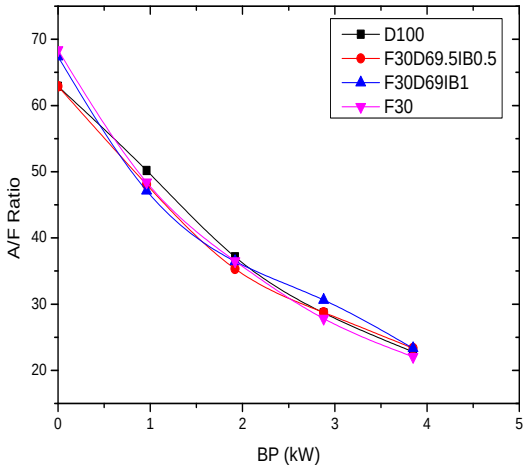

Fig. 3.6 Variation of Air Fuel Ratio with Brake Power Using Ignition Improver

3.2 EMISSION ANALYSIS USING OPTIMUM BLEND WITH IGNITION IMPROVER

The experiments are conducted on the four stroke single cylinder water cooled diesel engine at constant speed (1500 rpm) with varying loads. Various emission parameters in the sense of, the variation of Smoke density with Brake Power is shown in Fig. 3.7. The plot it is observed that the Smoke is nothing but solid soot particles suspended in exhaust gas. Figure 12 shows the variation of smoke level with brake power at various loads for different blends like F20, F30D69.5I5, and F30D69I10 tested fuels. It is observed that smoke is higher for optimum blend at full load conditions compared to ignition improver blends. Better and optimum fuel air mixture obtained for F30D69.5I5.The variation of *CO* emission with Brake Power is shown in Fig. 3.8. The plot it is observed that is interesting to note that the engine emits more CO for diesel as compared to biodiesel blends under all loading conditions. The CO concentration is decreases for the blends of F30D69.5I5 and F30D69I10 for all loading conditions. At lower biodiesel concentration, the oxygen present in the biodiesel aids for complete combustion. However as the biodiesel concentration increases, the negative effect due to high viscosity and small increase in specific gravity suppresses the complete combustion process, which produces small amount of CO. The variation of CO_2 emission with Brake Power is shown in Fig. 3.9. The plot it is observed that the CO_2 emission increased with increase in load for all blends. The lower percentage of biodiesel blends emits less amount of CO_2 in comparison with diesel. Blends F30D69.5I5 and F30D69I10 emit very low emissions. Using higher content biodiesel blends, an increase in CO_2 emission was noted, which is due to the high amount of oxygen in the specified fuel blends which converting CO emission into CO_2 emission contents. The variation of *HC* emission with Brake Power is shown in Fig. 3.10. The plot it is observed that the HC emission variation for different blends is indicated. That the HC emission decreases with increase in load for F30 and it is almost slightly decreases for adding ignition improver blends where some traces are seen at no load and full load. The variation of NO_x emission with Brake Power is shown in Fig. 3.11.

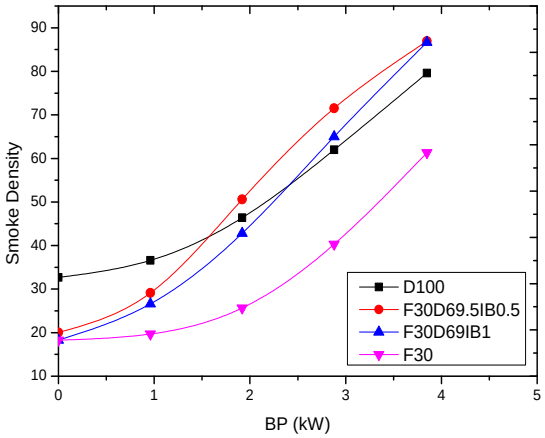

Fig. 3.7 Variation of Smoke Density with Brake Power Using Ignition Improver.

The plot it is observed that for different blends is indicated. The NO_x emission for all the fuels tested followed an increasing trend with respect to load. The reason could be the higher average gas temperature, residence time at higher load conditions. A reduction in the emission for all getting after adding the ignition improver blends as compared to optimum blend was noted. With increase in the fish oil content of the fuel, corresponding reduction in emission was noted and the reduction was remarkable for F30D69.5I5 and F30D69I10.The variation of unused oxygen emission with brake power is shown in Fig.3.12. From the plot reveals that the as load increases the unused oxygen decreases. At full load condition the unused oxygen obtained are 18.62%, 19.50%, 15.97% and 14.91% for the fuels of diesel, F30, F30D69.5I5 and F30D69I10 respectively. The decrement of unused oxygen is due to better combustion and CO emission converted into CO_2 emission.

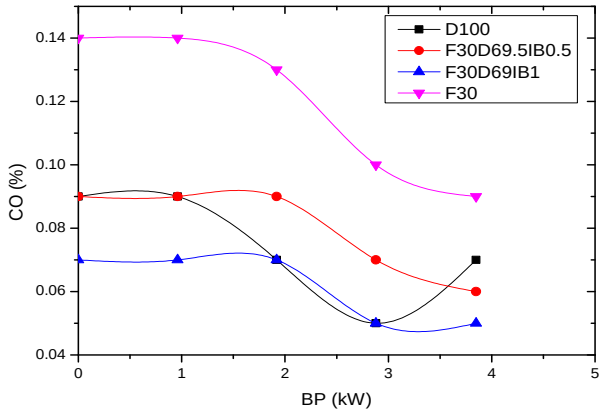

Fig. 3.8 Variation of Carbon Monoxide with Brake Power Using Ignition Improver

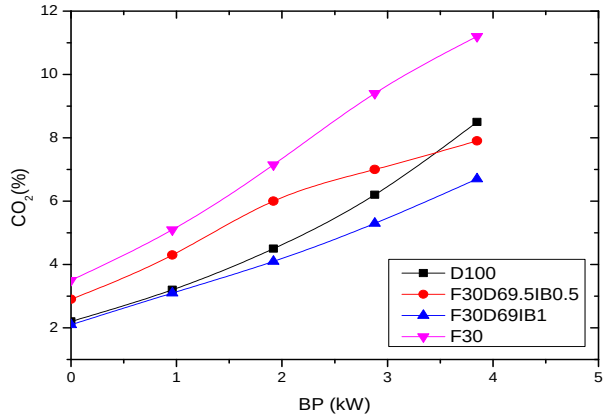

Fig. 3.9 Variation of Carbon Dioxide with Brake Power Using Ignition Improver

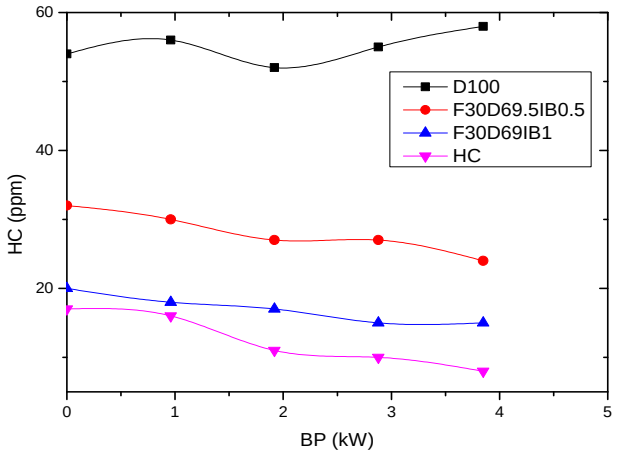

Fig. 3.10 Variation of Unburned Hydrocarbons with Brake Power Using Ignition Improver

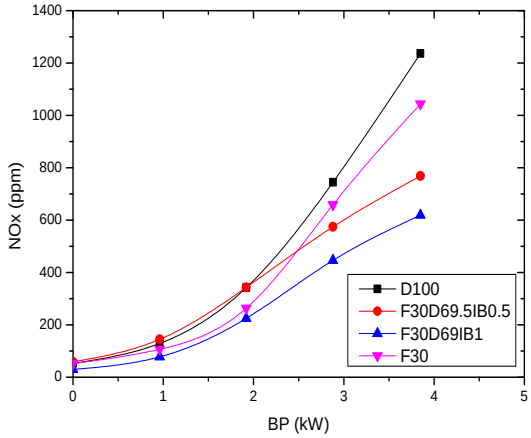

Fig. 3.11 Variation of NOx Emissions with Brake Power Using Ignition Improver

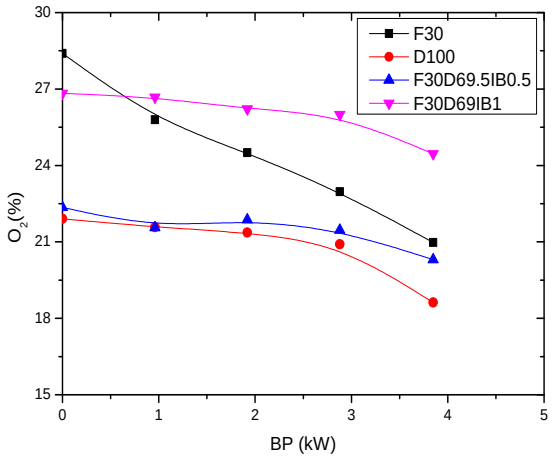

Fig. 3.12 Variation of Unused Oxygen with Brake Power Using Ignition Improver

IV. CONCLUSIONS

The test is conducted on the engine by taking the blend F30 along with the addition of ignition improver isobutanol in the quantity of 5ml (F30D69.5I5) and 10ml (F30D69I10) at the same operating conditions. Among these two compositions the one F30D69.5I5 has given the better performance in the following parameters.

- Brake thermal efficiency is observed as the BP increases there is considerable increase in the BTE. The BTE of diesel at full load is 32.82% while the blends of F30 is 34.08%, F30D69.5I5 is 35.14%, F30D69I10 is 34.01%, among the three the maximum BTE is 35.14% which is obtained for F30D69.5I5. The BTE of fish oil is increases up to 0.364% and 0.823% as compared with to fuels of optimum blend and diesel at full load condition.
- Brake specific fuel consumption is observed that as the load increases the fuel consumption decreases, the minimum fuel consumption is for F30D69.5I5is 0.25 kg/kW-hr as to that of F30 is 0.258 kg/kW-hr at full load condition.
- Smoke density is observed that smoke is higher for optimum blend at full load conditions compared to ignition improver blends. At full load condition the smoke density obtained are 79.6 HSU, 61.34 HSU, 86.92 HSU and 86.69HSU HSU for the fuels of diesel, F30, F30D69.5I5 and F30D69I10. It is observed that smoke is increases for fish oil blends at full load conditions as compared to optimum blend.
- Carbon monoxide is observed that is interesting to note that the engine emits more CO for diesel as compared to fish oil blends under all loading conditions. The CO concentration is increases for the blends of F30D69.I5 and same as the diesel for F30D69I10. At full load condition the CO emission obtained are 0.05%, 0.09%, 0.06% and 0.05% for the fuels of diesel, F30, F30D69.5I5 and F30D69I10 respectively.
- Unburned hydrocarbons are observed that the HC emission variation for different blends is indicated. At full load condition the unburned hydrocarbons are obtained 58ppm, 8ppm, 15ppm and 24ppm for the fuels of diesel, F30, F30D69.I5 and F30D69I10 respectively. The unburned hydrocarbons of after adding ignition improver of Fish oil decreases up to 24.44% as compared to diesel at full load condition.

- The NO_x emission for all the fuels tested followed a decreasing trend with respect to load. At full load condition the NOx emissions obtained are 1236ppm, 1044ppm, 769ppm and 619ppm for the fuels of diesel, F30, F30D69.I5 and F30D69I10 respectively.

REFERENCES

[1] M. Mani , C. Subash , G. Nagarajan, "Performance, Emission and Combustion Characteristics of a DI Diesel Engine Using Waste Plastic Oil", Applied Thermal Engineering , Vol. 29 ,2009, pp 2738–2744.

[2] Jagannath Balasaheb Hirkude a, Atul S. Padalkar "Performance and emission analysis of a compression ignition Engine operated on waste fried oil methyl esters", Applied Energy, Vol.90, 2012,pp 68–72.

[3] Sharanappa Godiganur b,, C.H. Suryanarayana Murthy c, Rana Prathap Reddy, "Cummins engine performance and emission tests using methyl ester mahua (Madhuca indica) oil/diesel blends" , Renewable Energy ,Vol.34, 2009,pp 2172–2177

[4] Sharanappa Godiganur a,, Ch. Suryanarayana Murthy b, Rana Prathap Reddy, "Performance and emission characteristics of a Kirloskar HA394 diesel engine operated on fish oil methyl esters", Renewable Energy,Vol.35, 2010,pp 355–359

[5] N.R. Banapurmath a,, P.G. Tewari a, V.S. Yaliwal b, Satish Kambalimath c, Y.H Basavarajappa, " Combustion characteristics of a 4-stroke CI engine operated on Honge oil, Neem and Rice Bran oils when directly injected and dual fuelled with producer gas induction", Renewable Energy, Vol.34, 2009, pp1877–1884

[6] Hary Sulistyo, Suprihastuti S. Rahayu, Gatot Winoto, I M. Suardjaja, "Biodiesel Production from High Iodine Number Candlenut Oil", World Academy of Science, Engineering and Technology.vol.no 48, 2008

[7] Xiaohu Fan, Rachel Burton and Greg Austic, "Preparation and Characterization of Biodiesel Produced from Recycled Canola Oil" **,**The Open Fuels & Energy Science Journal, Vol.2,2008,pp113-118

[8] S. Murugana, M.C. Ramaswamya and G. Nagarajan. "The use of tyre pyrolysis oil in diesel engines", Vol. 28, 2008, pp 2743-2749

[9] G Lakshmi Narayana Rao, S Sampath, K Rajagopal, "Experimental Studies on the Combustion and Emission Characteristics of a Diesel EngineFuelled with Used Cooking Oil Methyl Ester and its Diesel Blends", International Journal of Applied Science, Engineering and Technology vol no 4;1 2008

[10] Dennis Y.C. Leung , Xuan Wu, M.K.H. Leung ,"A review on biodiesel production using catalyzed transesterification", Applied Energy vol no:87 2010,pp.1083–1095

American Journal of Engineering Research (AJER)
e-ISSN : 2320-0847 p-ISSN : 2320-0936
Volume-02, Issue-10, pp-330-337
www.ajer.org

Research Paper Open Access

UNIVERSE IS LIKE SPACE SHIP

M.Arulmani, V.R.Hema Latha
B.E. (Engineer) (A New Theory on J-Hook and Anchor)
M.A., M.Sc., M.Phil.(Biologist)

Abstract: - A scientific research in this article focus that the whole Cosmo Universe shall be considered as a "SPACE SHIP". The Space Ship shall be considered as ANCHORED to the base of universe with three-in-one space elements SUN, EARTH, MOON for its stability and symmetry. Further the Anchor of Universe shall be considered fastened to the "J-Hook" through strong THREAD consists of three core or strand for its "Centre of Buoyancy".

The Space Ship shall be considered as a suspending pendulum. The base of the pendulum considered like Anchor which is fastened to J-Hook through a cable of three core and in "Standstill State".

The human populations, life organisms spread all over the EARTH shall be considered as Passengers. Other space objects such as Planets, Comets, Asteroids, Matters, Molecules having definite mass shall be considered as CARGO existing in the Upper Deck of Human Passengers and other life organisms.

The "J-Hook" shall be considered as having infinity energy level and any weight added to the base of space ship during the course of expanding universe shall not affect the centre of buoyancy of ship and the ship shall be considered as highly stable for ever (Highly Anchored) and become standstill.

Keywords: -
1) Philosophy of Absolute Symmetry.
2) Philosophy of J-Hook.
3) Philosophy of Anchor.
4) Philosophy of centre of Buoyancy
5) Philosophy of Noah's Ark.
6) Philosophy of Giza Pyramids.
7) Philosophy of Pure Science.
8) Philosophy of Space Ship.
9) Philosophy of Three core Thread
10) Philosophy of J-Radiation.

I. INTRODUCTION

This article focus that the space ship was highly stable in Prehistoric time and the centre of buoyancy of ship was well managed by proper aligning of Anchoring, when "Tamil based Indians" lived in "MARS" in Prehistoric time.

It is speculated that during the course of expanding universe the Prehistoric populations have been completely extinct at one stage and all the Prehistoric super high technology of "Space Management" might be completely destroyed (or) lost.

It is speculated that in modern time there is slight asymmetry in the Anchored base of universe due to asymmetry in relative position of SUN, EARTH, MOON and thereby the centre of buoyancy of ship might be slightly dislocated and there by the ship gets "WOBBLED".

It is speculated that he severe earth quake, unexpected cyclone, volcanic activity, unexpected sudden forest fire, severe atmospheric temperature rise etc might be due to dislocation of centre of buoyancy of the space ship.

II. PREVIOUS PUBLICATIONS

The philosophy of origin of first life and human, the philosophy of model Cosmo Universe, the philosophy of fundamental neutrino particles have already been published in various international journals mentioned below. Hence this article shall be considered as extended version of the previous articles already published by the same author.

[2] Cosmo Super Star – IJSRP, April issue, 2013
[3] Super Scientist of Climate control – IJSER, May issue, 2013
[4] AKKIE MARS CODE – IJSER, June issue, 2013

[5] KARITHIRI (Dark flame) The Centromere of Cosmo Universe – IJIRD, May issue, 2013
[6] MA-AYYAN of MARS – IJIRD, June issue, 2013
[7] MARS TRIBE – IJSER, June issue, 2013
[8] MARS MATHEMATICS – IJERD, June issue, 2013
[9] MARS (EZHEM) The mother of All Planets – IJSER, June issue, 2013
[10] The Mystery of Crop Circle – IJOART, May issue, 2013
[11] Origin of First Language – IJIRD, June issue, 2013
[12] MARS TRISOMY HUMAN – IJOART, June issue, 2013
[13] MARS ANGEL – IJSTR, June issue, 2013
[14] Three principles of Akkie Management (AJIBM, August issue, 2013)
[15] Prehistoric Triphthong Alphabet (IJIRD, July issue, 2013)
[16] Prehistoric Akkie Music (IJST, July issue, 2013)
[17] Barack Obama is Tamil Based Indian? (IJSER, August issue, 2013)
[18] Philosophy of MARS Radiation (IJSER, August 2013)
[19] Etymology of word "J" (IJSER, September 2013)
[20] NOAH is Dravidian? (IJOART, August 2013)
[21] Philosophy of Dark Cell (Soul)? (IJSER, September 2013)
[22] Darwin Sir is Wrong?! (IJSER, October issue, 2013)
[23] Prehistoric Pyramids are RF Antenna?!... (IJSER, October issue, 2013)
[24] HUMAN IS A ROAM FREE CELL PHONE?!... (IJIRD, September issue, 2013)
[25] NEUTRINOS EXIST IN EARTH ATMOSPHERE?!... (Under peer review)
[26] EARLY UNIVERSE WAS HIGHLY FROZEN?!... (Under peer review)

III. HYPOTHESIS

1. The whole Cosmo Universe shall be considered as a "SPACE SHIP". The base of ship is strongly anchored with star/Delta structure. The centre of Star Point of base of ship is considered connected to the far end in the "UPPER SPACE" through a strong cable containing Three Core Cable.
2. The SUN, EARTH, MOON shall be considered as Three-in-one Anchor having electromechanically actuated deriving Electric power through three core cable from J-Hook point. J-Hook point shall be considered as the source of "Energy transfer" for actuation of electro mechanical Anchor.

(i)

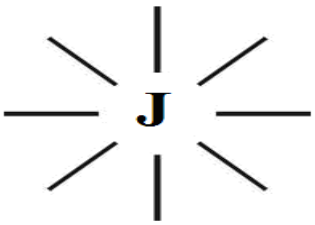

ii)

iii)

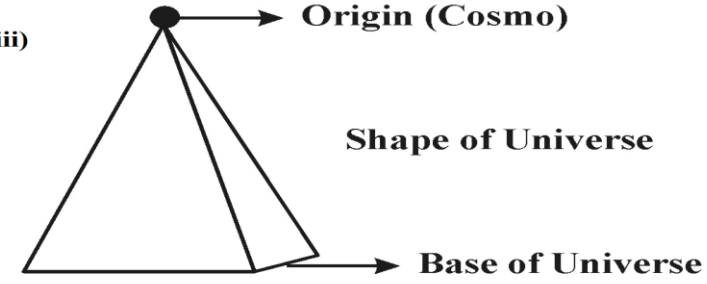

(ANCHOR)

(iv)

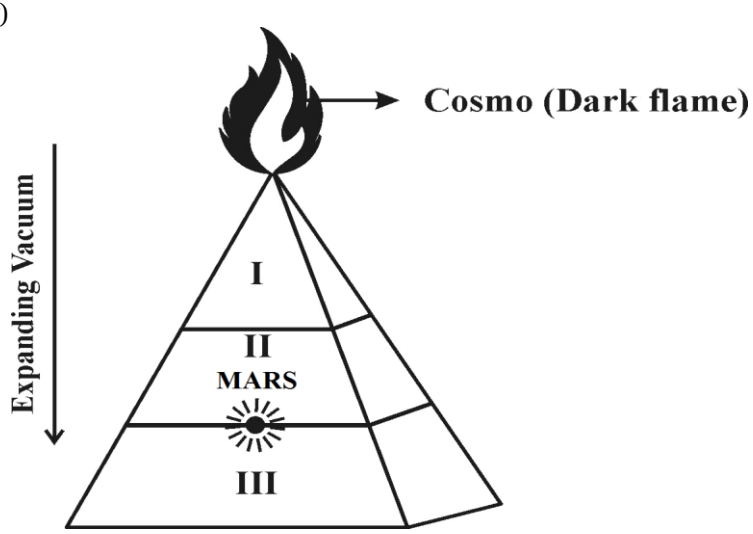

(MODEL COSMO UNIVERSE)

Region I – Perfect vacuum region (Anti-Neutrinos radiation)
Region II – Partial vacuum region (Neutrinos radiation)
Region III – Observable Vacuum region (EMR radiation)

3. The required electric energy shall be considered derived form the source of Three-in-one fundamental Neutrinos existing in the Upper region of Universe (Region-II). J-Hook shall be considered as the "Energy converter" (i.e) the three core cable shall be considered as the "WAVE GUIDE" for transmitting the electric energy in the form of Electro Magnetic Radiation. The electromagnetic radiation shall be considered as having transmitted through wave guides in the form of Optic, Electric, Magnetic component and travels in the absolute speed of Light (i.e) $3x10^8$ meter/sec. Further it is focused that the wave guide link shall be considered as strong chain link connecting both J-Hook and star point of Anchor. The Anchor shall be considered containing inbuilt "Antenna" for converting electromagnetic radiation wave into Electric energy required for actuating Armature of Anchor for revolving and exact positioning of SUN, EARTH, MOON on their axis.

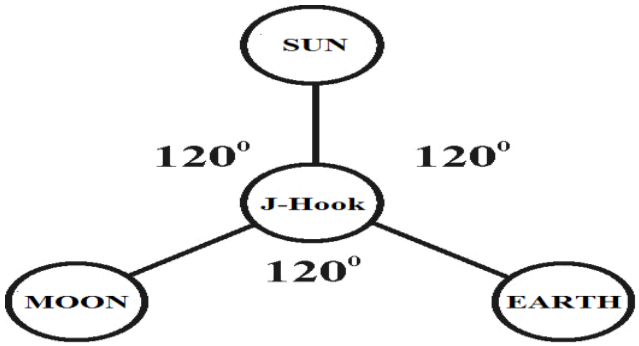

(ANCHOR ARMATURE)

IV. HYPOTHETICAL NARRATIONS

(a) Philosophy of J-Hook?

The J-Hook shall be considered as the point which is strongly fastened to the Cosmo origin point. In other words the J-Hook shall be considered as of strong GRAVITY BINDING with Cosmo origin. The Cosmo origin shall be considered as Highly "frozen" origin having very low temperature level or thousands of degree below the level of "Absolute Zero" point.

The philosophy of "J-Hook" shall be defined within the following scope.
1. J-Hook shall be considered as the point of bearing the Heavy load of entire material universe through "Neutrino thread" (3 core cable).

2. "J-Hook" shall be considered as the source of energy which transforms the energy from the fundamental Neutrinos Photon, Electron, Proton (Also called as God Particles) into Electromagnetic radiation (EMR).
3. "J-Hook" shall be considered as the point where the light travels at absolute speed of $3x10^8$ meter/sec.
4. "J-Hook" shall be considered as the point where the temperature of universe is maintained at "absolute Zero".
5. "J-Hook" shall be considered as the point where Prehistoric human (Star human) lived with super wisdom and with different genetic structure.
6. "J-Hook" shall be considered as the divine mechanism for executing the "law of super nature" (i.e) regulating the Arms of Anchor of material universe.
7. "J-Hook" shall be considered as the symbol of Absolute symmetry and confidence.

"The philosophy of "JACK" might be derived from the philosophy of "J-Hook"."

-Author

(b) Philosophy of Akkie?

The "Akkie" shall be considered as the Three-in-one Electromagnetic radiating source forming the base of whole Cosmo Universe. The Akkie shall be considered three-in-one "Mega star" of universe. The mega star shall also be called as "MAGI". The Prehistoric Tamil word MAGI shall mean "Cosmo Super Star" (MA+Akkie). Alternatively called as J+.

"Cosmo Super Star shall be considered as the CARGO of the Space Ship."
-Author The philosophy of MAGI shall be defined within the following scope.
1. "Magi" shall be considered as the "Electromagnetic base" of Cosmo Universe.
2. "Magi" shall be considered as three-in-one existence of SUN, EARTH, MOON connected in Star/Delta configuration.
3) "Magi" shall be considered as located in the Region-III of universe where light can travel maximum at the speed of 3.0×10^8 m/sec. In other words in Magi region the light can't travel more than the speed of 3×10^8 m/sec.
4) "Magi" shall be considered as the "three-in-one inbuilt arms" having characteristics of Optic, Electric magnetic property and the relative position of each arm shall be remote monitored and controlled by "J-Hook".
5) "Magi" shall be considered as the divine mechanism revolving on its axis at star/delta configuration connected to "master control" unit of "J-Hook" for precise positional control of Arms of Magi for precise control of center of buoyancy of Cosmo space ship

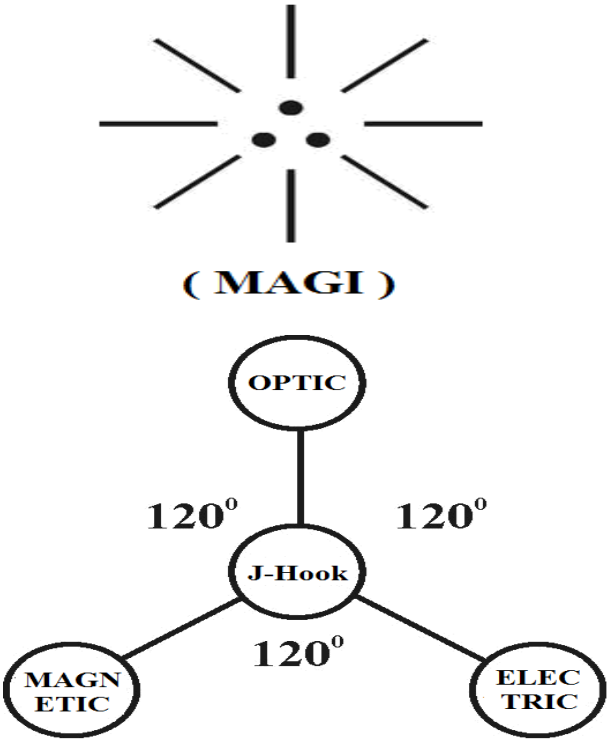

(ANCHOR BASE)

"The philosophy of "Anchor" might be derived from the philosophy of "MAGI" (ma-akkie).- Author

(c) Philosophy of Absolute symmetry?

It is hypothesized that the philosophy of Absolute symmetry shall be considered as the Three-in-one existence with angular displacement of 120^0. It is hypothesise3d that the fundamental Neutrinos Photon, Electron, Proton shall be considered as the super nature which make up the "Material Universe". All other particles such as Quarks, Muon, Electron, Tau, Supernova and other unknown particles shall be considered as "species" to the fundamental Neutrinos. "J-Hook" shall be considered as the located in Neutrino radiation (Region-II).

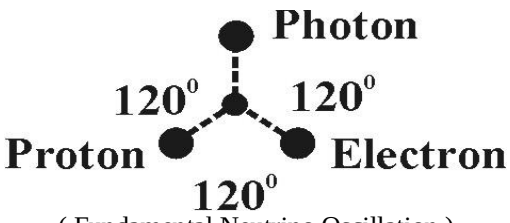

(Fundamental Neutrino Oscillation)

Further the fundamental Neutrinos shall be considered symmetrically displaced by 120^0 and have "SUSTAINED OSCILLATION". The existence of sustained Neutrinos oscillation shall be considered as responsible for the existence of three fundamental property Optic, Electric, Magnetic of Universe.

(d) Philosophy of NOAH'S ARK?...

It is hypothesized that the NOAH Origin (as evidenced from Biblical study) shall be considered as the 2^{nd} generation of Human populations who started living on EARTH at much later period with different genetic structure. The first generation of human populations shall be considered as prehistoric human lived in MARS Planet and expert in Astrophysics, Astronomy.

Further it is focused that the "NOAH'S Ark" shall be considered as "IMAGE" of "Cosmo Space Ship". In other words NOAH might have constructed the "ARK" based on the philosophy of Cosmo Space ship considering the relative position of SUN, EARTH, MOON and the Centro mere point of "J-Hook". "The Noah's Ark shall be considered as "ELECTROMAGNETIC SHIP" with super scientific technology rather than Mechanical type ship built by Modern scientists".

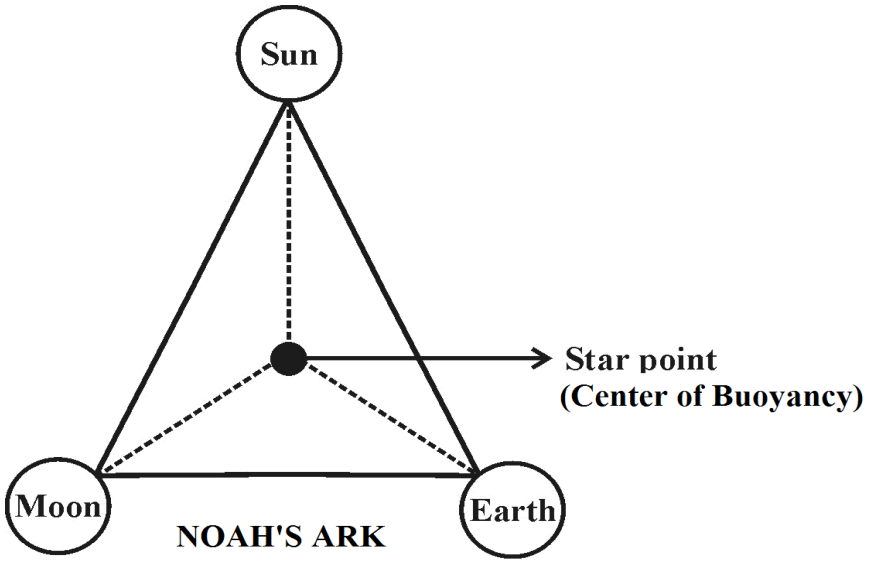

(e) Philosophy of Giza Great Pyramids?

It is hypothesized that the Great Pyramid and three associated Pyramids located along the same axial route shall be considered as the local energy transfer centre. In other words the Great Pyramid shall be considered as the Master energy transforming source (Master local Antenna) and the three other Pyramids shall be considered as Three-in-one "Armature" for controlling the relative position of Sun, Earth, Moon on its axis.
In Prehistoric time the existence of MON OLYMPUS Pyramid located in MARS shall be considered as the J-Hook point of material Universe. The Sun, Earth, Moon shall be considered as the TRINITY Pole of Universe.

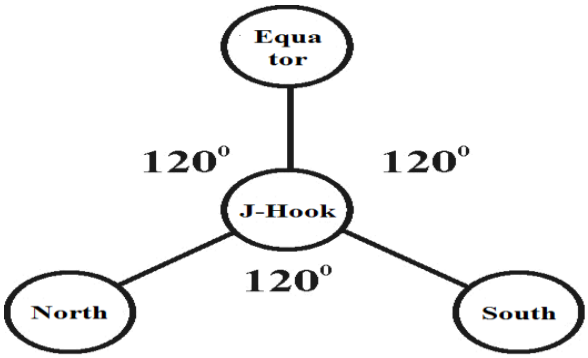

(TRIPOLE UNIVERSE)

"The Giza Great Pyramids shall be considered as the Energy transfer and local control units of the "Cosmo space ship" rather than "Memorial of Paraoah" of Egypt". -Author

(f) Characteristics of fundamental Neutrinos?

It is hypothesized that the three fundamental Neutrinos shall be considered as responsible for make up of whole Universe. Further the three Neutrinos shall be considered as having Optic, Electric, Magnetic Property which be considered as fundamental characteristics responsible for existence of Universe.

"No Fundamental Neutrinos shall mean N
No existence of Universe". - Author

(a) "J" Neutrino --- Proton (Magnetic)
(b) "K" Neutrino --- Electron (Electric)
(c) "A" Neutrino --- Photon (Optic)

(g) Etymology of word Jack?...

It is hypothesized that the word Jack might be derived from the Prehistoric Tamil phonetics "CHEI", "CHISU"

"CHEI, CHISU SHALL MEAN "INFANT";
INFANT SHALL mean EARLY UNIVERSE." - Author

It is speculated that in the early Universe the fundamental Neutrinos right have been evolved at one stage. The fundamental Neutrinos might have been called as "JAK" (Pronounced as JACK) JAK shall mean "three-in-one" fundamental Neutrinos (Minute Particles). The three Particles shall also be called as "TAMIL NEUTRINOS". The three fundamental Neutrinos shall be considered as having "Zero mass" but having definite charge property. The fundamental neutrinos shall also be called as JAK (God Particles).

(a) Proton Neutrino -- "J" (+ve polarity)
(b) Electron Neutrino -- "K" (-ve polarity)
(c) Photon Neutrino -- "A" (Neutral polarity)

(h) History of word "Jack"?...

The word Jack is believed to have originated from Hebrew origin pronounced as "JAK". JAK in Hebrew shall mean "God is gracious". Further the word Jack (JAK) is normally referred to applied to Male gender, Boy.

In English language slang "you don't know Jack" means "you don't know anything "Jack" in this situation. Further American President John F.Kennedy was more well known as "JACK". Case study shows that American actors Jack Nicholson, Jack Palance and Jack Lemmon are famous bearers of the name.

In Fiction, Literature, Music, Comics, Nursery rhymes, Video games also the word Jack has wide meanings and being applied. Further another way the word "Jack-s th" is used to denote a smaller version of something (ie) the word Jack-s th shall mean things of "SMALLER THAN THE NORMAL SIZE".

e.g. "Jack-bowl, Jack-brick, Jack-fish"

Further the word "Union JACK" shall mean "Redeem myself". Jack flag culture are small flags such as British Jack, French Jack, Dutch Jack used as ship signals to identify the nationality of the ship. In British use the Jack has been since 17th centenary.

(i) Philosophy of word "JACK"?...

It is hypothesized that the word "JACK" is more associated with Astrophysics, Astronomy meaning "MINUTE PARTICLES" rather than name of Person in human culture. The word Jack shall mean Dark Particles, Dark matter ("J-Akkie") "J-Akkie shall mean fundamental Neutrinos".

"JACK (JAK) shall alternatively means fundamental neutrinos (God Particles)" -Auhor

(j) Philosophy of pure science?

It is hypothesized that the philosophy of Pure science shall be considered as the Region-II of Universe where the Particles exist with Zero mass. The fundamental Neutrinos shall be considered as "God Particles" having Zero mass "J"-RADIATION shall be considered as the effect of God particles and the Region of Pure Science (also called as origin of Super science). The three branches Physical, Chemical, Mathematical science shall be considered as species to pure science. Further Pure science is the region where particles travel faster than speed of "Light".

"EMR shall be considered as species to J-Radiation" -Author

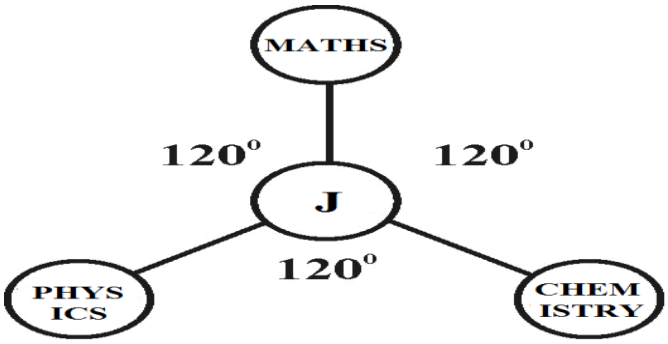

(J - The Pure Science)

(k) J-Radiation is matter?!...

It is hypothesized that J-Radiation shall be considered as the fundamental matter composed of particles having Zero mass. The three state of existence of matter solid, liquid, vapour shall be considered as species to J-Radiation and composed of particles having higher mass.

"The Existence of Matter in various form shall be due to Existence of EMR Particles in various angles." -Author

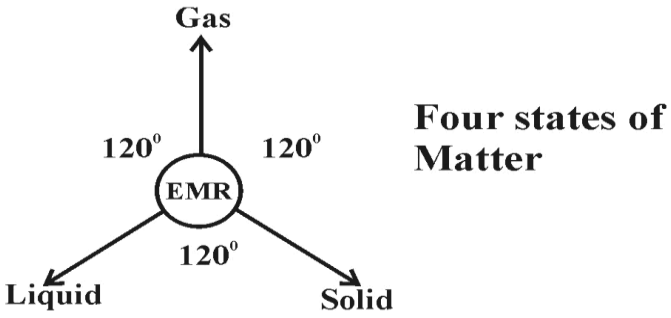

(l) Philosophy of evolution?!... Expanding Universe?!...

The process of evolution (or) Expanding Universe shall be considered as the continuous process when the Fundamental particles of Universe gaining mass under various environmental conditions (i.e) UV, visible, IR state.

"Evolution shall mean increase in Cell, Atom mass to the fundamental Cell and Atom." -Author

(m) "J-Hook" is Super symmetric Balance?

J-Hook shall be considered as the living divine mechanism of super symmetry balance and weighs the every form of matter and Energy with absolute accuracy level during the course of expanding Universe.

"Anchor" shall be considered as the divine mechanism having exactly in line with (Tuned) to "J-Hook" to maintain absolute centre of Buoyancy of "Cosmo Ship" for its stability and "everlasting Journey" towards the path of PEACE.

(n) J-Radiation travels faster than speed of Light?!...

J-Radiation shall be considered as the most fundamental matter having particles of Zero mass and travels faster than speed of Light.

"Dark Radiation (J-Radiation) shall be considered as upper region of Material Universe; EMR (White Radiation) shall be considered as bottom region of Material Universe".

V. CONCLUSION

J-Hook shall be considered as "SOUL" of every human, every matter existing in the Material Universe". Anchor shall be considered as stable life having absolute confidence. The whole Cosmo Universe shall be called as HUGE SPACE SHIP rather than as "BUBBLE UNIVERSE".

REFERENCE

[1] Intensive Internet "e-book" study through, Google search and wikipedia
[2] M.Arulmani, "3G Akkanna Man", Annai Publications, Cholapuram, 2011
[3] M. Arulmani; V.R. Hemalatha, "Tamil the Law of Universe", Annai Publications, Cholapuram, 2012
[4] Harold Koontz, Heinz Weihriah, "Essentials of management", Tata McGraw-Hill publications, 2005
[5] M. Arulmani; V.R. Hemalatha, "First Music and First Music Alphabet", Annai Publications, Cholapuram, 2012
[6] King James Version, "Holy Bible"
[7] S.A. Perumal, "Human Evolution History"
[8] "English Dictionary", Oxford Publications
[9] Sho. Devaneyapavanar, "Tamil first mother language", Chennai, 2009
[10] Tamilannal, "Tholkoppiar", Chennai, 2007
[11] "Tamil to English Dictionary", Suravin Publication, 2009
[12] "Text Material for E5 to E6 upgradaton", BSNL Publication, 2012
[13] A. Nakkiran, "Dravidian mother", Chennai, 2007
[14] Dr. M. Karunanidhi, "Thirukkural Translation", 2010
[15] "Manorama Tell me why periodicals", M.M. Publication Ltd., Kottayam, 2009
[16] V.R. Hemalatha, "A Global level peace tourism to Veilankanni", Annai Publications, Cholapuram, 2007
[17] Prof. Ganapathi Pillai, "Sri Lankan Tamil History", 2004
[18] Dr. K.K. Pillai, "South Indian History", 2006
[19] M. Varadharajan, "Language History", Chennai, 2009
[20] Fr. Y.S. Yagoo, "Western Sun", 2008
[21] Gopal Chettiar, "Adi Dravidian Origin History", 2004
[22] M. Arulmani; V.R. Hemalatha, "Ezhem Nadu My Dream" - (2 Parts), Annai Publications, Cholapuram, 2010
[23] M. Arulmani; V.R. Hemalatha, "The Super Scientist of Climate Control", Annai Publications, Cholapuram, 2013, pp 1-3

M.Arulmani, B.E. (Engineer)

V.R.Hema Latha, M.A., M.Sc., M.Phil.(Biologist)

American Journal of Engineering Research (AJER)
e-ISSN : 2320-0847 p-ISSN : 2320-0936
Volume-02, Issue-10, pp-338-343
www.ajer.org

Research Paper Open Access

Entropy and Enthalpy variations with Acoustic parameters of Cholesteryl oleyl carbonate

Jatinder Pal Singh, Rajesh Sharma
Department of Physics, Post-graduate government college sector-11, chandigarh, India

Abstract: - The ultrasonic velocity (U), density (ρ), viscosity (η) have been measured for Cholesteryl oleyl carbonate at different temperatures. From the experimental data, , Free Volume (VF)), Internal Pressure (πi), Relaxation time (τ), Gibbs Free Energy (ΔG), Absorption Coefficient (α) and Enthalpy (H), Entropy(S) have been calculated.Entropy is a thermodynamic state property, its value depends only on the state of a system, not on the history of the system. Therefore, to determine the change in entropy of a system from one state to another, it is sufficient to evaluate the change for a reversible process between those two states; the change in entropy for any other process connecting the same two states will be the same as the change for the reversible process The properties have been used to discuss the presence of significant interactions between the component molecules.

Keywords: - *Cholesteryl oleyl carbonate, Ultrasonic Velocity, Enthalpy(H), Entropy(S),Gibbs Free Energy (ΔG), Absorption Coefficient (α)*

I. INTRODUCTION

The study of intermolecular interaction plays an important role in the development of molecular sciences. A large number of studies have been made on the molecular interaction in liquid systems by various physical methods like Infrared [1,2], Raman effect [3,4], Nuclear Magnetic resonance, Dielectric constant[5], ultra violet[6] and ultrasonic method [7,8]. Cholesterol (**$C_{46}H_{80}O_3$, MOL WT-681.14**) is a steroid alcohol that is essentially insoluble in aqueous solutions. Cholesterol can be esterified with a fatty acid to form cholesteryl esters. The latter form discrete lipid droplets in cells, especially in cells of steroidogenic tissues, and in the lipid core of low-density lipoproteins in the blood. Cholesterol is a fatty lipid sparingly insoluble in water but soluble in a number of organic solvents. Cholesteric materials are temperature sensitive and have color changing ability upon temperature.Not only emulsifying and humectant properties but also liquid crystal properties of cholesterol and its derivatives (salts and esters) make them useful in the commercial applications of cosmetics and pharmaceuticals. Measurement of Ultrasonic Velocity is generally made either by continuous wave method or by pulse methods. In the present study, the ultrasonic velocity was measured using a multi ultrasonic Interferometer (Mittal Enterprises Make) for the observation of ultrasonic velocity (C) and knowing the frequency we can find out various parameters such as adiabatic compressibility, acoustic impedance and temperature variation using temperature bath. The density at room temperature was measured using specific gravity bottle and single pan microbalance. Acoustical parameters were calculated using the measure values of velocity, density. The values of ultrasonic velocity, Free Volume (VF)), Internal Pressure (πi), Relaxation time (τ), Gibbs Free Energy (G), Absorption Coefficient (α),Enthalpy(H), Entropy(S),of cholesteryl oleyl carbonate at different temperatures (303K to 323K) are given in Table 1. When a liquid freezes the mobile molecules of the liquid phase are forced to assume fixed positions in the solid phase This will normally reduce the molecular disorder of the system, so there will usually be an entropy decrease that accompanies freezing. Since entropy is a thermodynamic state property, its value depends only on the state of a system, not on the history of the system. Therefore, to determine the change in entropy of a system from one state to another, it is sufficient to evaluate the change for a reversible process between those two states; the change in entropy for any other process connecting the same two states will be the same as the change for the reversible process. At the transition temperature, any transfer of heat between the system and its surroundings is reversible, because the two phases in the system are in equilibrium.

II. SOME FORMULAE OF THE PARAMETERS TO BE CALCULATED

Gibbs free energy is calculated from acoustic relaxation time (τ) following Eyring rate process theory [19]:

$$\Delta G = RT \ln(KT\tau / h)$$

Where K = 1.23×10^{-23} J/K, T is the temperature, τ is the relaxation time, h = 6.626×10^{-34} Js (Planck's Constant) . Acoustic relaxation time (τ) is calculated using the following relation:

$\tau = 4\eta / 3\rho C^2$

Acoustical relaxation time indicates the the presence of interactions. The internal pressure is calculated from the free volume concept on the basis of statistical thermodynamics as,

$$\pi i = bRT [K\eta / C]^{1/2} [\rho^{2/3} / M^{7/6}]$$

Absorption coefficient (α) is calculated from the following equation $\alpha = \omega^2 \tau / 2C$ [19] where $\omega = 2\pi f$, C is the ultrasonic velocity, η is viscosity, ρ is the density and M is the molecular weight of the cholesteryl oleyl carbonate taken .The enthalpy (H) is calculated from the relation

$H = \pi i (Vf)$

Entopy(S) is calculated from the relation $G = H - T S$

Fig 1:

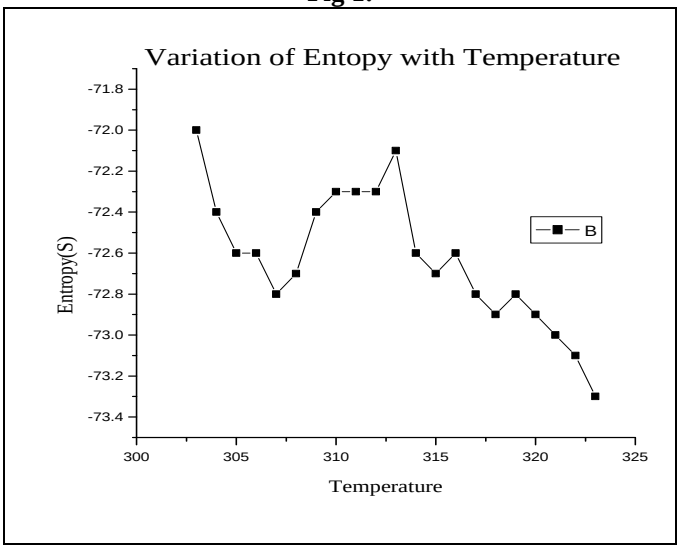

Fig 2:

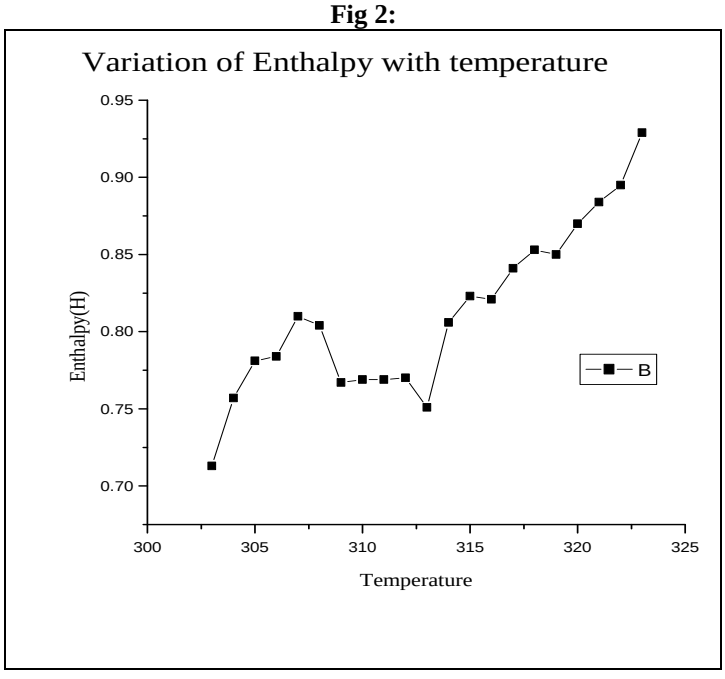

Fig 3:

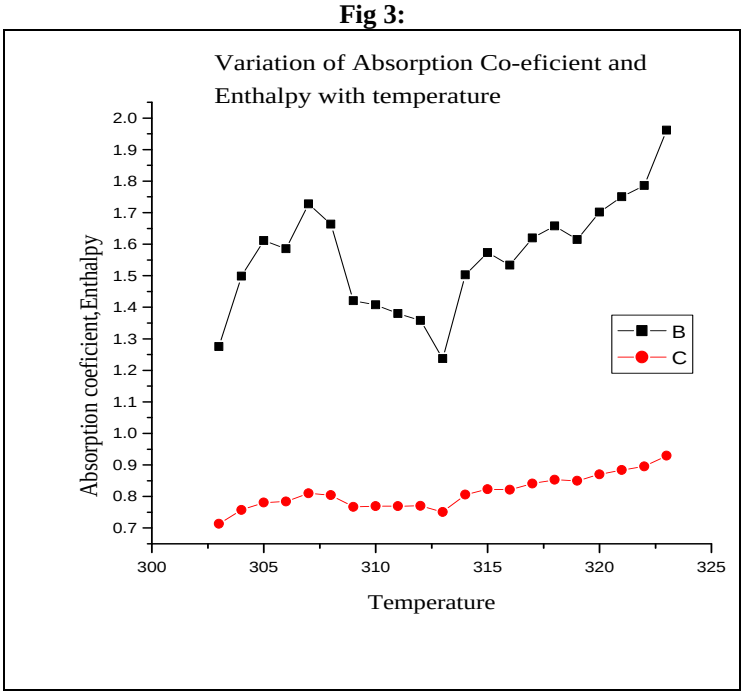

Table 1:

Abs. Temp	C m/s	τ (relaxation time)	ΔG	πi	α	Vf
303	1748	1.11E-09	2.20E+04	6.11E+05	1.275022155	1.17E-06
304	1568	1.17E-09	2.22E+04	5.95E+05	1.498288025	1.27E-06
305	1492	1.20E-09	2.24E+04	5.87E+05	1.611565767	1.33E-06
306	1504	1.19E-09	2.24E+04	5.88E+05	1.585643054	1.33E-06
307	1420	1.23E-09	2.26E+04	5.80E+05	1.727882688	1.40E-06
308	1456	1.21E-09	2.27E+04	5.84E+05	1.663199766	1.38E-06
309	1616	1.15E-09	2.26E+04	5.99E+05	1.420397546	1.28E-06
310	1624	1.14E-09	2.27E+04	6.00E+05	1.407639041	1.28E-06
311	1644	1.13E-09	2.27E+04	6.01E+05	1.379806776	1.28E-06
312	1660	1.13E-09	2.28E+04	6.03E+05	1.357724825	1.28E-06
313	1764	1.09E-09	2.28E+04	6.12E+05	1.237459938	1.23E-06
314	1548	1.16E-09	2.30E+04	5.92E+05	1.502899463	1.36E-06
315	1500	1.18E-09	2.32E+04	5.88E+05	1.573109748	1.40E-06
316	1524	1.17E-09	2.32E+04	5.90E+05	1.533663903	1.39E-06
317	1468	1.19E-09	2.33E+04	5.84E+05	1.619692135	1.44E-06
318	1444	1.20E-09	2.34E+04	5.82E+05	1.657627099	1.47E-06
319	1468	1.19E-09	2.35E+04	5.84E+05	1.614606747	1.46E-06
320	1416	1.20E-09	2.36E+04	5.79E+05	1.701693416	1.50E-06
321	1388	1.21E-09	2.37E+04	5.76E+05	1.750711048	1.53E-06
322	1368	1.22E-09	2.38E+04	5.74E+05	1.786463329	1.56E-06
323	1284	1.26E-09	2.40E+04	5.65E+05	1.961563587	1.65E-06

Fig 4:

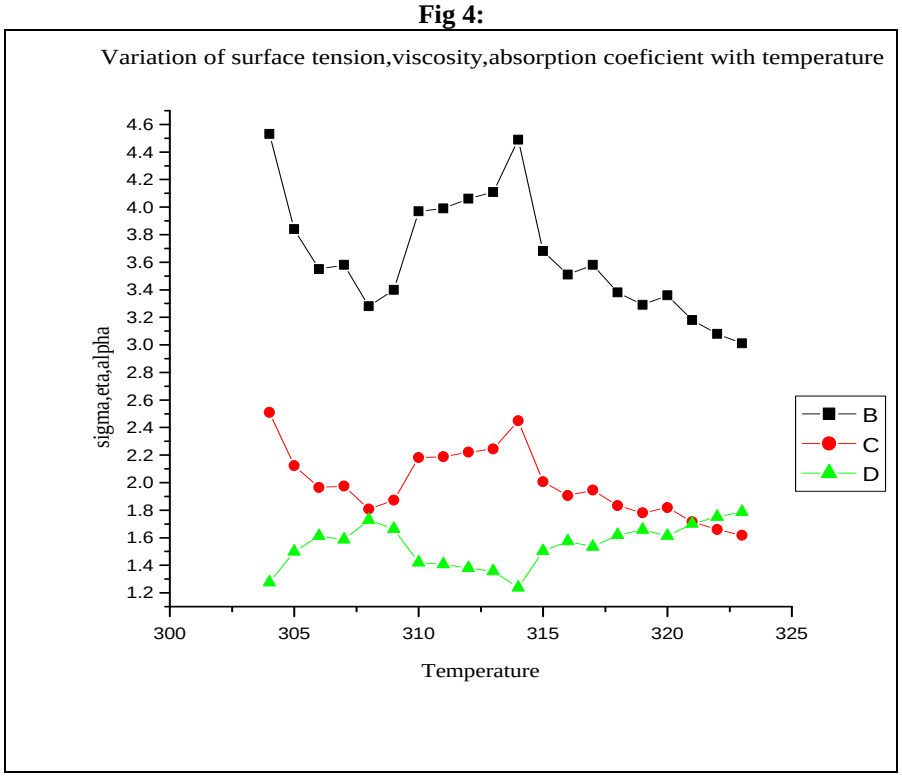

Table2:

Absolute Temp(T)	C(m/s)	Sigmax10^{-4}(σ)	Eta(η)	ρ □□k g/m3)	□ □ □ □ □ H □	S
303	1748	4.53	2.510051	982.9000	7.13E-01	-7.20E+01
304	1568	3.84	2.124227	980.7000	7.57E-01	-7.24E+01
305	1492	3.55	1.964224	978.6000	7.81E-01	-7.26E+01
306	1504	3.58	1.975388	976.5000	7.84E-01	-7.26E+01
307	1420	3.28	1.807604	974.3000	8.10E-01	-7.28E+01
308	1456	3.40	1.87161	972.2000	8.04E-01	-7.27E+01
309	1616	3.97	2.180629	970.1000	7.67E-01	-7.24E+01
310	1624	3.99	2.188548	968.0000	7.69E-01	-7.23E+01
311	1644	4.06	2.220686	965.9000	7.69E-01	-7.23E+01
312	1660	4.11	2.244912	963.9000	7.70E-01	-7.23E+01
313	1764	4.49	2.449869	961.8000	7.51E-01	-7.21E+01
314	1548	3.68	2.006363	959.7000	8.06E-01	-7.26E+01
315	1500	3.51	1.906749	957.7000	8.23E-01	-7.27E+01
316	1524	3.58	1.94553	955.7000	8.21E-01	-7.26E+01
317	1468	3.38	1.832349	953.6000	8.41E-01	-7.28E+01
318	1444	3.29	1.781042	951.6000	8.53E-01	-7.29E+01
319	1468	3.36	1.818934	949.6000	8.50E-01	-7.28E+01
320	1416	3.18	1.71683	947.6000	8.70E-01	-7.29E+01
321	1388	3.08	1.660052	945.6000	8.84E-01	-7.30E+01
322	1368	3.01	1.618347	943.6000	8.95E-01	-7.31E+01
323	1284	2.73	1.466207	941.6000	9.29E-01	-7.33E+01

An increase of entropy can cause numerous side-effects: Changes of volume, form, phase,magnetism,etc. Entropy decreses with temperature upto 307 K but there is maximum entropy at 313 K, which may point to BP II and BP I [3] phase transitions.

III. RESULTS AND DISCUSSION

Table 1 represents the experimentally measured values of ultrasonic velocity(U) , Gibbs free energy(ΔG), Classical Absorption Coefficient, Free Volume (VF) ,), Internal Pressure(πi), Relaxation time(τ), at different temperatures. Table 2 represents the variation of Enthalpy(H), Entropy(S),surface tension,viscosity,density. The excess values of relaxation time, internal pressure, and Gibbs free energy indicate that the interaction between the molecules does not seem to vary very much in strength with changing frequency. Hence, intermolecular interaction in the case of cholesteryl oleyl carbonate is large. However, with rise in temperature increase in free volume and decrease in internal pressure are noticed.From the table (1) Gibbs Free Energy, Classical Absorption Coefficient increases with the increase in temperature.Increase in Gibbs' free energy suggests shorter time for rearrangement of molecules. Relaxation time is the time taken for the excitation energy to appear as translational energy. The above fact confirms the minimum interaction between the molecules in cholesteryl oleyl carbonate . Viscous relaxation time and the Gibbs' free energy both decreases as temperature increases. As temperature increases, excitation energy increases and hence relaxation time decreases. Further, since the kinetic energy of the molecule increases, longer time is taken for rearrangement of molecules and this suggest a decrease in Gibbs' free energy. Free volume is the average volume in which the centre of a molecule can move due to the repulsion of the surrounding molecules. . This suggests that there is a closed packing of molecules inside the shield. Such an increase in internal pressure generally indicates association through hydrogen bonding and hence supports the present investigation. Figure 1 shows variation of entropy with temperature. From the graph it is observed that the entropy decreases with the increasing value of temperature, but a clearly visible change of the temperature evolution occurs at 307 and 313 , which may point to BP II and BP I [3] phase transitions. Recently the stabilization of blue phases over a temperature range of more than 60 K including room temperature (260–326 K) has been demonstrated [17,18] . Highly chiral liquid crystals, on the other hand, may exhibit one or more blue phases (BP) as they are heated from the helical phase to the isotropic phase. In addition, the blue phases possess a much higher viscosity than either the helical or isotropic phase. In both cases, it is likely that the crystalline ordering of the blue phases is responsible for giving these liquids properties which one usually associates with solids. The phase of a thermotropic liquid crystal is temperature dependent. As temperature is varied, the conditions on the translational and orientational order of the constituent molecules which produce the most energetically favorable system may also change.

IV. CONCLUSION

The results obtained for the present study indicate that the thermodynamic parameters are sensitive to the molecular interaction present in cholesteryl oleyl carbonate . From Ultrasonic velocity and related acoustical parameters for cholesteryl oleyl carbonate at varying temperature, it is concluded that there exists a strong molecular interaction due to hydrogen bonding.

REFERENCES

[1]. G.K. Johri, and R.C. Misra, Acustica, **67**, 292 (1989).
[2]. A.Ali and A.K. Nain, PRAMANA-journal of Phys1cs, **58**, No.4, 695 (2002).
[3] D.C. Wright and N.D. Mermin. "Crystalline liquids: the blue phases." *Rev. Mod. Phys.* **66**, 385 (1989).
[4] Mason W. P. (1965). Effect of Impurities and phonon processes on the ultrasonic attenuation of Germanium, Crystal Quartz and Silicon. In *Physical Acoustics IIIB.* W. P. Mason (Ed.). Academic Press Inc., New York, 235-285.
[5] Brugger, K. (1964). Thermodynamic definition of higher order elastic constants. Physical Review, 133., 6., A1611-A1612.
[6] P.K. Yadawa, D. Singh, D.K. Pandey & R.R. Yadav, *Elastic and acoustic properties of heavy rare-earth metals.*, The Open Acoustics Journal, 2., 80-86, 2009.
[7] C. S. Priya, S. Nithya, G. Velraj, A.N. Kanappan, *Molecular interactions studies in liquid mixtures using ultrasonic technique*, Int. J. Adv. Sci. and Tech, Vol. 18, 59-73, 2010.
[8] E. Freedman, J. Chem. Phys. **21**, 1784, (1955).
[9] A.N. Kanappan and V. Rajendran, Indian J. Pure and Appl. Phys., **30**, 176, (1992).
[10] V.K. Syal, Anita Chauhan and Suvarcha Chauhan, J.Pure. Appl. Ultrason., **27**, pp. 61-69 (2005).
[11] Rajesh Sharma, *Study of Dielectric and Ultrasonic Properties of Organic liquids and Liquid Crystals*, Ph.D. Thesis, directed by. Dr. G.K. Johri submitted to C.S.J.M. University, Kanpur, INDIA (2002).
[12] Deep Chandra Gupta, *Study of the Structure of Non-spherical Polar Molecules and Their Properties*, Ph.D. Thesis, directed by. Dr. G.K. Johri submitted to C.S.J.M. University, Kanpur, INDIA (1998).
[13] Mathieu Legay, Nicolas Gondrexon, Stéphane Le Person, Primius Boldo, and André Bontemps, *Enhancement of Heat transfer by ultrasound: Review and recent advances*, Int. J. Chem. Engg., Vol.2011, Article ID 670108.

[14] M. Nabeel Rashin and J. Hemalatha, *Acoustical study on the interaction of coconut oil based copper oxide nanofluid*, World Academy of Science, Engg. And Tech., Vol.64, 2012, pp. 201-205.
[15] S.Sh. Hosseini, Adam N.M. and Goudarzi K., *Effect of temperature increasing on nanofluid structure*, Australian J. Basic and App. Sci. Vol. 5(9), 2011, pp.979-984.
[16] R.R. Yadav, A.K. Gupta, S.K. Kor, and S. Ram, *Ultrasonic properties in Au nanoparticles reinforced PVA*
[17] S. Meiboom, J. P. Sethna, P. W. Anderson and W. F. Brinkman, "Theory of Blue Phase of Cholesteric Liquid Crystals." *Phys. Rev. Lett.* **46**, 1216 (1981).
[18] P. P. Crooker ,(1989): "Plenary Lecture. The blue phases. A review of experiments." Liquid Crystals, 5:3, 751-775 *solution*, Vol. 10. No. 4, 2007, pp. 398-401.
[19] Umadevi M.1, Kesavasamy R Thermodynamics and Transport Properties of Ester with Cyclohexane in Pentanol at 303**,.2** *Umadevi et al. Int. J. Res. Chem. Environ. Vol.2 Issue 3 July 2012(157-163)*

American Journal of Engineering Research (AJER)
e-ISSN : 2320-0847 p-ISSN : 2320-0936
Volume-02, Issue-10, pp-344-353
www.ajer.org

Research Paper Open Access

5G Wireless Communication Systems

Saddam Hossain
Department of Electronics & Telecommunication Engineering, The People's University of Bangladesh (PUB) Bangladesh

***Abstract*: -** As a subscriber becomes more aware of the mobile phone technology, he/she will seek for an appropriate package all together, including all the advanced features of a cellular phone can have. Hence, the search for new technology is always the main intention of the prime cell phone giants to out innovate their competitors. In addition, the main purpose of the fifth generation wireless networks (5G Wireless networks) is planned to design the best wireless world that is free from limitations and hindrance of the previous generations. 5G technologies will change the way most high bandwidth users access their Mobile Radio Communication (MRC). So, this paper represents, great evolution of 1G (First Generation) to 4G yield 5G, introduction to 5G technologies, why there is a need for 5G, advantages of 5G networks technology, exceptional applications, Quality of Service (QoS), 5G network architecture-The MasterCore as well as hardware and software for the 5G MasterCore technology.

Keywords: *- 5G, All IP Network, Cloud Computing , 5G architecture-The MasterCore, Quality of Service (QoS), 5G-IU, Parallel Multimode (PMM).*

I. INTRODUCTION

We are living in modern science. We can not think a single moment without science. Science makes our life easy and comfortable. Modern world is being compressed due to the development of science and its technologies. During the last few decades, the world has seen phenomenal changes in the telecommunications industry due to science and technology. We have different mobile and wireless communication technologies, which are mass deployed, such as WiMAX (IEEE 802.16 wireless and mobile networks) , Wi-Fi (IEEE 802.11 wireless networks), LTE (Long Term Evolution), 3G mobile networks (UMTS, cdma2000) and 4G as well as accompanying networks, such as personal area networks (e.g., Bluetooth, ZigBee) or sensor networks. Mobile terminals include variety of interfaces, such as GSM is one, which are based on old-fashioned circuit switching, the technology that is going into its last decade of existence. These technologies (mainly cellular generations) differ from each other based on four main aspects: radio access, data rates, bandwidth and switching schemes [1]. These differences have been noticed in previous generations (1G, 2G, 2.5G and 3G etc.). In accordance to, we are exploring the most advance cellular technology, could be 5G.

5G Technology stands for 5th Generation Mobile Technology. 5G technology has changed to use cell phones within very high bandwidth. 5G is a packet switched wireless system with wide area coverage and high throughput. 5G technologies use CDMA and BDMA and millimeter wireless that enables seed is greater than 100Mbps at full mobility and higher than1Gbps at low mobility. The 5G technologies include all types of advanced features which make 5G technology most powerful and in huge demand in the near future. It is not amazing, such a huge collection of technology being integrated into a small device. The 5G technology provides the mobile phone users more features and efficiency. A user of mobile phone can easily hook their 5G technology gadget with laptops or tablets to acquire broadband internet connectivity. Up till now following features of the 5G technology have come to surface- High resolution is offered by 5G for extreme mobile users, it also offers bidirectional huge bandwidth [2], higher data rates and the finest Quality of Service (QoS) (i.e. discussed below in the paper).

Now a days, all wireless and mobile networks are forwarding to all-IP principle, that means all data and signaling will be transferred via IP (Internet Protocol) on network layer [3].The purpose of the All-IP Network (AIPN) is to completely transform ("to change in composition or structure") the 100+ years of legacy network

infrastructure into a simplified and standardized network with a single common infrastructure for all services [15]. In order to implement 5G technology, MasterCore technique is needed to apply All-IP Network (AIPN) properly. Hence, the Mastercore is designed. The 5G MasterCore is a convergence of Parallel Multimode (PMM), Nanotechnology, Cloud Computing, and All IP Platform (Broadly mansion in section….) also 5G-IU technology. These technologies have their own impacts on existing wireless networks which make them into 5G.

II. EVOLUTION OF WIRELESS TECHNOLOGIES

This section mentions in short the evolution of wireless and cellular systems based on the four main key aspects: radio access, data rates, bandwidth and switching schemes.

2.1 Review of Previous Fourth Generations Systems

2.1.1 First-Generation Systems (1G)

The 1st generation was pioneered for voice service in early 1980's, where almost all of them were analog systems using the frequency modulation technique for radio transmission using frequency division multiple access (FDMA) with channel capacity of 30 KHz and frequency band was 824-894 MHz [6], which was based on a technology known as Advance Mobile Phone Service (AMPS).

2.1.2 Second Generation Systems (2G)

The 2nd generation was accomplished in later 1990's. The 2G mobile communication system is a digital system; this system is still mostly used in different parts of the world. This generation mainly used for voice communication also offered additional services such as SMS and e-mail. In this generation two digital modulation schemes are used; one is time division multiple access (TDMA) and the 2nd is code division multiple access (CDMA) [7] and frequency band is 850-1900 MHz. In 2G, GSM technology uses eight channels per carrier with a gross data rate of 22.8 kbps (a net rate of 13 kbps) in the full rate channel and a frame of 4.6 milliseconds (ms) duration [14].The family of this generation includes of 2G, 2.5G and 2.75G.

2.1.3 Third Generation Systems (3G)

Third generation (3G) services combine high speed mobile access with Internet Protocol (IP)-based services. The main features of 3G technology include wireless web base access, multimedia services, email, and video conferencing. The 3G W-CDMA air interface standard had been designed for "always-on" packet-based wireless service, so that computer, entertainment devices and telephones may all share the same wireless network and be connected internet anytime, anywhere [13]. 3G systems offer high data rates up to 2 Mbps, over 5 MHz channel carrier width, depending on mobility/velocity, and high spectrum efficiency. The data rate supported by 3G networks depends also on the environment the call is being made in; 144 kbps in satellite and rural outdoor, 384 kbps in urban outdoor and 2Mbps in indoor and low range outdoor [4]. The frequency band is 1.8 - 2.5 GHz [16].

2.1.4 Fourth Generation Systems (4G)

4G usually refers to the successor of the 3G and 2G standards. In fact, the 3GPP is recently standardizing LTE Advanced [8] as future 4G standard. A 4G system may upgrade existing communication networks and is expected to provide a comprehensive and secure IP based solution where facilities such as voice, streamed multimedia and data will be provided to users on an "Anytime, Anywhere" basis and at much higher data rates compared to previous generations. One common characteristic of the new services to be provided by 4G is their demanding requirements in terms of QoS. Applications such as wireless broadband access, Multimedia Messaging Service (MMS), video chat, mobile TV, HDTV content and Digital Video Broadcasting (DVB) are being developed to use a 4G network.

2.1.4.1 LTE advanced

LTE release 10, also referred to as LTE-Advanced, is claimed to be the true 4G evolution step. Earlier releases of LTE are included as integrated parts of LTE release 10, providing a more straightforward backwards compatibility and support of legacy terminals, for example. The main requirement specification for LTE advanced as approved in [8] are:

- Peak Downlink data rate: 1 Gbs, Peak Uplink data rate: 500 Mbps.
- Transmission bandwidth: Wider than approximately 70 MHz in DL and 40 MHz in UL.
- User throughput at cell edge 2 times higher than that in LTE.
- Average user throughput is 3 times higher than that in LTE.
- Spectrum efficiency 3 times higher than that in LTE; Peak spectrum efficiency downlink: 30 bps/Hz, Uplink: 15 bps/Hz.
- Mobility: Same as that in LTE.
- Coverage should be optimized or deployment in local areas/micro cell environments with Inter Site Distance (ISD) up to 1 km.

III. FIFTH GENERATION SYSTEMS (5G)

5G Wireless Communication System is not deployed yet. The big challenge for the design and deployment of 5G wireless system can be faced easily as proposed features and architecture (mentioned below) that will increase system capacity and quality within the limited available frequency spectrum, whose frequency band and Data Bandwidth will be '3-300GHz' and '1Gbps & higher (as demand)' successively. The remarkable issue, there don't have any limitation in 5G as respect to user demands in the next 200 years. The 5G also implies the whole wireless world interconnection (WISDOM—Wireless Innovative System for Dynamic Operating Mega communications concept), together with very high data rates of the Quality of Service (QoS) applications.

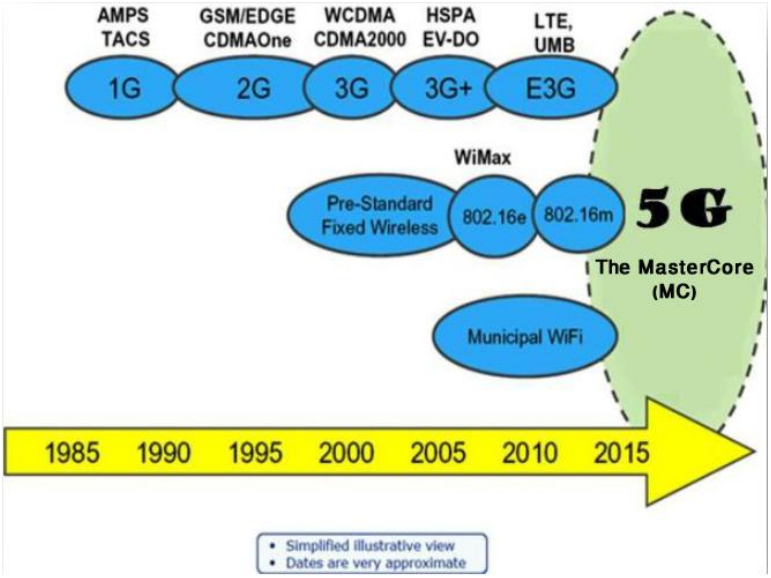

Figure 1: Evolution of Mobile Technologies

Table 1: Basic comparison among 3G, 4G and 5G Technology

Technology/ features	**3G**	**4G**	**5G**
Data Bandwidth	2Mbps	2Mbps to 1Gbps	1Gbps & Higher (as demand)
Frequency Band	1.8 - 2.5 GHz [16]	2 - 8 GHz [16]	3-300GHz [16],[18]
Standards	WCDMA CDMA-200 TD-SCDMA [19]	All access convergence including:OFMDA,MC-CDMA Network-LMPS [19]	CDMA & BDMA
Technology	Broad bandwidth CDMA,IP technology [19]	Unified IP And seamless combination of broadband LAN/WAN/ PAN and WLAN [19];	Unified IP and seamless combination of broadband, LAN/WAN/PAN/WLAN [19] and technologies for 5G new deployment (could be OFDM etc.);
Service	Integrated high quality audio, video and data	Dynamic information access, wear-able devices, HD streaming; global roaming;	Dynamic information access, wear-able devices, HD streaming; any demand of users; upcoming all technologies; global roaming smoothly;
Multiple Access	CDMA	CDMA	CDMA & BDMA
Core Network	Packet Network	All IP Network	Flatter IP Network & 5G Network Interfacing(5G-NI)
Definition	Digital Broadband, packet data	Digital Broad band, Packet data, All IP	Digital Broadband, Packet data All IP, Very high throughput
Hand off	Horizontal	Horizontal & Vertical	Horizontal & Vertical
Start from	2001 [12]	2010 [12]	2015 [12]

3.1 Why is there a need for 5G?

This paper mainly focuses on how a 5G network can provide more facilities approach to a common man to utilize his available possessions in an enormous way to make him to feel the real progress. As a user point of view, the major difference between current generations and expected 5G techniques must be something else than increased maximum throughput; other requirements include [1]:

- It could make better revenue for current global operators as well as interoperability will become more feasible.
- Improved and innovative data coding and modulation techniques, which includes filter bank multi carrier way in schemes.
- For wireless access and back haul use of millimeter wave frequencies is very useful.
- With the support of different conduction points with related coverage and surrounding the option of a supple usage of resources for up link and down link transmission in each cell is achieved by superior intrusion and mobility management.
- To make 5G practical for all sorts of radio access technologies there should be a common platform unique for all the technologies.
- Lower battery consumption.
- Lower outage probability.
- Better coverage and high data rates available at cell edge.
- Multiple concurrent data transfer paths.
- Possible to1Gbps and higher data rate in mobility.
- More secure; better cognitive radio/SDR Security.
- Higher system level spectral efficiency.
- World Wide Wireless Web (WWWW), wireless-based web applications that include full multimedia capability beyond 4G speeds.
- More applications combined with Artificial Intelligent (AI) as human life will be surrounded by artificial sensors which could be communicating with mobile phones.
- Not harmful to human health.
- Cheaper traffic fees due to low infrastructure deployment costs.
- Smart beam antenna systems.

5G is to be a new technology that will provide all the possible applications, by using only one universal device, and interconnecting most of the already existing communication infrastructures. The 5G terminals will be an upgradable multimode and cognitive radio- enabled. It will have software defined radio modulation schemes. All the required upgradable software should be downloaded from the Internet on the run. The 5G mobile networks will focus on the development of the user terminals where the terminals will have access to different wireless technologies at the same time and will consolidate various flows from various technologies. Besides, the terminal will make the ultimate choice among different wireless/mobile access network providers for a given service.

3.2 Advantages of 5G network of the MasterCore technology

The MasterCore technology has been designed for boundless wireless service; so that computer, entertainment devices and mobile phone may all share the same wireless network and can be connected with internet anytime, anywhere. It's designed for 5G communication system to fulfill the limitless target up to the next two centuries, the common features as following;

- Files can be downloaded (even movies) within seconds.
- Pages will upload almost instantly.
- Can play easily online games.
- 5G devices are comparatively less expensive than 3G and 4G devices.
- Using 5G the battery runs out very fast.
- Finest Quality of Service (QoS).
- All Networks can be gathered on a platform.
- Easily support previous generations.
- New deployments of 5G can be connected directly with The Mastercore by 5G -IU (5G Interfacing Unit) without All IP concept.
- No limitation as user demands.
- Ability to support the new services.

- World combination services are available.
- The MasterCore's hardware and software are upgradeable.
- Able to fill user's demand up to next century.
- Subscribers can store data in central storage.
- Remote PCs can be controlled by handsets.
- Subscriber can use application software without installation in own devices that provided by the MasterCore.
- Security is distributed several layers.
- The MasterCore can manage all securities of PSTNs, MSC, and BTS etc.
- The high quality services of 5G technology based on Policy to avoid error.

3.2.1 Quality of Service (QoS)

Next Generation Networks (NGN) consists of support functionalities for data transport, and control transport, as well as functionalities for support of services and applications. The measurement of traffic is a basic control activity in order to provide Quality of Service, [5]. In addition 5G communication system is designed by the finest Quality of Service (QoS).

Quality of Service (QoS) refers to a network's ability to achieve maximum bandwidth and deal with other network performance elements like latency, error rate and uptime. Quality of service also involves controlling and managing network resources by setting priorities for specific types of data (video, audio, files) on the network. QoS is exclusively applied to network traffic generated for video on demand, IPTV, VoIP, streaming media, videoconferencing and online gaming. The primary goal of quality of service is to provide priority to networks, including dedicated bandwidth, controlled jitter, low latency and improved loss characteristics. Its technologies supply the elemental building blocks that will be used for future business applications in campus, wide area networks and service provider networks. There are three fundamental components for basic QoS implementation [17]:

- Identification and marking techniques for coordinating QoS from end to end between network elements.
- QoS within a single network element.
- QoS policy, management, and accounting functions to control and administer end-to-end traffic across a network.

3.3 Exceptional applications

The 5G MasterCore has some exceptional applications with common features as;

- One can know weather, temperature, and location etc. of each other when conversation is going on.
- Students can attend any class of any institute of the world without going there (by WCSM).
- A doctor can treat patients of other countries from a place.
- Possible to monitor any place of the world from anywhere.
- Batteries can be charged by using network without charger.
- It could be possible to visualize lively all the planets and the Universe.
- One can complete his/her works without going to the office.
- One can be able to locate his/her child when she/he is unfortunately missed.
- One can be able to predict tsunami/earthquake before it occurs.

3.4 A proposed 5G Network Architecture

Terminals and network components are dynamically upgraded (and adapted) to new situation. Network operators use the upgradeability to introduce value-added services more easily. Upgradeability is based on cognitive radio. Cognitive radio technologies include the ability of devices to determine their location and location's information (i.e. temperature, weather etc.), sense spectrum used by neighboring devices, change frequency, adjust output power and even alter transmission parameters and characteristics. A cognitive radio is a transceiver (beam) that is able to understand and respond to its operating environment. Thus cognitive radio concerns mobile devices and networks which are computationally intelligent about radio resources and related communications to explore user communication needs and provide wireless services, be appropriate to those needs. Hence, the radio is aware and cognitive about changes in its environment and responds to these changes by adapting operating characteristics in some way to improve its performance. In addition, the appropriate proposed architecture of the 5G MasterCore technology is shown below in figure 2.

3.4.1The MasterCore

The 5G potential will require the design of a single wireless user terminal able to self-explanatory operate in different heterogeneous access networks.

A fully upgradable terminal changes its communication functions depending on network and/or user demands. In addition, the main challenge for an upgradable MasterCore is to deal with increasing number of different radio access technologies based on solid interoperability criteria and mechanisms. A core could be a convergence of the aforementioned nanotechnology, Parallel Multimode (PMM) technology, cloud computing and cognitive radio, upgradable and based on All IP Platform and 5G-IU is called the MasterCore. The 5G MasterCore is an upgradable and multi-technologies core. The MasterCore upgradability could be a self-adaptation and made adaptation to a dynamically-changing environment or mission oriented adaptation to meet a given set of mission requirements with the aim of improving service delivery and spectrum utilization. The MasterCore changes its communication functions depending on network status and/or user demands. Upgradability could be in both software and hardware. Hardware upgradability is mainly performed by operators, adding additional equipments to increase network capacity at a specific time. However, in software upgradability and with the power of SDR, network is dynamically upgradable, which means that the programs (running on the upgradable processing elements) as well as the communication links between the processing elements are upgraded at run-time. Upgradable hardware and software segments have been shown in the MasterCore Technology (MCT) in Figure 3. Different processing elements are used for different purposes. The general purpose processors are fully programmable to perform different computational tasks. The block diagram of the MasterCore architecture is shown in Figure 2.

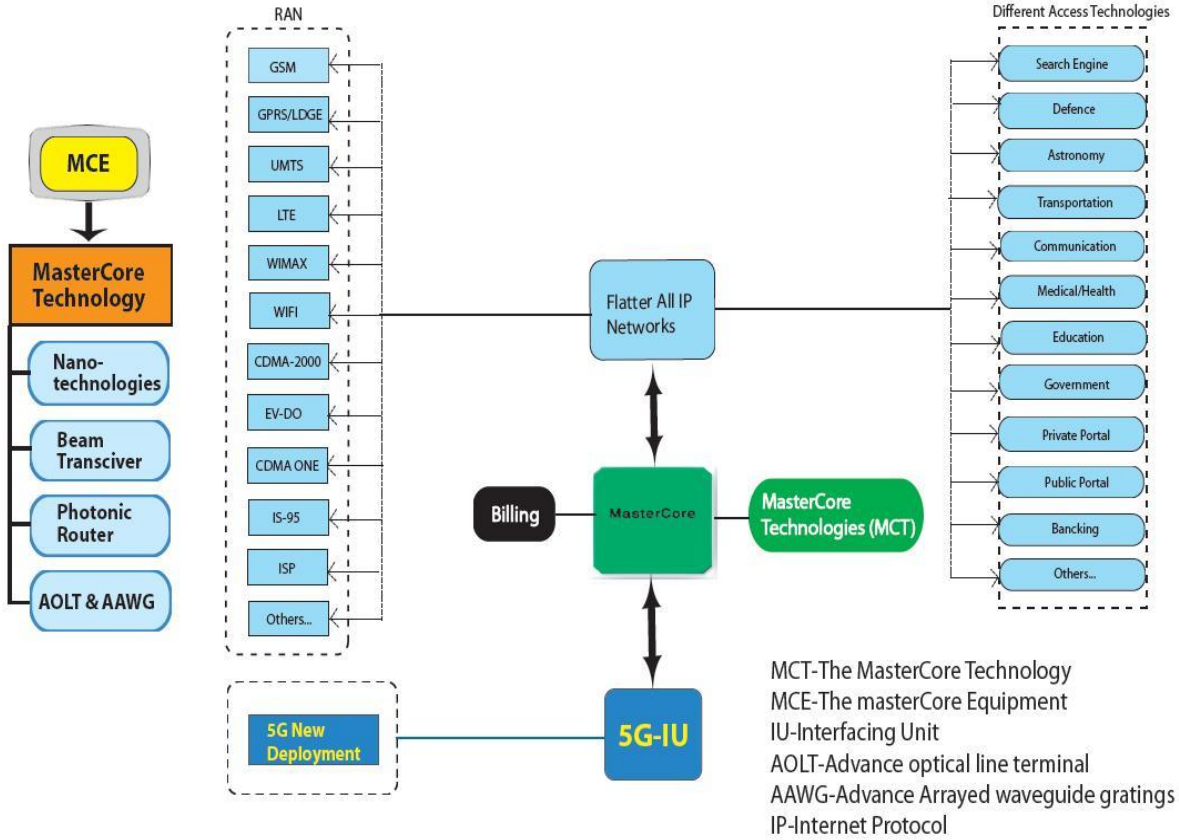

Figure 2: The MasterCore Architecture

3.4.2 The MasterCore Technologies (MCT)

The 5G MasterCore is a convergence of below mention technologies. These technologies have their own impact on exiting wireless network which makes them in to 5G. The different segments of the MasterCore Technology (MCT) are displayed below in figure 3.

3.4.2.1 Parallel Multimode (PMM)

In 5G Wireless Communication Systems, The MasterCore can be operated into parallel multimode such as All IP Network Mode, 5G Network Mode, where in All IP Network Mode controls all network technologies of RAN and DAT (Different Access Networks) up to 5G new deployments. 5G Network Mode manages all new deployments based on 5G as a result 5G network systems will be more efficiency, powerful and less complicated. Any service mode can be opened under 5G-NDM (New Deployment Mode) as WCSM (World Combination Service Mode).WCSM provides some services among subscribers that can be used in special purposes for example, a lecturer writes on white board that display on another board without video in

any country of the world and vice versa besides conversation and video. For Parallel Multimode, any new service can be added easily so that system of the network no needs to change. In fact all modes run at a time continuously (i.e. parallel).

3.4.2.2 All IP Network

The All-IP Network (AIPN) is an evolution of the 3GPP system to fulfill the increasing demands of the cellular communications market. It is a common platform valid for all sorts of radio access technologies. AIPN focused primarily on the enhancements of packet switched technology but now it provides a continued evolution and optimization in terms of both performance and cost. The key benefits of AIPN architecture includes a variety of different access systems' provision, lower costs, universal seamless access, and increased user-satisfaction and reduced system latency. But with the advantages of IP come some dangers: as data flow more freely and the internet is open not only to developers but also to all manner of criminals and viruses, developers and operators face new security challenges which should be solved properly.

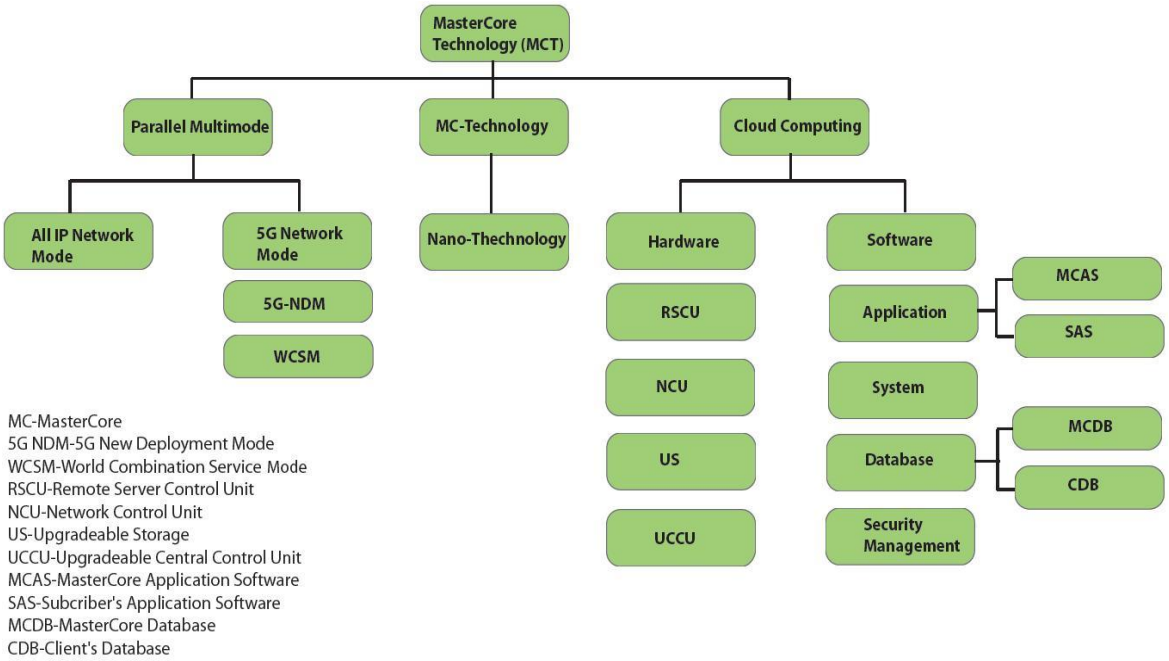

Figure 3: Segments of the MasterCore Technology (MCT)

3.4.2.3 Nanotechnology

Nanotechnology is the application of nanoscience to control process on nanometer scale between 0.1 to 100nm.The field is also known as Molecular Nanotechnology (MNT) where MNT deals with control of the structure of matter based on atom-by-atom and molecule by molecule engineering. Nanotechnology is considered as the next industrial revolution, and the telecommunications industry will be radically transformed by it in a few years. As the future applications will require more memory and computing power to offer higher data rates, current technologies can not resolve these challenges. Fortunately, nanotechnology could provide effective solutions for power efficient computing, sensing, memory enlargement, and humanmachine interaction, [9], [10].

Nanotechnology has shown its impact on both mobile as well as the core network as follows.

- The mobile device has become more than a communication device in modern world; computation and communication are ready to serve the user in an intelligent way. Mobile devices together with the intelligence, embedded in human environments, will create a new platform that enables ubiquitous sensing, computing, and communication. With nanotechnology mobile phones can act as intelligent sensors that have applications in many industries, among them transportation, communications, medicine and safety.
- The core network requires high speed and a reliable capacity to manipulate and interoperate increasing number of heterogeneous access technologies. At present, nanotechnologies are used in Digital Signal Processing (DSP) Fabrication, introducing new perceptions in DSP designing that increases the overall system speed & capacity.

Apart from this it has its own impact on sensor as well as security. This is considered as a most significant in telecommunication.

3.4.2.4 Cloud computing

"*Cloud computing is a model for enabling ubiquitous, convenient, on-demand network access to a shared pool of configurable computing resources (e.g., networks, servers, storage, applications, and services) that can be rapidly provisioned and released with minimal management effort or service provider interaction…" a definition from* [11]. Hence, cloud computing is a technology that uses the internet and central remote server to maintain data and applications. In 5G networks this central remote server could be a content provider. Cloud computing allows consumers and business to use applications without installation and access their personal files at any computer with internet access. The same concept is going to be used in multi-core technology where the user tries to access his private account form a global content provider through cloud computing.

3.5 MC Hardware and Software

3.5.1 Hardware

In MasterCore technology, assembly of hardware is set into several units to maintain whole network system properly, also to troubleshoot in core network instantly.

As a result, efficiency of the core is suitable with demanded services. Hardware classified into different units as:

a) Remote Server Control Unit (RSCU) provides a great opportunity to control remote server of users' networks. It indicates the immediate condition of remote server.

b) Network Control Unit (NCU) provides control of the communications among MS, BSC, MSC and PSTN.

c) Upgradeable Storage (US) refers to increase the storage as necessity as demand.

d) Upgradeable Central Control Unit (UCCU) provides the facilities to control all units centrally.

3.5.2 Software

Software Defined Radio (SDR) benefits from today's high processing power to develop multi-band, multi-standard base stations and terminals. Although in future the terminals will adapt the air interface to the available radio access technology, at present this is done by the infrastructure. Several infrastructure gains are expected from SDR. For example, to increase network capacity at a specific time (e.g. during a sports event), an operator will reconfigure its network adding several modems at a given. Base Transceiver Station (BTS). SDR makes this reconfiguration easy. In the context of 4G systems, SDR will become an enabler for the aggregation of multi-standard pico/micro cells. For a manufacturer, this can be a powerful aid to providing multi-standard, multiband equipment with reduced development effort and costs through simultaneous multi-channel processing.

1) 5G will be single unified standard of different wireless networks, including wireless technologies (e.g. IEEE 802.11), LAN/WAN/ PAN and WWWW, unified IP and seamless combination of broad band.

2) Software Defined Radio, Packet layer, implementation of packets, encryption, flexibility etc. In figure 2 are shown different classification segments of 5G software such as:

a) Application: The MasterCore Application Software (MCAS) refers to all application software are needed as to provide services and managements.

Subscriber's Application Software (SAS) is installed centrally so that subscriber runs a program without installing on his own devices. All services of application software are provided from central server.

b) System: System Software is an Operating System (OS) for the 5G MasterCore networking.

c) Database: The MasterCore Database (MCDB) software refers to manage and store all data of whole system those are needed. Client's Database (CDB) software manages all data of user's server those contain all essential information of users and users' networks.

d) Security Management: Securities (users to the Mastercore) will be managed centrally by Security Management (SM) software.

3.6 5G-IU

5G-IU (5G Interfacing Unit) acts to make the most powerful of 5G wireless communication system. Because, all sorts of radio access technologies are combined in a common platform is complex form of aggregation. It will be more complex in future when added new radio access technologies. This is why, 5G-IU is used between new deployments and core network so that 5G wireless communication system is easily manageable. It has some advantages are:

- Lower costs to establish networks.
- Lessen equipments.
- Improve network efficiency.
- Reduce complexity.
- Easily maintain high security.
- Impossible to occur any trouble.

3.7 The MasterCore Equipments (MCE)

Mobile phone has become more than a communication device in modern world it has turned into an identity of an individual. In 5G MasterCore these mobile and other devices (Laptop, local networking devices etc.) are referred as the MasterCore Equipments (MCE) as they are improved with nanotechnology, Beam Transceiver, Advance Optical Line Terminal (AOLT), Advance Arrayed Waveguide Gratings (AAWG). Nanotechnology refers NanoEquipments (NE) are Morph, Graphene's Transistor, GPS, Micro-Micro Phones, Liquid lens, Intelligent Batteries and Nanosensor [4]. We will broadly discuss about NE in our further papers. These are classified into two categories one is user's device and another is internal devices of user's networks. AOLT and AAWG are used in user's networks (LAN, WAN, MAN etc.) to increase faster data rate. We will be discussing about AOLT and AAWG in our further slides. One of the central visions of the wireless industry aims at ambient intelligence, computation and communication always available and ready to serve the user in an intelligent and efficient way. This requires that the devices are mobile. Mobile devices together with the intelligence and efficient that will be embedded in human environments – home, office, public places – will create a new platform that enables ubiquitous sensing, computing, and communication Specs of MasterCore Equipments given as follow:

- Self Cleaning – the phone cleans by itself.
- Self powered – the phone derives its energy/power from the sun, water, or air.
- Sense the environment – the phone will tell you the weather, the amount of air pollution present, etc.
- Flexible – bend but not break.
- More Reliable.
- Transparent – "see through" phones.

IV. FUTURE ENHANCEMENT

5G network technology will reveal a new era in mobile communication technology. The 5G mobile phones will have access to different wireless technologies at the same time and the terminal should be able to combine different flows from different technologies. 5G technology offer high resolution for crazy cell phone user. 5G technology will provide supper and perfect utilization of cellular communication in future. We can monitor any place of the world from anywhere, observe space and watch TV channels at HD clarity in our mobile phones without any interruption. There will be exciting amusement unbelievable services. The 5G mobile phones will be a tablet PC and amazing. Many mobile embedded technologies will evolve.

V. CONCLUSION

In this paper we have discussed the existing and future wireless mobile communication generations and cellular systems focusing on four main key factors: switching schemes, bandwidth, data rates, and radio access, also 5G main development challenges and explained the necessity for 5G. The 5G mobile technology will be implemented at the end of the current decade. We have proposed the MasterCore technology and its hardware and software implementation. We expect that this Paper helps to uplift stronger links between people working in different fields creating future concepts of mobile communication, Internet services, Quality of Service (QoS), Cloud computing, All IP network, Nanotechnologies and concept of the MasterCore. The new coming 5G technology is available in the market to fulfill user demands in affordable rates, bright and high peak future also much reliability as well as exceptional applications.

REFERENCES

Books, Journal Papers or Theses:

[1] Dr. Anwar M. Mousa, "Prospective of Fifth Generation Mobile Communications" *International Journal of Next-Generation Networks (IJNGN) Vol.4, No.3, September 2012*

2] Sapana Singh & Pratap Singh, "Key Concepts and Network Architecture for 5G Mobile Technology" *International Journal of Scientific Research Engineering & Technology (IJSRET)Volume 1 Issue 5 pp 165-170 August 2012*

[3] T. Janevski, "Traffic Analysis and Design of Wireless IP Networks", *Artech House Inc., Boston, USA, 2003.*

[4]. Imthiyaz Ali, "*5G the Nanocore" March 5, 2011*

[5] ITU-T, Y.2173, "*Management of performance measurement for NGN", September 2008.*

[6] Chen, YP; Yang, YH (2007), "*A new 4G architecture providing multimode terminals always best connected services," IEEE Wireless Communications, Volume: 14 Issue: 2 pp. 36-41.*

[7] Xichun Li, AbudullaGani, RosliSalleh, Omar Zakaria 2009," *The Future of Mobile Wireless Communication Networks,"2009 International Conference on Communication Software and Networks*

[8] *3GPP TSG RAN TR 36.913 v8.0.0, Requirements for Further Advancements for E-UTRA (LTEAdvanced).*

[9] Ermolov V. et al. "*Significance of Nanotechnology for future wireless devices and Communications", The 18th Annual IEEE International Symposium on PIMRC'07.*
[10] R.K.Jain, Risal Singh, "*Role of Nanotechnology in future wireless and communication systems", National seminar proceeding, Academy of Business & Engineering Science Ghaziabad, pp-19-28, 16-17th January 2009.*
[11] Peter Mell and Timothy Grance, *"The NIST Definition of Cloud Computing" US National Institute of Standards and Technology Special Publication 800-145, September 2011.*
[12] Engr. Muhammad Farooq, Engr. Muhammad Ishtiaq Ahmed, Engr. Usman M Al,*"Future Generations of Mobile Communication Networks" Academy of Contemporary Research Journal V II (I), 15-21, ISSN: 2305-865, January 2013*
[13] Theodore S. Rappaport, *"Wireless Communications Principle and Practice," published by Pearson Education (Singapore) Pte. Ltd,. Second Edition, Chapter Two;*
[14] Vijay K. Garg and Joseph E. Wilkes, "Principles & Applications of GSM," Published by Dopling Kindersley (India) Pvt. Ltd., licensees of Pearson Education in South Asia, First Impression, 2006;

URL:

[15] http://ytd2525.wordpress.com/category/all-ip-networks/
[16] http://www3.nd.edu/~mhaenggi/NET/wireless/4G/#3G%20Vs%204G%20
[17] http://www.techopedia.com/definition/9049/quality-of-service
[18] http://spectrum.ieee.org/telecom/wireless/millimeter-waves-may-be-the-future-of-5g-phones
[19] http://www.slideshare.net/noorec786/generations-of-network-1-g-2g-3g-4g-5g

Let's go ahead…..**To be continued…..**

American Journal of Engineering Research (AJER)
e-ISSN : 2320-0847 p-ISSN : 2320-0936
Volume-02, Issue-10, pp-354-362
www.ajer.org

Research Paper Open Access

Dependence of evaporation on meteorological variables at daily time-scale and estimation of pan evaporation in Junagadh region

Gundalia Manoj J., And Dholakia Mrugen B.
1 Asst. Prof., Department of Civil Engineering, Dr. Subhash Technical Campus, Junagadh, Gujarat (India)
2 Professor of Civil Engineering, L. D. College of Engineering, Ahmedabad, Gujarat (India)

Abstract: - The significance of six major meteorological factors, that influence the evaporation were evaluated at daily time-scale using the data from Junagadh station, Gujarat (India). The computed values were compared. The solar radiation, maximum air temperature and vapour pressure deficit were found to be the significant factors influencing pan evaporation (E_p). The negative correlation was found between relative humidity and (E_p), while wind speed and bright sunshine hours were found least correlated and no longer remained controlling factors influencing (E_p). The objective of the present study is to compare and evaluate the performance of four different methods to select the most appropriate equations for estimating (E_p).
The Nash-Sutcliffe efficiency coefficient (E) and refined Willmott's index (d_r) are used as performance criterion. The results show that the Jensen equation (radiation based) yielded the most reliable results in estimation of (E_p), especially for monsoon season. The Linacre equation (temperature based) produced reliable estimates for summer and post-monsoon season. The Penman equation (mass transfer based) and the Jensen equation resulted better for winter season while the Romanenko equation (humidity based) found comparatively less reliable. The prediction equations fitted for different seasons and annual basis can be recommended for estimating (E_p) in the study region.

Keywords: - *Pan evaporation; Meteorological variables; Evaporation estimation methods*

I. INTRODUCTION

Evaporation is influenced by number of agro-meteorological parameters and it is one of the integral major components of the hydrological cycle. Estimation of evaporation amount is very important for monitoring, survey and management of water resources, especially in arid and semi-arid areas where resources are scares and seriously endangered by overexploitation [22]. Usually, estimates of evaporation are needed in a wide array of problems in agriculture, hydrology, agronomy, forestry and land resources planning, such as water balance computation, irrigation management, crop yield forecasting model, river flow forecasting, ecosystem modelling. Irrigation can substantially increase crop yields, but again the scheduling of the water application is usually based on evaporation estimates. It depends on the supply of heat energy and the vapour pressure gradient, which, in turn, depends on meteorological factors such as temperature, wind speed, atmospheric pressure, solar radiation, quality of water, and the nature and shape of evaporation surface (e.g. [14]). These factors also depend on other factors, such as geographical location, season, time of day, etc. Thus, the process of evaporation is rather complicated.

Because of its nature, evaporation from water surfaces is rarely measured directly, except over relatively small spatial and temporal scales [12]. Evaporation can be directly measured from pan evaporation (E_p) and lysimeter. But, it is impractical to place evaporation pans in inaccessible areas where accurate instruments cannot be established or maintained. A practical means of estimating the amount of evaporation where no pans are available is of considerable significance to the hydrologists, agriculturists and meteorologists. Numerous investigators developed models for estimation of evaporation. Unfortunately, reliable estimates of evaporation are extremely difficult to obtain because of its complexity. Many methods for estimation of evaporation losses from free water surfaces were reported and it can be divided into several categories including: empirical methods (e.g. [24]), radiation (e.g. [2]), water budget methods (e.g. [33], [20]), energy budget methods (e.g. [10]), mass-transfer methods (e.g. [17]); temperature based (e.g. [4]; [18]); and

combination methods (e.g. [19]). In the direct method of measurement, the observation from Class A Pan evaporimeter and eddy correlation techniques were used [27], whereas in indirect methods, the evaporation is estimated from other meteorological variables like temperature, wind speed, relative humidity and solar radiation [23]. Overviews of many of these methods are found in review papers or books (e.g., [32]; [29]; [26]; [15] and [13]). Many equations for determining evaporation are available. The wide range of data types and expertise are needed to use these equations correctly, hence, it is difficult to select the most appropriate evaporation method for a given study. Therefore, there is a need to analyse and compare the different existing popular evaporation models and to develop a generalized model form.

In an earlier study, [30] evaluated and compared 13 evaporation equations, belonged to the category of mass-transfer method, and a generalized model form for that category was developed. [31] further examined the sensitivity of mass-transfer-based evaporation equations to evaluate errors in daily and monthly input data. [5] analysed the dependence of evaporation on various meteorological variables at different time scales. Radiation-based and temperature based evaporation methods were evaluated and generalised in the study of [6 and 7]. In this study, the existing methods are compared and evaluated, with their optimised parameters values. Finally, the overall applicability of the selected methods is examined in the order of their predictive ability for the study region.

II. STUDY AREA AND DATA COLLECTION

Data of the Junagadh meteorological station located in the Gujarat state of India were used in this study. This station is located at latitude of 21^0 31' N and a longitude of 70^0 33' E, 61 m msl. The region (Figure 1) is situated in semi-arid region; the mean annual precipitation for the region varies from a maximum of 1689.70 mm to minimum of 425 mm with an average value of 940 mm. The Junagadh region is characterized by a semi-arid climate, with warm and dry summers and mild winter conditions. Mean maximum temperature ranges from 33.23^0C to 34.91^0C and mean minimum temperature ranges from 19.44^0C to 29.67^0C. The highest annual wind speed was 13.6 km/h occurred in April, 2000 and 14.1 km/h in April, 2001 whereas the lowest annual wind speed was 8.6 km/h which occurred in October, 2001. The humidity has been changed between 88 % and 63%. Daily meteorological data, including air temperature, wind speed, relative humidity, bright sunshine hours and evaporation for 21 years (1992-2012) were collected from Agro meteorological Cell, Junagadh Agricultural University. The associate parameters like solar radiation, dew point temperature and vapour pressure deficit were computed with standard meteorological formula as described in FAO.

III. DEPENDENCE OF EVAPORATION ON METEOROLOGICAL VARIABLES

For better comparative evaluation, the dimensionless standardized values of each variable were computed and compared by using the transformation shown in equation (01).

$$Z_i = \frac{(X_i - \mu)}{\sigma} \qquad (01)$$

Where X is a variate, i is the i^{th} value, μ is the mean of X and σ is the standard deviation of X. In view of the above considerations, this paper first analyses and compares the roles of controlling variables influencing pan evaporation with daily time-scale. The dominating factors affecting evaporation for daily time-scales are determined, which then forms the basis for choosing the evaporation estimation method suitable for different seasons. After that, different methods, which include temperature, humidity, mass-transfer, and radiation methods, are examined and compared. The comparisons are shown in (Figure 2-7). (Figure 2-4), show that the radiation (R_s), maximum air temperature (T_{max}) and vapour pressure deficit (VPD) with R^2 values 0.86, 0.75 and 0.66 respectively, remain as controlling factors of evaporation. Hence, the radiation based, temperature based and mass transfer based methods for evaporation estimation comparatively give good results. The dependence of evaporation on relative humidity (RH) is shown in (Figure 5). A negative correlation exists between RH and (E_p) with R^2 value 0.25. It is perceived from (Figure 6) and (Figure 7) that wind speed (WS) (R^2 value 0.17) and bright sunshine hours (BSS) (R^2 value 0.38) are no longer remain a significant factors.

IV. EVAPORATION ESTIMATION METHODS

Many forms of the equation have been applied for estimating evaporation around the world. They can be categorised into five major types of approach - based on water budget methods, temperature methods, humidity methods, radiation methods, mass transfer (or aerodynamic) methods or combination (energy budget and aerodynamic) methods. Unfortunately, most of the reliable methods are parameter rich methods and therefore, not feasible for application in data scarce regions. On the other hand, accuracy and reliability of simple methods vary widely according to regional climate conditions. Therefore, it is difficult for many scientists to select the most suitable equation to use for a given study. Due to inaccuracy and unreliability in

estimation of the seepage rate, the water budget method was not used in the study. The equations and climatological data requirements of selected methods are shown in (Table 1).

V. STATISTICAL CRITERION

To assess the performances of selected methods, dimensionless statistic Nash-Sutcliffe efficiency coefficient (E) [21] is used. (E) is computed as shown in equation (02).

$$E = 1 - \frac{\sum_1^n (O_i - P_i)^2}{\sum_1^n (O_i - \overline{O_i})^2} \qquad (02)$$

Where O_i is the observed E_p at time t = i; P_i is simulated E_p at time i; $\overline{O_i}$ mean observed E_p and n is the number of observations. Values of (E) between 0.0 and 1.0 are generally viewed as acceptable levels of performance, whereas values less than 0.0 indicate unacceptable performance. (E) is recommended for two major reasons: (i) it is recommended by [1] and [8], and (ii) it provides extensive information on reported values.

The refined Willmott's index [3] method is applied to quantify the degree to which observed values of evaporation are captured by the selected methods. The refined Willmott's index (d_r) is expressed as shown in equation (03).

$$\begin{aligned} d_r &= 1 - \frac{\sum_1^n |O_i - P_i|}{2\sum_1^n |O_i - \overline{O_i}|}, \text{when} \\ \sum_1^n |O_i - P_i| &\le 2\sum_1^n |O_i - \overline{O_i}| \\ d_r &= \frac{2\sum_1^n |O_i - \overline{O_i}|}{\sum_1^n |O_i - P_i|} - 1, \text{when} \\ \sum_1^n |O_i - P_i| &> 2\sum_1^n |O_i - \overline{O_i}| \end{aligned} \qquad (03)$$

The range of (d_r) is from -1.0 to 1.0. A (d_r) of 1.0 indicates perfect agreement between model and observation, and a (d_r) of -1.0 indicates either lack of agreement between the model and observation or insufficient variation in observations to adequately test the model.

VI. PARAMETER ESTIMATION

In this study, the objective function of minimising sum of squares errors between observed and computed E_p (equation (04)) is selected to optimise the values of model parameters.

$$\mathbf{E_{min} = Min \sum_{i=1}^{n} \left| E_{po} - E_{pc} \right|^2} \qquad (04)$$

Where E_{po} is the observed E_p; E_{pc} is calculated E_p and n is the number of observations. The parameters of equations are computed and optimised using Microsoft Excel spread sheet, Microsoft Excel built-in optimisation tool Solver [16].

VII. RESULT AND DISCUSSION

The performances of [11], [25], [19] and [28] methods against observed pan evaporation data were evaluated by using Nash-Sutcliffe efficiency coefficient (E) and the refined Willmott's index (dr) statistical parameters and the results are presented in (Table 2). Mean daily values of evaporation are computed for different seasons with the four selected equations. The original empirical formulae may be reliable in the areas and over the periods for which they were developed, but large errors, can be expected when they are extrapolated to other climatic areas without recalibrating their parameters. Accordingly, modifications are made to the original equations used here to improve the results. The original and optimised parameter values of selected methods are presented in (Table 3).

It can be seen that the radiation based Jensen method is yielded the highest (E) and (d_r) values 0.96 and 0.90 respectively, especially for monsoon season. For summer and post-monsoon seasons, the temperature based Linacre method is earned (E) and (d_r) values 0.80, 0.76 and 0.18, 0.79 respectively. The Penman and Jensen methods are produced (E) and (d_r) values 0.82, 0.81 and 0.83, 0.80 respectively for winter season, which are much closer. The humidity based Romanenko method is yielded the lowest performance values for all seasons. This means humidity based method has a poor relationship with evaporation. When methods are compared on annual basis, the Penman method is found more appropriate that resulted (E) and (d_r) values 0.85 and 0.83 respectively. The high variability of weather variables indicates their responsibility to influence pan evaporation during different seasons (Fitzpatrick, 1963).

The fitted equations for different seasons with optimized parameter values are expressed as

Winter Season (Penman Equation)

$$E_p = 0.1293\,(1 + 0.24\,u_2)(e_s - e_o) \qquad (05)$$

Summer Season (Linacre Equation)

$$E_p == \frac{\frac{975.3827\ T_m}{(100-L)} + 5.4454\ (T_a - T_d)}{(80 - T_a)} \quad (06)$$

Post-monsoon Season (Linacre Equation)

$$E_p = \frac{\frac{475.3079\ T_m}{(100-L)} + 8.5453(T_a - T_d)}{(80 - T_a)} \quad (07)$$

Monsoon Season (Jensen Equation)

$$E_p = (0.2478\ T_a - 5.5146)R_s \quad (08)$$

When above equations are applied for annual basis, they produced (E) and (d_r) values 0.98 and 0.93 respectively (Figure 8).

VIII. CONCLUSION

The evaporation estimates obtained from four selected methods viz. Linacre, Jensen, Penman and Romanenko are compared to the observed pan evaporation for Junagadh region of Gujarat (India). Two statistical criterions (E) and (d_r) have been used to evaluate the performance of selected methods and establish the optimal parameters. From the above analysis, it can be concluded that there is no single method to cover all the seasons of the year in the study area. Among the selected four methods, the radiation based Jensen method is found to be the most suitable for estimating (E_p) for monsoon season in this study area based on the entire evaluation criterion. From a practical point of view, this method can be considered suitable to serve as a tool to estimate evaporation for hydrologic models. It is observed that for winter season the Jensen and Penman methods are best fitted while for summer and post-monsoon seasons, the Linacre method is found better. Consequently, Linacre method is good choice for calculating evaporation in the study region for summer and post-monsoon seasons. The Romanenko method has the lowest performance among all selected methods. The parameters we determined will indeed be provided useful information for estimating evaporation in Junagadh region. In view of the above we may infer that either and different methods need to be developed for this location which may hold for all seasons, or additional factors need to be included in conventional methods. It is hoped that the study, in general, will assist to select better methods in accordance to the availability of meteorological data.

IX. ACKNOWLEDGEMENT

The authors are grateful to Agro meteorological Cell, Junagadh Agricultural University, Junagadh (Gujarat), for providing all necessary meteorological data.

REFERENCES

[1] ASCE, "Criteria for evaluation of watershed models", *J. Irr. Drn. Eng.* 119(3): 429-442, 1993.
[2] C. H. B. Priestley, R. J. Taylor, "On the assessment of the surface heat flux and evaporation using large-scale parameters", *Monthly Weather Review* 100: 81–92, 1972.
[3] C. J. Willmott, S. M. Robeson and K. Matsuura, "A refined index of model performance", *Int. J. Climateol*., 32: 2088–2094, 2012.
[4] C. W. Thornthwaite, "An approach toward a rational classification of climate", *Geographical Review* 38: 55–94, 1948.
[5] C. Y. Xu and V. P. Singh, "Dependence of evaporation on meteorological variables at different time-scales and inter comparison of estimation methods", *Hydrological Processes* 12: 429–442, 1998.
[6] C. Y. Xu and V. P. Singh, "Evaluation and generalization of radiation-based methods for calculating evaporation", *Hydrological Processes* 14: 339–349, 2000.
[7] C. Y. Xu and V. P. Singh, "Evaluation and generalization of temperature-based methods for calculating evaporation", *Hydrological Processes* 15: 305–319, 2001.
[8] D. R. Legates and G. J. McCabe, "Evaluating the use of "goodness-of-fit" measures in hydrologic and hydro climatic model validation", *Water Resources Res*. 35(1): 233-241, 1999.
[9] E. A. Fitzpatrick, "Estimates of pan evaporation from mean maximum temperature and vapor pressure", *Journal of Applied Meteorology*, 2, 780-792, 1963.
[10] E. R. Anderson, "Energy-budget studies. In: Water Loss Investigations: Lake Hefner Studies", *U.S. Geological Survey Professional Paper*. 269: 71-119, 1954.
[11] E. T. Linacre E. T,"A simple formula for estimating evaporation rates in various climates, using temperature data alone", *Agricultural Meteorology*, 18: 409–424, 1977.
[12] F. E. Jones, "Evaporation of Water: with Emphasis on Applications and Measurement", *Lewis Publ., Inc.*, Chelsea, MI, 200 pp, 1992.

[13] F. I. Morton "Evaporation research — a critical review and its lessons for the environmental sciences", *Critical Reviews in Env. Sc. and Tech.* 24(3): 237–280, 1994.
[14] F. I. Morton, "Evaporation and Climate: A Study in Cause and Effect, Scientific". Series no. 4. *Inland Water Branch*, Department of Energy, Mines and Resources, Ottawa, Canada 31pp, 1968.
[15] F. I. Morton, "Studies in evaporation and their lessons for the environmental sciences", *Canadian Water Resources Journal* 15(3): 261–285, 1990.
[16] FrontLine, www. Solver.org. 8 November 2010.
[17] G. E. Harbeck "A practical field technique for measuring reservoir evaporation utilizing mass-transfer theory", *Geological Survey Professional Paper* 272-E: 101–105, 1962.
[18] H. F. Blaney, W. D. Criddle, "Determining Water Requirements in Irrigated Areas from Climatological Irrigation Data", *US Department of Agriculture, Soil Conservation Service*, Washington, D.C., (19): 48 pp, 1950.
[19] H. L. Penman, "Natural evaporation from open water, bare soil and grass. Proceedings, *Royal Society of London* 193: 120–145, 1948.
[20] J. C. Guitjens, "Models of Alfalfa Yield and Evapotranspiration, Journal of the Irrigation and Drainage Division", *Proceedings of the American Society of Civil Engineers* 108 (IR3): 212-222, 1982.
[21] J. E. Nash and J. V. Sutcliffe, "River flow forecasting through conceptual models: Part 1. A discussion of principles", *J. Hydrology* 10(3): 282-290, 1970.
[22] J. Shiri and K. Ozgur, "Application of Artificial Intelligence to Estimate Daily Pan Evaporation Using Available and Estimated Climatic Data in the Khozestan Province (South Western Iran)". *J. Irrig. Drain Eng*., 137 (7): 412-425, 2011.
[23] M. A. Benzaghta, T. A. Mohammed, A. H. Ghazali,and M. A. Mohd Soom, "Study on Simplified Model for Estimating Evaporation from Reservoirs", *Australian J. of Basic and Applied Sciences*, 4(12): 6473-6482, 2010.
[24] M. A. Kohler, T. J. Nordenson and W. E. Fox, "Evaporation from Pans and Lakes", *U.S. Dept. Com.Weather Bur*. Res. Paper 38. 21 pp, 1955.
[25] M. E. Jensen and H. R. Haise, "Estimating evapotranspiration from solar radiation", *J. Irrig. Drainage*, Div. ASCE, 89: 15-41, 1963.
[26] M. E. Jensen, R. D. Burman, R. G. Allen, "Evapotranspiration and Irrigation Water Requirements", *American Society of Civil Engineers*: New York, 1990.
[27] R. K. Linsley, M. A. Kohler& J. L. H. Paulhus, "Hydrology for Engineers". *McGraw-Hill*, 3rd edn. London, 1982.
[28] V. A. Romanenko, "Computation of the autumn soil moisture using a universal relationship for a large area. Proceedings Ukrainian" *Hydrometeorological Research Institute* (Kiev) 3, 1961.
[29] V. P. Singh, "Hydrologic Systems, Vol. II, Watershed Modelling". Prentice-Hall: Englewood Cliffs, New Jersey, 1989.
[30] V. P. Singh, C. Y. Xu, "Evaluation and generalization of 13 equations for determining free water evaporation". *Hydrological Processes* 11: 311–323, 1997a.
[31] V. P. Singh, C. Y. Xu, "Sensitivity of mass transfer-based evaporation equations to errors in daily and monthly input data", *Hydrological Processes* 11: 1465–1473, 1997b.
[32] W. Brutsaert, "Evaporation into the Atmosphere", D. Reidel: Dordrecht, 1982.
[33] W. J. Shuttleworth, "Evaporation from Amazonian rainforest, proceeding of the Royal society of London", Series B. *Biological sciences*, 233 (1272): 321-346, 1988.

Figure 1 Junagadh Region of Gujarat State

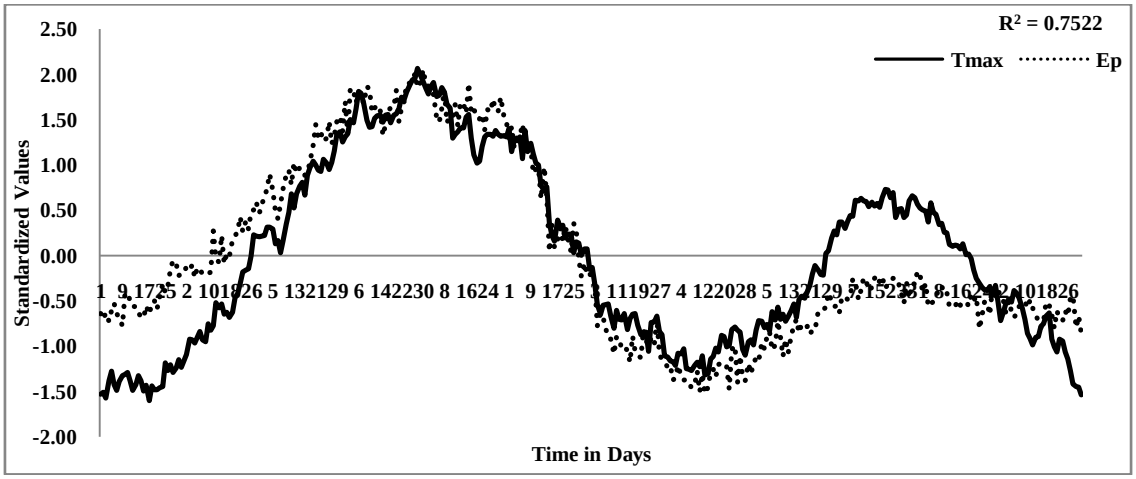

Figure 2 Dependence of E_p on T_{max} at Daily time-scale

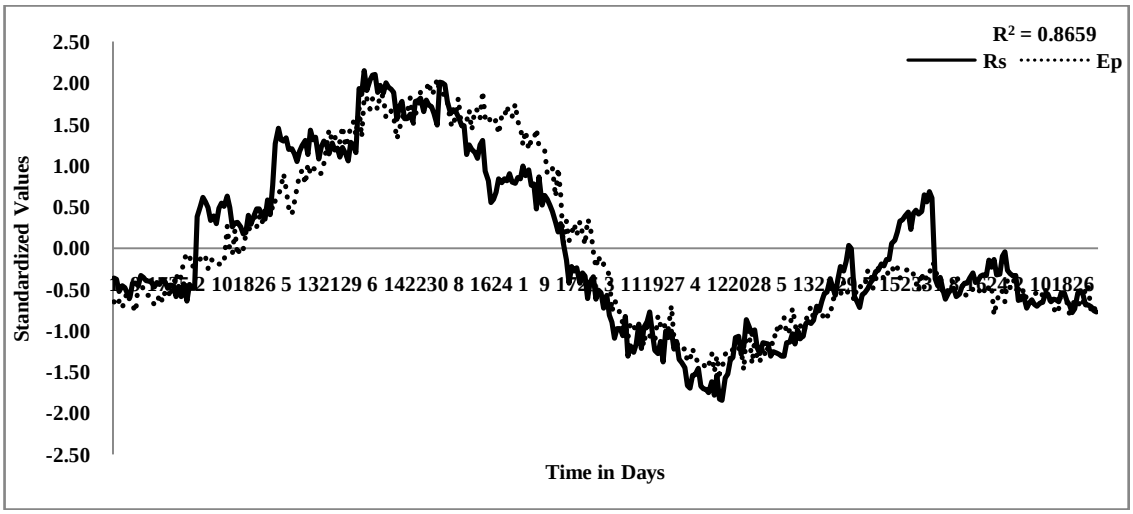

Figure 3 Dependence of E_p on R_s at Daily time-scale

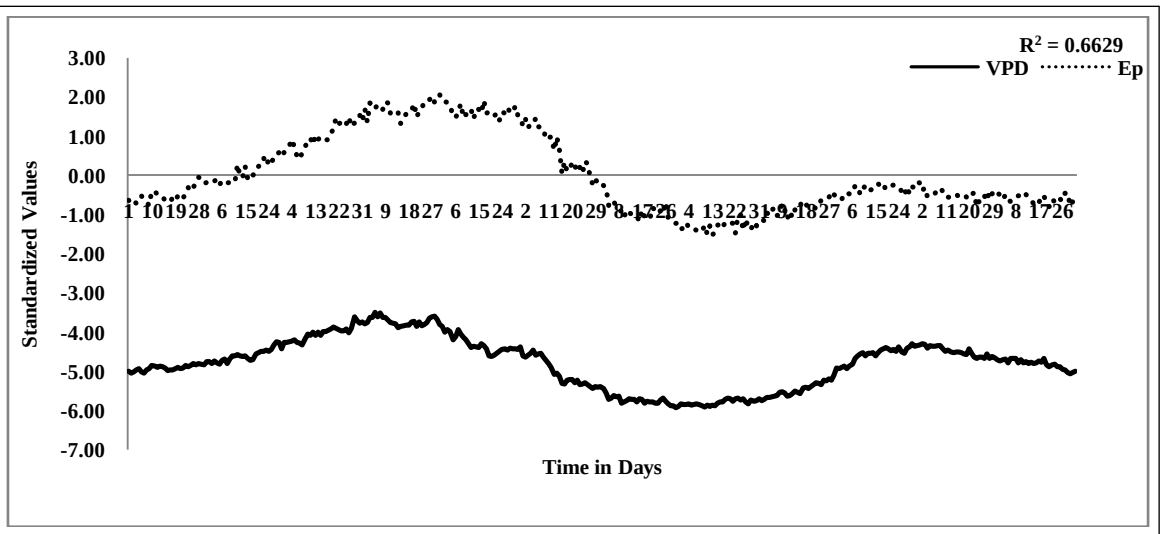

Figure 4 Dependence of E_p on VPD at Daily time-scale

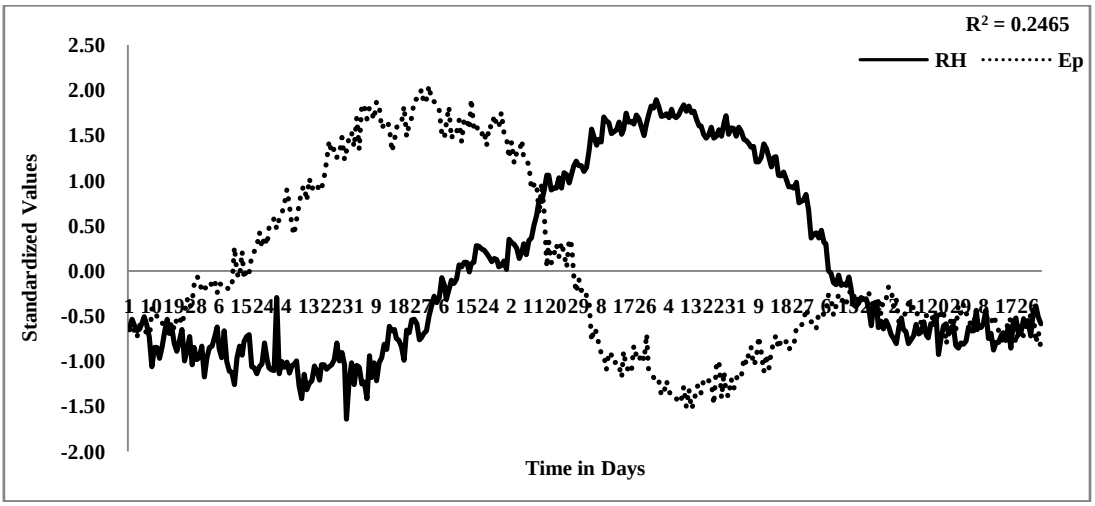

Figure 5 Dependence of E_p on RH at Daily time-scale

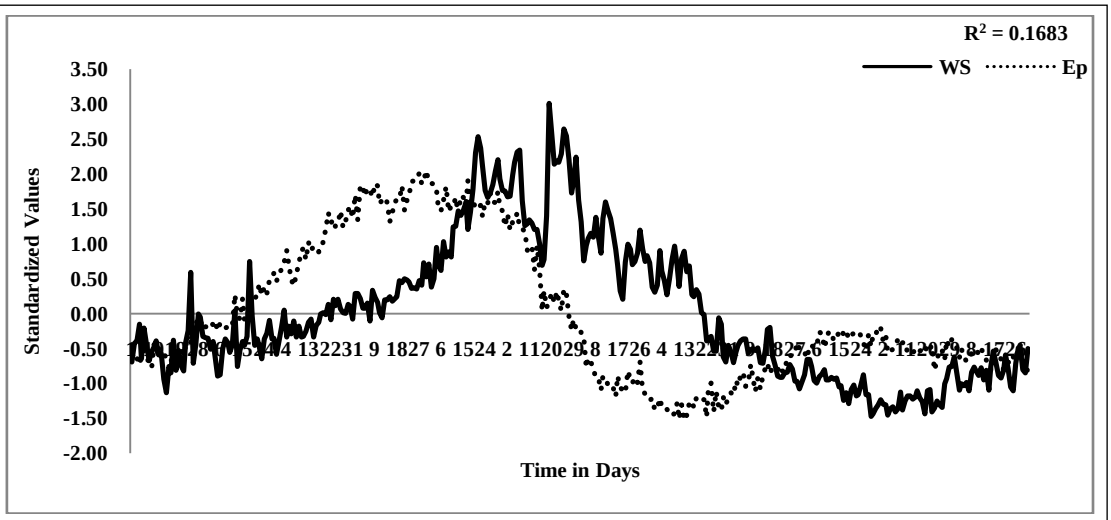

Figure 6 Dependence of E_p on WS at Daily time-scale

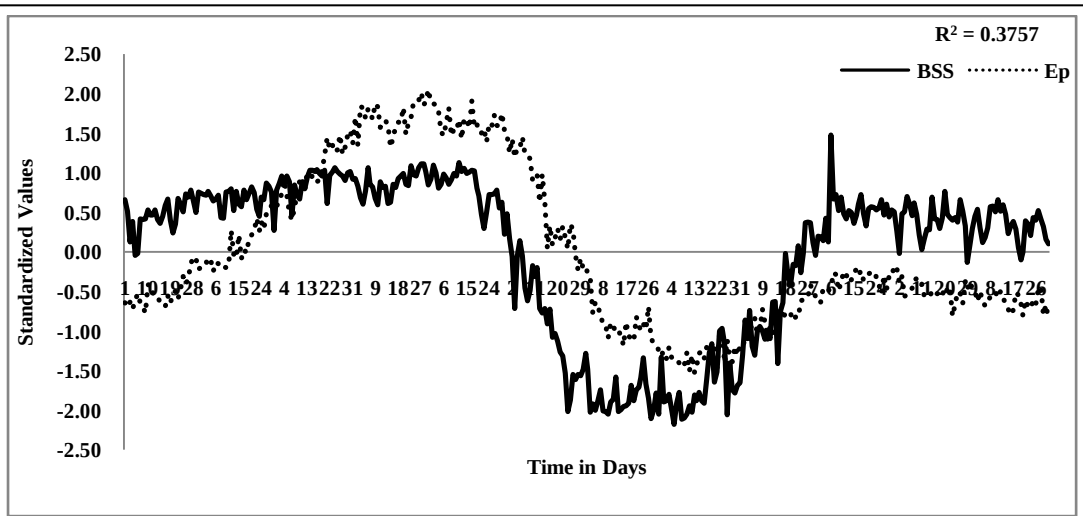

Figure 7 Dependence of E_p on BSS at Daily time-scale

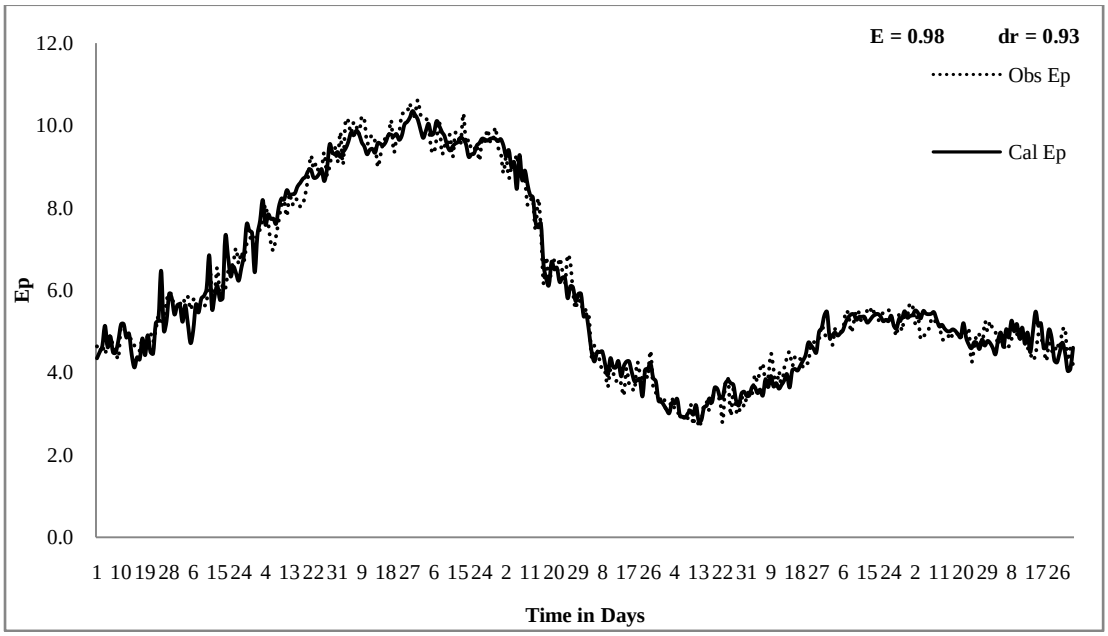

Figure 8 Performance of fitted equations for annual basis

Table 1. Equations and Climatological data requirements of selected methods for calculation of evaporation

Method	Reference	Equation	Climatological data requirements
Radiation	Jensen and Haise (1963)	$PE = (0.14\,T_a - 0.37)R_s$	Solar radiation and Temperature
Temperature	Linacre (1977)	$ET = \frac{\frac{500\,T_m}{(100-L)} + 15(T_a - T_d)}{(80 - T_a)}$	Temperature
Mass transfer	Penman (1948)	$ET = 0.35(1 + 0.24\,u_2)(e_s - e_o)$	Wind speed and vapour pressure
Humidity	Romanenko (1961)	$PE = 0.0018\,(25 + T_a)^2(100 - RH)$	Temperature and humidity

T_a = Air temperature in ^{0}C, R_s = Solar radiation in MJ/m^2/day, RH = Relative humidity in %, u_2 = Wind speed at 2 m height in m/s, e_s and e_o = Saturation and actual vapour pressure in mb, $T_m = (T_a + 0.006h)$, h = the elevation (m), L = the latitude (degree), T_d = Mean dew point, T_m and T_d are in ^{0}C, PE = Potential evaporation (mm) and ET = Free water evaporation (mm)

Table 2. Mean seasonal and annual estimated evaporation using selected methods for Junagadh region

Sr. No.	Season	Obs E_p mm	Jensen and Haise			Linacre			Penman			Romanenko		
			Cal E_p mm	E	d_r	Cal E_p mm	E	d_r	Cal E_p mm	E	d_r	Cal E_p mm	E	d_r
1	Winter	501.24	501.32	0.83	0.80	503.40	0.73	0.74	499.54	0.82	0.81	503.43	0.71	0.74
2	Summer	849.63	848.68	0.72	0.71	850.25	0.80	0.76	847.59	0.66	0.69	836.51	-2.13	0.01
3	Monsoon	547.28	547.09	0.96	0.90	550.97	0.83	0.79	489.52	0.58	0.65	538.52	0.82	0.79
4	Post-Monsoon	323.34	321.25	-1.04	0.32	322.95	0.18	0.57	322.46	-0.19	0.47	321.61	-1.26	0.26
5	Annual	2221.49	2262.21	0.78	0.76	2271.35	0.71	0.73	2112.80	0.85	0.83	2155.2	0.52	0.65

Table 3. Original and Optimised Parameter values of selected methods before and after calibration

	Jensen and Haise		Linacre		Penman	Romanenko
Original Values →	0.14	0.37	500	15	0.35	0.0018
Season	Optimised Values ↓					
Winter	0.0777	0.0000	196.8945	18.2719	0.1293	0.0013
Summer	0.0831	0.1493	975.3827	5.4454	0.1203	0.0018
Monsoon	0.2478	5.5146	232.5008	34.8545	0.1504	0.0022
Post-Monsoon	0.0606	0.0000	475.3079	8.5453	0.1263	0.0012
Annual	0.0735	0.0890	522.2668	13.3739	0.0016	0.0016

American Journal of Engineering Research (AJER)
e-ISSN : 2320-0847 p-ISSN : 2320-0936
Volume-02, Issue-10, pp-363-368
www.ajer.org

Research Paper Open Access

Haulage Vehicle Traffic and Runoff Effect on Gully Growth on Roadside Slopes of Unpaved Sand-Quarry Road, Uyo.

Obot Ekpo Essien*, Okon W. Emmanuel**
*Department of Agricultural and Food Engineering, University of Nigeria, P. O. Box 4309, Uniuyo Post Office, Uyo, Nigeria. Postal Code 520003.**
*Graduate, Department of Agric. and Food Engineering, University of Uyo, P.O.Box 1014, Uyo, Nigeria. ***

Abstract: - Rainfall runoff and sand haulage truck traffic count were quantified and regressed on gully soil loss and gully morphometric volume growth on unpaved haulage roadside erosion. The gully erosion on unpaved roadside was accelerated by the agency of runoff in splash wash from the road, and high axle sand haulage trucks traffic. The effect of the Runoff discharge and traffic count, as independent variables and cumulative quantities, on the cumulative soil loss from jagged side slope gullies, and the gully volume growth were very significant at $P < 0.01$ generally. Predictive coefficient of determination, significant at $P < 0.01$, were very perfect at R^2 = 88.8 to 98.9%. Different regimes of association were obtained such as: high runoff and high traffic count; high flow rate and low traffic count, and low runoff and high traffic count for effect ~~and~~ on gully loss and gully volume growth, and they gave accurate and significant relationship. Regulation of sand-mining over a catchment is recommended as it has otherwise destroyed landform and initiated unrestrained gullying.

Keywords: *- Sand haulage road, sand quarry, unpaved roadside/mechanized soil excavation, runoff, truck traffic count, gully soil loss, gully volume growth.*

I. INTRODUCTION

Destructive land use leads to land degradation and structural inability. One destructive landuse is an unplanned and unregulated sand mining that leads to gully initiation and growth. This is the case at Uyo peri-urban where the whole subcatchment is quarried daily for laterite sand used for the extensive construction and building projects in the urbanization expansion of the Uyo state capital, and some contiguous communities in the rural-urban fringe. The process of sand quarrying in the study area uses different stages of mechanization. Generally the land is cut into clods of sand heaped out before scooping with human labor into haulage trucks.

Soil surface vegetal cover and fallows and farms have been removed, and soil has been cut down to the sublayer for laterite; leaving jagged undulations of localized depressions for sedimentation or ponding of water. The haulage road was built up with the burrowed soil from the sand mine land to a height above the land mined fields, resulting in steep sides slopes of the road, which also is cleared of vegetal cover and top soil, so that no filtering strips was available to wedge runoff from the sides. The roadside slope is steep with no tuft or weed or runoff collecting drains to reduce runoff cascades down the side slope.

Usually there is some kind of erosion taking place along the roadside [1], especially where road was constructed by cut and fill method. Under rainfall characteristic and increase in slope length, soil erosion increases on roadside [2]. The process of gully erosion on the roadside of unpaved haulage road on the sand quarried landform involves the rainfall, the runoff, soil particle distribution and human factor – the high axle haulage truck traffic; however only the effect of runoff and truck traffic count are considered in the study, since rainfall and soil particles were considered in previous study [3].

When trucks of loaded laterite move up and down the haulage road, the loaded trucks tires cause abrasion of the wet or dry soil surface, dislodging particles, digging out ditches across the crown and eventually splash-washing the sediments laden water on traffic tyre impact to the roadsides, so that it flows down the road side slope. It causes levees at first, then the levees are broken by runoff wash off and rainfall impact [4]. Rills are created on the road crown across to the road side. Further runoff downstream finds the micro channels as easy drainage routes for flow rivulet to the sides. Steady rills are formed as weak parts of sediment on side

slopes break up, and, eventually, these grow bigger into gully and the growth rate of the gullies need to be determined as the degradation continues especially in the rainy season.

Roadside erosion could have been checked if tufting, sodding, pitching (agronomic method) or erection of retaining wall or bench terracing (permanent structure) of slope of filled road took place [1]. As the weed cover was removed during land mining and the road was unpaved and the side slope untamped and higher above the quarried land surface, a check in erosion, gully initiation and growth was hardly possible as no authority took functional responsibility on haulage road for sand quarrying, which is a private financial responsibility in haulage business.

Thus, ~~is~~ the causative factors are anthropogenic degradation of landform through erosion agencies of rainfall-runoff, splash wash and traffic abrasion. The objectives of these research aims to quantify these factors and correlate them with gully growth and soil loss for erosion control check in such vulnerable land use areas.

II. MATERIALS AND METHODS

2.1 Measurement of runoff discharge

A five-liter collector was used to fill a 20L container. A mouthpiece of metal plate was constructed and inserted on the scarp head of the gully and water flowed on it to the collector. The time taken to fill each 5L container was recorded using snap stop-watch. The total volume of container filled was divided by the total time taken, to give the discharge rate of runoff at respective gully line. Filling was so managed that no spillage was allowed. A fresh 5L – collector was waiting so as to change over and withdraw the filled sample collector without allowing it to brim nor overflow.

2.2 Determination of gully parameters

2.2.1 *Slope Length***.** The length of the main gully slope from the crest to the slope base on the road side slope was measured with a 30m linen tape and expressed in metres. Five measurements were made in each sampling location. The average value for each sampling area was computed.

2.2.2 ***Truck Traffic Count.***

A check point was mounted at the road entrance. The number of trucks entering and leaving the unpaved haulage routes were recorded, loaded or empty. A sentry was posted each day from 6am till 6pm.

2.3 Statistical Analysis

All data were organized into groups (see Results) and their description statistics, ANOVA, paired statistics, correlations and regression were carried out using SPSS software version 17.

III. RESULTS

The results are tabulated in tables below. Runoff discharge (RO) and Traffic count (TR) are independent variables.

Data collected were organized into three groups; namely:

(i) High traffic count (TR) and low runoff discharge (RO) and their combined effect on soil loss (SL) and on gully growth volume (both as dependent variables (Table 1).

(ii) High runoff discharge (RO) and low traffic count (TR) as independent variables and the recorded gully soil loss (SL) and on gully growth volume (GR) (Table 2);

(iii) High runoff discharge (RO) and high traffic count (TR) on gully soil loss (SL) and gully volume growth rate (GR) (Table 3).

The fourth and fifth groups are the mixed magnitudes of independent variables and the point values of each variable. These are too many to be presented here. Since the gully growth is additive geometric dimension or cumulative morphometric degradation over time, it is essential to relate the variables in cumulative values. Hence, the values in Tables 1 – 3 are presented as cumulative magnitudes of the variables.

Table 1. High traffic count and low runoff discharge effect on soil loss and gully volume growth rate.

S/N	High traffic count (TR)	Low runoff discharge (cumulative) (RO)	Soil loss (SL)
1.	18	1.1	4.25
2.	38	2.0	8.75
3.	90	2.7	12.13
4.	113	3.8	16.76
5.	135	4.4	19.21
6.	159	5.1	23.71
7.	189	5.9	27.21
8.	210	6.8	29.69
9.	245	7.4	32.69
10.	281	7.8	36.59
11.	304	8.6	40.07
12.	328	9.0	44.35
13.	348	9.8	47.70
14.	378	10.7	51.30
15	398	11.6	54.43
16.	435	12.3	58.23
17.	487	13.3	61.81
18.	532	14.1	64.69
19.	563	15.0	67.89
20.	617	16.0	71.44
21.	663	16.5	74.12
22.	699	17.8	76.70
23.	731	18.8	79.13
24.	781	19.6	81.88
25.	832	20.2	83.63
26.	872	20.9	88.26
27.	909	21.6	101.64
28.	937	22.2	106.39
29.	981	23.0	109.69
30.	1033	23.7	112.52
31.	1093	24.7	114.20
32.	1157	24.4	116.83

IV. DISCUSSION

4.1 Effect of gully growth

Gully growth is the cumulative dislodgement and transportation of soil particles from a location to a deposition at a distance. It is also erosive water effect which erosive water may not be constant in magnitude and force but vary in time and place. As such the infinitesimal or discrete change in morphometric dimension by successive current of erosive water (and or erosive rainfall) and abrasive tractive truck wheels (which grind the soil) enlarge or widen the gully geometry. By the cessation of the rains (i.e. erosive water current productive season), the resultant gully dimensional morphology is a cumulative geometric addition of the infinitesimal time dimensional increments.

Table 2. High runoff discharge and low traffic

High runoff discharge	Low truck traffic count	Soil loss	GV (Gully growth Volume)
40.7	1839	143.37	1,295,123
41.8	1867	148.14	1,375,917
42.5	1900	150.59	1,430,777
43.8	1944	158.59	1,584,954
48.3	2128	171.67	1,921,439
48.7	2154	175.95	2,031,056
47.5	2173	179.3	2,121,979
48.4	2201	182.9	2,259,261
49.4	2233	186.03	2,316,669
53.4	2432	203.04	3,003,833

Table 3. High amplitude regime

High runoff discharge (Cum RO)	High traffic count (CUM TR)	Soil loss CUM SL	Gully growth Volume (CU GV)
40.7	1839	143.37	1,295,123
41.8	1867	148.14	1,375,917
42.5	1900	150.59	1,430,777
43.8	1944	158.59	1,584,954
48.3	2128	171.67	1,921,439
48.7	2154	175.95	2,031,056
47.5	2173	179.3	2,121,979
48.4	2201	182.9	2,259,261
49.4	2233	186.03	2,316,669
53.4	2432	203.04	3,003,833
56.1	2567	211.7	3,236,993
55.3	2529	209.3	3,130,949
54.3	2475	206.7	3,003,833

N/B. Cum RO = Cumulative runoff discharge, cum TR – Cumulative vehicular traffic count, cum SL = Cumulative soil loss, Cum GR = Cumulative gully growth volume (cm^3)

$$\therefore Gully\ volume = \int_t (L + dt)(w + dw)(D + dd)dt$$

Where n is number of infinitesimal dimensional changes in the period (t) of the season. Thus, the ultimate gully geometry $[L.W.D]$.
= cumulative sum of changes in gully dimension in time interval dt under cumulative runoff, etc.

Tables 1-3 indicate the cumulative changes (continuous) of the four parameters (RO, TR, SL, GR) occurring within the rainy season. The values reflect the background of prior sand-mining of the road banks and filling of road with subsoils from the sand-quarried subcatchment.

The main difference in the groups is combining soil erosion factors.

4.1.1 Regression Relationship (soil loss).

1. High traffic count is a scene occurring under dry earth routes. Runoff is a scene under the threshold period of rainfall and dry season.

The effect of both Cum, RO and Cum.TR on soil loss was tested with a regression relationship, which gave:

$$Cum\ SL = 1.328 - 0.059 cum\ RO + 4.606 cum\ TR + 3.537\ @\ R^2 = 99.0\%, adj\ R^2 = 98.9\%.$$

Where estimated standard error of estimate is the constant 3.5375. (1)

The ANOVA indicated significant change at $P < 0.01$. The R^2 showed significant association of predictors to dependent variable (cum SL) @ $P < 0.01$. The coefficient of TR was also significant in predicting at $P < 0.01$ using t-statistics. The coefficient of the constant and RO were not significant, hence the error in estimation.

2.Case of high runoff and low traffic count (Table 2). This scene is usually observed under high rainfall amount in the months of July to October, which condition also reduces the traffic flow of haulage truck, even as constructive and building activities tend to subside.

The regression function relating their regime effect and gully soil loss was obtained as:

Cum SL = 2.479 cumRO – 0.060cumTR – 94.096 + 4.030 (2)
@ R^2 = 88.8%, adj R^2 = 85.6%.

Regression coefficient showed significant association @ $P < 0.01$ and significant difference of variance ($P < 0.01$) also.

ANOVA showed that the null hypothesis of variance homogeneity (of cum RO and cum TR) can be rejected at P<0.01 [5].
The coefficients for cumRO and cumTR showed significance at P<0.01

3. Case of high runoff discharge and high traffic count. This scene is usually in the post August break period with high intensity rainfall lasting for long hours (2 ½ -6 hours, [6]). The cumulative variable in regression relationship gave a predictive function as:

Cum SL = 2.348cum RO +0.143cum TR – 89.422 + 2.581. (3)
@ R^2 = 98.8%, adjusted R^2 = 97.3%, which were significant at P<0.01. ANOVA showed insignificance at P<0.01 indicating no homogeneity of variance; hence the variable variance were significantly different at P<0.01.
The accuracy of the relationship was significantly high @ P<0.01.

In general, using the cumulative criterion, the accuracy of the predictive association between the predictors (cumRO and cumTR) and the criterion (dependent) variable (cumSL) was very high and significant at P< 0.01.

4.1.2 Regression Relationship (Gully volume growth)
The gully volume growth (cum GR) is another criterion variable that depends on the predictor variables (cum RO, cum TR). Specific regimes were observed.

1. Case of high traffic count and low runoff.
   The effect of cumulative high traffic count (cum TR) and cumulative low runoff (cum RO) was established as:
   cum GR = 2140cumTR – 44940.50cumRO – 397276.450 – 3.2097E5 (4)
   @ R^2 = 89.9%, adj R^2 = 89.5% at P<0.01. ANOVA shows criterion variable and predictors have accurate association significant at P<0.01. The coefficient of the constant and cum TR were significant at P<0.01 and 0.1 respectively.
2. Case of high runoff and high traffic counts.
   The predictive association was obtained as:
   cumGR = 2636997.624cumRO – 56477.606cumTR – 450688.340 + 2.10891E6 (5)
   @ R^2 = 92.2%

The dependence of criteria variable (GR) on the predictors were 92.2% accurate. Only 7.8% of estimate could be said to depend on any other factor. There was a significant difference in the variable variances. The coefficients of the constant and predictors were, however, not significant at P<0.05.
The coefficients of the constant and predictors were, however, not significant at P<0.05.

3. The case of high runoff discharged and low traffic count.
   The predictive association was obtained as:
   cumGR = 4432.175cumTR – 79546.954cumRO – 3629338.062 + 61695.863 (6)
   @ R^2 = 99.0%; Adj R^2 = 98.7%

ANOVA: The F-ratio shows that we can reject the null hypothesis of the homogeneity of variances of cumRO and cumTR at P<0.01.

Also, the contribution of the constant, and the coefficients of cumRO and cumTR were significant at P<0.01, P = 0.05 and P<0.01 respectively.

V. CONCLUSION

Sand mining land use caused the onsite removal of soil vegetative cover and topsoil to the sublayer depths at a peri-urban sub catchment in Uyo for construction and building projects in adjoining areas. The unplanned and unregulated activity exposed the area and the unpaved haulage road to water and truck traffic erosion.
The gully erosion on unpaved roadside was accelerated by the agency of runoff in splash wash from the road, and high axle sand haulage trucks traffic.

The effect of the Runoff discharge and traffic count, as independent variables and in cumulative quantities, on the cumulative soil loss from jagged side slope gullies, and the gully volume growth were very significant at P<0.01 generally. Predicative coefficient of determination significant at P<0.01, were very perfect at R^2 = 88.8 to 98.9%. Different regimes of association were obtained such as: high runoff and high traffic count; high flow rate and low traffic count, and low runoff and high traffic count for effect and on gully loss and gully volume growth, and they gave accurate and significant relationship.

The case of using mixed magnitudes and point values of variables however, did not show accuracy and significance at R^2 = 12.4%. The growth of gully and its soil loss is really a cumulative addition of geometric changes over time in a given rainy season.

Regulation of sand-mining over a catchment is recommended as it has otherwise destroyed landform and initiated unrestrained gullying.

REFERENCES

[1]. Michael, M. A. and Ojha, T. P. (2006). Principles of Agricultural Engineering, Volume II. Jain Brothers, New Delhi 110005, 603-613.
[2]. Xu, X. L., Lin, W., Kong, V. P, Zhang, K. L, Yin, Bu and Chen, J. D. (2009). Runoff and water erosion on road sides: Effect of rainfall characteristics and slope length. Transportation Research Part D: Transportation and Environment, 14(7), 497 – 501.
[3]. Essien O. E., Okon, E. G. (2011). Rainfall characteristics, runoff rate and traffic flow on gully morphometric parameter growth and soil loss in sand-ruined peri-urban, Uyo, Nigeria. Journal of Geology and Mining Research, 3(7), 180 - 187.
[4]. Suresh, R. (2006). Soil and water conservation Engineering. Standard Publishers Distributors. Delhi 110 006. pp 404 – 522.
[5]. Ofo, J. E. (2001). Research methods and statistics, JOJA Educational Research and Publishers Ltd, Ikeja, Lagos, ISBN 978-2477-58-6, 311.
[6]. AKADEP (1995). Northern Akwa Ibom Swamps Development Study, Akwa Ibom Agricultural Development Project, Ministry of Agriculture and Natural Resources, Uyo, Nigeria

American Journal of Engineering Research (AJER)
e-ISSN: 2320-0847 p-ISSN : 2320-0936
Volume-02, Issue-10, pp-369-377
www.ajer.org

Research Paper Open Access

Estimating Time Loss Effects On Municipal Solid Waste Collection Using Haul Container System In Uyo Nigeria

Obot E. Essien[1], and J. C. Udo[2]
[1]*Department of Agricultural and Food Engineering, University of Uyo, Uyo, P.O. Box 1014, Uyo, Nigeria. Postal Code 52001.*
[2]*GIS Section, Department of Geography and Regional Studies, University of Uyo, Uyo, Nigeria.*

Abstract: - Time loss in time and motion study of the collection of municipal solid waste in Uyo metropolis was observed to affect the round-trip time, the solid waste generation rate and the collection efficiency of the haul container system of solid waste management, and hence needed information to drive control or reduction in the service. The result showed that its effects depended on the truck, route zone and operators skill in maneuvering the routes to reduce the dead ends and waste hours. Seven components of time losses with values ranging from 7 to 40 minutes per trip were measured, giving valuable total times loss per service truck per day as 2.0 hr for zones 2, 3 and 6, and 1.95hr for zone 4. The time loss for collection efficiency showed significant difference (P = 0.05) between zones and trucks, and varied as 19%, 20%, 7% and 30% for trucks 046, 053, 060 and 072 used in zones 03, 02, 04 and 06 respectively. Trucks for zones 05 and 01 were invalid. The available time was thus reduced. With average cycle time of 17.30 min to 24.21 min per trip, such loss time, in turn, reduced collection efficiency by 20 to 25% per truck thereby reducing the total trips and daily turnover. Recommendations include micro-routing principles, operators' motivation with team spirit and avoidance of observed start-up delays. Also route re-design of more dense zones and sparsely populated zones are recommended in order to bring trip time to near equality.

Key words: *- Time allowance, time loss, solid waste collection, municipal solid waste, collection efficiency, round trip time, route zones.*

I. INTRODUCTION

Efficiency of municipal solid waste collection is a time function of cycle time and loss time in an operation day. In solid waste collection operation of conventional haul-container system, one loop round trips or cycle time comprises the time spent on/or appropriated for lifting of one container load of generated solid wastes at a container station to the disposal site and return with an empty or used container to the waste generation site (i.e. pick-up station), then moving to the next station to repeat the same time-based set of motion and spot actions (activities) [1, 2].

Therefore in a nominal working day of fixed work period, the number of travel loops or cycle times completed within the work period is predicated on the deficiency factor or time allowance that quantitatively reduces the proportion of a working day available for the maximum travel cycles attainable. Thus a certain number of cycles of solid wastes collection, transportation and disposal is only optimum when the deficiency factor tends to zero. When repetitive work cycles or sequence of repeated work phases of short to long duration are involved, useless time consumption are studied and eliminated [3, 4]. The optimization of productive collection hour by deficiency factor tending to zero is what the evaluation and standardization of repetitive job standard cycle time evaluated aims at [4]; and this is applicable to collection operation of Haul Container System (HCS) since the method is not changing but repeated.

The time available for optimal cycles when deficiency factor tends to zero is a full working day. But as the deficiency factor (or loss time) is not zero where work is executed, then the maximum total cycles of waste collection to disposal per working day is diminished by total time allowance, or is subject to the total available cycle time which is the work period less the total time allowance [5], i.e.

Total available cycle	=	Total work period	-	Total time allowances	(1)

Hence, efficiency of solid waste collection service, which is the total available cycle time per work period, and, as such, is a productivity coefficient, is factored by the time allowance (time loss) in a daily solid waste collection, transport and disposal activities cycles.
Hence, from Equation 1, time-based solid waste collection efficiency is

Optimal Efficiency	=	$1 - \frac{Total\ Time\ Allowance}{Total\ Work\ period}$	(2)

Time allowance comprises different deficiency occurrences involving machine worthiness, environmental factors causing travel interruptions and delays, and human operators' factors (skill, integrity, diligence, fitness). These are not fixed values, hence their combination imposes unpredictable effect on the availability of time for actual solid waste collection service, which affects adversely collection efficiency under conventional haul-container system (HCS) of solid waste management, or any travel management system for that matter.

Efficiency means getting more for less: picking more solid wastes or recyclables using fewer trucks, fewer people or less time [6]. The implication of loss time is that it would need extension of time (working day) to collect the nominal quantity of waste or attain the nominal cycles of waste collection than could be achieved without occurrence of loss time or when loss time is negligible. Such extension of working day in the circumstance of waste collection would be counter-purpose to implied collection efficiency and haul container system management, and should not be contemplated upon. Since the primary aim of HCS is ensuring efficient collection by removal of generated garbage and other solid wastes from the community or locality to ensure elimination of environmental contamination and protect environmental aesthetics and public health in a less-costly operation, the uncertainty of time loss might make the realization of their aim and efficiency elusive. Hence, the rising need to investigate and quantify these impacts of loss time in the present system of haul container solid waste management in the metropolis since no standard data is available for any such service evaluation and improvement in order to benefit the environmental sanitation and public health, and work standardization [4].
Therefore, the time study objectives were to:

1. Measure the time loss in solid waste collection of HCS in the urban collection metropolis and
2. Evaluate the time loss impact on collection service capacity and efficiency, and
3. Ascertain prospects of improvement.

II. MATERIALS AND METHODS

Work measurement techniques was used. It consists of careful time measurement of the task with a time measurement instrument for a comprehensive time loss study. The time study, according to good practice guidelines for productive studies comprised, in addition to good setting, experimental design, time data collection, data analysis and discussion [7, 8].

1.1 Experimental Design: Time Study area.

The study was done in Uyo metropolis, the urban area of Akwa Ibom State capital territory, Nigeria. The expanding urban-rural fringe are not comprehensively addressed presently. Four (4) route zones out of the six (6) presently operating were plied. The other two route zones had certain un-cleared handicaps. One truck was assigned to each route zone per day. The process was to take a truck on a route zone to a municipal waste generating station, load off the solid waste into a container and haul it to a dumpsite; empty and hitch back an empty container to the generator location before moving to the next station to repeat the same set of component activities in the collection process. Thus, the task involves a repetitive set of activities of short or long duration with time losses in between them. These are to be measured and effects evaluated. For commonness purpose, timings for the first five trips were measured and used for time loss analysis. From here, projection for the number of trips per day was made and used for efficiency analysis. The initial five trips timing was replicated for 5 days to minimize or eliminate human error of visual observation of instrument dial.

1.2 Time data collection

Time and motion data were captured with an electronic stop-watch using the continuous stop-watch reading method [5, 8]. In the continuous method, the stop watch was allowed to tick continuously and at the end of each element of operation (motion or activity) reading of the stop watch was made and recorded in a time study register. The time required for each particular element of the operation, the previous reading (i.e. before

stepping into that activity) was subtracted from the next reading (i.e. reading at point of stepping out of that activity).

Set out rates
The set out capacity for each truck was the haul container heaped up or closed – cover volume, which was made up as follows;
Volume = length x width x height + ridged cover = $4.063m^3$

2.3 Evaluation of conventional HCS systems [8].
The round trip or cycle time for HCS collection of solid waste to disposal comprises the following in chronological order:
t_{pc} = time to pick up loaded or community bin of solid waste at first container Station
t_{h1} = time to haul loaded container from container station to disposal site
t_{ss} = time spent at disposal site (unloading waste container and re-attaching empty container)
t_{h2} = time spent returning empty container from disposal site back to some container station.
t_{uc} = time to un-mount empty container back at same container station
t_{dbl} = time to drive between container locations.

Therefore cycle or round trip time is

$$T_{cycle} = t_{pc} + t_{hi} + t_{ss} + t_{h2} + t_{uc} + t_{dbl} \quad (3)$$

III. EVALUATION OF TIME ALLOWANCE

The possible time losses encountered in a cycle of solid waste collection are as follows (IIE ANSI, 1982).
D_t = dispatch delay caused by sudden truck break down (maintenance factor time). This is incorporated in dispatch time, ti
D_b = extended break time by drivers to recover from fatigue (human factor time)
D_u = hold up along major (transit) roads (interruption time)
D_d = unnecessary delays (e.g. time for source sorting or scooping spilt waste at community bin station into the container haulage to disposal site. (This was very common).
D_v = delay in load evacuation, caused by insufficient trucks required to replace loaded container at disposal site
D_q = delay (or queuing time) enroute the narrow lane to dumpsite.
Unit of time was minutes. Then the loss times was

$$\text{Time Allowance} = D_b + D_d + D_l + D_q + D_u + D_v \quad (4)$$

2.4 Evaluation of efficiency
Collection efficiency (Ec) or service productivity (Cp) was computed as

Service productivity or productive hour Cp [5] is

$$Cp = \frac{\text{Total available cycle time, min/day}}{\text{Number of hours (or work period), hours}} \quad (5)$$

Total available time or round trip time was obtained from measurement and using equation (3)

Collection efficiency (Ec) is given as in equation (1) in terms of time allowance factor,

$$Ec = 1 - \frac{\text{Total time allowance}}{\text{Total work period}} \quad (1)$$

Total work period was 8 hours and total time allowance was obtained from measurement and using equation (4)

2.5 Evaluation of generation rate
Generation rate

$$K = \frac{\text{Collection load}}{\text{Total Available Time}} \quad (6)$$

Or in terms of loss time , (Tl),

K = Daily waste collection load per truck (7)
Total work period – Time loss (Tl)

When K >1, more trucks are needed.

Rate of solid waste collection and disposal (Qe).

Rate of municipal solid waste evacuation or collection and disposal by a collection truck per day was computed as

Qe = Average weight of solid waste x Number of trips
Average Cycle Time (tnet) (8)

IV. RESULTS

The measured and computed values of cycle time and loss time were as tabulated below.

3.1 Travel (Cycle) Time

The component time-based activities were measured and their time values are as given in Table 1.

Table 1: Summary of cycle time per trip for HCS collection trucks

Truck	Day/Trip	1	2	3	4	5	Avg/Trip	Sd
46	Mon	24.6	21.2	24.6	18.8	24.3	22.7-	2.61
53		24.3	23.4	23.4	23.6	20.6	23.06	1.42
60		24.8	29.4	23	25.4	24.4	25.40	2.40
72		18	14.8	17.6	14.3	15.3	16.00	1.69
Ag/Trip/Truck		22.93	22.20	22.15	20.53	21.15	21.7	-
Sd		3.29	6.03	3.11	5.00	4.28	-	-
t								
46	Tue	29.4	24.3	29.4	13.1	21.2	23.48	6.78
53		29.4	24.3	29.4	13.1	21.2	23.48	6.78
60		29.4	23.4	23.3	27.1	17.5	24.14	4.52
72		19.3	16.3	17.2	16.4	15.4	16.92	1.48
Ag/Trip/Truck		26.88	22.08	24.83	17.43	18.83	22.01	-
Sd		5.05	3.87	5.84	6.63	2.87	-	-
t								
46	Wed	29.9	21.4	26.9	13.2	21.4	22.56	6.38
53		26.3	36.5	26.5	22.1	24.5	27.18	5.50
60		25.64	24.5	25	23.1	23.5	24.35	1.05
72		16.5	17.1	16.4	18.6	16.3	16.98	0.96
Ag/Trip/Truck		24.59	24.88	23.70	19.25	21.43	22.7	-
Sd		5.71	8.32	4.93	4.47	3.65	-	-
t								
46	Thur.	27.4	22.3	27.4	17.6	22.7	23.48	4.10
53		-	-	-	-	-	-	-
60		20.4	24.3	25.1	25.1	24.3	23.84	1.96
72		23.1	17.3	16.3	16	16.2	17.78	3.02
Ag/Trip/Truck		23.63	21.30	22.93	19.57	21.07	21.7	-
Sd		3.53	3.61	5.86	4.86	4.29	-	-
t								
46	Fri.	25.4	29.6	25.4	22.3	24.1	25.36	2.69
53		-	-	-	-	-	-	-
60		18.2	24.4	23.2	21.4	20.2	21.48	2.44
72		19.4	16	19.1	19.5	20.2	18.84	1.64
		21.00	23.33	22.57	21.07	21.50	21.9	-
		3.86	6.86	3.20	1.43	2.25	-	-
Ag/Trip/Truck		23.96	22.80	23.28	19.48	20.73	-	-
Sd		4.39	5.48	4.27	4.52	3.30	-	-
t								

Note: sd = standard deviation, t = t-statistics. Ag/Trip/Truck = average cycle time per trip per truck.

3.2 Time losses

The following time losses (Time allowance) per day were recorded for Truck 060 in zone 4 and other trucks in solid waste collection using symbols in equation 4, they are:

Table 2: Time losses during HCS Municipal Solid Waste Collection to Disposal at Uyo Metropolis

Time loss1(w)	Values,	(min),	(hr)
T_L for Truck 060:			
U_d	10		0.167
H_u	25		0.417
D_t	7		0.117
D_l	40		0.667
B_t	20		0.333
D_2	2		0.033
D_e	20		0.333
Total for Truck 060 (T_L)	117		1.95 hr
Daily 5 trips avg.			1.50 hr
T_L for Truck 053, zone 3			2.0 hr
T_L for Truck 046, zone 2			2.0 hr
T_L for Truck 072, zone 6			2.0 hr

NB: T_L is sum of component time losses (equation (4)).

3.3 The loss effect on collection efficiency.

The efficiency is affected by the total time loss given as

$$T_{loss} = T_L + T_t \quad (9)$$

Where T_L is in equation 4 (time loss in operation), and T_t is dispatch time considered time loss because it also reduces day's operation or start up time outside collection to disposal activities [1].

Time loss varied significantly (P = 0.05) between the zones and truck operations, being 19% for truck 046, 20% for 053, 7% for 060 and 30% for truck 072. The lowest time loss for truck 072 is in line with the truck being the fastest evacuator of solid waste with mean cycle time of 17.75min.

Table 3: Average cycle time, theoretical and actual number of daily trips, Ae

Truck	Average T_{net}	Theoretical N_t	Actual N_t	Production hour	Production efficiency, %
046	24	20	15	-	75
053	25	20	16	-	80
060	24	20	15	-	75
072	17	28	21	-	75

V. DISCUSSION

4.1 Analysis of t_{net} data shows the following

For the cycle time (or t_{net}), the t_{net} values between daily trips time for trips 1 to 5 showed no significant difference (@ P < 0.05) between the trips (trips 1 to 5) on each day for each truck. That means that the t_{net} for each trips was specific to the truck, hence no significant variability per truck travel time. This suggests that the operators are conversant with their zonal routes layout, to reduce unchecked time at obstructions in the usual routes they plied in individual zones, and can create confidence in selecting zonal routes mean t_{net} as standard cycle times for the zonal routes.

Thus, the standard cycle times for zonal routes were as shown in Table 1.

The variability of the cycle times between trucks within each day was also checked. The sum of squares of t_{net} between 4 trucks and within each day, as given by ANOVA, was grossly less than the sum of squares within the t_{net} of each day; hence no significant difference in t_{net} (at P = 0.05) except on Tuesday that the difference was significant at P = 0.1. The 4th trip on Tuesday was the smallest t_{net} compared to other days, and might have contributed to the significant variance within days.

However for all groups, i.e. between all trucks and within all days' $t_{net,}$ the between trucks sum of squares was one-sixth the sum of squares for within groups or mean square for between trucks was 3.241 times of mean square for within group, hence making the variance significant at P = 0.05. That means the overall t_{net} had significant standard deviations within its values for the number of trips, days and trucks, or the mean t_{net} values for each truck for all days were significantly (P = 0.05) different from each other. Thus, in the overall truck performance, operator's skill, route size and loss time significantly affected individual truck's cycle time.

4.2 Cycle Time, Time Loss and Available Time

The cycle times in Table 1 are average sum of the component activity times in the circuitous road haulage of containerized MSW from generation point (container location) to disposal site and return. The cycle time for truck 072 was the least (Table 2) although its zonal area was 2.25 km2 and 1.125 times the size of zone 03 for truck 046, and 2.25 times the size of zone 02 for truck 053 and zone 4 for truck 060. It could mean that, in overall, that truck 072 was very frugal with time or very fast. This may be a coupled effect of the operator's skill, machine worthiness, operator's knowledge and the use of route for easy maneuverability, and perhaps a strategy of firstly evacuating the many containers at close proximity to the disposal site, freer routes at the start of collection when operator is fresher and clear-headed, and ending up with few distant containers in the mid-morning or early afternoon day when service routes are less busy [10, 11]. If that strategy is worthwhile then it can be so researched and then routes re-design undertaken to equalize zonal cycle times as much as possible. Cycle time seemed to vary with the collection vehicle trip number and day of operation. The intent satisfies the rule of micro-routing that collection from heavily travelled streets should not be carried out during rush hours; also collection should start as close to the garage or motor pool as possible taking into account heavily travelled and one-way streets where it is best to start near the upstream end of the street working down it through the looping process [10] 11]. The intent is to minimize driving time on the collection route through minimizing the dead head distance [10, 11].

However, apart from truck 072, there was no significant difference (P =0.05) between them. The variation of overall average round trip (cycle time) per day was not significantly different (P = 0.05) from the average trip cycle per truck for each day (Table 1) but varied as follows:

For Monday: average trip cycle time per day =
Average trip cycle time per truck = (21.75 mins)
For Tuesday = 22.01 mins; (22 mins)
For Wednesday = 22.76mins (23 mins)
For Thursday = 21.70 mins (22 mins)
For Friday = 21.89 mins (22 mins)

Thus, the cycle time for solid waste collection trip varied with the day of operation and the operation truck.

The mean cycle time (t_{net}) for each was computed as:

Average t_{net} = $(\sum$ mean daily $t_{net})/ n_d$

where n_d is number of days.

Using data in Table 1, the mean cycle time (Avg t_{net}) for the trucks varied as follows:

For 046, Avg t_{net} = 23.52 mins
For 053, Avg t_{net} = 24.57 mins
For 060, Avg t_{net} = 23.84 mins
For 072, Avg t_{net} = 17.30 mins

Number of cycle trips per day

The theoretical maximum number of collection trips per day is

Theoretical N_t = working hours/t_{net}

For an 8-hour working period

Theoretical N_t = 8 hour x 60 mins/$t_{net.\ us.}$

Using the t_{net} values above (in Table 1), theoretical N_t for the trucks were as in Table 3) as follows:

For 046, it was 20 ~ 20
For 053, it was 19.5 ~ 20
For 060, it was 20 ~ 20
For 072, it was 27.7 ~ 28

3 trucks (046, 060 and 053) had about the same N_t. However, the difference between mean cycle time for 072 and each or all the others was significant. The order of magnitude for overall average cycle time (t_{net}) was (Table 1): 053 (24.21 mins) > 046 (23.50 mins) > (23.84mins) > 072 (17.30 mins).

Above results show that, when rounded up t_{net} for 046, 053 and 060 would be the same as 24 min (Table 1), and t_{net} for 072 would be 0.75 x t_{net} of each of the other 3 truck i.e. t_{net} (072) ~ 75% t_{net} (046) or (053) or (060).

Time loss, T_L cut across all route zones and trucks' operation time. On the average T_L was of the order of magnitude as in Table 2, which was T_L (053) = T_L (046) = T_L (072) = 2.0 hr > T_L (060) = 1.95 T_L. Using T_L (060) for example, Dl(extended lunch break for operator adjustment to fatigue was the highest time loss of 0.667 hrs. The order of component losses (w) were: $D_l > H_u > B_t = D_e > U_d > D_t > D_q$. This suggests more special package of incentive and counseling of the operator, who was the main causal agent for De time loss [6].

The ratio of total T_L to total cycle times T for each service truck in a day was:

$$\text{T – T Ratio} = (\text{Time loss/cycle daily time}) = \frac{\text{Total time loss, } T_L}{\text{Number of trips x tnet}}$$

This shows that there is inherent time loss of time allowance in all cycle times for MSW collection to disposal either operator mental and physical fitness or machine worthiness of and environment both of them [5].

For truck 046, T – T ratio was 10%
For truck 053, T – T ratio was 10%
For truck 060, T – T ratio was 9.85%
For truck 072, T – T ratio was 7%

4.3 Time loss and total available time actual cycle time per truck and actual no. of trips per day

Time allowance + normal time = standard time []. Therefore time allowance or time loss affect the available time.
Thus, available time = standard time –time allowance
For truck 046 total available time is 8.0 – 2.0 = 6.0 hr, giving total number of trips per day as:
For truck 046 N_t is 15
For truck 053 N_t is 16.118 is 16
For truck 060 N_t is 15.233 is 15
For truck 0.72 N_t is 20.81 or 21

4.4 Collection Efficiency

Efficiency was considered in two aspects both resulting from effect of time.
As productive hour (Banga et al 2004), efficiency, by definition, is

$$E_f = \frac{Actual\ N_t}{Theoretical\ N_t}$$

Using the theoretical and actual N_t (Table 3), Efficiency was computed as follows: for 046, E_f = 15/20 or 75%; for 060, 072, E_f = 75%; while for 052, E_f = 80%. By order of magnitude, efficiency for truck 052 (80%) > 046 = 060 = 072.

Thus, the efficiency reduction by the effect of loss time varied between 20 and 25% per truck.

4.5 Daily Generation (Collection)

The total weight of collected load was the sum of the weight of load for each trip for each truck for the whole day. The daily generation rate was estimated as the total collected waste at the generation stations in the zone. The results are as recorded in Table 4.

Table 4. Rate of daily collection (or generated) solid waste load in Uyo metropolis

Trip	Haulage truck			
	046	**053**	**060**	**072**
1	400.00	400.0	400.0	400.0
2	450.0	450.0	450.0	450.0
3	200.0	200.0	300.0	200.0
4	200.0	200.0	200.0	200.0
5	150.0	200.0	200.0	150.0
Total, kg/day	1400.0	1450.0	1600.0	1400.0
Area, km^2	2.0	1.0	1.0	2.3
Waste Collection or generation rate kg/hr	175.00	181.3	200.0	175.0
Collection or generation density $kg/km^2/day$	700.00	1450.0	1600.0	622.1
Avg. collection per trip, kg/trip	280	290	320	280

* 1 day was 8 nominal operation hours.

The rate of generated solid waste was obtained as the rate of solid waste collection per day where nominal day was 8 nominal operation hours.

From the Table (Table 4), the highest solid waste collection rate, hence the highest solid waste generation with a collection area of only 1.0 km^2, resulted also in the solid waste highest generation density of 1600.00kg/km^2.

The least rate was 175 kg/day by truck 072 from the widest collection area (2.23km^2) in zone 6. This gave the least density of 622.1 kg/km^2. Actually, 046 also had the least generation rate 175 kg/day from the next larger area (2.0 km^2), giving the next lower collection or generation density of 700kg/km^2.

The set out rate or waste load per trip varied between 280 and 320 kg/trip, coming from truck 060 in one of the smallest area. This is so because the trucks were the same, the container capacity was the same, and the number of trip was the same.

Table 5. Effect of time loss on daily collection rate

Truck	**Zone**	**Nominal collection rate, kg/day**	**Loss time w, hr.**	**Unexpected collection rate kg/day**	**Percentage difference (%)**
046	2	175.0	2.0	233.3	33.3
053	3	181.3	2.0	242.0	33.5
060	4	200.0	1.5	213.3	7.0
072	6	175.0	2.0	233.3	33.3
Av. Per truck/day		182.8		230.5	26.2

Therefore, the difference was likely attributable to the packing and how full the containers were, and the level of decomposition of the bottom content. If the waste at the bottom has started decomposing in the waiting days before collection day, then it will lose moisture and so lose weight.

Also, it could be seen in the table (Table 5) that collection rate for 060 truck was the highest (200 kg/day) amongst the trucks set-out loads except 053 which was similar and as such had the next high collection rate (185 kg/day). For the smallest collection area to produce the highest collection rate and load/trip, it means the area (Zone 4) is a high solid waste generation zone in the metropolis; followed by zone 3 with truck 053. The larger areas 2.0 and 2.25 kg/m^2 produced lower generation rate of solid waste with the same lowest collection rate (175 kg/day) and load/trip (280kg/trip).

Effect of time loss on solid waste collection rate

The generation or collection rate was affected by loss time. Table 5 shows generation rate by between 7.0% and 33.5% of the nominal collection rate. The difference was significant at P = .05. The impact was greatest at 33.5% on truck 053 in zone 3 with area of 1.0 km^2, and the percentage difference was least (7.0%) for truck 060 in Zone 4. The loss time seemed to have extended the period for extra wastes to be thrown into the container thereby increasing the set out rate. Also the loss time reduced effective operation hours, thereby minimizing the daily operation hours.

VI. CONCLUSION AND RECOMMENDATIONS

Time losses components were identified and measured using continuous and snapback electronic stopwatches in the solid waste collection cycle in Uyo metropolis. Time loss affected the short duration round trip time. Four route zones at one haulage truck per zone were used in time and motion study of municipal solid waste collection with haul container system, and the data were statistically analyzed using SPSS version 17.

Time loss effect was observed on the short cycle time, time allowance, daily generation rate and daily truck collection efficiency; it depended on truck or operator's skill, route zonal area and density of community bins as well as on the collection week day – as affected by both load generation, and traffic density on collection routes.

The seven (7) components of time losses, including delays and extra time on lunch break and recuperation from fatigue constituted variable total loss on collection trip, reducing time allowance, efficiency which significantly varied with truck zone and day of operation and daily generation load.

Recommendations include measurement of cycle time for future new collection systems, reduction of startup loss of time by adequate garage preparation; route zone re-design for round-trip equality, and training of operators on skills of route management.

REFERENCES

[1]. Sincero A. P. and Sincero G. A. (2006), "Environmental engineering, a design approach", Prentice Hall of India, 517 – 581.

[2] McCreanor Dr (2008), "Solid Waste Collection", 27 – 42. Available @ http://.Faculty.mercer.edu pt/evc420/les.

[3]. ILO (1982), "Technical papers 8 and 9", ILO International Labour Organization.

[4]. Salvendry G. (Ed.) (2001), Handbook of Industrial Engineering Technology and operation management", 2nd Ed., New York: John Wiley and Sons, Chap. 54, 1410 – 1457.

[5]. Sharma S. C; Banga T. R. and Agarwal N. K. (2004), "Industrial engineering and management science", Delhi – 110006: Khanna Publishers, 49 – 89.

[6]. US EPA (1999), "Getting more for less: Improving collection efficiency", US EPA, EPA 530 – R- 199 – 038.

[7]. Maganotti N. and Spinelli R. (2012), Good Practice guidelines for biomass production studies". COST Action FP-0902, WG 2 Operations, Research and Measurement Methodologies, 1-44.

[8]. Wikipedia (2012), "Time and Motion Study", Wikipedia, The Free Encyclopedia.

[9]. IIE ANS (1982), "Industrial Engineering Terminology: ANSI Z940 – 1982", an American National Standard, Institute of Industrial Engineers, 1 – 10.

[10]. EPA (1974), "Heuristic routing for solid waste collection vehicles", US Environmental Protection Agency, Publication No. SW – 113.

[11]. Robert Bob (2011), "Solid Waste Routing Improving Efficiency in Solid Waste Collection Part 3". Available at http://wp.mc/p11k50.

American Journal of Engineering Research (AJER)
e-ISSN : 2320-0847 p-ISSN : 2320-0936
Volume-02, Issue-10, pp-378-384
www.ajer.org

Research Paper Open Access

Modified Multilevel Inverter Topology for Grid Connected Pv Systems

Dhivya Balakrishnan, Dhamodharan Shanmugam, K.Indiradevi
[1]*M.E-PED, Department OF EEE, Sri Shakthi Institute of Engineering and Technology, Coimbatore, Tamilnadu. INDIA.*
[2]*M.E-PED, Department OF EEE, Sri Shakthi Institute of Engineering and Technology, Coimbatore, Tamilnadu. INDIA.*
[3]*Asst.Prof (S)/Department OF EEE, Sri Shakthi Institute of Engineering and Technology, Coimbatore, Tamilnadu. INDIA.*

Abstract: - Multilevel converters offer high power capability, associated with lower output harmonics and lower commutation losses. Their main disadvantage is their complexity, requiring a great number of power devices and passive components, and a rather complex control circuitry. This paper proposes a single-phase seven- level inverter for grid connected PV systems, with a novel pulse width-modulated (PWM) control scheme. Three reference signals that are identical to each other with an offset that is equivalent to the amplitude of the triangular carrier signal were used to generate the PWM signals. The inverter is capable of producing seven levels of output-voltage levels from the dc supply voltage. This paper proposes a new multilevel inverter topology using an H-bridge output stage with two bidirectional auxiliary switches. The new topology produces a significant reduction in the number of power devices and capacitors required to implement a multilevel output using the Asymmetric Cascade configuration.

Keywords: - *Asymmetric cascade configuration, H-Bridge, multilevel inverter, pulse width Modulation.*

I. INTRODUCTION

The ever-increasing energy consumption, fossil fuels' soaring costs and exhaustible nature, and worsening global environment have created a booming interest in renewable energy generation systems, one of which is photovoltaic. Such a system generates electricity by converting the Sun's energy directly into electricity. Photovoltaic-generated energy can be delivered to power system networks through grid-connected inverters. A single-phase grid-connected inverter is usually used for residential or low-power applications of power ranges that are less than 10 kW [1]. Types of single-phase grid-connected inverters have been investigated [2]. A common topology of this inverter is full-bridge three-level. The three-level inverter can satisfy specifications through its very high switching, but it could also unfortunately increase switching losses, acoustic noise, and level of interference to other equipment. Improving its output waveform reduces its harmonic content and, hence, also the size of the filter used and the level of electromagnetic interference (EMI) generated by the inverter's switching operation [3].

Multilevel inverters are promising; they have nearly sinusoidal output-voltage waveforms, output current with better harmonic profile, less stressing of electronic components owing to decreased voltages, switching losses that are lower than those of conventional two-level inverters, a smaller filter size, and lower EMI, all of which make them cheaper, lighter, and more compact [3], [4]. Various topologies for multilevel inverters have been proposed over the years. Common ones are diode-clamped [5]–[10], flying capacitor or multicell [11]– [17], cascaded H-bridge [18]–[24], and modified H-bridge multilevel [25]–[29].

This paper recounts the development of a novel modified H-bridge single-phase multilevel inverter that has two diode embedded bidirectional switches and a novel pulse width modulated (PWM) technique. The topology was applied to a grid-connected photovoltaic system with considerations for a maximum-power-point tracker (MPPT) and a current-control algorithm.

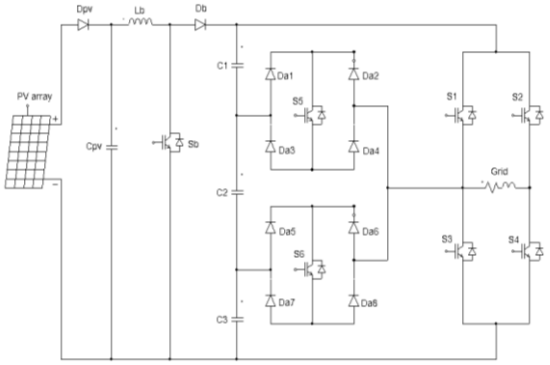

Fig. 1. Proposed single-phase seven-level grid-connected inverter for photovoltaic systems

II. PROPOSED SYSTEM

The proposed single-phase seven-level inverter was developed from the five-level inverter in [25]–[29]. It comprises a single-phase conventional H-bridge inverter, two bidirectional switches, and a capacitor voltage divider formed by $C1$, $C2$, and $C3$, as shown in Fig. 1. The modified H-bridge topology is significantly advantageous over other topologies, i.e., less power switch, power diodes, and less capacitor for inverters of the same number of levels. Photovoltaic (PV) arrays were connected to the inverter via a dc–dc boost converter. The power generated by the inverter is to be delivered to the power network, so the utility grid, rather than a load, was used. The dc–dc boost converter was required because the PV arrays had a voltage that was lower than the grid voltage. High dc bus voltages are necessary to ensure that power flows from the PV arrays to the grid. A filtering inductance Lf was used to filter the current injected into the grid. Proper switching of the inverter can produce seven output-voltage levels (Vdc, $2V$dc/3, Vdc/3, 0, $-V$dc, $-2V$dc/3, $-V$dc/3) from the dc supply voltage. The proposed inverter's operation can be divided into seven switching states, as shown in Fig. 2(a)–(g). Fig. 2(a), (d), and (g) shows a conventional inverter's operational states in sequence, while Fig. 2(b), (c), (e), and (f) shows additional states in the proposed inverter synthesizing one- and two-third levels of the dc-bus voltage. The required seven levels of output voltage were generated as follows.

1) Maximum positive output (Vdc): $S1$ is ON, connecting the load positive terminal to Vdc, and $S4$ is ON, connecting the load negative terminal to ground. All other controlled switches are OFF; the voltage applied to the load terminals is Vdc. Fig. 2(a) shows the current paths that are active at this stage.
2) 2) Two-third positive output ($2V$dc/3): The bidirectional switch $S5$ is ON, connecting the load positive terminal, and $S4$ is ON, connecting the load negative terminal to ground. All other controlled switches are OFF; the voltage applied to the load terminals is $2V$dc/3. Fig. 2(b) shows the current paths that are active at this stage.
3) One-third positive output (Vdc/3): The bidirectional switch $S6$ is ON, connecting the load positive terminal, and $S4$ is ON, connecting the load negative terminal to ground. All other controlled switches are OFF; the voltage applied to the load terminals is Vdc/3. Fig. 2(c) shows the current paths that are active at this stage.
4) Zero output: This level can be produced by two switching combinations; switches $S3$ and $S4$ are ON, or $S1$ and $S2$ are ON, and all other controlled switches are OFF; terminal ab is a short circuit, and the voltage applied to the load terminals is zero. Fig. 2(d) shows the current paths that are active at this stage.
5) One-third negative output ($-V$dc/3): The bidirectional switch $S5$ is ON, connecting the load positive terminal, and $S2$ is ON, connecting the load negative terminal to Vdc. All other controlled switches are OFF; the voltage applied to the load terminals is $-V$dc/3. Fig. 2(e) shows the current paths that are active at this stage.
6) Two-third negative output ($-2V$dc/3): The bidirectional switch $S6$ is ON, connecting the load positive terminal, and $S2$ is ON, connecting the load negative terminal to ground. All other controlled switches are OFF; the voltage applied to the load terminals is $-2V$dc/3. Fig. 2(f) shows the current paths that are active at this stage.
7) Maximum negative output ($-V$dc): $S2$ is ON, connecting the load negative terminal to Vdc, and $S3$ is ON, connecting the load positive terminal to ground. All other controlled switches are OFF; the voltage applied to the load terminals is $-V$dc. Fig. 2(g) shows the current paths that are active at this stage.

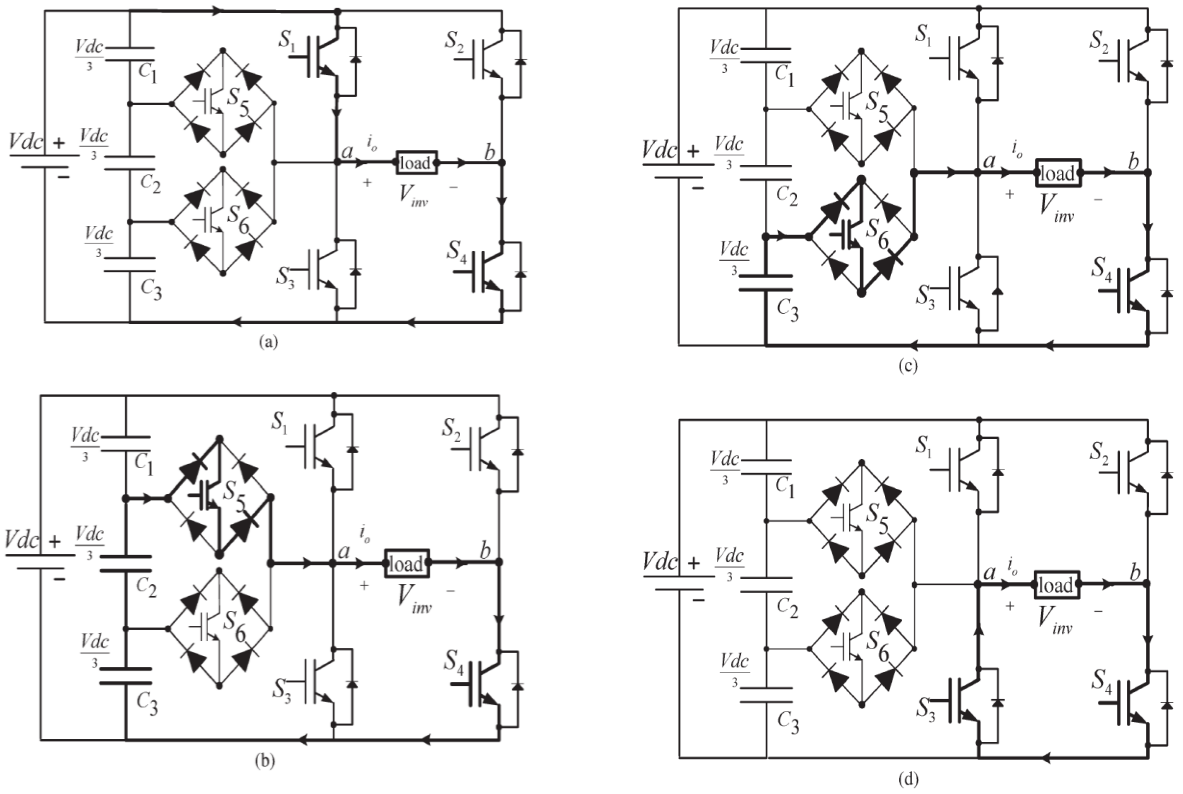

Fig. 2. Switching combination required to generate the output voltage (*V*ab). (a) *V*ab = *V*dc. (b) *V*ab = 2*V*dc/3. (c) *V*ab = *V*dc/3. (d) *Vab* = 0.

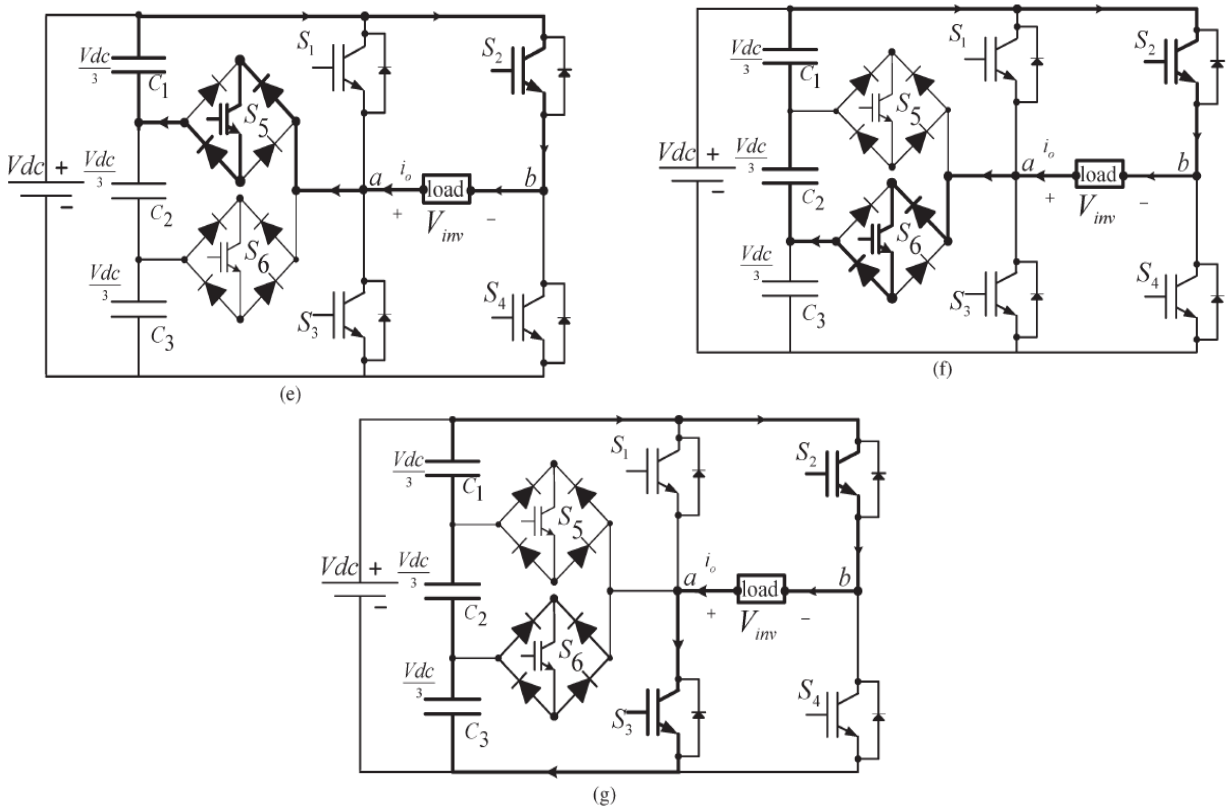

Fig. 2. (*Continued.*) Switching combination required to generate the output voltage (*V*ab). (e) *V*ab = −*V*dc/3. (f) *Vab* = −2*V*dc/3. (g) *V*ab = −*V*dc.

TABLE I: SWITCHING CONDITION

v_0	S_1	S_2	S_3	S_4	S_5	S_6
V_{dc}	on	off	off	on	off	off
$2V_{dc}/3$	off	off	off	on	on	off
$V_{dc}/3$	off	off	off	on	off	on
0	off	off	on	on	off	off
0*	on	on	off	off	off	off
$-V_{dc}/3$	off	on	off	off	on	off
$-2V_{dc}/3$	off	on	off	off	off	on
$-V_{dc}$	off	on	on	off	off	off

III. PWM MODULATION

A novel PWM modulation technique was introduced to generate the PWM switching signals. Three reference signals (*V*ref1, *V*ref2, and *V*ref3) were compared with a carrier signal (*Vcarrier*). The reference signals had the same frequency and amplitude and were in phase with an offset value that was equivalent to the amplitude of the carrier signal. The reference signals were each compared with the carrier signal. If *V*ref1 had exceeded the peak amplitude of *V*carrier, *V*ref2 was compared with *V*carrier until it had exceeded the peak amplitude of *V*carrier. Then, onward, *V*ref3 would take charge and would be compared with *V*carrier until it reached zero. Once *V*ref3 had reached zero, *V*ref2 would be compared until it reached zero. Then, onward, *V*ref1 would be compared with *V*carrier. Fig. 3 shows the resulting switching pattern. Switches *S*1, *S*3, *S*5, and *S*6 would be switching at the rate of the carrier signal frequency, whereas *S*2 and *S*4 would operate at a frequency that was equivalent to the fundamental frequency.

IV. CONTROL SYSTEM

The control system comprises a MPPT algorithm, a dc-bus voltage controller, reference-current generation, and a current controller. The two main tasks of the control system are maximization of the energy transferred from the PV arrays to the grid, and generation of a sinusoidal current with minimum harmonic distortion, also under the presence of grid voltage harmonics.

The proposed inverter utilizes the perturb-and-observe (P&O) algorithm for its wide usage in MPPT owing to its simple structure and requirement of only a few measured parameters. It periodically perturbs (i.e., increment or decrement) the array terminal voltage and compares the PV output power with that of the previous perturbation cycle. If the power was increasing, the perturbation would continue in the same direction in the next cycle; otherwise, the direction would be reversed. This means that the array terminal voltage is perturbed every MPPT cycle; therefore, when the MPP is reached, the P&O algorithm will oscillate around it.

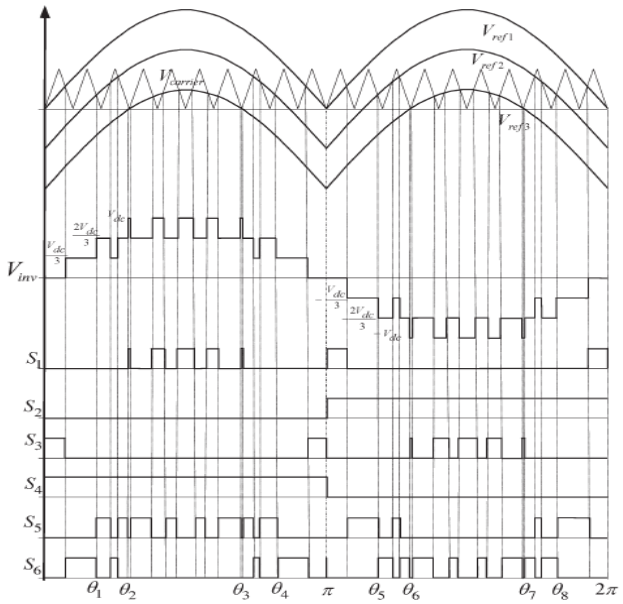

Fig. 3. Switching pattern for the single-phase seven-level inverter.

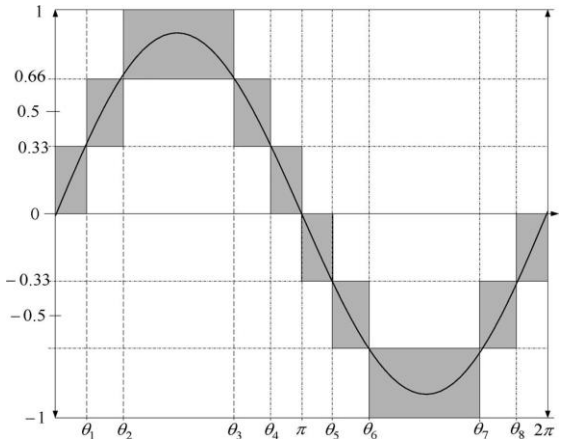

Fig. 4. Seven-level output voltage (*V*ab) and switching angles.

The P&O algorithm was implemented in the dc–dc boost converter. The output of the MPPT is the duty-cycle function. As the dc-link voltage *V*dc was controlled in the dc–ac seven level PWM inverter, the change of the duty cycle changes the voltage at the output of the PV panels. A PID controller was implemented to keep the output voltage of the dc–dc boost converter (*V*dc) constant by comparing *V*dc and *V*dc ref and feeding the error into the PID controller, which subsequently tries to reduce the error. In this way, the *V*dc can be maintained at a constant value and at more than √2 of *V*grid to inject power into the grid.

A PI algorithm was used as the feedback current controller for the application. The current injected into the grid, also known as grid current *I*grid, was sensed and fed back to a comparator that compared it with the reference current *I*gridref . *I*gridref is the result of the MPPT algorithm. The error from the comparison process of *I*grid and *I*gridref was fed into the PI controller. The output of the PI controller, also known as *V*ref , goes through an antiwindup process before being compared with the triangular wave to produce the switching signals for *S*1–*S*6. Eventually, *V*ref becomes *V*ref1; *V*ref2 and *V*ref3 can be derived from *V*ref1 by shifting the offset value, which was equivalent to the amplitude of the triangular wave. The mathematical formulation of the PI algorithm and its implementation in the DSP are discussed in detail in [28].

V. SIMULATION RESULTS

MATLAB SIMULINK simulated the proposed configuration before it was physically implemented in a prototype. The PWM switching patterns were generated by comparing three reference signals (*V*ref1, *V*ref2, and *V*ref3) against a triangular carrier signal. Subsequently, the comparing process produced PWM switching signals for switches *S*1– *S*6.

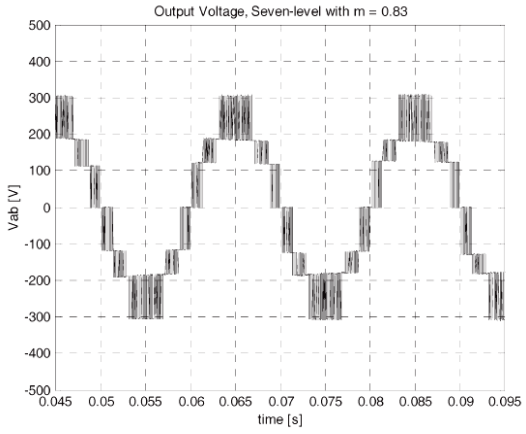

Fig. 5. Inverter output voltage (*V*inv).

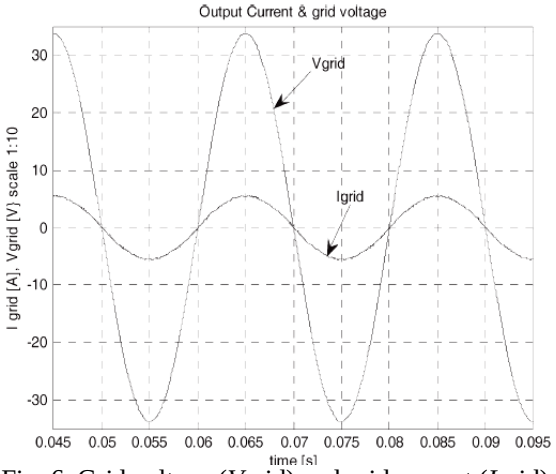

Fig. 6. Grid voltage (*V*grid) and grid current (*I*grid).

One leg of the inverter operated at a high switching rate that was equivalent to the frequency of the carrier signal, while the other leg operated at the rate of the fundamental frequency (i.e., 50 Hz). Switches *S*5 and *S*6 also operated at the rate of the carrier signal. Fig. 5 shows the simulation result of inverter output voltage *V*inv. The dc-bus voltage was set at 300 V ($> \sqrt{2}V$grid; in this case, *V*grid was 120 V). The dc-bus voltage must always be higher than $\sqrt{2}$ of *V*grid to inject current into the grid, or current will be injected from the grid into the inverter. Therefore, operation is recommended to be between $Ma = 0.66$ and $Ma = 1.0$. *V*inv comprises seven voltage levels, namely, *V*dc, 2*V*dc/3, *V*dc/3, 0, −*V*dc, −2*V*dc/3, and −*V*dc/3. The current flowing into the grid was filtered to resemble a pure sinewave in phase with the grid voltage (see Fig. 6). As *I*grid is almost a pure sinewave at unity power factor, the total harmonic distortion (THD) can be reduced compared with the THD in [28].

VI. CONCLUSION

Multilevel inverters offer improved output waveforms and lower THD. This paper has presented a novel PWM switching scheme for the proposed multilevel inverter. It utilizes three reference signals and a triangular carrier signal to generate PWM switching signals. The behavior of the proposed multilevel inverter was analyzed in detail. By controlling the modulation index, the desired number of levels of the inverter's output voltage can be achieved. The less THD in the seven-level inverter compared with that in the five- and three-level inverters is an attractive solution for grid-connected PV inverters.

REFERENCES

[1] M. Calais and V. G. Agelidis, "Multilevel converters for single-phase grid connected photovoltaic systems—An overview," in *Proc. IEEE Int. Symp. Ind. Electron.*, 1998, vol. 1, pp. 224–229.

[2] S. B. Kjaer, J. K. Pedersen, and F. Blaabjerg, "A review of single-phase grid connected inverters for photovoltaic modules," *IEEE Trans. Ind. Appl.*, vol. 41, no. 5, pp. 1292–1306, Sep./Oct. 2005.

[3] P. K. Hinga, T. Ohnishi, and T. Suzuki, "A new PWM inverter for photovoltaic power generation system," in *Conf. Rec. IEEE Power Electron. Spec. Conf.*, 1994, pp. 391–395.

[4] Y. Cheng, C. Qian, M. L. Crow, S. Pekarek, and S. Atcitty, "A comparison of diode-clamped and cascaded multilevel converters for a STATCOM with energy storage," *IEEE Trans. Ind. Electron.*, vol. 53, no. 5, pp. 1512– 1521, Oct. 2006.

[5] M. Saeedifard, R. Iravani, and J. Pou, "A space vector modulation strategy for a back-to-back five-level HVDC converter system," *IEEE Trans. Ind. Electron.*, vol. 56, no. 2, pp. 452–466, Feb. 2009.

[6] S. Alepuz, S. Busquets-Monge, J. Bordonau, J. A. M. Velasco, C. A. Silva, J. Pontt, and J. Rodríguez, "Control strategies based on symmetrical components for grid-connected converters under voltage dips," *IEEE Trans. Ind. Electron.*, vol. 56, no. 6, pp. 2162–2173, Jun. 2009.

[7] J. Rodríguez, J. S. Lai, and F. Z. Peng, "Multilevel inverters: A survey of topologies, controls, and applications," *IEEE Trans. Ind. Electron.*, vol. 49, no. 4, pp. 724–738, Aug. 2002.

[8] J. Rodriguez, S. Bernet, B. Wu, J. O. Pontt, and S. Kouro, "Multilevel voltage-source-converter topologies for industrial medium-voltage drives," *IEEE Trans. Ind. Electron.*, vol. 54, no. 6, pp. 2930–2945, Dec. 2007.

[9] M. M. Renge and H. M. Suryawanshi, "Five-level diode clamped inverter to eliminate common mode voltage and reduce dv/dt in medium voltage rating induction motor drives," *IEEE Trans. Power Electron.*, vol. 23, no. 4, pp. 1598–1160, Jul. 2008.
[10] E. Ozdemir, S. Ozdemir, and L. M. Tolbert, "Fundamental-frequencymodulated six-level diode-clamped multilevel inverter for three-phase stand-alone photovoltaic system," *IEEE Trans. Ind. Electron.*, vol. 56, no. 11, pp. 4407–4415, Nov. 2009.
[11] R. Stala, S. Pirog, M. Baszynski, A. Mondzik, A. Penczek, J. Czekonski, and S. Gasiorek, "Results of investigation of multicell converters with balancing circuit—Part I," *IEEE Trans. Ind. Electron.*, vol. 56, no. 7, pp. 2610–2619, Jul. 2009.
[12] R. Stala, S. Pirog, M. Baszynski, A. Mondzik, A. Penczek, J. Czekonski, and S. Gasiorek, "Results of investigation of multicell converters with balancing circuit—Part II," *IEEE Trans. Ind. Electron.*, vol. 56, no. 7, pp. 2620–2628, Jul. 2009.
[13] P. Lezana, R. Aguilera, and D. E. Quevedo, "Model predictive control of an asymmetric flying capacitor converter," *IEEE Trans. Ind. Electron.*, vol. 56, no. 6, pp. 1839–1846, Jun. 2009.
[14] M. F. Escalante, J.-C. Vannier, and A. Arzandé, "Flying capacitor multilevel inverters and DTC motor drive applications," *IEEE Trans. Ind. Electron.*, vol. 49, no. 4, pp. 809–815, Aug. 2002.
[15] A. Shukla, A. Ghosh, and A. Joshi, "Static shunt and series compensations of an SMIB system using flying capacitor multilevel inverter," *IEEE Trans. Power Del.*, vol. 20, no. 4, pp. 2613–2622, Oct. 2005.
[16] J. Huang and K. A. Corzine, "Extended operation of flying capacitor multilevel inverter," *IEEE Trans. Power Electron.*, vol. 21, no. 1, pp. 140– 147, Jan. 2006.
[17] F. Z. Peng, "A generalized multilevel inverter topology with self voltage balancing," *IEEE Trans. Ind. Appl.*, vol. 37, no. 2, pp. 611–617, Mar./Apr. 2001.
[18] E. Villanueva, P. Correa, J. Rodríguez, andM. Pacas, "Control of a singlephase cascaded H-bridge multilevel inverter for grid-connected photovoltaic systems," *IEEE Trans. Ind. Electron.*, vol. 56, no. 11, pp. 4399– 4406, Nov. 2009.
[19] L. M. Tolbert, F. Z. Peng, T. Cunnyngham, and J. N. Chiasson, "Charge balance control schemes for cascademultilevel converter in hybrid electric vehicles," *IEEE Trans. Ind. Electron.*, vol. 49, no. 5, pp. 1058–1064, Oct. 2002.
[20] K. A. Corzine, M. W. Wielebski, F. Z. Peng, and J. Wang, "Control of cascaded multilevel inverters," *IEEE Trans. Power Electron.*, vol. 19, no. 3, pp. 732–738, May 2004.
[21] J. I. Leon, S. Vazquez, S. Kouro, L. G. Franquelo, J. M. Carrasco, and J. Rodriguez, "Unidimensional modulation technique for cascaded multilevel converters," *IEEE Trans. Ind. Electron.*, vol. 49, no. 5, pp. 1058– 1064, Oct. 2002.
[22] C.-C. Hua, C.-W. Wu, and C.-W. Chuang, "A digital predictive current control with improved sampled inductor current for cascaded inverters," *IEEE Trans. Ind. Electron.*, vol. 56, no. 5, pp. 1718–1726, May 2009.
[23] S. Vazquez, J. I. Leon, L. G. Franquelo, J. J. Padilla, and J. M. Carrasco, "DC-voltage-ratio control strategy for multilevel cascaded converters fed with a single DC source," *IEEE Trans. Ind. Electron.*, vol. 56, no. 7, pp. 2513–2521, Jul. 2009.
[24] C. Cecati, F. Ciancetta, and P. Siano, "A multilevel inverter for photovoltaic systems with fuzzy logic control," *IEEE Trans. Ind. Electron.*, vol. 57, no. 12, pp. 4115–4125, Dec. 2010.
[25] G. Ceglia, V. Guzman, C. Sanchez, F. Ibanez, J. Walter, and M. I. Gimanez, "A new simplified multilevel inverter topology for DC–AC conversion," *IEEE Trans. Power Electron.*, vol. 21, no. 5, pp. 1311–1319, Sep. 2006.
[26] V. G. Agelidis, D. M. Baker, W. B. Lawrance, and C. V. Nayar, "A multilevel PWMinverter topology for photovoltaic applications," in *Proc. IEEE ISIE*, Guimäes, Portugal, 1997, pp. 589–594.
[27] S. J. Park, F. S. Kang,M.H.Lee, and C. U. Kim, "Anewsingle-phase fivelevel PWM inverter employing a deadbeat control scheme," *IEEE Trans. Power Electron.*, vol. 18, no. 3, pp. 831–843, May 2003.
[28] J. Selvaraj and N. A. Rahim, "Multilevel inverter for grid-connected PV system employing digital PI controller," *IEEE Trans. Ind. Electron.*, vol. 56, no. 1, pp. 149–158, Jan. 2009.
[29] N. A. Rahim and J. Selvaraj, "Multi-string five-level inverter with novel PWM control scheme for PV application," *IEEE Trans. Ind. Electron.*, vol. 57, no. 6, pp. 2111–2121, Jun. 2010.
[30] M. P. Kazmierkowski, R. Krishnan, and F. Blaabjerg, *Control in Power Electronics Selected Problems*. New York: Academic, 2002.

American Journal of Engineering Research (AJER)
e-ISSN : 2320-0847 p-ISSN : 2320-0936
Volume-02, Issue-10, pp-385-392
www.ajer.org

Research Paper Open Access

Exergy Analysis of Boiler In cogeneration Thermal Power Plant

Sarang j gulhane, Prof.Amit kumar thakur
**(scholar of mechanical department sagar institute of science and technology Bhopal.)*
** (Associate professor mechanical Engg sagar institute of science and technology Bhopal)*

***Abstract:* –** Effective energy utilization and its management for minimizing irreversibility has made human to look for efficient energy consumption & conversion. Based on several research activity and local power plant experience some key observation has made and is presented in this paper The aim of this paper is to be find out amount and source of irreversibilities gererated in boiler of 35 TPH boiler in 6 MW captive power plant so that any process in the system that having largest energy destruction can be identified that help designer to re design the system components.

***Key Words:* –** *Thermal Power Plant, energy utilization, Irreversibility.*

I. INTRODUCTION

Energy consumption is the most important problem in the today's era. In the present scenario per capita energy consumption determines the level of development of the nation. With the increased awareness that the world's energy resources are limited has caused many countries to reassess their energy policies and take measures for eliminating the waste. It has also ignited the interest in the scientists and researchers to take a close look at the energy conversion devices and to develop new techniques for better utilization of the available resources.

The First Law deals with the amounts of energy of various forms transferred between the system and its surroundings and with the changes in the energy stored in the system. It treats work and heat interactions as equivalent forms of energy in transit and offers no indication about the possibility of a spontaneous process proceeding in a certain direction. The first law places no restriction on the direction of a process, but satisfying the first law does not ensure that the process can actually occur. This inadequacy of the first law to identify whether a process can take place is remedied by introducing another general principle, the second law of thermodynamics

The exergy method of analysis is based on the Second law of thermodynamics and the concept of irreversible production of entropy. The fundamentals of the exergy method were laid down by Carnot in 1824 and Clausius in 1865. The energy-related engineering systems are designed and their performance is evaluated primarily by using the energy balance deduced from the First law of thermodynamics. Engineers and scientists have been traditionally applying the First law of thermodynamics to calculate the enthalpy balances for more than a century to quantify the loss of efficiency in a process due to the loss of energy. The exergy concept has gained considerable interest in the thermodynamic analysis of thermal processes and plant systems since it has been seen that the First law analysis has been insufficient from an energy performance stand point.

Keeping in view the facts stated above, it can be expected that performing an analysis based on the same definition of performance criteria will be meaningful for performance comparisons, assessments and improvement for thermal power plants. Additionally, considering both the energetic and exergetic performance criteria together can guide the ways of efficient and effective usage of fuel resources by taking into account the quality and quantity of the energy used in the generation of electric power in thermal power plants. The purpose of this study presented here is to carry out energetic and exergetic performance analyses, at the design conditions, for the existing coal and gas-fired thermal power plants in order to identify the needed improvement. For performing this aim, we summarized thermodynamic models for the considered power plants on the basis of mass, energy and exergy balance equations. The thermodynamic model simulation results are compared. In the direction of the comprehensive analysis results, the requirements for performance improvement are evaluated.

Energy And exergy analysis of caol fired cogeneration power plant with condensate extraction turbine

(A) Energy analysis of coal fired Cogeneration power plant with condensate extraction turbine.

In general coal based thermal plant works on Rankin cycle. Several advancement has made in recent thermal power plant to increase the energy output per unite mass of fuel burnt like reheating, regeneration etc. The design of any power plant is based on location, avaibility of fuel and it effectiveness. Since thermal power plant works on fossile fuel, it has made great interest to research to look for more efficient utilization of this fuel due to it's stock limitation under earth. Which results into no. of analysis based on energy losses and irreversibility, various attempts where made to over come this loss as and hence reheat cycle, regenerative cycle are the some fruitful outcome that came out for improvement.

II. DESCRIPTION OF COAL FIRED POWER PLANT

Several observed processes are considered for the analysis of a cumulative coal fixed thermal like lowering condenser pressure, superheating the to high temperatures, increasing the boiler pressure, reheat regenerative rankine cycle is used

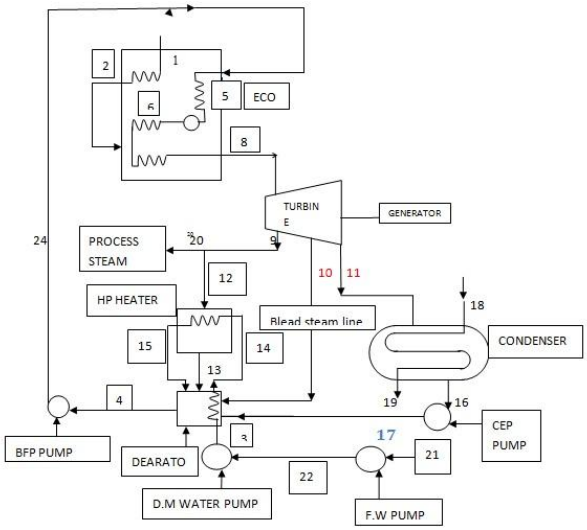

Fig.1 describs the detail part of cogeneration coal based with condensate extraction turbine consists of Boiler (B), Condensate extraction turbine with there stages (T) Pump (P), Decretory (D), a generator (S) , condense (c) high pressure feed water heater (HPH). The thermodynamic model of power plant are based on fundamental mass and energy balances. Using the energy and mass balance equation for each component in the power plant model, it is possible to compute energy and energy contents in terms of turbine power outputs, pump power consumptions boiler flow. for minimized the loss of dry flue gas.

Exergy analysis :-

useful work potential of a system is the amount of energy we extract as useful work. The useful work potential of a system at the specified state is called exergy. Exergy is a property and is associated with the state of the system and the environment. A system that is in equilibrium with its surroundings has zero exergy and is said to be at the dead state

It means available energy at a specified condition

Exergy analysis of boiler can be calculated by following formula which can be taken from research paper.

(1)Exergy analysis of fuel
(2)Exergy analysis of water
(3) Exergy analysis of Air
(4)Exergy analysis of flue gas
(5)Exergy analysis of economizer
(6)Exergy analysis of steam drum
(7)exrgy analysis of super heater

(1) Exergy analysis of fuel:-

Ultimate analysis of coal

COAL CONSITUTENT	UNIT	COAL SAMPLE
C	%	45
H	%	13
N	%	1.69
O	%	4.5
S	%	0.5
ASH	%	29.31
MOISTURE	%	9.82
VOLATILE MATTER	%	20.16
FIXED CARBON	%	34.71
CALORIFIC VALUE	KCAL/KG	4187

Exergy of fuel can be calculated by the equation proposes by shieh And fan for calculating the exergy of fuel
Exergy of fuel can be calculated by using a shieh and fan formula
f=34183016(C)+21.95(N)+11659.9(H)+18242.90(S)+13265.90(O)----------(1)
Accourding to the T.J kotas say that the ratio of exergy of fuel to caloric value of the fuel lies betn the 1.15 to 1.30 Accourding to the our ultimate analysis we get exergy of the fuel is =17683.84 kj/kg and calorific value is 17585.4 kj/kg thus ratio we get is 1.01 that is nearer to T.J kotas ratio.

Load in MW	Exergy of fuel in KW
5.6	32596.79
5.4	31480.92
4.9	30598.77
3.7	27927.78
1.1	13303.81

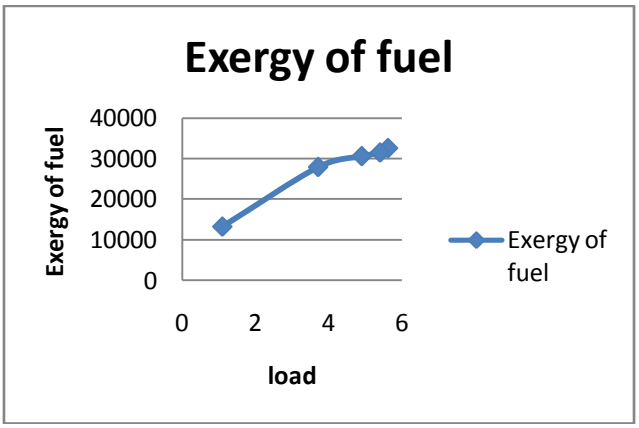

III. RESULTS AND DISCUSSION

From the above graph it shows as load increases the exergy of fuel is also increases So always run the plant in pick load
(2)The exergy of feed water
Before entering the water into the economizer ,the water is allowed to get heated in the deratator thus the temp of feed water is increased to higher temp
The temp water at economizer i/L from above table
Exergy of feed water can be calculated by

$$€\hat{w}=(c_{pw})\,(T_4-T_a)\text{- }T_a \text{Ln }\left(\frac{T_4}{T_a}\right)$$

Where
(Cp)w=specific heat of water =4.187 kj/kg
T4= temp of feed water

Ta= temp of ambient temp
While putting the above value , get following result

Load in MW	Exergy of water in KW
5.6	738.78
5.4	749.3812
4.9	656.7425
3.7	565.1152
1.1	74.30

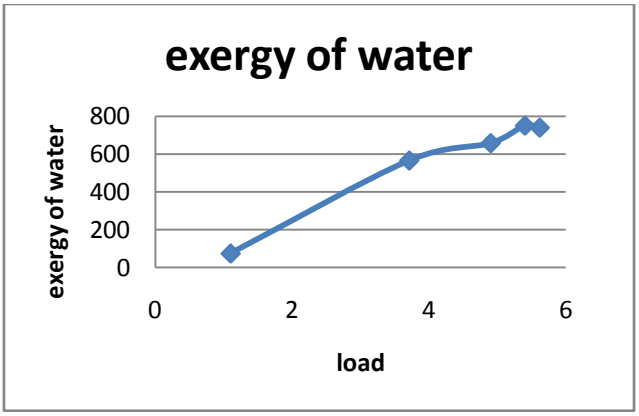

From the above graph it shows as load increases the exergy of water is also increases So always run the plant in pick load

(3)The exergy of Air

The exergy of air can be calculated by following
€a=(c_{pa}) $(T_2 - T_a)$- T_aLn $(\frac{T_2}{T_a})$
Where,
T2= temp of air after air pre heater
Ta= temp of ambient temp.

Load in MW	Exergy of Air in KW
5.6	115.075
5.4	127.077
4.9	139.212
3.7	159.925
1.1	32.77

The exergy of air is depend upon the combustion air temp as well as flue gas temp Due to that it is fund that exergy at full load i.e 5.6 MW is less as compared to the 3.7 MW s proper maintain the combustion air temp as well as flue gas temp

(4)The exergy of economizer :-
The water entering the economizer from deratator is already at higher temp is then heated almost saturated temp at that pressure but leaving the economizer remain in liquid without change in phase

€a=(c_{pw}) $(T_5 - T_4)$- T_4Ln $(\frac{T_5}{T_4})$

T5 & T4 are the temp of the ecomonizer inlet and outlet.

Load in MW	Exergy of Air in KW
5.6	927.45
5.4	940.758
4.9	893.339
3.7	725.191
1.1	211.862

It is also shows load increase exergy also increase

(5)The exergy of drum can be calculated

$€_{drum} = (h_6 - h_5)- T_6\ (s_{6-s_5})$

T6 = temp of drum

Load in MW	Exergy of drum
5.6	5123.369
5.4	5196.87
4.9	4741.2
3.7	3989.80
1.1	1408.98

As it also shows that load increase exergy of drum is also increase but in some case exergy is reduced due to steam flow is reduced as it depends upon the extraction steam or process steam

(7) The exergy of super heater

Super heater is place at end of boiler mounting and water ckt after super heater

Super heated steam is produced .the super heater for a given boiler is made up of three different component of super heater ,primary super heater is rise the temp by extracting the heat from flue gas is called as convective super heater, and second dary super heater is exposed to the flame to which heat is done by radiation thus caused radiating super heater ,temp rang for the turbine inlet is fix if the steam temp is rises above the rang it is found that attemptator or spary control valve is open ,after that steam goes to the bed super heater

Exergy rise in the drum=$(h_8 - h_6)$-$T_8(S_8 - S_6)$

As per the above diagram and reading table is found that

Load in MW	Exergy of super heater
5.6	2399.177
5.4	2103.43
4.9	2224.76
3.7	1456.16
1.1	669.21

It is also shows that load increase exergy rise of super heater also increase ,it is depend upon the temp of drum as well as temp of super heater temp.

(7)The exergy of flue gas

$€a=(c_{pg})\ (T_g - T_a)- T_a \text{Ln}\ (\frac{T_g}{T_a})$

Load in MW	Exergy of flue gas
5.6	194.14
5.4	200.228
4.9	263.251
3.7	220.324
1.1	163.797

AS load increase exergy of flue gas increase ,but it is again depend upon the temp of flue gas and boiler load if at particular load temp is less and boiler load is less then also exergy of flue gas is less.
Total exergy gain by the steam;

AS load increase exergy of flue gas increase ,but it is again depend upon the temp of flue gas and boiler load if at particular load temp is less and boiler load is less then also exergy of flue gas is less.
Total exergy gain by the steam;

Load in MW	Total exergy gain by steam
5.6	7711.21
5.4	7491.68
4.9	7203.08
3.7	5606.04
1.1	2215.74

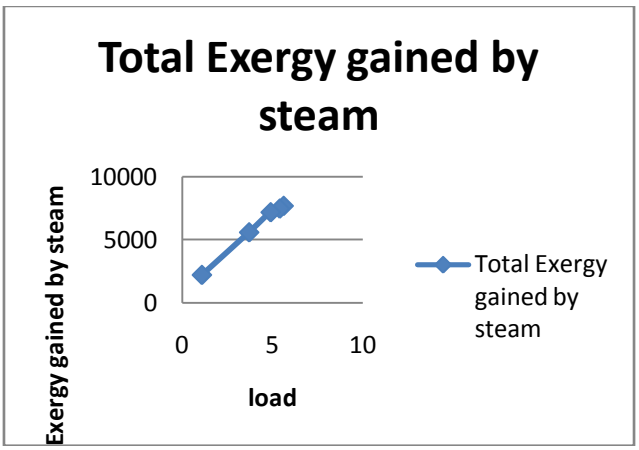

AS load increase total exergy of drum gain by the steam increase ,it is sum of exergy rise in ecomonizer and super heater
Efficiency of boiler = Total energy leaving the boiler to total energy entering the boiler

Load in MW	Efficiency of boiler as per 2 law
5.6	23.67
5.4	23.79
4.9	23.54
3.7	20.07
1.1	16.65

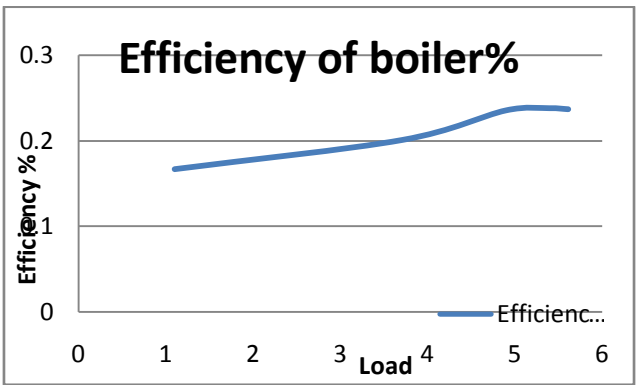

Result and discussion:-

Lot of precaution already taken for reducing the heat loss like insulation of boiler ,but still form observation boiler seem most exergy destruction part to which need to improve for 6 mw power plant analysis of exergy indicate that the boiler has exergy destruction at home load 1.1 mw is around 83.35% and as load

increases for highest load 5.6 mw the exergy destruction found to be 76.33%thus efficiency of 1 st law and 2 law increases with load ,we have to work on the peak load for reduce the irreversibility
The material capability study and exergy study on various component of boiler can b e the scop of the study, with the passage of time the technology getting matured and new material wi th higher capacity heat transfer rate like heat pipe and thermo sypon is used ,the data designer of the boiler can redesign the boiler with efficient auxiliary devices

IV. ACKNOWLEDGEMENTS

The author wish to thank Raymond India Limited, Yavatmal, for granting the permission to carry out work and their kind support during work.

REFERENCES

[1] A. Yunus and A. Michael, "Thermodynamics an Engineering Approach," Tata McGraw Hill, New Delhi, 2007.
[2] T. J. Kotas, "Exergy Criteria of Performance for Thermal Plant: Second of Two Papers on Exergy Techniques in Thermal Plant Analysis," International Journal of Heat and Fluid Flow, Vol. 2, No. 4, 1980, pp. 147-163.
[3] yongping yang “comprehensive exergy based evaluation and parametric study of a coal fired ultra super critical power plant
[4] P Regulagadda “energy analysis of a thermal power plant with measured boiler and turbine losses” applied thermal engineering vol 30-[2010]970-976
[5] T. Ganapathy, N. Alagumurthi, R. P. Gakkhar and K. Murugesan, "Exergy Analysis of Operating Lignite Fired Thermal Power Plant," Journal of Engineering Science and Technology Review, Vol. 2, No. 1, 2009, pp. 123-130.
[6] Seluk Atas “comparative energetic and exergetic performance analysis for coal fired thermal power plant in turkey” vol 48(2009)2179-2186
[7] S. C. Kamate and P. B. Gangavati, "Exergy Analysis of Cogeneration Power Plants in Sugar Industries," Applied Thermal Engineering, Vol. 29, No. 5-6, 2009, pp. 1187-1194.
[8] Arif hepbasil “Thermodynamic analysis of a building using exergy analysis method”
[9] A. Datta, S. Sengupta and S. Duttagupta, "Exergy Analysis of a Coal-Based 210 mw Thermal Power Plant," International Journal of Energy Research, Vol. 31, No. 1, 2007, pp. 14-28.
[10] M.K Gupta “exergy analysis and investigation for various feed water heater of direct steam generation solar thermal power plant
[11] I. H. Aljundi, "Energy and Exergy Analysis of a Steam Power Plant in Jordan," Applied Thrmal Engineering, Vol. 29, No. 2-3, 2009, pp. 324-328.
[12] Ankit patel “energy and exergy analysis of boiler with different fuels like Indian coal ,imported coal and L.H.H.S oil vol 8 oct 2012
[13] R saidur “energy and exergy economic analysis of industrial boiler” Vol 38(2010)2188-2197
[14] I. Dincer and M. A. Rosen, "Effect of Varying Dead-State Properties on Energy and Exergy Analyses of Thermal Systems,"
[15] International Journal of Thermal Sciences, Vol. 43, No. 3, 2004, pp. 121-133..
[16] R Jyothu naik “exergy analysis of 120MWcoal based thermal power plant ’’vol 2 4 apil 2013 issn 2278-0181
[17] M. A. Rosen, "Energy- and Exergy-Based Comparison of Coal-Fired and Nuclear Steam Power Plants," Exergy, Vol. 1, No. 3, 2001,
[18] pp. 180-192.
[19] M.k pal “energy and exergy analysis of boiler and turbine of a coal fired thermal power plant ’’vol 2 Issue 6 jun 2013
[20] I. Dincer and M. A. Rosen, "Effect of Varying Dead-State Properties on Energy and Exergy Analyses of Thermal Systems,"
[21] International Journal of Thermal Sciences, Vol. 43, No. 3, 2004, pp. 121-133.
[22] Alpesh mehata “thermodynamic analysis of gandhinagar thermal power station’’vol 3 oct –dec 2010
[23] H. Erdem, A. V. Akkaya., A. Dagdas, S. H. Sevilgen, B. Sahin, I. Tek, C. Gungor and S. Atas, "Comparative Energetic and Exergctic Performance Analyses for Coal-Fired Thermal Power Plants in Turkey." International Journal of Thermal Sciences, Vol. 48, No. 11, 2009,
[24] pp. 2179-2186.
[25] Amir vosough “improvement power plant efficiency with condenser pressure vol 2 No 3 june 2011
[26] i . H. Aljundi, "Energy and Exergy Analysis of a Steam Power Plant in Jordan," Applied Thrmal Engineering, Vol. 29, No. 2-3, 2009, pp. 324-328.

[27] A. Vidal, R. Best, R. Rivero and J. Cervantes. "Analysis of a Combined Power and Refrigeration Cycle by the Exergy Method," Energy, Vol. 31, No. 15, 2006, pp. 3401-3414,
[28] N. Arai, H. Taniguchi. K. Mouri and T. Nakahara. "Exergy Analysis on Combustion and Energy Conversion Processes," Energy, Vol. 30, No. 2-4. 2005. pp. 111-117.
[29] Nestor Garcia herando "energy and exergy analysis of an absorption power cycle"vol 55(2013)69-77
[30] Dincer and M. A. Rosen, "Exergy Analysis of Waste Emissions," International Journal of Energy Reserch, Vol. 23. No. 13, 1999. pp. 1153-1163.
[31] A. Khaliq and S. C. Kaushik, "Thermodynamic Performance Evaluation of Combustion Gas Turbine Cogeneration System w ith Reheat." Applied Thermal Engineering, Vol. 24. No. 13. 2004, pp. 1785-1795.
[32] G. M. Chen, S. K. Tyagi, Q. Wang and S. C. Kaushik. A New Thcrmoeconomic Approach and Parametric Study of an Irreversible Regenerative Brayton Refrigeration Cycle," International Journal of Refrigeration, Vol. 29. No. 7, 2006. pp. 1167-1174.
[33] S. C. Kaushik, S. K. Tyagi and M. K. Singhal. "Parametric Study of an Irreversible Regenerative Brayton Cycle with Isothermal Heat Addition," Energy- Conversion & Management, Vol. 44. No. 12. 2003, pp. 2013-2025.
[34] S M. Zubair and M A. Habib. "Second-Law-Based Thermodynamic Analysis of Regenerative-Reheat Rankine-Cycle Power Plants." Energy. Vol. 17, No. 3, 1992, pp. 295-301.
[35] M. Yilmaz, O. N. Sara and S. Karsli, "Performance Evaluation Criteria for Heat Exchangers Based on Second Law Analysis," Exergy, Vol. 1, No. 4, 2001, pp. 278-294.
[36] P. K. Nag. "Power Plant Engineering."

American Journal of Engineering Research (AJER)
e-ISSN : 2320-0847 p-ISSN : 2320-0936
Volume-02, Issue-10, pp-393-400
www.ajer.org

Research Paper Open Access

Modified Multiport Dc-Dc Converter Topology For Smart Grid

Dhamodharan Shanmugam, Dhivya Balakrishan, K.Indiradevi
[1]*M.E-PED, Department OF EEE, Sri Shakthi Institute of Engineering and Technology, Coimbatore, Tamilnadu. INDIA.*
[2]*M.E-PED, Department OF EEE, Sri Shakthi Institute of Engineering and Technology, Coimbatore, Tamilnadu. INDIA.*
[3]*Asst.Prof (S)/Department OF EEE, Sri Shakthi Institute of Engineering and Technology, Coimbatore, Tamilnadu. INDIA.*

Abstract: **-** The development of a Solid State Transformer (SST) that incorporates a DC-DC multiport converter to integrate both photovoltaic (PV) power generation and battery energy storage is presented in this dissertation. The DC-DC stage is based on a quad active-bridge (QAB) converter which not only provides isolation for the load, but also for the PV and storage. The AC-DC stage is implemented with a pulse-width-modulated (PWM) single phase rectifier. A unified gyrator-based average model is developed for a general multi-active-bridge (MAB) converter controlled through phase-shift modulation (PSM). Expressions to determine the power rating of the MAB ports are also derived. The developed gyrator-based average model is applied to the QAB converter for faster simulations of the proposed SST during the control design process as well for deriving the state-space representation of the plant. Both linear quadratic regulator (LQR) and single-input-single-output (SISO) types of controllers are designed for the DC-DC stage. A novel technique that complements the SISO controller by taking into account the cross coupling characteristics of the QAB converter is also presented herein. Cascaded SISO controllers are designed for the AC-DC stage. The QAB demanded power is calculated at the QAB controls and then fed into the rectifier controls in order to minimize the effect of the interaction between the two SST stages. The dynamic performance of the designed control loops based on the proposed control strategies are verified through extensive simulation of the SST average and switching models.

Keywords:- *DC–DC converter, distributed generation, multiport converter, smart grid, solid-state transformer.*

I. INTRODUCTION

In the last decade, the Smart Grid concept has drawn the attention of researchers and industry as a feasible solution to the challenges that the entire electrical system is facing due to the growth in load, the increasing penetration of renewables and the deployment of the distributed generation at the consumer end [1]. Currently, the Future Renewable Electric Energy Delivery and Management (FREEDM) Systems Center is working in several areas in its efforts to contribute with the modernization of the power distribution system and help develop the standards for the implementation and optimal operation of this portion of the future Smart Grid [2]. The power-electronics-based transformer, or so-called SST, is one of the key components of the FREEDM distribution system. In addition to serving as a regular distribution transformer, the SST provides ports for the proper integration of distributed energy resources (DER) and distributed energy storage (DES), thus enhancing the reliability of the distribution system [3]. Additionally, the SST enables the implementation of distributed intelligence through a secure communication network (COMM) to ensure stability and optimal operation of the distribution system. Another important component of the FREEDM distribution system is the Fault Identification Device (FID), which is a fast protection device deployed to enable Intelligent Fault Management (IFM) [4].

Besides the advantage of its reduced size and weight due to its high frequency (HF) transformer [5], the SST makes use of state-of-the-art Power Electronics devices that allows it to provide additional functionalities such as on-demand reactive power support to grid, power quality, current limiting, storage management and a DC bus for end use. Poor load power factor and harmonics are isolated from the distribution system, thus improving the overall system efficiency. Additionally, the selection of new generation materials for semiconductors and magnetics may help improve its efficiency when compared to a regular transformer of the

same ratings. Fig. 1 shows the SST interfacing photovoltaic (PV) generation, storage, electric loads as well as plug-in hybrid electric vehicles (PHEV).

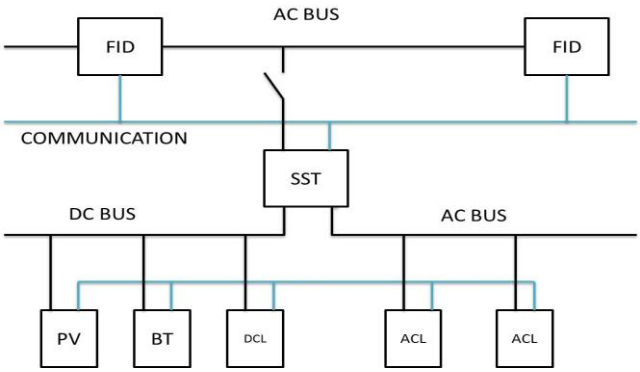

Figure. 1. Integration of DES, DER and intelligent loads through the SST.

The interest in renewable sources of energy has increase, considerably. They represent a potential solution to mitigate environmental issues and reduce the dependence on traditional sources of energy for electrical generation. The need of technology for adapting these non-traditional types of energy into the system has motivated the development of new generation power electronics converters. The future homes will make use of power converters to integrate all the available sources of electrical energy, including renewables as wind turbine (WT) and PV. These power converters have to meet efficiency, flexibility, power density, reliability and safety requirements.

A generation of power converters that has been proposed by researchers for the integration of distributed generation (DG) and storage is the family of multi-port DC-DC converters [6]. Their advantage lies in the integration of several sources with minimum DC-DC conversion stages. The traditional and integrated configurations introduced in [6] are shown in Fig. 2 and Fig. 3, respectively. The latter may require a reduced the number of components while providing galvanic isolation.

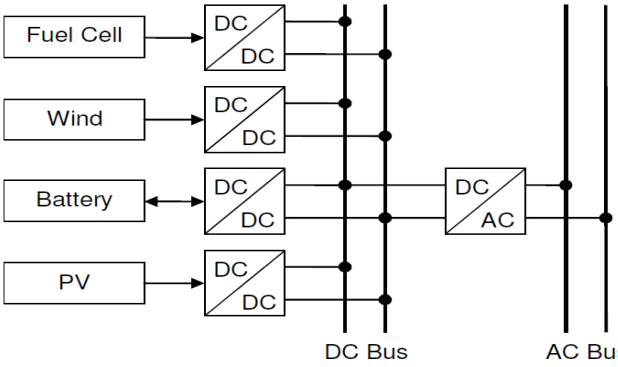

Figure. 2. Conventional power conversion through two-port DC-DC converters.

Since the SST and the multi-port converters are two key areas of research, the work presented herein has been motivated by the better integration that the SST can achieve with the use of multi-port converters. The three-stage configuration that has been identified as a potential candidate for the SST implementation relies on a DC bus for PV and storage integration.

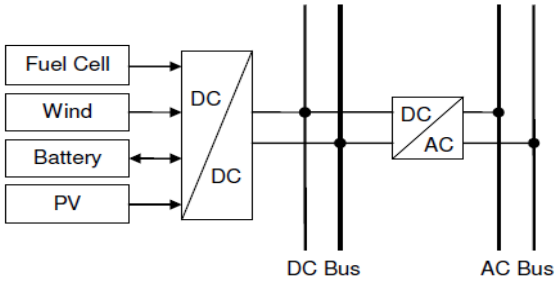

Figure. 3. Integrated power conversion through a multi-port DC-DC converter

This is achieved through separate DC-DC converters. Without isolation, the voltage ratings of these devices must be selected mainly based on the DC bus voltage rating. If voltage ratings are not compatible and/or isolation is required, then additional isolation is needed, thus increasing the size of the system. Furthermore, separate controllers for each DC-DC converter are to be designed. In this design process, the stability of the interconnected DC-DC converters must be ensured. The need of technology for integrating DG and storage into the distribution system has motivated the development of a new generation of power converters. A family of multiport dc–dc converters, which includes the multiactive-bridge (MAB) converters, has been proposed by researchers [6]. Their advantage lies in the integration of several sources with minimum dc–dc conversion stages, which yields a higher power density. Since the SST considered herein includes the grid, the load, the PV system, and the storage, a four-port dc–dc converter as the quad-active-bridge (QAB) converter is required.

II. PROPOSED SYSTEM

This paper proposes the development of a SST based on a QAB converter, to integrate DG and storage. The QAB converter, used in the implementation of the SST dc–dc stage, provides isolation for DG and storage through a single four-winding HF transformer as seen in Fig. 4 and the control design involves the analysis of only a single converter. The proposed SST is based on a particular type of multi-port converter, called quad-active-bridge (QAB) converter, to integrate PV and storage. This SST topology eliminates the need of additional isolation and only an integrated controller for the DCDC stage may be required.

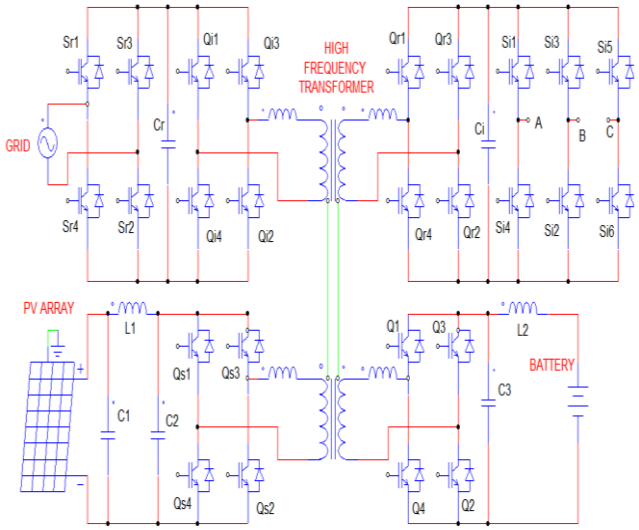

Figure. 4. QAB-based SST with PV and storage integrated through HF transformer.

The block representation of the proposed SST topology is shown in Fig. 5. Since little information is available on the literature for the QAB converter, a detailed analysis is required. Furthermore, an average model for any multi-active-bridge (MAB) converter is developed and expressions to calculate the rated power of any MAB port are derived. This is the basis for the dynamic analysis and control design of the DC-DC stage of the proposed SST topology.

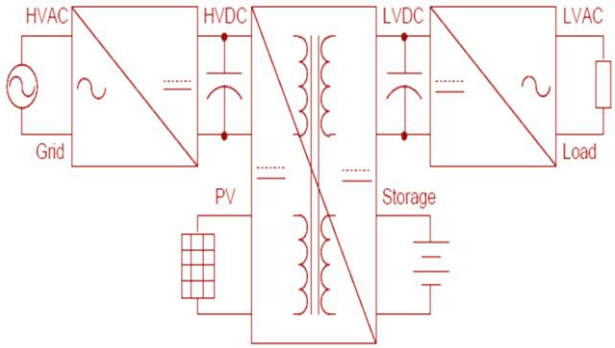

Figure 5. QAB-based SST with storage and PV.

The control design for the SST DC-DC stage is performed using both the conventional single-input-single-output (SISO) approach and a more modern multiple input- multiple-output (MIMO) approach. Furthermore, the SISO controller is complemented with a novel technique to deal with the cross-coupled characteristics of the QAB. Additionally, the control design for the SST AC-DC stage introduces a technique to deal with the interactions that result when the above two SST stages are interconnected. The performance of the controls is verified through extensive simulation of both switching and average models of the SST. Experimental results from the hardware implementation of a prototype SST are presented for validation purposes. Since no contributions are made on the SST DC-AC stage, it is modeled with a current source during its analysis and simulation, and implemented with an electronics load when testing the prototype SST.

III. QAB CONVERTER

Since the QAB converter has been selected for the implementation of the SST dc–dc stage, it will be analyzed herein following the approach developed for the MAB converter in the previous section. In [7], the authors briefly introduce the QAB converter; however, no experimental results have been provided to date. The switching model of the QAB converter is shown in Fig. 4 while its "Δ" equivalent ac circuit referred to port 1 is shown in Fig. 6, where the involved link inductances can be calculated with (1). Based on Fig. 6, the idealized steady-state QAB waveforms for unity-dc-conversion ratios are illustrated in Fig. 7. The bottom two plots show the currents *ij* at the dc side of the QAB ports, along with their corresponding CCA values *Ij*. The involved gyration gains can be calculated by using (2). When the max QAB link power has been reached between any two ports, the direction of the QAB power flow depends on the number of source, forwarding, and load ports [8] – [15].

$$L_{jk} = (L'_j + L_{\mathrm{TH}j})\left[L'_k\left(\frac{1}{L_m} + \sum_{l\neq j,k}^{n}\frac{1}{L'_l}\right) + 1\right] \quad \text{.....(1)}$$

$$g_{jk} = \frac{I_{jk}}{V_k} = \frac{N_1^2}{N_j N_k}\frac{1}{2\pi f_s L_{jk}}\phi_{jk}\left(1 - \frac{|\phi_{jk}|}{\pi}\right) \quad \text{.....(2)}$$

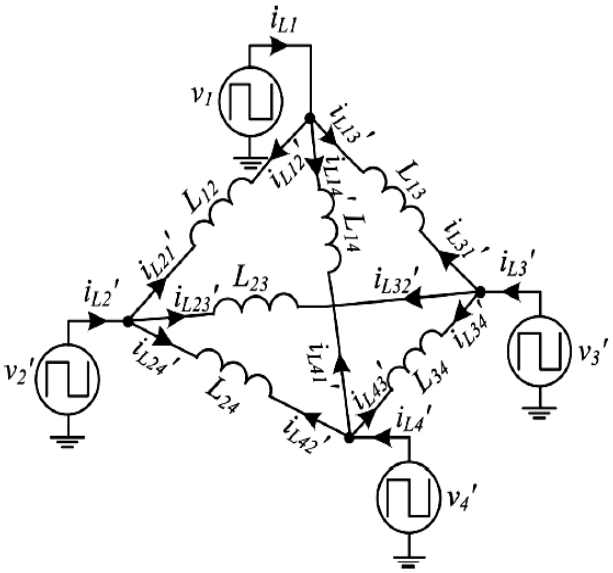

Figure 6. QAB "Δ" equivalent ac circuit referred to port 1.

IV. CONTROL SYSTEM

The block diagram in Fig. 8 shows the single-input-single output type of control loop for the PV voltage implemented herein. The gains associated with the feedback-signal conditioning, as well as the DSP digital-to-analog conversion and pulse width modulation (PWM) modules have been intentionally omitted for simplicity.

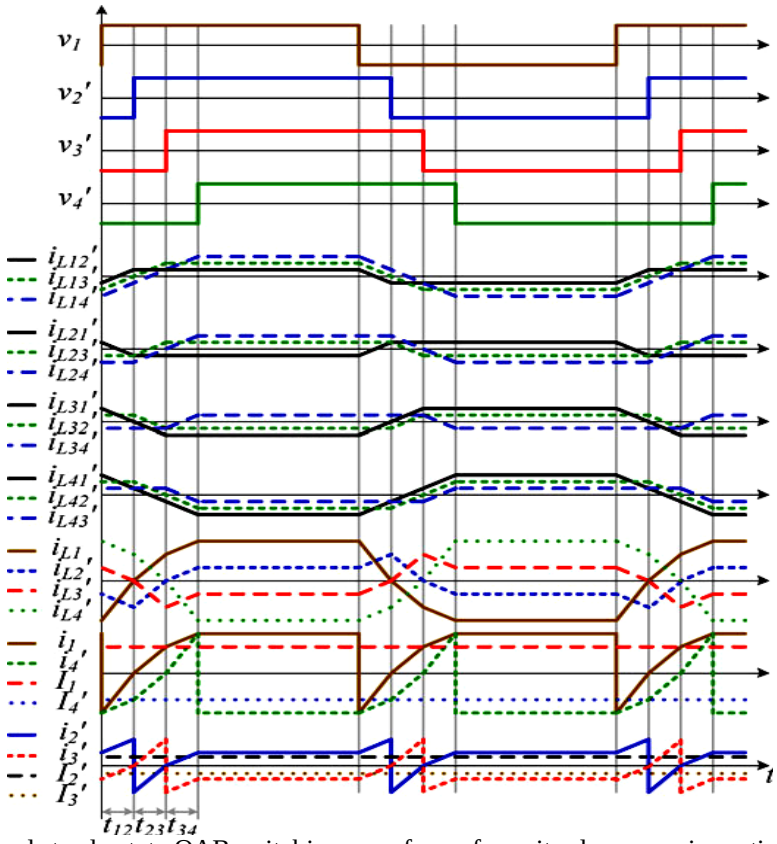

Figure 7. Idealized steady-state QAB switching waveforms for unity-dc conversion ratios and equal link inductances.

The control loops for the LVDC voltage and the battery current share the same structure. In the event that its saturation limits implemented on the DSP are reached, a controller may try to drive the phase-shift angles of the slower loops through the entries of the *KB* matrix. In order to avoid this, it may require forcing *KB* to be the identity matrix.

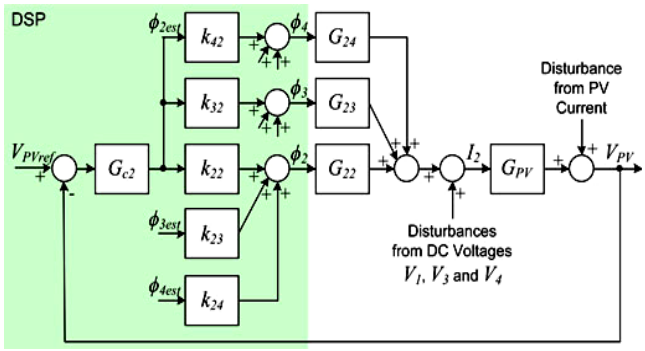

Figure 8. Simplified PV voltage control loop.

The entries of *GC* have been designed with the k-factor technique [16] with bandwidths of 200, 20, and 2 Hz for Gc3, Gc2, and Gc4, respectively, and phase margin of 60◦ for all of them. Alternatively, a multiple-input multiple- output type of control loop can be considered in order to incorporate the dc voltages as plant state variables [17], [18].

V. SIMULATION RESULTS

The selected simulation package is MATLAB/Simulink complemented with PLECS block set. Based on Fig. 4, the system electrical parameters are listed in Table I. The base inductance, obtained from the switching frequency, voltage, and current rating, is 76.4 μH. The QAB switching waveforms for $\varphi 2 = -38◦$, $\varphi 3 = -76◦$, and $\varphi 4 = -38◦$ are shown in Fig. 9.

TABLE I: SYSTEM ELECTRICAL PARAMETERS

Description	Symbol	Value
High-voltage-DC link voltage	V_{HVDC}	48 V
Low-voltage-DC link voltage	V_{LVDC}	48 V
PV voltage	V_{PV}	48 V
Battery voltage	V_{Batt}	48 V
Ports Current Rating	I_{Rating}	5 A
Port 1 leakage inductance	L_1	0.851 pu
Port 2 leakage inductance	L_2	0.851 pu
Port 3 leakage inductance	L_3	0.851 pu
Port 4 leakage inductance	L_4	0.851 pu
CLC filter inductance	L_{F1}	0.151 pu
LC filter inductance	L_{F2}	0.191 pu
High-voltage-DC link capacitance	C_{HVDC}	200 μF
CLC filter capacitance 1	C_{F1}	200 μF
CLC filter capacitance 2	C_{F2}	200 μF
Low-voltage-DC link capacitance	C_{F3}	200 μF
LC filter capacitance	C_{F4}	200 μF
Maximum phase-shift angle	ϕ	90°
Switching frequency	f_s	20 kHz

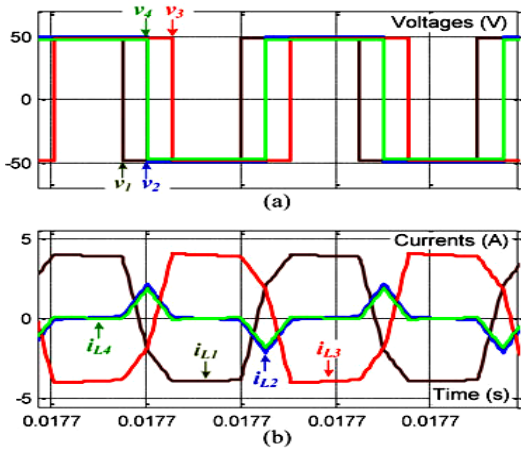

Fig. 9. Simulation results: QAB steady-state switching waveforms for $\varphi 2 = -38^\circ$, $\varphi 3 = -76^\circ$, and $\varphi 4 = -38^\circ$.

For the simulation of the close-loop operation, a step load at the LVDC link is applied to the system. The transient response when *KB* equals the identity matrix is seen in Fig. 10. It can be observed that, following the disturbance, the power variation is distributed among the remaining ports. This causes the PV voltage to dip. In steady state, the power is balanced by the HVDC link. When *KB* is selected to transfer the power variation onto the HVDC port, the transient response is seen in Fig. 11. It can be observed that the current from the HVDC link is forced to increase to meet the current demanded by the load with minimal undershoot on the PV and battery currents.

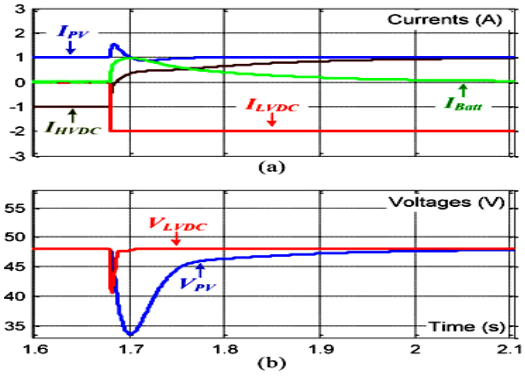

Fig. 10. Simulation results: SST dc–dec stage transient response to a step load when *KB* equals the identity matrix.

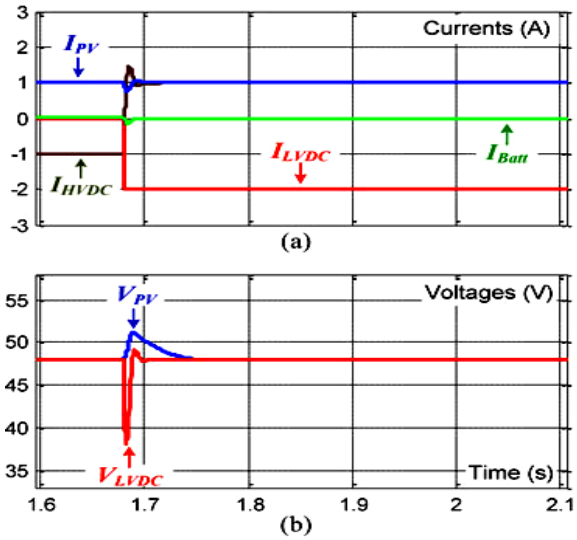

Fig. 11. Simulation results: SST dc–dc stage transient response to a step load when the power variation is transferred onto the HVDC link.

As a result, following the disturbance, the battery is forced to supply the current demanded by the load before slowly returning to its initial steady state. As seen from the simulation results, The QAB dc-side currents are directly controlled through the phase-shift angles both during transients as well as during steady state, thus ensuring the transformer amp-turn balancing at the QAB ac side. During transients, the QAB currents are shared depending on the selection of *KB*, as seen in Fig. 10 through Fig. 11. During steady state, the QAB currents are shared depending on the controls set point.

VI. CONCLUSION

A SST topology based on a QAB converter that provides isolation for the load, as well as DG and storage has been proposed herein. A gyrator-type large-signal average model has been developed for a general MAB converter and used to speed up the simulation of the dc–dc stage of the QAB-based SST. The expressions to determine the power rating of an MAB port have been derived and used to determine the power rating of the QAB ports considering the operating characteristics of the SST application. A control technique that takes into account the cross-coupling characteristics of the QAB converter has been introduced herein. This technique allows improving the dynamic performance of the HVDC voltage regulation of the SST. The dynamic performance of the control strategy has been verified through extensive simulation of both switching and average models.

REFERENCES

[1] Hassan, R.; Radman, G.; , "Survey on Smart Grid," *IEEE SoutheastCon 2010 (SoutheastCon), Proceedings of the* , vol., no., pp.210–213, 18–21 March 2010.

[2] Huang, A.Q.; Baliga, J.; , "FREEDM System: Role of power electronics and power semiconductors in developing an energy internet," *Power Semiconductor Devices & IC's, 2009. ISPSD 2009. 21st International Symposium on*, vol., no.pp.9–12, 14–18 June 2009.

[3] Heydt, G.T.; , "Future renewable electrical energy delivery and management systems: Energy reliability assessment of FREEDM systems," *Power and Energy Society General Meeting, 2010 IEEE* , vol., no., pp.1–4, 25–29 July 2010.

[4] Karady, G.G.; Xing Liu; , "Fault management and protection of FREEDM systems," *Power and Energy Society General Meeting, 2010 IEEE* , vol., no., pp.1–4, 25–29 July 2010.

[5] Tiefu Zhao; Liyu Yang; Jun Wang; Huang, A.Q., "270 kVA Solid State Transformer Based on 10 kV SiC Power Devices," *Electric Ship Technologies Symposium, 2007. ESTS '07. IEEE*, vol., no., pp.145–149, 21–23 May 2007.

[6] Tao, H.; Kotsopoulos, A.; Duarte, J.L.; Hendrix, M.A.M.; , "Family of multiport bidirectional DC-DC converters," *Electric Power Applications, IEE Proceedings* - , vol.153, no.3, pp. 451– 458, 1 May 2006.

[7] M. Qiang, W. Wei-yang, and X. Zhen-lin, "A multi-directional power converter for a hybrid renewable energy distributed generation system with battery storage," in *Proc. CES/IEEE 5th Int. Power Electron. Motion Control Conf.*, Aug. 14–16, 2006, vol. 3, pp. 1–5.
[8] G. Wang, S. Baek, J. Elliott, A. Kadavelugu, F. Wang, X. She, S. Dutta, Y. Liu, T. Zhao, W. Yao, R. Gould, S. Bhattacharya, and A. Q. Huang, "Design and hardware implementation of Gen-1 silicon based solid state transformer," in *Proc. 26th Annu. IEEE Appl. Power Electron. Conf. Expo.*, Mar. 6–11, 2011, pp. 1344–1349.
[9] H. Tao, A. Kotsopoulos, J. L. Duarte, and M. A. M. Hendrix, "Family of multiport bidirectional DC–DC converters," *IEE Proc.—Electric Power Appl.*, vol. 153, no. 3, pp. 451–458, May 2006.
[10] R. W. A. A. De Doncker, D. M. Divan, andM. H. Kheraluwala, "A threephase soft-switched high-power-density DC/DC converter for high-power applications," *IEEE Trans. Ind. Appl.*, vol. 27, no. 1, pp. 63–73, Jan./Feb. 1991.
[11] H. Tao, A. Kotsopoulos, J. L. Duarte, and M. A. M. Hendrix, "A softswitched three-port bidirectional converter for fuel cell and supercapacitor applications," in *Proc. IEEE 36th Power Electron. Spec. Conf.*, Jun. 2005, pp. 2487–2493.
[12] C. Zhao and J. Kolar, "A novel three-phase three-port UPS employing a single high-frequency isolation transformer," in *Proc. Power Electron. Specialists Conf.*, vol. 6, Jun. 2004, pp. 4135–4141.
[13] S. Falcones and R. Ayyanar, "Simple control design for a three-port DCDC converter based PV system with energy storage," in *Proc. 25th Annu.IEEE Appl. Power Electron. Conf. Expo.*, Feb. 21–25, 2010, pp. 2149–2153.
[14] Q. Chen, F. C. Lee, J. Z. Jiang, and M. M. Jovanovic, "A new model for multiple-winding transformer," in *Proc. 25th Annu. IEEE Power Electron. Spec. Conf. Rec.*, Jun. 20–25, 1994, vol. 2, pp. 864–871.
[15] M. Ehsani, I. Husain, and M. O. Bilgic, "Power converters as natural gyrators," *IEEE Trans. Circuits Syst. I: Fundam. Theory Appl.*, vol. 40, no. 12, pp. 946–949, Dec. 1993.
[16] N. Mohan, T. M. Undeland, and W. P. Robbins, *Power Electronics: Converters, Applications, and Design*, 2nd ed. New York: Wiley, 1995.
[17] A. A. Rodriguez, *Analysis and Design of Multivariable Feedback Control Systems*. Tempe, AZ: Control3D, LLC, 2003.
[18] D. S. Naidu, *Optimal Control Systems*. Boca Raton, FL: CRC Press, 2003.